AD_____

Award Number: W81XWH-06-1-0303

TITLE: BATTLE (Biomarker-based Approach of Targeted Therapy for Lung Cancer Elimination)

PRINCIPAL INVESTIGATOR: Waun Ki Hong, M.D.
Edward Kim, M.D.

CONTRACTING ORGANIZATION: University of Texas M. D. Anderson Cancer Center
Houston, TX 77030

REPORT DATE: April 2012

TYPE OF REPORT: Final

PREPARED FOR: U.S. Army Medical Research and Materiel Command
Fort Detrick, Maryland 21702-5012

REPORT DOCUMENTATION PAGE

Form Approved
OMB No. 0704-0188

1. REPORT DATE	2. REPORT TYPE	3. DATES COVERED
April 2012	Final	1 April 2006 – 31 March 2012

4. TITLE AND SUBTITLE

BATTLE (Biomarker-based Approach of Targeted Therapy for Lung Cancer Elimination)

5a. CONTRACT NUMBER

5b. GRANT NUMBER
W81XWH-06-1-0303

5c. PROGRAM ELEMENT NUMBER

6. AUTHOR(S)

Waun Ki Hong, M.D.
Edward Kim, M.D.

E-Mail: whong@mdanderson.org

5d. PROJECT NUMBER

5e. TASK NUMBER

5f. WORK UNIT NUMBER

7. PERFORMING ORGANIZATION NAME(S) AND ADDRESS(ES)

University of Texas M. D. Anderson Cancer Center
Houston, TX 77030

8. PERFORMING ORGANIZATION REPORT NUMBER

9. SPONSORING / MONITORING AGENCY NAME(S) AND ADDRESS(ES)
U.S. Army Medical Research and Materiel Command
Fort Detrick, Maryland 21702-5012

10. SPONSOR/MONITOR'S ACRONYM(S)

11. SPONSOR/MONITOR'S REPORT NUMBER(S)

12. DISTRIBUTION / AVAILABILITY STATEMENT
Approved for Public Release; Distribution Unlimited

13. SUPPLEMENTARY NOTES

14. ABSTRACT

The Program BATTLE seeks to establish individualized targeted therapy by prospectively examining patients' tumor biomarker profiles and assigning them to corresponding targeted therapies with the expectation to yield a better clinical outcome. Based on common altered signaling pathways in lung cancer, the BATTLE Program proposes to develop four phase II trials for chemorefractory, advanced NSCLC patients: erlotinib, ZD6474, bexarotene with erlotinib, and sorafenib which target, respectively, EGFR, VEGF / VEGFR, retinoid X receptor and cyclin D1, and Ras / Raf signaling pathways. A novel adaptive randomization statistical design will be applied to the clinical trials to accelerate the identification of best-fit treatment for patients. We propose also to study the molecular mechanisms of response or resistance to these targeted agents, identify novel molecular features in tumors and surrogate tissues to correlate with tumor response or resistance to the agents and, finally, explore other novel targeted agents (RAD001 and perifosine) in combination and their mechanisms of action by targeting mTOR and PI3K/Akt signaling, and develop phase I trials to test these combinations.

15. SUBJECT TERMS
Lung cancer, biomarker, targeted therapy, ZD6474, erlotinib, Sorafenib, bexarotene

16. SECURITY CLASSIFICATION OF:			17. LIMITATION OF ABSTRACT	18. NUMBER OF PAGES	19a. NAME OF RESPONSIBLE PERSON
a. REPORT	b. ABSTRACT	c. THIS PAGE			USAMRMC
U	U	U	UU	253	19b. TELEPHONE NUMBER *(include area code)*

TABLE OF CONTENTS

INTRODUCTION

Lung cancer is the leading cause of cancer-related death in both men and women in the United States. Chemotherapy has reached its limit in improving the survival of lung cancer patients. Therefore, a different strategy must be waged in the battle against lung cancer. Targeted therapy, a newly emerged therapeutic approach in lung cancer, has succeeded in some cancer types and demonstrated its initial success in the treatment of lung cancer when a class of targeted agents termed epidermal growth factor receptor (EGFR) tyrosine kinase inhibitors, such as gefitinib and erlotinib, improved tumor response rates in patients with advanced non-small cell lung cancer (NSCLC), with results strongly correlated to the presence of *EGFR* mutations in the tumors (Cappuzzo and Hirsch et al., 2004; Cappuzzo and Magrini et al., 2004; Gatzemeier et al., 2004; Herbst and Giaccone et al., 2004; Herbst and Prager et al., 2004; Herbst and Sandler et al., 2004; Lynch et al., 2004; Kobayashi et al., 2005; Miller et al., 2004; Pao et al., 2004; Paez et al., 2004; Shepherd et al., 2004; Shigematsu et al., 2005). This finding has demonstrated, for the first time, the importance of selecting patients for individualized targeted therapy in NSCLC.

The Program **BATTLE** (**B**iomarker-integrated **A**pproaches of **T**argeted **T**herapy for **L**ung Cancer **E**limination) seeks to establish individualized targeted therapy by prospectively examining patients' tumor biomarker profiles and assigning them to corresponding targeted therapies with the expectation to yield a better clinical outcome. This novel approach will be a proof-of-principle experiment to test the benefit of molecular-based individualized targeted therapy for lung cancer patients. Specifically, the objectives of the BATTLE program are:

1) To establish a clinical trial program using biomarkers to select individualized targeted therapy for patients with chemorefractory advanced NSCLC through the implementation of molecular classification based on the status of specific targeted biomarkers and adaptive randomization via hierarchical Bayes modeling.
2) To study the molecular mechanisms of response and resistance to targeted agents to discover new signaling pathways for test in future trials.
3) To identify molecular features in tumor tissues to correlate with tumor response or resistance, and identify serum biomarkers as surrogates.
4) To investigate other targeted agents in combination to overcome the resistance due to novel signaling pathways (e.g., mTOR and PI3K/Akt) and improve treatment efficacy.

BATTLE is composed of four Specific Aims with four phase II clinical trials and an umbrella protocol in Aim 1, six research projects in Aims 2 - 4, and two potential phase I trials in Aim 4. Here, we present our scientific progress of the BATTLE program for this sixth and final grant year.

PROGRESS REPORT

Aim 1 To establish a clinical trial program using biomarker assessment to select individualized targeted therapy for previously treated chemorefractory advanced NSCLC patients.

(PI, Co-PIs, and Investigators: Drs. Waun Ki Hong, Roy Herbst, Edward S. Kim, George Blumenschein, Anne Tsao, Hai Tran, Marshall Hicks, Rodolfo Morice, Bruce Johnson)

Specific Aim 1 has five clinical trials: one umbrella trial and four Phase II open-label trials. After screening, eligible patients are enrolled in the umbrella trial, and tumor biopsies are taken for

biomarker analysis conducted by the Biomarker Core. (For details, please see the Biomarker Core section of this report.) Biomarker results are analyzed by the Biostatistics and Data Management Core. (For details, please see the Biostatistics and Data Management Core section of this report.) There are two components of this study: 1) an equal randomization phase, where patients are randomized equally to the four trials after biomarker analysis; and 2) an adaptive randomization phase, where patients are enrolled to one of the four clinical trials based on their tumor biomarker characteristics. The four Phase II clinical trials are presented in the four sub-aims of Aim 1 described below and depicted in Figure 1. An update is provided following the list of subaims.

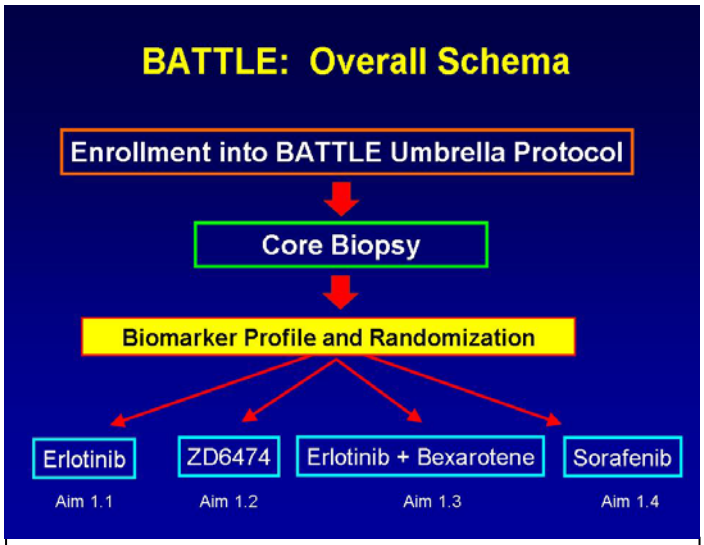

Figure 1. Overall Schema for BATTLE Trials.

Aim 1.1 To conduct a clinical trial with erlotinib in patients with previously treated advanced NSCLC whose tumors have EGFR mutations and / or overrepresentation.

Primary objective is to determine the 8-week progression-free survival (PFS) rate of patients with previously treated advanced NSCLC whose tumors have EGFR mutations and / or overrepresentation who are treated with erlotinib.

Secondary objectives are to 1) determine the overall survival rate, response rate, and toxicity profiles of patients with advanced NSCLC whose tumors have EGFR mutations and / or overrepresentation and treated with erlotinib, 2) determine the plasma and (if available) tumor tissue concentrations of erlotinib and their correlation with response and toxicity by using pharmacokinetics and pharmacodynamic modeling.

Aim 1.2 To conduct a clinical trial with ZD6474 in patients with previously treated advanced NSCLC whose tumors have increased VEGF and / or VEGFR-2.

Primary objective is to determine the 8-week PFS rate in patients with previously treated advanced NSCLC whose tumors have increased VEGF and / or VEGFR-2 who are treated with ZD6474.

Secondary objectives are to 1) determine the overall survival rate, response rates, and toxicity profiles of patients with advanced NSCLC whose tumors express increased VEGF and / or VEGFR-2 and treated with ZD6474, and 2) determine the plasma and (if available) tumor tissue levels of ZD6474 and their correlations with response and toxicity by using pharmacokinetics and pharmacodynamic modeling.

Aim 1.3 To conduct a clinical trial with the combination of bexarotene and erlotinib trial in patients with previously treated advanced NSCLC whose tumors have expressed RXRs and / or increased cyclin D1.

Primary objective is to determine the 8-week PFS rate in patients with previously treated advanced NSCLC whose tumors have expressed RXRs and / or increased cyclin D1 who are treated with the combination of Bexarotene and Erlotinib.

Secondary objectives are to 1) determine the overall survival rate, response rate, and toxicity profiles of patients with advanced NSCLC whose tumors have expressed RXRs and / or increased cyclin D1 and treated with the combination of bexarotene and erlotinib, 2) determine the plasma and (if available) tumor tissue concentrations of bexarotene and erlotinib and their correlation with response and toxicity by using pharmacokinetics and pharmacodynamic modeling.

Aim 1.4 To conduct a clinical trial with sorafenib trial in patients with previously treated advanced NSCLC whose tumors have mutated *K-ras* and / or *B-raf.*

Primary objective is to determine the 8-week PFS rate in patients with previously treated advanced NSCLC whose tumors have mutant *K-ras* and / or *B-raf* who are treated with sorafenib.

Secondary objectives are to 1) determine the overall survival rate, response rate, and toxicity profiles of patients with advanced NSCLC whose tumors have mutated K-ras and / or B-raf and treated with sorafenib, 2) determine the plasma and (if available) tumor tissue concentrations of sorafenib and their correlation with response and toxicity by using pharmacokinetics and pharmacodynamic modeling.

Summary of Research Findings

Specific Aim 1 was completed and results were extensively detailed in the previous annual report. Additional abstracts and publications related to the clinical trial and not previously reported have been listed in the "Abstracts and Publications" section of this report.

Specific Aim 2: To investigate molecular mechanisms of response and resistance to the targeted agents used in the BATTLE program.

Specific Aim 2.1. To validate the molecular mechanisms of response and resistance to erlotinib for patients with chemorefractory NSCLC.

(PI and Co-PI: Bruce Johnson, M.D., and Pasi Jänne, M.D., Ph.D.)

The association between somatic epidermal growth factor receptor (*EGFR*) mutations and clinical response to gefitinib in patients with non-small cell lung cancer (NSCLC) was published in 2004. This proposal builds on previous findings to further characterize *EGFR* mutations in subjects' tumors and in tumor cell lines and the relationship of these mutations, subject outcome, and *in vitro* behavior to different EGFR inhibitors. The data generated demonstrates that subjects whose NSCLC tumors have *EGFR* mutations typically respond to single-agent therapy with gefitinib, are treated for a median of 1 year or longer, and achieve a median overall survival duration longer than 2 years. This survival duration is 3-fold longer than that achieved with conventional chemotherapy in previously untreated subjects with NSCLC. The patients treated with gefitinib or erlotinib with increased copy number assessed by fluorescence in situ

hybridization (FISH) have a response rate of 20-30% and the patients live a median of approximately 2 years. The goal of this research is to confirm these initial observations in prospective cohorts of subjects with NSCLC and somatic *EGFR* mutations or increased copy number with erlotinib as the initial therapy. This proposal is generating translational information on somatic mutations and copy number, prospective validation of the outcome of patients with NSCLC and *EGFR* mutations or increased copy number treated with erlotinib, information on activation of the EGFR pathway in NSCLC and NSCLC cell lines, and information about mechanisms of resistance.

Objective 1: Establish estimates of the response and outcome of previously treated patients with prospectively identified somatic *EGFR* mutations treated with erlotinib.

Summary of Research Findings
This objective was completed and detailed in the previous annual report.

Objective 2: Determine effects of TGF-α, EGF, and AR on the growth of *EGFR*-mutant and wild-type cell lines.

Summary of Research Findings
This objective was completed and detailed in the previous annual report.

Objective 3: Determine effects of TGF-α, EGF, and AR on the cell cycle and apoptosis of *EGFR*-mutant and wild-type cell lines.

Summary of Research Findings
This objective was completed and detailed in the previous annual report.

Objective 4: Determine effects of different *EGFR* mutations and EGFR inhibitors on phosphorylation of EGFR and downstream signaling intermediates.

Summary of Research Findings
This objective was completed and detailed in the previous annual report.

Specific Aim 2.2. Insulin-like Growth Factor Receptor Signaling Pathways and Resistance to Gefitinib in Non Small-Cell Lung Cancer Cells

(PI: Ho-Young Lee, Ph.D.)

Non-small cell lung cancer (NSCLC) accounts for about 75%-80% of lung cancer cases and its dismal survival rate has not improved in the past 2 decades. The lack of effective therapy, the high proportion of patients with advanced disease at the time of diagnosis, and the rapidity of tumor progression are major contributors to lung cancer mortality, and raises the urgent need for novel strategies to treat this disease. Of many potential targets in adult solid tumors, the epidermal growth factor receptor (EGFR) has been extensively studied because overexpression of EGFR has been observed in a number of other common solid tumors including 40–80% of NSCLC (Jemal et al, 2003). Therefore, one therapeutic strategy was to use the agents targeting the EGFR pathway. However, negative results from several large-scale phase III clinical trials in lung cancer have been reported (Giaccone et al, 2002; Johnson, 2002), indicating the need for understanding the mechanisms that induce resistance to EGFR inhibitors. Accumulating evidence has implicated insulin-like growth factor receptor-I (IGF-IR) pathways in resistance to

chemotherapy, radiation therapy, and molecularly targeted agents (Kulik et al, 1997; Lin et al, 1999; DiGiovanni et al, 2000; Porras et al, 1998; Toker and Newton, 2000). Our objective is to investigate whether IGF-IR and downstream signaling mediators, such as PI3K/Akt and MAPK, are involved in the resistance to anti-EGFR therapies in NSCLC.

Objective 1: Determine whether inhibition of the IGF-1R–mediated signaling pathway augments the antiproliferative effects of erlotinib on NSCLC cells *in vitro,* and investigate the mechanism by which erlotinib leads NSCLC cells to activate the IGF-1R signaling pathway.

Objective 1 has been completed and was reported in the previous annual report.

Objective 2: Determine whether inhibition of the IGF-1R–mediated signaling pathway augments effects of erlotinib on the growth of human NSCLC xenograft tumors established in nude mice.

Objective 2 has been completed and was reported in the previous annual report.

Objective 3: Investigate whether IGF-1R activity influences the therapeutic activity of erlotinib in patients with NSCLC.

Summary of Research Findings

Objective 3 has been completed and was reported in the previous annual report.

Specific Aim 2.3. To investigate the molecular mechanisms of resistance to and biomarkers of the biologic activity of VEGF pathway inhibitors

(PI: John Heymach, M.D., Ph.D.)

The primary goals of this Aim were to develop biomarkers for the activity of VEGF inhibitors and investigate potential markers of therapeutic resistance. We have made significant progress towards these goals, and based on findings from BATTLE we are now poised to test and potentially validate these markers using samples from randomized phase III studies, and develop treatment regimens aimed at targeting resistance.

The initial primary focus of our efforts was blood-based biomarkers; however, through our efforts, and in collaboration with the laboratory of Dr. Wistuba, new tumor based biomarkers have emerged as well. Notable advances, detailed below, include the following: 1) Identification of KDR (copy number gain and protein levels) as a marker of A) recurrence after adjuvant chemotherapy, B) chemoresistance, C) VEGFR inhibitor benefit and, potentially, D) EGFR inhibitor resistance. 2) Identification of circulating HGF and osteopontin as potential markers of resistance to VEGFR inhibitors, and 3) Identification of circulating tumor endothelial cells (CTECs) as a potential biomarker.

Progress on these objectives is detailed below.

Objective 1: Quantitatively assess VEGFR (KDR) phosphorylation, downstream signaling, and biomarkers of angiogenesis in pre- and post-treatment tumor biopsy samples.

Summary of Research Findings

1. Role of tumor VEGFR2 (KDR) CNGs in NSCLC signaling and its role in promoting and invasive phenotype. As previously reported, in collaboration with Dr. Ignacio Wistuba, we found that tumor KDR CNGs (involving an amplicon on 4q12) were associated with increased levels of KDR protein, and increased levels of angiogenesis. Furthermore, KDR CNGs were associated with worse outcome in early stage NSCLC patients who received adjuvant platinum doublet chemotherapy, but not those who underwent resection alone. We observed a similar frequency of KDR copy gain in adenocarcinoma (26/85, 31%) and squamous cell carcinoma (19/54, 35%) histologies. Finally, we demonstrated that KDR CNGs were associated with chemoresistance in vitro. These results were published during the past year (Yang et al, Cancer Research, 2011).

We have completed this aim but extended these findings over the past year in several important ways. First, we demonstrated that tumor cell KDR promotes in vitro invasiveness, and that this invasiveness could be blocked by VEGFR tyrosine kinase inhibitors (TKIs) (Figure 1A). Furthermore, through an extensive proteomic analysis of pathways modulated by KDR or VEGF inhibitors, we identified that the PI3K pathway, HIF-1α, EZH2, and MET are all downstream targets associated with tumor KDR, and that KDR activation promotes MET phosphorylation, which may drive tumor cell invasiveness (Figure 1B-D).

One somewhat unexpected finding has emerged from the KDR analysis. As previously noted, tumor KDR was associated with improved outcome in patients treated with the VEGFR/EGFR pathway inhibitor vandetanib, but worse outcome in patients treated with erlotinib (Kim et al, Cancer Discovery, 2010). This finding suggested that tumor KDR may promote resistance to EGFR inhibitors. We have explored this pathway and found that, in fact, VEGF can promote EGFR-inhibitor resistance consistent with our earlier preclinical observations (Naumov et al, Clin Can Res, 2009). Investigations into the mechanism of this effect are still in progress, but our preliminary results suggest that VEGF may accelerate an epithelial-to-mesenchymal transition (EMT).

These observations have compelled us to further investigate KDR as a predictive marker for chemo- and EGFR-inhibitor resistance and/or VEGF inhibitor response. We have obtained independent funding from AstraZeneca, as well as the Lungevity Foundation, to investigate these and related markers; in fact, we will soon be conducting an analysis of tumor KDR using specimens from the randomized phase III trials of vandetanib vs. erlotinib (ZEST) and vandetanib with docetaxel vs. docetaxel (ZODIAC), as well as other potential trials. If these studies are positive, this work will define the first biomarkers for VEGF pathway inhibitors to be independently validated in a phase III trial. The potential clinical impact of these markers is enormous, and VEGF pathway inhibitors such as bevacizumab are approved for NSCLC, but there are currently no validated biomarkers for identifying which patients are likely to benefit from treatment.

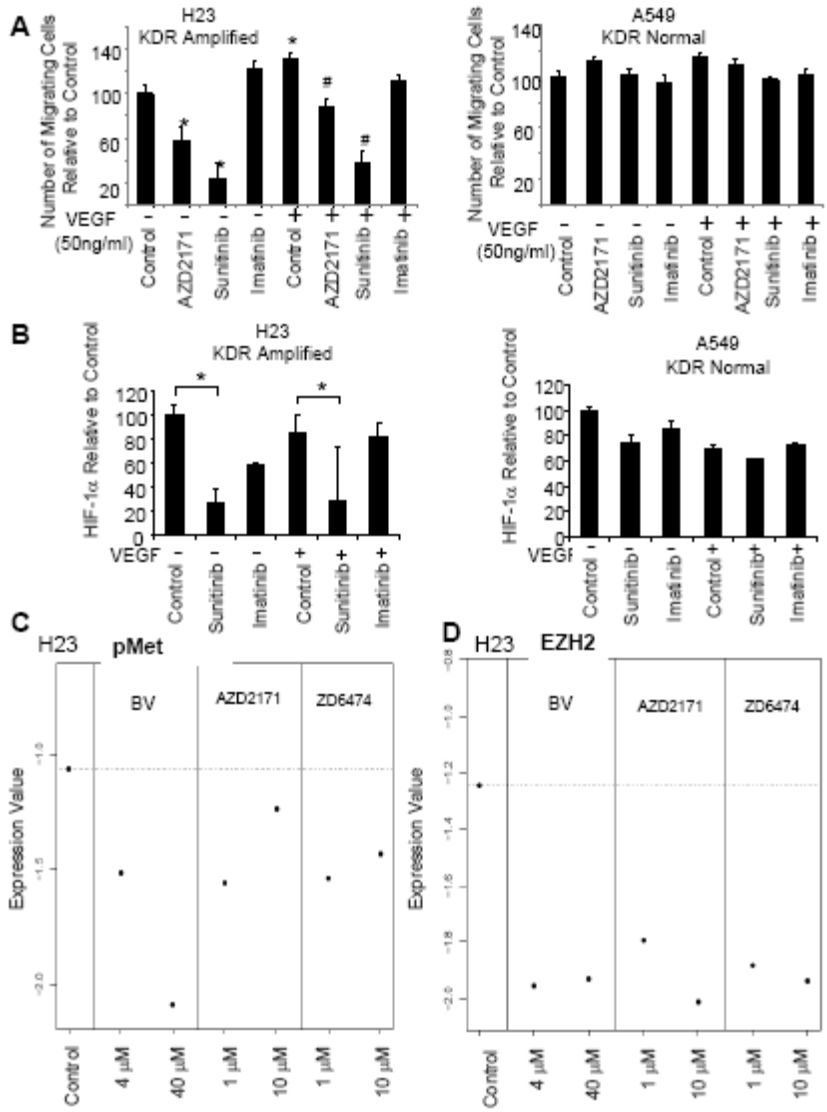

Figure 1. VEGFR TKIs modulate invasiveness, HIF-1α, and HIF-1α-regulated proteins in NSCLC cell lines with KDR amplification.

Objective 2: Investigate the utility of circulating endothelial cells (CECs), monocytes, and other cells in peripheral blood as biomarkers for antiangiogenic activity and inhibition of the VEGF pathway.

<u>Summary of Research Findings</u>

In our effort to improve circulating cellular biomarkers for VEGFR inhibitors, we have conducted preclinical and clinical investigations of new subtypes of circulating endothelial cells (CECs). We and others have investigated CECs as biomarkers in the past (e.g., Norden-Zfoni et al, CCR, 2007), but the field has been hampered by the lack of specificity of CECs, which may be shed by normal vasculature (mature CECs) or tumor endothelium, or even mobilized from bone marrow (circulating endothelial progenitors). To address this issue, we have investigated surface markers specific for tumor-associated (tumor endothelial markers, or TEMs) vs. normal endothelium. We demonstrated in preclinical models that we could detect TEMs on both tumor-associated endothelium and in CECs in mice bearing tumors, and have termed this population

circulating tumor endothelial cells (CTECs) (Figure 2A). We demonstrated that CTECs are present at higher levels in tumor-bearing mice compared to non-tumor-bearing mice, and that changes in CTECs are proportional to the efficacy of VEGF pathway inhibitors in preclinical models (Figure 2B).

We then investigated whether CTECs were present in NSCLC patients. We found that, in fact, CTECs were present in NSCLC patients and decreased after surgery (Figure 2C). We then recently conducted an analysis of CTECs in patients treated with vandetanib in the BATTLE trial (see Aim 1) using flow cytometry; analysis of these data is ongoing and will be completed in this grant period. A publication describing the preclinical and clinical identification of CTECs as a biomarker will be submitted in May 2012 (Khajavi, Nilsson et al, 2012).

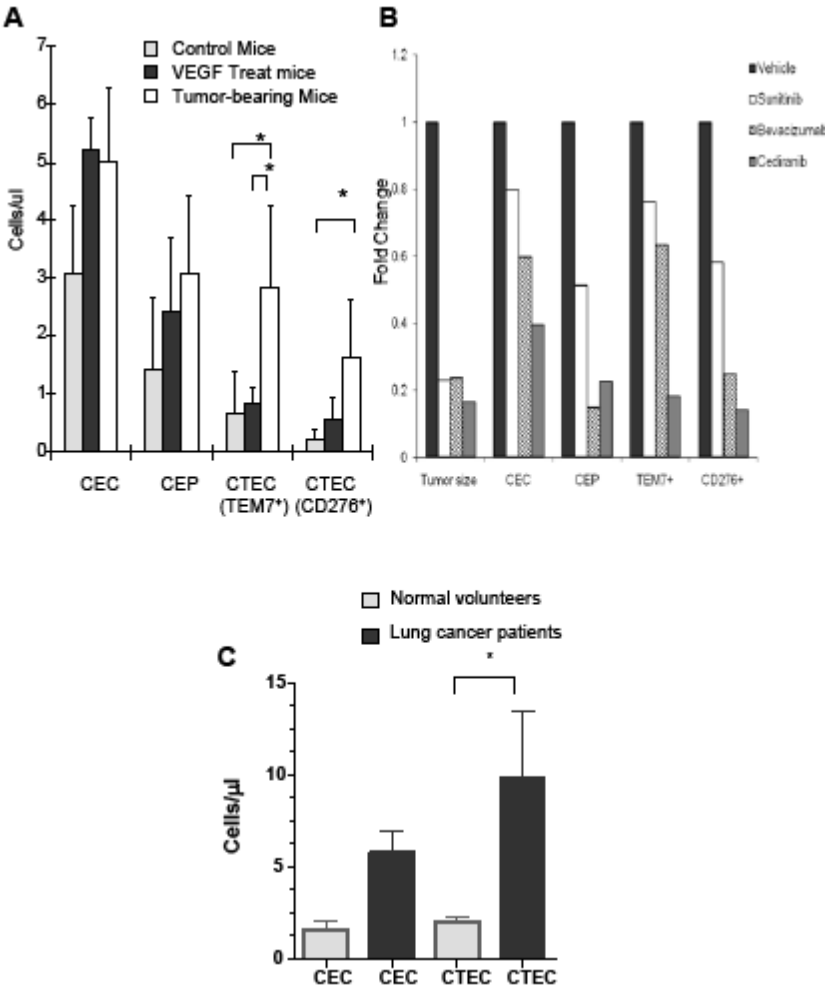

Figure 2. CTEC levels are elevated in tumor-bearing animals and correlate with VEGFR inhibitor activity in preclinical models of NSCLC. CTEC levels are also elevated in patients with NSCLC compared with healthy controls.

Objective 3: Systematically examine changes in the plasma and serum angiogenic profiles consisting of a panel of proangiogenic cytokines, targeted receptors, and potential biomarkers of endothelial damage.

<u>Summary of Research Findings</u>

As previously described, we conducted a broad profiling of cytokines and angiogenic factors (CA/Fs) using multiplex magnetic bead assays of the 185 baseline samples obtained from patients who consented to the optional blood collection and analysis. After the initial analysis, we detected significant batch effects due to manufacturing of the plates themselves and the analysis of these baseline samples was therefore redone to ensure the collection of satisfactory data. We have also assessed several CA/Fs by ELISA. In our preliminary analysis, we have identified several plasma factors associated with resistance to vandetanib including hepatocyte growth factor (HGF). To investigate whether HGF may actually promote resistance, we transfected HGF into NSCLC cell lines (H1975, HCC827, etc.) and found that HGF induced resistance to VEGF pathway inhibitors including bevacizumab and cediranib (AZD2171). A manuscript describing these findings will be submitted shortly (Cascone et al, 2012).

Key Research Accomplishments:

- Identified that KDR CNGs were present in NSCLC and predicted worse outcome in patients treated with adjuvant chemotherapy, as well as chemoresistance.
- Found that KDR upregulates pathways associated with angiogenesis and invasiveness (HIF, c-MET) in NSCLC tumor cells and, potentially, EGFR inhibitor resistance.
- Determined that in NSCLC cells with KDR CNGs, KDR inhibitors such as vandetanib could block invasiveness and down-regulate pathways associated with resistance, such as EZH2.
- Identified a new subpopulation of circulating endothelial cells (circulating tumor endothelial cells, or CTECs) and demonstrated that CTECs were a biomarker for VEGF pathway inhibitor response in NSCLC preclinical models, and were present in NSCLC patients.
- Identified CA/Fs associated with therapeutic resistance to drugs in the BATTLE study, including HGF as a marker of vandetanib resistance.

Conclusions

Our project investigating markers for VEGF pathway inhibitors in the BATTLE study has led to a candidate tumor marker, KDR CNGs, that is now undergoing validation using samples from phase III trials. If studies are positive, KDR CNGs would represent the first independently validated tumor marker for VEGFR inhibitors. Our data suggests that KDR CNGs may also be a useful biomarker for chemoresistance and EGFR inhibitor resistance, and we have demonstrated key signaling pathways downstream of KDR, including PI3K, HIF, EZH2, and c-MET.

We have also identified several novel blood-based biomarkers for VEGF/R inhibitors including CTECs as well as plasma CA/Fs such as HGF. We have gone on to validate HGF as a mechanism of resistance in preclinical models and, based on these findings, are now developing trials targeting c-MET and VEGF pathways simultaneously.

Specific Aim 2.4. To investigate the molecular mechanisms of the effects of the combination of bexarotene and erlotinib on NSCLC cells

(PI: Reuben Lotan, Ph.D.)

The need to discover and introduce more effective treatment agents and combinations is urgent, as is the need to improve the selection of the right agent or combination of agents for each patient on the basis of our understanding of the molecular targets. The combination of the retinoid X receptor (RXR)-selective ligand bexarotene and the epidermal growth factor receptor (EGFR) tyrosine kinase (TK) inhibitor erlotinib appears to be a promising approach, and will be

tested in patients with NSCLC in the BATTLE program. Some aspects of the mechanisms of action of these two agents are not fully resolved. Therefore, we propose to investigate how they exert their effects on NSCLC cells to improve their usefulness in future clinical trials.

Objective 1: To determine by immunohistochemical analysis the expression of nuclear receptors (retinoic acid receptors [RAR]-α, -β, and -γ; RXR-α, -β, and -γ; and PPAR-γ1 and PPAR-γ2) and cyclin D1 in NSCLC specimens obtained from patients to be enrolled in the BATTLE umbrella trial and from patients whose cancer progresses on treatment.

Summary of Research Findings
This objective was completed and detailed in the previous annual report.

Objective 2: Examine the effects of bexarotene, erlotinib, and rosiglitazone alone and in combination on the growth and apoptosis of NSCLC cells, cyclin D1 and PPAR-γ levels, and gene expression profiles.

Summary of Research Findings
This objective was completed and detailed in the previous annual report.

Objective 3: Determine whether RXRs, EGFR, and PPAR-γ are required to mediate the effects of bexarotene, erlotinib, and rosiglitazone, respectively, on cell growth control and apoptosis, and examine the functional significance of changes in gene expression induced by receptor agonists used singly or in combinations.

Summary of Research Findings
This objective was completed and detailed in the previous annual report.

Objective 4: Evaluate the growth inhibitory effects and mechanisms of action of novel RXR ligands AGN194204 and 9cUAB30 alone or combined with erlotinib and rosiglitazone on NSCLC cells.

Summary of Research Findings
This aim was closed as reported previously.

Specific Aim 3: To identify biomarkers as novel predictors of clinical end points and potential therapeutic targets

(PI: Ignacio Wistuba, M.D.)

Objective 1: Identify molecular features in tumor tissues that correlate with patients' responses to individual regimens used in the clinical trials of the proposed program.

Summary of Research Findings
As reported in the previous year, the BATTLE clinical trial completed accrual in October 2009, with subsequent follow-up identifying 244 evaluable patients in December 2009. We have previously reported the development of four gene expression signatures that predict 8-week

disease control (8-wk DC) for two of the four BATTLE treatment arms (Table 1). During the last unfunded extension year, in collaboration with Drs. John Heymach (BATTLE Co-Investigator), J. Jack Lee (Director, Biostatistics Core B), and Kevin Coombes (Bioinformatics), we have developed a robust signature for predicting 8-wk DC with sorafenib treatment (Saintigny et al, AACR 2012; Blumenschein et al, manuscript submitted), and we have submitted a manuscript to report the epithelial-mesenchymal transition (EMT) gene signature (Byers et al, manuscript submitted).

Table 1. Gene expression signatures developed and tested in the BATTLE NSCLC tumor specimens.

Signature	Samples Used to Derive Signature	Predictive of DC at 8 weeks in BATTLE		
		Yes/No	***Treatment Arms***	***Type of Tumors***
EGFR	Resected tumor tissues	No	None	--
EMT	Cell lines	Yes	Erlotinib	EGFR wild-type
5-gene	BATTLE tissues	Yes	Erlotinib	EGFR wild-type
"Sorafenib"	BATTLE tissues	Yes	Sorafenib	--

"Sorafenib" gene expression signature: The results from our BATTLE trial suggest that patients with chemorefractory, *EGFR*-wild-type NSCLC, including those with mutant *KRAS,* may benefit from sorafenib. Using 3 different approaches, we tested the hypothesis that gene expression profiles from wild-type *EGFR* tumors may predict sorafenib efficacy by capturing its effects on multiple targets. Baseline tumor biopsies from 37 BATTLE patients with *EGFR* wild-type tumors treated with sorafenib were profiled (Affymetrix Human Gene 1.ST), as well as 68 *EGFR* wild-type NSCLC cell lines with the available sorafenib IC50 (Illumina HumanWG-6 v3.0 expression beadchip). We first developed an "In vitro Sorafenib Signature (ISS)." Correlation of IC50s with each individual probe expression level was computed. The most significant probes were summarized by the first principal component (PC) analysis, and correlated with the IC50 of sorafenib. To validate the signature, the first PC was computed in BATTLE samples, and progression-free survival (PFS) of patients with high- vs. low-sensitivity signature was compared based on the median of the first PC. Then, alternatively, we developed a "Clinical Sorafenib Signature (CSS)" using BATTLE samples. We compared 23 (62%) patients who achieved 8-week disease control with 14 (38%) who did not (t-test). The most significant probe sets were summarized by the first PC, and PFS of patients with a high- vs. low-sensitivity signature were compared. To validate the signature, the first PC was computed in cell lines and correlated with IC50 of sorafenib. Finally, we tested a previously reported *KRAS* mutation gene expression signature derived by comparing genes differentially expressed in mutant vs. wild-type *KRAS* early stage resected lung adenocarcinomas in 124 BATTLE samples, including 24 mutant *KRAS*.

The ISS included 50 probes. The first PC was correlated with the IC50 of sorafenib (rho = -0.71, $P < 0.0001$). The ISS was then tested in BATTLE samples, and PFS was significantly different in patients with the high- (median PFS 3.61 months) vs. the low-sensitivity signature (median PFS 1.84 months, log-rank $P = 0.0263$). The CSS developed in BATTLE included 80 probe sets summarized using the first PC. PFS was significantly different in patients with the high- vs. the low-sensitivity signature (log-rank $P < 0.0001$). The CSS was then tested in cell lines and the first PC was significantly correlated with IC50 of sorafenib (rho = 0.24, $P = 0.0483$). Finally, the *KRAS* signature was significantly associated with *KRAS* mutation, but no association was observed with outcome in patients treated with sorafenib in BATTLE.

In conclusion, we have developed two gene expression signatures, ISS and CSS, that predicted benefit from sorafenib in patients with chemorefractory NSCLC and in vitro sensitivity to sorafenib, respectively (Saintigny et al, 2012 AACR Annual Meeting).

Objective 2: Determine the effect of targeted agents in tumor tissues, and identify novel molecular mechanisms of tumor response or progression.

Summary of Research Findings

The work of this objective has been completed, and the results were reported last year. During this last year of the unfunded extension, a manuscript describing the role of EMT as a mechanism of resistance to EGFR tyrosine kinase treatment in BATTLE patients was submitted for publication (Byers et al, manuscript submitted), and the paper describing the effect of *KRAS* oncogene-specific substitutions on protein behavior and implications for signaling and clinical outcome in sorafenib-treated BATTLE patients was published (Ihle et al, JNCI 2011).

Key Research Accomplishments:

- Developed two novel gene signatures that predicted 8-week disease control in patients with advanced and refractory NSCLC treated with sorafenib.
- Completed and submitted a manuscript describing the EMT novel gene signature that predicted 8-week disease control in patients with advanced and refractory NSCLC with wild-type *EGFR* tumors treated with the EGFR TKI erlotinib.
- Published our discovery that different therapeutic approaches might be required when treating patients with NSCLC harboring different mutant-*KRAS* amino acid substitutions.

Conclusions

We have further demonstrated that gene expression profiling from CNBs is a feasible approach for predicting response and identifying potential therapeutic targets in refractory NSCLC patients treated with targeted therapy. We have developed and refined gene expression signatures that predict 8-week disease control in the BATTLE patients with EGFR wild-type tumors who were treated with EGFR TKIs (EMT signature) and sorafenib. In addition, we published our discovery indicating that not all mutant-*KRAS* amino acid substitutions signal the effectors in a similar way in NSCLC.

Specific Aim 4: To explore new preclinical combinations and their mechanisms of action by targeting mTOR signaling and develop phase I trials to test these combinations.

(PI and Co-PIs: Suresh Ramalingam, M.D., Shi-Yong Sun, Ph.D., Haian Fu, Ph.D.)

The overall objective of Aim 4 is to study the efficacy of mTOR inhibitor combination therapies that co-target mTOR and PI3K/Akt signaling. Following is a summary of our research progress for Year 3:

Objective 1: To study the efficacy of mTOR inhibitor combination therapies that co-target mTOR and PI3K/Akt signaling.

Summary of Research Findings

The proposed studies in this objective have been completed and summarized in previous reports. The findings on enhanced anticancer activity by the combination of RAD001 and BEZ235 against human lung cancer in vitro and in vivo has been summarized and published (see Xu et al., PLoS ONE, 2011). In addition, the study on BEZ235 induction of autophagy, the

blockage of which enhances BEZ235's therapeutic efficacy against lung cancer both in vitro and in vivo, has also been published (see Xu et al., Cancer Biol Ther, 2011).

We also tested the effects of RAD001 in combination with the novel PI3K inhibitor, BKM120, in a panel of human lung cancer cell lines, and found that the combination synergistically inhibited the growth of lung cancer cells (combination indexes are < 1). The combination showed enhanced effects on G1 arrest (**Fig. 1**), but did not exhibit augmented effects on induction of apoptosis. In a long-term colony formation assay, we further showed that the combination of low concentrations of BKM120 and RAD001 was much more than either agent alone in inhibiting the formation and growth of lung cancer cell colonies (**Fig. 1**). Similarly, the combination was also more effectively than either agent alone in inhibiting the growth of lung cancer xenografts without apparently reducing mouse body weight (**Fig. 2**). All these results indicate that the combination of BKM120 and RAD001 effectively inhibits the growth of lung cancers cells in preclinical settings, warranting further clinical testing of this combination. These data are ready for summary and publication.

Using these results as preliminary data, we have submitted a new proposal (Project 1) for our lung cancer P01 renewal application in which we will elucidate the underlying mechanisms of these effects and validate our findings in animal models and in clinical trials. The first submission of this project received the best score among all projects, and the revised application has been recently submitted.

Based in part on the BATTLE data, the PI of this project submitted a R01 entitled "Therapeutic potential of mTOR kinase inhibitors in lung cancer," which received a potentially fundable score (7th percentile) and is pending a funding decision.

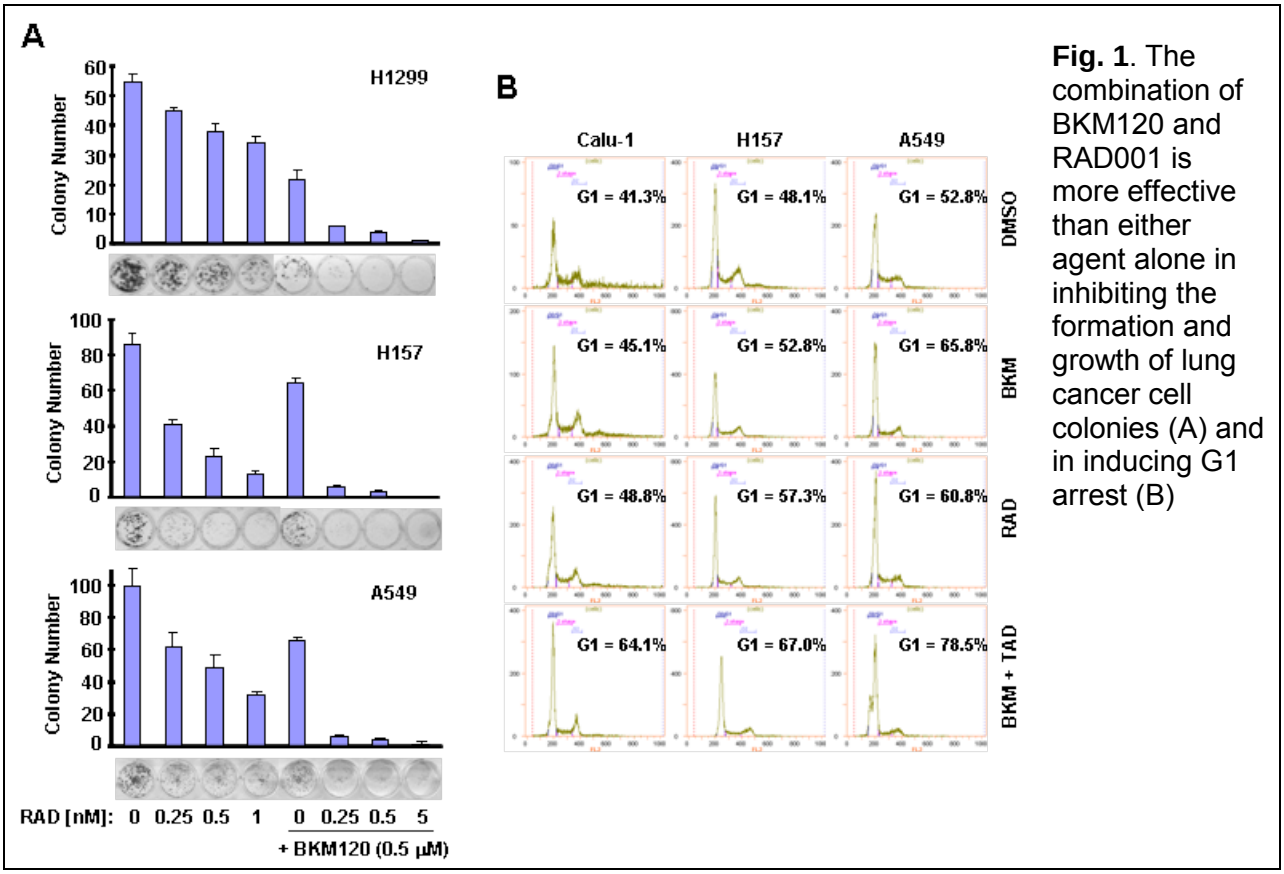

Fig. 1. The combination of BKM120 and RAD001 is more effective than either agent alone in inhibiting the formation and growth of lung cancer cell colonies (A) and in inducing G1 arrest (B)

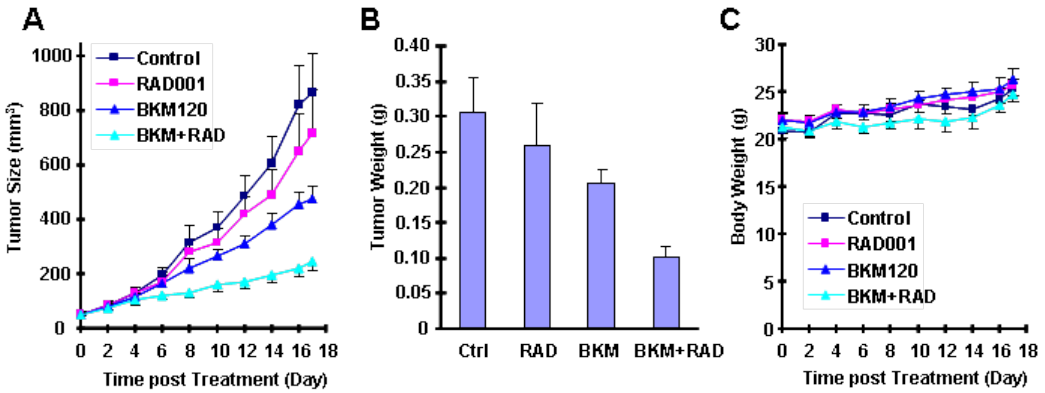

Fig. 2. The combination of BKM120 and RAD001 is more effective than either agent alone in inhibiting the growth of lung cancer xenografts in nude mice (A and B), without apparently reducing mouse body weight (C).

Objective 2: To examine whether rapamycin-induced Akt activation suppresses ASK1-mediated apoptosis and leads to decreased therapeutic efficacy.

Summary of Research Findings

Our studies have indicated a critical role of ASK2 in regulating ASK1 through recruiting 14-3-3 into the ASK1 protein complex. We have completed this study by demonstrating that phosphorylation of ASK2 at S964 induces 14-3-3 binding, which subsequently relays a survival signal to ASK1 through binding to phosphorylated ASK1 at S967. This work has been published in *Oncogene* (*2010*).

Our effort was then shifted to understand how upregulated Akt upon rapamycin treatment of cells suppresses the ASK1 function as proposed. We examined the functional interaction between Akt and ASK1, as ASK1 is known to be regulated by Akt directly through phosphorylation at S83 site. Interestingly, we discovered that activated Akt induces phosphorylation of ASK1 at S967, a 14-3-3 binding site associated with cell survival. In support of this finding, treatment of cells with IGF1, which activates Akt, triggers ASK1 phosphorylation at S967 and a pS967-mediated 14-3-3 association. On the other hand, inhibition of PI3K, an upstream activator of Akt, reduces S967 phosphorylation. Thus, Akt may exert its impact on ASK1 through a dual mechanism through S83 and S967. Our recent mechanistic studies have revealed the critical importance of IKK in mediating Akt-triggered phosphorylation of S967. This work has been summarized in a publication pending submission.

mTOR inhibition by rapamycin induces Akt activation, which not only provides a feedback survival mechanism, but also releases an inhibitory mechanism through phosphorylation of PRAS40. PRAS40 is an Akt substrate, which in its unphosphorylated state can suppress mTOR function. Our recent studies reveal that PRAS40 is upregulated in lung cancer cells. In particular, the phosphorylated form of PRAS40 is present in lung cancer cells and tumor tissues, as demonstrated by immunohistochemistry studies. We propose that phosphorylation of up-regulated PRAS40 allows mTOR signaling and promotes tumorigenesis. Indeed, we discovered that PRAS40 promotes tumorigenesis in part by enhancing Atg1-mediated autophagy. Taken together, our research suggests that Akt activation suppresses mTOR inhibitor's therapeutic efficacy possibly through multiple mechanisms, including ASK1 suppression and PRAS40 phosphorylation.

Objective 3: To conduct two phase I clinical trials to test the efficacy of the combination of an mTOR inhibitor with an Akt or an EGFR inhibitor in advanced NSCLC patients resistant to the front and second line therapy, and assess the modulation of targeted biomarkers from tumor tissues before and after the treatment.

Summary of Research Findings

In collaboration with investigators at MD Anderson Cancer Center and Dana Farber Cancer Center, a phase I study was first conducted to evaluate the combination of RAD001 with erlotinib. Subsequently, a randomized phase II study was performed to compare the combination against monotherapy with erlotinib alone in patients with advanced stage NSCLC. The combination was well tolerated, without undue increase in the incidence of adverse events. There was a trend towards improvement in PFS for the combination therapy, but the differences did not reach statistical significance. The disease control rate at 3 months was 39% for the combination compared to 28% for monotherapy with erlotinib. The results call for identification of biomarkers for patient selection. Based on the promising pre-clinical observations in objective 1, we will soon initiate a phase I study of RAD001 with BKM120, a PI3K inhibitor. This study will involve sequential biopsy collection to understand the molecular effects of the combination at the level of the tumor tissue.

Key Research Accomplishments:

1. The combination of RAD001 and BKM120 synergistically inhibits the growth of human lung cancer cells both in vitro and in vivo.
2. With results generated in the BATTLE project as preliminary data for a well-scored project, we have submitted the revision of our P01 renewal application.
3. Based on BATTLE data, we have submitted a new R01 and received a potentially fundable score (7^{th} percentile).

Biostatistics and Data Management Core

(Core Director: J Jack Lee, Ph.D.)

In close collaboration with the Biomarker Core, the clinical research team, and each of the basic science research components, the Biostatistics and Data Management Core (BDMC) for the Department of Defense (DoD) BATTLE lung cancer research program is a comprehensive, multi-lateral resource for designing clinical and basic science experiments; developing and applying innovative statistical methodology, data acquisition and management, and statistical analysis; and publishing translational research generated by this research proposal.

The main objectives of the BDMC are as follows:

1. Develop and implement a novel adaptive randomization scheme for assigning patients into the treatment arms with the highest probability of success.
2. Provide the statistical design, sample size, and power calculations for each project.
3. Develop a secure, internet-driven, web-based database network between UTMDACC and other research centers, including Emory University and the Dana-Farber Cancer Center, that integrates the clinical data generated by the five proposed clinical trials and

relating basic science research efforts of the BATTLE research project.
4. Develop a comprehensive, Web-based database management system for tissue specimen tracking and distribution and for a central repository of all biomarker data.
5. Provide all statistical data analyses, including descriptive analysis, hypothesis testing, estimation, and modeling of prospectively generated data.
6. Provide prospective collection, entry, quality control, and integration of data for the basic science, pre-clinical, and clinical studies in the BATTLE grant.
7. Provide study monitoring and conduct that ensures patient safety by timely reporting of toxicity and interim analysis results to various institutional review boards (IRBs), the UTMDACC data monitoring committee, the DoD, and other regulatory agencies.
8. Generate statistical reports for all projects.
9. Collaborate with all project investigators and assist them in publishing scientific results.
10. Develop and adapt innovative statistical methods pertinent to biomarker-integrated translational lung cancer studies.

Summary of Research Findings

In this unfunded extension period, the Biostatistics and Data Management Core continued to work with project investigators and provide biostatistics and database management support for all active projects and cores in the BATTLE program. Although the clinical trials have been completed, extensive effort has been devoted to the development of manuscripts for the various aspects of the proposed research and clinical trials. Evaluation and analysis of the clinical and scientific secondary endpoints continues.

(A) Biostatistics

The main clinical results of the BATTLE trial (Aim 1) were reported in Cancer Discovery (E Kim et al., April 2011). We have continued to work with clinical and basic science investigators with additional data analysis and manuscript writing. Notably, we have further characterized different types of *KRAS* mutation as a prognostic factor for lung cancer. Microarray data were analyzed in-depth to construct the EGFR-wild type signature, EMT signature, and the sorafenib signature reported in previous sections of this report. The manuscript detailing the results of the sorafenib study was submitted, and a vandetanib study-based manuscript is in preparation. A paper detailing the biopsy methods used in the BATTLE trial to acquire fresh tumor tissue was completed and submitted.

(B) Data Management

Database programming effort:

- Continue to work closely with the BATTLE research nurses make sure the data is meticulously updated, cleaned, and is accurate, including checking patient timelines for consent, randomization, response and off study, etc. Multiple iterations have taken place to achieve the goal. The updated data serve as the basis for the writing of several BATTLE manuscripts.
- Generated many reports for the Statistical Analyst on virtually all data captured to help with detailed analysis reports and statistics, including progression-free survival reports, off-study reports, tumor measurement data, and follow-pp data.
- Generated *KRAS* and *EGFR* biomarker reports for the labs to review and statistical analysis.

Key Research Accomplishments:

- Performed extensive statistical analysis on the study findings, including treatment efficacy, toxicity, compliance, pre-specified biomarkers, and discovery biomarkers, etc.
- Developed and maintained a secured, Web-based database application to assist with the data collection and analysis.
- A web-based database application is developed, deployed, and maintained at: https://insidebiostat/DMI_BATTLE/Common/Login.aspx.

Conclusions

In collaboration with clinical investigators, research nurses, the Biomarker Core, and basic scientists, the Biostatistics and Data Management Core have delivered the biostatistics and data management support as proposed.

Biomarker Core: Perform biomarker assessment to stratify patients into a particular arm of clinical trials and coordinate the distribution of clinical samples.

(Core Director: Ignacio Wistuba, M.D.)

The Biomarker Core, in close collaboration with the Clinical Trial team, Research Project Investigators and the other Cores, has played an important role in achieving the objectives proposed in the aims of the proposed BATTLE program by acquiring and processing lung cancer tissue specimens and performing biomarker analyses for the stratification of patients into clinical trial arms. In addition, the Core has played an important role in the discovery of novel molecular signatures and mechanisms of therapy resistance, by providing BATTLE tissue specimens to support the molecular profiling and mechanistic studies of response or resistance to targeted agents used in the BATTLE trials.

In conclusion, the Biomarker Core has successfully combined standard methods of histopathology processing and assessment of lung cancer tissue specimens with more advanced tools of molecular and genetic biomarker analyses.

Objective 1: To acquire, bank, process, and distribute tumor and blood specimens obtained from BATTLE enrolled patients for biomarker analyses and molecular mechanistic studies of targeted agents.

Summary of Research Findings

As previously reported, this Aim was completed last year.

Objective 2: To perform biomarker analyses and report results in a timely fashion for patient stratification in the BATTLE trials and molecular mechanistic studies of the targeted agents.

Summary of Research Findings

As previously reported, this Aim was completed last year.

Conclusions

As reported the previous year, in collaboration with other BATTLE investigators, we demonstrated that gene expression, miRNA, and protein profiling from tumor CNB is a feasible approach for predicting response in refractory NSCLC patients treated with targeted therapy. The Biomarker Core contributed significantly to many of the important discoveries by examining molecular abnormalities in the BATTLE tumor tissues. We have developed several predictive gene expression signatures in collaboration with investigators of **Specific Aim 3** and identified that, in NSCLC, not all mutant-*KRAS* amino acid substitutions signal the effectors in a similar way; thus, patients with *KRAS*-mutant tumors may require different therapeutic approaches (Ihle et al, JNCI, 2011).

KEY RESEARCH ACCOMPLISHMENTS

Specific Aim 2.3. To investigate the molecular mechanisms of resistance to and biomarkers of the biologic activity of inhibitors of the VEGF pathway

- Identified that KDR CNGs were present in NSCLC and predicted worse outcome in patients treated with adjuvant chemotherapy, as well as chemoresistance.
- Found that KDR upregulates pathways associated with angiogenesis and invasiveness (HIF, c-MET) in NSCLC tumor cells, and potentially EGFR inhibitor resistance.
- Determined that in NSCLC cells with KDR CNGs, KDR inhibitors, such as vandetanib, could block invasiveness and downregulate pathways associated with resistance, such as EZH2.
- Identified a new subpopulation of circulating endothelial cells (circulating tumor endothelial cells or CTECs) and demonstrated that CTECs were a biomarker for VEGF pathway inhibitor response in NSCLC preclinical models, and were present in NSCLC patients.
- Identified CA/Fs associated with therapeutic resistance to drugs in the BATTLE study, including HGF as a marker of vandetanib resistance.

Specific Aim 3: To identify biomarkers as novel predictors of clinical end points and potential therapeutic targets

- Developed two novel gene signatures that predicted 8-week disease control in patients with advanced and refractory NSCLC treated with sorafenib.
- Completed and submitted a manuscript describing the EMT novel gene signature that predicted 8-week disease control in patients with advanced and refractory NSCLC treated with the EGFR TKI erlotinib with wild-type *EGFR* tumors.
- Published our discovery that different therapeutic approaches might be required when treating patients with NSCLC harboring different mutant-*KRAS* amino acid substitutions.

Specific Aim 4: To explore new preclinical combinations and their mechanisms of action by targeting mTOR signaling and develop phase I trials to test these combinations.

- The combination of RAD001 and BKM120 synergistically inhibits the growth of human lung cancer cells both in vitro and in vivo.
- With results generated in the BATTLE project as preliminary data for a well-scored project, we have submitted the revision of our P01 renewal proposal.
- Based on BATTLE data, we have submitted a new R01 and received a potentially fundable score (7^{th} percentile).

Biostatistics and Data Management Core:

- Performed extensive statistical analysis on the BATTLE study findings, including treatment efficacy, toxicity, compliance, pre-specified biomarkers, and discovery biomarkers, etc.
- Developed and maintained a secured, Web-based database application to assist with the data collection and analysis.
- A Web-based database application is developed, deployed, and maintained at: https://insidebiostat/DMI_BATTLE/Common/Login.aspx.

PERSONNEL

A list of all personnel that have received funding from this research grant is included in Appendix A.

REPORTABLE OUTCOMES

Publications (Copies attached in Appendix B)

Kim WY, Prudkin L, Feng L, Kim ES, Hennessy B, Lee JS, Lee JJ, Glisson B, Lippman SM, Wistuba II, Hong WK, Lee HY. Epidermal growth factor receptor and K-Ras mutations and resistance of lung cancer to insulin-like growth factor 1 receptor tyrosine kinase inhibitors. Cancer. 2012 Feb 22. doi: 10.1002/cncr.26656. [Epub ahead of print] PubMed PMID: 22359227.

Kadara H, Kabbout M, Wistuba II. Pulmonary adenocarcinoma: a renewed entity in 2011. Respirology. 2012 Jan;17(1):50-65. doi: 10.1111/j.1440-1843.2011.02095.x. Review. PubMed PMID: 22040022.

Shirvani SM, Komaki R, Heymach JV, Fossella FV, Chang JY. Positron emission tomography/computed tomography-guided intensity-modulated radiotherapy for limited-stage small-cell lung cancer. Int J Radiat Oncol Biol Phys. 2012 Jan 1;82(1):e91-7. Epub 2011 Apr 12. PubMed PMID: 21489716.

Hirsch FR, Herbst RS. EGFR expression and the flexibility of FLEX. Lancet Oncol. 2012 Jan;13(1):3-5. Epub 2011 Nov 4. PubMed PMID: 22056020.

Shin DH, Min HY, El-Naggar AK, Lippman SM, Glisson B, Lee HY. Akt/mTOR counteract the antitumor activities of cixutumumab, an anti-insulin-like growth factor I receptor monoclonal antibody. Mol Cancer Ther. 2011 Dec;10(12):2437-48. Epub 2011 Oct 6. PubMed PMID: 21980128; PubMed Central PMCID: PMC3237768.

Tsao AS, Wei W, Kuhn E, Spencer L, Solis LM, Suraokar M, Lee JJ, Hong WK, Wistuba II. Immunohistochemical overexpression of platelet-derived growth factor receptor-beta (PDGFR-β) is associated with PDGFRB gene copy number gain in sarcomatoid non-small-cell lung cancer. Clin Lung Cancer. 2011 Nov;12(6):369-74. Epub 2011 May 17. PubMed PMID: 21729646.

Kim JS, Kim ES, Liu D, Lee JJ, Solis L, Behrens C, Lippman SM, Hong WK, Wistuba II, Lee HY. Prognostic impact of insulin receptor expression on survival of patients with nonsmall cell lung cancer. Cancer. 2011 Sep 22. doi: 10.1002/cncr.26492. [Epub ahead of print] PubMed PMID: 21952750; PubMed Central PMCID: PMC3298843.

Tsuta K, Kalhor N, Wistuba II, Moran CA. Clinicopathological and immunohistochemical analysis of spindle-cell carcinoid tumour of the lung. Histopathology. 2011 Sep;59(3):526-36. doi: 10.1111/j.1365-2559.2011.03966.x. Erratum in: Histopathology. 2011 Dec;59(6):1283. PubMed PMID: 22034892.

Kim MP, Chen Y, Bekele BN, Lopez A, Khanna A, Chen JQ, Spitz MR, Behrens C, Solis L, Wismach M, Ji L, Wistuba II, Roth JA, Katz RL. Activating enhancer-binding protein-2β nucleolar localization predicts poor survival after stage I non-small cell lung cancer resection. Ann Thorac Surg. 2011 Sep;92(3):1044-50. PubMed PMID: 21871297; PubMed Central PMCID: PMC3272351.

Xie Y, Xiao G, Coombes KR, Behrens C, Solis LM, Raso G, Girard L, Erickson HS, Roth J, Heymach JV, Moran C, Danenberg K, Minna JD, Wistuba II. Robust gene expression signature from formalin-fixed paraffin-embedded samples predicts prognosis of non-small-cell lung cancer patients. Clin Cancer Res. 2011 Sep 1;17(17):5705-14. Epub 2011 Jul 8. PubMed PMID: 21742808; PubMed Central PMCID: PMC3166982.

Heath EI, Blumenschein GR Jr, Cohen RB, Lorusso PM, Loconte NK, Kim ST, Ruiz-Garcia A, Chao RC, Wilding G. Sunitinib in combination with paclitaxel plus carboplatin in patients with advanced solid tumors: phase I study results. Cancer Chemother Pharmacol. 2011 Sep;68(3):703-12. Epub 2010 Dec 8. PubMed PMID: 21140147.

Kim JH, Choi DS, Lee OH, Oh SH, Lippman SM, Lee HY. Antiangiogenic antitumor activities of IGFBP-3 are mediated by IGF-independent suppression of Erk1/2 activation and Egr-1-mediated transcriptional events. Blood. 2011 Sep 1;118(9):2622-31. Epub 2011 May 6. PubMed PMID: 21551235; PubMed Central PMCID: PMC3167363.

Sandler A, Graham C, Baggstrom M, Herbst R, Zergebel C, Saito K, Jones D. An open-label, multicenter, three-stage, phase II study of s-1 in combination with cisplatin as first-line therapy for patients with advanced non-small cell lung cancer. J Thorac Oncol. 2011 Aug;6(8):1400-6. PubMed PMID: 21673602.

Sejpal S, Komaki R, Tsao A, Chang JY, Liao Z, Wei X, Allen PK, Lu C, Gillin M, Cox JD. Early findings on toxicity of proton beam therapy with concurrent chemotherapy for nonsmall cell lung cancer. Cancer. 2011 Jul 1;117(13):3004-13. doi: 10.1002/cncr.25848. Epub 2011 Jan 24. PubMed PMID: 21264827.

Adjei AA, Blumenschein GR Jr, Mandrekar S, Hillman S, Gatzemeier U, Heigener D. Long-term safety and tolerability of sorafenib in patients with advanced non-small-cell lung cancer: a case-based review. Clin Lung Cancer. 2011 Jul;12(4):212-7. doi: 10.1016/j.cllc.2011.03.021. Epub 2011 Apr 28. PubMed PMID: 21726819.

Tran HT, Zinner RG, Blumenschein GR Jr, Oh YW, Papadimitrakopoulou VA, Kim ES, Lu C, Malik M, Lum BL, Herbst RS. Pharmacokinetic study of the phase III, randomized, double-blind, multicenter trial (TRIBUTE) of paclitaxel and carboplatin combined with erlotinib or placebo in patients with advanced Non-small Cell Lung Cancer (NSCLC). Invest New Drugs. 2011 Jun;29(3):499-505. Epub 2010 Jan 22. PubMed PMID: 20094773.

Kim WY, Kim MJ, Moon H, Yuan P, Kim JS, Woo JK, Zhang G, Suh YA, Feng L, Behrens C, Van Pelt CS, Kang H, Lee JJ, Hong WK, Wistuba II, Lee HY. Differential impacts of insulin-like growth factor-binding protein-3 (IGFBP-3) in epithelial IGF-induced lung cancer development. Endocrinology. 2011 Jun;152(6):2164-73. Epub 2011 Mar 29. PubMed PMID: 21447628; PubMed Central PMCID: PMC3100627.

Herbst RS, Ansari R, Bustin F, Flynn P, Hart L, Otterson GA, Vlahovic G, Soh CH, O'Connor P, Hainsworth J. Efficacy of bevacizumab plus erlotinib versus erlotinib alone in advanced non-small-cell lung cancer after failure of standard first-line chemotherapy (BeTa): a double-blind, placebo-controlled, phase 3 trial. Lancet. 2011 May 28;377(9780):1846-54. PubMed PMID: 21621716.

Wu X, Ye Y, Rosell R, Amos CI, Stewart DJ, Hildebrandt MA, Roth JA, Minna JD, Gu J, Lin J, Buch SC, Nukui T, Ramirez Serrano JL, Taron M, Cassidy A, Lu C, Chang JY, Lippman SM, Hong WK, Spitz MR, Romkes M, Yang P. Genome-wide association study of survival in non-small cell lung cancer patients receiving platinum-based chemotherapy. J Natl Cancer Inst. 2011 May 18;103(10):817-25. Epub 2011 Apr 11. PubMed PMID: 21483023; PubMed Central PMCID: PMC3096796.

Tang X, Kadara H, Behrens C, Liu DD, Xiao Y, Rice D, Gazdar AF, Fujimoto J, Moran C, Varella-Garcia M, Lee JJ, Hong WK, Wistuba II. Abnormalities of the TITF-1 lineage-specific oncogene in NSCLC: implications in lung cancer pathogenesis and prognosis. Clin Cancer Res. 2011 Apr 15;17(8):2434-43. Epub 2011 Jan 21. PubMed PMID: 21257719; PubMed Central PMCID: PMC3078948.

Ihle NT, Byers LA, Kim ES, Saintigny P, Lee JJ, Blumenschein GR, Tsao A, Liu S, Larsen JE, Wang J, Diao L, Coombes KR, Chen L, Zhang S, Abdelmelek MF, Tang X, Papadimitrakopoulou V, Minna JD, Lippman SM, Hong WK, Herbst RS, Wistuba II, Heymach JV, Powis G. Effect of KRAS oncogene substitutions on protein behavior: implications for signaling and clinical outcome. J Natl Cancer Inst. 2012 Feb 8;104(3):228-39. Epub 2012 Jan 13. PubMed PMID: 22247021; PubMed Central PMCID: PMC3274509.

Xu CX, Li Y, Yue P, Owonikoko TK, Ramalingam SS, Khuri FR, Sun SY. The combination of RAD001 and NVP-BEZ235 exerts synergistic anticancer activity against non-small cell lung cancer in vitro and in vivo. PLoS One. 2011;6(6):e20899. Epub 2011 Jun 14. PubMed PMID: 21695126; PubMed Central PMCID: PMC3114848.

Xu CX, Zhao L, Yue P, Fang G, Tao H, Owonikoko TK, Ramalingam SS, Khuri FR, Sun SY. Augmentation of NVP-BEZ235's anticancer activity against human lung cancer cells by blockage of autophagy. Cancer Biol Ther. 2011 Sep 15;12(6):549-55. doi: 10.4161/cbt.12.6.16397. Epub 2011 Sep 15. PubMed PMID: 21738008; PubMed Central PMCID: PMC3218593.

Li Y, Fan S, Koo J, Yue P, Chen ZG, Owonikoko TK, Ramalingam SS, Khuri FR, Sun SY. Elevated expression of eukaryotic translation initiation factor 4E is associated with proliferation, invasion and acquired resistance to erlotinib in lung cancer. Cancer Biol Ther. 2012 Mar 1;13(5):272-80. Epub 2012 Mar 1. PubMed PMID: 22236867.

Abstracts (Attached in Appendix B**)**

Pierre Saintigny, George R. Blumenschein, Jr., Lixia Diao, Jing Wang, Kevin Coombes, Suyu Liu, Edward Kim, Anne Tsao, Roy Herbst, Christine Alden, Jack J. Lee, Ximing Tang, David Stewart, Merrill Kies, Frank Fossella, Hai Tran, Li Mao4, Marshall Hicks, Jeremy Erasmus, Sanjay Gupta, Luc Girard, Michael Peyton, Suzanne Davis, Scott Lippman, Waun Ki Hong, John Minna, Ignacio Wistuba, John Heymach. Gene-expression profiles predict sorafenib efficacy in wild-type EGFR non-small cell lung cancer (NSCLC). Proceedings of the 103rd Annual Meeting of the American Association for Cancer Research. Abstract 4819.

CONCLUSIONS

Aim 2.3: Our project investigating markers for VEGF pathway inhibitors in the BATTLE study has led to a candidate tumor marker, KDR CNGs, that is now undergoing independent validation using samples from phase III trials. If result is positive, KDR CNGs would represent the first independently validated tumor marker for VEGFR inhibitors. Our data suggest that KDR CNGs may also be a useful biomarker for chemoresistance and EGFR inhibitor resistance, and we have demonstrated key signaling pathways downstream of KDR, including PI3K, HIF, EZH2, and c-MET.

We have also identified several novel blood-based biomarkers for VEGF/R inhibitors including CTECs, and plasma CA/Fs, including HGF. We have gone on to validate HGF as a mechanism of resistance in preclinical models and, based on these findings, are now developing trials targeting c-MET and VEGF pathways simultaneously.

Aim 3: We have further demonstrated that gene expression profiling from CNBs is a feasible approach for predicting response and identifying potential therapeutic targets in refractory NSCLC patients treated with targeted therapy. We have developed and refined gene expression signatures that predict 8-week disease control in the BATTLE patients with *EGFR* wild-type tumors treated with EGFR TKIs (EMT signature) and sorafenib. In addition, we published our discovery indicating that in NSCLC, not all mutant-*KRAS* amino acid substitutions signal the effectors in a similar way.

Aim 4: In collaboration with investigators at MD Anderson Cancer Center and Dana Farber Cancer Center, a phase I study was first conducted to evaluate the combination of RAD001 with erlotinib. Subsequently a randomized phase II study was performed to compare the combination against monotherapy with erlotinib alone in patients with advanced stage NSCLC. The combination was well tolerated without undue increase in the incidence of adverse events. There was a trend towards improvement in PFS for the combination therapy, but the differences did not reach statistical significance. The disease control rate at 3 months was 39% for the combination compared to 28% for monotherapy with erlotinib. The results call for identification of biomarkers for patient selection. Based on the promising pre-clinical observations in objective 1, we will soon initiate a phase I study of RAD001 with BKM120, a PI3K inhibitor. This study will involve sequential biopsy collection to understand the molecular effects of the combination at the level of the tumor tissue.

Biostatistics and Data Management Core: In collaboration with clinical investigators, research nurses, the Biomarker Core, and basic scientists, the Biostatistics and Data Management Core delivered the biostatistics and data management support as proposed.

Biomarker Core: As reported the previous year, in collaboration with other BATTLE investigators, we demonstrated that gene expression, miRNA, and protein profiling from tumor CNB is a feasible approach for predicting response in refractory NSCLC patients treated with targeted therapy. The Biomarker Core contributed significantly to many of the important discoveries by examining molecular abnormalities in the BATTLE tumor tissues. We have developed several predictive gene expression signatures in collaboration with investigators of Specific Aim 3, and identified that in NSCLC, not all mutant-*KRAS* amino acid substitutions signal the effectors in a similar way; thus, patients with *KRAS*-mutant tumors may require different therapeutic approaches (Ihle et al, JNCI, 2011).

APPENDIX A

Personnel

DOD BATTLE EFFORT FUNDED PERSONNEL 04/01/06 - 03/31/12

Alden,Christine M
Barta,Peter
Brooks,Angela A
Carter,Kristina D
Cascone,Tina
Chen,Yulong
Choi,Dong Soon
Choi,Hyun Ho
Creel,Pamela S
Davis,Suzanne E
Deng,Jiong
Eddings,Teresa A
Fan,You-Hong
Fiorentino,Stefania
Fry,Nola J
George,John T
Gil,James M
Herynk,Matthew H
Hong,Waun K
Huang,Jian N
Huang,Jiannan
Jiang,Chengrong
Kalhor,Neda
Kim,Yoon Sung
LeBlanc,Laurie A
Lee,Ho-Young
Lee,Jiun-Kae Jack
Lewis,Dorothea A
Lewis,Jeffrey M
Li,Yuanyuan
Lin,Xiaofeng
Liu,Diane D
Liu,Suyu
Mao,Li
Martinez,Carmen R
McDowell,Christina L
Men,Taoyan
Min,Hye-Young
Price,Mellanie J
Ren,Hening
Rinsurongkawong,Waree
Saigal,Babita
Saintigny,Pierre
Smith,Beverly J
Smith,John Kendal
Song,Wei Sonya
Suraokar,Milind B
Tran,Hai T
Vilts,Raquel C
Weissferdt,Annikka
Willis,Veshae P

Wistuba,Ignacio Ivan
Woods,Denise M
Wu,Huakang
Xue,Yuwen
Yang,Bijun
Yin,Ming
Zhang,Guangcheng
Zhang,Li

APPENDIX B

Publications and Abstracts

Original Article

Epidermal Growth Factor Receptor and *K-Ras* Mutations and Resistance of Lung Cancer to Insulin-Like Growth Factor 1 Receptor Tyrosine Kinase Inhibitors

Woo-Young Kim, PhD[1]; Ludmila Prudkin, PhD[1]; Lei Feng, MS[2]; Edward S. Kim, MD[1]; Bryan Hennessy, MD[3]; Ju-Seog Lee, PhD[4]; J. Jack Lee, PhD[2,5]; Bonnie Glisson, MD[1]; Scott M. Lippman, MD[1]; Ignacio I. Wistuba, PhD[6]; Waun Ki Hong, MD[1]; and Ho-Young Lee, PhD[1,7]

BACKGROUND: Most patients with nonsmall cell lung cancer (NSCLC) have responded poorly to epidermal growth factor receptor (EGFR) tyrosine kinase inhibitors (TKIs). The authors investigated the involvement of insulinlike growth factor 1 receptor (IGF-1R) signaling in primary resistance to EGFR TKIs and the molecular determinants of resistance to IGF-1R TKIs. **METHODS:** Phosphorylated IGF-1R/insulin receptor (pIGF-1R/IR) was immunohistochemically evaluated in an NSCLC tissue microarray. The authors analyzed the antitumor effects of an IGF-1R TKI (PQIP or OSI-906), either alone or in combination with a small-molecular inhibitor (PD98059 or U0126) or with siRNA targeting *K-Ras* or mitogen-activated protein kinase/extracellular signal-regulated kinase kinase (MEK), in vitro and in vivo in NSCLC cells with variable histologic features and *EGFR* or *K-Ras* mutations. **RESULTS:** pIGF-1R/IR expression in NSCLC specimens was associated with a history of tobacco smoking, squamous cell carcinoma histology, mutant *K-Ras*, and wild-type (WT) *EGFR*, all of which have been strongly associated with poor response to EGFR TKIs. IGF-1R TKIs exhibited significant antitumor activity in NSCLC cells with WT EGFR and WT *K-Ras* but not in those with mutations in these genes. Introduction of mutant *K-Ras* attenuated the effects of IGF-1R TKIs on NSCLC cells expressing WT *K-Ras*. Conversely, inactivation of MEK restored sensitivity to IGF-TKIs in cells carrying mutant *K-Ras*. **CONCLUSIONS:** The mutation status of both *EGFR* and *K-Ras* could be a predictive marker of response to IGF-1R TKIs. Also, MEK antagonism can abrogate primary resistance of NSCLC cells to IGF-1R TKIs. ***Cancer* 2012;000:000–000.** © *2012 American Cancer Society.*

KEYWORDS: epidermal growth factor receptor, K-Ras, insulinlike growth factor 1 receptor, lung cancer, tyrosine kinase inhibitors.

INTRODUCTION

Lung cancer, usually caused by years of tobacco smoking, is the leading cause of cancer deaths in the United States.[1] Because conventional chemotherapy has limited efficacy against lung cancer, new targeted therapeutic approaches are being investigated. The epidermal growth factor receptor (EGFR) signaling pathway is an attractive target in the development of lung cancer treatments. However, treatment with erlotinib and gefitinib, the 2 EGFR tyrosine kinase inhibitors (TKIs) approved by the US Food and Drug Administration, has produced poor response rates in patients with nonsmall cell lung cancer (NSCLC).[2] Although a group of patients with somatic mutations in EGFR respond to these EGFR TKIs,[2-4] such mutations have been detected in only 5% of tumors from current or former smokers,[2] and a response rate to EGFR TKIs of only 3.9% has been reported in patients with NSCLC and a history of tobacco smoking compared with

Corresponding author: Ho-Young Lee, PhD, College of Pharmacy and Research Institute of Pharmaceutical Sciences, Seoul National University, Seoul 151-742, Republic of Korea; hylee135@snu.ac.kr

Woo-Young Kim's current address: College of Pharmacy, Sookmyung Women's University, Seoul, South Korea

[1]Department of Thoracic and Head and Neck Medical Oncology, The University of Texas MD Anderson Cancer Center, Houston, Texas; [2]Department of Biostatistics, The University of Texas MD Anderson Cancer Center, Houston, Texas; [3]Department of Gynecologic Medical Oncology, The University of Texas MD Anderson Cancer Center, Houston, Texas; [4]Department of Systems Biology, The University of Texas MD Anderson Cancer Center, Houston, Texas; [5]University of Texas Graduate School of Biomedical Sciences, Houston, Texas; [6]Department of Pathology, The University of Texas MD Anderson Cancer Center, Houston, Texas; [7]College of Pharmacy and Research Institute of Pharmaceutical Sciences, Seoul National University, Seoul, Republic of Korea

DOI: 10.1002/cncr.26656, **Received:** June 24, 2011; **Revised:** September 2, 2011; **Accepted:** September 2, 2011, **Published online** in Wiley Online Library (wileyonlinelibrary.com)

24.7% in NSCLC patients who have never smoked,[5] suggesting that EGFR may not be the appropriate target in NSCLC patients with a history of tobacco smoking.

Signaling through the insulinlike growth factor 1 receptor (IGF-1R) has an essential role in cell mitosis, survival, and transformation[6-9] and has been associated with higher risk of multiple neoplasms.[10-12] IGF-1 stimulates IGF-1R and the IGF-1R/insulin receptor (IGF-1R/IR) heterodimers. Recently, we demonstrated activation of the IGF-1R signaling axis during the early stages of lung carcinogenesis.[13] We found that activation of IGF-1R in the lungs of mice as a result of IGF-1 overexpression led to spontaneous lung tumor development that progressed to adenocarcinoma upon exposure to tobacco carcinogens. This early stage of lung cancer development was suppressed by administration of a selective IGF-1R TKI, *cis*-3-(3-[4 methyl-piperazin-l-yl]-cyclobutyl)-1-(2-phenyl-quinolin-7-yl)-imidazo(1,5-*a*)pyrazin-8-ylamine (PQIP).[13] Given the importance of IGF-1R signaling in most human cancers and the promising results of clinical trials targeting IGF-1R for cancer therapy,[14] we sought to evaluate the potential application of IGF-1R TKIs in a series of NSCLC cells with variable histologic and genetic characteristics to assess potential determinants of response or resistance to these drugs.

Here, we report that the activation of IGF-1R via tobacco smoking, constitutive activation of EGFR via somatic mutations, and IGF-1R–independent activation of signaling through mutant *K-Ras* are potential biomarkers of response or resistance of NSCLC cells to small-molecule IGF-1R TKIs, including PQIP and OSI-906. Our findings provide a rationale for the therapeutic use of IGF-1R TKIs, either singly or in combination with mitogen-activated protein kinase (MAPK)/extracellular signal-regulated kinase (MEK) inhibitors, in tobacco smoking-related NSCLC, particularly in tumors with *K-Ras* mutations.

MATERIALS AND METHODS

Cell Lines

NSCLC cell lines were obtained from American Type Culture Collection or provided by Dr. John Minna (University of Texas Southwestern Medical Center, Dallas, Texas). The cell lines were authenticated by the Genetic Resources Core Facility at Johns Hopkins University (Baltimore, Md) using DNA (short tandem repeat) profiling.

Protein Analysis

Antibodies detecting total IGF-1R (Santa Cruz, Calif), pIGF-1Rβ (Tyr1131/1146), pIGF-1Rβ (Tyr1135/1136), pErk1/2, pAkt, pIRS-1, total IRS-1, total Erk1/2, total Akt, actin, tubulin, or cleaved caspase-3 (all from Cell Signaling Technology, Danvers, Mass) were used for Western blotting. The culture medium without serum was harvested after 2 days of cell culture and concentrated with a Centricon centrifugal filter unit (Millipore, Billerica, Mass), and the free IGF-1 in the medium was measured with an enzyme-linked immunosorbent assay (ELISA) kit from Diagnostic Systems Laboratories (Webster, Tex). PQIP and OSI-906 were provided by OSI Pharmaceuticals (Melville, NY). Reverse-phase protein array was performed as previously described.[15]

Tissue Microarray of Primary Tumor Specimens and the Analysis

Primary NSCLC tumor specimens were collected from 354 patients who had been treated at our institution under an institutional review board–approved protocol and had given their informed consent. Demographic information for those patients was described previously.[16] Formalin-fixed, paraffin-embedded primary NSCLC sections (5 μm thick) were placed in a tissue microarray (TMA). Immunohistochemical (IHC) evaluation of the NSCLC TMA was performed as previously described.[16] Anti–pIGF-1R (Tyr 1135/1136)/IR (Tyr1162/1163) antibody (Biosource, Camarillo, Calif; diluted 1:200) or anti-pEGFR (Tyr1068) antibody (Zymed Laboratories, San Francisco, Calif; diluted 1:100) was used for staining. Immunostaining for IGF-1R, and pIGF-1R/IR (membrane) was quantified by a lung cancer pathologist who used a 4-value intensity score (0, 1+, 2+, and 3+), and the extent of reactivity was expressed as a percentage. A final staining score was calculated by multiplying the intensity score by the extent of reactivity value (range, 0-300). *EGFR* exons 18 to 21 and the *K-Ras* mutational hot spot codons 12, 13, and 61 were amplified as described previously.[3,4,17] Treated polymerase chain reaction (PCR) products were sequenced using a Big Dye Terminator v3.1 sequencing kit (Applied Biosystems, Foster City, Calif). Specimens with single or double *EGFR* and *K-Ras* mutations were confirmed using repeated PCR and sequencing, and the corresponding normal DNA was sequenced to verify that the mutations were somatic.

In Vitro Drug Sensitivity and Apoptosis Assays

The indicated NSCLC cells were treated with PQIP, either singly or in combination with MEK inhibitors, in 1% fetal bovine serum (FBS). Cell viability was

determined using a 3-(4,5-dimethylthiazol-2-yl)-2,5-diphenyltetrazolium bromide colorimetric assay as described previously.[18] At least 6 independent samples were used for the assay. Cell apoptosis was analyzed using immunofluorescence staining with cleaved caspase-3 antibody (BioVision, Mountain View, Calif) as described previously.[19] Adenovirus expressing dominant-negative MEK1/2 was described previously,[20] and siRNA against *K-Ras* was purchased from Dharmacon (Longmont, Colo). Anchorage-independent growth in 0.4% agarose with a 1% agarose underlay was measured as described previously.[13]

Animal Experiments

All animal procedures were performed in accordance with a protocol approved by The University of Texas MD Anderson Cancer Center Institutional Animal Care and Use Committee. Athymic nude mice (BALB/c) were obtained from Harlan Laboratories (Madison, Wis). Xenograft tumors were generated by subcutaneous injection of H226B–*K-Ras*. Briefly, nude mice were injected at a single dorsal flank site with 5×10^6 cells in 200 μL of phosphate-buffered saline. When tumors reached a volume of 50 to 200 mm^3, mice were treated orally with vehicle, OSI906 (40 mg/kg/d), U0126 (4 mg/kg, every other day), or both OSI-906 and U0126; the first day of drug treatment was termed day 0. Tumor size was measured every 2 days. Volumes were calculated by $0.5 \times a \times b^2$, in which a is the longer and b the shorter diameter. Mean tumor volumes and 95% confidence intervals were determined.

Statistical Analysis

For the TMA data, pIGF-1R expression levels for NSCLC patients with different clinical and demographic characteristics, including sex, history of tobacco smoking, tumor histologic type, and EGFR and *K-Ras* mutation status, were compared using Student t test, the Mann-Whitney U test, or analysis of variance. Correlations among TMA specimens stained for pIGF-1R/IR and pEGFR were identified using the Spearman rank correlation coefficient. For the drug sensitivity analysis, the 2-tailed Mann-Whitney U test was used to compare sensitivity between the mutant and wild-type (WT) *K-Ras* groups of cells. All analyses were conducted using SAS (SAS Institute, Cary, NC) or SPSS (SPSS Inc., Chicago, Ill). $P < .05$ was considered statistically significant.

RESULTS

Activation of IGF-1R/IR Is Associated With Histologic Features, History of Tobacco Smoking, and Mutations of EGFR and K-Ras in Human Lung Cancer

We evaluated the expression of pIGF-1R/IR in surgical tumor sections obtained from patients with NSCLC. pIGF-1R/IR staining was detected in the cell membrane (50%), cytoplasm (100%), and nucleus (100%). Given that the nature of IGF-1R as a membrane receptor and the role of nuclear IGF-1R staining are still unclear, we analyzed the membrane staining of pIGF-1R/IR.

Given the frequency of *EGFR* mutation (exons 18-21) in NSCLC patients who have never smoked, those with adenocarcinoma, and those with WT *K-Ras*[2,4,17,21-23] and the crosstalk between the EGFR and IGF-1R signaling pathways, we assessed the correlation of pIGF-1R/IR staining with the frequency of EGFR and *K-Ras* mutations in the NSCLC specimens. pIGF-1R/IR expression levels were higher in patients with squamous cell carcinoma than in those with adenocarcinoma ($P = .019$) and were higher in patients with a history of tobacco smoking (both former and current smokers) than in patients who had never smoked. pIGF-1R/IR level and EGFR mutation were negatively correlated, with a marginal significance (Table 1). In addition, pIGF-1R/IR levels were significantly higher in patients with mutant *K-Ras* than in those with WT *K-Ras*. The negative correlation between pIGF-1R/IR expression and mutant EGFR and the positive correlation between pIGF-1R/IR expression and mutant *K-Ras* were also observed in patients with adenocarcinoma (data not shown). These findings suggest that activation of the IGF-1R axis is strongly correlated with tobacco smoking–induced lung carcinogenesis.

NSCLC Cell Lines Carrying Mutant EGFR Are Independent of IGF-1R Signaling for Survival and Proliferation

Given the negative association between pIGF-1R/IR level and EGFR mutation, we sought to explore the impact of EGFR mutation on the sensitivity of NSCLC cells to PQIP, an IGF-1R/IR TKI.[24] We first examined whether the IGF-1R signaling pathway was functional in 6 NSCLC cell lines carrying mutant EGFR (L858R or Del746-750). IGF-1–induced activation of IGF-1R signaling was well preserved (Fig. 1A) and was effectively inhibited by PQIP (Fig. 1B) in the EGFR mutant cell lines. However, the viability and anchorage-independent colony-forming ability of these cells remained unchanged

Table 1. Tissue Levels of pIGF-1R/IR in Case Patients With Nonsmall Cell Lung Cancer

Variable	Category		pIGF-1R/IR	
		No.	Mean ± SD	*P*
Smoking	Never	50	8.8 ± 29.18	
	Former	134	28.28 ± 49.99	.008
	Current	82	30.85 ± 50.08	.027
Histology	Squamous	100	35.0 ± 53.04	
	Adenocarcinoma	168	19.75 ± 47.29	.019
EGFR	Mutant	25	8.0 ± 28.28	
	Wild type	159	24.78 ± 48.63	.066
K-Ras	Mutant	22	41.82 ± 53.06	
	Wild type	157	20.83 ± 45.99	.015

Abbreviations: pIGF-1R/IR, insulinlike growth factor 1 receptor/insulin receptor; SD, standard deviation.
Data represent analysis of variance test for smoking history, with *P* values comparing with never smoker; independent samples *t* test for histology; and Mann-Whitney test for *EGFR* mutation and *K-Ras* mutation.

after PQIP treatment (Fig. 1C). These findings suggest that the NSCLC cells carrying mutant EGFR harbor functional IGF-1R signaling but do not rely on the pathway for cell proliferation.

K-Ras *Mutation Is a Key Determinant of the Response of NSCLC Cell Lines carrying WT* EGFR *to IGF-1R Inhibitors*

Findings from the NSCLC TMA led us to hypothesize that NSCLC cell lines that are derived from lung epithelial cells exposed to tobacco smoke[25] could be dependent on IGF-1R signaling for survival and proliferation, thus providing a vulnerable point for pIGF-1R/IR—targeted inhibitors. To test this hypothesis, we examined a panel of 16 NSCLC cell lines carrying WT EGFR with various histologic features (squamous cell carcinoma, bronchioalveolar carcinoma, adenocarcinoma, and large-cell carcinoma) and mutations in *K-Ras* and *p53*. We assessed the effects of blockade of IGF-1R signaling by PQIP on the proliferation and viability of these NSCLC cells. When we tested the sensitivity to PQIP at different concentrations (0.2-10 μM), the 16 cell lines displayed differential sensitivity to PQIP treatment (Fig. 2A). We sought to identify predictive biomarkers of PQIP sensitivity in the cells. Although no obvious correlation was seen between PQIP sensitivity and the cells' histologic features (Fig. 2A) or expression levels of IGF-1R, IR, or pIGF-1R/IR (Fig. 2B), the NSCLC cells with mutant *K-Ras* (listed in black) tended to have poorer sensitivity to PQIP than did those with WT *K-Ras* (listed in blue) (Fig. 2A). Moreover, cell lines carrying mutant *K-Ras* (n = 7) showed significantly

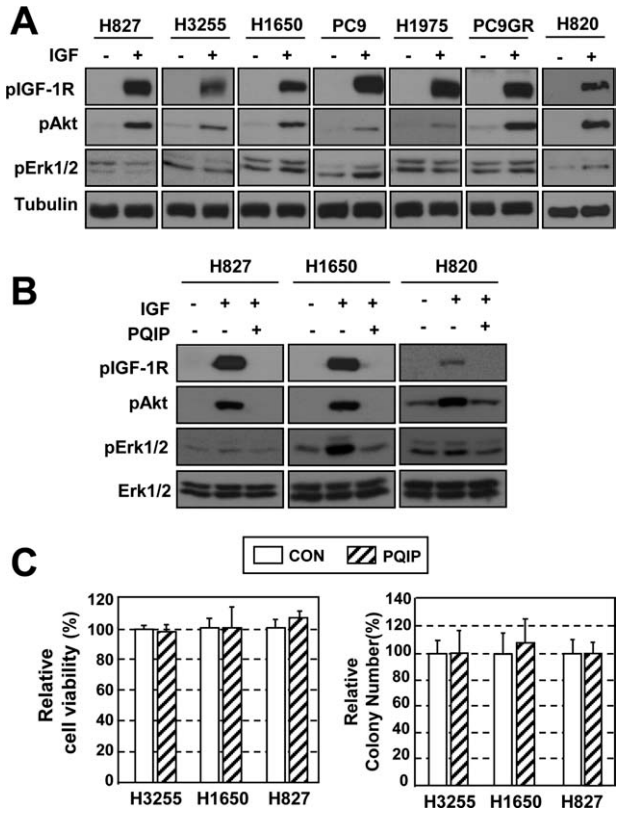

Figure 1. Response of nonsmall cell lung cancer cell lines carrying mutant *EGFR* to treatment with PQIP is shown. (A) The insulinlike growth factor 1 receptor (IGF-1R) signaling pathway is activated by IGF-1 in mutant *EGFR* cells. (B) PQIP inhibits IGF-1R phosphorylation (p), shown in a subset of mutant *EGFR* cell lines. (C) PQIP does not affect cell viability or anchorage-independent colony formation, shown in 3 mutant *EGFR* cell lines. Columns indicate means of 3 independent experiments; bars show standard deviation. CON, control.

higher viability than those carrying WT *K-Ras* (n = 5) at doses of 0.2 and 1.0 μM PQIP ($P < .05$; Fig. 2C).

To confirm the role of *K-Ras* mutation in PQIP resistance, we assessed the effects of PQIP on *K-Ras* mutant and WT cells. To investigate the mechanism by which *K-Ras* mutation rescues NSCLC cells from PQIP treatment, we examined the PQIP-induced antiproliferative activities of H460 and H157 cells after mutant *K-Ras* was knocked out by transfection with specific siRNA against *K-Ras*. Both H460 and H157 cells revealed a significantly enhanced PQIP sensitivity after *K-Ras* expression was silenced by transfection with specific siRNA (Fig. 2D, *Top*), indicating an essential role of mutant *K-Ras* in mediating PQIP resistance in the NSCLC cell lines. We next assessed the effects of PQIP on IGF-1R signaling in H596 cells, which carry WT *K-Ras*, and A549 cells, which carry mutant *K-Ras*. We found that PQIP treatment at 1 μM

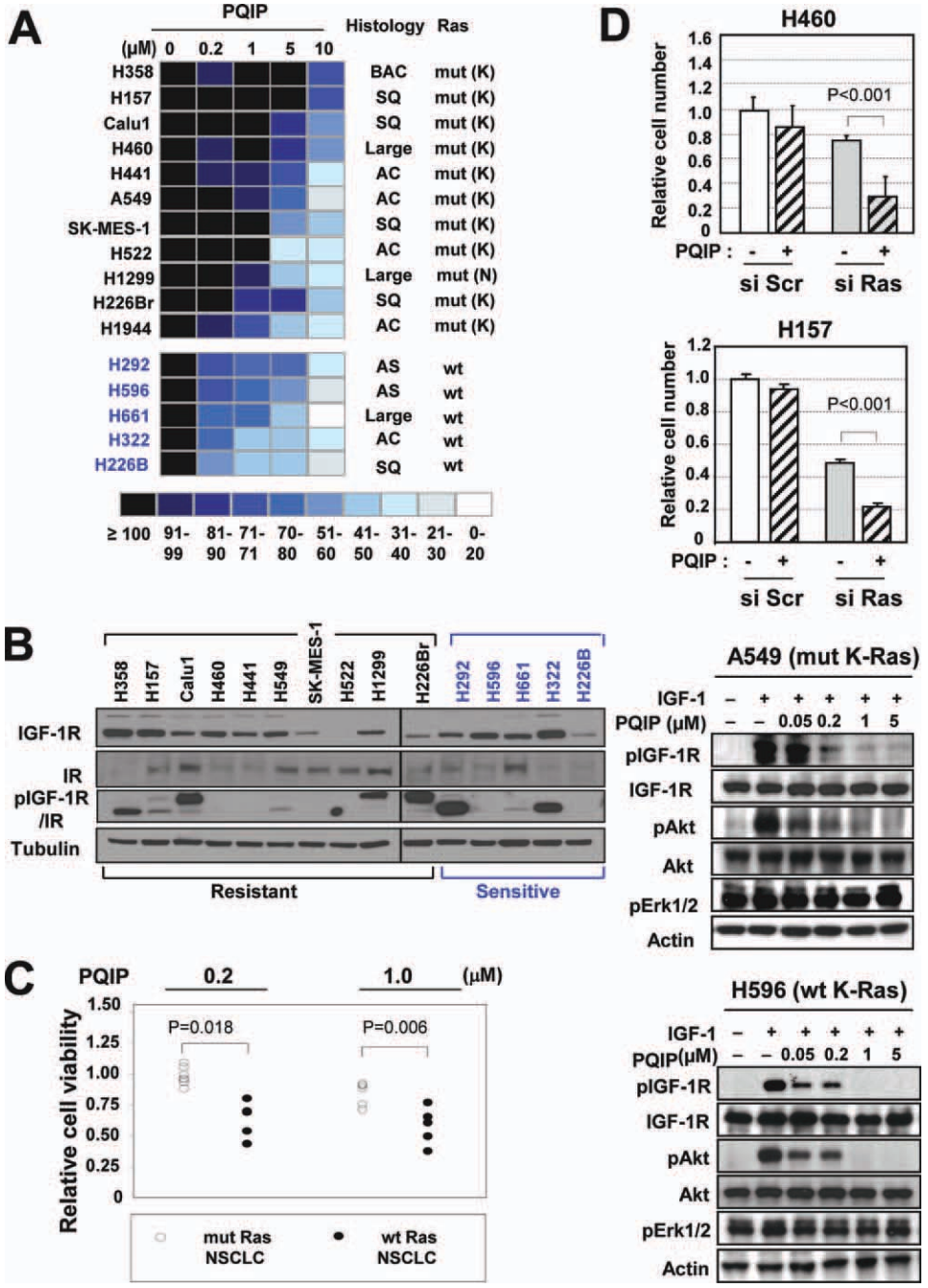

Figure 2. *K-Ras* mutation is associated with poor response to the insulinlike growth factor 1 receptor (IGF-1R) tyrosine kinase inhibitor PQIP in wild-type *EGFR* nonsmall cell lung cancer (NSCLC) cells. (A) Role of IGF signaling in NSCLC cells with mutant *K-Ras* (except H1299;*N-Ras*, listed in black) and wild-type *K-Ras* (listed in blue) is shown. The effect of PQIP on the survival/proliferation of NSCLC cells was examined (1% fetal bovine serum [FBS] in culture medium). Each result is displayed as a colored box; shades of blue represent the cell number relative to the control as a percentage. The most resistant cells are at the top and the most sensitive at the bottom. AC, adenocarcinoma; BAC, bronchioalveolar carcinoma; SQ, squamous cell carcinoma; Large, large-cell carcinoma, AS, adenosquamous carcinoma. (B) Relative expression of IGF-1R, insulin receptor (IR), and pIGF-1R/IR is shown in a panel of NSCLC cell lines. (C) Comparison of relative sensitivity to PQIP treatment is shown between the mutant (mut) and wild-type (wt) *K-Ras* groups. Relative cell viability decreased by ≥5% in response to treatment with 1 μM PQIP in each group. (D; *Top*) H460 and H157 cells, which carry mutant *K-Ras*, were transfected with *K-Ras* siRNA or Scr (scrambled) siRNA and then seeded in 96-well microplates. The cells were treated with PQIP for 3 days in RPMI containing 1% FBS and then subjected to 3-(4,5-dimethylthiazol-2-yl)-2,5-diphenyltetrazolium bromide assay. (*Bottom*) A549 and H596 cells, which carry mutant and wild-type K-*Ras*, respectively, were treated with the indicated concentrations of PQIP for 6 hours in the absence of FBS and then stimulated with IGF-1 for 30 minutes.

almost completely inhibited IGF-induced IGF-1R and Akt phosphorylation in H596 cells (Fig. 2D, *Bottom*). Similar results were found in A549 cells, indicating that PQIP is effective in blocking IGF-1R signaling in NSCLC cells regardless of *K-Ras* mutation status. These results indicate that the mechanism by which *K-Ras* mutation decreases NSCLC cell sensitivity to PQIP is independent of the ligand-induced phosphorylation of IGF-1R.

Mutant K-Ras *Activates IGF-1R/Akt Signaling but Leads to Resistance to IGF-1R/IR TKI*

Given the strong positive correlation between IGF-1R activation and *K-Ras* mutation in the human NSCLC TMA and the inverse correlation between PQIP sensitivity and *K-Ras* mutation in NSCLC cell lines, we further assessed the role of *K-Ras* mutation in the IGF-1R pathway and PQIP sensitivity in H226B and H596 cells in which Green Fluorescence Protein (GFP) or mutant *K-Ras* had been transduced by retroviral infection. H226B–*K-Ras* cells showed higher levels of pIGF-1R and pAkt and lower levels of IGF-1R than those in H226B-GFP cells (Fig. 3A). We also observed that H226B–*K-Ras* cells produced more IGF-1 than H226B-GFP cells did. To characterize further molecular sequelae triggered by mutant *K-Ras*, we performed a reverse-phase protein array. Unsupervised hierarchical clustering analyses demonstrated that the PI3K/Akt and Ras/MAPK pathways were activated by mutant *K-Ras* (Fig. 3B). Although PQIP treatment decreased pIGF-1R/IR and pAkt levels in both cell lines, phosphorylation of the downstream mediators of Akt, including pS6, and pGSK, was efficiently inhibited by PQIP treatment in H226B-GFP cells but not in H226B–*K-Ras* cells (Fig. 3C). Furthermore, H226B–*K-Ras* and H596–*K-Ras* cells were significantly less sensitive to PQIP treatment than the control cells were (Fig. 3D), suggesting that IGF-1R signaling is enhanced by mutant *K-Ras*; however, *K-Ras* mutation abrogates NSCLC cell sensitivity to PQIP by activating downstream signaling, including p70S6K.

Targeting MEK Overrides the Resistance of Mutant K-Ras *Cells to IGF-1R TKI*

Because p70S6K is known to be activated by the MEK/Erk pathway,[26] which can be constitutively activated by *K-Ras* mutation, we determined whether inactivation of MEK would restore the antitumor effects of PQIP or OSI-906 (a PQIP derivative currently undergoing a phase 1 clinical trial in our institute in NSCLC cell lines carrying mutant *K-Ras*). We found that cotargeting of MEK, either with a small-molecule MEK inhibitor (PD98059 or U0126) or with adenovirus expressing the dominant-negative form of MEK (Ad-MEK-DN), significantly enhanced the effects of PQIP on cell viability (Fig. 4A) and anchorage-independent colony-forming ability (Fig. 4B) in representative mutant *K-Ras* resistant cell lines. Furthermore, the percentage of apoptotic cells was significantly increased by the combined treatment (Fig. 4C). These results suggest that inactivation of MEK augments the apoptotic activities of PQIP in NSCLC cells carrying mutant *K-Ras*. We finally evaluated the combined effects of OSI-906 and U0126 in vivo. The mice treated with vehicle or OSI-906 alone showed similar H226B *K-Ras* tumor growth (Fig. 4D). Pharmacologic inhibition of MEK by administration of U0126 dramatically augmented the effects of OSI-906 on the growth of the tumors. On day 8 after the first dose, the mean tumor volume for mice that received combined OSI-906 and U0126 was significantly smaller than the mean tumor volume for mice that received vehicle, OSI-906 alone, or U0126 alone. IHC staining of Ki67 and cleaved caspase-3 in the tumors demonstrated that the combined treatment induced a decrease in cell proliferation in association with an increase in cell apoptosis in vivo (Fig. 4E). Taken together, these findings underscore the pivotal role of activation of the MEK/Erk pathway through *K-Ras* mutation in the primary resistance of NSCLC cells to IGF-1R TKIs.

DISCUSSION

In the present study, we elucidate potential predictive markers of response of NSCLC cells to IGF-1R TKIs. We show that: 1) the expression of IGF-1R/IR in NSCLC specimens is positively associated with a history of tobacco smoking, squamous cell carcinoma, WT *EGFR*, and mutant *K-Ras*; 2) somatic mutation of EGFR, which confers addiction to the EGFR signaling pathway, induces a lack of primary response to IGF-1R TKIs in NSCLC cells; and 3) *K-Ras* mutation causes increased production of IGF-1 and activation of the IGF-1R pathway but induces resistance to IGF-1R TKIs. Moreover, our findings provide a proof of principle that targeted inactivation of IGF-1R by a TKI, in combination with MEK inhibition, can achieve a favorable outcome in the treatment of NSCLC patients with a history of tobacco smoking and mutant *K-Ras*.

Several preclinical and clinical studies have shown encouraging therapeutic efficacy of EGFR TKI in NSCLC with mutant EGFR[2,3]; however, the limited response rates to EGFR TKIs underscore the need to

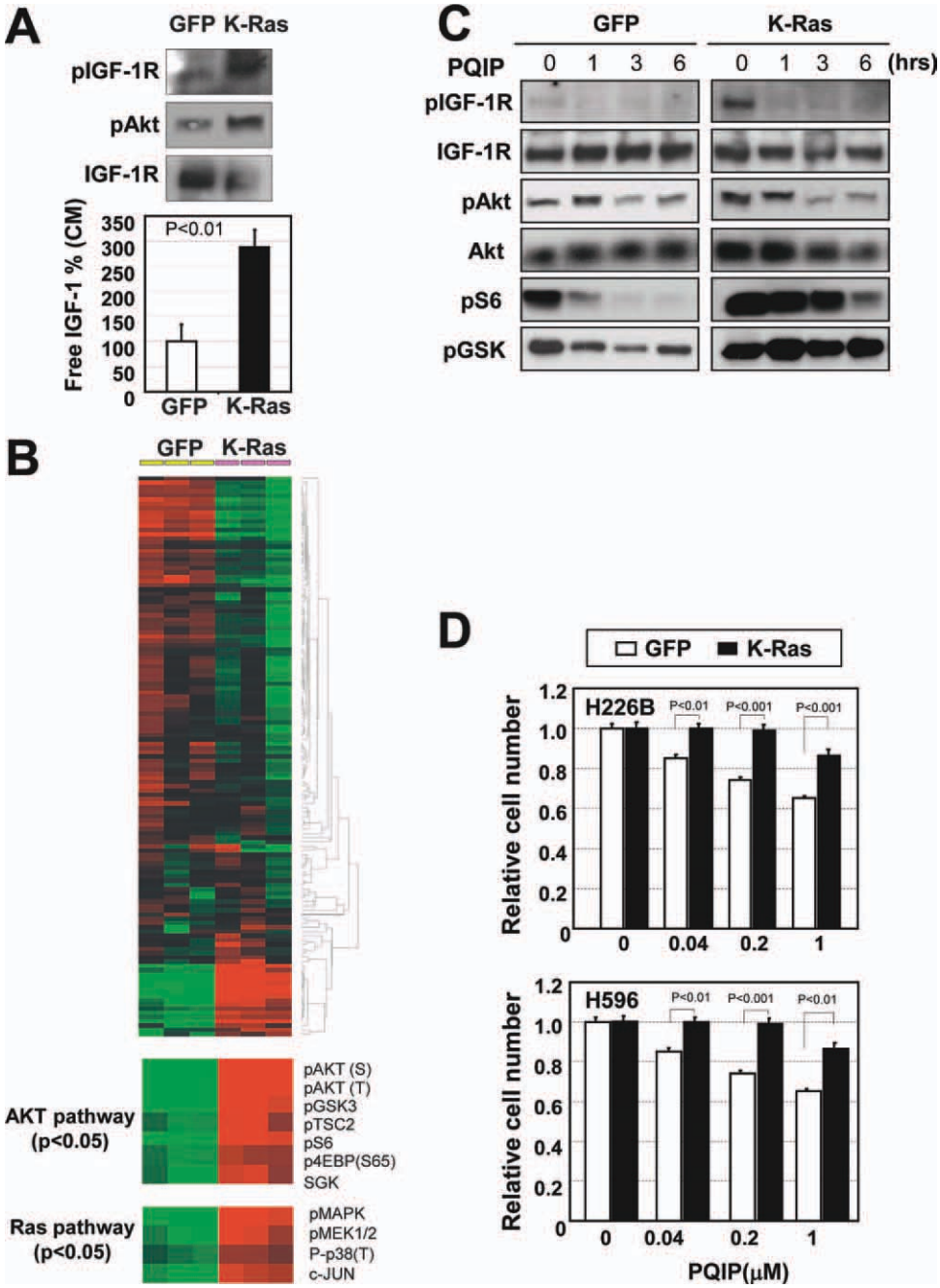

Figure 3. Mutant *K-Ras* is a determining factor of insulinlike growth factor 1 receptor (IGF-1R) tyrosine kinase inhibitor sensitivity of nonsmall cell lung cancer (NSCLC) cells. (A) The secreted IGF-1 level from NSCLC cells was enhanced by mutant K-*Ras*. H226B-GFP or H226B–K-*Ras* cells (H226B cells stably transduced with retrovirus expressing Green Fluorescence Protein (GFP) or mutant *K-Ras*, respectively) were cultured in 1% fetal bovine serum for 3 days. The conditioned media (CM) from H226B-GFP and H226B–*K-Ras* cells were applied to an IGF-1 enzyme-linked immunosorbent assay. (B) Hierarchical clustering of protein expression data from H226B-GFP and H226B–*K-Ras* cells is shown (n = 3 each). Reverse-phase protein array data are shown for 131 protein features. The data are presented in a matrix format: rows represent individual protein features, and columns represent individual samples. Each cell in the matrix represents the expression level of a protein feature in an individual cell sample. Red and green reflect relatively high and low expression levels, respectively. A total of 50 proteins showed differences with $P < .05$ by Student *t* test; of these, the molecules related to Akt signaling and Ras/MAPK signaling are shown in the bottom panels. The data were analyzed by using the Cluster and TreeView programs. (C) Molecular changes of the IGF-1R/Akt pathway by mutant *K-Ras* and PQIP are shown. H226B-GFP and H226-*K-Ras* cells were treated with PQIP (1 μM), and the cells were harvested at the indicated time point. (D) Mutant *K-Ras* enhanced the resistance of NSCLC cells to PQIP. Relative cell survival after PQIP treatment for 3 days is shown. Mutant *K-Ras* blunted the sensitivity of 226B and H596 cells to PQIP. Columns indicate means of 3 independent experiments; bars represent standard deviation.

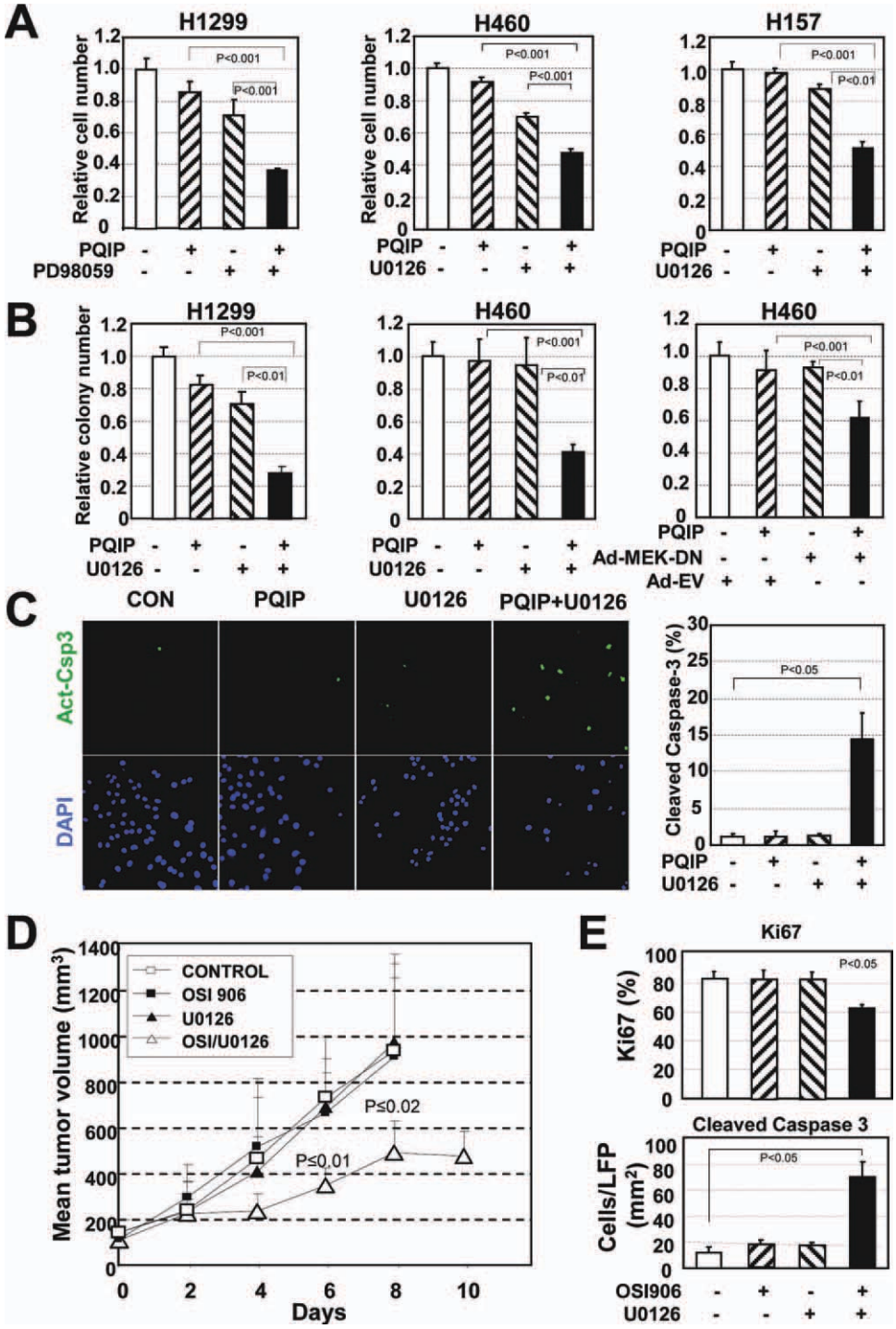

Figure 4. Cotargeting of insulinlike growth factor 1 receptor (IGF-1R) and *K-Ras* signaling overrides the resistance to IGF-1R tyrosine kinase inhibitor (TKI) driven by the *K-Ras* mutation in vitro and in vivo. (A) Relative cell survival of mutant *Ras* resistant non-small cell lung cancer (NSCLC) cells is shown after treatment with an IGF-1R TKI (PQIP, 5 μM), an mitogen-activated protein kinase/extracellular signal-regulated kinase (MEK) inhibitor (PD98059 [10 μM] or U0126 [2 μM or 1 μM]), or both. (B) Effect of combined IGF-1R and MEK inhibition on anchorage-independent colony-forming ability of NSCLC cells with mutant *Ras* is shown. The indicated NSCLC cells seeded in soft agar were treated with PQIP (1 μM), U0126 (2 μM), or both. Ad-MEK-DN, dominant negative form MEK expressing adenovirus; Ad-EV, empty adenovirus. The relative colony numbers are shown. (C) Synergistic apoptotic effect of combined treatment with PQIP (5 μM) and U0126 (1 μM) on apoptosis of mutant *K-Ras*–H157 NSCLC cells is shown. The active form of caspase-3 was stained, and the percentage of apoptotic cells is plotted. CON, control. (D) Mice bearing H226B–*K-Ras* xenograft tumors (2 tumors per mouse, 4 or 5 mice per group) were treated with vehicle (control), OSI-906 (40 mg/kg, once per day), U0126 (4 mg/kg, every other day), or both OSI-906 and U0126 as indicated. Day 0 represents the first day of drug treatment. Data are means and 95% confidence intervals. (E) Immunohistochemical staining of the xenograft tumors in D with Ki67 and cleaved caspase-3 antibody was performed, and results are shown for at least 4 tumors in each group. LFP, Lowe power field.

develop effective treatment strategies for patients with WT EGFR. Targeting the IGF-1R pathway is 1 emerging strategy. The 2 major approaches are small-molecule IGF-1R TKIs and anti–IGF-1R monoclonal antibodies. However, limited data are available about predictors of sensitivity to the anti–IGF-1R approaches. In this study, we identified predictors that could be used in clinical trials of IGF-1R TKIs in NSCLC patients. Previous studies have shown high levels of IGF-1R expression in squamous cell carcinoma histology.[27] By analyzing a TMA of specimens from 354 patients with NSCLC, we extended this observation, showing high levels of pIGF-1R/IR in patients with squamous cell carcinoma. These data suggest that squamous cell carcinoma may be more sensitive to IGF-1R TKIs than lung adenocarcinoma is. However, previous reports and our current results show that tumor histology is not a predictive marker of response to IGF-1R–targeted strategies. We also observed significantly elevated pIGF-1R/IR levels in patients with a history of tobacco smoking, those with mutant *K-Ras*, and those with WT EGFR, all of which have been strongly associated with poor response to EGFR TKIs.

Numerous studies have suggested that human cancer cells can be highly dependent on single or multiple pathways that are overly activated, conferring tumorigenic potential,[28-30] and successful anticancer therapeutic strategies would rely on the selection of patients harboring tumors that rely on those pathways for cell growth and survival. Our previous and current findings show that transformed lung epithelial cell lines induced by tobacco smoking components had an elevated expression of pIGF-1R/IR and were sensitive to the molecularly targeted strategies against the IGF-1R system.[31,32] Tobacco smoking components such as 4-(methylnitrosamino)-1- (3-pyridyl)-1-butanone have been shown to induce genetic changes in *p53* and *PTEN*, which regulate IGF-2 and IGF-1R expression.[33,34] NNK can also induce phosphorylation and degradation of p53 via activation of Akt.[35] Although we did not have mechanistic evidence for tobacco smoking-induced activation of IGF-1R/IR signaling in lung carcinogenesis, impact of the IGF-1R pathway in cell proliferation and survival suggested that targeting IGF-1R could be an effective therapeutic strategy for NSCLC patients with tobacco smoking history. This notion and our subsequent findings, including 1) the characteristics of patients with NSCLC harboring elevated pIGF-1R/IR levels were negatively correlated with those of patients harboring *EGFR* mutation, and (2) PQIP treatment effectively inhibited stimulation of the IGF-1R pathway but had little antitumor activity in mutant *EGFR*-expressing NSCLC cells, led us to hypothesize that a history of tobacco smoking and *EGFR* mutation are predictive biomarkers for absence of responsive to IGF-1R TKIs. However, we found that only a subset of human NSCLC cell lines with high pIGF-1R/IR levels and WT *EGFR* were sensitive to PQIP treatment. These observations suggest that *EGFR* mutation is not a predictive marker to response to IGF-1R TKI-based therapies.

Considering the potential mechanisms of crosstalk between EGFR and IGF-1R signaling,[18,36-38] inhibition of IGF-1R signaling could have been compensated for by enhanced activation through EGFR. However, NSCLC cells expressing mutant *Ras* did not exhibit significantly enhanced sensitivity in response to cotargeting of IGF-1R and EGFR by treatment with PQIP and the EGFR TKI erlotinib, whereas the same regimen significantly reduced cell viability in a subset of head and neck squamous cell carcinoma cell lines carrying WT *K-Ras* (data not shown).

It has been suggested that sensitivity of NSCLC cells to TKIs of IGF-1R and EGFR, either alone or their combination, is determined by the epithelial-to-mesenchymal transition.[36,39] However, epithelial-to-mesenchymal transition status was not a consistent predictive marker for insensitivity to antagonism against IGF-1R or to cotargeting IGF-1R and EGFR.[36] These findings indicate the involvement of additional biomolecules that differentiate the NSCLC cell response to IGF-1R TKIs.

Our current findings from several in vitro and in vivo experiments indicate that mutant *K-Ras* differentiates the response to IGF-1R inhibitors. In the current study, we found evidence that activation of the IGF-1R pathway is correlated with *K-Ras* mutation, which may increase IGF-1 production, as shown by significantly higher levels of IGF-1 in the conditioned media from H226B cells harboring mutant *K-Ras* compared with those harboring WT *K-Ras* (Fig. 3A). Therefore, *K-Ras* mutation could be a driving force for activation of the IGF-1R pathway and may thus be a predictive marker of sensitivity to IGF-1R blocking. However, our subsequent results clearly show that mutant *K-Ras* is a poor predictive marker of the therapeutic efficacy of the drugs: 1) mutant *K-Ras* led to increased resistance to PQIP in many assay systems, and 2) the inactivation of *K-Ras* or MEK by genomic approaches (siRNA targeting *K-Ras*, Ad-MEK-DN) or pharmacologic approaches (PD98059, U0126) induced antitumor activity of IGF-1R TKIs (PQIP, OSI-906) in vitro and in vivo in mutant *K-Ras* cell lines. These

findings highlight the need for stratification of patients on the basis of *K-Ras* mutation, in addition to history of tobacco smoking and *EGFR* mutation, when an IGF-1R–targeted therapeutic regimen is considered in clinical trials.

In summary, this study characterizes potential predictive markers of actions of IGF-1R TKIs. Our findings show that activation of IGF-1R/IR is mutually exclusive with activation of EGFR and is associated with tobacco smoking in NSCLC, suggesting that transformed lung epithelial cells and NSCLC cells are dependent on IGF-1R/IR signaling for survival and sustained proliferation. However, we also provide evidence for the first time that mutation in *K-Ras* is associated with activation of IGF-1R and the development of physiologically redundant signaling in patients with NSCLC, implicating mutant *K-Ras* as an important predictive marker to optimize the clinical efficacy of the IGF-1R–targeting strategy. Further investigation is warranted into the discovery of the predictive biomarkers for IGF-1R–targeted therapy and the exact mechanism of synergy between IGF-1R TKIs and MEK inhibitors.

FUNDING SOURCES

This work was supported by a grant from the National Research Foundation of Korea (NRF), Ministry of Education, Science and Technology (MEST), Republic of Korea (No. 2011-0017639) (H-Y. Lee), the Global Core Research Center (GCRC) grant (No. 2011-0035681) from NRF, MEST, Republic of Korea (H-Y. Lee), a National Institutes of Health grant R01 CA100816 (H-Y. Lee), and in part by the Department of Defense, through grants W81XWH-04-1-0142 VITAL and W8XWH-06-1-0303 BATTLE (to W.K.H.). We thank OSI Pharmaceuticals for providing PQIP, OSI-906, and erlotinib.

CONFLICT OF INTEREST DISCLOSURES

The authors made no disclosures.

REFERENCES

1. Jemal A, Siegel R, Ward E, Murray T, Xu J, Thun MJ. Cancer statistics, 2007. *CA Cancer J Clin*. 2007;57:43-66.
2. Pao W, Miller V, Zakowski M, et al. EGF receptor gene mutations are common in lung cancers from "never smokers" and are associated with sensitivity of tumors to gefitinib and erlotinib. *Proc Natl Acad Sci U S A*. 2004;101:13306-13311.
3. Lynch TJ, Bell DW, Sordella R, et al. Activating mutations in the epidermal growth factor receptor underlying responsiveness of non-small-cell lung cancer to gefitinib. *N Engl J Med*. 2004;350:2129-2139.
4. Paez JG, Janne PA, Lee JC, et al. EGFR mutations in lung cancer: correlation with clinical response to gefitinib therapy. *Science*. 2004;304:1497-1500.
5. Shepherd FA, Rodrigues Pereira J, Ciuleanu T, et al. Erlotinib in previously treated non-small-cell lung cancer. *N Engl J Med*. 2005;353:123-132.
6. Kozma LM, Weber MJ. Constitutive phosphorylation of the receptor for insulinlike growth factor I in cells transformed by the src oncogene. *Mol Cell Biol*. 1990;10:3626-3634.
7. Coppola D, Ferber A, Miura M, et al. A functional insulin-like growth factor I receptor is required for the mitogenic and transforming activities of the epidermal growth factor receptor. *Mol Cell Biol*. 1994;14:4588-4595.
8. Brodt P, Samani A, Navab R. Inhibition of the type I insulin-like growth factor receptor expression and signaling: novel strategies for antimetastatic therapy. *Biochem Pharmacol*. 2000;60:1101-1107.
9. Baserga R. The insulin-like growth factor-I receptor as a target for cancer therapy. *Expert Opin Ther Targets*. 2005;9:753-768.
10. Renehan AG, Atkin WS, O'Dwyer ST, Shalet SM. The effect of cigarette smoking use and cessation on serum insulin-like growth factors. *Br J Cancer*. 2004;91:1525-1531.
11. Yu H, Spitz MR, Mistry J, Gu J, Hong WK, Wu X. Plasma levels of insulin-like growth factor-I and lung cancer risk: a case-control analysis. *J Natl Cancer Inst*. 1999;91:151-156.
12. Papadimitrakopoulou VA, Brown EN, Liu DD, et al. The prognostic role of loss of insulin-like growth factor-binding protein-3 expression in head and neck carcinogenesis. *Cancer Lett*. 2006;239:136-143.
13. Kim WY, Jin Q, Oh SH, et al. Elevated epithelial insulin-like growth factor expression is a risk factor for lung cancer development. *Cancer Res*. 2009;69:7439-7448.
14. Pallis AG, Serfass L, Dziadziusko R, et al. Targeted therapies in the treatment of advanced/metastatic NSCLC. *Eur J Cancer*. 2009;45:2473-2487.
15. Kim WY, Chang DJ, Hennessy B, et al. A novel derivative of the natural agent deguelin for cancer chemoprevention and therapy. *Cancer Prev Res (Phila)*. 2008;1:577-587.
16. Kim WY, Kim MJ, Moon H, et al. Differential impacts of insulin-like growth factor-binding protein-3 (IGFBP-3) in epithelial IGF-induced lung cancer development. *Endocrinology*. 2011;152:2164-2173.
17. Tam IY, Chung LP, Suen WS, et al. Distinct epidermal growth factor receptor and KRAS mutation patterns in non-small cell lung cancer patients with different tobacco exposure and clinicopathologic features. *Clin Cancer Res*. 2006;12:1647-1653.
18. Morgillo F, Woo JK, Kim ES, Hong WK, Lee HY. Heterodimerization of insulin-like growth factor receptor/epidermal growth factor receptor and induction of survivin expression counteract the antitumor action of erlotinib. *Cancer Res*. 2006;66:10100-10111.
19. Woo JK, Choi DS, Tran HT, Gilbert BE, Hong WK, Lee HY. Liposomal encapsulation of deguelin: evidence for enhanced antitumor activity in tobacco carcinogen-induced and oncogenic K-ras-induced lung tumorigenesis. *Cancer Prev Res (Phila)*. 2009;2:361-369.
20. Lee HY, Moon H, Chun KH, et al. Effects of insulin-like growth factor binding protein-3 and farnesyltransferase inhibitor SCH66336 on Akt expression and apoptosis in non-small-cell lung cancer cells. *J Natl Cancer Inst*. 2004;96:1536-1548.
21. Pao W, Miller VA, Politi KA, et al. Acquired resistance of lung adenocarcinomas to gefitinib or erlotinib is associated

with a second mutation in the EGFR kinase domain. *PLoS Med*. 2005;2:e73.
22. Sugio K, Uramoto H, Ono K, et al. Mutations within the tyrosine kinase domain of EGFR gene specifically occur in lung adenocarcinoma patients with a low exposure of tobacco smoking. *Br J Cancer*. 2006;94:896-903.
23. Toyooka S, Tokumo M, Shigematsu H, et al. Mutational and epigenetic evidence for independent pathways for lung adenocarcinomas arising in smokers and never smokers. *Cancer Res*. 2006;66:1371-1375.
24. Ji QS, Mulvihill MJ, Rosenfeld-Franklin M, et al. A novel, potent, and selective insulin-like growth factor-I receptor kinase inhibitor blocks insulin-like growth factor-I receptor signaling in vitro and inhibits insulin-like growth factor-I receptor dependent tumor growth in vivo. *Mol Cancer Ther*. 2007;6:2158-2167.
25. Hecht SS. Tobacco smoke carcinogens and lung cancer. *J Natl Cancer Inst*. 1999;91:1194-1210.
26. Deguil J, Perault-Pochat MC, Chavant F, Lafay-Chebassier C, Fauconneau B, Pain S. Activation of the protein p7OS6K via ERK phosphorylation by cholinergic muscarinic receptors stimulation in human neuroblastoma cells and in mice brain. *Toxicol Lett*. 2008;182:91-96.
27. Gong Y, Yao E, Shen R, et al. High expression levels of total IGF-1R and sensitivity of NSCLC cells in vitro to an anti-IGF-1R antibody (R1507). *PLoS One*. 2009;4:e7273.
28. Haber DA, Bell DW, Sordella R, et al. Molecular targeted therapy of lung cancer: EGFR mutations and response to EGFR inhibitors. *Cold Spring Harb Symp Quant Biol*. 2005;70:419-426.
29. Weinstein IB, Joe A. Oncogene addiction. *Cancer Res*. 2008;68:3077-3080; discussion 3080.
30. Weinstein IB, Joe AK. Mechanisms of disease: oncogene addiction—a rationale for molecular targeting in cancer therapy. *Nat Clin Pract Oncol*. 2006;3:448-457.
31. Klein-Szanto AJ, Iizasa T, Momiki S, et al. A tobacco-specific N-nitrosamine or cigarette smoke condensate causes neoplastic transformation of xenotransplanted human bronchial epithelial cells. *Proc Natl Acad Sci U S A*. 1992;89:6693-6697.
32. Chun KH, Kosmeder JW Jr, Sun S, et al. Effects of deguelin on the phosphatidylinositol 3-kinase/Akt pathway and apoptosis in premalignant human bronchial epithelial cells. *J Natl Cancer Inst*. 2003;95:291-302.
33. Ohlsson C, Kley N, Werner H, LeRoith D. p53 regulates insulin-like growth factor-I (IGF-I) receptor expression and IGF-I-induced tyrosine phosphorylation in an osteosarcoma cell line: interaction between p53 and Sp1. *Endocrinology*. 1998;139:1101-1107.
34. Yi HK, Kim SY, Hwang PH, et al. Impact of PTEN on the expression of insulin-like growth factors (IGFs) and IGF-binding proteins in human gastric adenocarcinoma cells. *Biochem Biophys Res Commun*. 2005; 330:760-767.
35. West KA, Linnoila IR, Belinsky SA, Harris CC, Dennis PA. Tobacco carcinogen-induced cellular transformation increases activation of the phosphatidylinositol 3'-kinase/Akt pathway in vitro and in vivo. *Cancer Res*. 2004;64:446-451.
36. Buck E, Eyzaguirre A, Rosenfeld-Franklin M, et al. Feedback mechanisms promote cooperativity for small molecule inhibitors of epidermal and insulin-like growth factor receptors. *Cancer Res*. 2008;68:8322-8332.
37. Morgillo F, Kim WY, Kim ES, Ciardiello F, Hong WK, Lee HY. Implication of the insulin-like growth factor-IR pathway in the resistance of non-small cell lung cancer cells to treatment with gefitinib. *Clin Cancer Res*. 2007;13:2795-2803.
38. Barnes CJ, Ohshiro K, Rayala SK, El-Naggar AK, Kumar R. Insulin-like growth factor receptor as a therapeutic target in head and neck cancer. *Clin Cancer Res*. 2007;13:4291-4299.
39. Yauch RL, Januario T, Eberhard DA, et al. Epithelial versus mesenchymal phenotype determines in vitro sensitivity and predicts clinical activity of erlotinib in lung cancer patients. *Clin Cancer Res*. 2005;11(24 pt 1):8686-8698.

Official Journal of the Asian Pacific Society of Respirology
Respirology

INVITED REVIEW SERIES:
TRANSLATING RESEARCH INTO PRACTICE
SERIES EDITOR: JOHN E HEFFNER AND DAVID CL LAM

Pulmonary adenocarcinoma: A renewed entity in 2011

HUMAM KADARA,[1] MOHAMED KABBOUT[1] AND IGNACIO I. WISTUBA[1,2]

Departments of [1]Thoracic/Head and Neck Medical Oncology and [2]Pathology, The University of Texas MD Anderson Cancer Center, Houston, Texas, USA

ABSTRACT

Lung cancer, of which non-small-cell lung cancer comprises the majority, is the leading cause of cancer-related deaths in the United States and worldwide. Lung adenocarcinomas are a major subtype of non-small-cell lung cancers, are increasing in incidence globally in both males and females and in smokers and non-smokers, and are the cause for almost 50% of deaths attributable to lung cancer. Lung adenocarcinoma is a tumour with complex biology that we have recently started to understand with the advent of various histological, transcriptomic, genomic and proteomic technologies. However, the histological and molecular pathogenesis of this malignancy is still largely unknown. This review will describe advances in the molecular pathology of lung adenocarcinoma with emphasis on genomics and DNA alterations of this disease. Moreover, the review will discuss recognized lung adenocarcinoma preneoplastic lesions and current concepts of the early pathogenesis and progression of the disease. We will also portray the field cancerization phenomenon and lineage-specific oncogene expression pattern in lung cancer and how both remerging concepts can be exploited to increase our understanding of lung adenocarcinoma pathogenesis for subsequent development of biomarkers for early detection of adenocarcinomas and possibly personalized prevention.

Key words: airway epithelium, field cancerization, genetics, lung cancer, molecular biology.

INTRODUCTION

Lung cancer is the leading cause of cancer deaths in the United States and worldwide in both developing and developed regions.[1] The high mortality of this disease is in part due to the late diagnosis of the majority of lung cancers after regional or distant spread of the malignancy[2] and when only palliative treatment options are available.[3] Given that various epithelial tumours develop in a multi-stage stepwise fashion, it is plausible to assume that early diagnosis of lung cancer or intraepithelial lesions coupled with effective prevention strategies will improve survival of patients and reduce the significant health burden and mortality associated with this disease.[3] Despite recent encouraging findings from the National Lung Screening Trial (NLST),[4] early detection of lung cancer is challenging due to the lack of biomarkers for early diagnosis of the disease and to the presence of multiple neoplastic molecular pathways that mediate lung carcinogenesis. A better understanding of the molecular origins of lung cancer is expected to pave the way for unmet effective and personalized strategies for lung cancer prevention and treatment.

The two major forms of lung cancer are non-small-cell lung cancer (NSCLC), which accounts for approximately 85% of all diagnosed lung cancers, and small-cell lung cancer (SCLC), which constitute about 15% of lung neoplasms.[2] NSCLC is comprised of three major histological subtypes, squamous-cell carcinomas (SCC), lung adenocarcinomas and large-cell lung carcinomas.[2,5] Several major differences exist between adenocarcinomas and SCC, the two major subtypes of NSCLC. Compared with SCC and SCLC that arise from the major bronchi and are centrally located, pulmonary adenocarcinomas arise from small bronchi, bronchioles or alveolar epithelial cells, and are typically peripherally located as reviewed elsewhere.[2,5–7]

The Authors: Humam Kadara, PhD, is an instructor in the Department of Thoracic/Head and Neck Medical Oncology, Division of Cancer Medicine, The University of Texas MD Anderson Cancer Center. His research interests focus on lung cancer genomics, pathogenesis and prevention. Mohamed Kabbout, PhD, is a postdoctoral fellow in the same department researching on mutant Kirsten rat sarcoma oncogene-mediated lung cancer pathogenesis. Ignacio I. Wistuba, MD, is a Jeri and Lori Eisenberg Professor of Pathology in the Departments of Thoracic/Head and Neck Medical Oncology and Pathology and director of the Thoracic Molecular Pathology Laboratory at the University of Texas MD Anderson Cancer Center. His research interests focus on understanding the molecular pathology of lung cancer to guide or develop therapeutic and prevention strategies.

Correspondence: Humam Kadara, Department of Thoracic/Head and Neck Medical Oncology, The University of Texas MD Anderson Cancer Center, Houston, TX, USA, Email: hkadara@mdanderson.org

Received 10 October 2011; accepted: 11 October 2011.

Clinically, SCC and lung adenocarcinoma respond differently to chemotherapeutic agents, exemplified by the use of pemetrexed for treatment of the latter subtype and not for SCC.[8,9] Moreover, although smoking is the major causative factor in lung cancer pathogenesis, significant differences in smoking patterns are observed between the two major NSCLC histological subtypes. Whereas SCC pathogenesis is strongly linked to smoking, lung adenocarcinoma is the more common histological subtype in never-smoker patients.[10–13] Accumulating evidence suggests that lung adenocarcinoma arising in never-smokers is a disease with different pathological and epidemiological features compared with adenocarcinomas causally linked to cigarette smoking.[13] Specifically, never-smoker lung adenocarcinoma is more commonly diagnosed in females compared with males[14] and is more frequently found in eastern and southern parts of the Asian continent,[15] and displays better prognosis and survival compared with ever-smoker patients.[2,12,13] At the molecular level, and to date, two major pathways are thought to mediate lung adenocarcinoma development: an epidermal growth factor receptor (*EGFR*)-dependent pathway in never-smokers and a Kirsten rat sarcoma oncogene (*KRAS*)-dependent signalling module in smokers[16–23] (discussed further later). Further understanding of lung adenocarcinoma pathogenesis would be needed to unravel other pathways that play important roles in development of this major subtype of lung cancer.

Lung adenocarcinomas have a wide spectrum of clinical, molecular and histological features.[24] The 2004 World Health Organization (WHO) classification of lung tumours included four growth patterns for its adenocarcinoma classification: bronchioloalveolar (BAC; also known as lepidic), acinar, papillary and solid.[24] Most invasive lung adenocarcinomas are heterogeneous in nature and include more than one of these histological patterns.[24,25] The existing lung adenocarcinoma histological heterogeneity and the varying clinicopathological features (e.g. patient outcome) of the aforementioned histological patterns highlight the importance of incorporating histological pattern information into clinical management of this complex disease. More recently, the European Respiratory Society (ERS), the International Association for the Study of Lung Cancer (IASLC) and the American Thoracic Society (ATS) sponsored a new classification of lung adenocarcinoma.[26] The new classification study presented several modifications to the WHO 2004 criteria for diagnosis of resected adenocarcinoma specimens. Mainly, the consortium study suggested that the term BAC should be discontinued.[26] Instead, it is agreed that adenocarcinoma *in situ* (AIS) and minimally invasive adenocarcinoma (MIA) are to be used for small adenocarcinomas with either pure lepidic growth or predominant lepidic growth with less than 5 mm invasion, respectively.[26] Moreover, the new classification dropped the use of mixed subtype, and instead, adenocarcinomas are classified according to their predominant subtype.[26]

This review will describe advances in the molecular pathology of lung adenocarcinoma with emphasis on genomics and DNA alterations of this disease. Moreover, the review will describe recognized lung adenocarcinoma preneoplastic lesions and current concepts of the early pathogenesis and progression of the disease. We will also portray the field cancerization phenomenon and lineage-specific oncogene expression pattern in lung cancer and how both remerging concepts can be exploited to increase our understanding of lung adenocarcinoma pathogenesis for subsequent development of biomarkers for early detection of adenocarcinomas and possibly personalized prevention.

REVIEW

Molecular pathology of lung adenocarcinoma

Lung adenocarcinomas exhibit unique genomic aberrations compared with lung SCC, indicating that the molecular pathology of both NSCLC subtypes encompasses different molecular pathways of development and progression.[2] Earlier studies have shown that lung SCC exhibit higher frequencies of deletions at chromosomal regions 17p13 (*TP53*), 13q14 (*RB*), 9p21 (*CDKN2A*), 8p21–23 and 3p compared with lung adenocarcinomas.[27–29] Moreover, many of the aforementioned molecular abnormalities (e.g. allelic losses at 9p21 and 13q24) occur in the sequential multi-step progression of SCC but not of adenocarcinomas.[6,27] In contrast, mutations in the *KRAS*, *EGFR* and *HER2/NEU* oncogenes occur almost exclusively in adenocarcinomas.[2,20,22,23,30,31] Amplification of the embryonic stem cell (ESC) factor sex determining Y-box 2 (*SOX2*) is exclusive to SCC,[32,33] and increased gene dosage and protein expression of thyroid transcriptional factor–1/NK2 homeobox 1 (*TITF-1/NKX2-1*) is prevalent in lung adenocarcinoma, indicating that both transcriptional factors most likely function as lineage-specific genes in lung cancer.[34–36] This section will highlight molecular abnormalities, with special emphasis on genomics and DNA alterations, of lung adenocarcinoma that render this malignancy a unique entity.

Lung adenocarcinoma genomics

KRAS, a low molecular weight guanosine triphosphatase (GTPase) and the major upstream activator of the RAF-MEK-ERK pathway, is considered to be the most frequently mutated oncogene in lung adenocarcinomas.[19,21,37] As mentioned before, mutations in this oncogene are more common in adenocarcinomas arising in ever-smoker (former and current) lung cancer patients.[13,16,17,19,20,22,23,30] Most *KRAS* mutations involve replacing glycine 12 with other amino acids such as valine (G12V), aspartic acid (G12D) and glutamic acid (G12D), and replacing glycine 13, and are activating rendering the gene with reduced GTPase activity with subsequent potent activation of mitogenic and proliferative signalling through the RAF-MEK-ERK cascade.[19,37–39] Thus, it is plausible to assume that therapeutic strategies targeting *KRAS*

would be very beneficial in adenocarcinomas with activating mutations in this oncogene. However, there are currently no available treatment options for *KRAS*-mutant lung adenocarcinomas compared with tumours with mutations in other oncogenes,[40] as strategies targeting *KRAS* farnesylation, *MEK* activation and *BRAF* have either failed or yielded no responses.[41–43]

In contrast to *KRAS*, mutations in *EGFR* are strongly linked to lung adenocarcinomas arising in never-smokers and are suggested to molecularly drive the disease in this patient subpopulation.[13,14,17,18,22,23,30,37] It is important to note that *EGFR* mutations are more common in East Asian patients and in female gender.[2,13,22] Small in-frame deletions in exon 19 and missense mutations in exon 21 (L858R and L861Q) are the most common mutations detected in *EGFR*[44] and were shown by several ground-breaking studies to underlie sensitivity of lung adenocarcinoma patients to *EGFR*-targeting small tyrosine-kinase inhibitors (e.g. erlotinib and gefitinib).[18,45,46] These studies were the first to prove the feasibility of personalized medicine approaches for the management of lung adenocarcinoma and represent the landmark for the application of genomic medicine in this disease.

The discovery of fusions involving anaplastic large-cell lymphoma kinase (*ALK*) with the upstream partner echinoderm microtubule associated protein 4 (*EML4*) by Soda *et al*.[47] further opened new venues for genomic-driven personalized treatment strategies for lung adenocarcinoma.[48] Both *EML4* and *ALK* are located in chromosome 2p, and fusion of both involves small inversions within this region.[47] *EML4-ALK* fusion results in constitutive activation of the *ALK* kinase rendering cells and adenocarcinoma tumours expressing this oncogenic fusion protein sensitive to *ALK* inhibitors.[47–49] Like *EGFR* mutations, *EML4-ALK* fusion genes are prevalent in lung adenocarcinomas, younger patients and, in particular, in lifetime never-smoker patients or light smokers.[49,50] Importantly, *EML4-ALK* fusion genes are mutually exclusive from *EGFR* and *KRAS* mutations, indicating that such molecular defects function as drivers of pathogenesis, which is clinically important, as it increases potential of personalized treatment options that target driver oncogenes in this malignancy.[50]

Other mutually exclusive and, thus, potential oncogenic drivers have been identified in lung adenocarcinomas. Mutations in *HER2/NEU* were found by Stephens *et al*. to occur in lung adenocarcinomas.[31] Compared with mutations of *EGFR* oncogene, *HER2/NEU* mutations are less frequent[30] and have not been successfully exploited in the clinic for lung adenocarcinoma treatment.[51] Similar to *HER2/NEU*, mutations in *BRAF* also occur at low frequency in lung adenocarcinoma and are exclusive from *EGFR* and *KRAS* mutations, as well as from *EML-ALK* fusions.[50] There are yet no successful target-specific treatment strategies for lung adenocarcinoma with *BRAF* mutations. It is important to note that mutations in *HER2/NEU* and *BRAF* have not been found in lung SCC.[50]

The *TP53* tumour suppressor is the most frequently mutated gene in lung adenocarcinoma (65–70%). Various abnormalities in *TP53* were identified in lung adenocarcinoma almost two decades ago[52,53] and more recently in the tumour-sequencing project[37] and occur in similar pathways to those mediated by the oncogenic driver mutations mentioned earlier.[20,22,37] Mutations in the *CDKN2A* tumour suppressor have also been described in lung adenocarcinoma.[54,55] However, methylation[56] or focal DNA deletion[36,55] rather than mutation of this tumour suppressor seems to be more frequent and occurs earlier in lung cancer pathogenesis.[5] With the advent of various technologies including single nucleotide polymorphism (SNP) arrays, mass spectrometry mutational analysis and more recently second-generation sequencing, and the undertaking of large-scale studies such as the tumour-sequencing project,[37] our knowledge of the mutational spectrum of lung adenocarcinoma has substantially increased. New mutated oncogenes and tumour suppressor genes have been identified in lung adenocarcinoma and along with previously characterized mutated genes are outlined in Table 1 and have been reviewed in detail elsewhere.[50,51] It is important to note that many, if not

Table 1 Mutations in lung adenocarcinoma

—	Mutation rate (%)
Oncogenes	
KRAS	15–30
EGFR	5–40
ALK (fusion)	5–15
MET	14
KDR	5
EPHA3	5
MAP2K1	5
HER2/ERBB2	2–4
FGFR4	4
PDGFRA	4
NTRK1	4
NTRK3	4
EPHA5	4
ERBB4	4
LTK	3
PAK3	3
ERBB3	2
FGFR1	2
FGFR2	2
NRAS	2
PIK3CA	2
BRAF	2
AKT1	1
Tumour-suppressor genes	
TP53	50–70
STK1	20–30
LRP1B	9
NF1	7
ATM	7
APC	6
PTPRD	5
CDKN2A	5
RB1	4
PTEN	2

most, of these mutations are not mutually exclusive of other driver mutations and events such as *EGFR* mutations and *EML4-ALK* fusions. For example, *PIK3CA* mutations were always found together with *EGFR* mutations in never-smoker lung adenocarcinomas.[57] It is also worthwhile to mention that some of the outlined mutations have been detected in both lung adenocarcinomas and SCC (e.g. *PIK3CA* and *MET*) or only in the former subtype of NSCLC (e.g. *MEK1*, *HER2/NEU* and *BRAF*).[50] It is unknown for most of mutations occurring in lung adenocarcinomas and recently identified by exon-directing sequencing in the tumour-sequencing project, whether they also occur in lung SCC. The discovery of new oncogene and tumour suppressor mutations in lung adenocarcinoma occurring in mutually exclusive and inclusive cell signalling pathways expands the range of possible target-specific and even combinatorial personalized therapeutic strategies for this disease.

Copy-number alterations

Gene dosage variations occur in many pathological conditions. For example, in cancer, deletions and copy-number increases modulate the expression of tumour-suppressor genes and oncogenes, therefore contributing to tumourigenesis. Characterization of these DNA copy-number changes is vital for both the basic understanding of cancer and its diagnosis. Copy-number alterations are routinely assessed in laboratories by fluorescent *in situ* hybridization (FISH) techniques as well as genomic polymerase chain reaction (PCR), including quantitative PCR approaches. However, these approaches are labour-intensive and would hamper the discovery and complete understanding of the genome of tumours in large-scale studies. High-throughput and genome-wide analysis of DNA copy-number alterations was made possible by comparative genomic hybridization (CGH) approaches, which utilize differentially labelled test and reference genomic DNA that are co-hybridized to normal metaphase chromosomes.[58] CGH, however, exhibits limited mapping resolution even when compared with lower throughput higher resolution techniques, such as FISH.[59] Subsequently, high-resolution genome-wide analysis was successfully performed using cDNA microarray-based CGH and SNP arrays coupled with statistical methods to assess both the amplitude and the frequency of copy-number changes at each position in the genome.[59]

Genome-wide alterations in human lung adenocarcinoma tumours stemming from several major studies have assuredly increased our understanding of the molecular pathogenesis of this major malignancy.[36,60,61] Earlier chromosomal CGH studies have revealed in NSCLC recurrent gains at 1q31, 3q25–27, 5p13–14 and 8q23–24, and deletions at 3p21, 8p22, 9p21–22, 13q22 and 17p12–13.[62–66] Moreover, these early studies already highlighted genomic differences and similarities between lung adenocarcinomas and SCC; most prominent of which were gains in 3q mainly by lung SCC.[62–66] For example, Petersen *et al*. found genomic aberrations that characterize lung adenocarcinomas from SCC, namely gain of 1q23, and the deletion at 9q22 were significantly associated with adenocarcinomas, whereas the loss of chromosomal band 2q36–37 and gain of 3q were strongly associated with SCC.[66] Bjorkqvist *et al*. demonstrated that 94% (15/16) of lung SCC analysed had a gain in 3q, whereas only 24% (4/17) of the adenocarcinoma samples exhibited a gain in 3q, and high-level amplifications in 3q were only detected in SCC.[63] In addition, Luk *et al*. demonstrated that gains at 1q22–32.2, 15q, 20q and losses at 6q, 13q and 18q were more prevalent in lung adenocarcinomas, whereas SCC, as shown in earlier studies, exhibited gains/amplifications at 3q.[64] Moreover, Pei *et al*. showed that besides prevalent gain of 3q in lung SCC, gain of 20p13 and loss of 4q also were significantly higher in SCC, whereas gain of 6p was more common in adenocarcinomas.[65] Massion *et al*. utilized higher resolution analysis by array CGH to study copy-number alterations of known loci and found that the most distinct genomic aberration between both NSCLC subtypes was gain of 3q22–26 and loss of 3p by lung SCC.[67] Moreover, and in the same study, *PIK3CA* oncogene was found to be a member of the chromosome-3q amplicon with higher copy number and expression in SCC but not in adenocarcinomas.[67]

More recent studies utilized more advanced technologies to query the genome of lung adenocarcinoma and associate specific gene modulations with chromosomal and loci gain or losses. In the study by Tonon *et al*., high-resolution cDNA microarray-based CGH was utilized to study the genomic profiles of 18 lung adenocarcinomas and 26 SCC, as well as 14 NSCLC cell lines.[61] The study identified 93 focal copy-number alterations that mainly comprised previously uncharacterized recurrent high-amplitude amplifications and homozygous deletions.[61] Besides confirming previous findings by chromosomal CGH and highlighting known gains (e.g. 1q31 and 3q25–27) and known deletions (e.g. 3p, 8p22 and 13q22), the study by Tonon *et al*. was able to map specific genes to focal copy-number alterations including *CDKN2A* and *RB1* tumour-suppressor genes and *EGFR*, and *KRAS* oncogenes.[61] However, when comparing both adenocarcinomas and lung SCC, the study found that the only notable genomic difference between both NSCLC histological subtypes was the well-characterized gain of 3q26–29 in SCC that included *TP63*, well known for its role in squamous differentiation, and concluded that similar oncogene and tumour-suppressor gene aberrations drive lung adenocarcinoma and SCC pathogenesis.[61] The study by Tonon *et al*. was a major step in understanding the genomic profiles of NSCLC tumours despite the small number of lung adenocarcinomas and SCC analysed.

Later on, Weir *et al*. studied the genomic profiles of a large collection of primary lung adenocarcinomas ($n = 371$) by high-density SNP arrays using 238 000 probe sets.[36] The report by Weir *et al*. was a milestone in understanding the lung adenocarcinoma genome, as it unravelled previously uncharacterized amplified genes and loci that otherwise may have not been

identified using a small number of primary tumours. The study identified 39 large-scale chromosomal arm gain or loss, 26 of which were significantly recurrent across many lung adenocarcinomas. Importantly, the large-scale study by Weir *et al*. identified 31 recurrent focal events that included 24 amplifications and 7 homozygous deletions. Using dense SNP arrays coupled with statistical methods (genomic identification of significant targets in cancer), the group was able to associate specific genes to the focal events and rank significance of events based on both the amplitude and frequency of copy-number change,[36] similar to what was performed by Tonon *et al*.[61] to identify minimal common regions of copy-number alterations. The most significant focal regions of amplification included known oncogenes such as *MDM2* (12q15), *MYC* (8q24), *EGFR* (7p11), *CDK4* (12q14), *KRAS* (12p12), *CCNE1* (19q12), *ERBB2* (17q12), *CCND1* (11q13) and *TERT* (5p15).[36] It is important to note that three of these oncogenes, *EGFR*, *KRAS* and *ERBB2*, are mutated in lung adenocarcinoma, as discussed before, suggesting that amplification and mutation of these oncogenes may cooperate systematically in lung adenocarcinoma pathogenesis. The most significant focal regions of deletions also included known tumour-suppressor genes such as *CDKN2A* (9p21) and *PTEN* (10q23).[36] Although 5p was previously shown to be gained in lung adenocarcinomas, the identity of genes involved in this gain was unknown prior to the study by Weir *et al*. The application of more advanced technologies to characterize the genomic profile of lung adenocarcinomas enabled the group to highlight previously unknown associations between canonical cancer-associated genes and known loci copy-number alterations, as well as to identify potentially new oncogenes. For example, 10 genes, including *TERT*, were found in the study to be included in the 5p15 region.[36] Furthermore, the study highlighted previously uncharacterized amplification of *TITF-1/NKX2-1* (14q13.3) in lung adenocarcinomas and demonstrated the oncogenic role of this lineage-specific transcriptional factor in lung cancer cells evidenced by the effect of RNA interference-mediated knockdown of its expression on anchorage-independent growth of lung adenocarcinoma cell lines with amplification of this gene.[36] The amplification/copy-number gain of *TITF-1* in lung adenocarcinoma was later confirmed in different studies including that by Kwei *et al*. using array CGH.[34] However, it is important to mention that although *TITF-1* amplification is generally prevalent in lung adenocarcinoma and is thought to function as a lineage-specific oncogene in this subtype of NSCLC, it has also shown by FISH analysis in lung SCC, which will be discussed later in this review.

As mentioned before, numerous earlier studies have demonstrated that gain of 3q is a genomic feature of lung SCC. Similar to the aforementioned study by Weir *et al*., Bass and colleagues utilized high-density Affymetrix SNP arrays to analyse 40 oesophageal and 47 lung SCC, which confirmed that gain of 3q26 was the main focal amplification event in lung and oesophageal SCC.[32] Importantly, the same study revealed the presence of the ESC factor in this region, which was later on confirmed to be amplified in SCC and not in lung adenocarcinomas, and promoted the survival of cell lines of the former NSCLC subtype harbouring amplification of this transcriptional factor and further suggesting that lung adenocarcinomas are genetically different from SCC.

More recently, high-resolution array CGH was performed on never-smoker lung adenocarcinomas ($n = 60$) with known mutation status of *EGFR*.[68] This study identified 14 new minimal common regions of gain or loss and confirmed previously known copy-number alterations such as those involving *TERT* (5p), *TITF-1* (14q13), *EGFR* (7p) and *CDKN2B* (9p). Notably, the study revealed new genomic aberrations, namely the 16p11.2 region harbouring the *FUS* oncogene that functions in transcriptional splicing and DNA repair.[68] Gain of 16p11.2 was evident in greater than 20% of the never-smoker lung adenocarcinomas analysed and mRNA levels of *FUS* correlated with copy gain of 16p, as they were higher in tumours with gain of this region compared with tumours that did not exhibit 16p copy gain. Importantly, the study by Job *et al*. revealed genomic copy-number alterations that were highly associated with presence of *EGFR* mutation, an oncogenic driver of never-smoker lung adenocarcinoma pathogenesis.[68] Gains of 7p were significantly associated with presence of *EGFR* mutations and included *EGFR* gene, suggesting, as mentioned before, that copy-number alternations and mutations cooperate at the genomic level in lung adenocarcinoma pathogenesis. However, it cannot be ignored that *EGFR* copy gain or amplification may favour the detection of *EGFR* mutations in a heterogeneous tumour due to the mutant allele-specific imbalance phenomenon.[69] In a more recent study by Yuan *et al*. and also using array CGH technology, gains in 7p, including the *EGFR* gene, were common in *EGFR* mutant lung adenocarcinomas and predicted overall and recurrence-free survival in this disease population.[70] More importantly, in contrast to *EGFR* mutations, presence of genes (including *EGFR*) within the 7p gain predicted poorer response to tyrosine kinase inhibitors targeting *EGFR*.[70]

Gene expression profiling

Numerous studies have utilized microarray technology to analyse the global transcriptome of NSCLC for diagnosis (discussed later), molecular classification, response to therapy and prognosis. For the purpose of this review, we will discuss several key studies that investigated expression profiles of lung adenocarcinomas to further understand the molecular biology of this prevalent lung malignancy. Bhattacharjee and colleagues utilized arrays to study adenocarcinomas of lung origin ($n = 127$), SCC ($n = 21$), carcinoids ($n = 20$), SCLC ($n = 6$) and 17 normal samples.[71] The study found that differential expression profiles segregated the samples into different clusters based on histology, evidenced by the two-dimensional cluster

analysis. Genes associated with squamous differentiation such as keratin and *TP63* were overexpressed in SCC, and neuroendocrine markers were enriched in the SCLC cluster. Importantly, the study by Bhattacharjee *et al*. also analysed the adenocarcinomas alone by hierarchical clustering and demonstrated that the adenocarcinomas were heterogeneous in molecular make-up, being separated into various clusters with distinct clinical outcomes.[71] Similarly, Garber *et al*. utilized cDNA microarrays to study expression profiles of 41 adenocarcinomas, 16 SCC, 5 large-cell carcinomas and 5 SCLC, as well as 5 normal lung samples.[72] Again, lung adenocarcinomas were most heterogeneous and were divided into different clusters that were associated with clinicopathological variables such as tumour grade.[72] Later, Hayes *et al*. found that adenocarcinoma subtypes identified by the Bhattacharjee and Garber studies were reproducible in additional microarray datasets.[73] Several other studies have also demonstrated, using microarray expression profiling technology, the heterogeneity of lung adenocarcinomas and their distinction from other lung cancer subtypes. As reviewed by Yatabe, global gene expression profiling was able to subdivide lung adenocarcinomas into various clusters that correlated with *EGFR* mutation status, prognosis, expression of lung peripheral airway markers such as surfactant proteins (SP) and *CC10*, as well as enrichment of the BAC subtype.[44]

Lung adenocarcinoma preneoplasia

From biological and histopathological perspectives, NSCLC is a complex malignancy that develops through multiple preneoplastic pathways. Lung adenocarcinoma, a major subtype of NSCLC, has been increasing in incidence globally in both smokers and non-smokers[13] with a concurrent decrease in SCC frequency. It has been postulated that the increasing incidence of lung adenocarcinomas compared with SCC is in part due to the change in the type of cigarettes used (lower nicotine and tar) and smoking habits and behaviour.[11] Anatomical differences in the location of diagnosed lung adenocarcinomas and SCC strongly suggest that both NSCLC subtypes develop through different histopathological and molecular pathways and have different cells of origin; however, the specific respiratory epithelial cell type from which each lung cancer type develops has not been established with certainty.[5] Lung SCC is typically centrally located in the lung and is thought to arise from the major bronchi. In contrast, lung adenocarcinomas that are usually peripherally located are believed to arise from small bronchi, bronchioles or alveoli of the distant airways of the lung. The sequence of histopathological changes in bronchial epithelia that precede the development of lung SCC has been characterized.[6,27] However, the sequential preneoplastic changes, as well as the corresponding molecular abnormalities, leading to the development of lung adenocarcinomas are poorly documented.

Histopathological development of lung adenocarcinoma

Clara cells and the type II pneumocytes are believed to be the progenitor cells of the peripheral airways, and peripherally arising adenocarcinomas often express markers of these cell types.[44,74] Atypical adenomatous hyperplasias (AAH) are considered to be a precursor lesion for peripheral lung adenocarcinomas.[5,7] However, and until now, AAH is the only sequence of morphological change identified so far for the development of invasive lung adenocarcinomas, and there is consensus that the pathogenesis of many adenocarcinomas is largely unknown. The postulated progression of AAH to adenocarcinomas *in situ*, which is characterized by the growth of neoplastic cells along pre-existing alveolar structures without invasion, is supported by molecular studies.[75] Distinction between highly atypical AAH and what was known as BAC is sometimes difficult. Therefore, and as mentioned before, the ERS, IASLC and ATS sponsored a new classification of lung adenocarcinoma that presented several modifications to the WHO 2004 criteria for diagnosis of resected adenocarcinoma specimens. The term BAC was suggested to be discontinued and replaced with AIS and MIA used for small adenocarcinomas with either pure lepidic growth or predominant lepidic growth with less than 5 mm invasion, respectively. Importantly, the clinical features of both adenocarcinoma progression types are unique as patients with AIS or MIA have a 100% 5-year survival rate after respective surgery.[26]

The differentiation phenotype derived from immunohistochemical and ultrastructural features indicates that AAH originate from the progenitor cells of the peripheral airways.[26,44,74] Surfactant apoprotein and Clara cell-specific 10-kDd protein are expressed in almost all AAH. In addition, an increasing body of evidence suggests that AAH is the precursor of at least a subset of adenocarcinomas. For example, AAH is most frequently detected in lungs of patients bearing lung cancers (9–20%), especially adenocarcinomas (as many as 40%), compared with lung SCC (11%).[76] It is important to note that AAH is detected more frequently in East Asian patients relative to Western patients. In such studies, it has been suggested that AAH is involved in the linear progression of cells of the 'terminal respiratory unit' (TRU) to AIS and subsequently invasive adenocarcinomas[7,44,74] due to the expression of common genes between the TRU and the AAH, which is discussed later. Such studies have postulated that most, if not all, peripheral lung adenocarcinomas progress from alveoli through AAH as a preneoplastic lesion. As will be discussed further later, we have noted similar molecular abnormalities (e.g. *EGFR* mutations) between adenocarcinomas arising in never-smokers and small bronchioles within the localized and adjacent fields of the adenocarcinomas, suggesting that lung adenocarcinomas may arise from bronchiolar epithelium and small bronchi, and not only from alveoli.[77,78] In a recent review by Yatabe *et al*., a nonlinear progression schema for lung adenocarcinomas was suggested.[7] In this nonlinear schema, Yatabe *et al*. postulated that

lung adenocarcinomas of the TRU subtype, as named by the authors, develop through AAH. On the other hand, and according to the same nonlinear progression hypothesis, some lung adenocarcinomas arise through unknown preneoplastic precursors from other cells besides the TRU, which we believe may as well be the bronchiolar epithelium.[77,78]

Molecular pathogenesis of lung adenocarcinomas

Several molecular changes frequently present in lung adenocarcinomas are also present in AAH lesions, and they are further evidence that AAH may represent true preneoplastic lesions.[79] The most important finding is the presence of *KRAS* (codon 12) mutations in as many as 39% of AAH, which are also a relatively frequent alteration in lung adenocarcinomas.[6,80] Other molecular aberrations that were identified in AAH are overexpression of cyclin D1 (~70%), survivin (48%) and *HER2/neu* (7%) proteins.[5] Moreover, and as mentioned in the review by Wistuba and Gazdar, some AAH lesions were found to exhibit loss of heterozygosity (LOH) in chromosomes 3p (18%), 9p (*p16*^{INK4a}, 13%), 9q (53%), 17q and 17p (*TP53*, 6%).[5] It is noteworthy that most if not all of the aforementioned changes identified in AAH lesions are also frequently detected in lung adenocarcinomas. Later, AAH lesions were shown to exhibit LOH of tuberous sclerosis complex (TSC)-associated regions, activation of telomerase, loss of *LKB1*, overexpression of DICER, a key effector protein for small interfering RNA and miRNA function, and DNA methylation of *CDKN2A* and *PTPRN2*.[6,81,82] It is important to note that several studies have attempted to globally comprehend differential gene expression patterns and copy-number alterations between low-grade lesions (e.g. precursor lesions) or *in situ* adenocarcinomas and invasive tumours and found that amplification of the *EGFR* oncogene was the predominant differential molecular feature between the two different adenocarcinoma grade classes and occurred after mutations in the gene.[7] Importantly, as will be discussed in the next section of this review, *EGFR* mutations also preceded changes in copy number of the gene when studying histologically normal bronchiolar epithelia.[78]

KRAS and EGFR mutations in lung adenocarcinoma pathogenesis

Although there is only one sequence of morphological change characterized so far for the development of invasive lung adenocarcinomas, namely AAH, a large body of evidence suggests that at least two molecular pathways are involved, the *KRAS* and *EGFR* pathways in smoker and never-smoker adenocarcinoma subpopulations, respectively.[2,14,16,17,20–23,30] Mutations in *EGFR*, in particular, in-frame deletions of exon 19 and L858R and L861Q of exon 21, are strongly associated with never-smoking status, female gender and East Asian ethnicity, as well as predict favourable response to *EGFR* tyrosine kinase inhibitor.[2,12,13,17,22,23] On the other hand, mutations in *KRAS*, the most frequently mutated oncogene in lung adenocarcinoma, based on recent findings of the tumour-sequencing project, are strongly associated with development of adenocarcinomas linked to tobacco consumption.[2,16,17,20,21,23]

It has been suggested that the vast majority of AAH precursor lesions and adenocarcinomas *in situ* are associated with the TRU adenocarcinoma subtype that were found to express high levels of *TITF-1* and SP, leading to the conclusion that such adenocarcinomas are of the same lineage as terminal airway epithelial cells. In addition, it has been postulated that *EGFR* mutations are predominant in or specific to peripheral lung adenocarcinomas of the TRU subtype, which were suggested to arise from AAH lesions,[44,74,83] as 90 of 97 *EGFR* mutant adenocarcinomas were positive for *TITF-1*, and 91 of the 97 tumours were of the TRU subtype.[83] In addition, the hypothesis put forward that *EGFR* mutations are associated with or specific to the TRU subtype of lung adenocarcinomas is also in part due to the observation that the frequency of *EGFR* and *KRAS* mutations among AAH lesions, adenocarcinomas *in situ* and invasive adenocarcinomas is significantly different.[7,44] It was determined that whereas *KRAS* mutations decreased along adenocarcinoma progression, from 33% in AAH to 8% in adenocarcinomas, *EGFR* mutations were evenly distributed suggesting that *KRAS*-mutated AAH lesions rarely progress to adenocarcinomas. It is also important to mention, and as reviewed by Yatabe, that several studies performed gene expression profiling of lung adenocarcinomas and other histological subtypes of lung cancer and found that lung adenocarcinomas were heterogeneous and divided into different clusters.[44] Clusters with expression of *CC10* and features of alveolar signature such as *TITF-1* exhibited significantly better survival compared with adenocarcinomas in other clusters and comprised a higher frequency of *EGFR* mutations.

Mutations in the tyrosine-kinase domain of *EGFR* mutations were shown to be involved in the early pathogenesis of lung cancer, being identified in histologically normal epithelium of small bronchi and bronchioles adjacent to *EGFR* mutant adenocarcinomas[77] (discussed further in the next section of the review). *EGFR* mutations were detected in normal-appearing peripheral respiratory epithelium in 43% adenocarcinoma patients,[77] but not in patients without mutation in the tumour.[77] These findings may signify different cell types comprising the examined epithelia, which could represent sites of the cells of origin for *EGFR* mutant adenocarcinomas of the lung. Although the cell type having those mutations is unknown, our group has hypothesized that stem or progenitor cells of the bronchial and bronchiolar epithelium bear such mutations. It is also noteworthy that *EGFR* mutations were identified in only 3 of 40 AAH lesions examined[83,84] and were shown to be absent[22] or relatively infrequent in what was previously known as BAC of the lung.[84] These earlier observations support the argument that abnormalities of *EGFR* are not only relevant to the pathogenesis of alveolar-type lung

neoplasia but also may play drive peripheral lung adenocarcinoma from bronchiolar epithelium cells that are distinct from terminal respiratory and alveolar cells.[5,44] The different findings of *EGFR* mutation rates in AAH lesions may as well reflect the ethnicity (Asian vs Western) of the patients from which the lesions were isolated, as well as the standard practice of detection of small lesions such as AAH.

Field cancerization

Although the majority of lung cancer patients are current or former smokers (approximately 85%), a relatively small fraction of smokers (approximately 15%) develop primary lung tumours. Patients with early stage NSCLC, relative to other early stage malignancies, frequently exhibit recurrence or second primary tumour development after definitive treatment by surgery and removal of the original lung primary tumour. There is a large body of evidence that heavy smokers and patients who have survived an upper aerodigestive cancer comprise a high-risk population that may be targeted for early detection and chemoprevention efforts.[6] Although the risk of developing lung cancer decreases after smoking cessation, the risk never returns to baseline. Preneoplastic changes, namely dysplastic histological abnormalities, have been utilized as surrogate endpoints for chemopreventive studies. However, it was suggested that this 'shooting-in-the-dark' approach may explain the reasons behind the general failures of clinical chemoprevention studies.[3] It is also important to note that we are unable to predict which lifetime never-smokers or definitively treated never-smoker early-stage lung cancer patients will develop lung tumours or relapse. Therefore, novel approaches to identify the best population to be targeted for early detection and chemoprevention should be devised, and risk factors for lung cancer development or relapse need to be better defined. For these important purposes, a better understanding of the biology and molecular origins of lung cancer, for example, lung adenocarcinoma, is warranted. In this section of the review, we will describe the field cancerization phenomenon that herein refers to that occurring due to direct and indirect effects of smoking (field of injury) or independent of smoking in patients with and without cancer, with emphasis on aberrant molecular markers in histological normal epithelia that can be used to increase our understanding of lung cancer pathogenesis.

Smoking damaged epithelium and the lung field cancerization phenomenon

Earlier work by Danely Slaughter *et al*. in patients with oral cancer and oral premalignant lesions has suggested that histologically normal-appearing tissue adjacent to neoplastic and preneoplastic lesions display molecular abnormalities, some of which are in common with those in the tumours.[85] In 1961, a seminal report by Auerbach *et al*. suggested that cigarette smoke induces extensive histological changes in the bronchial epithelia in the lungs of smokers and that premalignant lesions are widespread and multifocal throughout the respiratory epithelium, suggestive of a field effect.[86] This phenomenon, coined 'field of cancerization', was later shown to be evident in various epithelial cell malignancies including lung cancer. Some degree of inflammation and inflammatory-related damage is almost invariably present in the central and peripheral airways of smokers and may precede the development of lung cancer.[87] Thus, the field of cancerization may be explained by both direct effect of tobacco carcinogens and initiation of inflammatory response. In this context, different theories for the origin of the field of cancerization or smoking-related field of injury have been put forward and will not be discussed here, as they have been nicely and extensively reviewed elsewhere by Steiling *et al*.[88]

Several studies focusing on the respiratory epithelium of lung cancer patients and smokers have demonstrated that multiple altered foci of bronchial epithelium are present throughout the airway.[27,28,89] A detailed analysis of histologically normal epithelium, and premalignant and malignant epithelia from lung SCC patients indicated that multiple, sequentially occurring allele-specific chromosomal deletions of LOH begin in dispersed clonally independent foci very early in the multi-stage pathogenesis of this smoking-related lung malignancy.[27,28] Notably, 31% of histologically normal epithelium and 42% of mildly abnormal (hyperplasia/metaplasia) specimens had clones of cells with allelic loss at one or more regions examined. Moreover, these molecular aberrations were also found in carcinomas *in situ* and SCC, and at a more advanced level.[27] Molecular changes involving LOH of chromosomal regions 3p (*DDUT* and *FHIT* genes), 9p (*CDKN2A*), genomic instability (increased microsatellite repeats) and *p16* methylation have all shown to commence in histologically normal or slightly abnormal tissue in SCC patients and in the sequence of pathogenesis of the disease.[5] As mentioned before, *KRAS* is the most mutated oncogene in lung adenocarcinomas.[37] Almost 15 years ago, Nelson *et al*. demonstrated that *KRAS* mutations are found in histologically normal lung tissue adjacent to lung tumours.[90] As will be discussed later, mutations in *EGFR* were also found in adjacent to tumour histologically normal epithelium.[77,78] Similar epigenetic and gene methylation patterns between tumours and adjacent histologically normal epithelia were described. An important study by Belinsky *et al*. reported aberrant promoter methylation of *p16*, which was described to be commonly methylated in lung tumours,[91] in at least one bronchial epithelial site from 44% of lung cancer patients examined.[92] Moreover, *p16* and death-associated protein kinase (DAPK) promoter methylation was observed frequently in bronchial epithelium from current and former smoker but not from never-smoker lung cancer patients and persisted after smoking cessation. Notably, 94% of lung tumours exhibited a concordant pattern of *p16* methylation with that in at least one bronchial epithelial site.[92]

The aforementioned molecular abnormalities were detected in histologically normal epithelia adjacent to archival surgically resected tumours from primary lung cancer patients. LOH and microsatellite alterations in multiple foci were also detected in distal histological normal bronchial epithelia of smokers without cancer.[93,94] Moreover, and importantly, these molecular abnormalities were detected in bronchial epithelia of cancer-free former smokers that appeared to have persisted for many years after smoking cessation. In addition, LOH was detected in DNA obtained from bronchial brushings of normal and abnormal lungs from patients undergoing diagnostic bronchoscopy and was detected in cells from the ipsilateral and contralateral lung.[95] Mutations in *TP53* were also described to occur in bronchial epithelia of cancer-free smokers in a widely dispersed manner.[96] Similar evidence also exists for promoter methylation and epigenetic changes in smoking-damaged lung epithelium of cancer-free patients. Methylation of various genes, including retinoic acid receptor 2 beta (*RAR-b2*), *H-cadherin*, *APC*, *p16* and *RASSFF1A* was described in bronchial epithelial cells of heavy smokers.[97] Moreover, methylation of *p16*, *GSTP1* and *DAPK* was reported to be evident in bronchial brushings of one third of the cancer-free smokers examined.[98] In the same study by Belinsky *et al.*, as mentioned before, methylation of *p16* was detected in epithelia of cancer-free smokers.[92] A more detailed list of aberrant gene promoter methylation in lung cancer patients and cancer-free smokers is nicely summarized and explained in the review by Heller *et al.*[99]

Gene expression profiling of the lung field cancerization

High-throughput microarray profiling was used by several groups to study the transcriptome of lung airways. Hackett *et al.* utilized microarrays to study the expression of 44 anti-oxidant-related genes using bronchial brushings from cancer-free current smokers and never-smokers, and found significant upregulation of 16 of the antioxidant genes in the airways of smokers compared with non-smokers.[100] Later, Spira *et al.* described global alterations in gene expression between normal-appearing bronchial epithelium of healthy cancer-free smokers and that of non-smokers.[101] In addition, and in the reports by Spira *et al.* and Beane *et al.*, irreversible changes in expression in airways of former smokers after years of smoking cessation were described that were thought to underlay the increased risk former smokers display, compared with never-smokers, for developing lung cancer long after they have discontinued smoking.[101,102] Schembri *et al.* also reported alterations in the expression of miRNA between large airways of current and never-smokers.[103] Notably, an 80-gene signature was derived from the transcriptome of large airway epithelial cells that can distinguish smokers without overt cancer from smokers with lung cancer and exhibited statistically significant utility characteristics of a lung cancer biomarker, despite originating from normal bronchial epithelia.[104] Moreover, the 80-gene signature, using publicly available microarray datasets, was able to distinguish lung tumours from corresponding normal lung tissues.[104] More recently, Gustafson *et al.* derived a phosphatidylinositol 3-kinase (*PI3K*) pathway activation signature using recombinant adenoviruses to express the 110α subunit of *PI3K* in primary human epithelial cells.[105] The same study then demonstrated that the *PI3K* pathway activation signature was elevated in cytologically normal bronchial airways of smokers with lung cancer and with dysplastic lesions.[105] Of substantial clinical importance, the study found that the signature was decreased in the airways of high-risk smokers whose dysplastic lesions regressed following treatment with the *PI3K* inhibitor myoinositol.[105]

Microarray and gene expression profiling methodologies were also used to demonstrate the wide anatomical spread of the lung field cancerization to epithelial regions that can be non-invasively sampled when devising approaches for early detection of lung cancer. Sridhar *et al.* highlighted common gene expression alterations in bronchial, nasal and buccal epithelia of smokers, in particular of various detoxification genes that perpetuate the field of cancerization due to tobacco consumption.[106] In addition, Zhang *et al.* identified 119 genes whose expression was affected by smoking similarly in both bronchial and nasal epithelium, including genes related to detoxification, oxidative stress and wound healing,[107] and the study by Boyle *et al.* highlighted significant similarities in expression changes between smokers and never-smokers in oral and bronchial epithelia.[108]

Lung adenocarcinoma field cancerization

To better understand the pathogenesis of *EGFR* mutant lung adenocarcinomas, Tang and colleagues investigated the presence of *EGFR* mutations in normal bronchial and bronchiolar epithelium adjacent to *EGFR* mutant tumours. As mentioned before, *EGFR* mutations were detected in histologically normal peripheral epithelia in 44% of lung adenocarcinoma patients with mutations but none in patients lacking mutations in the oncogene.[77] Moreover, the same study highlighted more frequent *EGFR* mutations in normal epithelium within the tumour (43%) than in adjacent sites (24%) suggests a localized field-effect phenomenon for this abnormality in the respiratory epithelium of the lung.[77] In addition, a higher frequency of mutations in cells obtained from small bronchi (35%) compared with bronchioles (18%) was detected.[77] More recently, *EGFR* protein overexpression, similar to mutation of the gene, also exhibited a localized field effect, as it was more frequent in normal bronchial epithelia sites within tumours than in sites adjacent to and distant from tumours.[78] Interestingly, *EGFR* copy-number alteration was not evident in normal bronchial epithelia, which is in accordance with findings that *EGFR* copy

number is relatively a late event in pathogenesis of adenocarcinomas.[7,78]

Field cancerization compartmentalization

The low frequency of molecular abnormalities detected in the centrally located bronchial respiratory epithelium in patients with peripheral lung adenocarcinomas, compared with specimens from patients with SCC and SCLC,[89] suggests the presence of two compartments in the lung with different degrees of smoking-related genetic damage. Thus, smokers who develop SCC have more smoking-related genetic damage in the respiratory epithelium of the central airway, whereas patients who develop adenocarcinoma have damage mainly in the peripheral airways (small bronchus, bronchioles and alveoli). While some molecular changes (e.g. inflammation and signalling pathways activation) have been detected throughout the lung airway and include both compartments (central and peripheral airway), other aberrations have been more frequently altered in either central (e.g. LOH, genetic instability evidenced by microsatellite repeats) or peripheral (e.g. *EGFR* mutations) airways.

Lineage-specific genes in lung cancer

The transformation of normal cells into tumourigenic counterparts is mediated by a complex array of intracellular signals, as well as genetic and epigenetic regulation. It has been suggested that lineage-specific genes, which play important roles in normal developmental processes such as organogenesis or tissue homeostasis and remain to be expressed or become amplified during an acquired pathological condition, are crucial for maintenance of the disease state.[32,109] Interestingly, lineage genes can discriminate different subtypes of the same cancer that rise from dissimilar cells/progenitors, for example, adenocarcinomas versus squamous tumours, and might offer new insights into crucial and therapeutically pliable tumour dependencies.[109] Various studies have highlighted the potential 'addiction' of tumour cells to aberrant and growth-promoting cell signalling mediated by lineage-specific oncogenes, for example, presence of the *BCR-ABL* fusion oncoprotein in chronic myelogenous leukemia,[110] mutations in the *KIT* oncogene in gastrointestinal stromal tumours,[111] amplification of the microphthalmia-associated transcriptional factor (*MITF*) in melanoma[112] and, more recently, amplification of *PAX8* in ovarian cancer.[113] Two lineage-specific oncogenes have been characterized in NSCLC. Recently, *TITF-1* amplification and protein expression were shown to be prevalent in lung adenocarcinomas and elicit growth-promoting signals in this malignancy.[34–36] The master ESC transcriptional factor *SOX2* was shown to be a member of the 3q locus (3q26.3) that is specifically amplified in lung and oesophageal squamous carcinomas.[32] These findings demonstrate that *TITF-1* and *SOX2* function as lineage-specific oncogenes in lung adenocarcinomas and SCC, respectively, and that targeting pathways downstream of those two master regulators may leverage new therapeutic strategies independently for each NSCLC subtype.

TITF-1

TITF-1 is a homeodomain-containing transactivating factor predominantly expressed in the terminal lung bronchioles and lung periphery in the developing and adult mouse.[114,115] In addition, *TITF-1* is crucial for branching morphogenesis during normal lung development[114–116] and transactivates the expression of the SP, such as SP-A, -B and -C, which are in turn typically expressed in the Clara cells and are important for the differentiation of alveolar type II pneumocyte cells in the peripheral lung.[117]

Several studies have demonstrated increased copy number and amplification of the 14q13.3 locus that harbours the *TITF-1* gene as well as paired box transcriptional factor family member 9 (*PAX9*) and *NKX2.8*.[34,36] It is postulated that *TITF-1* functions as a lineage-specific oncogene in lung adenocarcinoma as knockdown of *TITF-1* expression, in cells with amplification of the gene, by RNA interference results in lung adenocarcinoma cell-growth inhibition and apoptosis demonstrating a lineage-specific dependency of lung adenocarcinomas on *TITF-1*.[34–36] Kendall *et al*. demonstrated that co-amplified *TITF-1*, *PAX9* and *NKX2.8* exhibit oncogenic cooperation and cell prosurvival and proliferative properties.[118] Overexpression of both *TITF-1* and *NKX2.8* simultaneously in *BEAS-2B* immortalized human bronchial epithelial cells elicited the highest increase in cell colony growth compared with single-gene transfected cells.[118] Moreover, pathway gene signatures that overlap downstream of both *TITF-1* and *NKX2.8* defined lung adenocarcinoma patients with most dismal prognosis compared with signatures downstream of either transcriptional factor alone.[119] However, recently in *KRAS*(LSL-G12D/+);p53(flox/flox) mice, *TITF-1* was shown to suppress tumourigenesis and limit metastatic potential *in vivo*.[120]

Our group and others have demonstrated that *TITF-1* copy-number gain or amplification is associated with poor prognosis in NSCLC.[121,122] In contrast to the expected pro-survival properties of a cell-lineage oncogene and the association of *TITF-1* copy-number gain and amplification with poor survival, *TITF-1* protein expression by immunohistochemistry was shown to be a marker of favourable prognosis in NSCLC[122–125] including early stage (stage I) lung adenocarcinoma.[126] It is worthwhile to mention that *TITF-1* protein expression and *TITF-1* gene copy number were found to be associated with mutations in the *KRAS* and *EGFR* oncogenes, respectively.[122] As mutations in *EGFR* and *KRAS* occur almost mutually exclusively in lung adenocarcinomas[2] and were suggested to function in different lineages of lung adenocarcinomas,[109] it is possible that *TITF-1* expression is aberrantly differently controlled within different subsets of adenocarcinomas. It is also important to note that *TITF-1* copy-number gain was also

demonstrated in lung SCC.[34,122,125] It is plausible that *TITF-1* copy gain may only be a surrogate marker in SCC of another molecular defect in a gene nearby or within the 14q13.3 amplicon, for example, *NKX2.8* or *PAX9*. The significance of the infrequent copy number increase of *TITF-1* in lung SCC remains elusive.

SOX2

SOX2 was suggested to play key developmental roles in the formation of the lung, trachea and oesophagus based on its expression pattern in these tissues and organs.[127] Interestingly, *SOX2* was shown to be important for the morphogenesis of the trachea and oesophagus, and the differentiation of the oesophageal epithelium.[128] Moreover, the timing of *SOX2* expression in the foregut is tightly regulated, as it is only expressed in the main airways and non-branching bronchioles in the developing and adult mouse lung.[127,129,130] Heterozygote and homozygote transgenic mice with mutant *SOX2* have substantial defects in lung branching and morphogenesis during development.[129,130] Moreover, *SOX2* plays key roles in the maintenance of developing and adult tracheal cells evidenced by shorter and injured trachea in mice with knockout of both alleles of the transcriptional factor.[130] The numerous functions *SOX2* elicits in the differentiation of the conducting airways among other roles are reviewed in more detail by Whitsett and colleagues.[131] It is important to note that *SOX2* forms a core transcriptional factor complex with *OCT4* or *OCT1* and *TirNaNog*/*NANOG* that binds to enhancer sequences of various genes to regulate the inner cell mass or embryoblast within the blastocyst cavity in embryos.[132] Moreover, Boyer and colleagues demonstrated that *SOX2* along with *OCT4* and *NANOG* form a core regulatory transcriptional circuitry, signified by a *SOX2*/*OCT4*/*NANOG* expression signature, consisting of autoregulatory and feed-forward loops for the pluripotency and self-renewal of ESC.[133]

As mentioned earlier in the review, various studies have demonstrated that amplification of chromosomal region 3q (3q26.3) is almost specific to lung SCC.[61,63,64,66,67] The studies by Bass *et al*. and Hussenet and colleagues revealed that *SOX2* is amplified in this chromosomal region in lung SCC and squamous oesophageal cancers and promotes survival of SCC with amplification of this gene.[32,134] Subsequently, increased *SOX2* mRNA levels in lung SCC relative to adenocarcinomas was further evidenced by effective separation of both NSCLC subtypes by the previously characterized *OCT4*/*SOX2*/*NANOG* ESC expression signature,[133] following analysis of publicly available NSCLC microarray datasets.[33] In addition, SOX2 immunohistochemical protein expression was completely absent in lung adenocarcinoma pathogenesis, highly expressed in SCC development and significantly elevated in lung SCC relative to adenocarcinomas.[33] Interestingly, Maeir *et al*. later demonstrated that *SOX2* amplification was found in squamous carcinomas originating from other tissues and organs, such as those of the cervix, skin and penis.[135] It is noteworthy that SOX2 immunohistochemical protein expression in lung SCC and adenocarcinomas was also observed by other groups but in association with clinicopathological features including patient outcome. Interestingly, Wilbertz *et al*. reported the association of *SOX2* expression with favourable prognosis in lung SCC.[136] On the other hand, Sholl and colleagues demonstrated that *SOX2* immunohistochemical expression was an indicator of poor prognosis in lung adenocarcinomas.[137] Despite the equivocal associations of *SOX2* with lung cancer prognosis, various studies have highlighted tumour-promoting roles for this lineage-specific oncogene in lung cancer.[32,138,139]

McCaughan and colleagues specifically analysed 3q copy-number alteration in bronchial dysplasia of varying grades and severity and demonstrated that *SOX2* amplification was present in high-grade bronchial dysplasias but not in low-grade lesions and, importantly, was associated with clinical progression of high-grade preinvasive squamous lesions.[140] It is important to mention that Yuan *et al*. had found relatively high *SOX2* immunohistochemical protein expression in normal bronchial epithelia and alveolar bronchiolarization structures.[33] Congruent with the study by Yuan *et al*., the results by McCaughan and colleagues demonstrated the implication of *SOX2* in the early pathogenesis of lung SCC.[33,140] Given the high *SOX2* protein expression in histologically normal bronchial epithelia, amplification of *SOX2* in high-grade dysplasia may exacerbate signalling downstream of this transcriptional factor in the course of SCC development. It is unknown whether *SOX2* may be amplified in normal bronchial epithelia, in particular, those adjacent to lung SCC with increased dosage of the gene. The findings outlined earlier demonstrate that *SOX2* is another cell-lineage oncogene with dissimilar functions between SCC and lung adenocarcinomas.

FUTURE DIRECTIONS

Lung adenocarcinoma genomics

Studies addressing genomic profiles, including copy-number alterations and mutational spectrums, have substantially increased our understanding of the molecular make-up and biology of lung adenocarcinomas demonstrating that, genomically, this subtype of NSCLC is different from SCC. However, the heterogeneity within lung adenocarcinomas is still poorly understood. For example, it is unknown whether, for example, genomic copy-number alterations found in never-smoker adenocarcinomas are unique to this subtype or whether they are also found in smoker tumours. A large-scale side-by-side genomic analysis of never-smoker and smoker lung adenocarcinomas would shed light on copy-number alterations unique to both subtypes of lung adenocarcinomas. Moreover, it is not clear whether certain copy-number alterations can be clinically exploited for targeted therapy of lung adenocarcinoma. An important step in this direction was the demonstration by Yuan *et al*. that

lung adenocarcinomas with mutant *EGFR* and amplification of specific genes within the 7p region predict poor response to *EGFR* targeting tyrosine-kinase inhibitors.[70] It is tempting to speculate that an orthogonal study, largely encompassing both copy-number alterations and mutational spectrum and detecting focal amplification of oncogenes and loss of tumour-suppressor genes, would, for example, highlight potential targets of therapy in *EGFR*, *KRAS* and *ALK* wild-type lung adenocarcinomas for which there is an unmet need for therapeutic strategies.

Next-generation sequencing

Next-generation sequencing (NGS) technology, through whole-genome, whole-exome and whole-transcriptome approaches, holds great promise for providing invaluable insights into lung adenocarcinoma biology, diagnosis, prevention and therapy.[141] NGS enables the sequencing of expressed genes, exons and complete genomes providing data on levels of expression with a substantially larger dynamic range compared with array technology, sequence alterations, single nucleotide variations, as well as structural genomic aberrations.[141] A handful of studies have successfully applied NGS approaches to sequence one or two human lung tumour samples or cell lines demonstrating the feasibility of systematic, genome-wide characterization of rearrangements and alterations in complex human cancer genomes.[141–144] NGS analysis of a significant number of lung adenocarcinomas and/or NSCLC with characterized mutational status of known oncogenes (e.g. *EGFR* and *KRAS*) undoubtedly represents an important next step in furthering our comprehension of lung cancer biology. However, the application of NGS technology in clinical decision-making and personalized medicine is yet challenging.

Field cancerization and lung adenocarcinoma pathogenesis

Applying the same advanced high-throughput methodologies currently used in studying established tumours for the genetic analysis of lung adenocarcinoma preneoplasia and intraepithelial lesions, as well as histologically normal adjacent regions, is expected to expand our understanding of the biology of this prevalent disease. An important step in this direction was a recent study by Beane *et al.* in which RNA of bronchial airway epithelial cell brushings from healthy never-smokers and smokers with and without lung cancer was analysed by RNA sequencing.[145] The study highlighted transcripts whose expression was either not interrogated by or was not found to be significantly altered when using microarrays demonstrating that NGS, like in established lung tumours, has the potential to provide new insights into the biology of the airway field cancerization associated with smoking and lung cancer.[145]

Earlier findings demonstrated that centrally located lung SCC and peripherally located lung adenocarcinomas elicit and perpetuate differential effects on the airway epithelia. We believe that these effects overlap with those of the response of the host to tobacco exposure (reviewed by Steiling *et al.*[88]) but may be unique in several aspects. Changes in expression in the lung field of injury have shown to be similar in the large and small airways, and it is unknown whether they are associated with the development of the particular subtype of NSCLC. Addressing this question may be highly pertinent because both NSCLC subtypes display different genomic features, as previously discussed, and, therefore, are clinically managed by significantly dissimilar treatment strategies, let alone differences among various subtypes of lung adenocarcinomas. Moreover, a compartmental approach in studying the field of cancerization (Fig. 1) will shed

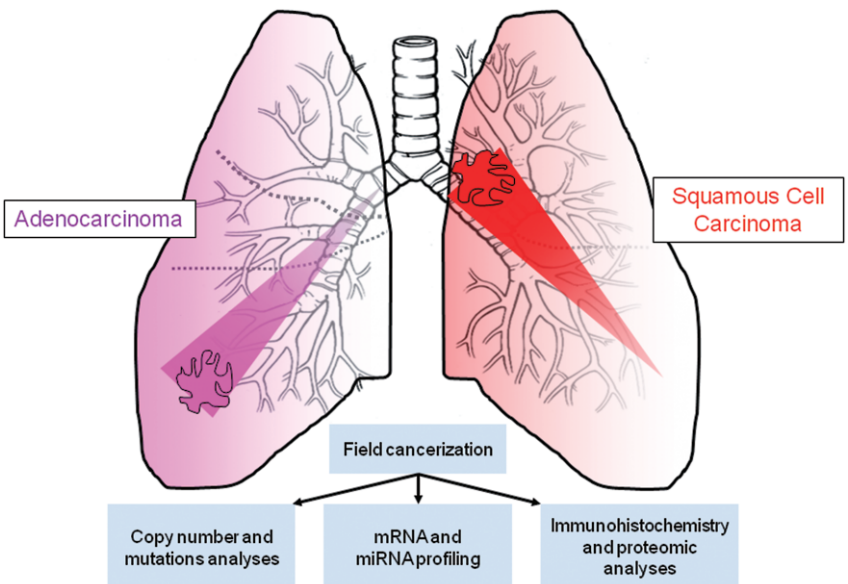

Figure 1 Molecular analysis of the lung field cancerization. It is unknown whether changes in expression in the lung field cancerization are associated with the development of a particular subtype of non-small cell lung cancer (NSCLC), that is, adenocarcinomas compared with squamous-cell carcinomas (SCC). Analysing local and distant field cancerization independently for lung adenocarcinomas and SCC may shed light on events common or unique to the molecular pathogenesis of the two major subtypes of NSCLC. Such a 'compartmental' approach in studying the field cancerization may unravel biomarkers that can guide personalized prevention strategies suitable for each different NSCLC subtype.

light on events in the early pathogenesis of lung adenocarcinomas versus SCC and unravel biomarkers that can be lineage specific and can guide personalized chemoprevention strategies suitable for each different NSCLC subtype, which may reduce the relatively high frequency of relapse of early stage patients.

PERSPECTIVE

Despite numerous efforts that have focused on increasing our understanding of the biology of lung adenocarcinomas, this subtype of NSCLC that is increasing in incidence compared with SCC, constitutes for approximately half of lung cancer deaths each year, which in turn comprise the biggest share of cancer-related deaths in the United States and worldwide. Compared with advances in targeted and personalized therapy of lung adenocarcinomas, little progress has been made in the tailored prevention of this fatal malignancy leading to a substantially decreased enthusiasm. This may change with the recent encouraging and significant findings of the NLST. Various molecular markers and expression classifiers previously described in the lung airways and in less invasive sites of the field cancerization, for example, nasal, sputum and exhaled breath condensates, can aid in selecting high-risk individuals best suited for CT screening for example. A comprehensive analysis of early molecular events in lung adenocarcinoma pathogenesis will undoubtedly unravel biomarkers that can, in the future, aid prevention through personalized strategies, deliver its longstanding promise to oppose this disease.

ACKNOWLEDGEMENTS

Funded in part by a Lung Cancer Research Foundation grant (HK) and DoD W81XWH-10-1-1007 (IIW).

REFERENCES

1 Jemal A, Bray F, Center MM *et al.* Global cancer statistics. *CA Cancer J. Clin.* 2010; **61**: 69–90.
2 Herbst RS, Heymach JV, Lippman SM. Lung cancer. *N. Engl. J. Med.* 2008; **359**: 1367–80.
3 Gold KA, Kim ES, Lee JJ *et al.* The BATTLE to personalize lung cancer prevention through reverse migration. *Cancer Prev. Res. (Phila.)* 2011; **4**: 962–72.
4 Aberle DR, Adams AM, Berg CD *et al.* Reduced lung-cancer mortality with low-dose computed tomographic screening. *N. Engl. J. Med.* 2011; **365**: 395–409.
5 Wistuba II, Gazdar AF. Lung cancer preneoplasia. *Annu. Rev. Pathol.* 2006; **1**: 331–48.
6 Wistuba II. Genetics of preneoplasia: lessons from lung cancer. *Curr. Mol. Med.* 2007; **7**: 3–14.
7 Yatabe Y, Borczuk AC, Powell CA. Do all lung adenocarcinomas follow a stepwise progression? *Lung Cancer* 2011; **74**: 7–11.
8 Scagliotti G, Brodowicz T, Shepherd FA *et al.* Treatment-by-histology interaction analyses in three phase III trials show superiority of pemetrexed in nonsquamous non-small cell lung cancer. *J. Thorac. Oncol.* 2011; **6**: 64–70.
9 Scagliotti GV, Parikh P, von Pawel J *et al.* Phase III study comparing cisplatin plus gemcitabine with cisplatin plus pemetrexed in chemotherapy-naive patients with advanced-stage non-small-cell lung cancer. *J. Clin. Oncol.* 2008; **26**: 3543–51.
10 Kabat GC, Wynder EL. Lung cancer in nonsmokers. *Cancer* 1984; **53**: 1214–21.
11 Khuder SA. Effect of cigarette smoking on major histological types of lung cancer: a meta-analysis. *Lung Cancer* 2001; **31**: 139–48.
12 Rudin CM, Avila-Tang E, Harris CC *et al.* Lung cancer in never smokers: molecular profiles and therapeutic implications. *Clin. Cancer Res.* 2009; **15**: 5646–61.
13 Sun S, Schiller JH, Gazdar AF. Lung cancer in never smokers—a different disease. *Nat. Rev. Cancer* 2007; **7**: 778–90.
14 Gazdar AF, Thun MJ. Lung cancer, smoke exposure, and sex. *J. Clin. Oncol.* 2007; **25**: 469–71.
15 Wakelee HA, Chang ET, Gomez SL *et al.* Lung cancer incidence in never smokers. *J. Clin. Oncol.* 2007; **25**: 472–8.
16 Le Calvez F, Mukeria A, Hunt JD *et al.* TP53 and KRAS mutation load and types in lung cancers in relation to tobacco smoke: distinct patterns in never, former, and current smokers. *Cancer Res.* 2005; **65**: 5076–83.
17 Mounawar M, Mukeria A, Le Calvez F *et al.* Patterns of EGFR, HER2, TP53, and KRAS mutations of p14arf expression in non-small cell lung cancers in relation to smoking history. *Cancer Res.* 2007; **67**: 5667–72.
18 Pao W, Miller V, Zakowski M *et al.* EGF receptor gene mutations are common in lung cancers from 'never smokers' and are associated with sensitivity of tumors to gefitinib and erlotinib. *Proc. Natl Acad. Sci. U.S.A.* 2004; **101**: 13306–11.
19 Reynolds SH, Anna CK, Brown KC *et al.* Activated protooncogenes in human lung tumors from smokers. *Proc. Natl Acad. Sci. U.S.A.* 1991; **88**: 1085–9.
20 Ridanpaa M, Karjalainen A, Anttila S *et al.* Genetic alterations in p53 and K-ras in lung-cancer in relation to histopathology of the tumor and smoking history of the patient. *Int. J. Oncol.* 1994; **5**: 1109–17.
21 Rodenhuis S, Slebos RJ, Boot AJ *et al.* Incidence and possible clinical significance of K-ras oncogene activation in adenocarcinoma of the human lung. *Cancer Res.* 1988; **48**: 5738–41.
22 Shigematsu H, Lin L, Takahashi T *et al.* Clinical and biological features associated with epidermal growth factor receptor gene mutations in lung cancers. *J. Natl Cancer Inst.* 2005; **97**: 339–46.
23 Tam IY, Chung LP, Suen WS *et al.* Distinct epidermal growth factor receptor and KRAS mutation patterns in non-small cell lung cancer patients with different tobacco exposure and clinicopathologic features. *Clin. Cancer Res.* 2006; **12**: 1647–53.
24 Travis WD, Garg K, Franklin WA *et al.* Bronchioloalveolar carcinoma and lung adenocarcinoma: the clinical importance and research relevance of the 2004 World Health Organization pathologic criteria. *J. Thorac. Oncol.* 2006; **1**: S13–9.
25 Motoi N, Szoke J, Riely GJ *et al.* Lung adenocarcinoma: modification of the 2004 WHO mixed subtype to include the major histologic subtype suggests correlations between papillary and micropapillary adenocarcinoma subtypes, EGFR mutations and gene expression analysis. *Am. J. Surg. Pathol.* 2008; **32**: 810–27.
26 Travis WD, Brambilla E, Noguchi M *et al.* International association for the study of lung cancer/American Thoracic Society/European Respiratory Society International Multidisciplinary Classification of Lung Adenocarcinoma. *J. Thorac. Oncol.* 2011; **6**: 244–85.
27 Wistuba II, Behrens C, Milchgrub S *et al.* Sequential molecular abnormalities are involved in the multistage development of squamous cell lung carcinoma. *Oncogene* 1999; **18**: 643–50.
28 Wistuba II, Behrens C, Virmani AK *et al.* High resolution chromosome 3p allelotyping of human lung cancer and preneoplastic/preinvasive bronchial epithelium reveals multiple, discontinuous sites of 3p allele loss and three regions of frequent breakpoints. *Cancer Res.* 2000; **60**: 1949–60.

29 Wistuba II, Behrens C, Virmani AK *et al.* Allelic losses at chromosome 8p21-23 are early and frequent events in the pathogenesis of lung cancer. *Cancer Res.* 1999; **59**: 1973–9.
30 Shigematsu H, Takahashi T, Nomura M *et al.* Somatic mutations of the HER2 kinase domain in lung adenocarcinomas. *Cancer Res.* 2005; **65**: 1642–6.
31 Stephens P, Hunter C, Bignell G *et al.* Lung cancer: intragenic ERBB2 kinase mutations in tumours. *Nature* 2004; **431**: 525–6.
32 Bass AJ, Watanabe H, Mermel CH *et al.* SOX2 is an amplified lineage-survival oncogene in lung and esophageal squamous cell carcinomas. *Nat. Genet.* 2009; **41**: 1238–42.
33 Yuan P, Kadara H, Behrens C *et al.* Sex determining region Y-Box 2 (SOX2) is a potential cell-lineage gene highly expressed in the pathogenesis of squamous cell carcinomas of the lung. *PLoS ONE* 2010; **5**: e9112.
34 Kwei KA, Kim YH, Girard L *et al.* Genomic profiling identifies TITF1 as a lineage-specific oncogene amplified in lung cancer. *Oncogene* 2008; **27**: 3635–40.
35 Tanaka H, Yanagisawa K, Shinjo K *et al.* Lineage-specific dependency of lung adenocarcinomas on the lung development regulator TTF-1. *Cancer Res.* 2007; **67**: 6007–11.
36 Weir BA, Woo MS, Getz G *et al.* Characterizing the cancer genome in lung adenocarcinoma. *Nature* 2007; **450**: 893–8.
37 Ding L, Getz G, Wheeler DA *et al.* Somatic mutations affect key pathways in lung adenocarcinoma. *Nature* 2008; **455**: 1069–75.
38 Barbacid M. Ras genes. *Annu. Rev. Biochem.* 1987; **56**: 779–827.
39 Campbell SL, Khosravi-Far R, Rossman KL *et al.* Increasing complexity of Ras signaling. *Oncogene* 1998; **17**: 1395–413.
40 Harris TJ, McCormick F. The molecular pathology of cancer. *Nat. Rev. Clin. Oncol.* 2010; **7**: 251–65.
41 Brunner TB, Hahn SM, Gupta AK *et al.* Farnesyltransferase inhibitors: an overview of the results of preclinical and clinical investigations. *Cancer Res.* 2003; **63**: 5656–68.
42 Hatzivassiliou G, Song K, Yen I *et al.* RAF inhibitors prime wild-type RAF to activate the MAPK pathway and enhance growth. *Nature* 2010; **464**: 431–5.
43 Haura EB, Ricart AD, Larson TG *et al.* A phase II study of PD-0325901, an oral MEK inhibitor, in previously treated patients with advanced non-small cell lung cancer. *Clin. Cancer Res.* 2010; **16**: 2450–7.
44 Yatabe Y. EGFR mutations and the terminal respiratory unit. *Cancer Metastasis Rev.* 2010; **29**: 23–36.
45 Lynch TJ, Bell DW, Sordella R *et al.* Activating mutations in the epidermal growth factor receptor underlying responsiveness of non-small-cell lung cancer to gefitinib. *N. Engl. J. Med.* 2004; **350**: 2129–39.
46 Paez JG, Janne PA, Lee JC *et al.* EGFR mutations in lung cancer: correlation with clinical response to gefitinib therapy. *Science* 2004; **304**: 1497–500.
47 Soda M, Choi YL, Enomoto M *et al.* Identification of the transforming EML4-ALK fusion gene in non-small-cell lung cancer. *Nature* 2007; **448**: 561–6.
48 Kwak EL, Bang YJ, Camidge DR *et al.* Anaplastic lymphoma kinase inhibition in non-small-cell lung cancer. *N. Engl. J. Med.* 2010; **363**: 1693–703.
49 Koivunen JP, Mermel C, Zejnullahu K *et al.* EML4-ALK fusion gene and efficacy of an ALK kinase inhibitor in lung cancer. *Clin. Cancer Res.* 2008; **14**: 4275–83.
50 Pao W, Girard N. New driver mutations in non-small-cell lung cancer. *Lancet Oncol.* 2011; **12**: 175–80.
51 Greulich H. The genomics of lung adenocarcinoma: opportunities for targeted therapies. *Genes Cancer* 2010; **1**: 1200–10.
52 Nigro JM, Baker SJ, Preisinger AC *et al.* Mutations in the p53 gene occur in diverse human tumour types. *Nature* 1989; **342**: 705–8.
53 Takahashi T, Nau MM, Chiba I *et al.* p53: a frequent target for genetic abnormalities in lung cancer. *Science* 1989; **246**: 491–4.
54 Hayashi N, Sugimoto Y, Tsuchiya E *et al.* Somatic mutations of the MTS (multiple tumor suppressor) 1/CDK4l (cyclin-dependent kinase-4 inhibitor) gene in human primary non-small cell lung carcinomas. *Biochem. Biophys. Res. Commun.* 1994; **202**: 1426–30.
55 Packenham JP, Taylor JA, White CM *et al.* Homozygous deletions at chromosome 9p21 and mutation analysis of p16 and p15 in microdissected primary non-small cell lung cancers. *Clin. Cancer Res.* 1995; **1**: 687–90.
56 Merlo A, Herman JG, Mao L *et al.* 5′CpG island methylation is associated with transcriptional silencing of the tumour suppressor p16/CDKN2/MTS1 in human cancers. *Nat. Med.* 1995; **1**: 686–92.
57 Sun Y, Ren Y, Fang Z *et al.* Lung adenocarcinoma from East Asian never-smokers is a disease largely defined by targetable oncogenic mutant kinases. *J. Clin. Oncol.* 2010; **28**: 4616–20.
58 Pinkel D, Segraves R, Sudar D *et al.* High resolution analysis of DNA copy number variation using comparative genomic hybridization to microarrays. *Nat. Genet.* 1998; **20**: 207–11.
59 Pollack JR, Perou CM, Alizadeh AA *et al.* Genome-wide analysis of DNA copy-number changes using cDNA microarrays. *Nat. Genet.* 1999; **23**: 41–6.
60 Kim TM, Yim SH, Lee JS *et al.* Genome-wide screening of genomic alterations and their clinicopathologic implications in non-small cell lung cancers. *Clin. Cancer Res.* 2005; **11**: 8235–42.
61 Tonon G, Wong KK, Maulik G *et al.* High-resolution genomic profiles of human lung cancer. *Proc. Natl Acad. Sci. U.S.A.* 2005; **102**: 9625–30.
62 Balsara BR, Testa JR. Chromosomal imbalances in human lung cancer. *Oncogene* 2002; **21**: 6877–83.
63 Bjorkqvist AM, Husgafvel-Pursiainen K, Anttila S *et al.* DNA gains in 3q occur frequently in squamous cell carcinoma of the lung, but not in adenocarcinoma. *Genes Chromosomes Cancer* 1998; **22**: 79–82.
64 Luk C, Tsao MS, Bayani J *et al.* Molecular cytogenetic analysis of non-small cell lung carcinoma by spectral karyotyping and comparative genomic hybridization. *Cancer Genet. Cytogenet.* 2001; **125**: 87–99.
65 Pei J, Balsara BR, Li W *et al.* Genomic imbalances in human lung adenocarcinomas and squamous cell carcinomas. *Genes Chromosomes Cancer* 2001; **31**: 282–7.
66 Petersen I, Bujard M, Petersen S *et al.* Patterns of chromosomal imbalances in adenocarcinoma and squamous cell carcinoma of the lung. *Cancer Res.* 1997; **57**: 2331–5.
67 Massion PP, Kuo WL, Stokoe D *et al.* Genomic copy number analysis of non-small cell lung cancer using array comparative genomic hybridization: implications of the phosphatidylinositol 3-kinase pathway. *Cancer Res.* 2002; **62**: 3636–40.
68 Job B, Bernheim A, Beau-Faller M *et al.* Genomic aberrations in lung adenocarcinoma in never smokers. *PLoS ONE* 2010; **5**: e15145.
69 Soh J, Okumura N, Lockwood WW *et al.* Oncogene mutations, copy number gains and mutant allele specific imbalance (MASI) frequently occur together in tumor cells. *PLoS ONE* 2009; **4**: e7464.
70 Yuan S, Yu SL, Chen HY *et al.* Clustered genomic alterations in chromosome 7p dictate outcomes and targeted treatment responses of lung adenocarcinoma with EGFR-activating mutations. *J. Clin. Oncol.* 2011; **29**: 3435–42.
71 Bhattacharjee A, Richards WG, Staunton J *et al.* Classification of human lung carcinomas by mRNA expression profiling reveals distinct adenocarcinoma subclasses. *Proc. Natl Acad. Sci. U.S.A.* 2001; **98**: 13790–5.
72 Garber ME, Troyanskaya OG, Schluens K *et al.* Diversity of gene expression in adenocarcinoma of the lung. *Proc. Natl Acad. Sci. U.S.A.* 2001; **98**: 13784–9.
73 Hayes DN, Monti S, Parmigiani G *et al.* Gene expression profiling reveals reproducible human lung adenocarcinoma subtypes in multiple independent patient cohorts. *J. Clin. Oncol.* 2006; **24**: 5079–90.
74 Yatabe Y, Mitsudomi T, Takahashi T. TTF-1 expression in pulmonary adenocarcinomas. *Am. J. Surg. Pathol.* 2002; **26**: 767–73.

75 Westra WH. Early glandular neoplasia of the lung. *Respir. Res.* 2000; **1**: 163–9.
76 Chapman AD, Kerr KM. The association between atypical adenomatous hyperplasia and primary lung cancer. *Br. J. Cancer* 2000; **83**: 632–6.
77 Tang X, Shigematsu H, Bekele BN *et al.* EGFR tyrosine kinase domain mutations are detected in histologically normal respiratory epithelium in lung cancer patients. *Cancer Res.* 2005; **65**: 7568–72.
78 Tang X, Varella-Garcia M, Xavier AC *et al.* Epidermal growth factor receptor abnormalities in the pathogenesis and progression of lung adenocarcinomas. *Cancer Prev. Res. (Phila.)* 2008; **1**: 192–200.
79 Kitamura H, Kameda Y, Ito T *et al.* Atypical adenomatous hyperplasia of the lung. Implications for the pathogenesis of peripheral lung adenocarcinoma. *Am. J. Clin. Pathol.* 1999; **111**: 610–22.
80 Westra WH, Baas IO, Hruban RH *et al.* K-ras oncogene activation in atypical alveolar hyperplasias of the human lung. *Cancer Res.* 1996; **56**: 2224–8.
81 Chiosea S, Jelezcova E, Chandran U *et al.* Overexpression of Dicer in precursor lesions of lung adenocarcinoma. *Cancer Res.* 2007; **67**: 2345–50.
82 Selamat SA, Galler JS, Joshi AD *et al.* DNA methylation changes in atypical adenomatous hyperplasia, adenocarcinoma in situ, and lung adenocarcinoma. *PLoS ONE* 2011; **6**: e21443.
83 Yatabe Y, Kosaka T, Takahashi T *et al.* EGFR mutation is specific for terminal respiratory unit type adenocarcinoma. *Am. J. Surg. Pathol.* 2005; **29**: 633–9.
84 Yoshida Y, Shibata T, Kokubu A *et al.* Mutations of the epidermal growth factor receptor gene in atypical adenomatous hyperplasia and bronchioloalveolar carcinoma of the lung. *Lung Cancer* 2005; **50**: 1–8.
85 Slaughter DP, Southwick HW, Smejkal W. Field cancerization in oral stratified squamous epithelium; clinical implications of multicentric origin. *Cancer* 1953; **6**: 963–8.
86 Auerbach O, Stout AP, Hammond EC *et al.* Changes in bronchial epithelium in relation to cigarette smoking and in relation to lung cancer. *N. Engl. J. Med.* 1961; **265**: 253–67.
87 Sin DD, Man SF, McWilliams A *et al.* Progression of airway dysplasia and C-reactive protein in smokers at high risk of lung cancer. *Am. J. Respir. Crit. Care Med.* 2006; **173**: 535–9.
88 Steiling K, Ryan J, Brody JS *et al.* The field of tissue injury in the lung and airway. *Cancer Prev. Res. (Phila.)* 2008; **1**: 396–403.
89 Wistuba II, Berry J, Behrens C *et al.* Molecular changes in the bronchial epithelium of patients with small cell lung cancer. *Clin. Cancer Res.* 2000; **6**: 2604–10.
90 Nelson MA, Wymer J, Clements N, Jr. Detection of K-ras gene mutations in non-neoplastic lung tissue and lung cancers. *Cancer Lett.* 1996; **103**: 115–21.
91 Belinsky SA, Nikula KJ, Palmisano WA *et al.* Aberrant methylation of p16(INK4a) is an early event in lung cancer and a potential biomarker for early diagnosis. *Proc. Natl Acad. Sci. U.S.A.* 1998; **95**: 11891–6.
92 Belinsky SA, Palmisano WA, Gilliland FD *et al.* Aberrant promoter methylation in bronchial epithelium and sputum from current and former smokers. *Cancer Res.* 2002; **62**: 2370–7.
93 Mao L, Lee JS, Kurie JM *et al.* Clonal genetic alterations in the lungs of current and former smokers. *J. Natl Cancer Inst.* 1997; **89**: 857–62.
94 Wistuba II, Lam S, Behrens C *et al.* Molecular damage in the bronchial epithelium of current and former smokers. *J. Natl Cancer Inst.* 1997; **89**: 1366–73.
95 Powell CA, Klares S, O'Connor G *et al.* Loss of heterozygosity in epithelial cells obtained by bronchial brushing: clinical utility in lung cancer. *Clin. Cancer Res.* 1999; **5**: 2025–34.
96 Franklin WA, Gazdar AF, Haney J *et al.* Widely dispersed p53 mutation in respiratory epithelium. A novel mechanism for field carcinogenesis. *J. Clin. Invest.* 1997; **100**: 2133–7.
97 Zochbauer-Muller S, Lam S, Toyooka S *et al.* Aberrant methylation of multiple genes in the upper aerodigestive tract epithelium of heavy smokers. *Int. J. Cancer* 2003; **107**: 612–6.
98 Soria JC, Rodriguez M, Liu DD *et al.* Aberrant promoter methylation of multiple genes in bronchial brush samples from former cigarette smokers. *Cancer Res.* 2002; **62**: 351–5.
99 Heller G, Zielinski CC, Zochbauer-Muller S. Lung cancer: from single-gene methylation to methylome profiling. *Cancer Metastasis Rev.* 2010; **29**: 95–107.
100 Hackett NR, Heguy A, Harvey BG *et al.* Variability of antioxidant-related gene expression in the airway epithelium of cigarette smokers. *Am. J. Respir. Cell Mol. Biol.* 2003; **29**: 331–43.
101 Spira A, Beane J, Shah V *et al.* Effects of cigarette smoke on the human airway epithelial cell transcriptome. *Proc. Natl Acad. Sci. U.S.A.* 2004; **101**: 10143–8.
102 Beane J, Sebastiani P, Liu G *et al.* Reversible and permanent effects of tobacco smoke exposure on airway epithelial gene expression. *Genome Biol.* 2007; **8**: R201.
103 Schembri F, Sridhar S, Perdomo C *et al.* MicroRNAs as modulators of smoking-induced gene expression changes in human airway epithelium. *Proc. Natl Acad. Sci. U.S.A.* 2009; **106**: 2319–24.
104 Spira A, Beane JE, Shah V *et al.* Airway epithelial gene expression in the diagnostic evaluation of smokers with suspect lung cancer. *Nat. Med.* 2007; **13**: 361–6.
105 Gustafson AM, Soldi R, Anderlind C *et al.* Airway PI3K pathway activation is an early and reversible event in lung cancer development. *Sci. Transl. Med.* 2010; **2**: 26ra5.
106 Sridhar S, Schembri F, Zeskind J *et al.* Smoking-induced gene expression changes in the bronchial airway are reflected in nasal and buccal epithelium. *BMC Genomics* 2008; **9**: 259.
107 Zhang X, Sebastiani P, Liu G *et al.* Similarities and differences between smoking-related gene expression in nasal and bronchial epithelium. *Physiol. Genomics* 2010; **41**: 1–8.
108 Boyle JO, Gumus ZH, Kacker A *et al.* Effects of cigarette smoke on the human oral mucosal transcriptome. *Cancer Prev. Res. (Phila.)* 2010; **3**: 266–78.
109 Garraway LA, Sellers WR. Lineage dependency and lineage-survival oncogenes in human cancer. *Nat. Rev. Cancer* 2006; **6**: 593–602.
110 Kantarjian H, Sawyers C, Hochhaus A *et al.* Hematologic and cytogenetic responses to imatinib mesylate in chronic myelogenous leukemia. *N. Engl. J. Med.* 2002; **346**: 645–52.
111 Demetri GD, von Mehren M, Blanke CD *et al.* Efficacy and safety of imatinib mesylate in advanced gastrointestinal stromal tumors. *N. Engl. J. Med.* 2002; **347**: 472–80.
112 Garraway LA, Widlund HR, Rubin MA *et al.* Integrative genomic analyses identify MITF as a lineage survival oncogene amplified in malignant melanoma. *Nature* 2005; **436**: 117–22.
113 Cheung HW, Cowley GS, Weir BA *et al.* Systematic investigation of genetic vulnerabilities across cancer cell lines reveals lineage-specific dependencies in ovarian cancer. *Proc. Natl Acad. Sci. U.S.A.* 2011; **108**: 12372–7.
114 Minoo P, Su G, Drum H *et al.* Defects in tracheoesophageal and lung morphogenesis in Nkx2.1(-/-) mouse embryos. *Dev. Biol.* 1999; **209**: 60–71.
115 Yuan B, Li C, Kimura S *et al.* Inhibition of distal lung morphogenesis in Nkx2.1(-/-) embryos. *Dev. Dyn.* 2000; **217**: 180–90.
116 Kimura S, Hara Y, Pineau T *et al.* The T/ebp null mouse: thyroid-specific enhancer-binding protein is essential for the organogenesis of the thyroid, lung, ventral forebrain, and pituitary. *Genes Dev.* 1996; **10**: 60–9.
117 Ikeda K, Clark JC, Shaw-White JR *et al.* Gene structure and expression of human thyroid transcription factor-1 in respiratory epithelial cells. *J. Biol. Chem.* 1995; **270**: 8108–14.
118 Kendall J, Liu Q, Bakleh A *et al.* Oncogenic cooperation and coamplification of developmental transcription factor genes in lung cancer. *Proc. Natl Acad. Sci. U.S.A.* 2007; **104**: 16663–8.

119 Hsu DS, Acharya CR, Balakumaran BS *et al.* Characterizing the developmental pathways TTF-1, NKX2-8, and PAX9 in lung cancer. *Proc. Natl Acad. Sci. U.S.A.* 2009; **106**: 5312–7.

120 Winslow MM, Dayton TL, Verhaak RG *et al.* Suppression of lung adenocarcinoma progression by Nkx2-1. *Nature* 2011; **473**: 101–4.

121 Barletta JA, Perner S, Iafrate AJ *et al.* Clinical significance of TTF-1 protein expression and TTF-1 gene amplification in lung adenocarcinoma. *J. Cell. Mol. Med.* 2009; **13**: 1977–86.

122 Tang X, Kadara H, Behrens C *et al.* Abnormalities of the TITF-1 lineage-specific oncogene in NSCLC: implications in lung cancer pathogenesis and prognosis. *Clin. Cancer Res.* 2011; **17**: 2434–43.

123 Barlesi F, Pinot D, Legoffic A *et al.* Positive thyroid transcription factor 1 staining strongly correlates with survival of patients with adenocarcinoma of the lung. *Br. J. Cancer* 2005; **93**: 450–2.

124 Berghmans T, Paesmans M, Mascaux C *et al.* Thyroid transcription factor 1—a new prognostic factor in lung cancer: a meta-analysis. *Ann. Oncol.* 2006; **17**: 1673–6.

125 Perner S, Wagner PL, Soltermann A *et al.* TTF1 expression in non-small cell lung carcinoma: association with TTF1 gene amplification and improved survival. *J. Pathol.* 2009; **217**: 65–72.

126 Anagnostou VK, Syrigos KN, Bepler G *et al.* Thyroid transcription factor 1 is an independent prognostic factor for patients with stage I lung adenocarcinoma. *J. Clin. Oncol.* 2009; **27**: 271–8.

127 Ishii Y, Rex M, Scotting PJ *et al.* Region-specific expression of chicken Sox2 in the developing gut and lung epithelium: regulation by epithelial-mesenchymal interactions. *Dev. Dyn.* 1998; **213**: 464–75.

128 Que J, Okubo T, Goldenring JR *et al.* Multiple dose-dependent roles for Sox2 in the patterning and differentiation of anterior foregut endoderm. *Development* 2007; **134**: 2521–31.

129 Gontan C, de Munck A, Vermeij M *et al.* Sox2 is important for two crucial processes in lung development: branching morphogenesis and epithelial cell differentiation. *Dev. Biol.* 2008; **317**: 296–309.

130 Que J, Luo X, Schwartz RJ *et al.* Multiple roles for Sox2 in the developing and adult mouse trachea. *Development* 2009; **136**: 1899–907.

131 Whitsett JA, Haitchi HM, Maeda Y. Intersections between pulmonary development and disease. *Am. J. Respir. Crit. Care Med.* 2011; **184**: 401–6.

132 Boiani M, Scholer HR. Regulatory networks in embryo-derived pluripotent stem cells. *Nat. Rev. Mol. Cell Biol.* 2005; **6**: 872–84.

133 Boyer LA, Lee TI, Cole MF *et al.* Core transcriptional regulatory circuitry in human embryonic stem cells. *Cell* 2005; **122**: 947–56.

134 Hussenet T, Dali S, Exinger J *et al.* SOX2 is an oncogene activated by recurrent 3q26.3 amplifications in human lung squamous cell carcinomas. *PLoS ONE* 2010; **5**: e8960.

135 Maier S, Wilbertz T, Braun M *et al.* SOX2 amplification is a common event in squamous cell carcinomas of different organ sites. *Hum. Pathol.* 2011; **42**: 1078–88.

136 Wilbertz T, Wagner P, Petersen K *et al.* SOX2 gene amplification and protein overexpression are associated with better outcome in squamous cell lung cancer. *Mod. Pathol.* 2011; **24**: 944–53.

137 Sholl LM, Barletta JA, Yeap BY *et al.* Sox2 protein expression is an independent poor prognostic indicator in stage I lung adenocarcinoma. *Am. J. Surg. Pathol.* 2010; **34**: 1193–8.

138 Lu Y, Futtner C, Rock JR *et al.* Evidence that SOX2 overexpression is oncogenic in the lung. *PLoS ONE* 2010; **5**: e11022.

139 Xiang R, Liao D, Cheng T *et al.* Downregulation of transcription factor SOX2 in cancer stem cells suppresses growth and metastasis of lung cancer. *Br. J. Cancer* 2011; **104**: 1410–7.

140 McCaughan F, Pole JC, Bankier AT *et al.* Progressive 3q amplification consistently targets SOX2 in preinvasive squamous lung cancer. *Am. J. Respir. Crit. Care Med.* 2010; **182**: 83–91.

141 Meyerson M, Gabriel S, Getz G. Advances in understanding cancer genomes through second-generation sequencing. *Nat. Rev. Genet.* 2010; **11**: 685–96.

142 Campbell PJ, Stephens PJ, Pleasance ED *et al.* Identification of somatically acquired rearrangements in cancer using genome-wide massively parallel paired-end sequencing. *Nat. Genet.* 2008; **40**: 722–9.

143 Lee W, Jiang Z, Liu J *et al.* The mutation spectrum revealed by paired genome sequences from a lung cancer patient. *Nature* 2010; **465**: 473–7.

144 Pleasance ED, Stephens PJ, O'Meara S *et al.* A small-cell lung cancer genome with complex signatures of tobacco exposure. *Nature* 2010; **463**: 184–90.

145 Beane J, Vick J, Schembri F *et al.* Characterizing the impact of smoking and lung cancer on the airway transcriptome using RNA-Seq. *Cancer Prev. Res. (Phila.)* 2011; **4**: 803–17.

Int. J. Radiation Oncology Biol. Phys., Vol. 82, No. 1, pp. e91–e97, 2012

0360-3016/$ - see front matter

ELSEVIER

doi:10.1016/j.ijrobp.2010.12.072

CLINICAL INVESTIGATION **Thoracic Cancer**

POSITRON EMISSION TOMOGRAPHY/COMPUTED TOMOGRAPHY-GUIDED INTENSITY-MODULATED RADIOTHERAPY FOR LIMITED-STAGE SMALL-CELL LUNG CANCER

Shervin M. Shirvani, M.D.,* Ritsuko Komaki, M.D.,* John V. Heymach, M.D., Ph.D.,† Frank V. Fossella, M.D.,† and Joe Y. Chang, M.D., Ph.D.*

Departments of *Radiation Oncology and †Thoracic/Head and Neck Medical Oncology, University of Texas M.D. Anderson Cancer Center, Houston, TX

Purpose: Omitting elective nodal irradiation from planning target volumes does not compromise outcomes in patients with non–small-cell lung cancer, but whether the same is true for those with limited-stage small-cell lung cancer (LS-SCLC) is unknown. Therefore, in the present study, we sought to determine the clinical outcomes and the frequency of elective nodal failure in patients with LS-SCLC staged using positron emission tomography/computed tomography and treated with involved-field intensity-modulated radiotherapy.

Methods and Materials: Between 2005 and 2008, 60 patients with LS-SCLC at our institution underwent disease staging using positron emission tomography/computed tomography before treatment using an intensity-modulated radiotherapy plan in which elective nodal irradiation was intentionally omitted from the planning target volume (mode and median dose, 45 Gy in 30 fractions; range, 40.5 Gy in 27 fractions to 63.8 Gy in 35 fractions). In most cases, concurrent platinum-based chemotherapy was administered. We retrospectively reviewed the clinical outcomes to determine the overall survival, relapse-free survival, and failure patterns. Elective nodal failure was defined as recurrence in initially uninvolved hilar, mediastinal, or supraclavicular nodes. Survival was assessed using the Kaplan-Meier method.

Results: The median age of the study patients at diagnosis was 63 years (range, 39–86). The median follow-up duration was 21 months (range, 4–58) in all patients and 26 months (range, 4–58) in the survivors. The 2-year actuarial overall survival and relapse-free survival rate were 58% and 43%, respectively. Of the 30 patients with recurrence, 23 had metastatic disease and 7 had locoregional failure. We observed only one isolated elective nodal failure.

Conclusions: To our knowledge, this is the first study to examine the outcomes in patients with LS-SCLC staged with positron emission tomography/computed tomography and treated with definitive intensity-modulated radiotherapy. In these patients, elective nodal irradiation can be safely omitted from the planning target volume for the purposes of dose escalation and toxicity reduction.

Small-cell lung cancer, Involved field radiation, Positron emission tomography, PET, Intensity-modulated radiotherapy, IMRT.

INTRODUCTION

The value of radiotherapy (RT) for local control of small-cell lung cancer (SCLC) confined to the thorax is indisputable (1, 2). Moreover, the use of concurrent chemotherapy with RT has resulted in an increased survival benefit and has become the standard of care for patients with limited-stage small cell lung cancer (LS-SCLC), yie-lding 5-year survival rates of about 28% (3). Nonetheless, most patients still experience recurrence and ultimately death from their disease. Evidence suggests that disease control in SCLC patients can be improved by even more aggressive therapy than that used currently, including radiation dose escalation. For example, in a multisite Phase I study evaluating different accelerated RT regimens with concurrent chemotherapy, the 18-month survival rate for the maximal tolerated dose of 61.2 Gy was 82%, significantly better than the rate achieved at the lowest dose of 50.4 Gy (25%) (4). However, enthusiasm among physicians for dose-escalated RT combined with chemotherapy must be tempered by the potential for significant toxic effects, including esophagitis, pneumonitis, and bone marrow suppression (4–7).

One strategy for escalating radiation doses without increasing toxicity is to diminish the targeted volume by omitting elective radiation fields, including uninvolved nodal stations. This strategy has proved useful for non–small-cell lung cancer and is associated with a minimal

Reprint requests to: Joe Y. Chang, M.D., Ph.D., Department of Radiation Oncology, Unit 97, University of Texas M.D. Anderson Cancer Center, 1515 Holcombe Blvd., Houston, TX 77030. Tel: (713) 563-2337; Fax: (713) 563-2366; E-mail: jychang@mdanderson.org

Presented at the 52nd Annual Meeting of the American Society for Radiation Oncology (ASTRO), San Diego, CA.

Conflict of interest: none.

Received Sept 24, 2010, and in revised form Nov 28, 2010. Accepted for publication Dec 15, 2010.

incidence of elective nodal recurrence (8–10). More recently, physicians have adopted this strategy for limited-stage SCLC (LS-SCLC); however, published data supporting its use for this disease are sparse. In one study, De Ruysscher *et al.* (11) found that among patients with LS-SCLC treated with involved-field RT guided by computed tomography (CT), the elective nodal failure (ENF) rate (11%) was unacceptably high. However, a similar study by the same group using positron emission tomography (PET) with CT (PET/CT) for target delineation produced better results, demonstrating an isolated ENF rate of only 3% (12). In the latter study, the investigators did not use four-dimensional (4D) CT-guided target delineation or treatment planning, respiratory gating, or intensity-modulated RT (IMRT); thus, the generalizability of their results is limited. The incorporation of these new technologies, including IMRT to PET/CT staging, co-uld offer an opportunity to further reduce toxicity but carry other risks. For example, incidental irradiation to nontargeted elective nodes might be different in IMRT than for three-dimensional conformal techniques and affect the rate of elective nodal failure. In the present study, we hypothesized that the clinical outcomes and rate of elective nodal failure would be acceptable using the combined approach of PET/CT staging and IMRT planning. Therefore, we conducted a retrospective study of our experience with, and report on the clinical outcomes and patterns of failure of, involved-field RT for LS-SCLC using IMRT guided by PET/CT.

METHODS AND MATERIALS

Patient selection

The clinical records of all consecutive patients with LS-SCLC who had undergone external beam RT initiated at the University of Texas M.D. Anderson Cancer Center between 2005 and 2008 were retrospectively reviewed. LS-SCLC was defined as disease confined to the thorax and regional nodes without malignant pleural effusion. The patients were included in the analysis if they had been diagnosed with histologically proven LS-SCLC that had not been treated previously with RT, had undergone staging using PET/CT before RT, had undergone definitive IMRT for the primary disease, and had complete RT records available. The patients who had been diagnosed initially with LS-SCLC and sc-heduled for induction chemotherapy but who subsequently developed distant metastasis before referral to the radiation oncology department were not included in the present analysis. Most (97%) of the patients received concurrent platinum-based chemotherapy. The M.D. Anderson institutional review board approved the present study.

Radiotherapy

The patients underwent IMRT using the Pinnacle CT-based treatment planning software program (Philips Medical Systems, Andover, MA). They underwent simulation and treatment in the supine position with their arms raised above their heads and were immobilized using a custom-made Vac-Lok cradle (Medtec, Orange City, IA). Most patients (73%) underwent 4D simulation. The gross tumor volume (GTV) included regions of primary disease and nodal metastasis defined by metabolically active regions on the patient's staging PET/CT scans. Involved nodal regions diagnosed by histologic evaluation of the biopsy samples obtained during mediastinoscopy or bronchoscopy were included in the GTV, regardless of the nodes' ^{18}F-fluorodeoxyglucose avidity on PET/CT scans. For 4D simulation, an internal GTV was defined as the sum envelope of GTVs extracted from the component images obtained in 10-breath phases (13). Typically, the clinical target volume (CTV) was defined as the internal GTV plus an 8-mm margin. The planning target volume (PTV) was defined as the CTV plus a 5–10-mm margin. In some cases, in lieu of the internal GTV covering the entire respiratory cycle, the treatment volumes were defined at deep inspiration, if necessary, to conform to normal tissue restraints. For the patients who underwent simulation during free breathing, the GTV was expanded by 0.8 cm to define the CTV, except for where the normal anatomic barriers and dose constraints required a smaller expansion. The CTV was then expanded by 1 cm to compensate for setup variability and target motion to generate the PTV. The plans were corrected for tissue inhomogeneity during treatment planning.

Radiation was delivered using photon beams of ≥6 MV from a linear accelerator. During RT, radiation oncologists evaluated the patients weekly to evaluate any acute toxic effects. Staging was repeated about 3 months after RT completion using contrast-enhanced CT. If no disease progression was observed, the patients were offered prophylactic cranial RT to a total dose of 25 Gy in 10 fractions. After completion of all treatment, the patients underwent repeat clinical examinations and imaging every 3 months for 2 years and then every 6 months for 3 years. Tumor recurrences were scored as separate, discrete events if they occurred ≥3 months apart.

Statistical analysis

The clinical endpoints examined included overall survival (OS), relapse-free survival (RFS), and patterns of failure. Recurrences were classified as in-field failures if most of the recurrent tumor volume or an obvious origin of recurrence was located in the treatment field PTV. In contrast, out-of-field failure was defined as a recurrence outside the PTV but within the lungs, pleura, mediastinum, or regional nodes. Elective nodal failure (ENF) represented a subset of out-of-field failure and was defined as a recurrence outside the PTV but within a hilar, mediastinal, or supraclavicular nodal basin. ENF was deemed to be isolated only in the absence of other sites of failure. Survival and the interval-to-failure durations were measured from the date of pathologic diagnosis of LS-SCLC, and the timing of the recurrences was defined as the time of the first imaging or clinical finding of recurrence. Survival probabilities were determined using the Kaplan-Meier method. Differences among the subgroups of patients were evaluated using the log–rank test. Toxicities were graded according to the Radiation Therapy Oncology Group criteria (14, 15).

RESULTS

Patient population and treatment

A total of 60 patients with LS-SCLC treated using IMRT guided by PET/CT between 2005 and 2008 were included in the present study (Table 1). Their median age was 63 years (range, 39–86). Most patients had a good performance status, with 85% of them having an Eastern Cooperative Oncology Group score of 0 or 1. Nearly all the patients (94%) had nodal disease at treatment, and approximately one-third of the patients had Stage N3 disease. Eight patients (13%) had involvement of an ipsilateral or contralateral

Table 1. Patient and treatment characteristics

Characteristic	Value
Patients *(n)*	60
Age (y)	
Median	63
Range	38–86
Gender *(n)*	
Male	25 (42)
Female	35 (58)
ECOG performance status *(n)*	
0	6 (10)
1	45 (75)
2	3 (5)
3	0 (0)
Not specified	6 (10)
Weight loss before treatment *(n)*	
None	23 (38)
<10 lb	10 (17)
≥10 lb	20 (33)
Not specified	7 (12)
Primary tumor size *(n)*	
≤3 cm	22 (37)
>3 cm	36 (60)
Primary tumor not identified	2 (3)
AJCC nodal stage *(n)*	
0	4 (7)
1	10 (17)
2	24 (40)
3	22 (37)
Chemotherapy *(n)*	
Induction	18 (30)
Concurrent	
Cisplatin/etoposide	40 (67)
Carboplatin/etoposide	11 (18)
Cisplatin/irinotecan	4 (7)
Unknown	3 (5)
None	2 (3)
RT *(n)*	
Simulation	
Four-dimensional	44 (73)
Free breathing	16 (27)
Dose *(n)*	
45 Gy, twice daily	41 (68)
Other	19 (32)
Prophylactic cranial irradiation *(n)*	
Yes	37 (62)
No	22 (37)
Unknown	1 (2)

Abbreviations: ECOG = Eastern Cooperative Oncology Group; AJCC = American Joint Committee on Cancer; RT = radiotherapy.
Data in parentheses are percentages.

supraclavicular nodal basin, and two (3%) had direct extension into adjacent bone; in all these cases, the treating oncologists classified the disease as limited stage at treatment planning.

Eighteen patients (30%) underwent induction chemotherapy, and 58 patients (97%) underwent concurrent chemotherapy, usually with a platinum agent and topoisomerase inhibitor. The most prescribed radiation dose was 45 Gy delivered in 30 twice-daily fractions; 68% of the patients received this treatment. Other prescribed total doses ranged from 40.5 Gy delivered in 27 fractions to 63.8 Gy delivered in a combination of daily and accelerated twice-daily fractions. Thirty-seven patients (62%) subsequently received prophylactic cranial RT after definitive therapy to the primary disease.

Clinical outcomes and patterns of failure

The median follow-up duration was 21 months (range, 4–58) in all patients and 26 months (range, 4–58) in survivors. The median actuarial overall survival time was 36 months (95% confidence interval [CI], 22–51), and the actuarial 2-year OS and RFS rate were 58% and 43%, respectively (Figs. 1 and 2).

Thirty patients (50%) had an observed recurrence. The leading cause of treatment failure was metastatic disease, which developed in 23 patients (38%) and accounted for 77% of all recurrences. Seven patients (12%) experienced locoregional failure. One patient (2%) had an isolated ENF, which represented 3% of all recurrences. The site of this nodal recurrence had <5 Gy of incidental radiation during the initial treatment (Fig. 3). We observed three other ENFs, with two occurring concurrently with in-field failures and one occurring concurrently with distant metastasis. Two ENFs occurred in the paratracheal nodes, and the other two occurred in the supraclavicular nodes. The sites of recurrence and their frequencies are listed in Table 2.

Toxicity

The rates of esophageal and pulmonary toxicities are presented in Table 3. A total of 14 (23%) and 4 (7%) patients experienced moderately symptomatic (Grade 3) acute radiation esophagitis and pneumonitis, respectively. No patients experienced Grade 4 or 5 acute esophagitis or pneumonitis. Neutropenic fever occurred in 10 patients (17%). No chronic Grade 3 esophageal or pulmonary toxicities were observed; one late Grade 4 toxicity occurred in a chronic smoker who required continuous oxygen by nasal

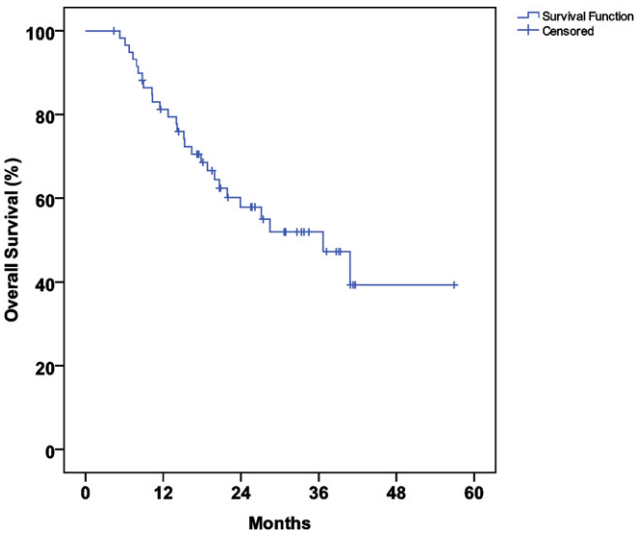

Fig. 1. Actuarial overall survival.

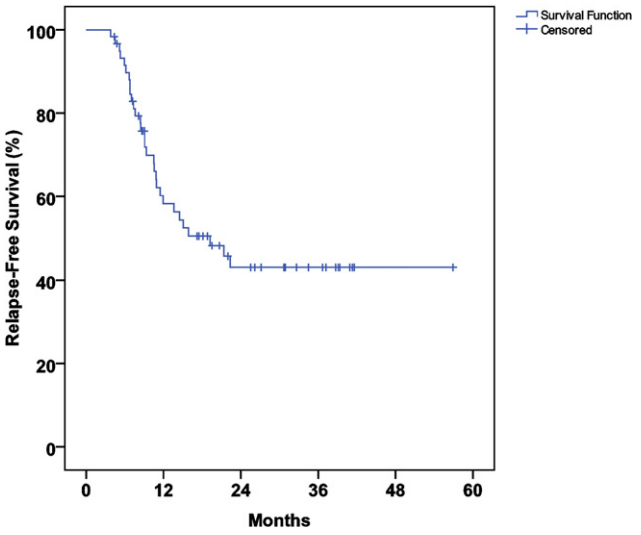

Fig. 2. Actuarial relapse-free survival.

cannula after developing severe pulmonary fibrosis following treatment.

PET/CT characteristics

Thirty-five patients (58%) underwent staging using PET/CT at our institution, and the remainder did so at another facility. The mean duration from the date of PET/CT to the start of RT was 38 days (range, 3–153; 95% CI, 30–47). In the patients for whom the standardized uptake value (SUV) was reported, the mean maximal SUV was 13.99 (range, 5.4–36.4; 95% CI, 12.1–15.9). Neither the setting in which the PET was performed nor the maximal SUV correlated with OS or RFS (data not shown). A period of <30 days from the date of PET/CT to the start of RT was associated with a nonsignificant trend toward improved RFS (p = .10) but not improved OS (Fig. 4).

DISCUSSION

In the early 1990s, emerging evidence demonstrated that small radiation target volumes did not adversely affect tumor control in the treatment of LS-SCLC (16–18). In fact, >80% of failures after RT during this period occurred in field, suggesting that inadequate radiation doses, rather than inadequate volumes, were the primary causes of intrathoracic recurrence (19). Therefore, the prevailing trend for RT in LS-SCLC during the past two decades has been to reduce the treatment field size while increasing the radiation dose. Small volumes have the additional benefit of sparing surrounding organs at risk from potentially life-threatening complications. The lungs, in particular, benefit from the reduced volumes, because the rate of pneumonitis approaches 33% once the lung volume receiving ≥20 Gy exceeds 40% (20). Thus, the treatment approach for SCLC at our institution has been to use image-guided RT to deliver escalated radiation doses to conformal treatment volumes (13). To that end, PET/CT scanning for staging and IMRT for treatment planning were incorporated at our institution for the treatment of LS-SCLC in 2005. We retrospectively reviewed the clinical outcomes and failure patterns, including the rate of ENF, in patients treated using these technologies. In our cohort of 60 patients, we observed a promising 2-year actuarial OS and RFS rate of 58% and 43%, respectively. We only observed one isolated elective nodal failure, and the dominant mode of recurrence in our data set was not locoregional failure but rather metastatic disease. The treatment was well tolerated by most patients, with Grade 3 acute esophagitis and pneumonitis occurring in 23% and 7% of patients, respectively.

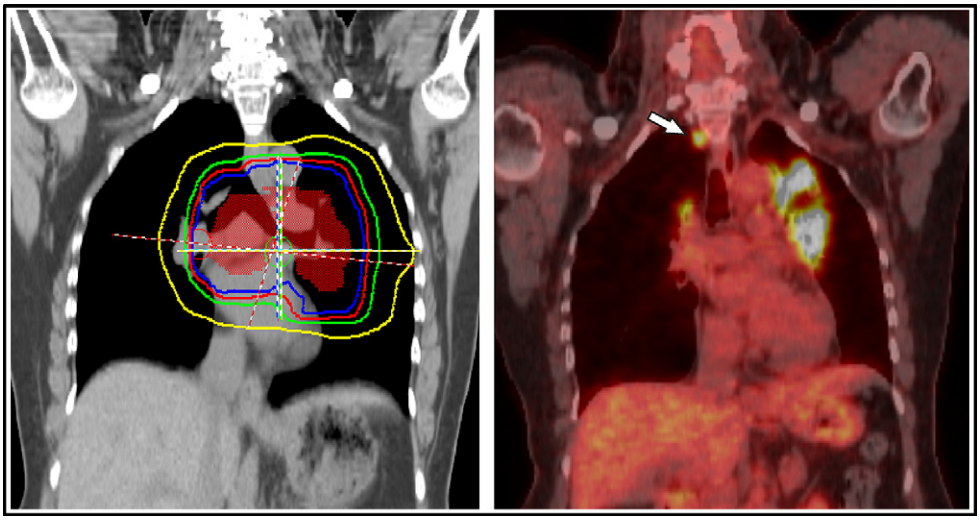

Fig. 3. Example of isolated elective nodal failure in our cohort. (Right) Intensity-modulated radiotherapy planning dose volumes for this patient, who received 45 Gy in 30 fractions given twice daily (orange, clinical target volume; blue, 45 Gy isodose line; red, 36 Gy; green, 20 Gy; yellow, 5 Gy). (Left) Elective nodal failure in right paratracheal lymph node (white arrow) observed on surveillance positron emission tomography/computed tomography scan obtained about 3 months after radiotherapy completion. Other areas of ^{18}F-fluorodeoxyglucose avidity on the image indicate inflammation and did not appear on subsequent scans.

Table 2. Patterns of failure for first recurrence

Recurrence	Patients with recurrence*(n)*
Total	30 (100)
Locoregional failure	7 (23)
In field	3 (10)
Out of field (includes elective nodes)	2 (7)
In field and out of field (includes elective nodes)	2 (7)
Distant failure	23 (77)
Distant metastases alone	18 (60)
In-field and distant metastases	2 (7)
Out-of-field and distant metastases	2 (7)
In-field, out-of-field, and distant metastases	1 (3)
Elective nodes	4 (13)
Pattern	
Isolated elective nodes	1 (3)
In-field and elective nodes	1 (3)
Distant metastases and elective nodes	2 (7)
Location	
Paratracheal	2 (7)
Supraclavicular	2 (7)

Data in parentheses are percentages.

Because of these findings, omitting elective nodal RT from the planning treatment volumes is reasonable and could improve local control without increasing toxicity by allowing dose escalation in a small field.

Positron emission tomography/CT is likely to be the most sensitive noninvasive method of delineating the extent of SCLC. Several series have shown that PET staging alters the presumed distribution of SCLC in 25–30% of patients previously staged using CT only (21–23). Therefore, the use of CT alone for target delineation in patients with LS-SCLC carries the risk of a geographic miss secondary to undetected disease. Confirming this hypothesis, a Phase II study of involved-field RT found a rather high rate of ENF (11%) in patients with SCLC staged using CT alone (11). In contrast, the addition of PET/CT staging to the diagnostic workup in a parallel study by the same investigators found a much

Table 3. Esophageal and pulmonary toxicities graded using Radiation Therapy Oncology Group criteria

	RTOG grade					
Toxicity	0	1	2	3	4	5
Acute *(n)*						
Esophageal	3 (5)	15 (25)	28 (47)	14 (23)	0 (0)	0 (0)
Pulmonary	38 (63)	12 (20)	6 (10)	4 (7)	0 (0)	0 (0)
Chronic *(n)*						
Esophageal	54 (90)	5 (8)	1 (2)	0 (0)	0 (0)	0 (0)
Pulmonary	40 (67)	9 (15)	10 (17)	0 (0)	1 (2)	0 (0)

Abbreviation: RTOG = Radiation Therapy Oncology Group.
Data in parentheses are percentages.

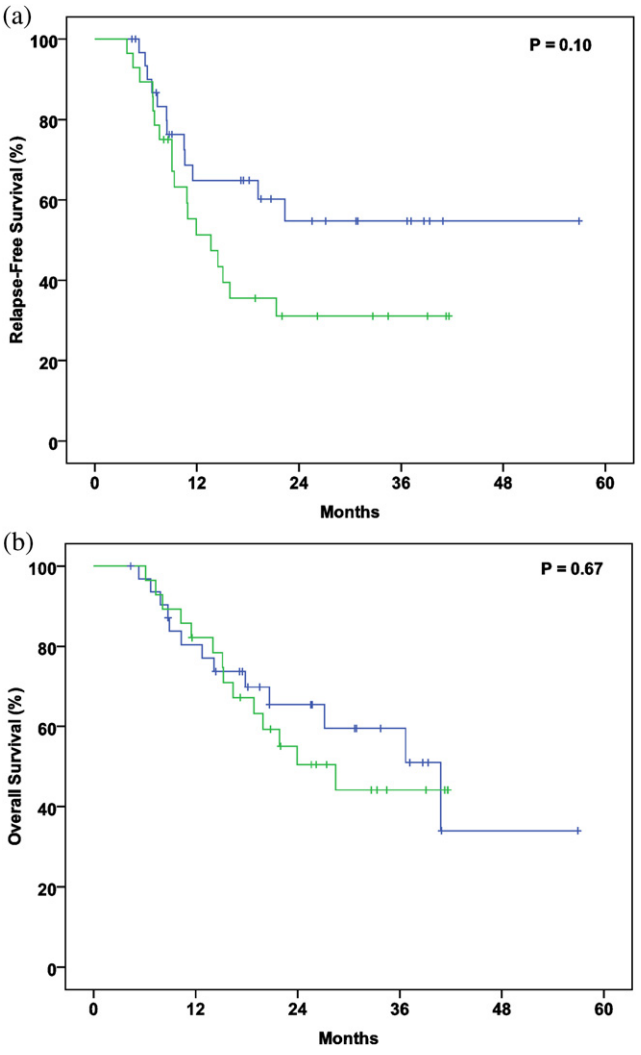

Fig. 4. (a) Relapse-free survival and (b) overall survival stratified by interval from positron emission tomography/computed tomography staging study to start of radiotherapy (green, ≥30 days; blue, <30 days).

improved rate of ENF (3%) (12). Additional improvements in PET techniques and logistics might further improve local control and survival in SCLC.

A natural hypothesis is that staging at or near simulation might result in improved disease coverage by preventing tumor progression in the PET-to-simulation interval. Our data suggest a trend toward improved RFS rates with PET-to-simulation intervals <30 days, making the conclusion that PET/CT ought to be performed at or near simulation a tempting one. However, patients with earlier RT simulations might have been healthier or had a better response to the initial treatment. Moreover, chemotherapy delivery affects the optimal timing of PET/CT. At many institutions, the standard practice is to have patients undergo simulation just before RT, at which time induction chemotherapy or the first dose of concurrent chemotherapy might have already been delivered (24). In these cases, PET/CT staging at simulation might be compromised by a diminished signal as a result of the systemic treatment. Therefore, additional studies are needed to determine

the optimal timing of PET/CT in relation to both the delivery of the first dose of chemotherapy and the start of RT.

We did not observe a difference in OS or RFS between the patients whose PET/CT scans were obtained at our institution and those whose scans were obtained at other facilities, despite suggestion in the literature that the quality of PET/CT studies can depend on the practice setting and training experience of the interpreting radiologist (25). Likewise, we did not detect any differences in the OS or RFS rate when we grouped patients according to the maximal SUVs on staging PET scans, which conflicts with recent data indicating that the SUV is prognostically relevant (26). The retrospective nature of our study and the heterogeneity of it with regard to the specific timing of PET/CT in relation to the delivery of chemotherapy might have diluted the effect of SUV on prognosis.

To our knowledge, this is the first study to examine the use of PET/CT and IMRT for involved-field RT for LS-SCLC. However, a recent study by van Loon *et al.* (12) in The Netherlands reported outcomes for a similar group of 60 patients with LS-SCLC treated using three-dimensional conformal techniques in place of IMRT. Strikingly, our series and theirs had nearly the same incidence of isolated ENF (2% and 3%, respectively), providing compelling corroboration of our primary finding that omission of elective nodal irradiation in pursuit of dose escalation and reduced toxicity is warranted. However, some important differences in outcomes of these two studies warrant attention. The 2-year actuarial OS and RFS rates in our study (58% and 43%, respectively) were greater than those (35% and 17%, respectively) reported by van Loon *et al.* (12). Our results also represent a modest improvement over that in the landmark Intergroup Trial 0096, in which the 2-year OS and RFS rate in the 45 Gy twice-daily arm was 47% and 29%, respectively.

The disparities in the study population and inherent selection bias were certainly responsible for some of the differences in outcomes seen between these studies. In addition, it is worth exploring other differences in study design and treatment technique that could also have had a bearing on the patient outcomes. Specifically, one explanation for the disparities between our results and those in the Dutch study is the use of different RT techniques, including IMRT and 4D-CT simulation in our study. Previously, we compared IMRT with three-dimensional conformal RT for advanced non–SCLC and found improved target coverage and reduced normal tissue exposure using the IMRT plans. Specifically, IMRT improved target conformality, delivered greater doses to the target, and reduced the mean lung volume receiving >20 Gy (27, 28). Also, most of our patients underwent 4D simulation for treatment planning. Liu *et al.* (29) previously demonstrated that during the respiratory cycle, one-half of all lung tumors moved >5 mm and one-tenth moved >1 cm. Our use of 4D simulation, therefore, might have reduced the rate of geographic misses during treatment caused by tumor motion. We observed a trend suggesting that patients who underwent 4D simulation had better RFS rates than those who underwent simulation with free breathing (data not shown); however, that analysis was limited because the free breathing scans were done in a small group of patients who underwent treatment at the beginning of our study period before 4D simulation was fully commissioned. We expect that the completion of ongoing lung cancer trials designed to clarify the use of technologies such as IMRT and 4D simulation in the treatment of lung cancer will shed more light on their contribution to improving outcomes.

One other issue worth considering is the potential role of incidental irradiation in the elective nodal failures seen in our study. Other investigators have studied incidental irradiation in three-dimensional conformal therapy of involved-field radiation in advanced non-SCLC and have reported that the median mean dose for thoracic nodal regions (Levels 1–11) was >40 Gy, except for at Levels 1, 3, and 7 in their series (30). It stands to reason that the treatment of LS-SCLC also results in high levels of incidental nodal irradiation, because this disease tends to be more centrally located near mediastinal nodal basins. Although beyond the scope of the present study, future investigations could clarify this issue by measuring the doses to incident nodes and relating them to rates of nodal control. It is notable that the 1 patient in our series with isolated elective nodal failure had negligible radiation dose at the site of paratracheal nodal failure (Fig. 3).

Our study was retrospective and thus had several important limitations that could explain the promising outcomes we observed. The improved sensitivity of PET/CT in detecting distant metastases might have excluded patients who otherwise would have been classified as having LS-SCLC in previous diagnostic eras, thereby improving the mean outcomes in our cohort. This stage-migration phenomenon might be responsible for our improved outcomes compared to Intergroup Trial 0096. Furthermore, because the patients were not prospectively followed up, selection bias and the loss of patients from our tertiary referral center to local follow-up might have contributed to an underestimation of the rates of recurrence and death. Finally, the follow-up in our study was limited both because of the recent advent of this treatment strategy at our institution and the relative rarity of LS-SCLC in the general population.

Despite these limitations, the data from evaluations of image-guided involved-field RT for LS-SCLC are scarce; thus, we believe that the present series of 60 patients is a significant addition to the published data and provides intriguing hypotheses for the future study of treatments of this disease. We hope that future prospective studies using strict protocols for patient stratification, diagnosis, and treatment will verify and build on the outcomes we have reported.

CONCLUSIONS

In the present cohort of 60 patients with LS-SCLC staged using PET/CT and undergoing definitive IMRT, only one isolated ENF occurred. We have concluded that for the purposes of dose escalation and reduced toxicity, elective nodal irradiation can be safely omitted from the PTV in patients who underwent staging and treatment using these techniques.

REFERENCES

1. Pignon JP, Arriagada R, Ihde DC, *et al*. A meta-analysis of thoracic radiotherapy for small-cell lung cancer. *N Engl J Med* 1992;327:1618–1624.
2. Warde P, Payne D. Does thoracic irradiation improve survival and local control in limited-stage small-cell carcinoma of the lung? A meta-analysis. *J Clin Oncol* 1992;10:890–895.
3. Turrisi AT III, Kim K, Blum R, *et al*. Twice-daily compared with once-daily thoracic radiotherapy in limited small-cell lung cancer treated concurrently with cisplatin and etoposide. *N Engl J Med* 1999;340:265–271.
4. Komaki R, Swann RS, Ettinger DS, *et al*. Phase I study of thoracic radiation dose escalation with concurrent chemotherapy for patients with limited small-cell lung cancer: Report of Radiation Therapy Oncology Group (RTOG) protocol 97-12. *Int J Radiat Oncol Biol Phys* 2005;62:342–350.
5. Choi NC, Herndon JE II, Rosenman J, *et al*. Phase I study to determine the maximum-tolerated dose of radiation in standard daily and hyperfractionated-accelerated twice-daily radiation schedules with concurrent chemotherapy for limited-stage small-cell lung cancer. *J Clin Oncol* 1998;16:3528–3536.
6. Murray N, Coy P, Pater JL, *et al*. Importance of timing for thoracic irradiation in the combined modality treatment of limited-stage small-cell lung cancer: The National Cancer Institute of Canada Clinical Trials Group. *J Clin Oncol* 1993;11:336–344.
7. Bradley J, Graham MV, Winter K, *et al*. Toxicity and outcome results of RTOG 9311: A phase I-II dose-escalation study using three-dimensional conformal radiotherapy in patients with inoperable non–small-cell lung carcinoma. *Int J Radiat Oncol Biol Phys* 2005;61:318–328.
8. De Ruysscher D, Wanders S, van Haren E, *et al*. Selective mediastinal node irradiation based on FDG-PET scan data in patients with non–small-cell lung cancer: A prospective clinical study. *Int J Radiat Oncol Biol Phys* 2005;62:988–994.
9. Rosenzweig KE, Sura S, Jackson A, *et al*. Involved-field radiation therapy for inoperable non small-cell lung cancer. *J Clin Oncol* 2007;25:5557–5561.
10. Sulman EP, Komaki R, Klopp AH, *et al*. Exclusion of elective nodal irradiation is associated with minimal elective nodal failure in non-small cell lung cancer. *Radiat Oncol* 2009;4:5.
11. De Ruysscher D, Bremer RH, Koppe F, *et al*. Omission of elective node irradiation on basis of CT-scans in patients with limited disease small cell lung cancer: a phase II trial. *Radiother Oncol* 2006;80:307–312.
12. van Loon J, De Ruysscher D, Wanders R, *et al*. Selective nodal irradiation on basis of (18)FDG-PET scans in limited-disease small-cell lung cancer: A prospective study. *Int J Radiat Oncol Biol Phys* 2010;77:329–336.
13. Chang JY, Dong L, Liu H, *et al*. Image-guided radiation therapy for non-small cell lung cancer. *J Thorac Oncol* 2008;3: 177–186.
14. Jemal A, Siegel R, Ward E, *et al*. Cancer statistics. *CA Cancer J Clin* 2007;2007(57):43–66.
15. Smith BD, Haffty BG, Smith GL, *et al*. Use of postmastectomy radiotherapy in older women. *Int J Radiat Oncol Biol Phys* 2008;71:98–106.
16. Schild SE, Curran WJ Jr.. Small cell lung cancer. In: Gunderson LL, Tepper JE, editors. Clinical radiation oncology. 2nd ed. Philadelphia: Elsevier Churchill Livingstone; 2007. p. 1827.
17. Kies MS, Mira JG, Crowley JJ, *et al*. Multimodal therapy for limited small-cell lung cancer: A randomized study of induction combination chemotherapy with or without thoracic radiation in complete responders; and with wide-field versus reduced-field radiation in partial responders: A Southwest Oncology Group Study. *J Clin Oncol* 1987;5:592–600.
18. Liengswangwong V, Bonner JA, Shaw EG, *et al*. Limited-stage small-cell lung cancer: Patterns of intrathoracic recurrence and the implications for thoracic radiotherapy. *J Clin Oncol* 1994; 12:496–502.
19. Brodin O, Rikner G, Steinholtz L, *et al*. Local failure in patients treated with radiotherapy and multidrug chemotherapy for small cell lung cancer. *Acta Oncol* 1990;29:739–746.
20. Graham MV, Purdy JA, Emami B, *et al*. Clinical dose–volume histogram analysis for pneumonitis after 3D treatment for non-small cell lung cancer (NSCLC). *Int J Radiat Oncol Biol Phys* 1999;45:323–329.
21. Bradley JD, Dehdashti F, Mintun MA, *et al*. Positron emission tomography in limited-stage small-cell lung cancer: A prospective study. *J Clin Oncol* 2004;22:3248–3254.
22. Niho S, Fujii H, Murakami K, *et al*. Detection of unsuspected distant metastases and/or regional nodes by FDG-PET [corrected] scan in apparent limited-disease small-cell lung cancer. *Lung Cancer* 2007;57:328–333.
23. van Loon J, Offermann C, Bosmans G, *et al*. ^{18}FDG-PET based radiation planning of mediastinal lymph nodes in limited disease small cell lung cancer changes radiotherapy fields: A planning study. *Radiother Oncol* 2008;87:49–54.
24. Spiro SG, James LE, Rudd RM, *et al*. Early compared with late radiotherapy in combined modality treatment for limited disease small-cell lung cancer: A London Lung Cancer Group multicenter randomized clinical trial and meta-analysis. *J Clin Oncol* 2006;24:3823–3830.
25. Blodgett T. Best practices in PET/CT: Consensus on performance of positron emission tomography-computed tomography. *Semin Ultrasound CT MR* 2008;29:236–241.
26. Lee YJ, Cho A, Cho BC, *et al*. High tumor metabolic activity as measured by fluorodeoxyglucose positron emission tomography is associated with poor prognosis in limited and extensive stage small-cell lung cancer. *Clin Cancer Res* 2009;15:2426–2432.
27. Liu HH, Wang X, Dong L, *et al*. Feasibility of sparing lung and other thoracic structures with intensity-modulated radiotherapy for non–small-cell lung cancer. *Int J Radiat Oncol Biol Phys* 2004;58:1268–1279.
28. Murshed H, Liu HH, Liao Z, *et al*. Dose and volume reduction for normal lung using intensity-modulated radiotherapy for advanced-stage non–small-cell lung cancer. *Int J Radiat Oncol Biol Phys* 2004;58:1258–1267.
29. Liu HH, Balter P, Tutt T, *et al*. Assessing respiration-induced tumor motion and internal target volume using four-dimensional computed tomography for radiotherapy of lung cancer. *Int J Radiat Oncol Biol Phys* 2007;68:531–540.
30. Kimura T, Togami T, Nishiyama Y, *et al*. Impact of incidental irradiation on clinically uninvolved nodal regions in patients with advanced non–small-cell lung cancer treated with involved-field radiation therapy: Does incidental irradiation contribute to the low incidence of elective nodal failure? *Int J Radiat Oncol Biol Phys* 2010;77:337–343.

HER2-positive breast cancer. Developing new treatment approaches in the early disease setting is not simple, and has been made more complicated by our recent successes. Conventional randomised adjuvant study designs require very large sample sizes when the expected outcome with standard therapy is quite favourable. In addition, these studies take many years to complete. An alternative to assessing promising new therapies in the adjuvant setting is to use preoperative study designs, as exemplified by Gianni and colleagues' study.[3] By using a surrogate endpoint—pCR—preoperative studies can be done much more rapidly and with far fewer patients than a typical adjuvant study. In addition, because patients who receive an investigational regimen in the preoperative setting can still receive standard of care therapy after surgery, the preoperative study design allows the assessment of novel targeted agents earlier in their development than would typically be possible in an adjuvant study. Preoperative study designs also provide a rich source of tumour tissue from which we can identify predictive biomarkers, assess pharmacodynamic properties of agents, and explore mechanisms of resistance in residual tumours. Together these features make the preoperative study design particularly well suited for assessing novel HER2-directed agents and combinations.

Nonetheless, despite the advantages of preoperative study designs, they remain inadequate for regulatory approval of new agents because there is no definitive evidence that differences in pCR will reliably translate into differences in long-term clinical outcome. The finding that ER-positive cancers have significantly lower rates of pCR than do ER-negative cancers, but generally have more favourable long-term disease control, indicates that the failure to obtain a pCR in a patient with an ER and HER2-positive tumour does not necessarily predict a particularly dire outcome. This observation highlights the need to develop better surrogate markers and underscores the importance of focusing on subgroups of patients with HER2-positive disease. Nevertheless, we believe that the preoperative setting holds great promise to identify early clinical signals, to interrogate tumour tissue for biomarkers that can predict treatment outcome, and ultimately for the purpose of drug approval. Large adjuvant studies continue to have a place in breast-cancer research, but they need to be complemented by innovative preoperative studies.

Ian Krop, Eric P Winer
Dana-Farber Cancer Institute, Boston, MA, USA
ikrop@partners.org

IK and EPW receive research support from Roche and Genentech.

1 Slamon D, Eiermann W, Robert N, et al. Adjuvant trastuzumab in HER2-positive breast cancer. *N Engl J Med* 2011; **365:** 1273–83.
2 Romond EH, Perez EA, Bryant J, et al. Trastuzumab plus adjuvant chemotherapy for operable HER2-positive breast cancer. *N Engl J Med* 2005; **353:** 1673–84.
3 Gianni L, Pienkowski T, Im Y-H, et al. Efficacy and safety of neoadjuvant pertuzumab and trastuzumab in women with locally advanced, inflammatory, or early HER2-positive breast cancer (NeoSphere): a randomised multicentre, open-label, phase 2 trial. *Lancet Oncol* 2012; **13:** 25–32.
4 Lee-Hoeflich ST, Crocker L, Yao E, et al. A central role for HER3 in HER2-amplified breast cancer: implications for targeted therapy. *Cancer Res* 2008; **68:** 5878–87.
5 Baselga J, Gelmon KA, Verma S, et al. Phase II trial of pertuzumab and trastuzumab in patients with human epidermal growth factor receptor 2-positive metastatic breast cancer that progressed during prior trastuzumab therapy. *J Clin Oncol* 2010; **28:** 1138–44.
6 Baselga J, Bradbury I, Eidtmann H, et al. First results of the NeoALTTO Trial (BIG 01-06 / EGF 106903): a phase III, randomized, open label, neoadjuvant study of lapatinib, trastuzumab, and their combination plus paclitaxel in women with HER2-positive primary breast cancer. San Antonio Breast Cancer Symposium; San Antonio, TX, USA Dec 8–12, 2010. S3–3.
7 Blackwell KL, Burstein HJ, Storniolo AM, et al. Randomized study of lapatinib alone or in combination with trastuzumab in women with ErbB2-positive, trastuzumab-refractory metastatic breast cancer. *J Clin Oncol* 2010; **28:** 1124–30.
8 Baselga J, Cortés J, Kim S-B, et al. Pertuzumab plus trastuzumab plus docetaxel for metastatic breast cancer. *N Engl J Med* 2011; published online Dec 8. DOI:10.1056/NEJMoa1113216.
9 Chang J, Mayer I, Forero-Torres A, et al. TBCRC 006: A multicenter phase II study of neoadjuvant lapatinib and trastuzumab in patients with HER2-overexpressing breast cancer. *Proc Am Soc Clin Oncol* 2011; **29:** abstr 505.

EGFR expression and the flexibility of FLEX

In *The Lancet Oncology*, Robert Pirker and colleagues[1] report on further analysis of the FLEX-study[2] where they calculate an immunohistochemistry score (H score) to provide a more detailed assessment of EGFR protein expression and how this affects response to treatment with cetuximab in patients with advanced non-small-cell lung cancer (NSCLC). The H score takes into account the percentage of cells (0–100%) in each intensity category (0–3+) and computes a final score, on a continuous scale between 0 and 300. Here,[1] a cutoff value of 200 was used to define high and low EGFR expressing groups. A similar immunohistochemistry scoring system (with a continuous scale between 0 and 400) for EGFR was introduced in 2003,[3] based on a

Published Online
November 4, 2011
DOI:10.1016/S1470-2045(11)70316-3

See Articles page 33

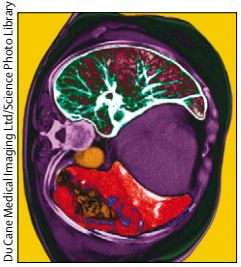
Du Cane Medical Imaging Ltd/Science Photo Library

prognostic discrimination for patients with early stage NSCLC. Patient's with high EGFR expression (score of ≥200) showed a trend to better prognosis without any systemic therapy. The FLEX study[2] compared chemotherapy with and without cetuximab as first-line treatment in patients with advanced NSCLC, who had tumours expressing even a minimum amount of EGFR (>1% cells). The study[2] showed better survival for the treatment with chemotherapy plus cetuximab (median survival 11·3 months *vs* 10·1 months, hazard ratio of death [HR] 0·87 [95% CI 0·76–1·00], p=0·04).[2] A similar study, the BMS-099 study,[4] in completely unselected patients with advanced NSCLC, did not show a significant outcome benefit with chemotherapy plus cetuximab (overall survival HR 0·89 [0·75–1·05]).[4] In both studies, the clinical benefit was marginal in these modestly selected or unselected patient populations.

The FLEX investigators refine their results by using a H score. In the original selection of patients to FLEX, 85% of them were eligible for therapy on the basis of EGFR screening. However, when using the H score, those patients categorised in the high-EGFR group comprised only 31% of the patients tested. The analyses for the group with EGFR expression above the cutpoint showed a median overall survival of 12·0 months (chemotherapy plus cetuximab) versus 9·6 months (HR 0·73 [95% CI 0·58–0·93], p=0·01). For caucasian patients with high EGFR (82%), the overall survival HR was 0·64 (0·49–0·83) with a survival difference of 3·5 months[5] in median overall survival in favour of chemotherapy plus cetuximab. In the adenocarcinoma subgroup, the median survival in the high EGFR-expressing group was 20·2 months for those given chemotherapy plus cetuximab versus 13·6 months for those given chemotherapy alone (HR 0·74 [0·48–1·14]). Thus, the H score assessment seems to help select a group of patients that might particularly benefit. Nearly 100% of the patients in the FLEX study had a H score assessment compared with 22% (148 of 676) of patients in the BMS-099.[6] However, both studies pointed in the same direction (BMS-099: high-EGFR group had overall survival HR of 0·93 *vs* 1·28 in low-EGFR group, and objective response in 40% of patients in high group *vs* 18% of those in low group).[6]

Several crucial questions remain about the reproducibility of the H score. Results from a reproducibility study were recently presented,[7] which showed that by training pathologists, reproducibility among different observers increased from a concordance of 76% (κ=0·52) to 91% (κ=0·81).[7] Thus, the H scoring system seems reproducible among pathologists after specific training.

Is further prospective validation of the FLEX findings necessary? Even if the H score system was prespecified in the FLEX study,[2] the cutoff value of 200 for high expression versus low expression was not. The use of the sub-population treatment effect pattern plot (STEPP) method, without a validation set, raises issues of reproducibility. This concern could be mitigated by showing that the cases of high versus low expression are reproducible at multiple sites and in multiple datasets. Therefore, further prospective validation is essential and is currently planned in a large ongoing prospective phase 3 study comparing chemotherapy with and without cetuximab (SWOG 0819 study). Whether automated assessment of EGFR protein-expression (ie, AQUA assessment),[8] or other digital quantitative scoring systems (ie, ACIS, APERIO, or LEICA) can improve the selection of patients for the use of cetuximab, or other EGFR antibodies, needs to be addressed in future studies.

Clearly, the use of targeted drugs requires specific criteria for patient selection based on the assessment of a molecular target. For patients with advanced NSCLC, we have now identified *EGFR* mutations (in 10% of caucasian patients) and anaplastic lymphoma kinase (*ALK*)-gene rearrangements (3%) as crucial determinants for EGFR tyrosine-kinase inhibitors and ALK-inhibitor therapies, respectively. Use of EGFR immunohistochemistry in the FLEX study seems to be an encouraging step towards personalised medicine for patient subgroups with advanced lung cancer who will potentially receive cetuximab.

**Fred R Hirsch, Roy S Herbst*
Departments of Medicine and Pathology, University of Colorado Cancer Center, Aurora, CO, USA (FRH); Department of Medicine, Yale Cancer Center, Smilow Cancer Hospital, New Haven, CT, USA (RSH)
fred.hirsch@ucdenver.edu

FRH has served as consultant to Merck Serono, Bristol-Myers Squibb, Lilly-Imclone, Pfizer, OSI/Roche/Genentech, Celgene, and Boehringer-Ingelheim. He is co-inventor of a University of Colorado owned patent, *Methods for prediction of clinical outcome to epidermal growth factor receptor inhibitors by cancer*, patent licensed to Abbot. RSH has served as a consultant for Bristol-Myers Squibb and OSI/Roche/Genentech.

1 Pirker R, Pereira JR, von Pawel J, et al. EGFR expression as a predictor of survival for first-line chemotherapy plus cetuximab in patients with advanced non-small-cell lung cancer: analysis of data from the phase 3 FLEX study. *Lancet Oncol* 2011; published online Nov 4. DOI:10.1016/S1470-2045(11)70318-7.

2 Pirker R, Pereira JR, Szczesna A, et al, on behalf of the FLEX Study Team. Cetuximab plus chemotherapy in patients with advanced non-small-cell lung cancer (FLEX): an open label randomised phase III trial. *Lancet* 2009; **373:** 1525–31.
3 Hirsch FR, Varella-Gracia M, Bunn PA Jr, et al. Epidermal growth factor receptor in non-small-cell lung carcinoma: correlation between gene copy number and protein expression and impact on prognosis. *J Clin Oncol* 2003; **21:** 3798–807.
4 Lynch TJ, Patel T, Dreisbach L, et al. Cetuximab and first-line taxane/carboplatin chemotherapy in advanced non-small-cell lung cancer: results of the randomized multicenter phase III trial BMS099. *J Clin Oncol* 2010; **28:** 911–17.
5 O'Byrne K, Paz-Ares L, Pereira JR, et al. Epidermal Growth Factor Receptor (EGFR) expression as a pedictive biomarker of survival in patients with advanced non-small cell lung cancer (NSCLC) receiving first-line therapy with cetuximab combined with chemotherapy in the FLEX Trial. The European Multidisciplinary Cancer Congress; Stockholm; Sept 23–27, 2011. Abstract 9000.
6 Lynch TJ, Bhagavatheeswaran P, Mukhopadhyay P, Khambata-Ford S, Harbison CT. A retrospective subgroup analysis of EGFR immunohistochemistry (IHC) expression by Histo-Score correlated to outcomes from the BMS099 1st line phase III NSCLC trial of cetuximab (cet) plus carbopalatin/taxane. The European Multidisciplinary Cancer Congress; Stockholm; Sept 23–27, 2011. Abstract 9001.
7 Ruschoff J, Kerr KM, Buttner R, et al. Round robin test to evaluate the reproducibility of a therapeutically relevant immunohistochemical score for the categorization of non-small cell lung cancer (NSCLC) into tumours with high and low epidermal growth factor receptor (EGFR) expression. The European Multidisciplinary Cancer Congress; Stockholm; Sept 23–27, 2011. Abstract 9002.
8 Mascaux C, Wynes MW, Kato Y, et al. EGFR protein expression in non-small cell lung cancer predicts response to an EGFR tyrosine kinase inhibitors—a novel antibody immunhistochemistry or AQUA technology. *Clin Cancer Res* 2011; published online Oct 12. DOI:10.1158/1078-0432.CCR-11-0209.

Hypofractionated radiotherapy for prostate cancer

Published **Online** December 13, 2011 DOI:10.1016/S1470-2045(11)70347-3

See **Articles** page 43

In radiobiology, the α-β ratio, defined as the dose at which killing of cells by linear (α) and quadratic (β) components are equal, is used to quantify the fractionation sensitivity of tissues and tumours. With data from low-dose-rate brachytherapy and external-beam radiotherapy series, Brenner and Hall[1] were the first to report a low α-β ratio of 1·5 for prostate cancer; many investigators have since recorded similar values (lower than those of surrounding normal tissues, such as the rectum and bladder). As a result, the hypofractionation approach to radiotherapy—ie, few, large doses—has potential therapeutic advantages for tissues with low α-β ratios and hence high radiation-fraction sensitivity.

In *The Lancet Oncology*, David Dearnaley and colleagues[2] report preliminary safety results from the conventional versus hypofractionated high-dose intensity-modulated radiotherapy in prostate cancer (CHHiP) randomised trial. CHHiP is an important multi-institutional trial comparing conventional 2 Gy fractions to a total of 74 Gy in 37 fractions with hypofractionated high-dose radiotherapy in 3 Gy fractions to totals of 60 Gy in 20 fractions or 57 Gy in 19 fractions. With a median follow-up of 50·5 months, both hypofractionation schedules were well tolerated without any increase in toxicity when compared with controls. These results are promising, but long-term toxicity outcomes and data for freedom from biochemical failure or recurrence of prostate cancer are awaited. Data for secondary endpoints, such as development of metastases, cause-specific and overall survival, quality of life, and health economics, will also be important.

Although an α-β ratio of less than two for prostate cancer is widely accepted, some reports suggest values of more than three.[3] Confounding factors for α-β ratio estimates are poorly matched groups, hypoxia, different definitions of biochemical failures, inaccurate assumptions, disease heterogeneity, high-grade disease, retrospective data, and insufficient follow-up. A prospective randomised trial such as CHHiP helps to establish the true α-β ratio for prostate cancer and thus could advance understanding of prostate-cancer biology. However, the use of hormonal therapy in this trial could be a potential confounding factor. Even if the α-β ratio of prostate cancer is not as low as 1·5, hypofractionation might be a viable option to reduce overall treatment duration without adverse toxic effects or reductions in effectiveness. A decrease of 3·5 weeks in overall treatment time (7·5 weeks for conventional group *vs* 3·8–4 weeks for hypofractionated groups) would have substantial effects on quality of life and health economics.

The first randomised trials of hypofractionation had moderate radiation doses of 64–66 Gy, which were below the standard-of-care radiation doses of 74–80 Gy.[2,4-6] So-called extreme hypofractionation has since been developed, and uses stereotactic body radiotherapy. This treatment uses five fractions of 6–10 Gy. However, follow-up for trials of such techniques is still short and no data from randomised trials are available. The CHHiP investigators used moderate hypofractionation, with three-dimensional conformal and intensity-modulated radiotherapy. Another three randomised trials have been undertaken in the USA[4,5] and Italy.[6] The control doses

Published OnlineFirst October 6, 2011; DOI:10.1158/1535-7163.MCT-11-0235

Molecular Medicine in Practice

Molecular Cancer Therapeutics

Akt/mTOR Counteract the Antitumor Activities of Cixutumumab, an Anti-Insulin–like Growth Factor I Receptor Monoclonal Antibody

Dong Hoon Shin[1], Hye-Young Min[3], Adel K. El-Naggar[2], Scott M. Lippman[1], Bonnie Glisson[1], and Ho-Young Lee[1,3]

Abstract

Recent reports have shown limited anticancer therapeutic efficacy of insulin-like growth factor receptor (IGF-1R)-targeted monoclonal antibodies (mAb), but the resistance mechanisms have not been completely identified. Because cooperation between epidermal growth factor receptor (EGFR) and IGF-IR could cause resistance to inhibitors of individual receptor tyrosine kinases, we investigated the involvement of EGFR signaling in resistance to IGF-1R mAb and the underlying mechanisms of action. Most head and neck squamous cell carcinoma (HNSCC) tissues had coexpression of total and phosphorylated IGF-1R and EGFR at high levels compared with paired adjacent normal tissues. Treatment with cixutumumab (IMC-A12), a fully humanized IgG1 mAb, induced activation of Akt and mTOR, resulting in *de novo* synthesis of EGFR, Akt1, and survivin proteins and activation of the EGFR pathway in cixutumumab-resistant HNSCC and non–small cell lung cancer (NSCLC) cells. Targeting mTOR and EGFR pathways by treatment with rapamycin and cetuximab (an anti-EGFR mAb), respectively, prevented cixutumumab-induced expression of EGFR, Akt, and survivin and induced synergistic antitumor effects *in vitro* and *in vivo*. These data show that resistance to IGF-1R inhibition by mAbs is associated with Akt/mTOR-directed enhanced synthesis of EGFR, Akt1, and survivin. Our findings suggest that Akt/mTOR might be effective targets to overcome the resistance to IGF-1R mAbs in HNSCC and NSCLC. *Mol Cancer Ther; 10(12); 2437–48. ©2011 AACR.*

Introduction

Head and neck squamous cell carcinoma (HNSCC) is the fifth most common malignancy, and non–small cell lung cancer (NSCLC) is the leading cause of cancer-related death (1). Despite decades of research and treatment advances, the 5-year survival rates for both have improved little, and local and distant metastases remain significant barriers to disease eradication (2). Recent advances in developing molecularly targeted cancer therapeutic agents that block specific receptors or signaling proteins may lead to promising new treatments for these cancers.

Authors' Affiliations: Departments of [1]Thoracic/Head and Neck Medical Oncology and [2]Pathology, The University of Texas MD Anderson Cancer Center, Houston, Texas; and [3]College of Pharmacy, Seoul National University, Seoul, Republic of Korea

Note: Supplementary data for this article are available at Molecular Cancer Therapeutics Online (http://mct.aacrjournals.org/).

Corresponding Author: Ho-Young Lee, College of Pharmacy, Seoul National University, 599 Gwanak-ro, Gwanak-gu, Seoul 151-742, Republic of Korea. Phone: 82-2-880-9277; Fax: 82-2-6280-5327; E-mail: hylee135@snu.ac.kr

doi: 10.1158/1535-7163.MCT-11-0235

The insulin-like growth factor (IGF) axis plays a pivotal role in regulating tumor cell growth, differentiation, tumor angiogenesis, metastasis, apoptosis, and MDR (3). The IGF axis is composed of ligands, receptors, and IGF-binding proteins (4). The balance between expression and activity of these molecules is tightly controlled under normal physiologic conditions; changes in this balance can cause numerous molecular events that can ultimately lead to malignancy (5). Increased IGF-1 receptor (IGF-1R) and circulating IGF-1 expression is associated with an elevated risk for numerous cancer types and rapid disease progression, including HNSCC and NSCLC (6, 7). Increased bioactive IGF-II levels also result from reduced expression of IGF-binding protein or inactivation of the type 2 IGF receptor that mediates IGF-II degradation (8, 9). These changes can result in high local IGF tissue concentrations. In addition, the binding of IGFs to IGF-IR initiates conformational changes, transmembrane receptor tyrosine kinase (RTK) autophosphorylation, and Ras-Raf-mitogen–activated protein kinase and phosphoinositide 3-kinase (PI3K)/AKT signaling cascade activation, leading to the phosphorylation of several downstream substrates that are involved in cell proliferation, survival and apoptosis, inflammation, genomic instability, and angiogenesis (3). Thus, IGF-1R signaling has been considered as a promising target for cancer therapy. Indeed, IGF-1R inactivation by gene

Published OnlineFirst October 6, 2011; DOI:10.1158/1535-7163.MCT-11-0235

disruption, antisense oligonucleotides, neutralizing antibodies, dominant-negative mutants, small molecule IGF-IR kinase inhibitors, and IGF-binding proteins has resulted in antitumor activity (10). However, several clinical trials with anti–IGF-1R monoclonal antibodies (mAb) have shown modest therapeutic efficacy in clinical trials, and the mechanisms involved in resistance to the drug have not been clearly defined. In a previous study, IGF and epidermal growth factor (EGF) stimulation both resulted in a physical association between the two receptors in a TU159 HNSCC cell line protein complex (7). We and others have shown cross-talk between RTKs of EGF receptor (EGFR) and IGF receptor, wherein a inhibition of tyrosine kinase inhibitor (TKI) of one RTK is compensated by enhanced activity of the reciprocal RTK; thus, one suspected IGF-1R resistance mechanism is cross-talk with EGFR or other kinase receptors (11–13). However, to our knowledge, the involvement of the EGFR pathway in resistance to IGF-1R mAb-based anticancer therapy has not been defined. In this article, we report that inhibition of the IGF-1R pathway by cixutumumab (IMC-A12), a fully humanized IgG1 mAb (14), results in stimulation of the Akt/mTOR pathway through increasing synthesis of EGFR, Akt1, and antiapoptotic survivin proteins. In addition, suppression of mTOR-mediated protein synthesis or inactivation of EGFR renders cixutumumab-resistant cells sensitive to the drug. These results present a drug resistance mechanism of an IGF-1R–targeted agent as well as molecular targets to restore its antitumor activity.

Materials and Methods

Cell culture and reagents

All human HNSCC (SqCC/Y1, HN30, LN686, FADU, UMSCC1, UMSCC2, UMSCC4, UMSCC6, UMSCC11A, UMSCC14A, UMSCC38, TR146, and OSC19) were kindly provided by Dr. Jeffrey Myers (MD Anderson Cancer Center, Houston, TX). NSCLC (H226Br, H226B, H596, H460, A549, and H1299) cell lines were kindly provided by Jack Roth (Department of Thoracic and Cardiovascular Surgery, the University of Texas MD Anderson Cancer Center, Houston, TX) or purchased from the American Type Culture Collection. Cells were cultured in DMEM, Ham's F12 or RPMI 1640 medium supplemented with 10% FBS (Life Technologies, Inc.). Cells were validated by analysis of their short tandem repeat profile. We used specific antibodies against the following antigens: phospho-Akt (pAkt, S473), Akt, Akt1, Akt2, Akt3, pIGF-1R (Y1131), pmTOR (S2248), mTOR, pEGFR (Y1068), EGFR, PARP, cleaved caspase-3, survivin (Cell Signaling Technology), IGF-1Rβ, pERK (T202/204), and ERK (Santa Cruz). Rapamycin was purchased from MBL International Corporation. Cixutumumab and C225 [cetuximab (Erbitux)] were provided by Imclone Systems, Inc.

Cell viability assay

Poly-HEMA (poly-2-hydroxyethyl methacrylate)-coated plates (PCP) were prepared as previously described (15). For the cell viability assay, 2×10^3 cells were plated on 96-well PCPs or ultralow attached plates (UAP). After 3 days of drug treatment, cell proliferation was measured with the MTT and the MTS assay. Six replicate wells were used for each analysis; at least 3 independent experiments were conducted.

Reverse transcriptase PCR

Total RNA was isolated and reverse transcriptase PCR (RT-PCR) was done as described elsewhere (12), using the following primer sequences: (sense) 5′-GGAGAACTGCCAGAAACTGACC-3′ and (antisense) 5′-GCCTGCAGCACACTGGTTG-3′ for EGFR; (sense) 5′-AGCGACGTGGCTATTGTGAAG-3′ and (antisense) 5′-GCCGCCAGGTCTTGATGTAC-3′ for Akt1; and (sense) 5′-CCTCTATGCCAACACAGTGC-3′ and (antisense) 5′-CATCGTACTCCTGCTTGCTG-3′ for (beta-actin). The following thermocycler conditions were used for amplification: 94°C for 6 minutes (hot start), followed by 28 to 33 cycles of 94°C for 45 seconds, 56°C to 60°C for 45 seconds, and 72°C for 1 minute.

Metabolic labeling

Metabolic labeling was done as described elsewhere (12). Briefly, LN686 cells were treated with cixutumumab (25 μg/mL) in the presence of rapamycin (1 μmol/L) for 72 hours and incubated with medium lacking methionine and cysteine for 1 hour. The cells were labeled with [^{35}S] methionine-cysteine and cixutumumab and harvested at the indicated time points. Equal amounts of protein were used for immunoprecipitation with antibodies against EGFR, Akt1, Akt2, and Akt3, and the immunoprecipitates were separated by SDS-PAGE. Laser densitometry was done to quantify the band intensity.

Western blot analysis

We carried out a biochemical analysis of 8 head and neck tumor and 8 healthy adjacent tissue specimens from patients with head and neck cancer who had undergone surgical resection at The University of Texas MD Anderson Cancer Center (Houston, TX). This study was approved by the MD Anderson Cancer Center institutional review board. All tissue specimens had been frozen in liquid nitrogen immediately after being resected. Total protein isolation and Western blot analysis were done as described previously (12).

Soft agar assays

An anchorage-independent colony formation assay was done as previously described (12). To determine the effect of the combined drug treatment, we estimated potentiation by multiplying the percentage of cells remaining (% growth) for each agent. The classification index was calculated as described previously (16).

Caspase-3/CPP32 colorimetric assay

Caspase-3/CPP32 activity was determined as described elsewhere (17) using cells that had been treated

Published OnlineFirst October 6, 2011; DOI:10.1158/1535-7163.MCT-11-0235

with cixutumumab, rapamycin, C225, or their combinations for 3 days. Fold-increase in CPP32 activity was determined by comparing these results with the level of the uninduced control. Six replicate wells were used for each analysis; at least 3 independent experiments were done.

In vivo model

All animal procedures were done in accordance with a protocol approved by the MD Anderson Institutional Animal Care and Use Committee. Xenograft tumors were generated by subcutaneously injecting nude mice with 1×10^6 of LN686 cells. When tumors reached a volume of 80 to 100 mm^3 (termed day 0 for our experiments), we treated control mice with an intraperitoneal injection of sterile PBS and xenografted mice with cixutumumab (10 mg/kg, once a week), C225 (10 mg/kg, once a week), and rapamycin (5 mg/kg, daily); cixutumumab and C225 (10 mg/kg each, once a week); or cixutumumab (10 mg/kg, once a week) and rapamycin (5 mg/kg, daily). Tumor volumes were measured every 3 days.

Statistical analysis

The data acquired from the MTT assay were analyzed using Student *t* test. All means and 95% CIs from 8 samples were calculated using Microsoft Excel software (Microsoft Corporation). Statistical significance of differences in tumor growth in the combination treatment group and in the single-agent treatment groups were analyzed by ANOVA. All means from triplicate to 8 samples and 95% CIs were calculated using SAS software (release 8.02; SAS Institute). In all statistical analyses, 2-sided *P* values of less than 0.05 were considered statistically significant.

Results

IGF-1R and pIGF-1R expressions in human HNSCC tissue

To have the rationale to target both IGF-1R and EGFR signalings, we determined total and phosphorylated IGF-1R and EGFR expression levels in HNSCC tissue. Seven (#1–7) of the 8 tumor specimens had high levels of IGF-1R and phosphorylated IGF-1R (pIGF-1R) expression, and all of the tumor specimens had high levels of EGFR and phosphorylated EGFR (pEGFR) expression compared with normal tissue specimens from the same patients (Fig. 1). All of the specimens with high levels of IGF-1R and pIGF-1R expressions also had higher levels of pEGFR and EGFR expression than did normal tissue. These findings indicated coexpression and coactivation of IGF-1R and EGFR at high levels in HNSCC, suggesting the potential value of cotargeting the IGF-1R and EGFR pathways.

Resistance to cixutumumab-induced growth inhibition is correlated with EGFR/PI3K/AKT pathway activation in HNSCC and NSCLC cells grown in a 3-dimensional mimic environment

Several studies have reported the difference of cellular responses in a 3-dimensional (3D) environment and the higher sensitivities of a number of cancer cell lines to certain anticancer drugs in 3D culture systems compared with the response of the same cell lines grown in monolayers (18–20). Hence, we determined effects of cixutumumab on HNSCC cells grown on poly-HEMA-coated plates (PCP) and UAPs, known as 3D-mimetic culture systems. Cells cultured under the conditions grew and formed spherical colonies. Representative results from LN686 and OSC19 cells grown in PCPs and UAPs are shown (Fig. 2A). Cixutumumab treatment completely inhibited 10% FBS or IGF induced, but not insulin induced, IGF-1R phosphorylation (Fig. 2A, bottom and Supplementary Fig. S1), indicating that only IGF-1R–mediated signaling could participate in the action of cixutumumab. We then carried out an MTS assay on 13 HNSCC and 6 NSCLC cell lines in 10% FBS with or without cixutumumab for 72 hours. We observed differential sensitivity of tested cells to cixutumumab treatment, and 2 HNSCC (UMSCC38 and OSC19) and NSCLC (H1299 and A549m) cell lines had more than 60% inhibition in viability (Fig. 2B). Consistent with the results in cells grown on PCPs, cixutumumab treatment strongly suppressed the growth of UMSCC38, OSC19, H1299, and A549m cells in UAPs, whereas the remaining cells showed moderate responses to treatment (Fig. 2C). These results

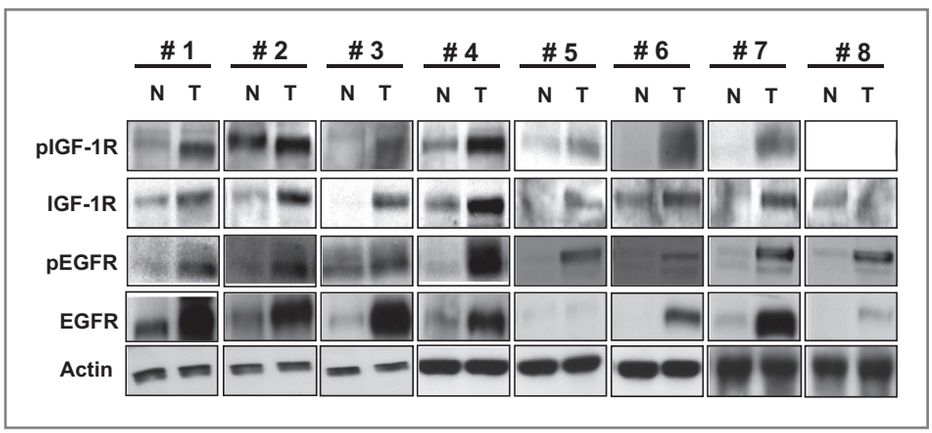

Figure 1. The activities and expression of IGF-1R and EGFR in paired squamous cell carcinoma and normal tissue specimens from patients with HNSCC. Proteins were extracted from HNSCC and healthy normal tissue and subjected to Western blot analysis to determine expressions of total and phosphorylated IGF-1R and EGFR. N, normal; T, tumor.

Published OnlineFirst October 6, 2011; DOI:10.1158/1535-7163.MCT-11-0235

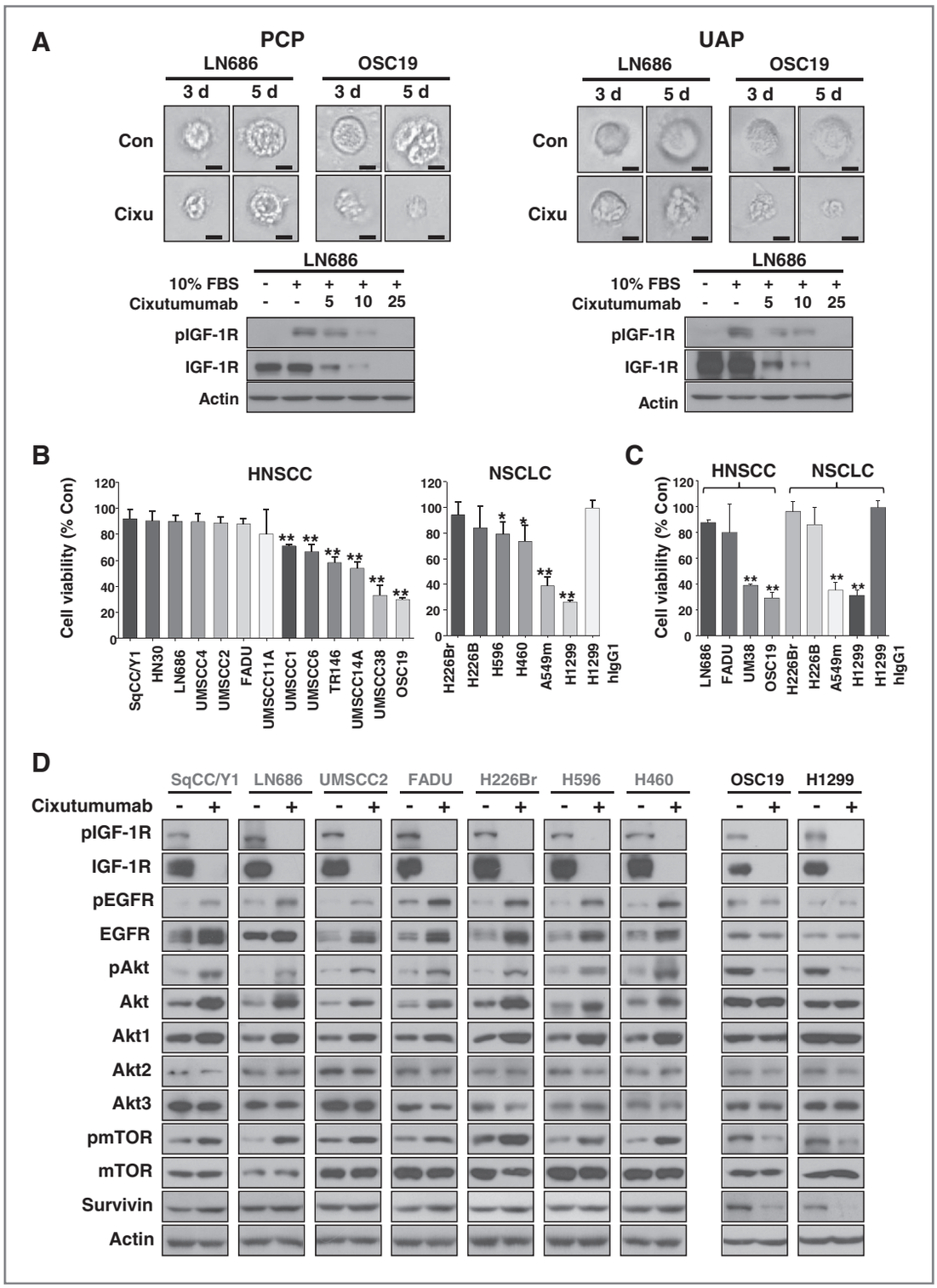

Figure 2. HNSCC and NSCLC cell lines display differential sensitivities to cixutumumab in the 3D mimic condition. Indicated HNSCC and NSCLC cells cultured in poly(HEMA)-coated plates (PCP) and in ultralow attached plates (UAP) were treated with hIgG$_1$ (25 μg/mL) or IMC-cixutumumab (25 μg/mL) for 3 (A, C, and D) or 5 days (B) in the presence of FBS or for 6 hours in the absence of FBS and then stimulated with 10% FBS for 30 minutes (A, bottom). A, representative morphologies of LN686 and OSC19 cells (Con, control; Cixu, cixutumumab). A (bottom) and D, Western blot was done for the indicated proteins. B and C, cell viabilities were measured by using MTS assay and were determined as percentages of each control groups. Independent experiments were repeated 3 times. Bars represent mean ± SD ($n = 6$); *, $P < 0.05$ and **, $P < 0.01$. The statistical significance was determined by using Student t test.

Published OnlineFirst October 6, 2011; DOI:10.1158/1535-7163.MCT-11-0235

suggest that antitumor effects of cixutumumab are limited to specific HNSCC and NSCLC cell lines.

We investigated the mechanisms involved in cixutumumab resistance in HNSCC and NSCLC cells. Because we did not find obvious difference between the results from PCP and UAP, additional studies were done in PCP, as a representative of 3D-mimic 2D system. We correlated total (Supplementary Fig. S2A) and phosphorylated IGF-1R and EGFR (Supplementary Fig. S2B) with resistance to cixutumumab and found no obvious correlation between them. Furthermore, IGF-1R mRNA levels were not changed after the drug treatment (data not shown). However, cixutumumab increased phosphorylation of EGFR and its downstream mediators, including Akt and mTOR, in all cixutumumab-resistant HNSCC (SqCC/Y1, LN686, UMSCC2, and FADU) and NSCLC (H226Br, H596, and H460) cell lines, but not in cixutumumab-sensitive HNSCC (OSC19) and NSCLC (H1299) cell lines after 3 days of treatment (Fig. 2D). Of note, cixutumumab-resistant cell lines had increased EGFR and Akt1 levels, with no changes in Akt2 and 3, suggesting that activation of the EGFR pathway could have been due to the increased expressions of EGFR and Akt1. Cixutumumab-resistant cells also showed slightly increased level of survivin expression, a member of inhibitor of apoptosis proteins known to decrease the sensitivity of tumor cells to chemotherapeutic drugs (21). In contrast, cixutumumab-sensitive lines showed obviously decreased levels of survivin. These findings suggest that induced expression of EGFR, Akt1, and survivin protein provide cixutumumab-resistant cell lines with ability to proliferate after the drug treatment.

mTOR pathway induces *de novo* EGFR and Akt protein synthesis

We assessed the mechanisms of cixutumumab-mediated increase in EGFR and Akt1 protein expression using LN686 and FADU cells grown in PCPs. No detectable changes were observed in EGFR and Akt1 mRNA levels (Fig. 3A), suggesting cixutumumab-induced posttranscriptional upregulation of EGFR and Akt expressions in the drug-resistant cells. Therefore, we monitored the kinetics of cixutumumab-induced phosphorylation of EGFR, Akt, and mTOR in cixutumumab-resistant LN686 cells. Cixutumumab (25 μg/mL) induced decreases in pIGF-1R, pAkt, and pERK1/2 levels as early as 30 minutes after treatment (Fig. 3B). However, pAkt induction was evident after 1 hour of cixutumumab treatment, followed by delayed increases in pEGFR and survivin expressions after 1 day. Obvious increases in EGFR and Akt1 protein expressions were observed after 3 days treatment of the drug. Given the role of Akt/mTOR pathway in protein synthesis, we determined effects of cixutumumab on EGFR and Akt1 protein synthesis rates by metabolically labeling LN686 cells with [^{35}S] Met-Cys. As shown in Fig. 3C, the [^{35}S]-labeled EGFR and Akt1 synthesis rate was remarkably higher in cixutumumab-treated LN686 cells than in untreated cells. In contrast, Akt2 and Akt3 protein synthesis was not detectably affected by cixutumumab treatment. We further confirmed cixutumumab-induced *de novo* synthesis of EGFR and Akt1 proteins was prevented by combined treatment with rapamycin, an mTOR inhibitor. Together, these findings suggest that inhibition of cixutumumab of IGF-1R signaling resulted in initial activation of the Akt/mTOR pathway followed by increased synthesis of EGFR and Akt proteins, leading to activation of the EGFR pathway in cixutumumab-resistant cells.

Cotargeting IGF-1R and mTOR or EGFR enhances antitumor activity of cixutumumab in cixutumumab-resistant cells

We next asked whether increased AKT/mTOR activity compensates for loss of IGF-1R signaling by increasing EGFR and Akt1 protein synthesis and thus EGFR signaling activation. To this end, we tested the effects of single or combined treatment with cixutumumab and rapamycin, an mTOR inhibitor on proliferation of cixutumumab-resistant cells grown in PCPs. Rapamycin (1 μmol/L) induced a complete suppression of 10% FBS-induced phosphorylation of mTOR after 6 hours of treatment (Supplementary Fig. S3A) and significant decrease in cell proliferation after 3 days treatment (Supplementary Fig. S3B). The rapamycin treatment inhibited mTOR and $p70^{S6K}$ phosphorylation in both cixutumumab-resistant (LN686, SqCC/Y1) and cixutumumab-sensitive (OSC19, H1299) cells (Fig. 4A). Rapamycin is known as an allosteric inhibitor of mTORC1 (22), and p70S6 kinase is a major effector of the of mTOR phosphorylation (Ser2448; ref. 23), suggesting that inactivation of p70S6 kinase by rapamycin via mTOR regulation led to dephosphorylation of mTOR. Synergistic antiproliferative effect was found in cixutumumab-resistant cells treated with cixutumumab and rapamycin combination compared with those treated with each single agent (Fig. 4B and Supplementary Table S1). Moreover, the cotreatment showed significantly enhanced caspase-3/CPP32 activity and PARP and caspase-3 cleavages in these cells (Fig. 4C). Treatment with rapamycin also prevented cixutumumab-induced increases in EGFR and Akt. The cotreatment suppressed basal as well as cixutumumab-induced upregulation of pEGFR, survivin, pAkt, and pmTOR expressions with no detectable impact in protein levels of mTOR in these cells (Fig. 4D), suggesting that inactivation of mTOR inhibits cixutumumab-induced activation of Akt/mTOR pathway and *de novo* EGFR and Akt protein expressions, resulting in restoration of apoptotic activity of cixutumumab in the drug-resistant cell lines.

We next tested the effects of single or combined treatment with cixutumumab and C225, an EGFR-neutralizing antibody, on proliferation of cixutumumab-resistant cells grown in PCPs. C225 treatment (25 μg/mL) induced a complete suppression of 10% FBS- or EGF (100 ng/mL)-stimulated EGFR phosphorylation after 6 hours (Supplementary Fig. S4A) and a significant decrease in cell proliferation after 3 days of treatment (Supplementary

Published OnlineFirst October 6, 2011; DOI:10.1158/1535-7163.MCT-11-0235

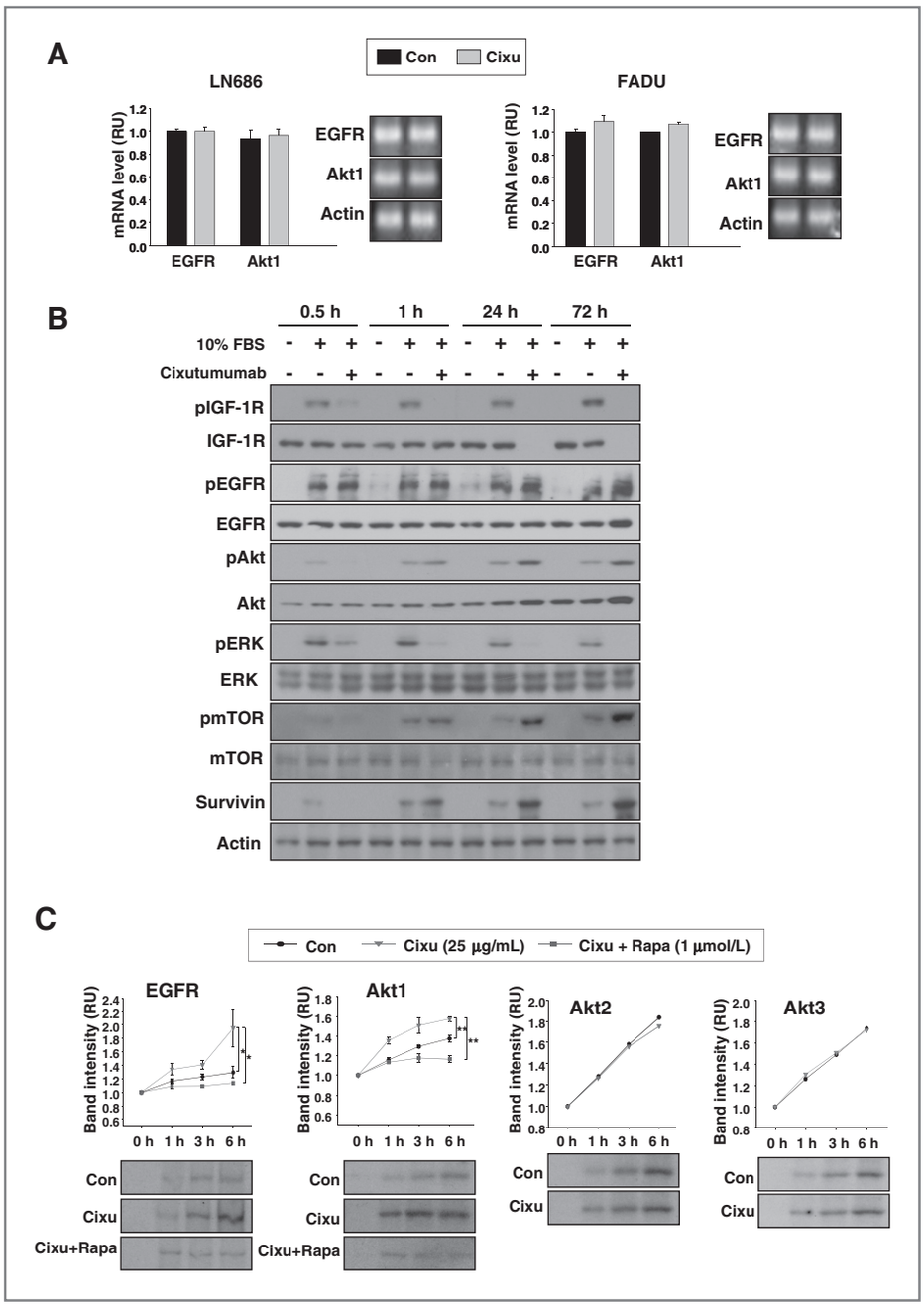

Figure 3. Cixutumumab induced the activities and expression levels of EGFR and Akt is through mTOR-mediated protein synthesis. A, RT-PCR analysis of LN686 and FADU cells grown in PCPs in the presence of vehicle (Con) or cixutumumab (Cixu) for 3 days. B, LN686 cells grown in PCP were treated with cixutumumab in the absence of FBS for indicated time period and then stimulated with 10% FBS for 30 minutes before harvest. The indicated proteins were detected by Western blot analysis. C, LN686 cells grown in PCP in the presence of vehicle (Con) or cixutumumab (Cixu) with or without rapamycin (Rapa) or 3 days were metabolically pulse-labeled with *trans* ^{35}S-methionine and cysteine and then chased with media containing methionine and cysteine for the indicated time periods. Immunoprecipitation was done using antibodies against EGFR, Akt1, Akt2, and Akt3. Densitometry was done to quantify the density of each band compared with that at time 0 hour. Student *t* test, average ± SD; $n = 3$. *, $P < 0.05$ and **, $P < 0.01$. RU, relative unit.

Fig. S4B). The C225 treatment led to decreases in pEGFR, EGFR, and pAkt expressions in both cixutumumab-resistant and cixutumumab-sensitive NSCLC and HNSCC cells, with no effects on pIGF-1R, IGF-1R, and IR expressions (Fig. 5A). The addition of C225 prevented a cixutumumab-induced increase in EGFR and Akt protein expressions in cixutumumab-resistant cells (Fig. 5B). Furthermore, the C225 treatment completely blocked cixutumumab-induced phosphorylation of EGFR, Akt, and mTOR in the presence of FBS (Fig. 5B) or IGF-1 (Supplementary Fig. S5). Combined treatment with cixutumumab and C225 induced synergistically enhanced antiproliferative activities (Fig. 5C, top, Supplementary Table S1) with increased apoptosis, as shown by increased caspase-3/CPP32 activity (Fig. 5C, bottom) and PARP cleavage (Fig. 5B, Supplementary Fig. S4), indicating that reduced cell viability by the cotreatment was due to increased cell death. We also observed that cixutumumab-resistant cells grown in soft agar showed synergistically increased sensitivity to the cotreatment than to the single treatment (Fig. 5D, Supplementary Table S2). Enhanced apoptosis was also observed after cotreatment with cixutumumab

Published OnlineFirst October 6, 2011; DOI:10.1158/1535-7163.MCT-11-0235

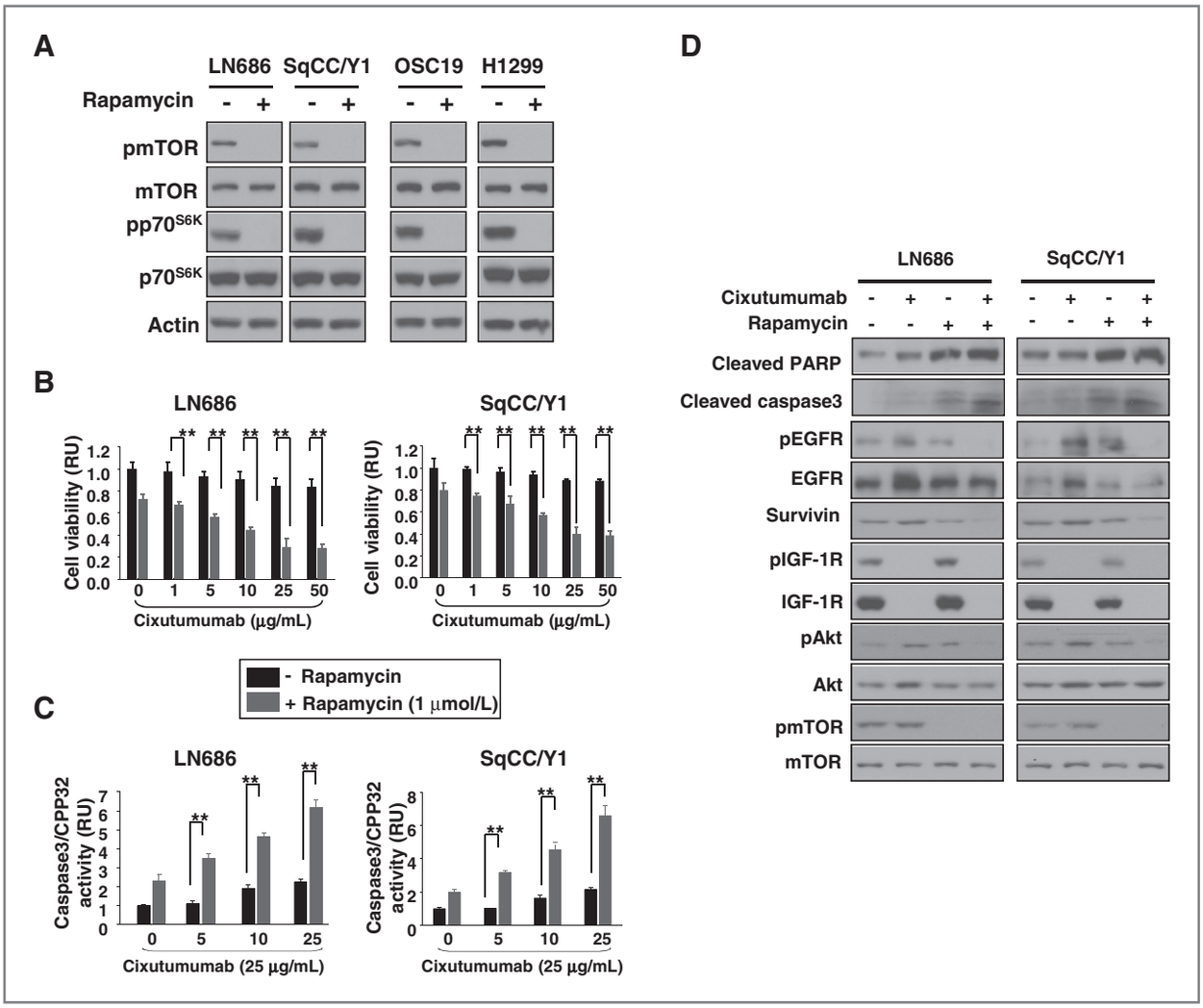

Figure 4. The combination between cixutumumab and rapamycin exhibits synergistic effects on cell viability and caspase-3 activity in HNSCC. A, Western blot on the regulation of mTOR and p70S6K by rapamycin treatment in cixutumumab-resistant (LN686 and SqCC/Y1) and cixutumumab-sensitive (OSC19 and H1299) cells. Cells were treated with vehicle (Con) or rapamycin for 3 days in PCPs and stimulated with 10% FBS for 30 minutes. B and C, LN686 and SqCC/Y1 cells grown in PCP were treated with cixutumumab in the presence (gray columns) or absence (black columns) of rapamycin for 3 days and then cell viability and caspase-3/CPP32 activity was measured. Student *t* test, average ± SD; $n = 6$. **, $P < 0.001$. RU, relative unit. D, LN686 and SqCC/Y1 cells were treated with cixutumumab, rapamycin, or their combination in PCPs for 3 days and stimulated with 10% FBS. Cell lysates were analyzed by Western blot.

with LY294002 (PI3K/Akt inhibitor) or erlotinib (an EGFR TKI; Supplementary Fig. S6). These findings suggest that, when the IGF-1R pathway is inactivated by cixutumumab, the Akt/mTOR pathway–derived EGFR activation by the drug provides an alternative proliferation or survival signaling.

Effects of cixutumumab, C225, rapamycin, and their combinations on the growth of cixutumumab-resistant HNSCC xenograft tumors

To determine whether EGFR and mTOR signaling inhibition enhances antitumor activity of cixutumumab *in vivo*, we tested the effects of cixutumumab, rapamycin, and C225 alone or in combination on the growth of cixutumumab-resistant LN686 xenograft tumors established in nude mice. Single treatment of cixutumumab with 10 mg/kg (once a week; Fig. 6A, left) or with higher doses (25 or 50 mg/kg, twice a week; data not shown) showed modest effects on the tumor growth. Significant smaller tumors were found in mice treated with cixutumumab and rapamycin or C225 than those in control mice and in mice treated with single agent alone (Fig. 6A). Cixutumumab treatment alone or in combination with rapamycin did not exhibit significant toxic effects, including weight loss (data not shown). Western blot analysis on the tumor tissues revealed that Akt, mTOR, and EGFR activity was effectively blocked by combined treatment with cixutumumab and rapamycin, or with cixutumumab and C225 (Fig. 6B). In addition, cixutumumab and C225 or rapamycin led to increased levels of terminal

Published OnlineFirst October 6, 2011; DOI:10.1158/1535-7163.MCT-11-0235

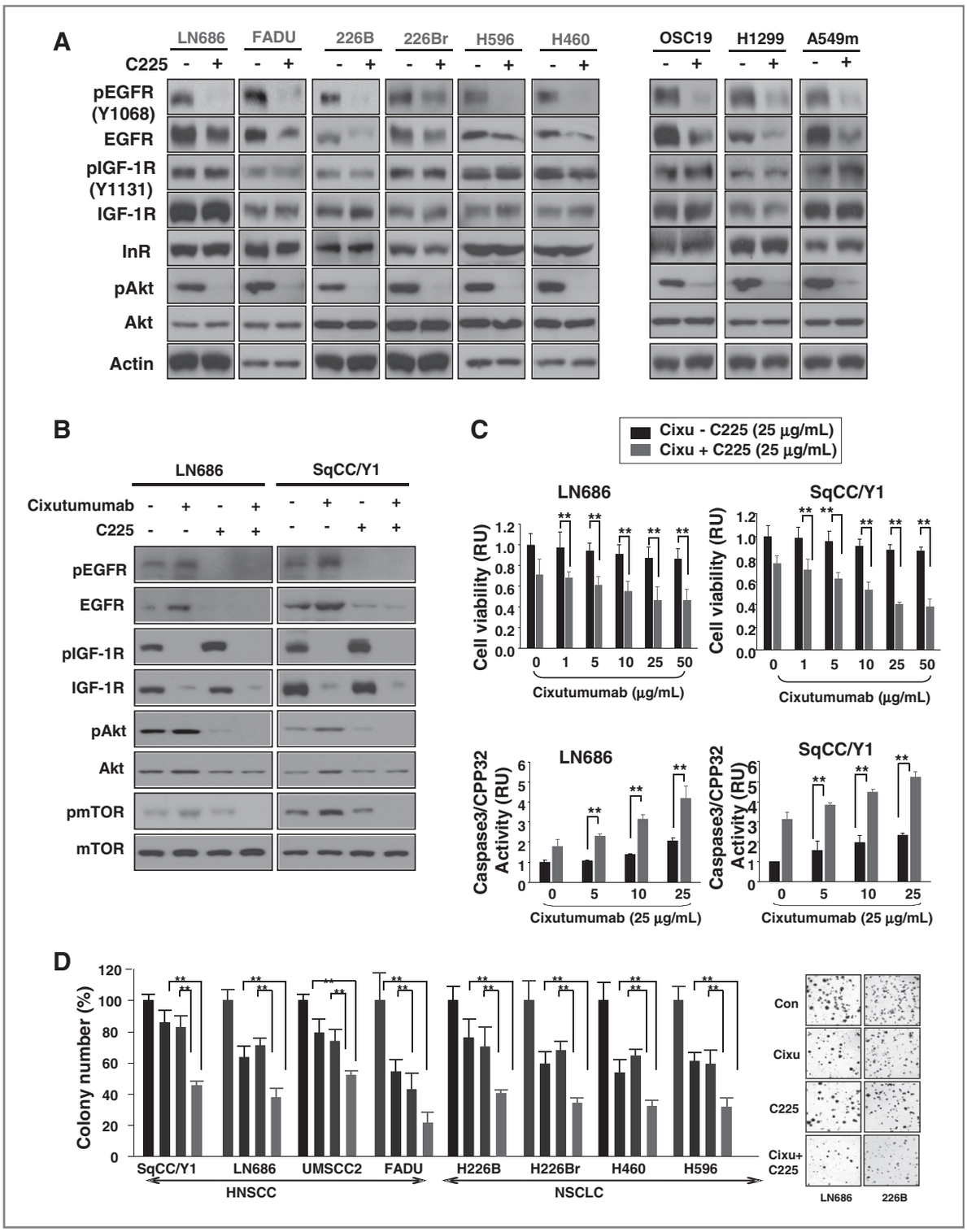

Figure 5. The cotreatment with cixutumumab and C225 exerts synergistic effects on colony formation and caspase-3 activity. A and B, Western blot on the indicated cixutumumab-resistant and cixutumumab-sensitive cells treated with vehicle (−), C225, cixutumumab, or their combination for 3 days and stimulated with 10% FBS. C, viability and caspase-3/CPP32 activity were measured in the indicated cells grown in PCPs with indicated doses of cixutumumab in the presence (gray columns) or absence (black columns) of C225 for 3 days. Student *t* test, average ± SD; $n = 6$. **, $P < 0.001$. RU, relative unit. D, the indicated cell lines grown in soft agar were treated with cixutumumab, C225, or their combination. Colonies were stained and then counted. Student *t* test, average ± SD; $n = 6$. *, $P < 0.05$ and **, $P < 0.01$ (left). Representative images are shown in the right.

Published OnlineFirst October 6, 2011; DOI:10.1158/1535-7163.MCT-11-0235

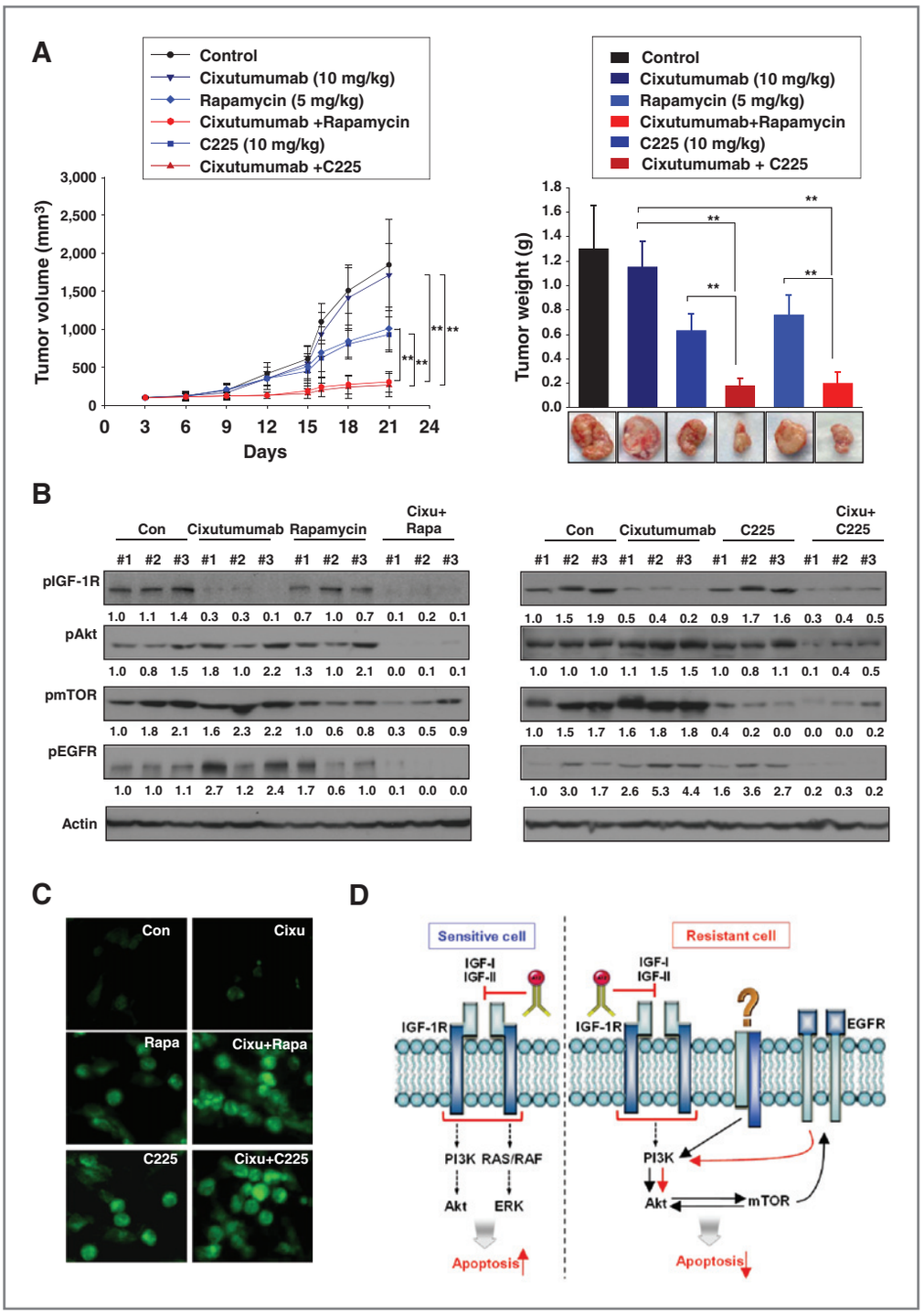

Figure 6. The cotargeting IGF-1R and mTOR or EGFR exhibits potent antitumor properties *in vivo* in HNSCC. A, mice bearing LN686 xenograft tumors were administrated with vehicle (control), cixutumumab, C225, rapamycin, or their combination. Tumors were measured every 3 days. Results are expressed as mean tumor volume (calculated from 8 mice) relative to the tumor volume at day 0. Student *t* test, average ± SE; $n = 8$. *, $P < 0.05$ and **, $P < 0.001$. B, Western blot analysis on the expression of pAkt, pEGFR, pmTOR, and actin. C, TUNEL staining of the xenografts tissues. D, schematic model of resistance mechanism to cixutumumab.

deoxynucleotidyl transferase–mediated dUTP-biotin nick-end labeling (TUNEL) staining (Fig. 6C). These findings suggest that combined treatment with cixutumumab and rapamycin or C225 enhances *in vivo* antitumor activity by decreasing cixutumumab-induced Akt, mTOR, and EGFR activity and by inducing apoptosis.

Published OnlineFirst October 6, 2011; DOI:10.1158/1535-7163.MCT-11-0235

Discussion

In this study, we show that (i) blocking IGF-1R signaling by cixutumumab induces activation of EGFR signaling in cixutumumab-resistant HNSCC and NSCLC cells through Akt/mTOR-mediated *de novo* synthesis of EGFR and Akt1, leading to activation of the EGFR pathway; (ii) activation of the Akt/mTOR pathway also results in induction of survivin protein expression, contributing to increase in antiapoptotic potential in the cixutumumab-resistant cells; and (iii) blocking the mTOR or EGFR signaling pathway restores proapoptotic activity of cixutumumab in HNSCC cells, both *in vitro* and *in vivo* (Fig. 6D). These results provide a first mechanistic evidence for a cross-talk between the IGF-1R and the EGFR signaling pathways as a consequence of cixutumumab-mediated inactivation of the IGF-1R signaling. Overall, these findings suggest that Akt/mTOR-mediated synthesis of proteins involved in cell proliferation and survival is involved in resistance of HNSCC and NSCLC cells to anti–IGF-IR mAbs, indicating the potential clinical use of cotargeting IGF-IR and mTOR as well as cotargeting IGF-1R and EGFR in patients with HNSCC or NSCLC.

IGF-1R- and IGF-1R/IR-targeting drug candidates, which are mainly composed of anti–IGF-1R mAbs and small molecule inhibitors, have shown a variety of antitumor activities in several preclinical studies (24, 25). However, the clinical response rates to IGF-1R mAbs, alone and with chemotherapeutic agents, have been lower than expected (26). To develop effective anticancer therapeutic strategies with anti–IGF-1R mAbs, we determined the mechanisms that induce primary resistance to the anti–IGF-1R mAb cixutumumab, a fully humanized IgG1 mAb that is being clinically evaluated for the treatment of several cancers, including HNSCC and NSCLC (14, 26). It has been suggested that activation of the IGF-IR pathway after EGFR TKI treatment counteracted the antitumor activity of drugs in several cancer cell types (11–13). Conversely, in a recent report, IGF-IR inhibition by TKI promoted EGFR activation (27). Given the interplay and considerable functional similarities between functions of EGFR and IGF-1R, we hypothesized that switching to EGFR signaling allows cells to resist cixutumumab treatment. Our data showed that cixutumumab induced EGFR, Akt, and mTOR phosphorylation, which was well correlated with resistance of HNSCC and NSCLC cells to cixutumumab treatment. Hence, we sought to identify the pathways involved in the activation of the EGFR pathway in HNSCC and NSCLC cells by cixutumumab treatment.

Resistance to anticancer drugs has been associated with genetic alterations, quantitative protein changes, truncation, posttranslational modification(s), and subcellular localization of selected proteins (28, 29). For example, *EGFR* T790M mutation, *c-MET*, and *K-Ras* gene amplification, loss of PTEN expression, and c-MET expression and phosphorylation have been suggested to cause resistance to TKIs of EGFR or MET (30–33). However, activation mutation and amplification of IGF-1R have not been reported, and we observed no detectable changes in IGF-1R mRNA levels after drug treatment. Our *in vitro* kinetic study show that cixutumumab treatment induced initial activation of the Akt/mTOR pathway, followed by increase in EGFR, Akt1, and survivin protein levels and EGFR phosphorylation in drug-resistant cells. The induced activation of the Akt/mTOR pathway seemed to increase survivin expression in cixutumumab-resistant cells. The Akt/mTOR pathway plays a major role in regulating the translation of mRNA subsets, many of which encode for proteins involved in cell proliferation, growth, and angiogenesis (34). We previously showed that treatment with EGFR TKIs results in mTOR-mediated *de novo* synthesis of EGFR and survivin proteins, protecting NSCLC cells from antiproliferative effects of EGFR TKIs (12). It is plausible that cixutumumab-induced increase in Akt/mTOR activities could have contributed to resistance to the drug through increased expression of EGFR signaling components and antiapoptotic protein, compensating for loss of the IGF-1R pathway. Indeed, blocking mTOR activity suppressed synthesis of these proteins and restored apoptotic activity of cixutumumab in cixutumumab-resistant HNSCC cells both *in vitro* and *in vivo*. These findings suggest that the ability of HNSCC and NSCLC cells to resist EGFR- and IGF-1R–targeting agents and adapt to a stressful environment is, at least in part, from their capacity to stimulate mTOR-mediated protein synthesis involved in cell proliferation and survival. In this study, we did not determine the mechanism by which cixutumumab treatment induces initial activation of the Akt/mTOR pathway. Given that the insulin receptor (IR) has been implicated in acquired resistance to anti–IGF-1R therapeutic agents, IR signaling may be one such pathway. In cell cultures, IR downregulation suppressed cancer cell proliferation and metastasis and reversed cixutumumab resistance, and inhibition of function of IR was required for antitumor activity of cixutumumab in a mouse neuroendocrine tumor model (35, 36). Active investigations are underway to determine whether activation of IR signaling or other pathways are involved in cixutumumab-mediated initial activation of the Akt/mTOR pathway.

Although additional mechanisms underlying activation of EGFR signaling by cixutumumab should be explored (such as whether upregulation of ligand, availability of adaptor proteins, or changes in EGFR confirmation with other EGFR family members), our *in vitro* and *in vivo* results provide a mechanistic model in which cixutumumab stimulates PI3K/Akt, resulting in mTOR-mediated *de novo* protein expression of EGFR and Akt1 proteins. Increased expressions of EGFR and Akt1 could have been involved in stimulation of the EGFR pathway, and induced expression of survivin protein could have protected HNSCC and NSCLC cells from apoptosis. This newly identified resistance mechanism against IGF-1R mAbs could provide new avenues for therapeutic strategy. First, combination regimens of EGFR inhibitors and IGF-1R mAbs may be effective if the IGF-1R

Published OnlineFirst October 6, 2011; DOI:10.1158/1535-7163.MCT-11-0235

overexpressing tumors have high levels of EGFR. Indeed, inhibition of EGFR activation by treatment with C225, an anti-EGFR mAb, abolished resistance to cixutumumab and induced apoptosis in cixutumumab-resistant cells *in vitro* and *in vivo*. Second, a combined treatment with mTOR inhibitor seems to benefit IGF-1R mAb–resistant patients. It is well known that mTOR inhibition activates PI3-K/Akt by upregulating IGF-1R signaling, and therapeutic inhibition of the IGF-1R pathway as a strategy to overcome resistance to mTOR inhibitor has been suggested in a variety of cancers, including HNSCC (37, 38), in which mTOR overexpression has been observed (39). Although the rationale for cotargeting mTOR and IGF-1R/Akt is different, the previous findings and our current results support the hypothesis that combination regimens of mTOR and IGF-1R inhibitors could be better therapeutically for the treatment of IGF-1R overexpressing tumors with high levels of mTOR. In light of this notion, we found that combined treatment with cixutumumab and rapamycin suppressed EGFR, Akt and survivin expression, decreased proliferative activities, and induced apoptosis in cixutumumab-resistant cells *in vitro* and *in vivo*.

In conclusion, we have described for the first time that the Akt/mTOR pathway has a specific role in inducing cell survival against an anti–IGF-1R mAb, cixutumumab. Further investigations are warranted to validate mTOR expression as a prognostic marker or predictor of resistance to IGF-1R mAb-based therapy and to determine the detailed mechanism by which cixutumumab mediates Akt/mTOR activation. In addition, clinical trials are needed to determine whether cixutumumab in combination with an mTOR inhibitor would enhance objective response and survival rates in HNSCC patients.

Disclosure of Potential Conflicts of Interest

No potential conflicts of interest were disclosed.

Grant Support

This research was supported by the National Research Foundation of Korea (NRF) grant funded by the Korea government (MEST; No. 2011-0017639; H-Y. Lee), NIH grant R01 CA100816 (H-Y. Lee), the second phase of the Brain Korea 21 Program in 2011 (H-Y. Lee), and P50 CA097007 (S.M. Lippman).

The costs of publication of this article were defrayed in part by the payment of page charges. This article must therefore be hereby marked *advertisement* in accordance with 18 U.S.C. Section 1734 solely to indicate this fact.

Received April 2, 2011; revised August 8, 2011; accepted September 22, 2011; published OnlineFirst October 6, 2011.

References

1. Jemal A, Siegel R, Xu J, Ward E. Cancer statistics, 2010. CA Cancer J Clin 2010;60:277–300.
2. Chin D, Boyle GM, Porceddu S, Theile DR, Parsons PG, Coman WB. Head and neck cancer: past, present and future. Expert Rev Anticancer Ther 2006;6:1111–8.
3. Samani AA, Yakar S, LeRoith D, Brodt P. The role of the IGF system in cancer growth and metastasis: overview and recent insights. Endocr Rev 2007;28:20–47.
4. Pollak MN, Schernhammer ES, Hankinson SE. Insulin-like growth factors and neoplasia. Nat Rev Cancer 2004;4:505–18.
5. Khandwala HM, McCutcheon IE, Flyvbjerg A, Friend KE. The effects of insulin-like growth factors on tumorigenesis and neoplastic growth. Endocr Rev 2000;21:215–44.
6. Yu H, Spitz MR, Mistry J, Gu J, Hong WK, Wu X. Plasma levels of insulin-like growth factor-I and lung cancer risk: a case-control analysis. J Natl Cancer Inst 1999;91:151–6.
7. Barnes CJ, Ohshiro K, Rayala SK, El-Naggar AK, Kumar R. Insulin-like growth factor receptor as a therapeutic target in head and neck cancer. Clin Cancer Res 2007;13:4291–9.
8. Zhan S, Shapiro D, Zhang L, Hirschfeld S, Elassal J, Helman LJ. Concordant loss of imprinting of the human insulin-like growth factor II gene promoters in cancer. J Biol Chem 1995;270:27983–6.
9. Jamieson TA, Brizel DM, Killian JK, Oka Y, Jang HS, Fu X, et al. M6P/IGF2R loss of heterozygosity in head and neck cancer associated with poor patient prognosis. BMC Cancer 2003;3:4.
10. Bahr C, Groner B. The insulin like growth factor-1 receptor (IGF-1R) as a drug target: novel approaches to cancer therapy. Growth Horm IGF Res 2004;14:287–95.
11. Adams TE, McKern NM, Ward CW. Signalling by the type 1 insulin-like growth factor receptor: interplay with the epidermal growth factor receptor. Growth Factors 2004;22:89–95.
12. Morgillo F, Woo JK, Kim ES, Hong WK, Lee HY. Heterodimerization of insulin-like growth factor receptor/epidermal growth factor receptor and induction of survivin expression counteract the antitumor action of erlotinib. Cancer Res 2006;66:10100–11.
13. Morgillo F, Kim WY, Kim ES, Ciardiello F, Hong WK, Lee HY. Implication of the insulin-like growth factor-IR pathway in the resistance of non-small cell lung cancer cells to treatment with gefitinib. Clin Cancer Res 2007;13:2795–803.
14. Rowinsky EK, Youssoufian H, Tonra JR, Solomon P, Burtrum D, Ludwig DL. IMC-A12, a human IgG_1 monoclonal antibody to the insulin-like growth factor I receptor. Clin Cancer Res 2007;13:5549–55s.
15. Fukazawa H, Mizuno S, Uehara Y. A microplate assay for quantitation of anchorage-independent growth of transformed cells. Anal Biochem 1995;228:83–90.
16. Goldstein D, Bushmeyer SM, Witt PL, Jordan VC, Borden EC. Effects of type I and II interferons on cultured human breast cells: interaction with estrogen receptors and with tamoxifen. Cancer Res 1989;49:2698–702.
17. Junttila TT, Akita RW, Parsons K, Fields C, Lewis Phillips GD, Friedman LS, et al. Ligand-independent HER2/HER3/PI3K complex is disrupted by trastuzumab and is effectively inhibited by the PI3K inhibitor GDC-0941. Cancer Cell 2009;15:429–40.
18. Mizushima H, Wang X, Miyamoto S, Mekada E. Integrin signal masks growth-promotion activity of HB-EGF in monolayer cell cultures. J Cell Sci 2009;122:4277–86.
19. Pickl M, Ries CH. Comparison of 3D and 2D tumor models reveals enhanced HER2 activation in 3D associated with an increased response to trastuzumab. Oncogene 2009;28:461–8.
20. Hirschhaeuser F, Leidig T, Rodday B, Lindemann C, Mueller-Klieser W. Test system for trifunctional antibodies in 3D MCTS culture. J Biomol Screen 2009;14:980–90.
21. Altieri DC. Survivin in apoptosis control and cell cycle regulation in cancer. Prog Cell Cycle Res 2003;5:447–52.
22. Choo AY, Blenis J. Not all substrates are treated equally: Implications for mTOR, rapamycin-resistance and cancer therapy. Cell Cycle 2009;8:567–72.
23. Chiang GG, Abraham RT. Phosphorylation of mammalian target of rapamycin (mTOR) at Ser-2448 is mediated by p70S6 kinase. J Biol Chem 2005;280:25485–90.
24. Allen G, Armstrong E, Modhia F, Ludwig D, Hicklin D, Harari P. Inhibition of insulin-like growth factor-1 receptor signaling impairs proliferation of head and neck, lung, prostate and breast cancer cells. Proc Amer Assoc Cancer Res 2005;46:#5041.

Published OnlineFirst October 6, 2011; DOI:10.1158/1535-7163.MCT-11-0235

25. Gualberto A, Pollak M. Emerging role of insulin-like growth factor receptor inhibitors in oncology: early clinical trial results and future directions. Oncogene 2009;28:3009–21.
26. Reidy DL, Vakiani E, Fakih MG, Sanif MW, Hecht JR, Goodman-Davis N, et al. Randomized, phase II study of the insulin-like growth factor-1 receptor inhibitor IMC-A12, with or without cetuximab, in patients with cetuximab- or panitumumab-refractory metastatic colorectal cancer. J Clin Oncol 2010;28:4240–6.
27. Buck E, Eyzaguirre A, Rosenfeld-Franklin M, Thomson S, Mulvihill M, Barr S, et al. Feedback mechanisms promote cooperativity for small molecule inhibitors of epidermal and insulin-like growth factor receptors. Cancer Res 2008;68:8322–32.
28. Janne PA, Gray N, Settleman J. Factors underlying sensitivity of cancers to small-molecule kinase inhibitors. Nat Rev Drug Discov 2009;8:709–23.
29. Onitsuka T, Uramoto H, Nose N, Takenoyama M, Hanagiri T, Sugio K, et al. Acquired resistance to gefitinib: the contribution of mechanisms other than the T790M, MET, and HGF status. Lung Cancer 2010;68:198–203.
30. Bianco R, Shin I, Ritter CA, Yakes FM, Basso A, Rosen N, et al. Loss of PTEN/MMAC1/TEP in EGF receptor-expressing tumor cells counteracts the antitumor action of EGFR tyrosine kinase inhibitors. Oncogene 2003;22:2812–22.
31. Cepero V, Sierra JR, Corso S, Ghiso E, Casorzo L, Perera T, et al. MET and KRAS gene amplification mediates acquired resistance to MET tyrosine kinase inhibitors. Cancer Res 2010;70:7580–90.
32. Skalnikova H, Martinkova J, Hrabakova R, Halada P, Dziechciarkova M, Hajduch M, et al. Cancer drug-resistance and a look at specific proteins: Rho GDP-dissociation inhibitor 2, Y-box binding protein 1 and HSP70/90 organising protein in proteomics clinical application. J Proteome Res 2011;10:404–15.
33. Benedettini E, Sholl LM, Peyton M, Reilly J, Ware C, Davis L, et al. Met activation in non-small cell lung cancer is associated with de novo resistance to EGFR inhibitors and the development of brain metastasis. Am J Pathol 2010;177:415–23.
34. Rao JS, Gondi C, Chetty C, Chittivelu S, Joseph PA, Lakka SS. Inhibition of invasion, angiogenesis, tumor growth, and metastasis by adenovirus-mediated transfer of antisense uPAR and MMP-9 in non-small cell lung cancer cells. Mol Cancer Ther 2005;4:1399–408.
35. Dunn SE, Ehrlich M, Sharp NJ, Reiss K, Solomon G, Hawkins R, et al. A dominant negative mutant of the insulin-like growth factor-I receptor inhibits the adhesion, invasion, and metastasis of breast cancer. Cancer Res 1998;58:3353–61.
36. Sachdev D, Singh R, Fujita-Yamaguchi Y, Yee D. Down-regulation of insulin receptor by antibodies against the type I insulin-like growth factor receptor: implications for anti-insulin-like growth factor therapy in breast cancer. Cancer Res 2006;66:2391–402.
37. Clark C, Shah S, Herman-Ferdinandez L, Ekshyyan O, Abreo F, Rong X, et al. Teasing out the best molecular marker in the AKT/mTOR pathway in head and neck squamous cell cancer patients. Laryngoscope 2010;120:1159–65.
38. Liu FY, Zhao ZJ, Li P, Ding X, Zong ZH, Sun CF. Mammalian target of rapamycin (mTOR) is involved in the survival of cells mediated by chemokine receptor 7 through PI3K/Akt in metastatic squamous cell carcinoma of the head and neck. Br J Oral Maxillofac Surg 2010;48:291–6.
39. Stadler ME, Patel MR, Couch ME, Hayes DN. Molecular biology of head and neck cancer: risks and pathways. Hematol Oncol Clin North Am 2008;22:1099–124, vii.

Immunohistochemical Overexpression of Platelet-Derived Growth Factor Receptor–Beta (PDGFR-β) is Associated With *PDGFRB* Gene Copy Number Gain in Sarcomatoid Non–Small-Cell Lung Cancer

Anne S. Tsao,[1] Wei Wei,[2] Elisabetta Kuhn,[1,3] Loreto Spencer,[1,3] Luisa M. Solis,[1,3] Milind Suraokar,[1,3] J. Jack Lee,[2] Waun Ki Hong,[1] Ignacio I. Wistuba[1,3]

Abstract

Sarcomatoid non-small cell lung cancer (NSCLC) is an uncommon histologic variant that has not been molecularly well-characterized. We conducted immunohistochemical and fluorescence in situ hybridization studies of PDGF-B/PDGFR-b on archived surgically resected specimens and showed high PDGFR-b IHC expression and gene copy number gain. Further studies are warranted to determine whether PDGFR-b is a feasible therapeutic target in this population.

Introduction: Sarcomatoid non-small cell lung cancer (NSCLC) is an uncommon histologic variant that has not been molecularly well-characterized. We hypothesized that the PDGF-B/PDGF-Rβ pathway may be dysregulated in sarcomatoid lung cancer. **Methods:** We conducted immunohistochemical (IHC) and gene copy number gain studies of PDGF-B/PDGFR-β on archived surgically resected specimens, 43 sarcomatoid NSCLCs and 42 control NSCLCs that were age, gender and stage-matched. Biomarkers were correlated to patient demographics, tumor characteristics, and survival. **Results:** Sarcomatoid tumors had higher PDGFR-β IHC expression than control NSCLC (median score 2.69 vs. 1.93; $P < 0.0001$). No difference was seen between the two groups of PDGF-B IHC expression; and neither PDGF-B nor PDGFR-β IHC levels correlated with gender, age, clinical or pathologic TNM status, or overall survival. *PDGFRB* gene copy number was evaluated by FISH using three ways: presence of amplification, gene copy number gain, and gene copy ratio between tumor and normal tissue. *PDGFRB* gene copy number gain was associated with sarcomatoid histology ($P = 0.006$), lower clinical and pathologic T-stage ($P = 0.07$, $P = 0.048$), and higher pathologic N-stage ($P = 0.013$). Sarcomatoid NSCLC patients ($P = 0.006$) and female patients ($P = 0.03$) had higher gene copy ratios above 1.83. Higher PDGFR-β IHC expression in tumor cells was associated with gene copy number gain ($P = 0.021$) and higher gene copy ratio status ($P = 0.005$). **Conclusion:** This is the first study to demonstrate high PDGFR-β IHC expression and gene copy number gain in sarcomatoid NSCLC tumors and suggests that further studies are warranted to determine whether PDGFR-β is a feasible therapeutic target in this population.

Clinical Lung Cancer, Vol. 12, No. 6, 369-74
Keywords: PDGFR-β, PDGFRB, Sarcomatoid NSCLC

Introduction

Sarcomatoid non–small-cell lung cancer (NSCLC) is a rare tumor variant that comprises approximately 1.5% of all lung cancers.[1] Because of their rare incidence, these tumors are often called by several names such as spindle-cell carcinoma, carcinosarcoma, giant-cell carcinoma, or sarcomatoid carcinoma. Sarcomatoid NSCLCs are histologically heter-

[1]Department of Thoracic and Head and Neck Medical Oncology, University of Texas M.D. Anderson Cancer Center, Houston, TX
[2]Department of Biostatistics, University of Texas M.D. Anderson Cancer Center, Houston, TX
[3]Department of Pathology, University of Texas M.D. Anderson Cancer Center, Houston, TX

Submitted: Dec 20, 2010; Revised: Feb 03, 2011; Accepted: Feb 22, 2011

Address for correspondence: Anne S. Tsao, MD, Associate Professor, University of Texas M.D. Anderson Cancer Center, 1515 Holcombe Blvd. Unit 432, Houston, TX 77030
Tel: 713-792-6363; Fax: 713-792-1220; e-mail contact: astsao@mdanderson.org

1525-7304/$ - see frontmatter
doi: 10.1016/j.cllc.2011.02.002

ogeneous and have varying levels of epithelial and mesenchymal features. The most common definition of sarcomatoid NSCLC consists of the tumor containing at least 10% sarcomatoid features based on immunohistochemical markers and histologic appearance.

Although rare, cases involving sarcomatoid NSCLC have been reported to have more aggressive clinical phenotypes with higher recurrence rates and subsequently worse prognoses.[2] This aggressive nature is speculated in part to potentially be caused by augmented angiogenesis, as prior studies note that lung metastases from sarcomas have higher microvessel density than carcinomatous metastases.[3,4]

Platelet-derived growth factor (PDGF) and receptor-β (PDGFR-β) have critical roles in angiogenesis and tumor-cell proliferation. There have been several studies in resected lung cancer tumors evaluating PDGF and PDGFR (α, β) in tumor cells and stroma.[5-7] Although these studies have differed in opinion on the prognostic significance of PDGF/ PDGFR-β immunohistochemistry in unselected NSCLC, it is clear that the pathway has a role in regulating angiogenesis via potentiation of vascular endothelial growth factor.[5-7] Given the hypothesis that sarcomatous and more aggressive tumors may have higher requirements of angiogenesis and that some studies in unselected NSCLC have shown prognostic significance for PDGF-B/ PDGFR-β, we sought to characterize the presence of PDGFR-β expression and gene copy number in a large series of resected sarcomatoid NSCLC.

Table 1 Patient Demographics

Patients N = 95	Sarcomatoid NSCLC N = 43	NSCLC N = 42
Female Gender	43%	43%
Median Age	57	57
Histology		
Adenocarcinoma	N/A	21
Squamous-Cell Carcinoma	N/A	21
Stage		
I	10	5
II	18	18
III	12	19
IV	3	0
T1	4	5
T2	14	18
T3	19	19
T4	6	0
N0	30	30
N1	5	8
N2	8	3
N3	0	1
M0	40	42
M1	3	0

Material and Methods

Tumor Tissue Specimens

Archived sarcomatoid lung cancer cases were selected from a review of the University of Texas M.D. Anderson Cancer Center Thoracic Tissue Bank from 1984 to 2004. A total of 59 cases were identified and 43 tumor blocks had adequate tissue to perform the analyses. The diagnosis of sarcomatoid NSCLC was confirmed by an independent histopathology review and tissue markers. Comparison control cases were selected from the same Thoracic Tissue Bank and were matched to the sarcomatoid NSCLC patients by the following characteristics: age, gender, and stage. Equal numbers of adenocarcinoma and squamous-cell carcinoma were chosen and will be subsequently referred to as the control NSCLC.

Immunohistochemistry

We performed standard immunohistochemical (IHC) studies of the PDGF-B ligand and PDGFR-β on 43 sarcomatoid lung cancers and 42 control NSCLCs that had been surgically resected. Sarcomatoid lung cancers were carefully selected and the IHC studies were performed on the sarcomatoid carcinoma areas. The histology sections were incubated with primary antibodies against PDGF-B (N-30, dilution 1:200, Santa Cruz Biotechnology, Inc, Santa Cruz, Calif) and PDGFR-β (P-20, dilution 1:300, Santa Cruz Biotechnology, Inc) for 65 minutes at room temperature. Tissue sections were then incubated with the secondary antibody (EnVision Dual Link+; DAKO, Carpinteria, Calif) for 30 minutes, after which diaminobenzidine chromogen was applied for 5 minutes. PDGF-B and PDGFR-β protein expressions were measured from three different areas of the tumor specimen and given a labeling score (intensity × % of tumor involvement). The average of the three scores was assigned to each tumor specimen, and the averages were categorized as: low (0-1), intermediate (>1-2), or high (>2-3). These data were correlated to clinical information, and a comparison between the two populations was completed. IHC expression was evaluated in the tumor cells, vasculature, and stroma.

Fluorescence In Situ Hybridization for Analysis of Gene Copy Number

In addition, the *PDGFRB* gene copy number was evaluated in tumor tissue. We analyzed the gene copy number per cell using a dual-color fluorescence in situ hybridization (FISH) assay. Sarcomatoid lung cancers were carefully selected and the FISH studies for gene copy number analyses were performed on the sarcomatoid carcinoma areas. The *PDGFRB* probe was prepared from the Vysis LSI CSF1R probe (5q33-34) SpectrumOrange (Abbott Molecular, Ill). A similar probe Vysis LSI D5S23, D5S721 SpectrumGreen Probe mapping to chromosome 5p was used as an internal control. The 4-μm thick sections were incubated from 2 hours to overnight at 56°C, deparaffinized in Citri-Solv (Fisher, Waltham, Mass) and washed in 100% ethanol. The slides were sequentially incubated in 2x saline-sodium citrate buffer (SSC) at 75°C for 18 to 23 minutes, digested in 0.5mg/mL proteinase K/2x SSC at 45°C for 18 to 23 minutes, washed in 2x SSC for 5 minutes, and dehydrated in ethanol. DNA denaturation was performed for 15 minutes at 85°C and hybridization was allowed to occur at 37°C for 36 to 48 hours. Chromatin was counterstained with 4',6-diamidino-2-phenyldole (0.3 μg/mL in Vectashield mounting medium; Vector Laboratories, Burlingame, Calif). Gene copy number analysis was performed in approximately 50 nuclei per tumor in at least four areas, and the selection of the area was guided by the hema-

Figure 1 Representative Microphotographs of Two Sarcomatoid Lung Carcinomas. (*A*) Pleomorphic Subtype, and (*D*) Giant Cell (Hematoxilyn-Eosin Stain) With Strong Cytoplasmic Expression of PDGF-B (*B*, *E*; *Black Arrows*) and PDGFR-β (*C*, *F*; *Blue Arrows*) in Highly Atypical Malignant Cells. Tumor Stromal Cells and Blood Vessel Endothelial Cells Show PDGFR-β IHC Expression (*Red Arrow*). (Original Magnification x 200.)

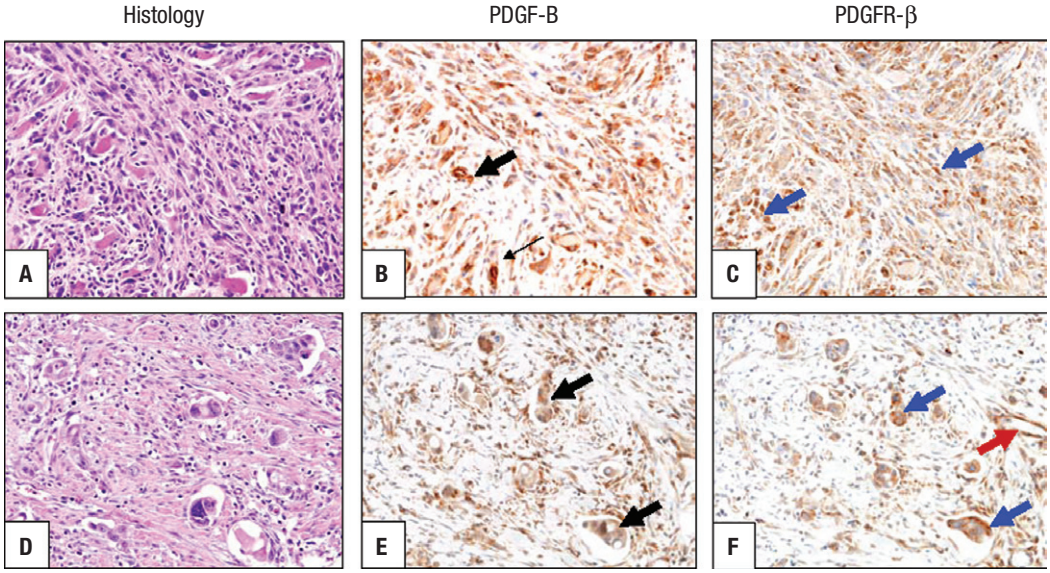

toxylin-and-eosin–stained section. The *PDGFRB* gene copy number was evaluated using three methods: (1) gene amplification, defined as presence of loose or tight gene cluster or *PDGFRB* gene to centromeric probe 5 radio ≥2; (2) copy number gain, defined as ≥4 copies in >40% cells or presence of gene amplification; and, (3) the gene copy ratio between tumor and normal cells. The definition of gene copy number gain (> 4 copies in > 40% of cells) was established in a prior publication by Varella-Garcia et al.[8]

Statistical Analysis

Biomarker expression was correlated to patient demographics, tumor characteristics, and overall survival. Control NSCLC tumor specimens, which consisted of equal numbers of adenocarcinoma and squamous-cell carcinoma, were age-, gender-, and stage-matched to the archived sarcomatoid specimens. The *PDGFRB* gene copy number was evaluated using presence of amplification, FISH positivity, and the gene copy ratio between tumor and normal tissue. Demographic and IHC outcomes were summarized using mean, standard deviation, range if continuous, or using frequency tables and percentages if categorical. Comparisons of raw IHC outcomes between patient groups were performed using the Wilcoxon rank sum test. Comparisons of categorized IHC outcomes between patient groups were performed using the Fisher exact test. Overall survival was estimated using the Kaplan-Meier curves. Comparisons of overall survival between patient groups were made using the log-rank test. All tests were two-sided and*P* values of .05 or less were considered statistically significant. Statistical analysis was performed using SAS version 9 (SAS Institute, Cary, NC).

Figure 2 Box Plots Showing the Distribution of Biomarkers by Histologic Subtype NSCLC Versus Sarcomatoid Lung Cancer. The White Cross Showing the Mean Immunohistochemical (IHC) Score and the White Bar Indicating the Median IHC Score by (A) a Statistically Significant Difference by Wilcoxon Rank Sum Test in PDGFRβ IHC ($P < .0001$) and no Significant Difference in (B) PDGF-B IHC ($P = .16$)

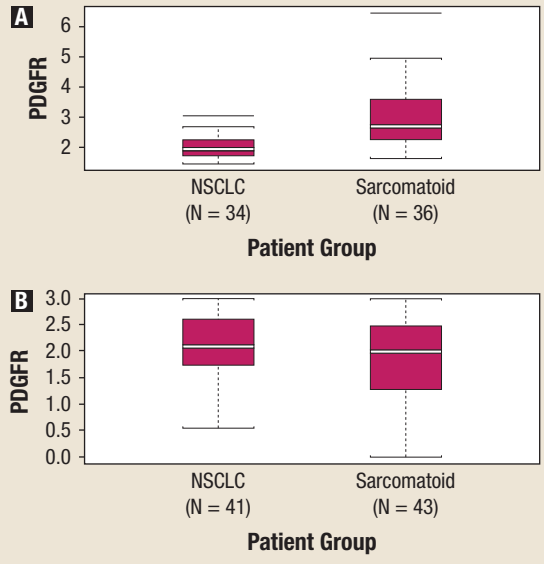

Table 2 Overall and Progression-Free Survival Results by PDGFR-β IHC Biomarker Results[a]

Patient Population	PDGFRβ IHC Level	N	Median OS (mo)	2-year OS Rate (%)	5-year OS Rate (%)	*P* Value	Median PFS (mo)	2-year PFS Rate (%)	5-year PFS Rate (%)	*P* Value
All Patients	Low	35	33.6	59	43	.36	18.0	41%	41%	.29
	Intermediate	27	25.9	51	30		9.6	35%	18%	
	High	21	10.1	41	41		4.9	40%	40%	
Sarcomatoid	Low	4	61.8	59	43	.48	59.7	41%	41%	.73
	Intermediate	20	35.3	51	30		8.1	35%	18%	
	High	19	9.7	41	41		4.9	40%	40%	
Control NSCLC	Low	31	33.6	97	88	.39	18.2	91%	85%	.22
	Intermediate	7	13.3	100	88		9.6	96%	78%	
	High	2	n/a*	81	76		n/a*	80%	50%	

[a] No patients have died yet and median survival results cannot be obtained.

Figure 3 Representative Microphotographs of Two Sarcomatoid Lung Carcinomas Examined by FISH Showing Normal *PDGFRB* Copies (*A*) and Gene Amplification (*B*) in Malignant Cells. (Original Magnification × 1,000.) Red Signals (*White Arrows*) Represent *PDGFRB* Gene Copies and Green Signals (*Green Arrows*) Represent the Chromosome 5 Centromeric Probe. (Cell Nuclei Stained With 4',6-diamidino-2-phenyldole.)

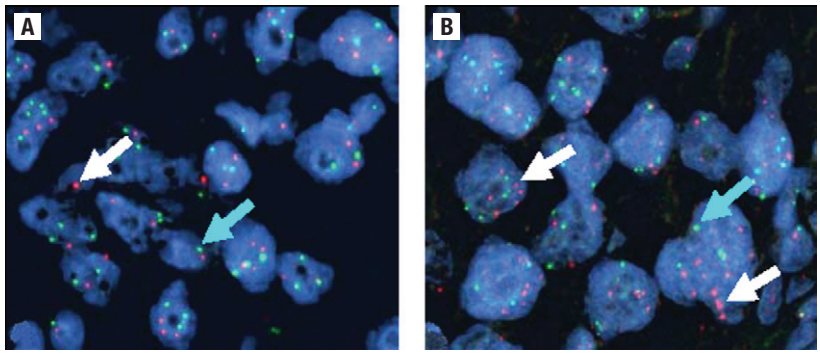

Results

Patient Demographics

The median age was 57, and women comprised 43% of each group. There was no significant difference in T and N stage between the two groups, but three sarcomatoid patients had M1 disease (Table 1).

PDGF-B and PDGFR-β Immunohistochemical (IHC) Results

PDGF-B/PDGFR-β IHC expression was evaluated in tumor cells, vasculature, and in the stroma. There was no significant difference in IHC expression of PDGF-B or PDGFR-β between sarcomatoid or the control NSCLC in the vasculature or stroma. However, sarcomatoid lung carcinoma tumor cells had higher expression of PDGFR-β than NSCLC tumors (median score, 2.69 versus 1.93; $P < .0001$), with 91% of sarcomatoid lung tumors having intermediate or high PDGFR-β staining compared to 24% of NSCLCs ($P <$ .0001). This analysis was conducted using the Wilcoxon rank sum test and treated the IHC results as a continuous variable and by Fisher exact test where the IHC scores were grouped into low (0 - <1), intermediate (>1-<2), and high (>23) scores (Figs 1 and 2). There was no difference in IHC expression of ligand PDGF-B between the two tumor groups when evaluating the scores as a continuous variable (2 versus 2.1, $P = .16$). Also, there was no difference in PDGFR-β IHC expression between the various histologic patterns of sarcomatoid lung tumors (ie, giant-cell, pleomorphic, spindle-cell).

Neither PDGF-B nor PDGFR-β IHC tumor levels correlated with gender, age, TNM status, or overall pathologic stage of tumor in either the sarcomatoid or control populations. After a median follow-up time of 1.4 years, PDGF-B and PDGFR-β IHC levels in the tumor cells did not significantly impact overall or progression-free survival in either population; however, a numerical trend was seen between low PDGFR-β IHC expression and improved median over-

Table 3 Overall and Progression-Free Survival Results by PDGFR Copy Number Gain Biomarker Results

Patient Population	PDGFR Copy Number Gain	N	Median OS (mo)	2-Year OS Rate (%)	5-Year OS Rate (%)	*P* Value	Median PFS (mo)	2-Year PFS Rate (%)	5-Year PFS Rate (%)	*P* Value
All Patients	Positive	14	39.1	55	N/A[a]	.82	10.1	46	N/A[a]	.77
	Negative	55	25.5	50	40		11.5	38	33	
Sarcomatoid	Positive	12	14.3	55	N/A[a]	.66	7.2	46	N/A[a]	.58
	Negative	24	25.9	50	40		9.7	38	33	
Control NSCLC	Positive	2	N/A[a]	86	79	.31	N/A[a]	77	69	.3
	Negative	31	22.4	96	85		12.1	93	76	

[a] No patients have died yet and a median survival results cannot be obtained.

all and progression-free survival (Table 2). When comparing overall survival between the two populations, patients with stage 2 sarcomatoid lung tumors had a trend toward worse survival than stage 2 NSCLC patients ($P = .066$).

PDGFRB Gene Copy Number

The *PDGFRB* gene copy number was evaluated using FISH for the presence of amplification, gene copy number gain, and the gene copy ratio between tumor and normal tissue (Fig 3). Gene copy number gain was defined as ≥4 gene copies in >40% cells or presence of gene amplification.[8] We identified *PDGFRB* gene amplification in six patients with sarcomatoid histology and only two in the control NSCLC group ($P = .26$). Six additional patients with sarcomatoid NSCLC histology had > 4 gene copies in more than 40% of cells compared to none in the control NSCLC group. These patients were more likely to have advanced nodal N2 disease ($P = .0006$). Thus, there were 12 patients with sarcomatoid histology who had the *PDGFRB* gene copy number gain compared to two patients in the NSCLC control group ($P = .006$).

PDGFRB gene copy number gain was associated with sarcomatoid histology ($P = .006$), lower clinical and pathologic T stage ($P = .07$, $P = .048$), and higher pathologic N stage ($P = .013$). Sarcomatoid NSCLC patients had higher gene copy ratios (greater than 1.83) compared to the control NSCLC patients (25 patients versus 9 patients, $P = .0004$). Female patients also had higher gene copy ratios compared to men ($P = .03$). There was no significant association between *PDGFRB* gene copy number gain and other histologic subtypes of NSCLCs (ie, adenocarcinoma, squamous-cell carcinoma). There was no correlation between gene copy number gain and overall or progression-free survival outcomes (Table 3).

High PDGFR-β IHC protein expression in tumor cells was associated with gene copy number gain ($P = .021$) and higher gene copy ratio (tumor versus normal) status ($P = .005$). This association was identified when evaluating the IHC scores as a continuous variable and also with the low, intermediate, and high cut-offs. There was also a trend towards higher gene copy ratio correlating to a higher IHC expression of PDGFR-β in the stroma ($P = .048$).

Discussion

Sarcomatoid NSCLC is a rare histologic variant, yet it appears to have a more aggressive phenotype,[9-17] with one prior study reporting a worse 5-year overall survival rate (24.5% versus 46.3%, $P = .01$) and shorter time to recurrence compared to stage-matched NSCLC.[2] Because of the rarity of sarcomatoid NSCLC, there have been few tissue-based studies evaluating tumor biomarkers and controversial results regarding the natural history of this disease.[3,5,18] However, this variant clearly has a unique biology and as treatment options are limited in the metastatic setting, identifying targets for systemic therapy is essential.

There have been some retrospective studies evaluating PDGF (various isoforms)/ PDGFR (α, β) in NSCLC tumor tissue and cell lines[5,6,19] which have suggested that NSCLC tumor cells that express PDGF had a worse prognosis. However, most prior studies report that NSCLC tumor cells do not express PDGFR (α, β) and that the receptors' expression is reserved in the surrounding vasculature and stroma.[6] An exception to these, Donnem et al[5] reported that PDGFR-α expression in NSCLC had a negative prognostic effect for disease-specific survival. However, none of the prior studies have evaluated PDGFR in the unique sarcomatoid histologic variant of NSCLC. We are the first to report in this present study that PDGFR-β expression is highly upregulated in sarcomatoid NSCLC tumors and that it is associated with high *PDGFRB* gene copy number when compared to control NSCLC. This is consistent with a prior hypothesis that sarcomatoid variants of epithelial tumors may require enhanced angiogenesis to promote their aggressive phenotype.[3,4]

The implications of this finding suggest that anti-angiogenic therapy, specifically PDGFR inhibitors, may be of significance in the treatment of sarcomatoid NSCLC. McDermott et al[20] recently identified lung and sarcoma cell lines that were highly sensitive to a PDGFR kinase inhibitor and had focal gene amplification of *PDGFRA* gene and the *PDGFC* gene. There appeared to be co-dependency of *PDGFC* activation of *PDGFRA* and RNA interference of either protein prevented cell proliferation. As there may be a direct anti-tumor effect with PDGFR inhibition for sarcomatoid tumors, PDGFR inhibition has also been hypothesized to decrease tumor interstitial fluid pressure and potentially enable increased chemotherapy uptake.[21]

The lack of correlation of higher PDGFR-β IHC and copy number to overall survival outcome found in our study does not necessarily argue against developing PDGF/PDGFR inhibitors in this subtype of lung cancer or in evaluating these biomarkers for prognostic/predictive value to systemic therapy. Any definitive conclusions regarding this are limited by the retrospective nature of this

analysis and the fact that our study's tumor specimens were collected from patients whose subsequent adjuvant therapy varied significantly. There were also three sarcomatoid patients who were subsequently found to have M1 disease shortly after resection, which in a small study such as this, could impact the results by diminishing the overall survival outcomes. When matching and comparing the stage 2 control NSCLC and sarcomatoid patients, the sarcomatoid lung cancer patients had a trend towards worse overall survival. All of these variables factor into the analyses of the overall survival data and potentially prevent a rigorous assessment of survival outcomes and the PDGFR-β IHC/gene copy number biomarkers. A prospective clinical trial that is designed to target the angiogenesis and PDGF/PDGFR pathway would be the optimal setting to determine whether PDGFR-β IHC or gene copy number has potential as a predictive or prognostic biomarker.

Conclusion

This is the first study to show high PDGFR-β IHC expression and increased gene copy number in sarcomatoid NSCLC tumors. Further studies are warranted to determine whether PDGFR-β is a feasible therapeutic target in sarcomatoid lung cancers that overexpress PDGFR-β by IHC or have high *PDGFRB* gene copy number. In addition, assessment of these biomarkers for prognostic or predictive value in a prospective trial for sarcomatoid NSCLC would be reasonable.

Clinical Practice Points

Sarcomatoid non-small cell lung cancer (NSCLC) is an uncommon histologic variant that has not been molecularly well-characterized and is often refractory to standard chemotherapeutics. It was hypothesized that the PDGF-B/PDGF-Rb pathway may be dysregulated in sarcomatoid lung cancer; and we conducted a study to evaluate protein expression and gene copy number between age, gender, and stage-matched NSCLC and sarcomatoid NSCLC surgically resected tumors. PDGFRB gene copy number gain was associated with sarcomatoid histology, lower clinical and pathologic T-stage, and higher pathologic N-stage. Higher PDGFR-b IHC expression in tumor cells was associated with gene copy number gain and higher gene copy ratio status. This is the first study to demonstrate high PDGFR-b IHC expression and gene copy number gain in sarcomatoid NSCLC tumors and suggests that further studies are warranted to determine whether PDGFR-b is a feasible therapeutic target in this population.

Acknowledgment

This study is supported by the National Institutes of Health grant number 5 K12 CA088084 05(PP-9).

References

1. Brambilla E, Travis WD, Colby TV, et al. The new World Health Organization classification of lung tumours. *Eur Respir J* 2001; 18:1059-68.
2. Martin LW, Correa AM, Ordonez NG, et al. Sarcomatoid carcinoma of the lung: a predictor of poor prognosis. *Ann Thorac Surg* 2007; 84:973-80.
3. Pelosi G, Fraggetta F, Nappi O, et al. Pleomorphic carcinomas of the lung show a selective distribution of gene products involved in cell differentiation, cell cycle control, tumor growth, and tumor cell motility: a clinicopathologic and immunohistochemical study of 31 cases. *Am J Surg Pathol* 2003; 27:1203-15.
4. Veronesi G, Landoni C, Pelosi G, et al. Fluoro-deoxi-glucose uptake and angiogenesis are independent biological features in lung metastases. *Br J Cancer* 2002; 86: 1391-5.
5. Donnem T, Al-Saad S, Al-Shibli K, et al. Prognostic impact of platelet-derived growth factors in non-small cell lung cancer tumor and stromal cells. *J Thorac Oncol* 2008; 3:963-70.
6. Kawai T, Hiroi S, Torikata C. Expression in lung carcinomas of platelet-derived growth factor and its receptors. *Lab Invest* 1997; 77:431-6.
7. Shikada Y, Yonemitsu Y, Koga T, et al. Platelet-derived growth factor-AA is an essential and autocrine regulator of vascular endothelial growth factor expression in non-small cell lung carcinomas. *Cancer Res* 2005; 65:7241-8.
8. Varella-Garcia M, Diebold J, Eberhard DA, et al. EGFR fluorescence in situ hybridisation assay: guidelines for application to non-small-cell lung cancer. *J Clin Pathol* 2009; 62:970-7.
9. Venissac N, Pop D, Lassalle S, et al. Sarcomatoid lung cancer (spindle/giant cells): an aggressive disease? *J Thorac Cardiovasc Surg* 2007; 134:619-23.
10. Fishback NF, Travis WD, Moran CA, et al. Pleomorphic (spindle/giant cell) carcinoma of the lung. A clinicopathologic correlation of 78 cases. *Cancer* 1994; 73: 2936-45.
11. Koss MN, Hochholzer L, Frommelt RA. Carcinosarcomas of the lung: a clinicopathologic study of 66 patients. *Am J Surg Pathol* 1999; 23:1514-26.
12. Ro JY, Chen JL, Lee JS, et al. Sarcomatoid carcinoma of the lung. Immunohistochemical and ultrastructural studies of 14 cases. *Cancer* 1992; 69:376-86.
13. Terzi A, Gorla A, Piubello Q, et al. Biphasic sarcomatoid carcinoma of the lung: report of 5 cases and review of the literature. *Eur J Surg Oncol* 1997; 23:457.
14. Wick, MR, Ritter JH, Humphrey PA. Sarcomatoid carcinomas of the lung: a clinicopathologic review. *Am J Clin Pathol* 1997; 108:40-53.
15. Raveglia F, Mezzetti M, Panigalli T, et al. Personal experience in surgical management of pulmonary pleomorphic carcinoma. *Ann Thorac Surg* 2004; 78:1742-7.
16. Mochizuki T, Ishii G, Nagai K, et al. Pleomorphic carcinoma of the lung: clinicopathologic characteristics of 70 cases. *Am J Surg Pathol* 2008; 32:1727-35.
17. Rossi G, Cavazza A, Sturm N, et al. Pulmonary carcinomas with pleomorphic, sarcomatoid, or sarcomatous elements: a clinicopathologic and immunohistochemical study of 75 cases. *Am J Surg Pathol* 2003; 27:311-24.
18. Nakajima M, Kasai T, Hashimoto H, et al. Sarcomatoid carcinoma of the lung: a clinicopathologic study of 37 cases. *Cancer* 1999; 86:608-16.
19. Antoniades HN, Galanopoulos T, Neville-Golden J, et al. Malignant epithelial cells in primary human lung carcinomas coexpress in vivo platelet-derived growth factor (PDGF) and PDGF receptor mRNAs and their protein products. *Proc Natl Acad Sci U S A* 1992; 89:3942-6.
20. McDermott U, Ames RY, Iafrate AJ, et al. Ligand-dependent platelet-derived growth factor receptor (PDGFR)-alpha activation sensitizes rare lung cancer and sarcoma cells to PDGFR kinase inhibitors. *Cancer Res* 2009; 69:3937-46.
21. Pietras K, Rubin K, Sjoblom T, et al. Inhibition of PDGF receptor signaling in tumor stroma enhances antitumor effect of chemotherapy. *Cancer Res* 2002; 62: 5476-84.

Original Article

Prognostic Impact of Insulin Receptor Expression on Survival of Patients with Nonsmall Cell Lung Cancer

Jin-Soo Kim, MD[1]; Edward S. Kim, MD[1]; Diane Liu, MS[2]; J. Jack Lee, PhD, MS, DDS[2]; Luisa Solis, MD[3]; Carmen Behrens, MD[1]; Scott M. Lippman, MD[1]; Waun Ki Hong, MD[1]; Ignacio I. Wistuba, MD[1,3]; and Ho-Young Lee, PhD[1,4]

BACKGROUND: The purpose of this study was to characterize insulin receptor (IR) and insulin-like growth factor-1 receptor (IGF-1R) expression in patients with nonsmall cell lung cancer (NSCLC). **METHODS:** A total of 459 patients who underwent curative resection of NSCLC were studied (median follow-up duration, 4.01 years). Expression of the IR and IGF-1R protein in tumor specimens was assessed immunohistochemically using tissue microarrays. **RESULTS:** The cytoplasmic IR score was higher in patients with adenocarcinoma (ADC) than in those with squamous cell carcinoma (SCC), whereas cytoplasmic IGF-1R score was higher in patients with SCC than those with ADC. Neither IR nor IGF-1R expression was associated with sex, smoking history, or clinical stage. Patients with positive IR or IGF-1R expression levels had poor recurrence-free (RFS) (3.8 vs 3.3 years; 3.8 vs 2.0 years, respectively), but similar overall survival (OS). Patients with high expression levels of IR and IGF-1R had shorter RFS and OS compared with those with low levels of IR and/or IGF-1R expression. Finally, a multivariate analysis revealed the impact of IR, but not of IGF-1R, as an independent predictive marker of NSCLC survival: hazard ratio (HR) for OS, 1.005 (95% confidence interval [CI], 1.001-1.010], HR for RFS, 1.005 (95% CI, 1.001-1.009), when IR score was tested as a continuous variable. **CONCLUSIONS:** Overexpression of IR predicts a poor survival among patients with NSCLC, especially those with SCC. These results might serve as future guidance to the clinical trials involving IR or IGR-1R targeting agents. *Cancer* **2011;000:000–000.** © *2011 American Cancer Society.*

KEYWORDS: carcinoma, nonsmall cell lung, receptor, insulin, receptor, IGF type 1, prognosis, survival.

INTRODUCTION

Nonsmall cell lung cancer (NSCLC) is the leading cause of cancer-related deaths in the United States, and current systemic therapies for NSCLC have limited efficacy, indicating the need for novel treatment strategies.[1] One potentially effective strategy is targeting the insulin-like growth factor (IGF)/insulin signaling pathway. The IGF/insulin system is composed of ligands (insulin, IGF-I, and IGF-II), receptors (insulin receptor [IR], IGF-1R, and IGF-2R), and IGF-binding proteins 1-6. The IR and IGF-1R are highly homologous heterotetrameric molecules composed of 2 extracellular α-subunits with binding capacity and 2 transmembrane β-subunits with tyrosine kinase activity that are activated in response to ligand binding.[2] The IR and IGF-1R can homodimerize as well as heterodimerize with each other and have selective affinities to ligands, such as IGF-I, IGF-II, and insulin.[3] Whereas IGF-I and insulin bind to IGF-1R and the IR, respectively, with high selectivity, IGF-II binds to IGF-1R as well as an alternative splicing variant of the IR, termed IR-A.[4] Also, whereas insulin has direct access to its receptors, the bioavailability of IGF-I is influenced by IGF-binding proteins.[2]

The IGF-1R and IR interact and share similar downstream signaling pathways, including mitogen-activated protein kinase and phosphatidylinositol 3-kinase. The IGF-1R and IR participate in mitogenic and antiapoptotic signaling in normal and neoplastic epithelia. In mammals, the IR and IGF-1R have also evolved to exert different biological functions. Specifically, the IR plays a central role in glucose homeostasis, whereas IGF-IR is a regulator of body growth.[5]

Corresponding author: Ho-Young Lee, PhD, College of Pharmacy, Seoul National University, 599 Gwanak-ro, Gwanak-gu, Seoul 151-742, Republic of Korea; Fax: +82-2-872-1795; hylee135@snu.ac.kr

[1]Department of Thoracic/Head & Neck Medical Oncology, The University of Texas MD Anderson Cancer Center, Houston, Texas; [2]Department of Biostatistics, The University of Texas MD Anderson Cancer Center, Houston, Texas; [3]Department of Pathology, The University of Texas MD Anderson Cancer Center, Houston, Texas; [4]College of Pharmacy, Seoul National University, Seoul, Republic of Korea

This study was presented at the 102nd Annual Meeting of the American Association for Cancer Research, April 2-6, 2011, Orlando, Florida.

DOI: 10.1002/cncr.26492, **Received:** March 14, 2011; **Revised:** June 26, 2011; **Accepted:** July 18, 2011, **Published online** in Wiley Online Library (wileyonlinelibrary.com)

Interestingly, expression of IR-A, often referred to as the fetal isoform of the IR, is elevated in several human cancers.[6] In patients with breast cancer, total level of the IR expression was indicative of poor survival, whereas total IGF-IR expression was not.[7,8] Furthermore, IR down-regulation has shown to inhibit polyoma virus middle T antigen-induced tumor growth in vivo.[9] Insulin may be involved in the growth of malignancies.[5] Aberrant IR expression sensitized cancer cells to the pleiotropic effects of circulating insulin, leading to acquire resistance to both conventional and targeted therapies, especially in hyperinsulinemic patients.[10,11] Given the impact of IGF-1R/IR signaling on the development and progression of several types of cancer, researchers have long studied the prognostic value of IGF-1R protein expression in patients with NSCLC[12-14] or small-cell lung cancer.[15] Researchers have also studied the impact of the epidermal growth factor receptor (EGFR) pathway, which is suggested to crosstalk with the IGF-1R pathway, on survival in patients with lung cancer.[16,17] Despite the data indicating the potential prognostic significance of IR overexpression, information about IR expression in lung cancer cases is very limited.

The aim of this study was to analyze IR and IGF-1R expression in correlation with clinicopathological parameters in NSCLC patients and to evaluate the prognostic impact of the expression on the survival of these patients.

MATERIALS AND METHODS

Patient Characteristics

The study patients' baseline characteristics are listed in Table 1. Detailed clinical and pathological information was available for most of the patients and included their demographic data, smoking history (never-smokers va ever-smokers [patients who had smoked at least 100 cigarettes in their lifetimes]), pathological TNM stage, and overall survival (OS) and recurrence-free survival (RFS) duration. The numbers of patients per sex were well balanced, and almost two-thirds of the patients had adenocarcinoma (ADC). Most of the patients had early-stage NSCLC and were ever-smokers. Tissue banking and research conduct were approved by The University of Texas MD Anderson Cancer Center institutional review board. All patients provided their informed consent to participate in the study, and all identifying information was removed from the database.

Case Selection and Tissue Microarray Construction

For this study, archived formalin-fixed, paraffin-embedded specimens of NSCLC were obtained from previously described tissue banks at MD Anderson.[18] The tissue specimens were originally collected from 1997 to 2005 and were classified using the 2004 World Health Organization classification system.[19] A tissue microarray (TMA) set comprising 511 NSCLC specimens (334 ADCs and 177 squamous cell carcinomas [SCCs]) obtained from patients who underwent surgery at MD Anderson from 2003 to 2005 was constructed. Only patients with available staging information were included in our analysis ($n = 459$). After histological examination of the NSCLC specimens, the NSCLC TMAs were constructed by obtaining 3 1-mm-diameter cores from each tumor at 3 different sites (periphery, intermediate, and central tumor). The TMAs were prepared using a manual tissue arrayer (Advanced Tissue Arrayer ATA100; Chemicon International, Tumecula, Calif).

Immunohistochemical Analysis of Tumor Specimens

Expression of IGF-1R, and IR in TMAs was measured using immunostaining. Primary antibodies used in immunohistochemical (IHC) analysis were purchased from Cell Signaling Technology (Danvers, Mass) (IGF-1R) or Santa Cruz Biotechnology (Santa Cruz, Calif) (IR). Details of the IHC analysis were described previously.[18] The expression of IGF-1R and IR was quantified by 2 independent observers (C.B. and I.I.W.) who were unaware of the patients' outcomes. Cytoplasmic, membranous, and nuclear expression was quantified using a 4-value intensity scoring system (0, 1+, 2+, and 3+) and the percentage (0%-100%) of the extent of reactivity. Next, the expression score was calculated by multiplying the intensity value by the reactivity extension value (range, 0-300). Tumors with IHC score equal to or higher than 1 were considered positive staining for the markers.

Statistical Analysis

Summary statistical analysis of biomarker expression levels according to patient baseline characteristics was performed. Wilcoxon rank sum and Kruskal-Wallis tests were performed to compare the biomarker expression in different subgroups defined by categorical variables, such as histology and smoking history. Spearman rank correlation coefficients were used to determine the correlation among biomarkers. Student *t* test and Pearson correlation coefficient were used to analyze gene expression data. The OS and RFS durations in each subgroup of patients were then determined using the Kaplan-Meier method and compared using the log-rank test. Cox proportional

Table 1. Patients Characteristics

Feature	NSCLC Histologic Type[a]		
	Adenocarcinoma (n = 298)	Squamous Carcinoma (n = 161)	Total (n = 459)
Median age (range), y	66 (32-88)	66 (43-89)	66 (32-89)
Sex			
Male	133 (44.6%)	96 (59.6%)	231 (50.3%)
Female	165 (55.4%)	65 (40.4%)	228 (49.7%)
Smoking status[b]			
Never	47 (15.8%)	1 (0.6%)	48 (10.5%)
Former	132 (44.3%)	76 (47.2%)	208 (45.3%)
Current	118 (39.6%)	83 (51.6%)	201 (43.8%)
Unknown	1 (0.3%)	1 (0.6%)	2 (0.4%)
Race			
Caucasian	272 (91.3%)	146 (90.7%)	418 (91.1%)
Others	26 (8.7%)	15 (9.3%)	41 (8.9%)
T category[c]			
1	120 (40.3%)	57 (35.4%)	177 (38.6%)
2	145 (48.7%)	83 (51.6%)	228 (49.7%)
3	11 (3.7%)	11 (6.8%)	22 (4.8%)
4	22 (7.4%)	10 (6.2%)	32 (7%)
N category[c]			
0	212 (71.1%)	104 (64.6%)	316 (68.8%)
1	42 (14.1%)	37 (23.0%)	79 (17.2%)
2	43 (14.4%)	19 (11.8%)	62 (13.5%)
x	1 (0.3%)	1 (0.6%)	2 (0.4%)
Final stage[c]			
I	184 (61.7%)	90 (55.9%)	274 (59.7%)
II	83 (27.9%)	58 (36.0%)	141 (30.7%)
III	20 (6.7%)	10 (6.2%)	30 (6.5%)
IV	11 (3.7%)	3 (1.9%)	14 (3.1%)

Abbreviation: NSCLC, nonsmall cell lung cancer.
[a] Values are number of cases unless otherwise indicated.
[b] Smoking history was assigned based on the CDC definitions (Accessed on Jun 29, 2010. http://www.cdc.gov/nchs/nhis/tobacco/tobacco_glossary.htm).
Never smoker: an adult who has never smoked, or who has smoked less than 100 cigarettes in his or her lifetime.
Former smoker: an adult who has smoked at least 100 cigarettes in his or her lifetime but who had quit smoking at the time of interview.
Current smoker: an adult who has smoked 100 cigarettes in his or her lifetime and who currently smokes cigarettes.
[c] According to the American Joint Committee on Cancer Staging Manual, 6th edition.

hazards models were used for multivariate analysis. All statistical tests were 2 sided, and *P* values of no more than .05 were considered statistically significant.

RESULTS

Expression of the IR and Correlation with Expression of IGF-1R

IHC staining of the tissue specimens obtained from the 459 patients revealed quantifiable expression of the IR and IGF-1R in most of the NSCLCs (Fig. 1). The expression of the IR, IGF-1R was mainly cytoplasmic with modest membraneous staining; we did not detect nuclear staining of these proteins. The expression levels at cytoplasmic and membranous locations for each marker were well correlated with each other (data not shown). Cytoplasmic IR expression levels were significantly higher in ADC specimens than in SCC specimens ($P = 2.4$ E-4, Fig. 2A), but the membranous IR expression levels were similar. The levels of IR expression according to sex, stage, and smoking history were similar (Table 2). Cytoplasmic and membraneous expressions of IGF-1R ($P = 4.7$ E-05, Fig. 2B) were significantly associated with SCC. Expression of the IR and that of IGF-1R were not correlated

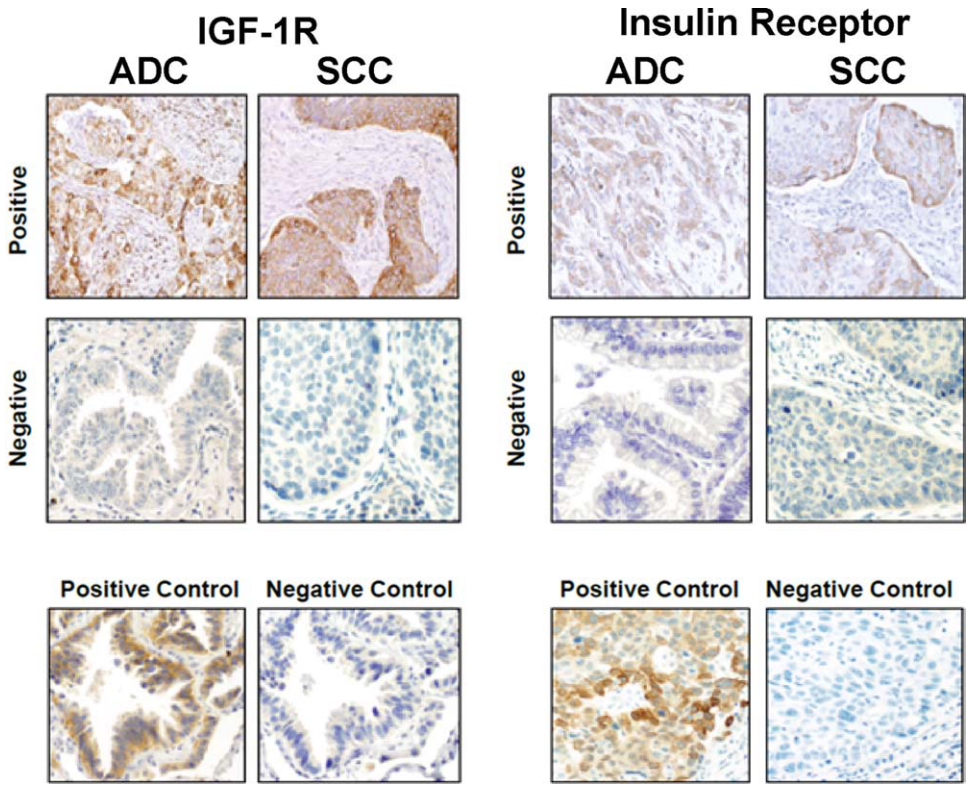

Figure 1. This shows examples of insulin receptor (IR) and insulin-like growth factor-1 receptor (IGF-1R) immunohistochemical staining. Representative photomicrographs of IR and IGF-1R expression in lung adenocarcinoma (ADC) and squamous cell carcinoma (SCC).

with each other, and expression of pIGF-1R/IR was not significantly correlated with that of the IR and IGF-1R (data not shown). When we compared expression of IR and IGF-1R using gene expression and clinical data retrieved from the Gene Expression Omnibus (GSE3141; http://www.ncbi.nlm.nih.gov/geo/),[20] which include 58 patients with ADC and 53 with SCC, normalized expression of IR (probe ID: 213792_s_at and 226450_at) were significantly higher in ADC than in SCC ($P = .057$ and .0010, respectively, Fig. 2C), whereas those of IGF-1R (probe ID: 225330_at and 203627 at) were significantly higher in SCC than in ADC ($P = 3.5$ E-7 and 1.3 E-9, respectively, Fig. 2D). The expression of 2 probes in each genes were strongly correlated with each other (Pearson correlation coefficient [R_P]: 0.773, $P = 2.6$ E-23 for IR, and R_P: 0.830, $P = 2.1$ E-29 for IGF-1R). We confirmed these differential expression patterns using an independent dataset with 138 patients (GSE8894).[21]

RFS and OS

After a median follow-up duration of 4.1 years for the censored observations (data cutoff: September 2010), RFS durations in patients with positive membraneous IR expression levels were significantly shorter than those in patients with negative IR expression levels (median: 3.8 years vs 3.3 years, $P = .044$ [log-rank test]) (Fig 3A). In contrast, the OS durations were similar in patients with positive versus negative IR expression levels ($P = .430$ [log-rank test]) (Fig 3B). Cytoplasmic IGF-1R and IR expression did not have impacts on RFS and OS in univariate analysis. Although membraneous IR expression levels were not significantly different between ADC and SCC, SCC patients with positive IR expression had shorter RFS and OS durations than those with negative IR expression (Fig. 3C and D), whereas IR expression in ADC patients did not make any difference in survival (Fig. 3E and F). When we performed a subgroup analysis by gender, there were similar OS in both IR positive and negative groups, whereas we observed prolonged RFS in IR negative groups in both gender (log rank test, $P = .085$ and .047 for male and female, respectively). Patients with positive membraneous IGF-1R expression showed poor RFS compared with those with negative expression ($P = .044$), whereas there was a similar OS between these

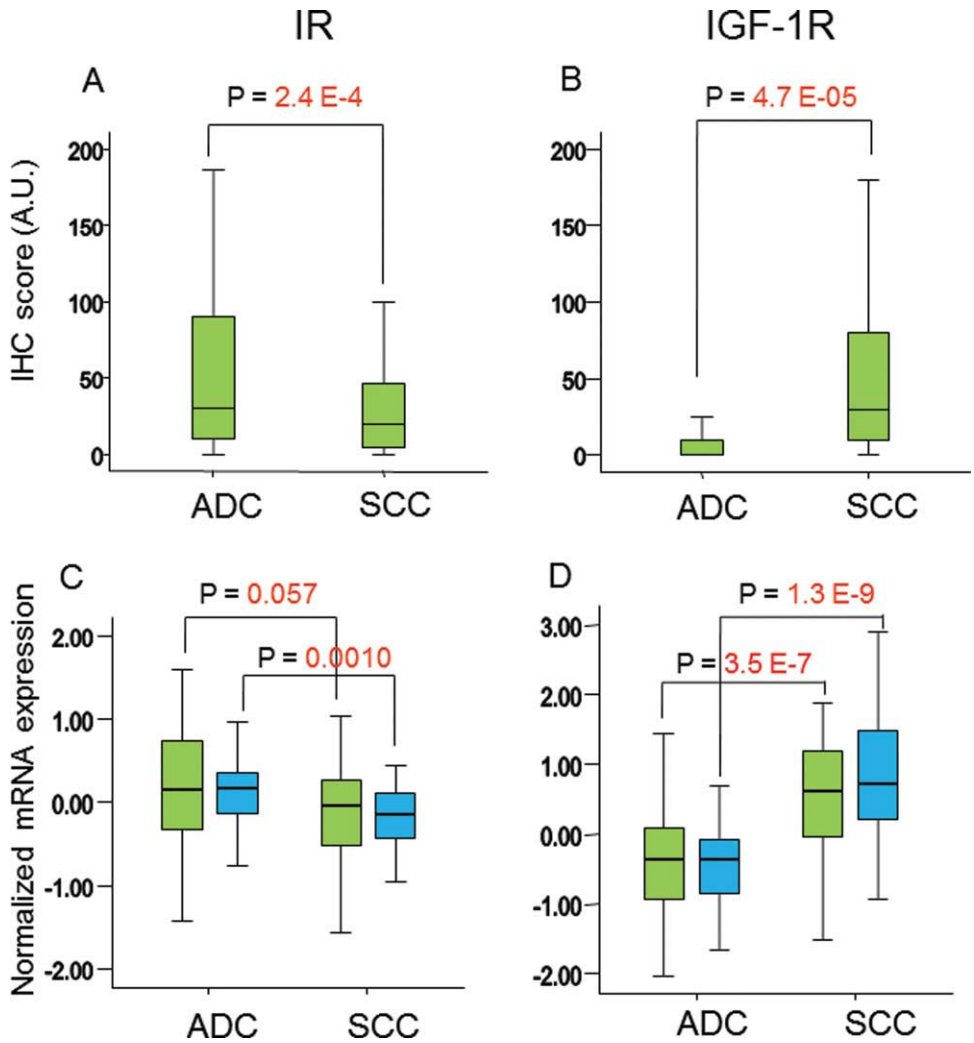

Figure 2. This shows expression pattern of IR and IGF-1R according to histology. immunohistochemical (IHC) score and normalized mRNA expression level on microarray data (GSE3141) were compared by Wilcoxon rank sum test in lung adenocarcinoma (ADC) and squamous cell carcinoma (SCC). IHC score (A) of IR was significantly higher in tumors from ADC (P = 2.4 E-4), and normalized mRNA expression levels of IR (C) were significantly higher in tumors from ADC (green: probe number 213792_s_at P = .057, and blue: probe number 226450_at P = .0010, respectively). IHC score of IGF-1R (2B) were significantly higher in tumors from SCC (P = 4.7 E-05) and normalized mRNA expression levels of IGF-1R (D) were significantly higher in tumors from SCC (green: probe number 225330_at, P = 3.5 E-7, and blue: probe number 203627_at P = 1.3 E-9).

groups (Fig. 4A and B). In the subgroup analysis by histology, SCC patients with positive or negative IGF-1R had a similar OS and RFS (Fig. 4C and D), whereas ADC patients with positive IGF-1R expression (N = 11) had poor OS and RFS compared with those with negative IGF-1R expression (Fig. 4E and F). Interestingly, patients with positive membraneous IGF-1R and IR expression levels (N = 23) had shorter RFS and OS durations than did all of the other patients (Fig. 5). When tested as continuous variables, the IGF-1R scores were not associated with differences in survival duration (data not shown). In contrast, the IR IHC score significantly impacted RFS and OS durations when tested as a continuous variable (hazard ratio [HR] for OS, 1.0045 [95% confidence interval [CI], 1.0001-1.0089]; P = .0470; HR for RFS, 1.0052 [95% CI, 1.0005-1.0100]; P = .0311). We confirmed the prognostic value of the IR IHC score regarding RFS and OS in the multivariate analysis (Table 3). When we performed the multivariate analysis in each histology subgroup, the negative impact of IR was significant only in patients with SCC (HR for OS: 1.009 [1.002-1.016], P = .014 and HR for RFS: 1.007 [1.001-1.014], P = .027) (Table 4). In the multivariate model with IGF-1R, IR only retained the significance. Unfortunately, we were

Table 2. Patients Characteristics According to IR Expression

		Negative IR (N = 274)	Positive IR (N = 180)	*P*[a]
Age Median age (range), y		66 (32-88)	66 (42-89)	.810
Gender	Female	130 (47.4%)	97 (53.9%)	.174
	Male	144 (52.6%)	83 (46.1%)	
Race	Caucasian	245 (89.4%)	168 (93.3%)	.154
	Noncaucasian	29 (10.6%)	12 (6.7%)	
Histology	Adenocarcinoma	172 (62.8%)	123 (68.3%)	.224
	Squamous cell carcinoma	102 (37.2%)	57 (31.7%)	
Smoking	Never smoker	34 (12.4%)	14 (7.8%)	.265
	Former smoker	119 (43.4%)	86 (47.8%)	
	Current smoker	120 (43.8%)	79 (43.9%)	
	Unknown	1 (0.4%)	1 (0.6%)	
T category[b]	T1	100 (36.5%)	72 (40.0%)	.892
	T2	140 (51.1%)	88 (48.9%)	
	T3	14 (5.1%)	8 (4.4%)	
	T4	20 (7.3%)	12 (6.7%)	
N category[b]	N0	191 (69.7%)	122 (67.8%)	.861
	N1	45 (16.4%)	33 (18.3%)	
	N2	37 (13.5%)	25 (13.9%)	
	Nx	1 (0.4%)	0 (0%)	
Final stage[b]	I	162 (59.1%)	109 (60.6%)	.930
	II	86 (31.4%)	54 (30.0%)	
	III and IV	26 (8.5%)	17 (9.4%)	

Abbreviation: IR, insulin receptor.
[a] *P* values are calculated by Mann-Whitney test for age, and by chi-square test for all of the other variables.
[b] According to the American Joint Committee on Cancer Staging Manual, 6th edition.

not able to show the survival difference from gene expression databases, mainly because of lack of statistical power from small sample size.

DISCUSSION

Recent evidences imply that the IR expression has a role in cancer cell proliferation, angiogenesis, lymphangiogenesis, and metastasis in patients with various cancers.[5,22-24] However, firm studies of IR expression in primary human cancers are surprisingly scarce. In this article, we have demonstrated, to our knowledge for the first time, the survival impact of IR expression in patients with NSCLC. The results described herein provide evidence that IR expression in tumor specimen is an independent prognostic factor for OS and RFS in patients with resected NSCLC. The impact of IR expression on survival is substantial, even though the HRs for OS and RFS look small. Considering the IHC scores were put as a continuous variable in the multivariate model, the increase of HRs per 1 IR score is almost comparable to those per 1 year of age (Tables 3 and 4). Our data suggest that IR is a potential target in cancer therapy and that patients with NSCLC should be stratified based on IR expression in future clinical trials with IGF-1R/IR-targeted agents. Additional information can be retrieved from completed clinical trials of IGF-1R- or IR-targeted agents via retrospective analysis to determine whether differences in IR expression level among treatment groups affect outcomes and thus have therapeutic implications.

Because the IGF-1R pathway is frequently deregulated in human tumors, including NSCLC, investigators have assessed the role of IGF-1R expression as a prognostic factor. Previous studies have shown that IGF-1R expression is consistently associated with SCC.[12-14] However, these previous studies do not consistently support a definite impact of IGF-1R protein expression on survival of NSCLC.[12-14] Because it is well known that IGF-1R and IR are structurally similar and functionally interact to promote cell proliferation and survival,[5] we sought to determine whether expression of IGF-1R, IR, or their coexpression have prognostic impacts in NSCLC. Our data confirm previous findings of IGF-1R expression in association with histological feature of SCC.[12-14] We also show previously unidentified results, including: 1) IR expression was consistently associated with ADC; 2) patients with IGF-1R-positive or IR-positive tumors showed significantly shorter RFS than those with IGF-1R-negative tumors or IR-negative tumors, respectively (Figs. 3A and 4A); 3) IGF-1R and IR expressions were negatively correlated with survival duration of patients with ADC and

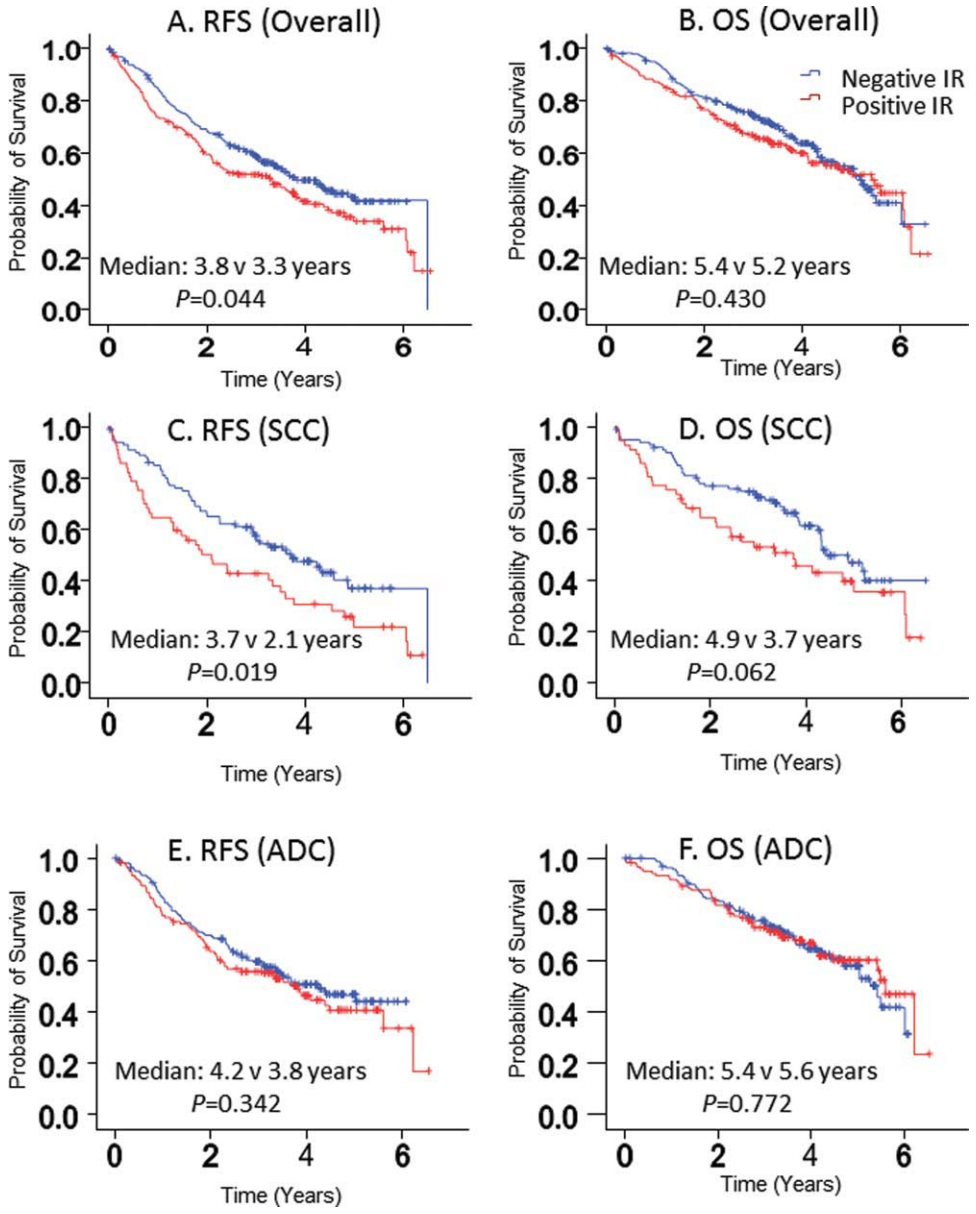

Figure 3. This shows Kaplan-Meier estimates of survival among the study population, according to insulin receptor (IR) expression levels. Recurrence-free survival (RFS) and overall survival (OS) in overall population (A, B), in patients with squamous cell carcinoma (SCC) (C, D) and in patients with adenocarcinoma (ADC) (E, F). Data on RFS and OS are shown according to stratification on the basis of IR expression levels. Overall, patients with IR-negative tumors had significantly better RFS than did patients with IR-positive tumors ($P = .044$ for RFS and $P = .430$ for OS by the 2-sided log-rank test) (A, B). Subgroup analysis shows the impact of IR expression on RFS or OS is confined to patients with squamous cell carcinoma (SCC) (C-F).

SCC, respectively (Figs. 3C and D and 4E and F), although the number of patients with ADC was not enough to draw a firm conclusion about the correlation; and 4) patients with positive IR and IGF-1R expression levels had significantly shorter survival durations than did patients with negative IR and/or negative IGF-1R expression levels, although the number of patients in the positive expression group was relatively small. Interestingly, we observed similar survival durations in patients with negative IR and/or negative IGF-1R (Fig. 5). These data suggest that IR and IGF-1R could have independent roles in the prognosis of lung cancer patients. Further, these 2 receptors could function as potential prognostic factors dependent on the histological feature of patients. In a

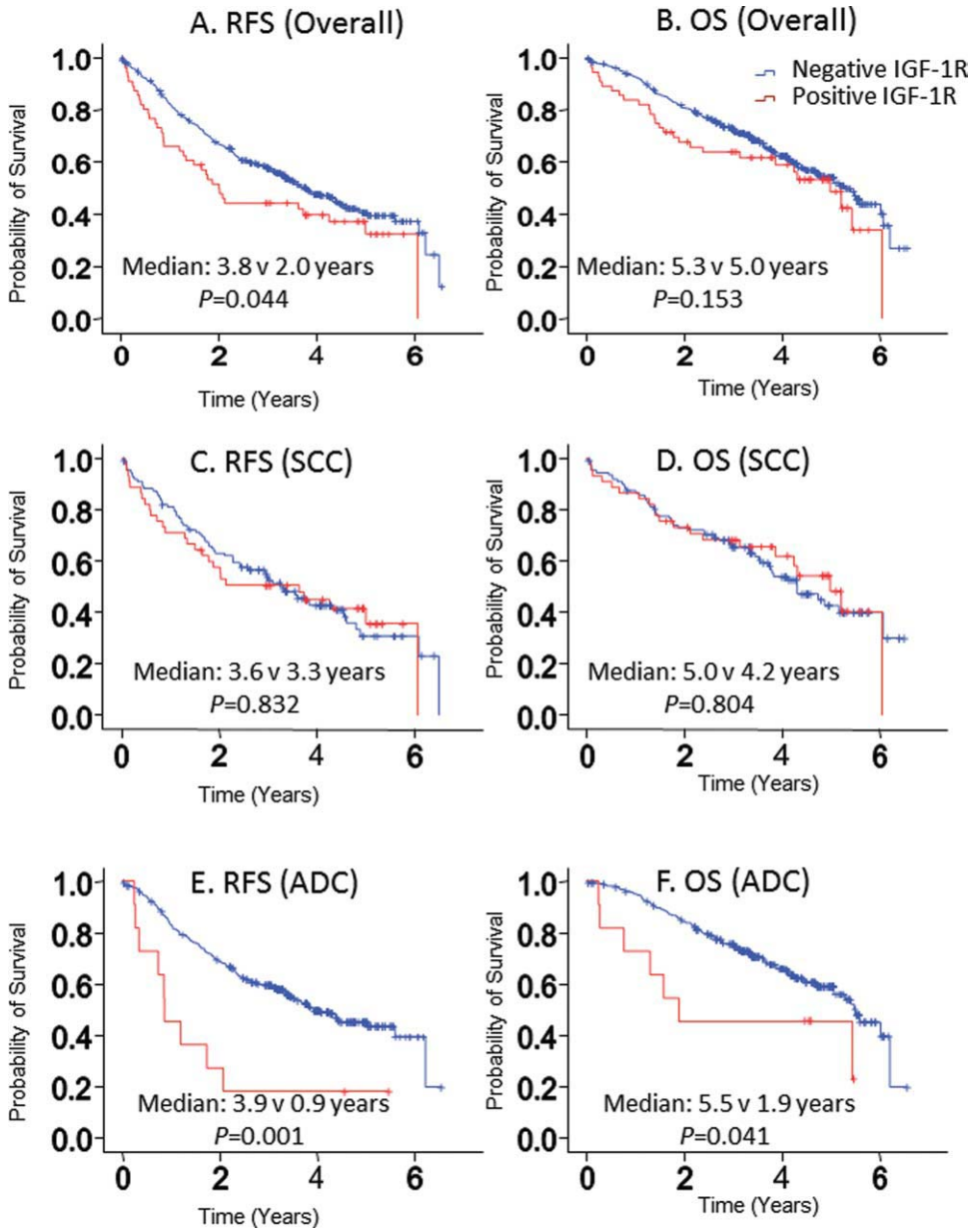

Figure 4. This shows Kaplan-Meier estimates of survival among the study population, according to insulin-like growth factor 1 receptor (IGF-1R) expression levels. Recurrence-free survival (RFS) and overall survival (OS) in overall population (A, B), in patients with squamous cell carcinoma (SCC) (C, D) and in patients with adenocarcinoma (ADC) (E, F). Data on OS and RFS are shown according to stratification on the basis of IGF-1R expression levels. Patients with high IGF-1R tumors had significantly poor RFS and similar OS than did patients with low IGF-1R IHC score (*P* values are as indicated in the figures and calculated by the 2-sided log-rank test). Overall, patients with IGF-1R-negative tumors had significantly better RFS than did patients with IGF-1R-positive tumors ($P = .044$ for RFS and $P = .430$ for OS by the 2-sided log-rank test) (A, B). Subgroup analysis shows the impact of IR expression on RFS or OS is confined to patients with adenocarcinoam (ADC) (C-F).

multivariate analysis, however, IGF-1R did not retain a significant hazard ratio for RFS and OS, whereas IR did, suggesting a definite impact of IR expression, not IGF-1R expression, on survival of NSCLC.

Based on our findings that IGF-1R expression was greater in ever-smokers than in never-smokers[25] and in patients with SCC than in those with ADC and whereas IR expression was higher in patients with ADC than in those with SCC, we could suggest that cotargeting of the IR and IGF-1R may have broader coverage than targeting of IGF-1R alone. Of interest, some anti-IGF-1R antibody-based clinical trials, which have shown initial benefit

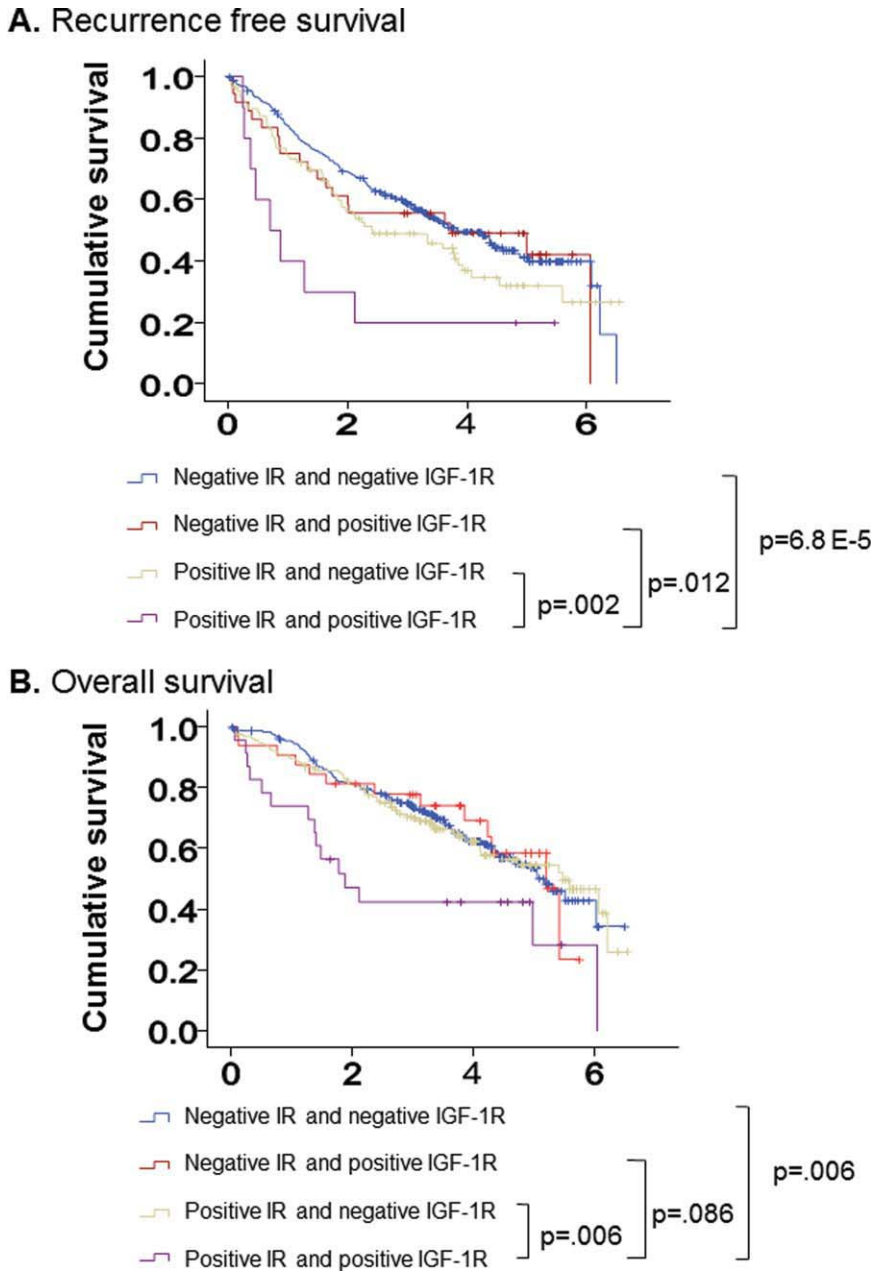

Figure 5. This shows Kaplan-Meier estimates of survival among the study population, according to insulin receptor (IR) and insulin-like growth factor 1 receptor (IGF-1R) expression levels. Data on overall survival (OS) and recurrence-free survival (RFS) are shown according to stratification on the basis of IR and IGF-1R expression levels. Patients with high IR and IGF-1R tumors had significantly poor RFS and OS than did patients with low IR and/or low IGF-1R IHC score (*P* values are as indicated in the figures and calculated by the 2-sided log-rank test).

in patients with SCC, revealed limitations in therapeutic efficacy.[26] More importantly, recent phase III trials of the anti-IGF-1R antibody figitumumab were terminated prematurely because of an increase in the number of serious adverse events and excess mortality in the experimental arm. The resistance to anti-IGF-1R antibody could be explained by the possibility that reduced IGF-1R availability in hybrid IGF-1R/IR receptors may result in increased numbers of IR homodimers, leading to unwanted enhanced IR signaling. Also, anti-IGF-1R antibodies may not effectively block signaling from hybrid IGF-1R/IR. In previous studies, down-regulation of IGF-1R expression did not affect the IR expression levels but, interestingly, sensitized cells to insulin activation of

Table 3. Multivariate Analysis of Survival for Overall Population

Variable	HR for OS (95% CI)	*P*	HR for RFS (95% CI)	*P*
Age	1.013 (0.998-1.029)	.089	1.009 (0.996-1.022)	.169
Gender				
(Male vs female)	1.577 (1.172-2.123)	.003	1.439 (1.110-1.866)	.006
Histology (SCC vs ADC)	1.279 (0.947-1.726)	.109	1.179 (0.904-1.538)	.224
Stage				
II vs I	1.837 (1.330-2.537)	<.001	1.846 (1.392-2.449)	<.001
III/IV vs I	2.294 (1.471-3.576)	<.001	2.214 (1.478-3.315)	<.001
IR expression[a]	1.005 (1.001-1.010)	.028	1.005 (1.001-1.009)	.019

Abbreviations: ADC, adenocarcinoma; CI, confidence interval; HR, hazard ratio; IR, insulin receptor; OS, overall survival; RFS, recurrence-free survival; SCC, squamous cell carcinoma.
P values are calculated by Cox Proportional Hazard Model.
[a] Membraneous IR IHC score was used as a continuous variable.

Table 4. Multivariate Analysis of Survival for Patients With Squamous Cell Carcinoma

Variable	HR for OS (95% CI)	*P* Value	HR for RFS (95% CI)	*P* Value
Age	1.005 (0.980-1.029)	.718	1.002 (0.981-1.024)	.850
Gender				
(Male vs Female)	1.133 (0.713-1.801)	.598	1.125 (0.736-1.718)	.586
Stage				
II vs I	1.536 (0.920-2.563	.101	1.701 (1.075-2.691)	.023
III/IV vs I	2.561 (1.258-5.213)	.010	2.874 (1.472-5.611)	.002
IR expression[a]	1.009 (1.002-1.016)	.014	1.007 (1.001-1.014)	.027

Abbreviations: ADC, adenocarcinoma; CI, confidence interval; HR, hazard ratio; IR, insulin receptor; OS, overall survival; RFS, recurrence-free survival; SCC, squamous cell carcinoma.
P -values are calculated by Cox Proportional Hazard Model.
[a] Membraneous IR IHC score was used as a continuous variable.

downstream signaling pathways in several breast cancer cell lines[27] or osteoblasts.[28] In a pancreatic neuroendocrine tumor model in which the researchers treated tumors with the anti-IGF-1R antibody IMC-A12, elevated IR signaling before and after treatment may have manifested as intrinsic and adaptive resistance to anti-IGF-1R Ab-based therapies.[29] Also, authors have noted that hyperinsulinemia is a compensatory mechanism to IGF-1R inhibitors,[30,31] which may directly activate IR signaling pathways. In these regard, small-molecule tyrosine kinase domain inhibitors (TKI) of IGF-1R, which are under investigation in clinical trials, could be a better strategy to target IGF-1R/IR signaling, as IGF-1R monoclonal antibody induced a compensatory increase of IR phosphorylation, which could be abolished by IGF-1R TKI.[32] A challenge to the development of IGF-1R-targeted kinase inhibitors may be the similarity of the catalytic domain to that of the IR.[33-35] Inhibition of the IR in normal cells could have brought significant undesired effects on glucose homeostasis, and chronic treatment may result in symptoms of diabetes.[36] However, little data on the tolerability and efficacy of the small-molecule inhibitors of IGF-1R are currently available.[37] Further investigation of the role of targeting IR in lung cancer is warranted.

A recent study examined the role of insulin and phosphorylated IR (pIR) in patients with NSCLC.[38] The researchers confirmed the intracellular presence of insulin in 30 of 112 patients using IHC analysis and observed a significant correlation with pIR expression. Although the results of both DFS and OS analyses were not statistically significant, the investigators observed a trend of longer survival durations in patients with insulin-positive tumors than in those with insulin-negative tumors. One of the possible explanations for the increased survival durations in these patients is the close relationship of insulin reactivity with unaggressive, highly differentiated forms in the study population; however, we cannot conclude the significance of the survival difference because of the lack of statistical significance and relatively small number in the study. Furthermore, the researchers in this previous study correlated intracellular insulin levels, not pIR expression

levels, with patient survival, which only suggested that noncirculatory ligands impacted survival.

In conclusion, we demonstrated that IGF-1R expression was higher in patients with SCC or ever-smokers than in those with ADC or never-smokers. On the other hand, IR expression was higher in patients with ADC than those with SCC. In addition, we show the prognostic impact of IR expression on survival in patients with resected NSCLC. Given our current observations and the previous reports supporting a possible role of IR expression in the resistance mechanisms to IGF-1R–targeted agents, clinical trials are warranted to assess the therapeutic efficacy of co-targeting both IGF-1R and IR. We believe that the roles of the IR in lung cancer biology and tumorigenesis should be important subjects of future research.

FUNDING SUPPORT

This work was supported by National Institutes of Health Grant R01 CA100816 and the National Research Foundation of Korea (NRF) grant funded by the Korea government (MEST) (No. 2011-0017639) (to H.-Y.L.) and by Department of Defense Grant W81XWH-04-1-0142-01-VITAL and W8XWH-06-1-0303 BATTLE (to W.K.H.).

CONFLICT OF INTEREST DISCLOSURES

The authors made no disclousres

REFERENCES

1. Janku F, Stewart DJ, Kurzrock R. Targeted therapy in non-small cell lung cancer—is it becoming a reality? *Nat Rev Clin Oncol*. 2010;7:401-414.
2. Pollak M. Insulin and insulin-like growth factor signalling in neoplasia. *Nat Rev Cancer*. 2008;8:915-928.
3. Ryan PD, Goss PE. The emerging role of the insulin-like growth factor pathway as a therapeutic target in cancer. *Oncologist*. 2008;13:16-24.
4. Camidge DR, Dziadziuszko R, Hirsch FR. The rationale and development of therapeutic insulin-like growth factor axis inhibition for lung and other cancers. *Clin Lung Cancer*. 2009;10:262-272.
5. Frasca F, Pandini G, Sciacca L, et al. The role of insulin receptors and IGF-I receptors in cancer and other diseases. *Arch Physiol Biochem*. 2008;114:23-37.
6. Denley A, Wallace JC, Cosgrove LJ, Forbes BE. The insulin receptor isoform exon 11- (IR-A) in cancer and other diseases: a review. *Horm Metab Res*. 2003;35:778-785.
7. Mathieu MC, Clark GM, Allred DC, Goldfine ID, Vigneri R. Insulin receptor expression and clinical outcome in node-negative breast cancer. *Proc Assoc Am Physicians*. 1997; 109:565-571.
8. Law JH, Habibi G, Hu K, et al. Phosphorylated insulin-like growth factor-i/insulin receptor is present in all breast cancer subtypes and is related to poor survival. *Cancer Res*. 2008; 68:10238-10246.
9. Novosyadlyy R, Vijayakumar A, Lann D, Fierz Y, Kurshan N, LeRoith D. Physical and functional interaction between polyoma virus middle T antigen and insulin and IGF-I receptors is required for oncogene activation and tumour initiation. *Oncogene*. 2009;28:3477-3486.
10. Belfiore A, Frasca F, Pandini G, Sciacca L, Vigneri R. Insulin receptor isoforms and insulin receptor/insulin-like growth factor receptor hybrids in physiology and disease. *Endocr Rev*. 2009;30:586-623.
11. Ma J, Li H, Giovannucci E, et al. Prediagnostic body-mass index, plasma C-peptide concentration, and prostate cancer-specific mortality in men with prostate cancer: a long-term survival analysis. *Lancet Oncol*. 2008;9:1039-1047.
12. Cappuzzo F, Tallini G, Finocchiaro G, et al. Insulin-like growth factor receptor 1 (IGF1R) expression and survival in surgically resected non-small-cell lung cancer (NSCLC) patients. *Ann Oncol*. 2010;21:562-527.
13. Gong Y, Yao E, Shen R, et al. High expression levels of total IGF-1R and sensitivity of NSCLC cells in vitro to an anti-IGF-1R antibody (R1507). *PLoS One*. 2009;4:e7273.
14. Dziadziuszko R, Merrick DT, Witta SE, et al. Insulin-like growth factor receptor 1 (IGF1R) gene copy number is associated with survival in operable non-small-cell lung cancer: a comparison between IGF1R fluorescent in situ hybridization, protein expression, and mRNA expression. *J Clin Oncol*. 2010;28:2174-2180.
15. Chang MH, Lee J, Han J, et al. Prognostic role of insulin-like growth factor receptor-1 expression in small cell lung cancer. *APMIS*. 2009;117:861-869.
16. Herbst RS, Heymach JV, Lippman SM. Lung cancer. *N Engl J Med*. 2008;359:1367-1380.
17. Kim SJ, Rabbani ZN, Dong F, et al. Phosphorylated epidermal growth factor receptor and cyclooxygenase-2 expression in localized non-small cell lung cancer. *Med Oncol*. 2010;27: 91-97.
18. Yuan P, Kadara H, Behrens C, et al. Sex determining region Y-Box 2 (SOX2) is a potential cell-lineage gene highly expressed in the pathogenesis of squamous cell carcinomas of the lung. *PLoS One*. 2010;5:e9112.
19. Travis WD, Brambilla E, Muller-Hermelink HK, Harris CC. Tumours of the lung. In: Travis WD, Brambilla E, Muller-Hermelink HK, Harris CC, editors. Pathology and Genetics: Tumours of the Lung, Pleura, Thymus and Heart. Lyon: International Agency for Research on Cancer (IARC); 2004:9-124.
20. Bild AH, Yao G, Chang JT, et al. Oncogenic pathway signatures in human cancers as a guide to targeted therapies. *Nature*. 2006;439:353-357.
21. Lee ES, Son DS, Kim SH, et al. Prediction of recurrence-free survival in postoperative non-small cell lung cancer patients by using an integrated model of clinical information and gene expression. *Clin Cancer Res*. 2008;14:7397-7404.
22. Zhang H, Fagan DH, Zeng X, Freeman KT, Sachdev D, Yee D. Inhibition of cancer cell proliferation and metastasis by insulin receptor downregulation. *Oncogene*. 2010;29: 2517-2527.
23. Cox ME, Gleave ME, Zakikhani M, et al. Insulin receptor expression by human prostate cancers. *Prostate*. 2009;69: 33-40.
24. Avnet S, Sciacca L, Salerno M, et al. Insulin receptor isoform A and insulin-like growth factor II as additional treatment targets in human osteosarcoma. *Cancer Res*. 2009;69: 2443-2452.

25. Kim J, Kim ES, Liu D, et al. Comprehensive analysis of expression patterns of insulin-like growth factor and Src pathway in patients with non-small cell lung cancer: two large, independent series of tissue microarray. *J Clin Oncol*. 2010;28:15s (abstr 10531).
26. Gualberto A, Dolled-Filhart M, Gustavson M, et al. Molecular analysis of non-small cell lung cancer (NSCLC) identifies subsets with different sensitivity to insulin like growth factor I receptor (IGF-IR) inhibition. *Clin Cancer Res*. 2010;16:4654-4665.
27. Zhang H, Pelzer AM, Kiang DT, Yee D. Down-regulation of type I insulin-like growth factor receptor increases sensitivity of breast cancer cells to insulin. *Cancer Res*. 2007;67: 391-397.
28. Fulzele K, DiGirolamo DJ, Liu Z, Xu J, Messina JL, Clemens TL. Disruption of the insulin-like growth factor type 1 receptor in osteoblasts enhances insulin signaling and action. *J Biol Chem*. 2007;282:25649-25658.
29. Ulanet DB, Ludwig DL, Kahn CR, Hanahan D. Insulin receptor functionally enhances multistage tumor progression and conveys intrinsic resistance to IGF-1R targeted therapy. *Proc Natl Acad Sci USA*. 2010;107:10791-10798.
30. Karp DD, Paz-Ares LG, Novello S, et al. Phase II study of the anti-insulin-like growth factor type 1 receptor antibody CP-751,871 in combination with paclitaxel and carboplatin in previously untreated, locally advanced, or metastatic non-small-cell lung cancer. *J Clin Oncol*. 2009;27:2516-2522.
31. Haluska P, Carboni JM, Loegering DA, et al. In vitro and in vivo antitumor effects of the dual insulin-like growth factor-I/insulin receptor inhibitor, BMS-554417. *Cancer Res*, 2006;66:362-371.
32. Buck E, Gokhale PC, Koujak S, et al. Compensatory insulin receptor (IR) activation on inhibition of insulin-like growth factor-1 receptor (IGF-1R): rationale for cotargeting IGF-1R and IR in cancer. *Mol Cancer Ther*. 2010;9:2652-2664.
33. Sabbatini P, Rowand JL, Groy A, et al. Antitumor activity of GSK1904529A, a small-molecule inhibitor of the insulin-like growth factor-I receptor tyrosine kinase. *Clin Cancer Res*. 2009;15:3058-3067.
34. Wahner Hendrickson AE, Haluska P, Schneider PA, et al. Expression of insulin receptor isoform A and insulin-like growth factor-1 receptor in human acute myelogenous leukemia: effect of the dual-receptor inhibitor BMS-536924 in vitro. *Cancer Res*. 2009;69:7635-7643.
35. Wood ER, Shewchuk L, Hassel A, et al. Discovery of an inhibitor of insulin-like growth factor 1 receptor activation: implications for cellular potency and selectivity over insulin receptor. *Biochem Pharmacol*. 2009;78:1438-1447.
36. Dziadziuszko R, Camidge DR, Hirsch FR. The insulin-like growth factor pathway in lung cancer. *J Thorac Oncol*. 2008; 3:815-818.
37. Gridelli C, Rossi A, Bareschino MA, Schettino C, Sacco PC, Maione P. The potential role of insulin-like growth factor receptor inhibitors in the treatment of advanced non-small cell lung cancer. *Expert Opin Investig Drugs*. 2010;19: 631-639.
38. Mattarocci S, Abbruzzese C, Mileo AM, et al. Intracellular presence of insulin and its phosphorylated receptor in non-small cell lung cancer. *J Cell Physiol*. 2009;221:766-770.

Histopathology 2011, **59**, 526–536. DOI: 10.1111/j.1365-2559.2011.03966.x

Clinicopathological and immunohistochemical analysis of spindle-cell carcinoid tumour of the lung

Koji Tsuta,[1,2] Neda Kalhor,[1] Ignacio I Wistuba[1,3] & Cesar A Moran[1]
[1]*Department of Pathology, The University of Texas M. D. Anderson Cancer Center, Houston, TX, USA,* [2]*Division of Pathology, National Cancer Center Hospital, Tokyo, Japan, and* [3]*Department of Thoracic/Head and Neck Medical Oncology, The University of Texas M. D. Anderson Cancer Center, Houston, TX, USA*

Date of submission 8 April 2010
Accepted for publication 13 September 2010

Tsuta K, Kalhor N, Wistuba I I & Moran C A
(2011) *Histopathology* **59**, 526–536

Clinicopathological and immunohistochemical analysis of spindle-cell carcinoid tumour of the lung

Aims: To analyse the clinicopathological features and immunohistchemical profile of spindle-cell carcinoid tumours (SCCT) of the lung.
Methods and results: Using a cut-off value of ≥50% spindle cells for defining SCCT, 13 were indentified among 80 consecutively resected carcinoid cases. SCCTs are asymptomatic and are peripherally located, well-demarcated tumours. Tumour cells were composed of elongated spindle cells, with scant to moderate amounts of cytoplasm and uniform nuclei with fine granular chromatin. Immunohistochemical analysis revealed that all 13 cases were positive for three neuroendocrine markers (chromogranin A, synaptophysin and CD56). Four tumours (30.7%) were positive for broad-spectrum cytokeratin (CK) and nine tumours (69.2%) were positive for thyroid transcription factor 1. All epithelial components were negative for vimentin, but 12 tumours (92.3%) were positive for stellate-shaped cells (so-called sustentacular cells).
Conclusions: SCCTs are clinically asymptomatic, peripherally located, well-demarcated tumours, and patients with SCCTs have a favourable outcome. The immunoreactivity pattern of SCCT (low reactivity of broad-spectrum CK and reactivity for vimentin in intratumoral sustentacular cells) might result in a misdiagnosis of SCCT as mesenchymal tumour; therefore, pathologists need to be familiar with this pattern.

Keywords: carcinoid tumour, lung, spindle cell

Abbreviations: CK, cytokeratin; EMA, epithelial membrane antigen; SCLC, small cell carcinoma of the lung; SCCT, spindle-cell carcinoid tumours; TTF, thyroid transcription factor

Introduction

Carcinoid tumours of the lung are composed of a homogeneous cellular proliferation with an organoid and trabecular structure. They are composed of small- to medium-sized round to polygonal cells with scant to moderate amounts of eosinophilic cytoplasm, and centrally located, round to oval nuclei with fine granular chromatin. However, a variety of morphological features can be observed in these tumours, including spindle, acinic, signet-ring, mucin-producing and oncocytic cells.[1]

Carcinoid tumours consisting predominantly of spindle cells are relatively uncommon. Felton *et al.*[2] reported the first case of spindle-cell carcinoid tumour (SCCT) in 1953. Although the definitions of SCCT have differed, approximately 100 cases of SCCT have been reported since this original description.[1,3–27] Most reports of lung SCCT have been case reports or brief

Address for correspondence: C A Moran, Department of Pathology, Unit 85, The University of Texas M. D. Anderson Cancer Center, 1515 Holcombe Boulevard, Houston, TX 77030, USA.
e-mail: CesarMoran@mdanderson.org.

references to SCCT in general accounts of pulmonary neuroendocrine carcinomas. In series analyses of neuroendocrine carcinomas, SCCTs have been observed to comprise 4.5–30.2% of all carcinoid tumours.[1,9,14,22,26]

Clinically, SCCTs are peripherally located asymptomatic tumours showing clinical behaviour ranging from extremely indolent[8,9,16,21,23] to more aggressive[10,13] than non-spindle cell carcinoid tumours. Histologically, SCCTs are arranged in a vague organoid pattern with sharply circumscribed borders and are composed of elongated spindle cells with scant to moderate amounts of cytoplasm and poorly defined cell borders. The nuclei are uniform, with fine granular chromatin and inconspicuous nucleoli.

Because of the characteristic morphological features of SCCT, the differential diagnosis includes many possibilities. Among them, small cell carcinoma of the lung (SCLC) is one of the most important in the differential diagnosis, because the clinical behaviour and treatment modalities of SCLCs are quite different from those of SCCTs.[15,16,25] Primary and metastatic mesenchymal tumours also enter into the differential diagnosis.[11,16,25,27] With those considerations, immunohistochemical analysis is useful in the differential diagnosis.[28] However, few articles have been published on analysing the immunohistochemical profile of a series of SCCTs.[23,26]

Eighty consecutively resected cases of carcinoid tumours were analysed to determine the clinicopathological significance of a spindle-cell component with the tumours grouped as spindle-cell component-negative (spindle-cell components <5%), spindle-cell minor (≥5 to <50%) and spindle-cell predominant (SCCT, ≥50%)

Material and methods

CASE SELECTION

Tumour specimens from patients who were diagnosed with neuroendocrine carcinomas between 1990 and 2005 were reviewed retrospectively. Tumour specimens were obtained from samples deposited in the files of The University of Texas M. D. Anderson Cancer Center Lung SPORE Tissue Bank (Houston, TX, USA). This was approved by the institutional review board. The patients' clinical information was collected, including age, gender, presenting symptoms, smoking history, tumour location (which lobe and whether central or not), maximum tumour size (in cm), lymph node status, treatment modalities, site of any tumour recurrence and duration of recurrence or survival.

HISTOLOGICAL EXAMINATION

All available haematoxylin and eosin-stained slides in each case were examined and assessed for the parameters described below; the researchers were unaware of any clinical details for any patient. The histological diagnosis of carcinoid tumour was based on the classification schema of the latest edition of the World Health Organization classification.[29] The carcinoid tumours were divided into three groups: spindle-cell component-negative (spindle-cell components <5%), spindle-cell minor (≥5 to <50%) and spindle-cell predominant (SCCT, ≥50%). Thirteen cases of SCCT were thereby identified. The following pathological features were evaluated for all specimens: the infiltrative growth of the adjacent normal architecture, the presence of blood or lymphatic vessel invasion and the presence of necrosis. The stroma between the tumour nests was rich in capillary or fibrous tissue, and the presence of bone formation was noted. The histological features of the tumour cells were also evaluated, including the nuclear to cytoplasmic ratio, the presence of giant cells (more than one cell/10 high-power fields), chromatin pattern (which was categorized as fine, granular or coarse) and the presence of conspicuous nucleoli.

IMMUNOHISTOCHEMICAL EXAMINATION

Immunohistochemical analysis was performed on the 13 SCCT cases. For immunohistochemistry, 4-μm-thick sections were deparaffinized. Heat-induced epitope retrieval with target retrieval solution (Dako, Carpinteria, CA, USA) was performed. Slides were allowed to cool at room temperature for about 30 min and then rinsed with deionized water. The slides were then treated with 3% hydrogen peroxide for 20 min to block endogenous peroxidase activity, followed by washing in deionized water for 2–3 min. The slides were then incubated with primary antibodies against chromogranin A (1:100, DAK-A3; Dako), synaptophysin (1:200, polyclonal; Dako), CD56 (1:200, 123C3.D5; Neomarkers, Fremont, CA, USA), broad-spectrum cytokeratin (1:100, MNF116; Dako), cytokeratin 7 (CK7; 1:100, OV-TL 12/30; Dako), epithelial membrane antigen (EMA; 1:100, E29; Dako), thyroid transcription factor 1 (TTF-1; 1:100, 8G7G3/1; Dako), vimentin (1:200, V9; Dako), E-cadherin (1:100, G10; Santa Cruz Biotechnology, Heidelberg, Germany) and Ki-67 (1:100, MIB1; Dako). Immunoreactions were detected using the EnVison-Plus system (Dako) and visualized with 3,3′-diaminobenzidine, followed by

counterstaining with haematoxylin. Appropriate positive and negative controls were used for each antibody.

The immunostaining results were evaluated on a four-point scale, with 1+ being reactivity in 5–25% of the tumour cell population, 2+ in 26–50% of the cells, 3+ in 51–75% of the cells and 4+ in >76% of the cells. Staining in rare scattered individual cells (<5%) was considered as a negative result. Ki-67 immunoreactivity was evaluated in positive nuclei of the highest labelling region (so-called hot spots) of 1000 tumour nuclei. Disagreements regarding the histological and immunohistochemical factors were resolved by means of a joint review of the slides using a multiheaded microscope.

STATISTICAL ANALYSIS

All statistical analyses were performed using SPSS version 12.0 software for Windows (SPSS, Chicago, IL, USA). The Wilcoxon rank-sum test was used to analyse the continuous variables and Fisher's exact test to analyse other clinicopathological data. The recurrence-free survival curves were derived using the Kaplan–Meier method and the curves compared using the log-rank test. $P \leq 0.05$ was considered to be significant.

Results

CLINICAL FEATURES OF SCCT

The clinicopathological summary of the 13 cases of SCCT is shown in Table 1. There were 11 cases of typical and two cases of atypical carcinoid tumour. The patients consisted of four men and nine women, with a mean age (at the time of diagnosis) of 54.4 years (range 33–74 years). Presenting symptoms were documented in one of 11 patients. Smoking history was documented in 12 cases, with four patients each being never, former and present smokers. The tumour size ranged from 1.0 to 13.0 cm (mean 3.20 cm). The tumour was located in the right-upper lobe in three patients, the right-middle lobe in five, the right-lower lobe in one, the left-upper lobe in two and the left-lower lobe in two. The tumour was located in the central portion (second-order bronchi) of the lung in six patients and in the intermediate (third- or fourth-order bronchi) or peripheral portion (further distal bronchi) in seven patients. Lymph node metastasis was observed

Table 1. Clinicopathological summary of 13 cases of spindle-cell carcinoid tumour

No.	Sex	Age (years)	Symptom	Smoking	Size (cm)	Site		LN	Preope diag	Final diag	Outcome (month)	Spindle cell (%)
1	F	37	–	Present	3.1	RUL	C	M	Meta of sarcoma	TC	1	50
2	F	50	–	Never	4.5	LLL	C	S	–	TC	60	50
3	M	72	–	Former	2.5	LUL	P	0	TC	TC	60	60
4	M	44	Haemoptysis	Former	4.0	RML	P	0	–	TC	66	60
5	F	43	–	Present	1.4	LLL	C	0	TC	AC	94	60
6	F	65	–	Former	4.0	RLL	C	0	TC	TC	41	70
7	F	73	–	Present	1.0	RUL	P	0	–	TC	169	80
8	M	40	–	Present	13	RML	P	0	TC	TC	129	90
9	F	74	–	Never	1.6	RML	P	0	TC	TC	116	90
10	F	40	–	Never	1.6	RML	P	0	SCLC	TC	99	90
11	F	66	NA	NA	1.6	LUL	P	S	SCLC or AC	AC	55	100
12	F	70	–	Never	1.8	RML	C	0	TC	TC	100	100
13	M	33	–	Former	1.6	RUL	C	0	–	TC	31	100

LN, Lymph node metastasis; Preope, preoperative; Diag, diagnosis; M, male; F, female; NA, not assessed; RUL, right upper lobe; RML, right middle lobe; RLL, right lower lobe; LUL, left upper lobe; LLL, left lower lobe; C, central portion; P, non-central portion; TC, typical carcinoid; AC, atypical carcinoid; SCLC, small cell carcinoma; Meta, metastasis.

in three patients. Nine patients received a preoperative diagnosis at the primary hospital; of these, six had a diagnosis of typical carcinoid tumour, one had a diagnosis of SCLC or atypical carcinoid tumour, one a diagnosis of SCLC and one a diagnosis of metastasis of sarcoma (this patient had a history of leiomyosarcoma of the uterus). All 13 patients were alive without disease recurrence at the time of analysis.

HISTOLOGICAL FEATURES OF SCCT

Spindle-cell components were observed in 22 cases (27.5%), with SCCT then diagnosed in 13 cases (16.3%). The spindle-cell components were 10–100% (average 56.6%) in all carcinoid tumours and were 50–100% (average 76.9%) in the SCCTs. Three of 13 cases (23%) consisted of only spindle cells. SCCTs were arranged in a vague organoid pattern with sharply circumscribed borders (Figure 1A). These tumour cells were composed of elongated spindle cells, with scant to moderate amounts of cytoplasm and poorly defined cell borders, and with uniform nuclei with fine granular chromatin and inconspicuous nucleoli (Figure 1B,C).

Three cases with lymph node metastasis were composed of only spindle cells in two cases (primary site; the spindle-cell component was 100% in one case and 50% in the other) and mixed with spindle cells and non-spindle cells in one case (primary site; spindle-cell component was 50%).

CLINICOPATHOLOGICAL DIFFERENCES AMONG TUMOURS CONSIDERED BY SPINDLE-CELL GROUPING

Clinicopathological differences among the tumours grouped as spindle-cell component negative (spindle-cell components <5%), spindle-cell minor (≥5 to <50%) and spindle-cell predominant (SCCT, ≥50%) are shown in Table 2. The presence of symptoms at diagnosis was observed less frequently in patients with SCCTs ($P = 0.088$). Spindle-cell minor tumours and SCCTs tended to occur in peripheral lesions ($P = 0.059$). There were no statistical differences in occurrence age of occurrence, gender, smoking history, tumour size, lymph node metastasis or pathological stage among these three groups.

Among the histological features, SCCTs showed less infiltrative growth ($P = 0.002$), a high nuclear cytoplasmic ratio ($P = 0.001$) and a fine chromatin pattern ($P = 0.034$). There were no statistical differences in blood and lymph vessel invasion, gender, presence of necrosis, pattern of the stroma, bone formation, presence of giant tumour cells or presence of conspicuous nucleoli. The mean follow-up time for all 80 patients

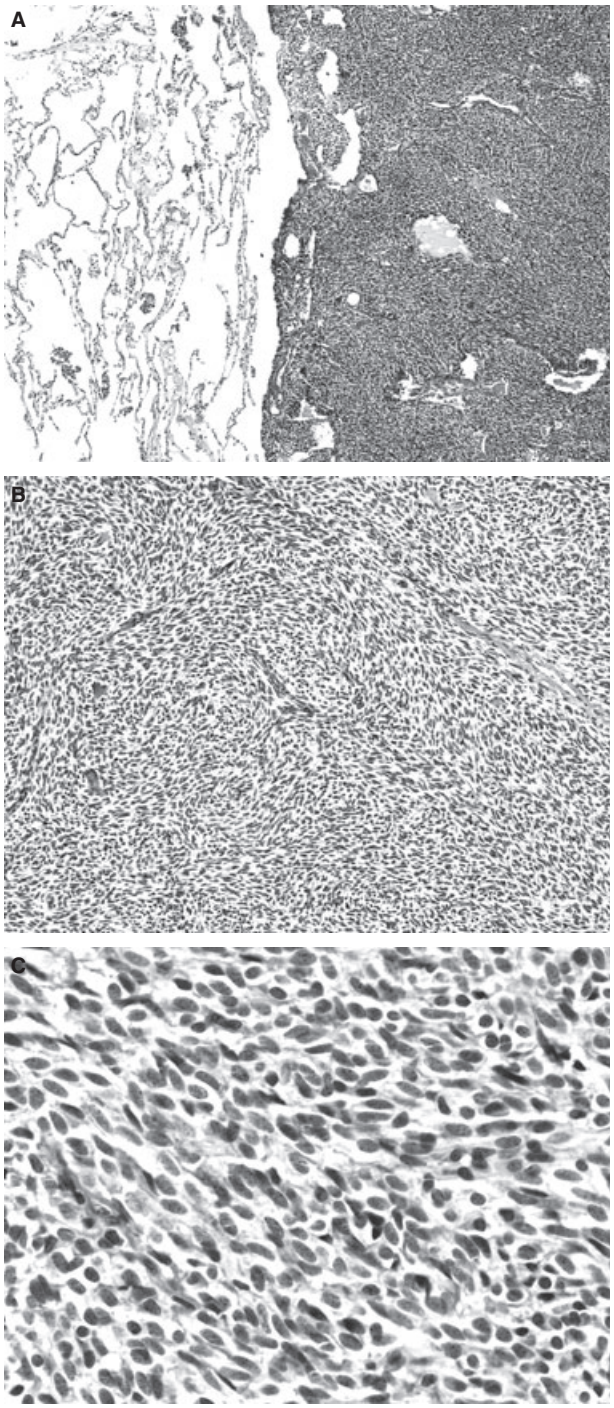

Figure 1. Microscopic features of spindle-cell carcinoid tumour. **A**, Spindle-cell carcinoid tumour (SCCT) shows sharply circumscribed borders [haematoxylin and eosin (H&E)-stained]. **B**, SCCT is arranged in a vague organoid pattern. These tumour cells are composed of elongated spindle cells with scant to moderate amounts of cytoplasm and poorly defined cell borders (H&E-stained). **C**, The tumour nuclei are uniform, with fine granular chromatin and inconspicuous nucleoli (H&E-stained).

Table 2. Comparison of clinicopathological features of 13 cases of spindle-cell carcinoid tumour

	Spindle-cell component			
	Negative <5%	Minor ≥5 to <50%	Predominant ≥50%	*P*-value
Diagnosis				
Typical	50	7	11	0.804
Atypical	8	2	2	
Age (years)	53.1	61.7	54.4	0.253
Gender				
Female	33	7	9	0.397
Male	25	2	4	
Symptom				
None	35	4	11	0.088
Present	22	4	1	
Smoking				
Never	25	3	4	0.282
Former	23	5	4	
Present	8	0	4	
Lobe				
Right upper	7	1	3	0.106
Right middle	5	0	5	
Right lower	20	5	1	
Left upper	9	2	2	
Left lower	16	1	2	
Left main	1	0	0	
Location				
Central	40	3	6	0.059
Non-central	18	6	7	
Tumour size (cm)	2.98	2.41	3.21	0.700
Lymph node metastasis				
Absent	46	6	10	0.951
Present	12	2	3	
Pathological stage				
I and II	46	5	10	0.682
III and IV	5	1	0	
Infiltrative growth				
Absent	20	2	11	0.002
Present	38	7	2	

Table 2. (*Continued*)

	Spindle-cell component			
	Negative <5%	Minor ≥5 to <50%	Predominant ≥50%	*P*-value
Blood-vessel invasion				
Absent	31	7	8	0.370
Present	27	2	5	
Lymph-vessel invasion				
Absent	37	5	9	0.806
Present	21	4	4	
Neoplastic necrosis				
Absent	54	8	13	0.530
Present	4	1	0	
Stroma				
Capillary	40	8	9	0.463
Fibrous	18	1	4	
Bone formation				
Absent	43	9	11	0.180
Present	15	0	2	
Nuclear cytoplasmic ratio				
Low to moderate	48	6	4	0.001
High	10	3	9	
Giant cell				
Absent	45	9	11	0.261
Present	13	0	2	
Chromatin pattern				
Fine	29	7	11	0.034
Coarse	29	2	2	
Nucleolus				
Inconspicuous	45	8	12	0.387
Conspicuous	13	1	1	

was 78 months (range 1–169 months). There were no statistical differences ($P = 0.5174$) in the 5-year recurrence-free survival among patients with SCCT (100%), carcinoid with spindle-cell minor (88.9%) and spindle-cell negative (90.2%) carcinoid tumours (Figure 2).

IMMUNOHISTOCHEMICAL FINDINGS

The immunohistochemical results for the SCCTs are shown in Table 3 and Figure 3. All 13 cases were positive for three neuroendocrine markers: chromogranin A, synaptophysin and CD56. However, the distribution of positive cells for these three neuroendocrine markers was variable, with chromogranin A being the best marker for diagnosing SCCT (Figure 4A). Immunoreactivity of broad-spectrum cytokeratin (NMF116) was observed in only four cases (30.7%), with three of these four cases showing focal (<50%) reactivity (Figure 4B). CK7 was positive in 10 cases (76.2%), with four cases showing diffuse (≥50%)

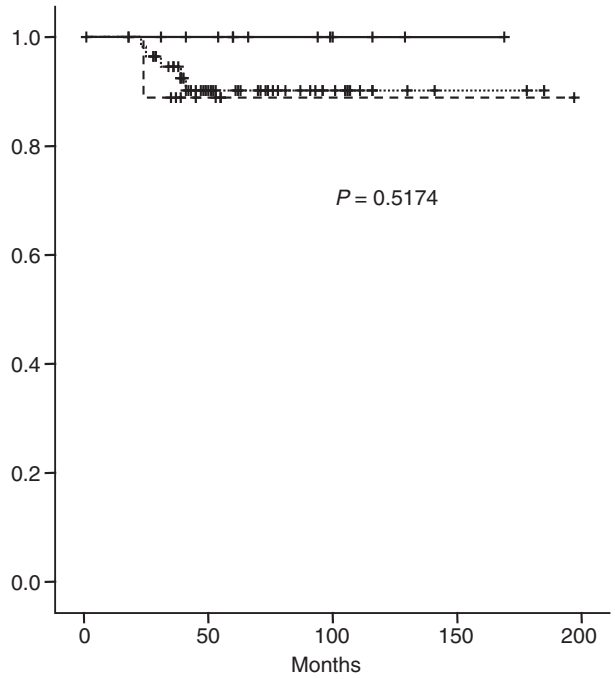

Figure 2. The recurrence-free survival rates for patients with spindle-cell carcinoid tumour (SCCT). The 5-year recurrence-free survival rates for cases with SCCT (solid line; 100%), carcinoid with spindle-cell minor (dashed line; 88.9%), and spindle-cell negative (square-dot line; 90.2%) carcinoid tumours, respectively.

reactivity (Figure 4C). EMA was positive in seven cases (53.8%), but all seven cases showed focal (<50%) reactivity. Twelve cases showed at least partial reactivity for broad-spectrum CK, CK7 or EMA. However, one case was negative for these three markers. TTF-1 was positive in nine cases (69.2%) but only one case showed diffuse (≥50%) reactivity (Figure 4D). TTF-1 was also positive in the one case that was negative for all three epithelial markers. All epithelial components were negative for vimentin, but 12 cases (92.3%) were positive for stellate-shaped cells (sustentacular cells). Some vimentin-positive areas occupied about half the tumour nests (both epithelial and sustentacular cells; Figure 5A,B). Membranous E-cadherin immunoreactivity was observed in 10 cases (76.2%), but nine of the 10 cases showed focal (<50%) reactivity. The mean proliferative index, assessed by Ki-67 staining, was 1.80% (range 0.1–9.5%).

Discussion

In the present study, we report on the clinicopathological and immunohistochemical characteristics of SCCTs. Spindle-cell components were observed in 27.5% of the cases. We set the cut-off value for defining SCCT at ≥50% spindle cells within the tumour

Table 3. Immunohistochemical results of spindle-cell carcinoid tumour

No.	Chromogranin A	Synaptophysin	CD56	CK	CK7	EMA	TTF-1	Vimentin	E-cadherin	Ki-67 (%)
1	4	2	3	0	0	1	2	SC2	1	9.5
2	4	2	2	0	3	2	1	SC1	2	2.1
3	4	2	4	0	0	0	1	SC1	0	0.3
4	4	3	4	0	1	2	4	SC2	1	1.8
5	4	4	4	0	1	0	1	SC1	3	1.3
6	3	3	3	0	3	0	2	SC2	1	2.3
7	4	3	3	1	2	1	0	SC1	0	0.3
8	4	4	4	3	2	2	2	0	1	1.8
9	4	4	4	0	1	0	1	SC1	2	0.1
10	3	4	4	0	3	1	0	SC1	1	1.5
11	4	4	4	1	0	0	0	SC2	0	1.1
12	4	3	4	2	2	0	2	SC1	1	0.2
13	4	4	4	0	3	1	0	SC2	1	1.1

CK, Cytokeratin; EMA, epithelial membrane antigen; TTF-1, thyroid transcription factor-1; SC, sustentacular cell.

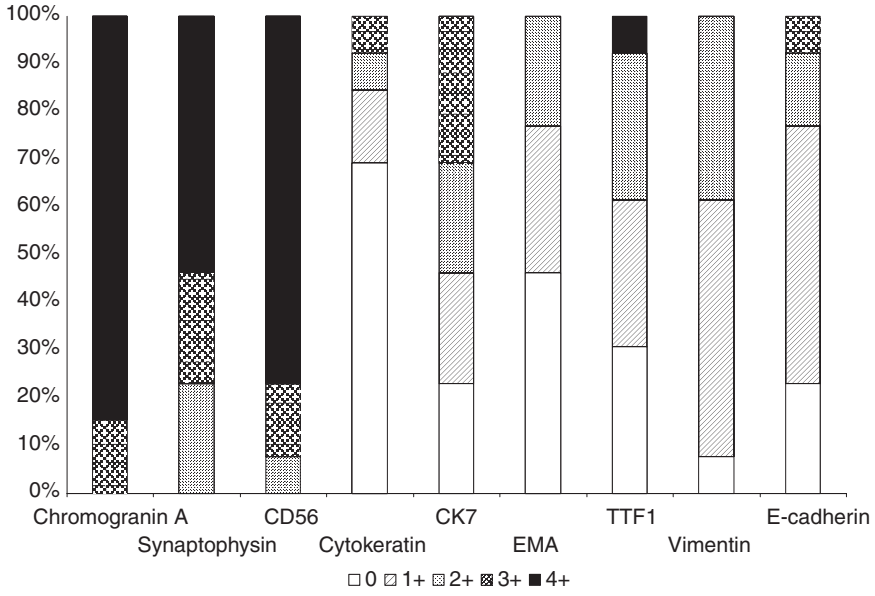

Figure 3. Bar graphs depicting the comparative percentages of positive immunohistochemical results for each distribution, with 1+ being reactivity in 5–25% of the tumour cell population, 2+ in 26–50% of cells, 3+ in 51–75% of cells and 4+ in >76% of cells.

and then found 13 cases (16.3%) among 80 surgically resected carcinoid cases. It is of note that this tumour exhibited an unusual immunostaining pattern despite the epithelial tumour: low reactivity for the epithelial marker of broad-spectrum CK and reactivity for mesenchymal markers of vimentin in intratumoral sustentacular cells.

Clinically, the SCCTs were asymptomatic, peripherally located tumours. We found no differences in unfavourable outcomes (recurrence, death and lymph node metastasis) between patients with SCCTs and those with non-SCCTs. Some authors have reported that SCCTs have a more aggressive clinical course than non-SCCTs.[10,13] However, other single case reports and series analyses of SCCTs have reported an indolent clinical course for SCCTs.[16,21,23] In addition, we also found no differences in histological features of tumour aggressiveness (presence of blood and/or lymphatic vessel invasion) between SCCTs and non-SCCTs. A high Ki-67 index is a known unfavourable factor in pulmonary carcinoid tumours.[30] For the SCCT cases we studied, the mean Ki-67 index was 1.80%, which is within the range of previously reported Ki-67 indices for typical carcinoid tumours.[31] These results indicate that the presence of a spindle-cell component is not in itself an unfavourable factor.

Because of their spindle-cell and neuroendocrine morphology, SCCTs need to be differentiated from SCLCs.[15,16,25] Among the patients in our study who received a preoperative diagnosis at the primary hospital, two of nine cases were misdiagnosed (one as SCLC and one as metastasis of sarcoma). SCLCs are seen most often in male smokers.[32] However, eight of 12 cases in our cohort were former or active smokers. Tumour location (central in SCLC, peripheral in SCCT) might be a factor in the differential diagnosis. However, our data and previous reports have shown that some SCCTs occur in the central portion.[14–16,26] Furthermore, approximately 5% of SCLCs occur in a peripheral portion.[32] Therefore, information regarding smoking habits and tumour locations is less informative for differential diagnosis. Histologically, the key factors for distinguishing SCLCs from SCCTs correctly are the presence of mitoses and necrosis and the chromatin pattern. However, several authors have reported that it is difficult to distinguish between SCLCs and carcinoid tumours in small biopsy tissue fragments or cytological samples.[33,34] In such cases, our data and previous reports have shown that a low (<20%) Ki-67 index is one of the most helpful diagnostic markers.[33]

Mesenchymal tumours must also be considered in the differential diagnosis of SCCTs. Although SCCT is an epithelial tumour we found that vimentin, which is used widely as a mesenchymal marker, was positive in 12 cases (92.3%). In some cases vimentin-positive areas occupied about half of the tumour nests. Similarly, one case report showed diffuse immunoreactivity of vimentin in SCCT, and these authors emphasized the resemblance to monophasic synovial sarcoma.[27] Most of the vimentin-positive cells in our study were considered to be sustentacular cells, because the positive cells had a stellate shape and several authors have reported that 18–82% of pulmonary carcinoid tumours contain sustentacular cells.[35,36] We have

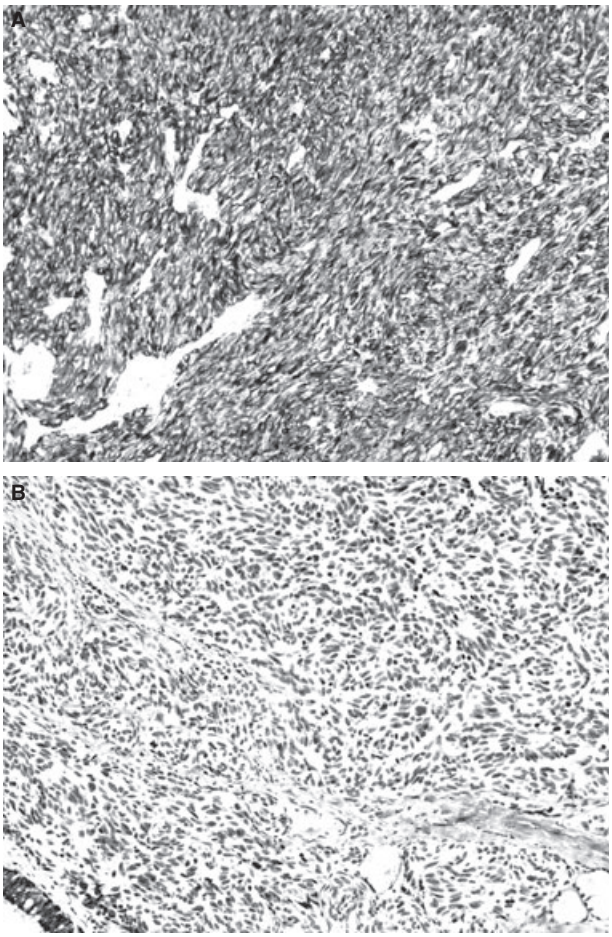

Figure 4. Immunohistochemical results for spindle-cell carcinoid tumours (SCCT). **A**, SCCT are strongly diffusely positive for chromogranin A. **B**, SCCT are negative for broad-spectrum cytokeratin, but bronchial epithelia are positive (left lower corner). **C**, SCCT are positive for cytokeratin 7. **D**, SCCT are positive for thyroid transcription factor-1.

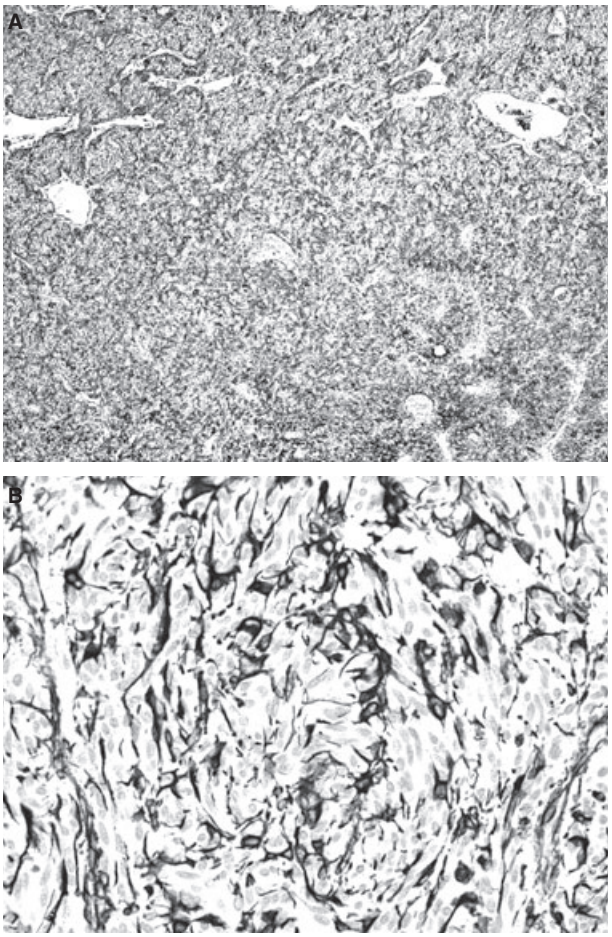

Figure 5. **A**, Vimentin-positive area occupies about half the area in the tumour. **B**, Vimentin-positive cells have a stellate shape with long slender cytoplasmic processes. Epithelial components are negative for vimentin.

found recently that the presence of sustentacular cells differs in the morphological subtypes of carcinoid tumour, with spindle-cell types being the most prevalent subtype.[37] This immunostaining pattern of SCCTs with regard to intratumoural sustentacular cells might result in a misdiagnosis of mesenchymal tumour.

In the diagnosis of undifferentiated tumours, broad-spectrum CK is one of the most useful markers in a preliminary immunohistochemical panel.[28] Immunoreactivity of broad-spectrum CK (NMF116) for SCCT was observed in only four cases (30.7%) in our study, and three of these showed focal (<50%) reactivity. Previous studies have shown that about half of carcinoid cases are positive for broad-spectrum CK, despite their epithelial origin,[1] and SCCT is negative for broad-spectrum CK.[23,27] When tumours that are highly suspected of being epithelial in origin are negative for broad-spectrum CK, antibodies for EMA and/or Cam5.2 are recommended for the second panel to determine their origin.[28] In the present study, we found that EMA was not useful when used in conjunction with broad-spectrum CK to diagnose SCCT. Instead, we found that CK7 was positive in 10 cases (76.2%), and four cases showed diffuse (≥50%) reactivity. CK7 expression rates for pulmonary carcinoid tumours have been reported to be 22–63%.[38,39] However, there are no reports regarding CK7 expression in SCCTs. Twelve cases showed at least partial reactivity for broad-spectrum CK, CK7 or EMA. However, one case was negative for these three markers.

TTF1 expression in pulmonary carcinoid tumours is a matter of debate. The incidence of TTF-1 expression in pulmonary carcinoid tumour has been reported to

range from 0% to 94%.[26,32,40] We found that TTF-1 was positive in nine cases (69.2%), but only one case showed diffuse (≥50%) reactivity. Furthermore, TTF-1 positive cases included only the one case in which all three epithelial markers were negative. Du *et al.*[26] found a low incidence of TTF-1 positivity in typical carcinoid tumours (27.8%), but they found a high TTF-1-positive incidence (85.7%) in their cases with spindle-cell morphology. These immunohistochemical results support the recommendation to use broad-spectrum CK, CK7 and/or TTF-1 antibodies for the diagnosis of peripherally located spindle-cell lesions of the lung.

Of the three neuroendocrine markers for which all 13 cases were positive (chromogranin A, synaptophysin and CD56), we recommend the use of chromogranin A for diagnosing pulmonary spindle-cell tumours, not only for its sensitivity but also to avoid misdiagnosis. CD56 is a well-known and highly sensitive neuroendocrine marker, but it also shows reactivity in synovial sarcoma.[41] A recent study has shown that the lung is the second most frequent location for synovial sarcoma after the extremities. Owing to similarities in not only morphological features, but also clinical features (younger age at occurrence compared with lung carcinoma, and occurrence at peripheral locations), monophasic synovial sarcoma is the most important consideration in the differential diagnosis of SCCT.[27]

Conflict of interests

No potential conflicts of interest were disclosed.

Acknowledgements

We would like to thank Susan Cweren and Denise Woods for their skilful technical assistance and the Department of Scientific Publications at M. D. Anderson Cancer Center for their help with English editing. This work was supported in part by a grant from the US Department of Defense PROSPECT W81XWH-07-1-0306.

References

1. Travis WD, Linnoila RI, Tsokos MG *et al.* Neuroendocrine tumors of the lung with proposed criteria for large-cell neuroendocrine carcinoma: an ultrastructural, immunohistochemical, and flow cytometric study of 35 cases. *Am. J. Surg. Pathol.* 1991; **15;** 529–553.
2. Felton WL, Liebow AA, Lindskog GE. Peripheral and multiple bronchial adenomas. *Cancer* 1953; **6;** 555–567.
3. Kay S. Histologic and histogenetic observations on the peripheral adenoma of the lung. *AMA Arch. Pathol.* 1958; **65;** 395–402.
4. Sobota JT, Reed RJ. Multiple bronchial adenomas, Cushing's syndrome and hypokalemic alkalosis. *Dis. Chest* 1964; **46;** 367–371.
5. Heimburger IL, Kilman JW, Battersby JS. Peripheral bronchial adenomas. *J. Thorac. Cardiovasc. Surg.* 1966; **52;** 542–549.
6. Gmelich JT, Bensch KG, Liebow AA. Cells of Kultschitzky type in bronchioles and their relation to the origin of peripheral carcinoid tumor. *Lab. Invest.* 1967; **17;** 88–98.
7. Dube VE. Peripheral bronchial carcinoid with a spindle-cell pattern. Report of a case. *Arch. Pathol.* 1970; **89;** 374–377.
8. Arrigoni MG, Woolner LB, Bernatz PE. Atypical carcinoid tumors of the lung. *J. Thorac. Cardiovasc. Surg.* 1972; **64;** 413–421.
9. Salyer DC, Salyer WR, Eggleston JC. Bronchial carcinoid tumors. *Cancer* 1975; **36;** 1522–1537.
10. Bonikos DS, Bensch KG, Jamplis RW. Peripheral pulmonary carcinoid tumors. *Cancer* 1976; **37;** 1977–1998.
11. Churg A. Large spindle cell variant of peripheral bronchial carcinoid tumor. *Arch. Pathol. Lab. Med.* 1977; **101;** 216–218.
12. Heilman E, Feiner H. The role of electron microscopy in the diagnosis of unusual peripheral lung tumors. *Hum. Pathol.* 1978; **9;** 589–593.
13. Gillespie JJ, Luger AM, Callaway LA. Peripheral spindled carcinoid tumor: a review of its ultrastructure, differential diagnosis, and biologic behavior. *Hum. Pathol.* 1979; **10;** 601–606.
14. Cooney T, Sweeney EC, Luke D. Pulmonary carcinoid tumours: a comparative regional study. *J. Clin. Pathol.* 1979; **32;** 1100–1109.
15. McDonnell L, Sweeney EC. Spindle cell atypical bronchial carcinoid. *Ir. J. Med. Sci.* 1980; **149;** 66–69.
16. Ranchod M, Levine GD. Spindle-cell carcinoid tumors of the lung: a clinicopathologic study of 35 cases. *Am. J. Surg. Pathol.* 1980; **4;** 315–331.
17. Craig ID, Finley RJ. Spindle-cell carcinoid tumor of lung. Cytologic, histopathologic and ultrastructural features. *Acta Cytol.* 1982; **26;** 495–498.
18. Geller SA, Gordon RE. Peripheral spindle-cell carcinoid tumor of the lung with type II pneumocyte features. An ultrastructural study with comments on possible histogenesis. *Am. J. Surg. Pathol.* 1984; **8;** 145–510.
19. el-Salhy M, Lundqvist M, Wilander E. Bronchial carcinoids and phaeochromocytomas. A comparative study with special emphasis on S-100 protein, serotonin and neuron-specific enolase (NSE) immunoreactivity. *Acta Pathol. Microbiol. Immunol. Scand A* 1986; **94;** 229–235.
20. Szyfelbein WM, Ross JS. Carcinoids, atypical carcinoids, and small-cell carcinomas of the lung: differential diagnosis of fine-needle aspiration biopsy specimens. *Diagn. Cytopathol.* 1988; **4;** 1–8.
21. Abdi EA, Goel R, Bishop S, Bain GO. Peripheral carcinoid tumours of the lung: a clinicopathological study. *J. Surg. Oncol.* 1988; **39;** 190–196.
22. Hasleton PS, al-Saffar N. The histological spectrum of bronchial carcinoid tumours. *Appl. Pathol.* 1989; **7;** 205–218.
23. Fekete PS, Cohen C, DeRose PB. Pulmonary spindle cell carcinoid. Needle aspiration biopsy, histologic and immunohistochemical findings. *Acta Cytol.* 1990; **34;** 50–56.
24. Min KW. Diagnostic usefulness of sustentacular cells in paragangliomas: immunocytochemical and ultrastructural investigation. *Ultrastruct. Pathol.* 1998; **22;** 369–376.
25. Hummel P, Cangiarella JF, Cohen JM, Yang G, Waisman J, Chhieng DC. Transthoracic fine-needle aspiration biopsy of pulmonary spindle cell and mesenchymal lesions: a study of 61 cases. *Cancer* 2001; **93;** 187–198.

26. Du EZ, Goldstraw P, Zacharias J *et al.* TTF-1 expression is specific for lung primary in typical and atypical carcinoids: TTF-1-positive carcinoids are predominantly in peripheral location. *Hum. Pathol.* 2004; **35;** 825–831.
27. Zhong Y, Wu S, Andaz S, Danovich S, Lin J. Pulmonary carcinoid tumor masquerading as a synovial sarcoma. *Int. J. Surg. Pathol.* 2011; **19;** 71–74.
28. Bahrami A, Truong LD, Ro JY. Undifferentiated tumor: true identity by immunohistochemistry. *Arch. Pathol. Lab. Med.* 2008; **132;** 326–348.
29. Travis WD, Colby T, Corrin B *et al.* Tumors of the lung. In Kleihues P, Sobin LH, eds. *WHO classification of tumors. pathology and genetics of tumors of the lung, pleura, thymus and heart*. Lyon, France: IARC Press, 2004: 9–124.
30. Costes V, Marty-Ané C, Picot MC *et al.* Typical and atypical bronchopulmonary carcinoid tumors: a clinicopathologic and KI-67-labeling study. *Hum. Pathol.* 1995; **26;** 740–745.
31. Rugge M, Fassan M, Clemente R *et al.* Bronchopulmonary carcinoid: phenotype and long-term outcome in a single-institution series of Italian patients. *Clin. Cancer Res.* 2008; **14;** 149–154.
32. Travis WD, Colby TV, Corrin B *et al. World Health Organization international histological classification of tumors: histological typing of lung and plural tumors*. Heidelberg: Springer, 1999.
33. Pelosi G, Rodriguez J, Viale G, Rosai J. Typical and atypical pulmonary carcinoid tumor overdiagnosed as small-cell carcinoma on biopsy specimens: a major pitfall in the management of lung cancer patients. *Am. J. Surg. Pathol.* 2005; **29;** 179–187.
34. Renshaw AA, Haja J, Lozano RL, Wilbur DC, Cytology Committee, College of American Pathologists. Distinguishing carcinoid tumor from small cell carcinoma of the lung: correlating cytologic features and performance in the College of American Pathologists Non-Gynecologic Cytology Program. *Arch. Pathol. Lab. Med.* 2005; **129;** 614–618.
35. Al-Khafaji B, Noffsinger AE, Miller MA *et al.* Immunohistologic analysis of gastrointestinal and pulmonary carcinoid tumors. *Hum. Pathol.* 1998; **29;** 992–999.
36. Gosney JR, Denley H, Resl M. Sustentacular cells in pulmonary neuroendocrine tumours. *Histopathology* 1999; **34;** 211–215.
37. Tsuta K, Raso MG, Kalhor N, Liu DC, Wistuba II, Moran CA. Sox10-positive sustentacular cells in neuroendocrine carcinoma of the lung. *Histopathology* 2011; **58;** 276–285.
38. Chu P, Wu E, Weiss LM. Cytokeratin 7 and cytokeratin 20 expression in epithelial neoplasms: a survey of 435 cases. *Mod. Pathol.* 2000; **13;** 962–972.
39. Cai YC, Banner B, Glickman J, Odze RD. Cytokeratin 7 and 20 and thyroid transcription factor 1 can help distinguish pulmonary from gastrointestinal carcinoid and pancreatic endocrine tumors. *Hum. Pathol.* 2001; **32;** 1087–1093.
40. Oliveira AM, Tazelaar HD, Myers JL, Erickson LA, Lloyd RV. Thyroid transcription factor-1 distinguishes metastatic pulmonary from well-differentiated neuroendocrine tumors of other sites. *Am. J. Surg. Pathol.* 2001; **25;** 815–819.
41. Hartel PH, Fanburg-Smith JC, Frazier AA *et al.* Primary pulmonary and mediastinal synovial sarcoma: a clinicopathologic study of 60 cases and comparison with five prior series. *Mod. Pathol.* 2007; **20;** 760–769.

Activating Enhancer-Binding Protein-2β Nucleolar Localization Predicts Poor Survival After Stage I Non-Small Cell Lung Cancer Resection

Min P. Kim, MD, Ying Chen, MD, PhD, B. Nebiyou Bekele, PhD, Adriana Lopez, MS, Abha Khanna, MA, Jie Qing Chen, MD, Margaret R. Spitz, MD, Carmen Behrens, MD, Luisa Solis, MD, Marnie Wismach, MD, Lin Ji, PhD, Ignacio I. Wistuba, PhD, Jack A. Roth, MD, and Ruth L. Katz, MD

Departments of Thoracic and Cardiovascular Surgery, Pathology, Biostatistics, Melanoma Medical Oncology, Epidemiology and Thoracic, Head and Neck Medical Oncology, University of Texas MD Anderson Cancer Center, Houston, Texas

Background. **Activating enhancer-binding protein-2β (AP2β) is a transcription factor involved in apoptosis. The purpose of the current study was to assess the cellular location and level of AP2β in non-small cell lung cancer (NSCLC) and normal lung tissue and investigate whether the level and localization of AP2β expression is predictive of overall survival in patients with stage I NSCLC.**

Methods. **We performed immunohistochemical analysis of tissue microarrays (TMAs) prepared from stage I NSCLC specimens with adjacent normal lung tissue from two independent sets of patients who underwent lung resection with curative intent at our institution. The AP2β intensity was assessed in TMAs, and AP2β staining patterns were classified as either diffuse or nucleolar in the TMAs. The AP2β intensity and localization were analyzed for correlation with patients' survival.**

Results. **Immunohistochemical analysis of TMAs showed that the intensity of AP2β immunohistochemical staining did not correlate with overall survival. When location of AP2β was analyzed in TMAs, all of the normal lung tissue had diffuse pattern of AP2β. In the first set of NSCLC, patients with nucleolar pattern had a significantly lower 5-year survival rate than patients with diffuse pattern (67% versus 100%; $p = 0.004$); this finding was confirmed in the second set (64% versus 91%; $p = 0.02$). Multivariate analysis revealed that nucleolar pattern was an independent predictor of poor overall survival in both sets.**

Conclusions. **The AP2β, which is located in the nucleoplasm in normal lung tissue, is found in either nucleoplasm or nucleoli in NSCLC. The patients with AP2β in the nucleoli had poor survival compared with patients with AP2β in the cytoplasm.**

(Ann Thorac Surg 2011;92:1044–50)

The overall 5-year survival rate among patients with stage I non-small cell lung cancer (NSCLC) who undergo resection with curative intent ranges from 55% to 72% [1]. This poor survival for the early stage cancer suggests that lung cancer is very aggressive, and that identifying the biomarkers that underlie the aggressiveness of NSCLC could be used to identify patients at high risk of recurrence and death, and subsequently guide adjuvant therapy decisions to improve overall survival.

One known prognostic factor in patients with stage I NSCLC is human telomerase reverse transcriptase (hTERT), an important component of human telomerase, the enzyme that lengthens chromosome ends to prevent apoptosis in cancer cells. When hTERT is not expressed in a cancer cell, the cell will reach its Hayflick limit and eventually undergo apoptosis; when hTERT is overexpressed, telomere length is maintained, and the cancer cell avoids apoptosis. The hTERT may localize in the nucleoli of cancer cells, or it may localize in the nucleoplasm, where its telomere-lengthening activity occurs [2, 3]. In NSCLC patients, hTERT expression has been associated with lower rates of overall and disease-free survival [4]. The hTERT expression, as well as the expression of several other oncogenes [5], is regulated by the transcription factor activating enhancer-binding protein-2β (AP2β) [6], which is involved in development, differentiation, and carcinogenesis in mammals [7-10]. Gene knockout experiments with AP2β have shown that AP2β-deficient mice die shortly after birth owing to collecting duct and distal tubular epithelia defects caused by massive renal epithelial cell apoptosis [11]. These findings suggests that AP2β is important in preventing cell death and that AP2β expression in NSCLC may lead to tumors that are resistant to signals for apoptosis.

In the current study, we investigated whether hTERT and AP2β colocalize in the nuclei of NSCLC cells and

Accepted for publication April 6, 2011.

Address correspondence to Dr Kim, Department of Surgery, The Methodist Hospital, 6550 Fannin St, SM1661, Houston, TX 77030; e-mail: mpkim@tmhs.org.

Published by Elsevier Inc

0003-4975/$36.00
doi:10.1016/j.athoracsur.2011.04.029

whether the level and localization of AP2β expression is predictive of overall survival in patients with stage I NSCLC.

Material and Methods

Assessing AP2β Expression in Lung Cancer Cells

WESTERN BLOT ANALYSIS. Immortalized normal human bronchial epithelial cells (HBECs) and H1299 and A549 NSCLC cells were grown to 80% confluence under cell culture conditions as described previously [12]. Cell lysate was prepared in 1x Lamini/urea buffer containing 62.5 mM Tris-HCl (pH 6.8), 2% SDS (w/v), 5% glycerol, 6 M urea, and complete protease inhibitors (Roche Applied Science, Indianapolis, IN). Protein concentrations were determined using the BCA Protein Assay Kit (Thermo Scientific, Waltham, MA). Next, 50 μg of crude protein extracts were loaded onto a 10% SDS-PAGE gel and run for approximately 150 minutes at 130 V. The separated proteins were then transferred to a nitrocellulose membrane and run for 1 hour at 100 V. The membrane was incubated with blocking buffer containing 5% milk in phosphate-buffered saline (PBS) for 1 hour at room temperature. After blocking, the membrane was incubated simultaneously with AP2β and β-actin antibodies at dilutions of 1:2500 and 1:10000, respectively, in Tris-buffered saline with 0.1% Tween-20 and 5% milk. Odyssey secondary antibodies (goat anti-rabbit IRDye 800 and goat anti-mouse IRDye 680; Li-COR Biosciences, Lincoln, NE) were added according to the manufacturer's instructions. Blots were imaged using an Odyssey Infrared Imaging System (Li-COR Biosciences).

IMMUNOHISTOCHEMICAL ANALYSIS. For immunohistochemistry of the immortalized HBECs and H1299 and A549 NSCLC cells, 5-μm-thick, paraffin-fixed cell-block sections were deparaffinized in xylene and rehydrated with graded alcohols. Antigen retrieval was carried out using BORG decloaker buffer (Biocare Medical, Concord, CA). Endogenous peroxidase activity was quenched by immersion in 3% hydrogen peroxide (Sigma-Aldrich, St. Louis, MO) or methanol at room temperature. Nonspecific primary antibody binding was blocked by incubating the sections with 10% normal goat serum. The sections were then incubated with a rabbit polyclonal antibody against AP2β (1:150 dilution [Santa Cruz Biotechnology, Santa Cruz, CA]) overnight at 4°C. Next, the slides were incubated with secondary anti-rabbit IgG-biotin antibody (1:200 dilution [Vectastain Elite ABC Kit; Vector laboratories, CA]) for 1 hour at room temperature. Visualization was performed using chromogen 3,3′-diaminobenzidine (Dako, Carpinteria, CA). The slides were counterstained with hematoxylin and coverslipped with PerMount. Cell block sections that were incubated without the primary antibody were used as negative controls.

Patients and Tissue Samples

This retrospective study was approved by the University of Texas MD Anderson Cancer Center Institutional Review Board. We looked at two independent sets of patients with stage I lung cancer as the median follow-up in our first set of patient was very short. We considered that analysis in a second group of patients with longer median follow-up would strengthen our conclusions.

PATIENT SETS. Two independent sets that were created by two different departments at the MD Anderson Cancer Center were analyzed for the study. The first set of tissue microarray was created from NSCLC specimens (stage I squamous cell carcinoma and stage I adenocarcinoma) from 126 patients who underwent lung resection with curative intent at MD Anderson Cancer Center between 2002 and 2008. Normal lung tissue specimens adjacent to tumor were available for 86 of these patients. The second set of tissue microarray was composed of NSCLC specimens (stage I squamous cell carcinoma and stage I adenocarcinoma) from 115 patients who underwent lung cancer resection with curative intent at MD Anderson Cancer Center between 1994 and 2004. Although there was 2-year overlap between the sets, there were no patients who were in both sets. NSCLC stage was determined according to the seventh edition of the American Joint Committee on Cancer lung cancer staging [13]. Patients' clinicopathologic data were obtained from a clinical database derived from patient charts and electronic medical record.

IMMUNOHISTOCHEMICAL ANALYSIS. Immunohistochemical analysis was performed to assess the intensity and location of AP2β and location of hTERT in the NSCLC and location of AP2β in adjacent normal lung tissue in first patient set and location of AP2β in second patient set. Tissue microarrays were incubated with 0.3% hydrogen peroxide for 5 minutes to inactivate the endogenous peroxidase and then in 5% normal goat serum for 1 hour at room temperature to eliminate nonspecific protein binding. The microarrays were then incubated with a rabbit polyclonal antibody against AP2β (1:150 dilution [Santa Cruz Biotechnology]) and a mouse monoclonal antibody against hTERT (1:40 dilution [Novus Biological, Littleton, CO]) overnight at 4°C. Next, the microarrays were washed with PBS for 5 minutes and then incubated with a biotinylated second antibody at room temperature for 1 hour. The microarrays were then washed with PBS for 5 minutes, incubated with rabbit Extra Avidin peroxidase reagent (Sigma-Aldrich) for 30 minutes, and washed again with PBS for 10 minutes. Color was developed using 0.05% 3,3 diaminobenzine hydrochloride (Sigma-Aldrich) and 0.0006% hydrogen peroxide in PBS. The microarrays were then counterstained with Mayer's hematoxylin, dehydrated, cleared, and mounted. Microarrays of NSCLC and normal lung tissue incubated with PBS containing 1% bovine serum albumin without the primary antibodies were used as negative controls.

Two investigators (R.K. and Y.C.) independently assessed the intensity and pattern of AP2β staining and the pattern of hTERT staining in the NSCLC and normal lung tissue specimens. The AP2β staining intensity scores were calculated by multiplying the percentage of cells stained the nucleoplasm or nucleoli by the intensity

score (1, 2, 3, or 4) of the stain. Staining of the nucleoplasm without nucleoli staining was labeled as diffuse, and staining of several small nucleoli or a single large macronucleoli with or without nucleoplasm staining was labeled as nucleolar.

Statistical Analysis

Statistical analyses were performed on the two independently assessed datasets of AP2β staining intensity and pattern and hTERT staining pattern. Identical statistical methods were applied for both sets. The AP2β staining patterns, staining intensity score, and histology were correlated with patients' clinicopathologic data. The AP2β and hTERT staining patterns were analyzed for correlation using Fisher's exact initial. The Wilcoxon rank sum initial was used to analyze the distribution of age, tumor size, and clinicopathologic features according to AP2β staining pattern and intensity. The Kruskal-Wallis rank sum test was used to assess the distribution of AP2β intensity scoring by tumor differentiation. Fisher's exact test was used to assess relationships between AP2β staining patterns and sex, histology, stage, differentiation, and smoking status. Pearson correlation was calculated to assess the relationship between AP2β intensity and age and tumor size. The Kaplan-Meier method was used to estimate patients' overall survival rate, and the log rank test was used to compare the survival distributions in patients with diffuse AP2β staining and patients with nucleolar AP2β staining. Univariate analysis was performed on age, sex, smoking history, histology, tumor differentiation, size of tumor, AP2β intensity, and AP2β pattern for survival, and multivariate analysis was performed using standard criteria. Because no deaths occurred among the patients in the initial set whose disease had diffuse AP2β staining, Firth's penalized maximum likelihood bias reduction method for the Cox proportional hazards regression model was used for multivariate analysis of overall survival in these patients. All p values less than 0.05 were considered statistically significant. Hazard ratios (HR) and 95% confidence intervals (CI) were calculated for the multivariate analysis for overall survival. All statistical analyses were performed using SAS version 9.2.0 and S-PLUS version 7 (SAS Institute, Cary, NC).

Results

AP2β Expression in Lung Cancer Cells

Immunohistochemistry and Western blot revealed that AP2β levels were higher in the H1299 and A549 NSCLC cells than in the HBECs (Fig 1).

First Patient Set

The first patient set included 59 men and 67 women. The mean age was 67 years. Fifteen patients (12%) were never-smokers. Most tumors were adenocarcinomas (69%), and most tumors were either moderately (47%) or poorly (39%) differentiated. The mean follow-up time was 23 months.

The AP2β intensity scores did not correlate with patients' sex, age, or smoking status, or tumor size, histology, or differentiation (Table 1). The log rank test did not reveal an association between AP2β intensity and 5-year overall survival rate (HR, 1.001; 95% CI, 0.99 to 1.01). Thirty-five patients had a diffuse AP2β pattern, and 91 patients had a nucleolar AP2β pattern (Fig 2). We found no significant differences in patient age, tumor size, or tumor histology between patients with diffuse AP2β staining and patients with nucleolar AP2β staining; however, we did find that significantly more women than men had a diffuse AP2β staining pattern ($p = 0.046$; Table 2). Moreover, significantly more patients with poorly differentiated adenocarcinomas had a nucleolar AP2β

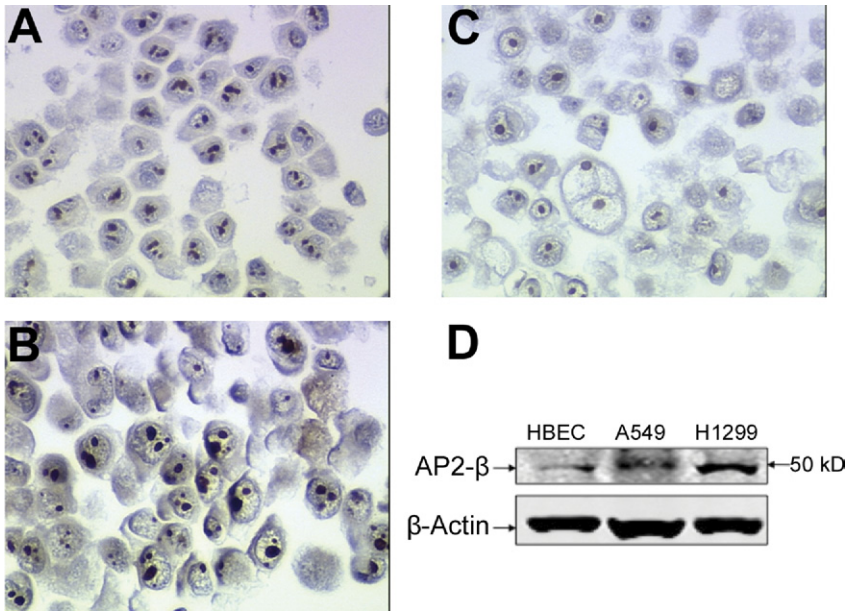

Fig 1. Both (A) A549 and (B) H1299 (b) lung cancer cells have more activating enhancer-binding protein-2β (AP2β) staining compared with (C) control immortalized human bronchial epithelial cells (HBEC). (D) Western-blot analysis showed that AP2β protein expression is upregulated in the A549 and H1299 lung cancer cells compared with control immortalized HBEC. (Original magnification in panels A, B, and C, X100.)

Table 1. Relationship Between Activating Enhancer-Binding Protein-2β (AP2β) Staining Intensity in Stage I Non-Small Cell Lung Cancer and Patients' Clinicopathologic Features in First Patient Set

Characteristic	No. of Patients	AP2β Staining Intensity Mean ± SD	Median (Range)	*p* Value
Sex				
Male	59	263 ± 67	270 (88–380)	0.52
Female	67	255 ± 63	270 (102–380)	
Tumor histology				
Adenocarcinoma	87	258 ± 65	275 (101–380)	0.92
Squamous cell carcinoma	39	262 ± 65	270 (88–380)	
Smoking status				
Never	15	258 ± 71	285 (140–370)	0.82
Ever	111	259 ± 64	270 (88–380)	
Tumor differentiation[a]				
Well	11	252 ± 56	275 (175–360)	0.6
Moderate	59	263 ± 69	277 (88–380)	
Poor	49	253 ± 63	261 (102–380)	

[a] Tumor differentiation data for 7 patients were unavailable.

pattern than a diffuse AP2β pattern ($p = 0.011$), and significantly more never-smokers had a diffuse AP2β pattern than a nucleolar AP2β pattern ($p = 0.029$). All 86 normal lung tissue specimens had diffuse AP2β staining (Fig 2).

The Kaplan-Meier survival plot revealed that patients with a nucleolar AP2β staining pattern had a significantly lower 5-year survival rate (67%) than patients with a diffuse AP2β staining pattern (100%; $p = 0.004$; Fig 3). Multivariate analysis revealed that cellular AP2β location was an independent predictor of 5-year survival ($p = 0.004$; HR, 13.9; 95% CI, 1.9 to 1756). We determined the cellular location of hTERT in 96 patients. Twenty-seven patients had a diffuse pattern of hTERT staining, and 69 patients had a nucleolar pattern of hTERT staining. The hTERT localization and AP2β localization were correlated ($p < 0.0001$).

Second Patient Set

The second set included 57 men and 58 women. The mean age was 68 years, and the majority of tumors were adenocarcinomas (72%). Twenty patients (17%) were never-smokers, 50 patients (43%) had a poorly differentiated tumor, and 93 patients (81%) underwent lobectomy for NSCLC. The mean follow-up time was 83 months.

Thirty-five patients had a diffuse AP2β staining pattern, and 80 patients had a nucleolar AP2β staining pattern. We found no significant differences in age, tumor size, tumor histology, smoking status, tumor differentiation, race, or surgery type between patients with a diffuse AP2β pattern and patients with a nucleolar AP2β pattern (Table 3). However, significantly more women than men had a diffuse AP2β pattern ($p = 0.04$).

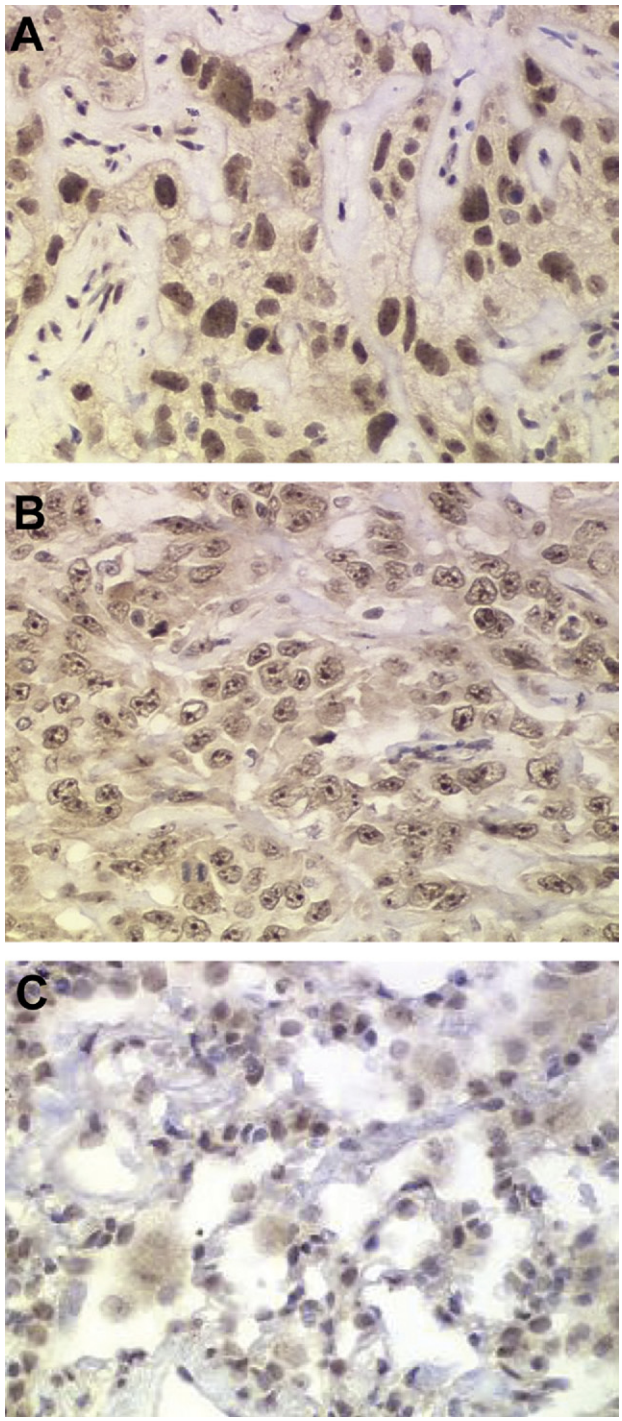

Fig 2. (A) Diffuse nuclear activating enhancer-binding protein-2β (AP2β) staining characterized by nucleoplasm staining without nucleoli staining in non-small cell lung cancer. (B) Nucleolar AP2β staining characterized by the staining of several small nucleoli or a single large macronucleoli with or without nucleoplasm staining in non-small cell lung cancer. (C) All tumor-adjacent normal lung tissue specimens had diffuse nuclear AP2β staining. (Original magnification in panels A, B, and C, X200.)

Table 2. Relationship Between Activating Enhancer-Binding Protein-2β (AP2β) Staining Pattern in Stage I Non-Small Cell Lung Cancer and Clinicopathologic Features of the First Patient Set[a]

Characteristic	Total n = 126	AP2β Staining Pattern: Diffuse n = 35	AP2β Staining Pattern: Nucleolar n = 91	*p* Value
Mean age ± SD, years		66 ± 18	64 ± 16	0.31
Sex				
Male	59 (47)	11 (31)	48 (53)	0.04
Female	67 (53)	24 (69)	43 (47)	
Smoking				
Never	15 (12)	8 (23)	7 (8)	0.03
Ever	111 (88)	27 (77)	84 (92)	
Histology				
Squamous cell carcinoma	39 (31)	8 (23)	31 (34)	0.28
Adenocarcinoma	87 (69)	27 (77)	60 (66)	
Differentiation[b]				
Well	11 (9)	7 (20)	4 (4)	0.01
Moderate	59 (47)	17 (49)	42 (46)	
Poor	49 (39)	9 (26)	40 (44)	
Mean tumor size ± SD, cm		2.7 ± 1	3.2 ± 1.7	0.24

[a] Data are given as number of patients (%) unless otherwise indicated. [b] Tumor differentiation data for 7 patients were unavailable.

Table 3. Relationship Between Activating Enhancer-Binding Protein-2β (AP2β) Staining Pattern in Stage I Non-Small Cell Lung Cancer and Clinicopathologic Features of Second Patient Set[a]

Characteristic	Total n = 115	AP2β Staining Pattern: Diffuse n = 35	AP2β Staining Pattern: Nucleolar n = 80	*p* Value
Sex				
Male	57 (50)	12 (34)	45 (49)	0.04
Female	58 (50)	23 (66)	35 (38)	
Mean age ± SD, years		66 ± 10	68 ± 11	0.32
Smoking				
Never	20 (17)	8 (23)	12 (15)	0.57
Former	55 (48)	15 (43)	40 (50)	
Current	40 (35)	12 (34)	28 (35)	
Histology				1.00
Squamous cell carcinoma	32 (28)	10 (29)	22 (24)	
Adenocarcinoma	83 (72)	25 (71)	58 (64)	
Differentiation				
Well	32 (28)	10 (29)	22 (24)	0.30
Moderate	33 (29)	11 (31)	22 (24)	
Poor	50 (43)	14 (40)	36 (40)	
Mean tumor size ± SD, cm		3.1 ± 1	2.8 ± 0.9	0.07

[a] Data are given as number of patients (%) unless otherwise indicated.

The Kaplan-Meier survival plot revealed that patients with a diffuse AP2β pattern had a significantly higher 5-year survival rate than did patients with a nucleolar AP2β pattern (91% versus 64%; $p = 0.0211$; Fig 4). Univariate and multivariate analyses revealed that AP2β staining pattern ($p = 0.037$; HR, 2.18; 95% CI, 1.05 to 1.47) and patient age ($p = 0.001$; HR, 1.07; 95% CI, 1.03 to 1.11) were independent predictors of 5-year survival.

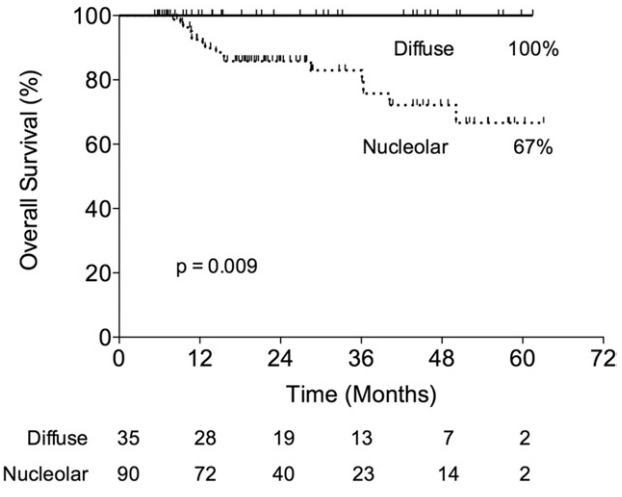

Fig 3. In the initial set, patients who had non-small cell lung cancer with a nucleolar activating enhancer-binding protein-2β (AP2β) pattern had a significantly lower 5-year survival rate than patients who had non-small cell lung cancer with a diffuse AP2β pattern (67% versus 100%; p = 0.009).

Comment

The AP2β is a transcription factor that plays an important role in regulating apoptosis and control cell division [14];

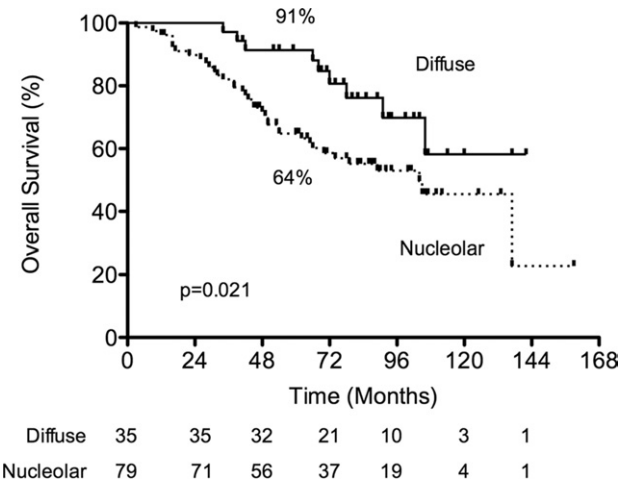

Fig 4. In the validation set, patients who had non-small cell lung cancer with a nucleolar AP2β pattern had a significantly lower 5-year survival rate than patients who had non-small cell lung cancer with a diffuse AP2β pattern (64% versus 91%; p = 0.0211).

however, there is limited information about its role in lung cancer. In our study, the AP2β that is located in the nucleoplasm in normal lung tissue was found in either nucleoplasm or nucleoli in NSCLC, and the patients with AP2β in the nucleoli had poor survival. Most prognostic markers for NSCLC are identified by assessing the level of RNA or a specific protein in the tumor and then determining whether that level correlates with survival.

Immunohistochemistry studies have shown that Ki-67, p53, and Bcl-2 are important in NSCLC and may provide some prognostic information [15]. We took a similar approach and investigated the level of AP2β and its relation to survival. Since presence of hTERT has been associated with survival in NSCLC patients [4], we expected that the hTERT promoter AP2β would also be associated with survival. Surprisingly, we found no relationship between the level of AP2β and survival. Although AP2β was expressed in normal lung tissue as well as in NSCLC and higher AP2β levels were expressed in the NSCLC cell lines than in the normal cells, AP2β level was not a predictor of survival. The difference may be due to how hTERT levels were determined in previous study [4]. Wang and coworkers [4] found the hTERT level by performing in situ hybridization for hTERT mRNA expression. They looked at the presence of the hTERT mRNA in the cytoplasm of NSCLC cells and found that only 33% of the samples expressed hTERT. In the current study, we found that hTERT was expressed in 76% of the samples studied, which is much closer to 86% of samples identified in other studies [16]. Thus, the in situ hybridization method that was used in Wang and colleagues [4] might not reflect the protein levels, and protein levels may not provide prognostic information.

However, in both sets of patients, the cellular location of AP2β was a prognostic marker for survival. In normal lung tissue cells, AP2β was diffusely expressed in the nucleoplasm; in contrast, in the NSCLC cells, AP2β was either diffusely expressed in the nucleoplasm or expressed in the nucleoli. In both patient sets, AP2β localization in the nucleoli, which plays an important role in ribosome biogenesis, was found to be an indicator of poor prognosis. These findings suggest that NSCLC tumors are more resistant to cell death when the AP2β is localized in the nucleoli. Other studies have shown that apoptosis-related proteins are present in the nucleoli after the induction of cell death [17]. Because AP2β knockout mice die from massive apoptosis [11], the presence of AP2β in the nucleoli may indicate that this protein is present to prevent cell death and allowing the tumor to grow without any controls.

The current study was not without its limitations. One potential limitation was that the current study was retrospective; thus, some data were unavailable for analysis such as type of resection, morbidity of the operation, type of recurrence, and cause of death. A larger issue stemming from the retrospective nature of the study was that the patient groups were not balanced. In the first set of patients, more women, never-smokers, and patients with well-differentiated tumors were in the diffuse staining group than in the nucleolar staining group, whereas in the second set of patients, more women were in the diffuse staining group than in the nucleolar staining group. To account for the unbalanced group, we used univariate and multivariate analyses, which accounts for these factors, to analyze the relationship between different factors and survival, and we found that AP2β nucleolar localization was an independent predictor of poor survival. Moreover, in the second patient set, age was also an independent predictor of survival, suggesting that patients who undergo lung cancer resection are at a higher risk of dying from other causes such as cardiovascular disease. Thus, later deaths among patients in the validation set may have been due to factors that were independent of tumor aggressiveness but associated with advanced age and its comorbidities. Moreover, our use of two independent groups of patients strengthened the study, with findings in the first set also seen in the second set of patients.

In conclusion, the current study's findings show that AP2β colocalizes with hTERT in either the nucleoplasm or nucleoli of NSCLC cells. Moreover, the AP2β nucleolar localization was associated with very poor survival. The current standard of care for patients with stage I NSCLC is surgical resection. If the AP2β nucleolar pattern is indeed an indicator of poor prognosis, these patients may benefit from adjuvant therapy to improve their survival. Additional studies are needed to confirm our findings, identify the exact mechanism of nucleolar localization of the AP2β and aggressiveness of tumor, and determine whether adjuvant therapy prolongs survival in patients predicted to have poor prognosis.

This work was supported in part by the National Institutes of Health through MD Anderson's Cancer Center Support Grant CA-016672—Lung Program, Biostatistics CCSG Shared Resource; Specialized Program of Research Excellence Grant CA-070907 (J. Roth); and Department of Defense Vanguard Investigations of Therapeutic Approaches to Lung Cancer Grant W81XWH-04-1-0142 (I. Wistuba). We thank Joe Munch in MD Anderson's Department of Scientific Publications for editing the manuscript.

References

1. Nesbitt JC, Putnam JB, Walsh GL, et al. Survival in early-stage non-small cell lung cancer. Ann Thorac Surg 1995;60:466–72.
2. Yan P, Benhattar J, Seelentag W, et al. Immunohistochemical localization of hTERT protein in human tissues. Histochem Cell Biol 2004;121:391–7.
3. Etheridge KT, Banik SS, Armbruster BN, et al. The nucleolar localization domain of the catalytic subunit of human telomerase. J Biol Chem 2002;277:24764–70.
4. Wang L, Soria JC, Kemp BL, et al. hTERT expression is a prognostic factor of survival in patients with stage I non-small cell lung cancer. Clin Cancer Res 2002;8:2883–9.
5. Eckert D, Buhl S, Weber S, et al. The AP-2 family of transcription factors. Genome Biol 2005;6:246.
6. Ma H, Urquidi V, Wong J, et al. Telomerase reverse transcriptase promoter regulation during myogenic differentiation of human RD rhabdomyosarcoma cells. Mol Cancer Res 2003;1:739–46.
7. Ding X, Fan C, Zhou J, et al. GAS41 interacts with transcription factor AP-2beta and stimulates AP-2beta-mediated transactivation. Nucleic Acids Res 2006;34:2570–8.

8. Williams T, Admon A, Luscher B, et al. Cloning and expression of AP-2, a cell-type-specific transcription factor that activates inducible enhancer elements. Genes Dev 1988;2:1557–69.
9. Moser M, Imhof A, Pscherer A, et al. Cloning and characterization of a second AP-2 transcription factor: AP-2 beta. Development 1995;121:2779–88.
10. Bosher JM, Totty NF, Hsuan JJ, et al. A family of AP-2 proteins regulates c-erbB-2 expression in mammary carcinoma. Oncogene 1996;13:1701–7.
11. Moser M, Pscherer A, Roth C, et al. Enhanced apoptotic cell death of renal epithelial cells in mice lacking transcription factor AP-2beta. Genes Dev 1997;11:1938–48.
12. Nishizaki M, Sasaki J, Fang B, et al. Synergistic tumor suppression by coexpression of FHIT and p53 coincides with FHIT-mediated MDM2 inactivation and p53 stabilization in human non-small cell lung cancer cells. Cancer Res 2004;64:5745–52.
13. Goldstraw P, Crowley J, Chansky K, et al. The IASLC Lung Cancer Staging Project: proposals for the revision of the TNM stage groupings in the forthcoming (seventh) edition of the TNM classification of malignant tumours. J Thorac Oncol 2007;2:706–14.
14. Hilger-Eversheim K, Moser M, Schorle H, et al. Regulatory roles of AP-2 transcription factors in vertebrate development, apoptosis and cell-cycle control. Gene 2000;260:1–12.
15. Zhu CQ, Shih W, Ling CH, et al. Immunohistochemical markers of prognosis in non-small cell lung cancer: a review and proposal for a multiphase approach to marker evaluation. J Clin Pathol 2006;59:790–800.
16. Albanell J, Lonardo F, Rusch V, et al. High telomerase activity in primary lung cancers: association with increased cell proliferation rates and advanced pathologic stage. J Natl Cancer Inst 1997;89:1609–15.
17. Horky M, Kotala V, Anton M, et al. Nucleolus and apoptosis. Ann NY Acad Sci 2002;973:258–64.

INVITED COMMENTARY

This study by Kim and colleagues analyzes the prognostic importance of activating enhancer-binding protein-2β (AP2β) in patients with lung cancer [1]. AP2β, a transcription factor that plays an important role in regulating apoptosis and cell division, is normally located in the nucleoplasm in normal lung tissue. In this study AP2β was found in either the nucleoplasm or nucleoli in lung tumors, and the patients with AP2β in the nucleoli had inferior survival. Understanding how biological factors function in lung cancer (such as AP2β in this study) may improve prognostic stratification of patients after surgery; however this understanding may also improve the selection of patients for adjuvant therapy and the development of specific biological agents.

The paradigm for the treatment of non-small cell lung cancer (NSCLC) continues to shift in favor of analyzing biological factors to estimate prognosis, select therapy, and predict treatment response. Although the seventh edition of the American Joint Commission on Cancer (AJCC) recognizes a nonanatomic factor (histologic grade [G]) in the staging classification for esophageal cancer [2], the most recent AJCC staging guidelines remain confined by the tumor (T), nodal (N), and metastases (M) descriptors [3]. Recent and ongoing trials may yet have an impact however. The majority of pulmonary adenocarcinomas have at least 1 identifiable oncogenic mutation, such as epidermal growth factor (EGFR), KRAS, anaplastic lymphoma kinase (ALK), BRAF, and others; moreover the majority of these oncogenes have a corresponding effective pharmacologic inhibitor [4]. Oral tyrosine kinase inhibitors to EGFR have already been established as the treatment of choice (over cytotoxic chemotherapy) for first-line treatment of stage IV NSCLC in patients with EGFR mutation [5] and are currently being tested in the adjuvant setting in patients with completely resected NSCLC [6]. Similarly, patients with stage IV disease with ALK mutations may also preferentially benefit from the ALK inhibitor crizotinib [7], an advantage that may also be translated to the treatment of early-stage disease.

Until recently the biological characteristics of NSCLC had been defined only by histologic type: adenocarcinoma, squamous cell carcinoma, large-cell carcinoma, and other subtypes. Until recently the treatment of NSCLC has been guided only by the anatomic parameters of TNM staging. That era has ended for many patients with metastatic NSCLC; it should be coming to a close for patients with resectable NSCLC as well. This study and others that seek to define the importance of oncogenic mutations are the pathway to the future.

Thomas A. D'Amico, MD

Section of General Thoracic Surgery
Duke University Medical Center, Box 3496
Duke South, White Zone, Rm 3589
Durham, NC 27710
e-mail: damic001@mc.duke.edu

References

1. Kim MP, Chen Y, Bekele BN, et al. Activating enhancer-binding protein-2β nucleolar localization predicts poor survival after stage I non-small cell lung cancer resection. Ann Thorac Surg 2011;92:1044–50.
2. Edge SB, Byrd DR, Compton CC, et al, eds. AJCC Cancer Staging Manual. 7th ed. New York, NY: Springer-Verlag; 2009:103–15.
3. Goldstraw P, Crowlye J, Chansky K, Giroux DJ. The IASLC Lung Cancer Staging Project: Proposals for the revision of the TNM stage groupings in the forthcoming (seventh) edition of the TNM classification of malignant tumours. J Thorac Oncol 2007;2:706–14.
4. Sharma SV, Haber DA, Settleman J. Cell line–based platforms to evaluate the therapeutic efficacy of candidate anticancer agents. Nature Rev Cancer 2010;10:241–53.
5. Mok TS, Wu Y-L, Thongprasert S, et al. Gefitinib or carboplatin–paclitaxel in pulmonary adenocarcinoma. N Engl J Med 2009;361:947–57.
6. Janjigian YY, Park BJ, Zakowski MF, et al. Impact on disease-free survival of adjuvant erlotinib or gefitinib in patients with resected lung adenocarcinomas that harbor EGFR mutations. J Thorac Oncol 2011;6:569–75.
7. Bang Y, Kwak EL, Shaw AT, et al. Clinical activity of the oral ALK inhibitor PF-02341066 in ALK-positive patients with non-small cell lung cancer (NSCLC)[abstract]. J Clin Oncol 2010;28 (suppl):18s.

0003-4975/$36.00
doi:10.1016/j.athoracsur.2011.04.075

Published OnlineFirst July 8, 2011; DOI:10.1158/1078-0432.CCR-11-0196

Clinical Cancer Research

Imaging, Diagnosis, Prognosis

Robust Gene Expression Signature from Formalin-Fixed Paraffin-Embedded Samples Predicts Prognosis of Non–Small-Cell Lung Cancer Patients

Yang Xie[1,2], Guanghua Xiao[1], Kevin R. Coombes[6], Carmen Behrens[7], Luisa M. Solis[8], Gabriela Raso[8], Luc Girard[4,5], Heidi S. Erickson[7], Jack Roth[9], John V. Heymach[7], Cesar Moran[8], Kathy Danenberg[10], John D. Minna[2,3,4,5], and Ignacio I. Wistuba[7,8]

Abstract

Purpose: The requirement of frozen tissues for microarray experiments limits the clinical usage of genome-wide expression profiling by using microarray technology. The goal of this study is to test the feasibility of developing lung cancer prognosis gene signatures by using genome-wide expression profiling of formalin-fixed paraffin-embedded (FFPE) samples, which are widely available and provide a valuable rich source for studying the association of molecular changes in cancer and associated clinical outcomes.

Experimental Design: We randomly selected 100 Non–Small-Cell lung cancer (NSCLC) FFPE samples with annotated clinical information from the UT-Lung SPORE Tissue Bank. We microdissected tumor area from FFPE specimens and used Affymetrix U133 plus 2.0 arrays to attain gene expression data. After strict quality control and analysis procedures, a supervised principal component analysis was used to develop a robust prognosis signature for NSCLC. Three independent published microarray datasets were used to validate the prognosis model.

Results: This study showed that the robust gene signature derived from genome-wide expression profiling of FFPE samples is strongly associated with lung cancer clinical outcomes and can be used to refine the prognosis for stage I lung cancer patients, and the prognostic signature is independent of clinical variables. This signature was validated in several independent studies and was refined to a 59-gene lung cancer prognosis signature.

Conclusions: We conclude that genome-wide profiling of FFPE lung cancer samples can identify a set of genes whose expression level provides prognostic information across different platforms and studies, which will allow its application in clinical settings. *Clin Cancer Res; 17(17); 5705–14. ©2011 AACR.*

Introduction

Lung cancer is the leading cause of death from cancer for both men and women in the United States and in most parts of the world, with a 5-year survival rate of 15% (1). Non–small-cell lung cancer (NSCLC) is the most common cause of lung cancer death, accounting for up to 85% of such deaths (2). Clinicopathologic staging is the standard prognosis factor for lung cancer used in clinical practice but does not capture the complexity of the disease so that heterogeneous clinical outcomes within the same stage are commonly seen. Several randomized clinical trials showed that adjuvant chemotherapy improves survival in resected NSCLC (3–7). The effect of adjuvant chemotherapy on prolonging survival is modest—only 4% to 15% improvement in 5-year survival—although such treatment is associated with serious adverse effects (6, 8). Therefore, it is of considerable clinical importance to have a robust and accurate prognostic signature for lung cancer, especially in early stage lung cancer to improve the current clinical decisions on whether an individual lung cancer patient should receive adjuvant chemotherapy or not.

Genome-wide expression profiles have been used to identify gene signatures to classify lung cancer patients with different survival outcomes (9–16). However, the requirement of frozen tissues for microarray experiments limits the clinical usage of these gene signatures.

Authors' Affiliations: Departments of [1]Clinical Sciences, [2]Simmons Cancer Center, [3]Internal Medicine, [4]Pharmacology, and [5]Hamon Center for Therapeutic Oncology Research, The University of Texas Southwestern Medical Center, Dallas; Departments of [6]Bioinformatics and Computational Biology, [7]Thoracic/Head and Neck Medical Oncology, [8]Pathology and [9]Thoracic and Cardiovascular Surgery, The University of Texas MD Anderson Cancer Center, Houston, Texas; and [10]Response Genetics, Inc., Los Angeles, California

Note: Supplementary data for this article are available at Clinical Cancer Research Online (http://clincancerres.aacrjournals.org/).

Corresponding Author: Ignacio I. Wistuba, Departments of Pathology and Thoracic/Head and Neck Medical Oncology, Unit 85, The University of Texas MD Anderson Cancer Center, 1515 Holcombe Boulevard, Houston, TX 77030. Phone: 713-563-9184; Fax: 713-792-0309; E-mail: iiwistuba@mdanderson.org

doi: 10.1158/1078-0432.CCR-11-0196

Published OnlineFirst July 8, 2011; DOI:10.1158/1078-0432.CCR-11-0196

Translational Relevance

This article is the first study to develop a robust prognosis signature for non–small cell lung cancer (NSCLC) on the basis of genome-wide expression profiling of clinically available formalin-fixed and paraffin-embedded (FFPE) samples. Although clinical FFPE tumor samples are widely available, the genome-wide expression profiling of FFPE samples has been hampered because of the degradation of RNAs extracted from them. In this article, we show that NSCLC FFPE-derived signature is strongly associated with clinical outcome of the patients, is independent of clinical prognostic variables, and can be validated in several independent studies. We showed that, after strict quality control and analysis procedures, genome-wide profiling of FFPE samples can actually provide a unique opportunity to identify a set of genes whose expression level is less sensitive to the environmental changes. This gene signature is more robust across different platforms and studies, which is critical for the successful application of gene signatures in real clinical settings.

Furthermore, prognostic gene signatures for NSCLC developed by different groups show minimal overlap and are often difficult to reproduce by independent groups (17, 18). To address the problem of requirement for frozen issues, we designed this study to test the feasibility of developing lung cancer prognosis gene signatures by using genome-wide expression profiling of formalin-fixed paraffin-embedded (FFPE) samples, which are widely available and provide a valuable rich source for studying the association of molecular changes in cancer and associated clinical outcomes. We derived a prognosis signature for NSCLC from FFPE samples and validated it in several independent studies. To facilitate other researchers to reproduce all results in this study, we have provided a literate programming R package.

Materials and Methods

Tissue specimens

The overall study design and the flow chart of the derivation and validation of the robust gene signature are described in Figure 1. We randomly selected 100 NSCLC FFPE samples with annotated clinical information from the UT-Lung SPORE Tissue Bank from 2001 to 2005. From these samples, 75 samples passed the mRNA quality control criteria (Supplementary Methods). Among these 75 samples, 48 samples are adenocarcinomas and 27 are squamous cell carcinomas. The median follow-up time is 2.8 years and the maximum follow-up time is 6.9 years; the characteristics of these patients are summarized in Supplementary Table S1. The samples were obtained under approval of the Institutional Review Boards at MD Anderson Cancer Center.

Sample microdissection and RNA extraction

FFPE tumor specimens were cut into serial sections with a thickness of 10 μm. For the pathologic diagnosis, one slide was stained with H&E and evaluated by a pathologist. Other sections were stained with nuclear fast red (NFR; American MasterTech Scientific Inc.) to enable visualization of histology. Tumor tissue was isolated by using manual macrodissection when the tumor area was more than 0.5×0.5 mm^2 or laser capture microdissection (P.A.L.M. Microlaser Technologies AG) in cases of smaller tumor areas. At least 50 mm^2 of tumor tissue was collected from each FFPE block. The extraction of RNA from tissue samples was done by a proprietary procedure of Response Genetics, Inc. (United States Patent Application 20090092979) designed to optimize the yield of higher molecular weight RNA fragments from FFPE specimens.

Microarray data preprocessing and quality control

Total RNA was processed for analysis on the Affymetrix U133 plus 2.0 arrays according to Affymetrix protocols for first- and second-strand synthesis, biotin labeling, and fragmentation. The quality control procedure for microarray data analysis was based on the percentage of present calls calculated by the MAS5 package. We selected arrays with at least 15% of probe sets present; 55 of 75 arrays passed this quality control criterion and will be used for the analysis. We selected probe sets that are present on all 55 arrays; 1,400 genes passed this criterion. These 1,400 genes were referred as the robust gene set (RGS), because the mRNA expression of these genes is robust to FFPE processing. The 55 samples and the 1,400 genes were used to develop gene signatures.

After microarray analysis QC, we used the RMA background correction algorithm (19) to remove nonspecific background noise. A robust regression model (20) was fitted to the probe level data, and the fitted expression values for the probes at the 3′ end were used to summarize the probe set expression values. Quantile–quantile normalization was used to normalize all the arrays. Consortium microarray raw data (13) was downloaded from caArray database of the National Cancer Institute (NCI) and preprocessed by RMA background correction and quantile–quantile normalization. All gene expression values were log transformed (on a base 2 scale).

Supervised classification by using supervised principal component analysis

Classification was done by using supervised principal component analysis (21, 22), a widely used classification method in biomedical research (23–26). As a supervised classification method, each prediction model was trained in a training dataset and then the performance was tested in an independent test dataset. We used an R package (version 2.81), Superpc (version 1.05), to implement the prediction algorithm, and the default parameters were used. The implementation details can be found in the Supplementary Sweave Report. The training and testing sets for each

Published OnlineFirst July 8, 2011; DOI:10.1158/1078-0432.CCR-11-0196

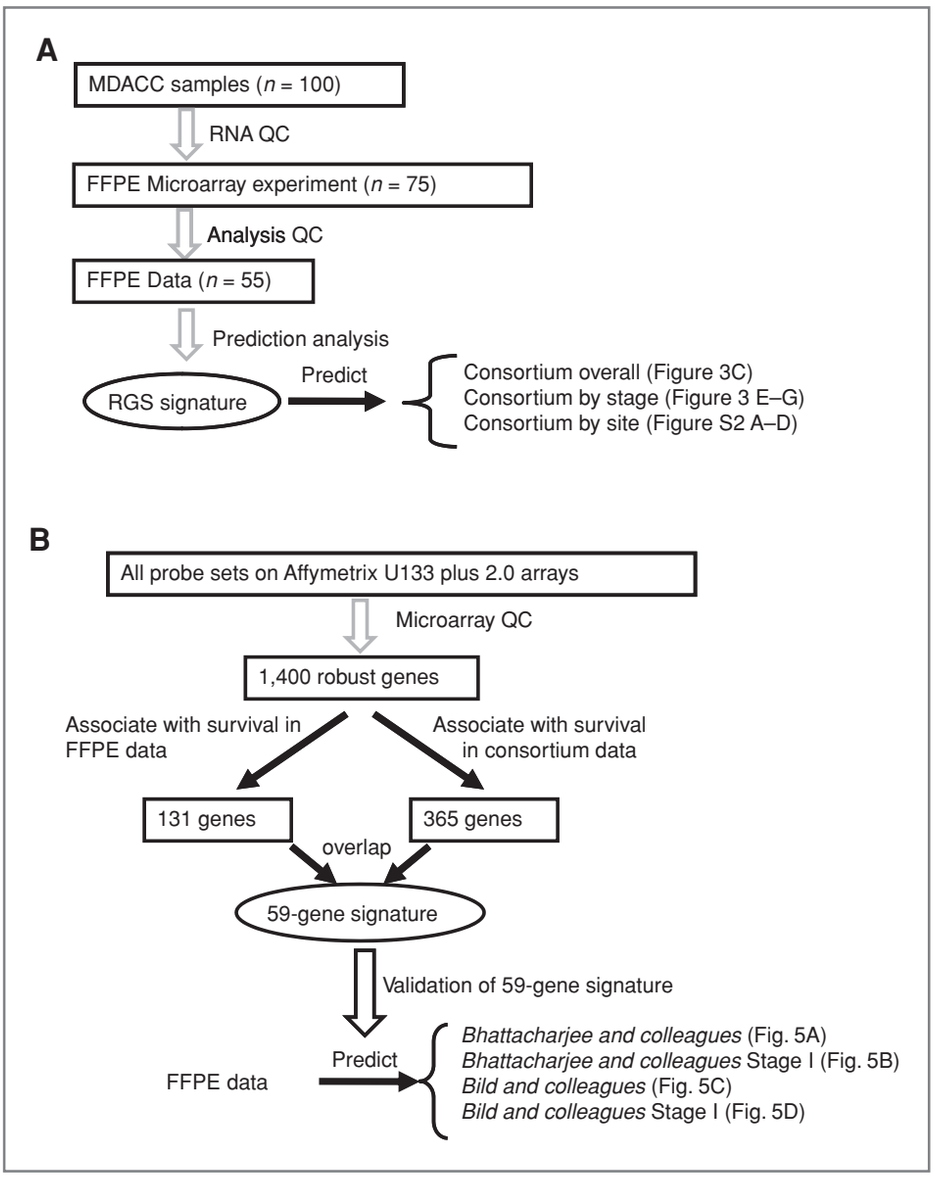

Figure 1. A, flow chart of the derivation and validation of the robust gene signature from FFPE samples collected from MD Anderson UT-Lung Cancer SPORE tissue bank (MDACC). B, flow chart of the derivation and validation of 59-gene prognosis signature.

prediction model are summarized in Supplementary Table S2.

Survival analysis

Overall survival time was calculated from the date of surgery until death or the last follow-up contact. Survival curves were estimated by using the product-limit method of Kaplan–Meier (27) and were compared by using the log-rank test. The maximum follow-up time for the FFPE patient cohort is less than 7 years, whereas some patients in the consortium cohort have been followed for up to 17 years. To avoid the extrapolation of the prediction model, the comparison of survival time between predicted groups are truncated at 7 years. The analysis results without truncation can be seen in Supplementary Sweave Report. Univariate and multivariate Cox proportional hazards analysis (28) were also done, with survival as the dependent variable.

Results

The robust gene set defines two tumor groups

The expression of these 1,400 genes divided the 55 patients into 2 groups on the basis of unsupervised clustering analysis (with Euclidean distance and complete linkage for the hierarchical clustering algorithm; Fig. 2). Interestingly, group 1 has significantly shorter survival time compared with group 2 (Fig. 2B; HR = 3.6, P = 0.017), and multivariate Cox proportional hazards analysis showed that the association between RGS groups

Published OnlineFirst July 8, 2011; DOI:10.1158/1078-0432.CCR-11-0196

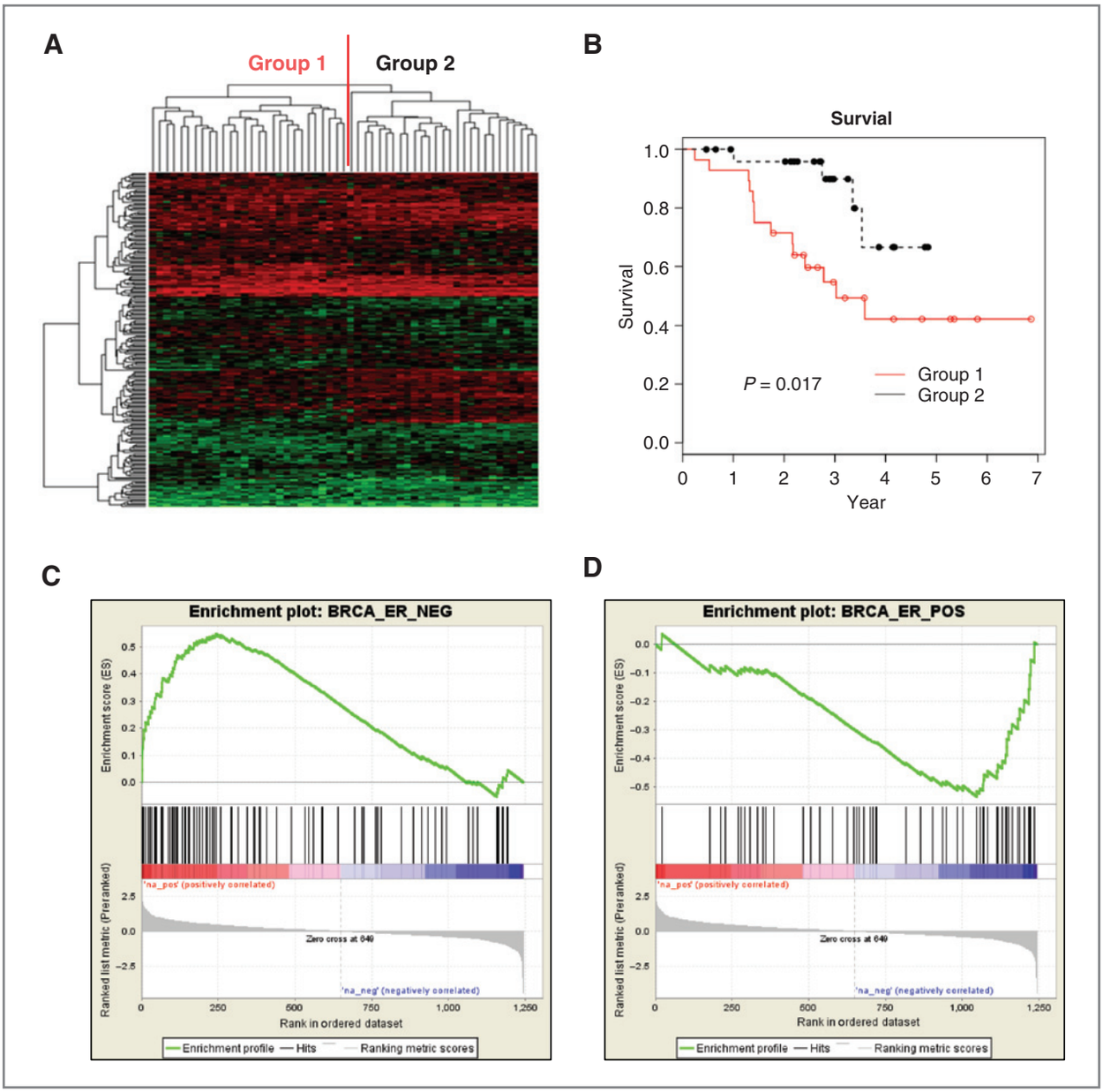

Figure 2. Microarray analysis of the gene expression profiles from FFPE lung tumor samples. A, unsupervised cluster analysis of the 55 FFPE lung cancer patient cohort by using the expression profile of 1,400 robust genes that pass the microarray quality control criterion. Vertical and horizontal axes represent robust genes and lung cancer patient clusters, respectively. B, Kaplan–Meier plot showing the association of the expression of robust genes with patient survival *P* values were obtained by using the log-rank test. Red color represents sample cluster I and black color represents sample cluster II defined by unsupervised clustering algorithm by using robust gene profiling data. ● indicates censored samples. Gene set enrichment analysis found that the ER-negative signature derived from breast cancer patients is enriched in group 1 defined by RGS expression (C), and the ER-positive signature derived from breast cancer patients is enriched in group 2 defined by RGS expression (D). The y-axis shows running enrichment scores for the specific gene set on the 1,400 preranked genes. The x-axis shows the rank in the ordered dataset. The vertical lines represent the locations of the genes that are in the specific gene set.

and survival ($P = 0.012$) is independent of stage. Notably, group 1 was dominated by squamous cell carcinoma (23/28), whereas group 2 was dominated by adenocarcinomas (25/27; $P < 0.0001$; Supplementary Table S3). The other clinical characteristics including gender, age, and smoking status were not significantly different between the 2 groups. To explore whether the association between RGS groups and survival is due to the histologic difference between two groups, we drew Kaplan–Meier curves by both histology and RGS groups (Supplementary Fig. S1),

Published OnlineFirst July 8, 2011; DOI:10.1158/1078-0432.CCR-11-0196

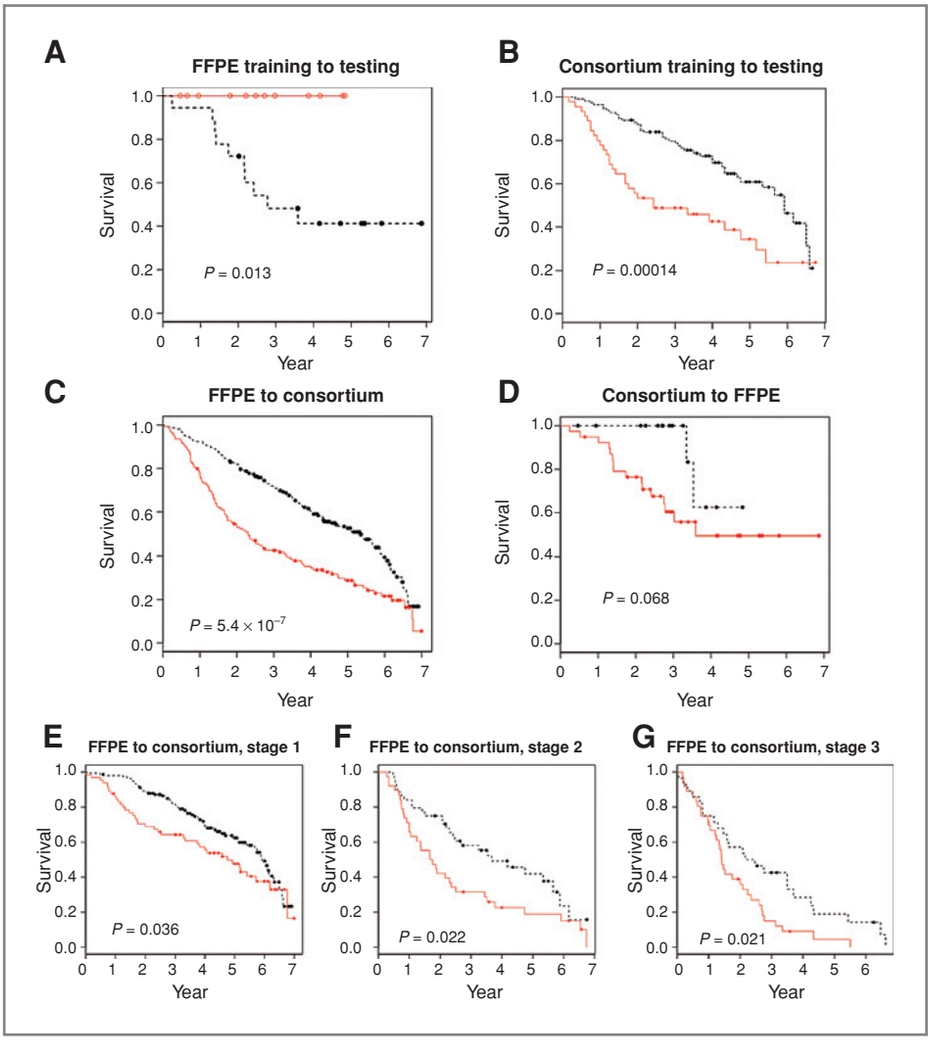

Figure 3. Kaplan–Meier plots showing the predictive power of the robust gene signatures. Fifty-five FFPE tumor samples from MD Anderson Cancer Center were randomly divided into training (25 samples) and testing (30 samples) sets (A). Independent validation of the robust gene signature in the 442 frozen sample cohort from multi-institute consortium. The microarray datasets were divided into 2 groups, one for the training and the other for the testing cohort according to the original paper (B). The training data were 55 FFPE tumor samples and the testing dataset were 442 frozen sample cohort from multi-institute consortium. The testing was done for all patients (C), stage I patients (E), stage II patients (F) and stage III patients (G) separately. The training data were the consortium dataset with 442 frozen samples and the testing data were 55 FFPE samples from MD Anderson Cancer Center (D). *P* values were obtained by the log-rank test. Red and black lines represent predicted high- and low-risk groups, respectively. ● indicates censored samples.

and it shows clearly that RGS can distinguish high- and low-risk groups within both adenocarcinoma and squamous groups, indicating the association of RGS groups and survival is independent of histology groups.

We used gene set enrichment analysis to identify the enriched gene sets in both RGS groups. Interestingly, an estrogen receptor (ER)–negative signature in breast cancer (29) is enriched in RGS group 1, meanwhile, an ER-positive signature in breast cancer (29) is enriched in RGS group 2 (Fig. 2C and D), indicating the relationship between the ER signatures and the RGS groups. The other enriched gene sets are summarized in Supplementary Table S4; notably, genes enriched in group 1 are also enriched in mouse neural stem cells and embryonic stem cells.

Construct and validate RGS prognosis signatures

FFPE samples training to testing. The strong associations between RGS groups and survival outcomes motivated us to explore whether RGS expression profile can be used to construct prognosis signature. We randomly divided 55 patients into training (25 samples) and testing (30 samples) sets and constructed a prediction model by using 1,400 robust gene expression values in the training set through a supervised principle component approach (21). Figure 3A shows that the predicted low-risk group has significant longer survival time than the predicted high-risk group ($P = 0.013$) in the testing set. To test whether this association was not random, we randomly split the data into training and testing sets 200 times, repeated the same prediction and testing procedures for each set, and found that the prognosis performance of RGS signature is significantly better than random ($P = 0.02$).

Frozen samples training to testing. We then tested whether this robust gene set can be used to construct prognosis signature in frozen samples. The largest independent public available lung cancer microarray dataset is the recently published NCI Director's Consortium for study of lung cancer involving 442 resected adenocarcinomas

Published OnlineFirst July 8, 2011; DOI:10.1158/1078-0432.CCR-11-0196

(13). From that study, Affymetrix U133A microarray data for the 1,012 robust genes were excerpted with 388 less genes than our FFPE data because of the microarray platform difference. We used the same training and testing strategy as in the original analyses of these data (13) for constructing and validating prognosis signature through supervised principal component approach. The training set included samples from University of Michigan Cancer Center (UM) and Moffitt Cancer Center (HLM), and the testing set included the Memorial Sloan-Kettering Cancer Center (MSKCC) and Dana-Farber Cancer Institute (DFCI) samples. This analysis revealed that the predicted low-risk group has significant longer survival time than the predicted high-risk group (HR = 2.44, $P = 0.00014$) in the testing dataset (Fig. 3B).

FFPE to frozen samples and vice versa. Next, we used our FFPE and the consortium datasets as frozen samples to investigate whether the predication model built from one type of sample can be validated in another type of sample. Again, the same supervised principal component method was used to construct the prediction model. The prediction model built from FFPE samples can significantly distinguish the high- and low-risk groups in frozen samples (Fig. 3C; HR = 1.95, $P = 5.4 \times 10^{-7}$), and the prediction model built from frozen samples can also distinguish the high- and low-risk groups in FFPE samples but with marginal significance (Fig. 3D; HR = 3.59, $P = 0.068$). We also tested the performance of FFPE prediction model on 4 individual datasets in consortium study and found that the predicted low-risk groups have longer survival time compared with the predicted high-risk groups for all sets: MSKCC dataset (median survival time 6.5 vs. 3.3 years; HR = 2.31, $P = 0.0093$), DFCI dataset (median survival time 5.9 vs. 0.9 years; HR = 2.62 $P = 0.0076$), HLM dataset (median survival time 3.4 vs. 2.2 years; HR = 1.25, $P = 0.4$) and UM dataset (median survival time 5.4 vs. 2.2 years; HR = 1.98, $P = 0.0011$; Supplementary Fig. S2). Next, we compared the performance of RGS signature with previous published lung cancer prognosis signatures by using the same consortium dataset as testing set. Shedden and colleagues (13) showed that the HRs for Method A signature (the best signature in their study) and Chen and colleagues (11) signatures range from 1.10 to 1.83 for the MSKCC test set, whereas the HR for our RGS signature is 2.89 on the same MSKCC test set. For the DFCI test set, the HRs range from 1.76 to 2.30 by using the published signatures, whereas the HR for our RGS signature on the same DFCI test set is 2.39. Therefore, the prognosis performance of RGS prognosis is at least as good as other published signatures in the microarray dataset.

The RGS prognosis signature is independent of clinical variables

To test whether RGS is an independent prognosis signature, we fitted a multivariate Cox regression model including RGS risk scores, age, gender, stage, smoking status, adjuvant chemotherapy usage, and clinical sites as covariables for the consortium dataset. The RGS risk scores were calculated from the prediction model built from the FFPE samples set. Table 1 shows that the RGS signature is significantly associated with the survival time after adjusting for other clinical variables (HR = 1.3, $P = 0.007$). Pathologic stages based on international staging system is the most widely used and important prognosis variable for lung cancer patients (30); here we tested whether RGS signature can further refine the prognosis within each stage. The RGS prognosis signature from FFPE samples was tested within each stage of the consortium dataset. The results show clearly that the RGS signature is significantly associated with survival outcome within each stage (Fig. 3E–G; HR = 1.54, $P = 0.036$ for stage I, HR = 1.81, $P = 0.022$ for stage II and HR = 1.90, $P = 0.021$ for stage III), indicating that the RGS signature can refine the prognosis for lung cancer patients. The RGS prognosis signature from FFPE samples was further tested for patients with or without adjuvant chemotherapy separately, and the results show that the RGS signature is significantly associated with survival for both groups (Supplementary Fig. S3A and B; HR = 1.95, $P = 0.015$ for patients with chemotherapy, HR = 1.99, $P = 0.00062$ for patients without chemotherapy).

Table 1. The association between characteristics of patients and RGS risk scores and survival time for consortium patients on the basis of multivariate Cox regression model

Variables	HR (95% CI)	*P*
RGS risk scores	1.300 (1.074–1.574)	0.0070
Gender (female vs. male)	0.803 (0.576–1.119)	0.19
Age (continuous in unit of 10 y)	1.571 (1.321–1.868)	<0.0001
Smoking (current/former vs. never)	1.356 (0.791–2.322)	0.27
Stage		
Stage II vs. stage I	2.116 (1.433–3.126)	0.0002
Stage III vs. stage I	4.855 (3.164–7.449)	<0.0001
Adjuvant chemotherapy (yes vs. no)	1.688 (1.172–2.431)	0.0049
Study sites		
DFCI vs. UM	1.295 (0.741–2.264)	0.36
HLM vs. UM	1.632 (1.094–2.434)	0.016
MSKCC vs. UM	0.657 (0.419–1.031)	0.068

NOTE: RGS scores were calculated from the prediction model built from MD Anderson Cancer Center FFPE samples.

Refine to 59-gene prognosis signature

Among all the RGS genes, 131 genes are associated with survival ($P < 0.05$) in the FFPE dataset, and 365 genes are associated with overall survival ($P < 0.05$) in the consortium dataset by univariate Cox regression analysis. There is significant overlap between these two gene lists (Fig. 4A; 59 common genes; $P = 0.0008$, hypergeometric test). More significant genes were found in the consortium data

Published OnlineFirst July 8, 2011; DOI:10.1158/1078-0432.CCR-11-0196

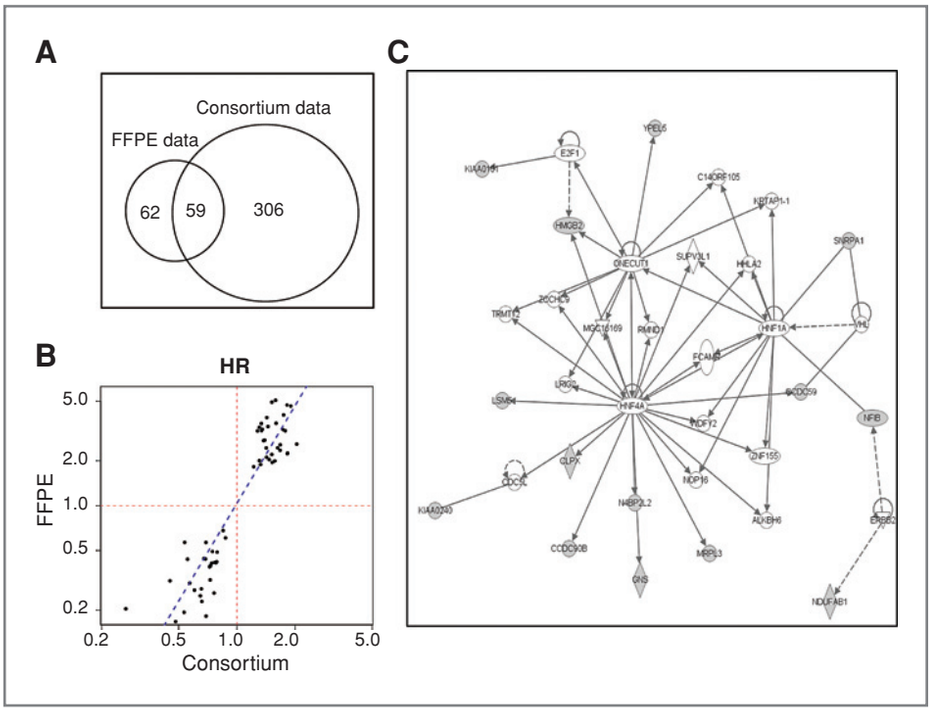

Figure 4. Comparison of individual gene effect across FFPE samples from MD Anderson Cancer Center and 442 frozen samples from consortium. A, Venn diagram of genes associated with overall survival ($P < 0.05$ in univariate Cox regression models). It shows 59 genes are significantly associated with survival in both FFPE data and consortium data. B, the HRs from univariate Cox regression models for the 59 genes common in both sets are consistent between FFPE set and consortium set. C, regulatory gene and protein interaction networks defined by the 59 predictors. Computational molecular interaction network prediction on the basis of genes and proteins associated with the significant pathways in the Ingenuity Pathways Knowledge Base (IPKB) by IPA. Interactions between the different nodes are given as solid (direct interaction) and dashed (indirect interaction) lines (edges). This network received the highest score by IPA and is mostly centered on the transcription factors *HNF4A* and *HNF1A*, and *ONECUT1*. The shaded genes are the genes belonging to 59-gene signature.

compared with the FFPE data, which is likely due to the larger sample size ($n = 442$) of the consortium dataset compared with the FFPE dataset sample size ($n = 55$). Surprisingly, HRs from the two datasets are very consistent with each other. All 59 genes have the same direction of effects (positive or negative) on the survival between the 2 datasets and the HRs from 2 datasets are highly correlated (Pearson's correlation = 0.86; Fig. 4B), indicating the high consistency of expressions of these genes across datasets. These results motivated us to hypothesize that these 59 genes (Supplementary Table S5) alone can be used for lung cancer prognosis. To test this hypothesis, we applied supervised principal component analysis to these 59 genes by using the FFPE dataset to construct a 59-gene prognosis signature. Because the selection of these 59 genes used information from both FFPE and consortium datasets, we used another 2 independent lung cancer datasets, including the Bild and colleagues ($n = 111$; ref. 9) dataset and the Bhattacharjee and colleagues dataset ($n = 117$; ref. 31) downloaded from the literature to validate our 59-gene signature. The 59-gene prediction model built from FFPE samples can significantly distinguish the high- and low-risk groups for both the Bhattacharjee and colleagues and Bild and colleagues datasets (Fig. 5A; HR = 1.81, $P = 0.016$ and Fig. 5C; HR = 2.10, $P = 0.02$, respectively). Furthermore, this signature can also significantly distinguish the high- and low-risk groups within stage I patients for both datasets (Fig. 5B and D), indicating that this 59-gene signature can refine the prognosis for lung cancer patients within stage I patients. Because of the small sample size for stage II and stage III patients in Bild and colleagues and Bhattacharjee and colleagues studies, the 59-gene prognosis signature was not tested for stage II and stage III patients. We also found that 59-gene prediction model built from the consortium dataset can also distinguish the high- and low-risk groups for the Bild and colleagues and Bhattacharjee and colleagues datasets (Supplementary Fig. S4A–D).

To understand the potential biological relevance of these 59 genes significantly associated with survival in the FFPE and consortium datasets, we used Ingenuity Pathway Analysis (IPA) to explore which known regulatory networks are enriched in this 59-gene set. IPA analysis revealed the most significant molecular networks to be cancer, tumor morphology, and respiratory disease. This network (Fig. 4C) includes 14 genes of the 59-gene set and is centered on transcription factors *HNF4A*, *HNF1A*, and *ONECUT1* (*HNF6A*). This hepatocellular network has been implicated in hepatocellular carcinoma as determined by *in vitro* study

Published OnlineFirst July 8, 2011; DOI:10.1158/1078-0432.CCR-11-0196

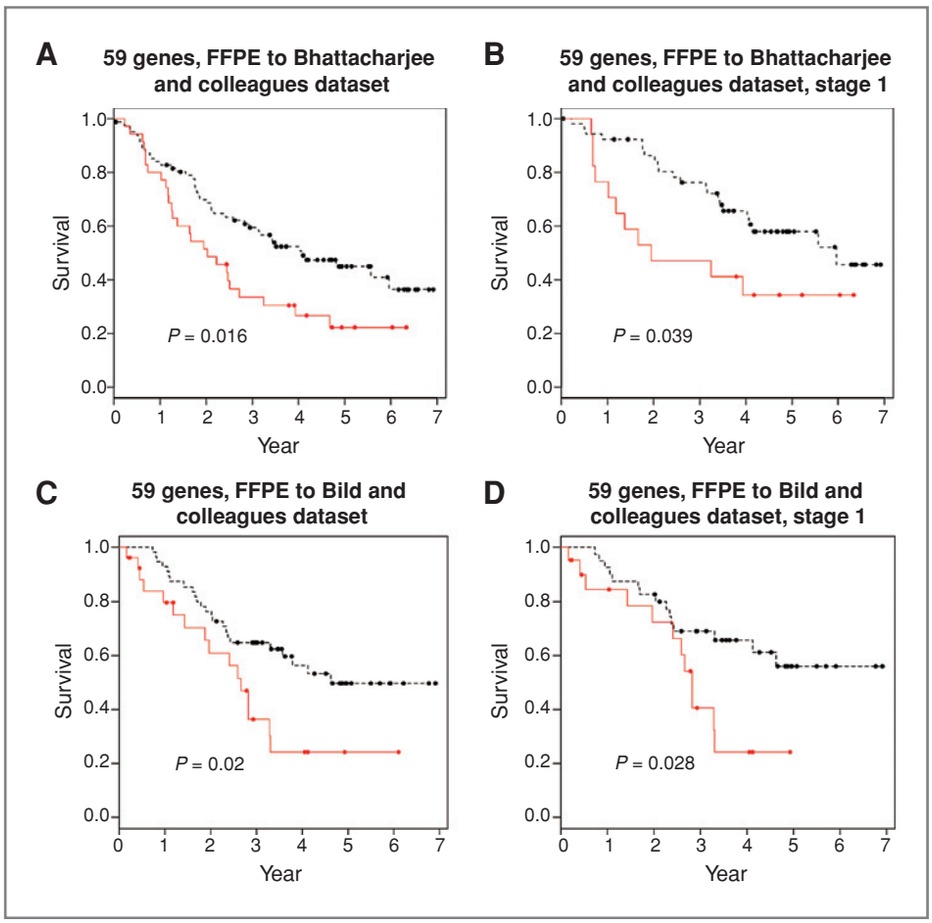

Figure 5. Kaplan–Meier plots showing the predictive power of the 59-gene signature for 2 independent validation sets. The training data were 55 FFPE tumor samples from MD Anderson Cancer Center and the testing dataset was frozen samples from lung cancer patients from Bhattacharjee and colleagues (31) dataset (A), the stage I patients from Bhattacharjee and colleagues dataset (B), frozen samples from lung cancer patients from Bild and colleagues (9) dataset (C), and the stage I patients from Bild and colleagues dataset (D). *P* values were obtained by the log-rank test. Red and black lines represent predicted high- and low-risk groups, respectively. • indicates censored samples.

(32) and molecular interactions in this network are putatively involved in lung cancer survival.

Discussion

In this study, we tested the feasibility of deriving a lung cancer prognosis gene signature from FFPE tumor samples on the basis of genome-wide mRNA expression profiling. Although reverse transcriptase PCR methods have been used to measure gene expression level from FFPE samples (33–35), the selection of genes for testing are limited to the current knowledge base which is incomplete and inconsistent (36). Because of degradation and chemical alteration of RNA extracted from FFPE samples, the use of microarray analysis of gene expression from FFPE samples has been hampered (36). New technology and methodologies developed to extract RNA from FFPE samples coupled with new array platforms have made it possible to measure gene expression from FFPE samples (33, 37–40). A recent study showed the feasibility of using DNA-mediated annealing, selection, extension, and ligation arrays with 6,100 preselected genes to profile mRNA expression from hepatocellular carcinoma tissue (41). No prognosis signature for other types of cancer has been developed by using microarray analysis of gene expression from FFPE extracted RNA. In this study, we built a robust gene signature for NSCLC on the basis of microarray analysis of FFPE samples. We claim that this is a robust gene signature because it has been validated in 6 independent published datasets, including 4 sets from the consortium study and 2 additional studies from DFCI and Duke. We also built a prediction model by using the same set of robust genes from frozen samples and validated the model in both frozen and FFPE samples.

Most published gene signatures identified from different studies are usually very different and with little overlap. However, we found that there is significant overlap among the robust genes associated with survival outcomes between the FFPE dataset and the consortium dataset ($P = 0.008$). More impressively, the HRs, indicating the strength of the association of genes expression and survival time, are highly consistent between 2 independent datasets. Our interpretation for this consistency across studies is that the gene expression variation across studies is a major contribution to signature differences across studies. In this study, we used strict quality steps to exclude genes that were not expressed in our FFPE samples. This allowed for analysis of the remaining genes

Published OnlineFirst July 8, 2011; DOI:10.1158/1078-0432.CCR-11-0196

which had more stable expression patterns and were more robust to environment changes. Validation of our novel 59-gene signature prognostic for NSLC survival in 2 additional independent datasets further confirmed the robustness of these genes.

By grouping our RGS of 1,400 genes by gene expression, we found that the group expression levels correlated with survival. Interestingly, group 1 had a shorter survival and contained an ER-negative breast cancer signature. Group 2 had a longer survival and contained an ER-positive breast cancer signature. This correlation with ER status and survival has been shown previously in breast cancer and shown to have predictive power for prognosis (29). In addition to ER status, the RGS groups were separated by the presence of stem cell signatures (embryonic stem cell signature and neural stem cell signature), with group 1 (shorter survival) having 2 stem cell signatures, whereas group 2 (longer survival) did not. The embryonic stem cell signature has previously been shown to be associated with poor prognosis of NSCLC (42). In addition, in mouse models, a hematopoietic and neural stem cell–like signature in primary tumors has been shown to be a predictor of poor prognosis in 11 types of cancer, including lung (43). These ER status and stem cell signature data support our RGS expression groupings and their correlation with survival prognosis.

Besides the prognostic signature, the predictive signatures to determine the optimal chemotherapy regimen for individual patients also have tremendous clinical benefit. Tumor samples from clinical trials data are important to develop predictive signatures to reduce the selection bias for evaluating treatment efficacy within signature groups. However, very limited frozen tumor samples are available from completed clinical trials. Our study showed the feasibility of using FFPE samples for genome-wide mRNA profiling. Therefore, this study provides an important step to construct and validate predictive signatures for chemotherapy response by using the available FFPE samples from clinical trials in the future.

Disclosure of Potential Conflicts of Interest

No potential conflicts of interest were disclosed.

Grant Support

This study was supported in part by grants from the Department of Defense (W81XWH-07-1-0306 03 to J.D. Minna and I.I. Wistuba), the Specialized Program of Research Excellence in Lung Cancer Grant (P50CA70907 to J.D. Minna, J. Roth, and I.I. Wistuba), the NCI (1R01CA152301-01 to Y. Xie and I.I. Wistuba, Cancer Center Support Grant CA-16672), the NIH (5R21DA027592 to G. Xiao), and the NSF (DMS0907562 to G. Xiao).

The costs of publication of this article were defrayed in part by the payment of page charges. This article must therefore be hereby marked *advertisement* in accordance with 18 U.S.C. Section 1734 solely to indicate this fact.

Received January 26, 2011; revised June 10, 2011; accepted June 29, 2011; published OnlineFirst July 8, 2011.

References

1. Jemal A, Siegel R, Ward E, Hao Y, Xu J, Thun MJ. Cancer statistics, 2009. CA Cancer J Clin 2009;59:225–49.
2. Tsuboi M, Ohira T, Saji H, Miyajima K, Kajiwara N, Uchida O, et al. The present status of postoperative adjuvant chemotherapy for completely resected non-small cell lung cancer. Ann Thorac Cardiovasc Surg 2007;13:73–7.
3. Douillard JY, Rosell R, De Lena M, Carpagnano F, Ramlau R, Gonzales-Larriba JL, et al. Adjuvant vinorelbine plus cisplatin versus observation in patients with completely resected stage IB-IIIA non-small-cell lung cancer (Adjuvant Navelbine International Trialist Association [ANITA]): a randomised controlled trial. Lancet Oncol 2006;7:719–27.
4. Kato H, Ichinose Y, Ohta M, Hata E, Tsubota N, Tada H, et al. A randomized trial of adjuvant chemotherapy with uracil-tegafur for adenocarcinoma of the lung. N Engl J Med 2004;350:1713–21.
5. Arriagada R, Bergman B, Dunant A, Le Chevalier T, Pignon JP, Vansteenkiste J. Cisplatin-based adjuvant chemotherapy in patients with completely resected non-small-cell lung cancer. N Engl J Med 2004;350:351–60.
6. Winton T, Livingston R, Johnson D, Rigas J, Johnston M, Butts C, et al. Vinorelbine plus cisplatin vs. observation in resected non-small-cell lung cancer. N Engl J Med 2005;352:2589–97.
7. Strauss GM, Herndon JE 2nd, Maddaus MA, Johnstone DW, Johnson EA, Harpole DH, et al. Adjuvant paclitaxel plus carboplatin compared with observation in stage IB non-small-cell lung cancer: CALGB 9633 with the Cancer and Leukemia Group B, Radiation Therapy Oncology Group, and North Central Cancer Treatment Group Study Groups. J Clin Oncol 2008;26:5043–51.
8. Olaussen KA, Mountzios G, Soria JC. ERCC1 as a risk stratifier in platinum-based chemotherapy for nonsmall-cell lung cancer. Curr Opin Pulm Med 2007;13:284–9.
9. Bild AH, Yao G, Chang JT, Wang Q, Potti A, Chasse D, et al. Oncogenic pathway signatures in human cancers as a guide to targeted therapies. Nature 2006;439:353–7.
10. Boutros PC, Lau SK, Pintilie M, Liu N, Shepherd FA, Der SD, et al. Prognostic gene signatures for non-small-cell lung cancer. Proc Natl Acad Sci U S A 2009;106:2824–8.
11. Chen HY, Yu SL, Chen CH, Chang GC, Chen CY, Yuan A, et al. A five-gene signature and clinical outcome in non-small-cell lung cancer. N Engl J Med 2007;356:11–20.
12. Lu Y, Lemon W, Liu PY, Yi Y, Morrison C, Yang P, et al. A gene expression signature predicts survival of patients with stage I non-small cell lung cancer. PLoS Med 2006;3:e467.
13. Shedden K, Taylor JM, Enkemann SA, Tsao MS, Yeatman TJ, Gerald WL, et al. Gene expression-based survival prediction in lung adenocarcinoma: a multi-site, blinded validation study. Nat Med 2008;14:822–7.
14. Sun Z, Wigle DA, Yang P. Non-overlapping and non-cell-type-specific gene expression signatures predict lung cancer survival. J Clin Oncol 2008;26:877–83.
15. Hsu DS, Balakumaran BS, Acharya CR, Vlahovic V, Walters KS, Garman K, et al. Pharmacogenomic strategies provide a rational approach to the treatment of cisplatin-resistant patients with advanced cancer. J Clin Oncol 2007;25:4350–7.
16. Hayes DN, Monti S, Parmigiani G, Gilks CB, Naoki K, Bhattacharjee A, et al. Gene expression profiling reveals reproducible human lung adenocarcinoma subtypes in multiple independent patient cohorts. J Clin Oncol 2006;24:5079–90.
17. Coombes KR, Wang J, Baggerly KA. Microarrays: retracing steps. Nat Med 2007;13:1276–7; author reply 7–8.
18. Ioannidis JP, Allison DB, Ball CA, Coulibaly I, Cui X, Culhane AC, et al. Repeatability of published microarray gene expression analyses. Nat Genet 2009;41:149–55.

Published OnlineFirst July 8, 2011; DOI:10.1158/1078-0432.CCR-11-0196

19. Bolstad BM, Irizarry RA, Astrand M, Speed TP. A comparison of normalization methods for high density oligonucleotide array data based on variance and bias. Bioinformatics 2003;19:185–93.
20. Huber PJ. 1972 Wald Lecture - Robust Statistics - Review. Ann Math Stat 1972;43:1041-67.
21. Bair E, Tibshirani R. Semi-supervised methods to predict patient survival from gene expression data. PLoS Biol 2004;2:E108.
22. Breiman L, Friedman J, Stone JC, Olshen RA. Classification and regression trees. New York: Chapman & Hall/CRC; 1984.
23. Garzotto M, Beer TM, Hudson RG, Peters L, Hsieh YC, Barrera E, et al. Improved detection of prostate cancer using classification and regression tree analysis. J Clin Oncol 2005;23:4322–9.
24. Hess KR, Abbruzzese MC, Lenzi R, Raber MN, Abbruzzese JL. Classification and regression tree analysis of 1000 consecutive patients with unknown primary carcinoma. Clin Cancer Res 1999;5:3403–10.
25. Koziol JA, Zhang JY, Casiano CA, Peng XX, Shi FD, Feng AC, et al. Recursive partitioning as an approach to selection of immune markers for tumor diagnosis. Clin Cancer Res 2003;9:5120–6.
26. Valera VA, Walter BA, Yokoyama N, Koyama Y, Iiai T, Okamoto H, et al. Prognostic groups in colorectal carcinoma patients based on tumor cell proliferation and classification and regression tree (CART) survival analysis. Ann Surg Oncol 2007;14:34–40.
27. Kaplan ELM P. Nonparametric estimation from incomplete observations. J Am Stat Assoc 1958;53:457–81.
28. Collett D. Modelling survival data in medical research. Boca Raton: Chapman & Hall/CRC; 2003.
29. van 't Veer LJ, Dai H, van de Vijver MJ, He YD, Hart AA, Mao M, et al. Gene expression profiling predicts clinical outcome of breast cancer. Nature 2002;415:530–6.
30. Mountain CF. The new International Staging System for Lung Cancer. Surg Clin North Am 1987;67:925–35.
31. Bhattacharjee A, Richards WG, Staunton J, Li C, Monti S, Vasa P, et al. Classification of human lung carcinomas by mRNA expression profiling reveals distinct adenocarcinoma subclasses. Proc Natl Acad Sci U S A 2001;98:13790–5.
32. Hatzis P, Talianidis I. Regulatory mechanisms controlling human hepatocyte nuclear factor 4alpha gene expression. Mol Cell Biol 2001;21:7320–30.
33. Farragher SM, Tanney A, Kennedy RD, Paul Harkin D. RNA expression analysis from formalin fixed paraffin embedded tissues. Histochem Cell Biol 2008;130:435–45.
34. Cronin M, Pho M, Dutta D, Stephans JC, Shak S, Kiefer MC, et al. Measurement of gene expression in archival paraffin-embedded tissues: development and performance of a 92-gene reverse transcriptase-polymerase chain reaction assay. Am J Pathol 2004;164:35–42.
35. Gianni L, Zambetti M, Clark K, Baker J, Cronin M, Wu J, et al. Gene expression profiles in paraffin-embedded core biopsy tissue predict response to chemotherapy in women with locally advanced breast cancer. J Clin Oncol 2005;23:7265–77.
36. van't Veer LJ, Bernards R. Enabling personalized cancer medicine through analysis of gene-expression patterns. Nature 2008;452:564–70.
37. Loudig O, Milova E, Brandwein-Gensler M, Massimi A, Belbin TJ, Childs G, et al. Molecular restoration of archived transcriptional profiles by complementary-template reverse-transcription (CT-RT). Nucleic Acids Res 2007;35:e94.
38. Penland SK, Keku TO, Torrice C, He X, Krishnamurthy J, Hoadley KA, et al. RNA expression analysis of formalin-fixed paraffin-embedded tumors. Lab Invest 2007;87:383–91.
39. Ravo M, Mutarelli M, Ferraro L, Grober OM, Paris O, Tarallo R, et al. Quantitative expression profiling of highly degraded RNA from formalin-fixed, paraffin-embedded breast tumor biopsies by oligonucleotide microarrays. Lab Invest 2008;88:430–40.
40. Roberts RA, Sabalos CM, LeBlanc ML, Martel RR, Frutiger YM, Unger JM, et al. Quantitative nuclease protection assay in paraffin-embedded tissue replicates prognostic microarray gene expression in diffuse large-B-cell lymphoma. Lab Invest 2007;87:979–97.
41. Hoshida Y, Villanueva A, Kobayashi M, Peix J, Chiang DY, Camargo A, et al. Gene expression in fixed tissues and outcome in hepatocellular carcinoma. N Engl J Med 2008;359:1995–2004.
42. Hassan KA, Chen G, Kalemkerian GP, Wicha MS, Beer DG. An embryonic stem cell-like signature identifies poorly differentiated lung adenocarcinoma but not squamous cell carcinoma. Clin Cancer Res 2009;15:6386–90.
43. Glinsky GV, Berezovska O, Glinskii AB. Microarray analysis identifies a death-from-cancer signature predicting therapy failure in patients with multiple types of cancer. J Clin Invest 2005;115:1503–21.

Cancer Chemother Pharmacol (2011) 68:703–712
DOI 10.1007/s00280-010-1536-1

ORIGINAL ARTICLE

Sunitinib in combination with paclitaxel plus carboplatin in patients with advanced solid tumors: phase I study results

Elisabeth I. Heath · George R. Blumenschein Jr · Roger B. Cohen · Patricia M. LoRusso · Noelle K. LoConte · Sindy T. Kim · Ana Ruiz-Garcia · Richard C. Chao · George Wilding

Received: 1 September 2010 / Accepted: 15 November 2010 / Published online: 8 December 2010

Abstract
Purpose To evaluate the maximum tolerated dose (MTD), safety, and antitumor activity of sunitinib combined with paclitaxel and carboplatin.
Methods Successive cohorts of patients with advanced solid tumors received oral sunitinib (25, 37.5, or 50 mg) for 2 consecutive weeks of a 3-week cycle (Schedule 2/1) or as a continuous daily dose for 3-week cycles (CDD schedule) in combination with paclitaxel (175–200 mg/m^2) plus carboplatin (AUC 6 mg min/ml) on day one of each of 4 cycles. Dose-limiting toxicities (DLTs) and adverse events (AEs) were evaluated to determine the MTD. Efficacy parameters were analyzed in patients with measurable disease.
Results Forty-three patients were enrolled ($n = 25$ Schedule 2/1; $n = 18$ CDD schedule). Across all doses, 6 DLTs were observed [grade 4 papilledema, grade 5 GI hemorrhage, grade 3 neutropenic infection, and grade 4 thrombocytopenia ($n = 3$)]. The MTD for Schedule 2/1 was sunitinib 25 mg plus paclitaxel 175 mg/m^2 and carboplatin AUC 6 mg min/ml. The MTD was not determined for the CDD schedule. Treatment-related AEs included neutropenia (77%), thrombocytopenia (56%), and fatigue (47%). Of 38 evaluable patients, 4 (11%) had partial responses and 12 (32%) had stable disease. PK data indicated an increase in maximum and total plasma exposures to sunitinib and its active metabolite when given with paclitaxel and carboplatin compared with sunitinib monotherapy.
Conclusions Myelosuppression resulting in prolonged dose delays and frequent interruptions was observed, suggesting that this treatment combination is not feasible in the general cancer population.

Keywords Sunitinib · Phase I · Solid tumor · NSCLC · Antiangiogenesis · Chemotherapy

E. I. Heath (✉) · P. M. LoRusso
Karmanos Cancer Institute, 4100 John R,
Detroit, MI 48201, USA
e-mail: heathe@karmanos.org

G. R. Blumenschein Jr
The University of Texas M.D. Anderson Cancer Center,
Houston, TX, USA

R. B. Cohen
Fox Chase Cancer Center, Philadelphia, PA, USA

N. K. LoConte · G. Wilding
University of Wisconsin Carbone Cancer Center,
Madison, WI, USA

S. T. Kim · A. Ruiz-Garcia · R. C. Chao
Pfizer Oncology, Clinical Development,
La Jolla, San Diego, CA, USA

Introduction

Carboplatin and paclitaxel are frequently combined to treat a broad range of solid tumor types, including ovarian cancer and non-small-cell lung cancer (NSCLC). Efficacy of chemotherapy is limited, however, especially in advanced cancer [1, 2]. Consequently, there is considerable interest in developing innovative treatment strategies, with one common approach being the combination of agents with different mechanisms of action such as chemotherapy with molecularly targeted drugs.

Vascular endothelial growth factor (VEGF) and platelet-derived growth factor (PDGF) signaling pathways play a critical role in angiogenesis and have been identified as therapeutic targets for multiple solid tumors [3, 4]. The targeted antiangiogenic agent bevacizumab, an anti-VEGF monoclonal antibody, has shown encouraging antitumor

activity when combined with chemotherapy in patients with solid tumors [5–7]. In a randomized phase III study in NSCLC, overall survival was improved in patients treated with paclitaxel, carboplatin, and bevacizumab compared to patients treated with paclitaxel/carboplatin alone [8].

In addition to inhibition of VEGF, evidence suggests that inhibiting multiple signaling pathways in parallel, such as VEGF and PDGF pathways, may be more effective than inhibiting single pathways in isolation [9, 10]. Sunitinib malate (SUTENT®) is an oral multitargeted tyrosine kinase inhibitor (TKI) of VEGF and PDGF receptor (VEGFR and PDGFR) subtypes, stem cell factor receptor (KIT), FMS-like tyrosine kinase (FLT3), glial cell line-derived neurotrophic factor (REarranged during Transfection [RET]), and colony-stimulating factor 1 receptor (CSF-1R) [11, 12]. Sunitinib is currently approved for treatment of advanced renal cell carcinoma (RCC) and imatinib-resistant/imatinib-intolerant gastrointestinal stromal tumor (GIST) [13–15].

The primary objective of this phase I study was to assess the maximum tolerated dose (MTD) and overall safety of sunitinib administered on two different schedules in combination with paclitaxel and carboplatin, for the treatment of patients with advanced solid tumors. Secondary objectives included evaluation of the pharmacokinetics (PK) of the combination and antitumor activity in patients with measurable disease.

Materials and methods

Patient eligibility

Patients ≥18 years with advanced solid tumors refractory to standard therapy or for which no curative therapy exists were eligible if they were considered suitable for treatment with standard doses of carboplatin and paclitaxel and had a life expectancy of ≥12 weeks. A maximum of two prior chemotherapy regimens was permitted. Additional inclusion criteria included an Eastern Cooperative Oncology Group performance status (ECOG PS) of 0 or 1 and adequate organ function. Exclusion criteria included prior treatment with high-dose chemotherapy requiring stem cell rescue or prior irradiation to ≥25% of bone marrow; and surgery, systemic therapy, or any investigational agent within 4 weeks prior to starting study treatment (except palliative radiotherapy). Other exclusion criteria included history of untreated brain metastases and severe acute or chronic cardiovascular abnormalities.

Study design and treatment

In this phase I, open-label, multicenter, dose-finding study (3 + 3 design), patients were scheduled to receive sunitinib in combination with paclitaxel and carboplatin for 4 cycles. A treatment cycle consisted of 3 weeks of once-daily dosing of oral sunitinib given on either Schedule 2/1 (2 weeks on treatment followed by 1 week off treatment) or on a continuous daily dosing (CDD) schedule, in combination with intravenous (iv) paclitaxel and carboplatin administered once every 21 days. The starting doses of each drug were sunitinib 25 mg/day, paclitaxel 175 mg/m^2, and carboplatin area under the curve (AUC) 6 mg min/ml.

The MTD was defined as the highest dose at which 0/6 or 1/6 patients experienced a dose-limiting toxicity (DLT) during the first cycle, with at least 2/3 or 2/6 patients experiencing a DLT at the next higher dose level. In general, treatment-related grade 3 or 4 toxicities were considered DLTs including: grade 4 neutropenia lasting ≥7 days, febrile neutropenia lasting >24 h, neutropenic infection, grade ≥3 thrombocytopenia with bleeding or grade 4 thrombocytopenia lasting ≥7 days, lymphopenia accompanied by an infection, and grade 3 or 4 non-hematologic toxicities lasting ≥7 days. Persistent nausea, vomiting, or diarrhea (despite maximal medical therapy) were also considered DLTs.

Escalating doses of sunitinib and paclitaxel and carboplatin were first studied on sunitinib Schedule 2/1 starting at dose level 1 (Table 1). According to the protocol, once the DLT assessment period was completed on dose level 1 of Schedule 2/1, the sunitinib CDD schedule was evaluated, starting at dose A (Table 1). Dose escalation occurred as summarized in Table 1. Once the MTD was determined for both sunitinib treatment schedules, additional patients were to be enrolled at the MTD(s) to better characterize safety and antitumor activity. In addition, there was the option to enroll further subjects at specific dose levels to further explore the observed toxicity and PK profile. Further details relating to the dose-escalation decisions made during the trial are described in the "Results" section.

Patients could be treated with 4 cycles of combination therapy until disease progression, unacceptable toxicity, or withdrawal of consent. Dose reductions were permitted at the discretion of the investigators. Patients deriving clinical benefit upon completion of 4 cycles could continue to receive sunitinib alone under a separate continuation protocol.

All patients provided written informed consent. The study was performed with institutional ethics committee approval, and in accordance with International Conference on Harmonization Good Clinical Practice guidelines, the Declaration of Helsinki (1996 Version), and applicable local and Federal regulatory requirements and laws.

Study endpoints and assessments

The primary endpoints were the MTD and overall safety of the combination. Secondary endpoints included PK

Table 1 Planned dose levels and observed dose-limiting toxicities

Dose level[a]	Paclitaxel (mg/m^2)	Carboplatin (mg min/ml)	Sunitinib (mg)	*n* (*n* evaluable for DLT)	DLTs
Schedule 2/1[b]					
1	175	6	25	9 (7)	Grade 4 papilledema ($n = 1$)
2	175	6	37.5	13 (10)	Grade 5 gastrointestinal hemorrhage ($n = 1$)
					Grade 4 thrombocytopenia ($n = 2$)
					Grade 3 neutropenic infection ($n = 1$)
3	200	6	37.5	3 (3)	None
CDD schedule[c]					
A	175	6	25	3 (3)	None
B	175	6	37.5	9 (9)	None
C[d]	175	6	50	2 (2)	Grade 4 thrombocytopenia ($n = 1$)
B1[d]	200	6	25	4 (4)	None

CDD continuous daily dosing, *DLT* dose-limiting toxicity

[a] Patients started sunitinib on day 3 and chemotherapy on day 1 of cycle 1. During subsequent cycles, patients started both chemotherapy and sunitinib on day 1

If 0/3 patients experienced a DLT during cycle 1, subjects were enrolled onto the next dose level

If 1/3 subjects experienced a DLT during cycle 1, the cohort was expanded to a total of $n = 6$ patients. If 1/6 subjects experienced a DLT, then dose escalation continued and subjects were enrolled in the next dose level

If ≥ 2 subjects in any cohort experienced a DLT during cycle 1, then the MTD had been exceeded and cohorts in preceding dose levels could be expanded to a total of $n = 6$ patients until the MTD was identified

If there was interest in further exploring the toxicity profile observed at a specific dose level and 2 DLTs were observed in the initial 6 patients enrolled, an additional 3 patients could be enrolled. If no additional DLTs were observed, dose escalation could continue after discussion between the sponsors and investigators

[b] On Schedule 2/1, the MTD was determined as sunitinib 25 mg/day plus paclitaxel 175 mg/m^2 and carboplatin AUC 6 mg min/ml

[c] MTD was not determined on the CDD schedule

[d] Patients were enrolled concurrently onto doses C and B1

parameters and assessment of antitumor activity. Safety was assessed by recording adverse events (AEs), graded using National Cancer Institute Common Terminology Criteria for Adverse Events (NCI CTCAE), version 3.0. Hematology and blood chemistry parameters were also monitored at baseline and throughout the study. Other safety assessments included physical examinations and vital signs, and 12-lead electrocardiograms (ECG) performed at screening, during cycle 1, and at end of treatment.

Tumor assessments were performed at screening and at the end of cycles 2 and 4, and whenever disease progression was suspected according to Response Evaluation Criteria In Solid Tumors (RECIST) [16]. Objective tumor response was assessed in patients with measurable disease.

Full PK profiles were obtained on Schedule 2/1 from 5 patients receiving dose level 1, 4 patients receiving dose level 2, and 2 patients receiving dose level 3. On the CDD schedule, full PK profiles were obtained from 1 patient receiving dose level A and 5 patients receiving dose level B (dose levels described in Table 1). Plasma samples for PK analyses were analyzed using validated analytical methods. Sunitinib and its primary metabolite, SU12662, were assayed using LC–MS/MS (assay dynamic range was 0.100–60.0 ng/ml for sunitinib and 0.100–20.0 ng/ml for SU12662). Paclitaxel was assayed using LC–MS/MS with solid phase extraction; the assay had a dynamic range of 10.0–2,000 ng/ml. Carboplatin was assayed using ICP/MS (assay dynamic range was 2.00–1,000 ng/ml).

PK parameters for sunitinib, SU12662, total drug (sunitinib plus SU12662), paclitaxel, and carboplatin are reported for paired observations. On Schedule 2/1, patients received a single dose of sunitinib 7 days prior to the start of cycle 1 (day–7). Following this dose, 24-h plasma samples were taken to assess sunitinib and SU12662 PK. During cycle 1, paclitaxel and carboplatin were given on day 1 and sunitinib was started on day 3 and given through cycle 1, day 16. This dosing schedule allowed PK data to be collected for sunitinib alone (day 7), paclitaxel and carboplatin alone (cycle 1, day 1), and sunitinib plus paclitaxel and carboplatin (cycle 2, day 1). From cycle 2 onwards, sunitinib plus paclitaxel and carboplatin were administered starting on day 1 of each cycle. On the CDD schedule, sunitinib was started on day 3 in cycle 1. This allowed PK analysis of paclitaxel and carboplatin alone (cycle 1, day 1), sunitinib alone at steady state (cycle 1, day 15), and paclitaxel and carboplatin plus steady-state

Table 2 Patient demographics

	Schedule 2/1 ($n = 25$)	CDD schedule ($n = 18$)	Total ($n = 43$)
Sex, *n* (%)			
Male/female	17 (68)/8 (32)	12 (67)/6 (33)	29 (67)/14 (33)
ECOG performance status, *n* (%)			
0/1	6 (24)/19 (76)	5 (28)/13 (72)	11 (26)/32 (74)
Primary disease sites			
NSCLC	4 (16)	6 (33)	10 (23)
Esophageal adenocarcinoma	1 (4)	3 (17)	4 (9)
Pancreatic carcinoma	4 (16)	0 (0)	4 (9)
SCLC	3 (12)	1 (6)	4 (9)
Malignant melanoma	3 (12)	0 (0)	3 (7)
Mesothelioma	2 (8)	1 (6)	3 (7)
Other[a]	8 (32)	7 (39)	22 (51)
Prior treatments			
Chemotherapy[b]	20 (80)	8 (44)	28 (65)
Cancer-related surgery	23 (92)	16 (89)	39 (91)
Radiotherapy	12 (48)	5 (28)	17 (40)
Immunotherapy	3 (12)	0 (0)	3 (7)
Hormonal therapy	1 (4)	0 (0)	1 (2)
Unspecified	1 (4)	0 (0)	1 (2)

CDD continuous daily dosing, *ECOG* Eastern Cooperative Oncology Group, *NSCLC* non-small-cell lung cancer, *SCLC* small-cell lung cancer

[a] Carcinoid, pleural mesothelioma, neuroendocrine carcinoma, metastatic neoplasm unknown primary, thyroid cancer [all $n = 2$ (4.7%)], adrenocortical carcinoma, transitional cell carcinoma bladder, breast cancer, mesothelioma, ovarian cancer, malignant hepatic neoplasm, seminoma, and metastases to peritoneum [all $n = 1$ (2.3%)]

[b] Includes prior targeted therapies: erlotinib ($n = 2$), bevacizumab, BSI-201, figitumumab, sorafenib, and vorinostat (each $n = 1$)

sunitinib (cycle 2, day 1). From cycle 2 onwards, sunitinib plus paclitaxel and carboplatin were administered starting on day 1 of each cycle.

Statistical methods

The observed safety profile on each schedule determined the number of patients per dose level and number of dose escalations. Due to the exploratory nature of this study, no inferential analyses were planned.

Results

Patient characteristics

Forty-three patients were enrolled into the trial: 25 patients on Schedule 2/1 and 18 patients on the CDD schedule. The median age of patients was 58 years (range: 32–76). Baseline characteristics are summarized in Table 2.

Subject evaluation groups

The doses of study treatment evaluated are shown in Table 1. The sponsor and investigators agreed to further expand dose level 2 for Schedule 2/1 and dose level B for the CDD schedule to better characterize the safety profile of the combination regimens. Initially, 6 patients were enrolled in the first cohort at dose level 1 on Schedule 2/1 (including 2 patients who were not evaluable for DLT: $n = 1$ developed a hypersensitivity reaction to paclitaxel; $n = 1$ experienced disease progression prior to cycle 1 day 1). One DLT (grade 4 papilledema) was observed and this cohort was expanded to 9 patients, resulting in 7 patients evaluable for DLTs. Because no additional DLTs were observed, patients were next enrolled at dose level 2 and, among 3 patients initially enrolled who were evaluable for DLTs (1 further patient discontinued early due to disease progression prior to cycle 1, day 1), one DLT was observed; this cohort was then expanded to 13 patients. While the dose level 2 cohort was being expanded, the protocol was amended to allow concurrent enrollment into Schedule 2/1 and the CDD schedule. Three patients were enrolled onto dose level 3 and no DLTs were observed. Following enrollment into dose level 3, further DLTs were observed in the expanded dose level 2 cohort. On the CDD schedule starting at dose level A, 3 patients were enrolled and no DLTs were observed. Enrollment of the CDD schedule cohorts continued as described in Table 1.

A total of 13 patients (30%) completed the study (receiving the 4 planned cycles of study treatment) and 30 patients discontinued before completion. Of the 13 patients who completed, 12 ($n = 4$ from Schedule 2/1 cohorts, $n = 8$ from CDD cohorts) enrolled in a continuation protocol and received sunitinib as a single agent. One additional patient who was discontinued from the study due to AEs after cycle 1 was also enrolled in the continuation protocol. Twenty of the 25 patients (80%) on Schedule 2/1 discontinued treatment early: 11 patients due to insufficient clinical response and 9 due to AEs, including 6 who had AEs that were considered treatment-related [papilledema, gastrointestinal (GI) hemorrhage, syncope, pyrexia, pneumonia, leukopenia, and hemoptysis (all $n = 1$ each), anemia ($n = 3$), thrombocytopenia ($n = 3$), and neutropenia ($n = 2$)]. Ten of the 18 patients (56%) on the CDD schedule discontinued treatment early: 6 patients due to insufficient clinical response; 2 due to AEs (1 patient had AEs considered to be treatment-related: neutropenia, anemia, and thrombocytopenia); 1 patient on the CDD schedule died due to disease progression; and 1 patient withdrew consent.

The number of sunitinib treatment cycles started ranged between 0–4 and 1–5 on Schedule 2/1 and the CDD schedule, respectively. One patient on the CDD schedule received 5 cycles of sunitinib on the study, receiving an additional cycle of treatment while awaiting enrollment in the continuation protocol. In total, 11 patients received all three drugs through to the start of cycle 2 without dose reductions, dose delays, or dose interruptions (Schedule 2/1 dose level 1, $n = 2$; dose level 2 $n = 2$; CDD schedule dose B, $n = 5$; dose B1, $n = 2$).

Of the 25 patients on Schedule 2/1, 10 (40%) required sunitinib dose delays and 2 (8%) required dose reductions. Of the 18 patients on the CDD schedule, 8 (44%) required sunitinib dose delays and 3 (17%) required dose reductions. In all but 2 patients, sunitinib dose delays were attributed to neutropenia, thrombocytopenia, or leukopenia (all grades). The duration of sunitinib dose delays was most commonly $\geq$3 weeks ($n = 18$ patients overall).

In the Schedule 2/1 cohorts, 10 patients experienced dose delays for paclitaxel and 10 patients experienced dose delays for carboplatin. Five patients experienced at least one dose reduction of paclitaxel and 1 patient experienced $\geq$2 dose reductions of carboplatin. In the CDD cohorts, 9 and 8 patients experienced dose delays for paclitaxel and carboplatin, respectively, and 3 and 1 patients experienced at least one dose reduction of paclitaxel and carboplatin, respectively.

Determination of MTD

Across all schedules, DLTs occurring in the first treatment cycle were reported in 6 patients (14%; Table 1). All DLTs were reported as serious AEs (SAEs) and considered to be related to sunitinib and/or paclitaxel and carboplatin treatment. On Schedule 2/1, the MTD was determined as sunitinib 25 mg/day plus paclitaxel 175 mg/m^2 and carboplatin AUC 6 mg min/ml. The MTD was not determined for the CDD schedule.

Other safety findings

Treatment-emergent (all-causality) non-hematologic AEs occurring in $\geq$10% of patients across all treatment combinations are shown in Table 3. Most non-hematologic AEs were grade 1 or 2 in severity. The most common were fatigue (58%), nausea (44%), alopecia (30%), and dyspnea (28%).

Overall, 35/43 patients (81%) experienced at least one AE (grade $\geq$ 3) considered related to study treatment. The most common treatment-related AEs were neutropenia [77%; grade 3 (23%) or 4 (42%)], thrombocytopenia [56%; grade 3 (19%) or 4 (14%)], and fatigue [47%; grade 3 (7%)]. The frequency of treatment-related AEs was similar for Schedule 2/1 and the CDD schedule, although the incidence of treatment-related thrombocytopenia was higher for patients on the CDD schedule (11/18 subjects, 61%) compared with Schedule 2/1 (13/25 subjects, 52%).

All-causality hematologic AEs reported in all cycles and cycle 1 are shown in Table 4. Neutropenia (79%) and thrombocytopenia (74%) were the most frequent events. Hematologic laboratory abnormality shifts from grade $\leq$2 to grade $\geq$3 (all patients, both schedules) included neutropenia (70%), leukopenia (49%), thrombocytopenia (40%), lymphopenia (35%), and anemia (23%). No patient experienced grade 4 lymphopenia. One patient experienced a shift to grade 4 anemia.

Cardiovascular disorders occurred infrequently. Grade 3 thrombosis, grade 1 sinus tachycardia, and grade 1 tachycardia were reported in 1 patient each. None of these AEs was considered related to study treatment. One patient receiving dose level 2 on Schedule 2/1 experienced grade 3 syncope deemed treatment-related by the investigator. There were no clinically significant changes at any timepoints for the mean heart rate, blood pressure, and ECG parameters.

Three patients died on study. Two deaths were attributed to disease progression [bladder cancer ($n = 1$) and esophageal adenocarcinoma ($n = 1$)]. The third patient, a 59-year-old male patient with pancreatic carcinoma who was receiving treatment on Schedule 2/1 dose level 2, died due to GI hemorrhage and hypotension, which were considered possibly related to study treatment.

Antitumor activity

Of the 38 patients with measurable disease at baseline and evaluable for response, 4 patients achieved a partial

Table 3 Most common all-causality non-hematologic adverse events (≥10% incidence cut-off) in all cohorts

Adverse event	All patients ($n = 43$)				
	Grade 1 *n* (%)	Grade 2 *n* (%)	Grade 3 *n* (%)	Grade 4 *n* (%)	Total *n* (%)
Fatigue	12 (30)	9 (21)	4 (9)	0 (0)	25 (58)
Nausea	13 (30)	6 (14)	0 (0)	0 (0)	19 (44)
Alopecia	7 (16)	6 (14)	0 (0)	0 (0)	13 (30)
Dyspnea	4 (9)	6 (14)	2 (5)	0 (0)	12 (28)
Diarrhea	6 (14)	5 (12)	0 (0)	0 (0)	11 (26)
Constipation	8 (19)	2 (5)	0 (0)	0 (0)	10 (23)
Vomiting	8 (19)	2 (5)	0 (0)	0 (0)	10 (23)
Anorexia	5 (12)	3 (7)	1 (2)	0 (0)	9 (21)
Arthralgia	9 (21)	0 (0)	0 (0)	0 (0)	9 (21)
Pyrexia	7 (16)	2 (5)	0 (0)	0 (0)	9 (21)
Cough	6 (14)	2 (5)	0 (0)	0 (0)	8 (19)
Epistaxis	8 (19)	0 (0)	0 (0)	0 (0)	8 (19)
Headache	8 (19)	0 (0)	0 (0)	0 (0)	8 (19)
Neuropathy peripheral	7 (16)	1 (2)	0 (0)	0 (0)	8 (19)
Dehydration	2 (5)	3 (7)	2 (5)	0 (0)	7 (16)
Dysgeusia	6 (14)	1 (2)	0 (0)	0 (0)	7 (16)
Dizziness	6 (14)	0 (0)	0 (0)	0 (0)	6 (14)
Dyspepsia	6 (14)	0 (0)	0 (0)	0 (0)	6 (14)
Hypomagnesemia	3 (7)	2 (5)	0 (0)	1 (2)	6 (14)
Myalgia	6 (14)	0 (0)	0 (0)	0 (0)	6 (14)
Rash	6 (14)	0 (0)	0 (0)	0 (0)	6 (14)
Weight decreased	5 (12)	1 (2)	0 (0)	0 (0)	6 (14)
Aspartate aminotransferase increased	1 (2)	3 (7)	1 (2)	0 (0)	5 (12)
Chills	5 (12)	0 (0)	0 (0)	0 (0)	5 (12)
Hemoptysis	4 (9)	0 (0)	1 (2)	0 (0)	5 (12)

There was one grade 5 event (gastrointestinal hemorrhage)

Table 4 All-causality hematologic adverse events in all cohorts (occurring in cycle 1 and in all cycles)

Adverse event	All patients ($n = 43$)				
	Grade 1 *n* (%)	Grade 2 *n* (%)	Grade 3 *n* (%)	Grade 4 *n* (%)	Total *n* (%)
Cycle 1					
Anemia	2 (5)	4 (9)	5 (12)	3 (7)	14 (33)
Leukopenia	0 (0)	8 (19)	7 (16)	4 (9)	19 (44)
Neutropenia	0 (0)	5 (12)	8 (19)	14 (33)	27 (63)
Thrombocytopenia	3 (7)	5 (12)	5 (12)	8 (19)	21 (49)
All cycles					
Anemia	1 (2)	10 (23)	9 (21)	3 (7)	23 (54)
Leukopenia	0 (0)	6 (14)	10 (23)	5 (12)	21 (49)
Neutropenia	1 (2)	4 (9)	11 (26)	18 (42)	34 (79)
Thrombocytopenia	5 (12)	7 (16)	10 (23)	10 (23)	32 (74)

response (PR) for an objective response rate of 10.5% [95% confidence interval (CI): 2.9%, 24.8%] across all cohorts. Two PRs occurred on Schedule 2/1 (one at dose level 1 and the other at dose level 2). Two PRs occurred on the CDD schedule (one at dose level B and the other at dose level B1). Patients with PRs had the following primary diagnoses: SCLC ($n = 1$), NSCLC ($n = 2$), and peritoneal carcinomatosis ($n = 1$), and 2 patients had

received prior chemotherapeutic regimens (carboplatin plus etoposide and topotecan; carboplatin plus paclitaxel; and carboplatin plus gemcitabine).

Across both dosing schedules, stable disease (SD) with duration ≥42 days after the first dose of study drug was observed in 12 patients ($n = 6$ on Schedule 2/1 and $n = 6$ on the CDD schedule). Twelve patients (32%) experienced progressive disease (PD) as their best response (6 on Schedule 2/1 and 6 on the CDD schedule). Response status could not be determined for 10/38 evaluable patients because post-baseline scans were not available (patients either discontinued early or lesions identified at baseline were not assessed).

Pharmacokinetics

AEs prevented many patients from taking sunitinib daily on both schedules. On the CDD schedule, plasma concentration profiles at steady state were collected for only 5 patients (paired observations) at sunitinib 37.5 mg/day plus paclitaxel 175 mg/m^2 and carboplatin AUC 6 mg min/ml (dose level B), and 1 patient at sunitinib 25 mg/day plus paclitaxel 175 mg/m^2 and carboplatin AUC 6 mg min/ml (dose level A). Therefore, PK parameters are presented only for the dose levels on both treatment schedules with a sufficient number of evaluable patients: sunitinib 37.5 mg/day plus paclitaxel 175 mg/m^2 and carboplatin AUC 6 mg min/ml (dose levels 2 and B; Table 1). The data indicated an increase in maximum and total plasma exposures to sunitinib and its active metabolite SU12662 when sunitinib was given with paclitaxel and carboplatin compared with sunitinib monotherapy (Table 5). No notable difference in PK was observed between Schedule 2/1 and the CDD schedule.

Discussion

The objective of this phase I, dose-finding PK study was to determine the MTD and overall safety of sunitinib plus paclitaxel and carboplatin in patients with solid tumors for whom curative therapy was not available. Sunitinib was investigated on intermittent (Schedule 2/1, 2 weeks on treatment, 1 week off treatment) and CDD schedules. The MTD on Schedule 2/1 (investigated in 25 patients) was determined to be sunitinib 25 mg/day plus paclitaxel 175 mg/m^2 and carboplatin AUC 6 mg min/ml. The MTD for the CDD schedule was not determined (investigated in 18 patients) because the study was stopped before formal determination of the MTD, based upon the toxicity patterns observed in the sunitinib Schedule 2/1 cohort. Frequent and sometimes prolonged dose delays and dose interruptions also made assessment of the MTD challenging. In total, 11 patients (Schedule 2:1 $n = 4$; CDD schedule $n = 7$) received all three drugs through to the start of cycle 2 without dose reductions, dose delays, or dose interruptions.

Most non-hematologic AEs reported with sunitinib plus paclitaxel and carboplatin were grade 1 or 2 in severity. No unexpected AEs were reported and no significant cardiac abnormalities were noted during this study. Even though AEs greater than grade 1 or 2 in severity were infrequent, the cumulative effect of multiple grade 1/2 side effects in individual patients and the prolonged duration of these toxicities resulted in the need for dose interruptions and treatment delays in a significant proportion of patients and suggested that the regimens studied were ultimately unfeasible. Similar observations have been reported in clinical trials of other targeted therapies when combined with each other or cytotoxic chemotherapy [17].

The most common non-hematologic AEs were fatigue, nausea, alopecia, and dyspnea. The AE profile in this study was generally similar to that of other studies of a taxane plus carboplatin [18–20], single-agent sunitinib [21–23], or sunitinib in combination with chemotherapy [24–26]. However, grade 3/4 neutropenia and thrombocytopenia (laboratory abnormalities) occurred in 70% and 40% of patients, respectively, which is a higher incidence than has been reported in trials of other targeted agents in combination with carboplatin and paclitaxel in patients with solid tumors [8, 27–29]. Temporary sunitinib dose interruptions/delays were needed by almost half of the patients enrolled in this study and were attributed to neutropenia, thrombocytopenia, or leukopenia (all grades) at one or more times in all but 2 of these patients. Based on the investigators' observations, chemotherapy-naïve patients appeared to tolerate the treatment better than chemotherapy-refractory patients. Delays or interruptions in the dosing of paclitaxel and carboplatin were also frequent during this trial, further limiting the feasibility of this treatment regimen. Additionally, the majority of patients (70%) discontinued study treatment before receiving the 4 planned cycles: 80% of patients on Schedule 2/1 and 56% on the CDD schedule. In-line with the investigators' observations on tolerability, the imbalance in discontinuation rates between the two schedules might have been related to the fact that the majority of patients on Schedule 2/1 (80%) had received prior chemotherapy, whereas over half of patients on the CDD schedule were chemotherapy-naïve (56%).

Complete PK data based on small sample sizes (4 and 5 patients in Schedule 2/1 and CDD cohorts, respectively) suggest that administration of sunitinib with paclitaxel and carboplatin led to an increase in maximum and total plasma exposures to sunitinib and its active metabolite SU12662 compared with sunitinib administered alone. This may have been the result of inhibition of the CYP3A4 metabolic pathway and/or P-glycoprotein (P-gp) efflux system

Table 5 Pharmacokinetic parameters (subjects with paired observations only) at sunitinib 37.5 mg/day plus paclitaxel 175 mg/m^2 and carboplatin 6 AUC mg min/ml

	Alone mean (%CV) [median]	Combination mean (%CV) [median]	Geometric mean ratio (combination/alone)
Schedule 2/1 ($n = 4$)			
Sunitinib			
T_{max} (h)[a]	6.0 (4.0–8.0)	16.0 (6.0–24.0)	N/A
C_{max} (ng/ml)	19.1 (23) [20.0]	28.4 (51) [26.1]	1.37
AUC_{0-24} (ng h/ml)	332 (27) [342]	501 (42) [503]	1.44
SU12662			
T_{max} (h)[a]	4.0 (2.0–6.0)	24.0 (4.0–24.0)	N/A
C_{max} (ng/ml)	3.11 (45) [2.99]	6.61 (68) [5.51]	1.93
AUC_{0-24} (ng h/ml)	54.1 (48) [52.9]	96.5 (61) [86.0]	1.68
Total drug			
T_{max} (h)	6.0 (4.0–8.0)	15.0 (4.0–24.0)	N/A
C_{max} (ng/ml)	22.1 (23) [23.9]	33.2 (52) [30.6]	1.38
AUC_{0-24} (ng h/ml)	386 (29) [408]	597 (44) [607]	1.48
Paclitaxel			
T_{max} (h)[a]	3.0 (3.0–3.0)	3.0 (3.0–3.0)	N/A
C_{max} (μg/ml)	4.45 (23) [4.58]	5.00 (27) [5.49]	1.11
AUC_{∞} (μg h/ml)	15.5 (17) [16.3]	16.8 (22) [18.02]	1.08
Clearance (l/h)	21.1 (33) [18.4]	19.8 (41) [16.2]	0.92
$t_{1/2}$ (h)	8.80 (15) [8.36]	8.23 (17) [8.54]	N/A
Total platinum			
T_{max} (h)[a]	3.5 (3.5–4.0)	3.5 (3.5–3.5)	N/A
C_{max} (μg/ml)	20.6 (29) [19.2]	22.6 (20) [21.2]	1.11
AUC_{0-24} (μg h/ml)	65.1 (23) [60.4]	60.3 (10) [60.3]	0.94
Free platinum			
T_{max} (h)[a]	3.5 (3.5–4.0)	3.5 (3.5–3.5)	N/A
C_{max} (μg/ml)	25.2 (37) [24.9]	21.3 (9) [20.7]	0.89
AUC_{∞} (μg h/ml)	50.7 (25) [49.5]	43.0 (6) [42.8]	0.87
Clearance (l/h)	13.3 (39) [11.2]	13.2 (22) [12.4]	1.02
$t_{1/2}$ (h)	4.72 (24) [4.89]	5.27 (4) [5.27]	N/A
CDD schedule ($n = 5$)			
Sunitinib			
T_{max} (h)[a]	8.0 (6.0–10.0)	6.0 (4.0–10.0)	N/A
C_{max} (ng/ml)	42.1 (12) [43.7]	47.0 (15) [44.4]	1.11
AUC_{0-24} (ng h/ml)	874 (13) [918]	983 (18) [897]	1.12
SU12662			
T_{max} (h)[a]	8.0 (4.0–10.0)	6.0 (4.0–10.0)	N/A
C_{max} (ng/ml)	13.4 (39) [15.7]	19.2 (39) [19.8]	1.44
AUC_{0-24} (ng h/ml)	279 (39) [326]	395 (37) [430]	1.43
Total drug			
T_{max} (h)[a]	8.0 (6.0–10.0)	6.0 (4.0–10.0)	N/A
C_{max} (ng/ml)	55.3 (14) [50.9]	65.2 (17) [68.3]	1.17
AUC_{0-24} (ng h/ml)	1,153 (14) [1,115]	1,379 (15) [1,351]	1.19
Paclitaxel			
T_{max} (h)[a]	3.0 (2.0–3.0)	3.0 (3.0–3.0)	N/A
C_{max} (μg/ml)	3.96 (40) [3.62]	5.24 (50) [4.92]	1.28
AUC_{∞} (μg h/ml)	14.3 (31) [13.2]	15.9 (33) [13.6]	1.11
Clearance (l/h)	26.5 (34) [29.8]	23.6 (32) [27.4]	0.89

Table 5 continued

	Alone mean (%CV) [median]	Combination mean (%CV) [median]	Geometric mean ratio (combination/alone)
$t_{1/2}$ (h)	8.89 (14) [8.69]	7.84 (29) [6.90]	N/A
Total platinum			
T_{max} (h)[a]	3.5 (3.5–4.0)	3.5 (3.5–4.0)	N/A
C_{max} (μg/ml)	23.1 (20) [24.5]	22.8 (13) [24.7]	1.00
AUC_{0-24} (μg h/ml)	67.6 (7) [65.5]	60.6 (11) [64.0]	0.89
Free platinum			
T_{max} (h)[a]	4.0 (3.5–4.0)	3.5 (3.5–4.0)	N/A
C_{max} (μg/ml)	20.7 (15) [19.3]	22.0 (16) [22.5]	1.06
AUC_{∞} (μg h/ml)	48.3 (9) [49.2]	43.1 (9) [42.4]	0.89
Clearance (l/h)	17.1 (26) [16.5]	18.9 (22) [21.1]	1.11
$t_{1/2}$ (h)	5.18 (6) [5.09]	4.16 (26) [4.80]	N/A

Total drug sunitinib + SU12662, C_{max} maximum plasma concentration, $t_{1/2}$ terminal phase half-life, *AUC* area under the plasma concentration–time profile for time zero to infinity (AUC_{∞}) or 24 h (AUC_{0-24}), *CV* coefficient of variation, *N/A* not applicable, *CDD* continuous daily dosing

[a] T_{max} = time for C_{max}; median (min, max)

(during absorption or elimination) by paclitaxel. Both sunitinib and SU12662 are substrates for CYP3A4 [30]; SU12662 is also a substrate for P-gp. Paclitaxel at higher concentrations has the potential to inhibit both CYP3A4 and the P-gp transport system [31–35]. Carboplatin, on the other hand, is very unlikely to inhibit either of these pathways. The administration of sunitinib with paclitaxel and carboplatin did not appear to affect the PK of either paclitaxel or carboplatin. The observed drug–drug interaction between sunitinib and paclitaxel may have contributed to some of the toxicities observed in this study, including neutropenia and thrombocytopenia resulting in dose interruptions/delays. However, other variables such as patient selection or overlapping mechanisms of action may have contributed.

Of the 38 evaluable patients with measurable disease at baseline, 4 patients (with tumor types typically treated with paclitaxel and carboplatin) had confirmed PRs, 2 of whom where chemotherapy-naïve. Given the short duration of treatment (4 cycles) and limited patient numbers in this phase I trial, no time-to-event analysis was performed and no definitive conclusions can be drawn regarding the antitumor activity of the triple combination regimen.

In summary, a potential drug–drug interaction may have led to an increase in levels of sunitinib and SU12662, resulting in increased myelosuppression and consequent dose interruptions/delays, which limit the dose intensity and potential utility of this combination.

Acknowledgments The authors thank all of the participating patients and their families, as well as the global network of investigators, research nurses, study coordinators, and operations staff. This study was sponsored by Pfizer Inc. Statistical support was provided by Patricia Stephenson at Rho, Inc. (Chapel Hill, NC). Medical writing support was provided by Siân Marshall at ACUMED (Tytherington, UK) and was funded by Pfizer Inc.

Conflict of interest S. T. Kim, R. C. Chao, and A. Ruiz-Garcia are employees of Pfizer Inc. and hold stock in Pfizer Inc., the makers of SUTENT®. P. LoRusso and R. Cohen have provided consultancy/advisory support for Pfizer and received funding support from Pfizer. E. Heath has received funding support from Pfizer. G. Wilding, G. Blumenschein Jr, and N. LoConte have no potential conflicts of interest to disclose.

References

1. Keedy VL, Sandler AB (2007) Inhibition of angiogenesis in the treatment of non-small cell lung cancer. Cancer Sci 98:1825–1830
2. National Comprehensive Cancer Network (2009) NCCN clinical practice guidelines in oncology: NSCLC v.2.2009. Available via http://www.nccn.org/professionals/physician_gls/PDF/nscl.pdf
3. Khosravi SP, Fernandez PI (2008) Tumoral angiogenesis: review of the literature. Cancer Invest 26:104–108
4. Tallquist M, Kazlauskas A (2004) PDGF signaling in cells and mice. Cytokine Growth Factor Rev 15:205–213
5. Saltz LB, Clarke S, az-Rubio E et al (2008) Bevacizumab in combination with oxaliplatin-based chemotherapy as first-line therapy in metastatic colorectal cancer: a randomized phase III study. J Clin Oncol 20:2013–2019
6. Robert NJ, Dieras V, Glaspy J et al (2009) RIBBON-1: randomized, double-blind, placebo-controlled, phase III trial of chemotherapy with or without bevacizumab (B) for first-line treatment of HER2-negative locally recurrent or metastatic breast cancer (MBC). J Clin Oncol 27(15s):1005 Abstract
7. Nghiemphu PL, Liu W, Lee Y et al (2009) Bevacizumab and chemotherapy for recurrent glioblastoma: a single-institution experience. Neurology 72:1217–1222
8. Sandler A, Gray R, Perry MC et al (2006) Paclitaxel-carboplatin alone or with bevacizumab for non-small-cell lung cancer. N Engl J Med 355:2542–2550

9. Homsi J, Daud AI (2007) Spectrum of activity and mechanism of action of VEGF/PDGF inhibitors. Cancer Control 14:285–294
10. Bergers G, Song S, Meyer-Morse N, Bergsland E, Hanahan D (2003) Benefits of targeting both pericytes and endothelial cells in the tumor vasculature with kinase inhibitors. J Clin Invest 111:1287–1295
11. Abrams TJ, Lee LB, Murray LJ, Pryer NK, Cherrington JM (2003) SU11248 inhibits KIT and platelet-derived growth factor receptor beta in preclinical models of human small cell lung cancer. Mol Cancer Ther 2:471–478
12. Mendel DB, Laird AD, Xin X et al (2003) In vivo antitumor activity of SU11248, a novel tyrosine kinase inhibitor targeting vascular endothelial growth factor and platelet-derived growth factor receptors: determination of a pharmacokinetic/pharmacodynamic relationship. Clin Cancer Res 9:327–337
13. Motzer RJ, Hutson TE, Tomczak P et al (2006) Phase III randomized trial of sunitinib malate (SU11248) versus interferon-alfa (IFN-a) as first-line systemic therapy for patients with metastatic renal cell carcinoma (mRCC). Proc Am Soc Clin Oncol 24:2s
14. Motzer RJ, Figlin R, Hutson TE et al (2007) Sunitinib versus interferon-alfa (IFN-a) as first-line treatment of metastatic renal cell carcinoma (mRCC): updated results and analysis of prognostic factors. J Clin Oncol ASCO Annual meeting proceedings part I. vol 25, no. 18S (20 June Suppl):(Abstract 5024)
15. Demetri GD, van Oosterom AT, Garrett CR et al (2006) Efficacy and safety of sunitinib in patients with advanced gastrointestinal stromal tumour after failure of imatinib: a randomised controlled trial. Lancet 368:1329–1338
16. Therasse P, Arbuck SG, Eisenhauer EA et al (2000) New guidelines to evaluate the response to treatment in solid tumors. J Natl Cancer Inst 92:205–216
17. Edgerly M, Fojo T (2008) Is there room for improvement in adverse event reporting in the era of targeted therapies? 1. J Natl Cancer Inst 100:240–242
18. Rigas JR (2004) Taxane-platinum combinations in advanced non-small cell lung cancer: a review. Oncologist 9 Suppl 2: 16–23
19. Custodio Carretero AB, Garcia Saenz JA, Gonzalez Larriba JL et al (2008) Adjuvant chemotherapy for early-stage non-small-cell lung cancer. Single-centre experience and literature review. Clin Transl Oncol 10:560–571
20. Perez EA (2004) Carboplatin in combination therapy for metastatic breast cancer. Oncologist 9:518–527
21. Burstein HJ, Elias AD, Rugo HS et al (2008) Phase II study of sunitinib malate, an oral multitargeted tyrosine kinase inhibitor, in patients with metastatic breast cancer previously treated with an anthracycline and a taxane. J Clin Oncol 26:1810–1816
22. Socinski MA, Novello S, Brahmer JR et al (2008) Multicenter, phase II trial of sunitinib in previously treated, advanced non-small-cell lung cancer. J Clin Oncol 26:650–656
23. Kulke M, Lenz HJ, Meropol N et al (2008) Activity of sunitinib in patients with advanced neuroendocrine tumors. J Clin Oncol 26:3403–3410
24. Kozloff M, Chuang E, Starr A et al (2010) An exploratory study of sunitinib plus paclitaxel as first-line treatment for patients with advanced breast cancer. Ann Oncol 21:1436–1441
25. Robert F, Sandler A, Schiller JH et al (2010) Sunitinib in combination with docetaxel in patients with advanced solid tumors: a phase I dose-escalation study. Cancer Chemother Pharmacol 66:669–680
26. Chiorean EG, Sweeney CJ, Verschraegen CF et al (2008) Tolerability/safety of sunitinib (SU) on schedule 2/1 in combination with capecitabine (C) in patients (pts) with advanced solid tumors (STs): a phase I dose-finding study. J Clin Oncol 26: 2008 (20 May suppl; abstract 3562)
27. Fountzilas G, Kalofonos HP, Dafni U et al (2004) Paclitaxel and epirubicin versus paclitaxel and carboplatin as first-line chemotherapy in patients with advanced breast cancer: a phase III study conducted by the Hellenic cooperative oncology group 1. Ann Oncol 15:1517–1526
28. Karp DD, Novello S, Cardenal F et al (2009) Continued high activity of figitumumab (CP-751,871) combination therapy in squamous lung cancer. J Clin Oncol 27 (15s) 8072: 15s (suppl; abstract)
29. Leong S, Cohen RB, Gustafson DL et al (2009) Mapatumumab, an antibody targeting TRAIL-R1, in combination with paclitaxel and carboplatin in patients with advanced solid malignancies: results of a phase I and pharmacokinetic study 1. J Clin Oncol 27:4413–4421
30. Pfizer Inc. (2008) Data on file
31. Beulz-Riche D, Robert J, Riche C, Ratanasavanh D (2002) Effects of paclitaxel, cyclophosphamide, ifosfamide, tamoxifen and cyclosporine on the metabolism of methoxymorpholinodoxorubicin in human liver microsomes. Cancer Chemother Pharmacol 49:274–280
32. Nielsen TL, Rasmussen BB, Flinois JP, Beaune P, Brosen K (1999) In vitro metabolism of quinidine: the (3S)-3-hydroxylation of quinidine is a specific marker reaction for cytochrome P-4503A4 activity in human liver microsomes. J Pharmacol Exp Ther 289:31–37
33. Walsky RL, Gaman EA, Obach RS (2005) Examination of 209 drugs for inhibition of cytochrome P450 2C8. J Clin Pharmacol 45:68–78
34. Rochat B, Morsman JM, Murray GI, Figg WD, McLeod HL (2001) Human CYP1B1 and anticancer agent metabolism: mechanism for tumor-specific drug inactivation? J Pharmacol Exp Ther 296:537–541
35. Baumhakel M, Kasel D, Rao-Schymanski RA et al (2001) Screening for inhibitory effects of antineoplastic agents on CYP3A4 in human liver microsomes. Int J Clin Pharmacol Ther 39:517–528

blood

2011 118: 2622-2631
Prepublished online May 6, 2011;
doi:10.1182/blood-2010-08-299784

Antiangiogenic antitumor activities of IGFBP-3 are mediated by IGF-independent suppression of Erk1/2 activation and Egr-1 –mediated transcriptional events

Jai-Hyun Kim, Dong Soon Choi, Ok-Hee Lee, Seung-Hyun Oh, Scott M. Lippman and Ho-Young Lee

Blood (print ISSN 0006-4971, online ISSN 1528-0020), is published weekly by the American Society of Hematology, 2021 L St, NW, Suite 900, Washington DC 20036.

Antiangiogenic antitumor activities of IGFBP-3 are mediated by IGF-independent suppression of Erk1/2 activation and Egr-1–mediated transcriptional events

*Jai-Hyun Kim,[1] *Dong Soon Choi,[1] Ok-Hee Lee,[1] Seung-Hyun Oh,[1] Scott M. Lippman,[1] and Ho-Young Lee[1,2]

[1]Department of Thoracic/Head and Neck Medical Oncology, The University of Texas M D Anderson Cancer Center, Houston, TX; and [2]Research Institute of Pharmaceutical Sciences, College of Pharmacy, Seoul National University, Seoul, Korea

Most antiangiogenic therapies currently being evaluated in clinical trials target the vascular endothelial growth factor pathway; however, the tumor vasculature can acquire resistance to vascular endothelial growth factor-targeted therapy by shifting to other angiogenesis mechanisms. Insulin-like growth factor binding protein-3 (IGFBP-3) has been reported to suppress tumor growth and angiogenesis by both IGF-dependent and IGF-independent mechanisms; however, understanding of its IGF-independent mechanisms is limited. We observed that IGFBP-3 blocked tumor angiogenesis and growth in non–small cell lung cancer and head and neck squamous cell carcinoma. Conditioned media from an IGFBP-3–treated non–small cell lung cancer cell line displayed a significantly decreased capacity to induce HUVEC proliferation and aortic sprouting. In cancer cells, IGFBP-3 directly interacted with Erk1/2, leading to inactivation of Erk1/2 and Elk-1, and suppressed transcription of early growth response protein 1 and its target genes, basic fibroblast growth factor and platelet-derived growth factor. These data suggest that IGF-independent Erk1/2 inactivation and decreased IGFBP-3–induced Egr-1 expression block the autocrine and paracrine loops of angiogenic factors in vascular endothelial and cancer cells. Together, these findings provide a molecular framework of IGFBP-3's IGF-independent antiangiogenic antitumor activities. Future studies are needed for development of IGFBP-3 as a new line of antiangiogengic cancer drug. (*Blood*. 2011; 118(9):2622-2631)

Introduction

Angiogenesis, the formation of new capillaries from existing blood vessels, is essential to carcinogenic processes, including solid tumor formation, growth, invasion, and metastasis.[1] Most tumors can stimulate angiogenesis by switching on the production of numerous cytokines and growth factors, including fibroblast growth factors (FGFs), vascular endothelial growth factors (VEGFs), and platelet-derived growth factors (PDGFs).[2] Several antiangiogenic agents are in various phases of clinical trials for human cancer; however, most of these agents target the VEGF signaling pathway.[3] Therefore, other potential therapeutic agents that block non-VEGF angiogenic pathways need to be evaluated.

Insulin-like growth factor-binding protein-3 (IGFBP-3), a member of a family of 6 IGFBPs, has demonstrated antiproliferative, proapoptotic, antiangiogenic, and antimetastatic activity in a variety of cancer cells.[4-8] It may also have IGF-independent antitumor activities through cell-surface or intracellular protein interaction, its nuclear translocation, or its transcriptional regulation.[7,9-12] However, the mechanisms that mediate IGFBP-3's IGF-independent antitumor activity have not been clearly defined.

The 82-kDa phosphoprotein transcription factor early growth response protein 1 (Egr-1), an immediate early gene product, has been implicated in multiple cellular processes, including cell growth, apoptosis, wound healing, and angiogenesis. Mitogenic stimuli, including serum, PDGF, peptide growth factors, and B-Raf, and nonmitogenic stresses, including γ-irradiation and hypoxia, activate Egr-1 expression through serum response elements (SREs) in the *Egr-1* promoter, where serum response factor (SRF) and ternary complex factors form transcriptionally active ternary complexes.[13] Once activated, Egr-1 binds to GC-rich, *cis*-acting promoter elements and controls the expression of multiple genes that encode growth factors, cytokines, adhesion molecules, and proteases, including IGF-1, IGF-2, TGF-β1, fibronectin, urokinase-type plasminogen activator, VEGF-1R, VEGF, PDGF-A and -B, and basic FGF (bFGF), which are believed to have important functions in cancer cell survival, apoptosis, angiogenesis, invasion, and metastasis.[14,15] The association between Egr-1 and tumor angiogenesis has been observed in various tumor types.[16-18] A DNA-based enzyme and a siRNA that target Egr-1 suppress bFGF expression and tumor angiogenesis and growth in various cancer cell types.[18-21]

In this study, we determined the mechanisms by which IGFBP-3 exerts its IGF-independent antiangiogenic antitumor activity. Our findings reveal that IGFBP-3's engagement of Erk1/2 inactivates Erk1/2 and Elk1 in an IGF-independent manner, resulting in inhibited binding of Elk1 to SRE sites in the *Egr-1* upstream promoter and reduced transcription of *Egr-1* and its target genes, including *PDGF* and *bFGF*. Egr-1, bFGF, and PDGF proteins were highly down-regulated in our non–small cell lung cancer (NSCLC) mouse models; we also observed angiogenesis suppression. These data suggest that increase in IGFBP-3 level could lead to inhibition of tumor angiogenesis.

Submitted August 10, 2010; accepted April 17, 2011. Prepublished online as *Blood* First Edition paper, May 6, 2011; DOI 10.1182/blood-2010-08-299784.

*J.-H.K. and D.S.C. contributed equally to this work.

The online version of this article contains a data supplement.

The publication costs of this article were defrayed in part by page charge payment. Therefore, and solely to indicate this fact, this article is hereby marked "advertisement" in accordance with 18 USC section 1734.

Methods

Cell culture, animals, and other reagents

H460, H1299, A549 (NSCLC cell lines), UMSCC38 (head and neck squamous cell carcinoma [HNSCC] cell lines), and HUVEC (Cambrex Bio Science) cell lines were cultured as previously described.[8] NSCLC cell lines (H1299, A549, and H460) and HUVEC were cultured in RPMI 1640 with 10% FBS and in EGM (Lonza Walkersville Inc), respectively, in a humidified environment with 5% CO_2. Six-week-old female athymic nude mice (10 mice for each group) and chick eggs (Harlan-Sprague-Dawley and Charles River laboratories) were maintained in a defined pathogen-free environment. All animal procedures were performed in accordance with a protocol approved by the M. D. Anderson Institutional Animal Care and Usage Committee.

Tumor xenograft model and immunohistochemical analysis

Ad-BP-3's antiangiogenic effects on established H1299 subcutaneous or UMSCC38 HNSCC orthotopic tumor models were determined as described elsewhere.[8,11,22] In brief, after the H1299 xenograft tumor volume reached ~ 75 mm^3, mice (n = 5) were given single intratumoral injections (1×10^{10} particles) of IGFBP-3–expressing (Ad-BP-3) or empty viruses (Ad-EV). Tumors embedded in paraffin were subjected to immunohistochemical staining by the use of an ABC staining kit (Vector Laboratories) with anti-bFGF (1:400 dilution), anti-PDGF (1:400 dilution), and anti–Egr-1 (1:400 dilution) antibodies. For CD31 staining, frozen tumor tissue sections were stained with anti-CD31 antibody (1:100 dilution).

Matrigel plug assay

The in vivo mouse Matrigel plug assay was performed with A549 NSCLC cells infected with Ad-BP-3 (50 pfu/cell) or Ad-EV (50 pfu/cell). Each treatment group included 10 mice. The number of blood vessels per field was analyzed by microscopy at 10× magnification.

Cell proliferation, migration, invasion, and tube-formation assay

The in vitro migration, invasion, and tube-formation assays were performed as described elsewhere.[8,23,24] In brief, in the coculture assay with H460 cells, HUVECs (4×10^4) were seeded onto the cell culture inserts (1-μm pore size; Becton Dickinson) and H460 cells (2×10^5) transfected with pBP-3, pBP-3-ggg, or pEgr1 were transferred to the bottom of a 12-well plate. Three days later, HUVEC proliferation was assessed by use of the MTT assay. To determine IGFBP-3's effects on NSCLC cells' angiogenesis-stimulating effects, we infected H1299, H460, and A549 cells with Ad-BP-3 (50 pfu/cell) or Ad-EV or treated them with rBP-3 or control vehicle, as previously described.[25] Conditioned media (CM) were collected from NSCLC cells and added to HUVECs for cell proliferation or tube formation or to check aortas for endothelial cell sprouting, as previously described.[8,24] HUVEC tube formation was scored after 8 hours, and cell proliferation was analyzed by the MTT assay after 3 days, as previously described.[26] Each condition was tested in 6 wells. The details are described in supplemental Methods (available on the *Blood* Web site; see the Supplemental Materials link at the top of the online article).

Transcription analysis

Quantitative RT-PCR was performed as described elsewhere.[27] The primer sequences used are described in supplemental Methods. To avoid amplification of genomic DNA, each gene primer was chosen from different exons. To analyze the *bFGF* promoter, we amplified the 5′-flanking region (−590 to +26) of the human *bFGF* gene (GenBank accession number: NM_002006) from human genomic DNA (Sigma-Aldrich) and cloned into the *SmaI* site of the luciferase reporter vector pGL3-Basic (Promega). The detailed methods used to construct the mutant *Egr-1* promoter vectors, transfect plasmids and siRNAs, and perform the luciferase reporter assay are described in supplemental Methods.

ChIP

A ChIP assay was performed with H460 cells infected with Ad-BP-3 or Ad-EV or treated with rBP-3 or control vehicle. Extracts from equal numbers of cells were immunoprecipitated with antibodies against Elk-1, SRF, IGFBP-3, or preimmune serum as a negative control. PCR was performed with the use of primers encompassing the SRE elements, as depicted in Figure 5A, and an exon 1 primer was used as a negative control. All PCR primers and conditions are described in the supplemental Methods. An aliquot of the whole-cell protein-DNA complex (2% of the immunoprecipitated volume) was subjected to PCR analysis to confirm the protein-bound DNA sequence.

Immunoprecipitation, in vitro pull, and Western blot analyses

H1299 cells were transfected with 5 μg of control (EV) or pCMV6-IGFBP-3-Flag (pBP-Flag). After they were starved of serum, the cells were stimulated with 10% FBS for 0 and 20 minutes. Whole-cell lysates were prepared, and Western blotting was performed as described elsewhere.[28] For immunoprecipitation, total cell lysates were precleared with the appropriate protein-G or protein-A beads and then incubated with goat antibody (1 μg) against Erk1/2 or rabbit antibody against p38α and protein-G or protein-A beads. IGFBP-3-Flag binding was detected with a mouse anti-Flag antibody. For the in vitro pulldown assay, rBP-3 (1 μg) conjugated to NTA-agarose beads (50 μL, 50% slurry) was incubated with H1299 cell lysate (150, 300, and 450 μg) and then washed with PBS and 10mM imidazole. The beads were then boiled in 2× sample buffer for 10 minutes and used for the Western blot analysis. For the negative control, blank BSA-coated NTA beads were incubated with 450 μg of cell lysate.

Immunofluorescence staining

H1299 cells were seeded on cover slips (Deckgläser; Menzel-Gläser) coated with rat tail collagen type I (100 μg/mL; BD Biosciences). After being incubated overnight, the cells were serum-starved for 3 hours and treated with rhIGFBP-3 at 10 μg/mL in a serum-free medium (RPMI 1640) and fixed at 0, 10, 30, and 60 minutes in 4% paraformaldehyde in PBS for 3 minutes. After being thoroughly washed with PBS, the cells were treated with methanol on ice and washed with PBS. After blocking with 5% BSA, primary rabbit anti-IGFBP-3 (Santa Cruz Biotechnology) and mouse anti-Erk1/2 (Cell Signaling Technology) antibodies were added to the cells overnight at 4°C. After being washed in PBS, the cells were stained with donkey anti–rabbit antibodies conjugated with Alexa Fluor 568 and donkey anti–mouse antibodies conjugated with Alexa Fluor 488. During the washing steps, the cells were stained with Hoechst 33342. The cover slips were mounted and imaged with the use of an Olympus IX71 FV 500 laser confocal microscope with Fluoview Version 5.0 software. All images were obtained with a 60× objective lens with 2× optical zoom. The colocalization analysis was performed by use of the colocalization finder function of ImageJ software (NIH).

Statistical analysis

Data are given as the mean ± SD. To determine the statistical significance between groups, we used paired Student *t* tests and 95% confidence intervals. In all statistical analyses, 2-sided *P* values $< .05$ were considered statistically significant.

Results

IGFBP-3 inhibits NSCLC and HNSCC tumor growth and angiogenesis

We previously demonstrated that IGFBP-3 overexpression inhibits the growth of H1299 NSCLC xenografts in nude mice.[11] To determine whether IGFBP-3's antiangiogenic activity contributes to its antitumor activities, we performed a series of experiments by using adenoviral (Ad-BP-3) and recombinant (rBP-3) IGFBP-3.

We first determined Ad-BP-3's effect on tumor growth and angiogenesis in 1299 NSCLC xenograft tumors established in athymic nude mice. Ad-BP-3 induced significant decreases in

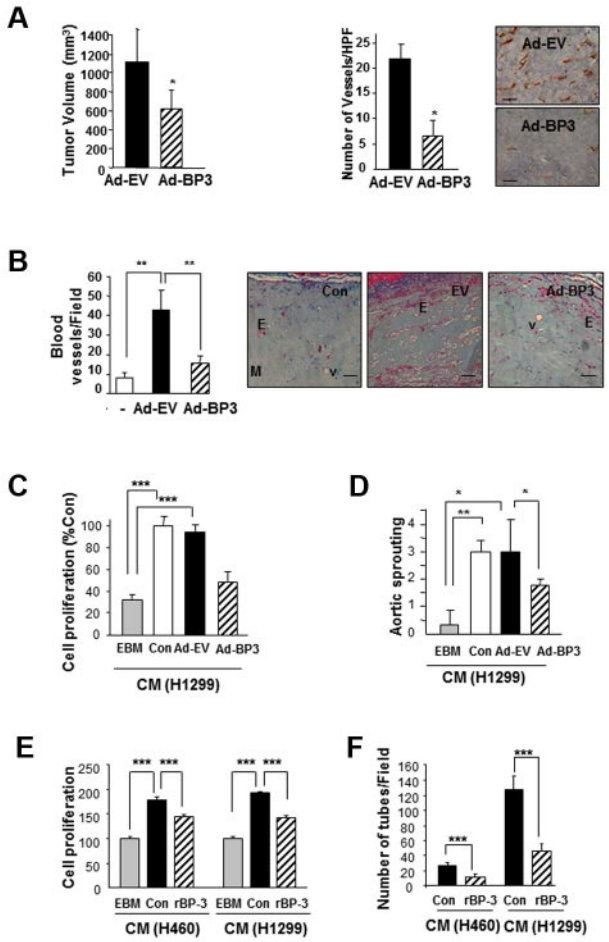

Figure 1. IGFBP-3 suppresses tumor growth and angiogenesis in NSCLC xenografts and vascular endothelial cells. (A) H1299 xenograft tumor growth (left) 10 days after injection with IGFBP-3–expressing adenoviruses (Ad-BP-3) or empty viruses (Ad-EV). Tumor growth is expressed as the mean ± SEM. An immunohistochemical analysis of CD31 (right) was performed in xenograft tissues, and the number of CD31-immunoreactive vessels per high-power field was counted. The results represent the mean calculated from 5 mice (bars, SDs). *$P < .05$ compared with the control group. Representative CD31 immunostaining in H1299 xenograft tissues is included. (B) Matrigel plug assay with A549 cells. Gross observed results of blood vessels are expressed as the mean of 5 tumors ± SEM, **$P < .01$. (C-D) Effect of CM from indicated NSCLC cell lines that had been infected with Ad-EV or Ad-BP-3 (C-D) or treated with rBP-3 (E-F) on HUVEC proliferation (C,E), chick aortic sprouting (D), and HUVEC tube formation (F). The results represent the means (bars, SDs) of 5 identical wells. *$P < .05$; **$P < .01$; ***$P < .001$.

H1299 NSCLC xenograft tumor growth (Figure 1A). Anti-CD31 staining of the tumor tissues injected with Ad-BP-3 revealed significantly decreased tumor vascularization compared with those injected with control viruses (AD-EV; Figure 1A right). The Matrigel plugs that contained Ad-BP-3–infected A549 cells had significantly fewer blood vessels than did those containing Ad-EV cells ($P < .01$; Figure 1B). These findings suggest that IGFBP-3 has antiangiogenic and antitumor activity in NSCLC.

Tumor angiogenesis is partly mediated by tumor-secreted angiogenic growth factors that interact with their receptors expressed on endothelial cells.[29] To determine whether IGFBP-3 suppresses the secretion of angiogenic factors from NSCLC, we collected CM from Ad-EV– or Ad-BP-3–infected H1299 cells after incubating them in a serum-free medium for 1 day. As shown in Figure 1C, HUVECs that had been treated with CM from untreated (Con) or Ad-EV–infected cells, but not from Ad-BP-3–infected cells, demonstrated significantly greater proliferation than did those treated with endothelial cell basal medium only. The ex vivo chick aortic ring arch assay showed similar results; the CM from untreated or Ad-EV–infected cells, but not the CM from Ad-BP-3–infected cells, significantly stimulated the formation of endothelial cell sprouts (Figure 1D).

Because protein expression induced by adenoviruses can be much greater than that seen under real-life conditions, we further determined the effects of exogenously added recombinant IGFBP-3 (rBP-3), which has a cytosolic half-life of 3 hours.[28] We performed a Western blot analysis to confirm that no residual rBP-3 was present in the CM (data not shown). HUVECs that had been treated with the CM from BP-3–pretreated cancer cells also showed significantly reduced proliferation (Figure 1E) and tube formation (Figure 1F) compared with those treated with CM from untreated NSCLC cells. These findings suggest that IGFBP-3 has antiangiogenic and antitumor activity in NSCLC, at least partly because of its effects on NSCLC cells' secretion of angiogenic factors.

IGFBP-3 induces down-regulation of the bFGF-Egr-1 transcription loop

We assessed the angiogenic factors that are regulated by IGFBP-3. Consistent with previous findings in which IGFBP-3 was found to mediate the antiangiogenic action of the farnesyl transferase inhibitor SCH66336, which suppresses VEGF expression in NSCLC and HNSCC cells,[8,30] Ad-BP-3 reduced VEGF expression in H1299 and A549 NSCLC cells (unpublished data). We determined IGFBP-3's effects on bFGF expression. Ad-BP-3 led to decreased bFGF expression in H1299, A549, and H460 NSCLC cells and UMSCC38 HNSCC cells (Figure 2A) over the range of doses used in the cell-based experiments described in Figure 1. IGFBP-3's

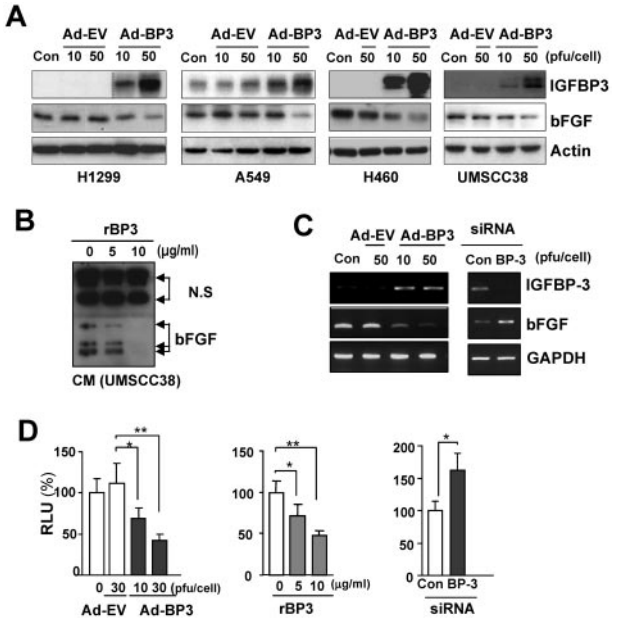

Figure 2. IGFBP-3 down-regulates *bFGF* transcription. (A) Western blot analysis of IGFBP-3 and bFGF expression in NSCLC and HNSCC cells 2 days after infection with Ad-EV or Ad-BP-3. (B) Reduced bFGF levels in the CM from rBP-3–treated UMSCC38 cells. N.S. indicates nonspecific bands. (C) Semiquantitative RT-PCR analysis of *bFGF* expression in H460 cells infected with Ad-EV or Ad-BP-3 (left) or transfected with scrambled (Con) or IGFBP-3 (BP-3) siRNA (right). (D) Luciferase assay to determine the effect of IGFBP-3 on *bFGF* promoter activity in H460 cells transiently transfected with bFGF-Luc in association with Ad-BP-3 or Ad-EV infection at the indicated doses (left), rBP-3 treatment (middle), or scrambled (Con) or IGFBP-3 (BP-3) siRNA cotransfection (right). The results represent the means (bars, SDs) of triplicate results. *$P < .05$; **$P < .01$; ***$P < .001$.

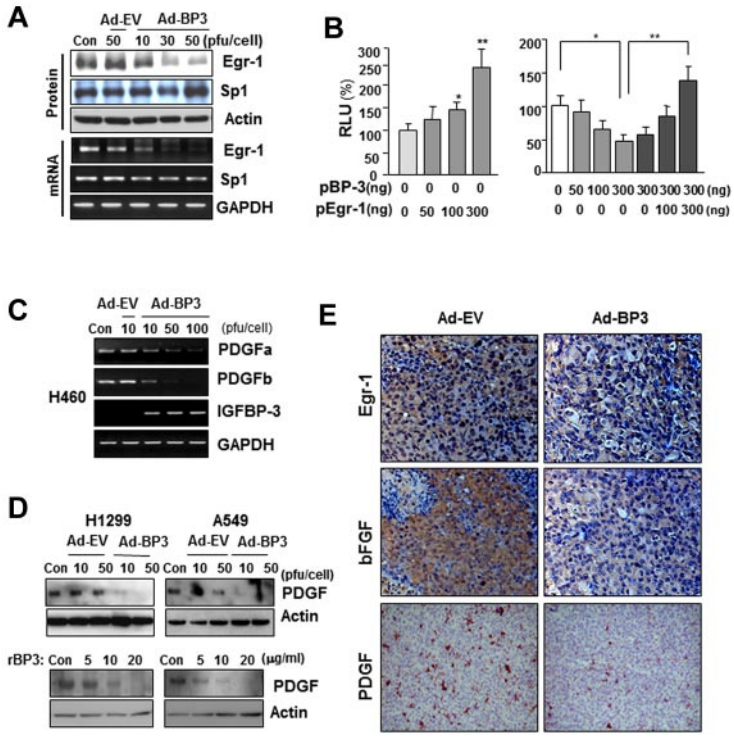

Figure 3. IGFBP-3 down-regulates *bFGF* expression promoter activity by regulating *Egr-1* transcription. (A) Western blot (top) and semiquantitative RT-PCR (bottom) analyses of IGFBP-3's effect on Egr-1 and Sp-1 protein and mRNA expression in H460 cells that had been infected with Ad-BP-3 or Ad-EV for 2 days. (B) Luciferase assay to determine Egr-1's effect on bFGF expression. H460 cells transiently transfected with bFGF-Luc and pEgr-1, pBP-3, or both; $^{*}P < .05$, $^{**}P < .01$. (C-D) RT-PCR analysis of *PDGFa* and *PDGFb* mRNA expression in H460 cells (C) and Western blot analysis of PDGF protein expression in H1299 and A549 cells (D) after infection with Ad-EV or Ad-BP-3 or treatment with rBP-3. (E) Immunohistochemical analysis of Egr-1, bFGF, and PDGF expression in H1299 xenografts 10 days after injection with Ad-EV or Ad-BP-3.

ability to reduce bFGF protein expression was further confirmed by a Western blot analysis of rBP-3–treated H1299 cells (supplemental Figure 1). A CM analysis from UMSCC38 cells revealed that rBP-3 reduced bFGF secretion (Figure 2B). Ad-BP-3 negatively regulated *bFGF* transcription in H460 cells (Figure 2C). Conversely, IGFBP-3 knockdown by siRNA led to increased *bFGF* mRNA levels. We then determined IGFBP-3's effects on *bFGF* promoter activity by transiently transfecting H460 cells with a pGL3-basic luciferase reporter construct that contained the 5′-flanking promoter region of human *bFGF* (−589 to +26). *bFGF* promoter activity was significantly reduced after Ad-BP-3 infection or rBP-3 treatment but increased after IGFBP-3 siRNA transfection (Figure 2D). Together, these data demonstrate the inhibitory effects of IGFBP-3 on *bFGF* transcription.

We next determined which transcription factors are involved in IGFBP-3–regulated *bFGF* promoter activity. The Egr-1 and Sp-1 transcription factors have long been recognized as MAPK-dependent activators of *bFGF* transcription.[13,31,32] Therefore, we determined IGFBP-3's effects on Egr-1 and Sp-1 expression. Infection of H460 cells with Ad-BP-3 dramatically reduced Egr-1 expression at the protein and mRNA levels, with no detectable changes in Sp-1 expression of (Figure 3A). RT-PCR (supplemental Figure 2A) and Northern blot (supplemental Figure 2B) analyses further confirmed rBP-3's and Ad-BP-3's ability to reduce *bFGF* and *Egr-1* mRNA levels. A band shift analysis revealed a reduction in nuclear complexes bound to the *Egr-1* gene promoter in Ad-BP-3–infected H460 cells compared with in Ad-EV–infected cells (supplemental Figure 2C). These findings suggest that IGFBP-3 inhibits Egr-1 expression, leading to reduced *bFGF* promoter activity and attenuated bFGF expression.

To determine Egr-1's effect on IGFBP-3–mediated antiangiogenic activity in NSCLC cells, we transiently cotransfected H460 cells with the *bFGF* luciferase reporter construct and an *Egr-1* expression vector, an *IGFBP-3* expression vector (p*BP-3*), or both. As shown in Figure 3B, Egr-1 expression led to a dose-dependent increase in *bFGF* promoter activity (left) and attenuated IGFBP-3's inhibitory effects on promoter activity (right). These results indicate that Egr-1 plays a specific role in IGFBP-3–mediated suppression of *bFGF* transcription. IGFBP-3 also inhibited the expression of PDGF, another Egr-1–regulated angiogenic factor, as shown by the results of an RT-PCR analysis of *PDGF-a* and *-b* mRNA levels in H460 cells (Figure 3C) and a Western blot analysis of PDGF protein expression in H1299 and A549 cells (Figure 3D) that had been infected with Ad-BP-3 or treated with rBP-3. An immunohistochemical analysis of H1299 xenografts injected with Ad-BP-3 (Figure 1A) also demonstrated reduced Egr-1, bFGF, and PDGF staining (Figure 3E). Collectively, these results demonstrate that IGFBP-3–mediated Egr-1 suppression results in decreased bFGF and PDGF expression.

IGFBP-3 suppresses Egr-1 promoter activity in an IGF-independent manner

The conventional function of IGFBP-3 is to regulate cell growth and promote apoptosis by sequestering free IGFs. However, studies have shown that IGFBP-3 also has IGF-independent antitumor activity.[4,33] To determine whether *Egr-1* transcription regulation by IGFBP-3 is IGF dependent, we cotransfected H460 cells with a human *Egr-1* reporter construct and expression vectors carrying *K-ras* (V12) or *H-ras* (V12), along with pBP-3 or an empty vector control.

Transfection with pBP-3 resulted in substantial loss of the *Egr-1* promoter activity that had been stimulated by *K-ras* (V12) and *H-ras* (V12; Figure 4A). *Egr-1* transcription is known to be activated by environmental stresses, such as hypoxia and radiation.[34,35] *Egr-1* promoter activity, stimulated by γ-radiation (8 Gy) or incubation in 1% O_2, was significantly suppressed by pBP-3 (Figure 4A right). We also found that pBP-3-ggg, a mutant IGFBP-3 with a substitution of 3 glycine residues ($Gly^{56}Gly^{80}Gly^{81}$) that are critical for the IGF binding domain,[33] inhibited the *Egr-1* promoter activity stimulated by IGF-1, FBS, or constitutively

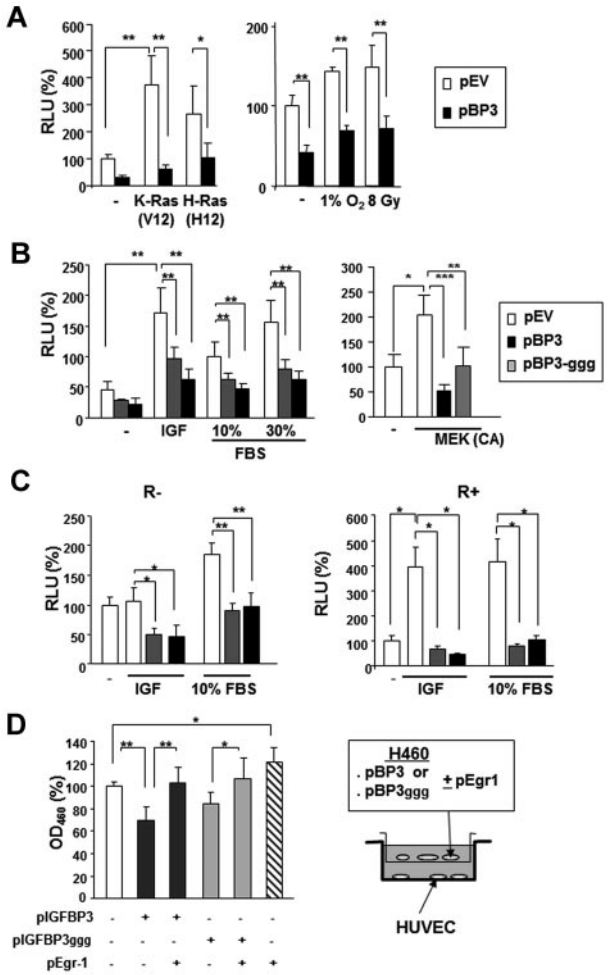

Figure 4. IGFBP-3 inhibits Egr-1 expression independently IGF-1. (A-B) The wild-type 1.2-kb *Egr-1* promoter reporter construct (Egr1-A-Luc) was transiently transfected, with or without pBP-3 or pBP-3-ggg, into NSCLC H460 cells. (A) Cells were stimulated by cotransfection of plasmids containing mutants of *K-Ras* (V12) or *H-Ras* (V12) or by exposure to hypoxia (1% O_2) or γ-radiation (8 Gy). (B) Cells were stimulated by IGF-1 (50 ng/mL) or FBS (10% and 30%) for 24 hours or cotransfected with plasmids expressing CA *MEK*. (C) R^- (IGF-1R null mouse fibroblasts) and R^+ (R^- cells transfected with IGF-1R) cell lines were cotransfected with Egr1-A-Luc and pBP-3 or pIGFBP-3-ggg and then stimulated by IGF-1 (50 ng/mL) or FBS (10%) for 24 hours. The data are the mean ± SD from 3 independent experiments, with 4 replicates per experiment. $^*P < .05$, $^{**}P < .01$. (D) In vitro evaluation of the antiangiogenic potential of IGFBP-3. pBP-3–transfected H460 cells show less stimulatory activity for HUVEC proliferation than untransfected H460 cells in a coculture assay system. The values are the mean ± SD from 2 separate experiments, with 3 replicates per experiment. $^*P < .05$, $^{**}P < .01$, $^{***}P < .001$.

active MAPK kinase (MEK; ΔN3/S218E/S222D) (Figure 4B).[36] pBP-3 and pBP-3-ggg reduced IGF-1– and 10% FBS-stimulated *Egr-1* promoter activity in both R^- (mouse embryonic fibroblasts from an IGF-1R–null mouse) and R^+ (R^- cells transfected with IGF-1R) cells (Figure 4C).[37] These findings suggest that the effects of IGFBP-3 on *Egr-1* promoter activity are IGF-1 independent.

We then determined whether this IGFBP-3–induced decrease in Egr-1 expression affected IGFBP-3–mediated antiangiogenic activity. To this end, we cocultured HUVECs with H460 cells cotransfected with pEgr-1 and pBP-3 or pBP-3-ggg. As shown in Figure 4D, HUVECs that had been cocultured with H460 cells transfected with Egr-1 and pBP-3 or pBP-3ggg had significantly reduced proliferation compared with those cultured with H460 cells transfected with pBP-3 or pBP-3-ggg alone, indicating attenuation of the antiangiogenic effects of pBP-3 and pBP-3ggg by Egr-1 expression. Taken together, these results demonstrate that IGFBP-3 has antiangiogenic activity in NSCLC cells by inhibiting *Egr-1* promoter activity through IGF-1–independent pathways.

IGFBP-3 inhibits Erk phosphorylation and subsequent Elk-1 activation, leading to a reduction in Elk-1 binding to SREs in the *Egr-1* promoter

The promoter region (−935 to +12) of *Egr-1* contains AP-1, Sp-1, cAMP response element, and SREs and their adjacent Ets binding sites.[13] To identify the promoter elements that are involved in IGFBP-3–regulated *Egr-1* promoter activity, we assessed a 1.2-kb *Egr-1* promoter construct (A) and several 5′-truncated deletion mutant constructs (B to V)[13] for promoter activity in H460 cells that had been transiently cotransfected with pBP-3. Deletion of the 2 AP-1 binding sites and 3 Sp-1 binding sites (C construct) or the CRE sites and two 3′-SREs (SRE 1 and 2; D construct) had little effect on promoter activity compared with the A construct, and the promoter activities of these 3 constructs (A, C, and D) were strongly inhibited by cotransfection with pBP-3 (Figure 5A). In

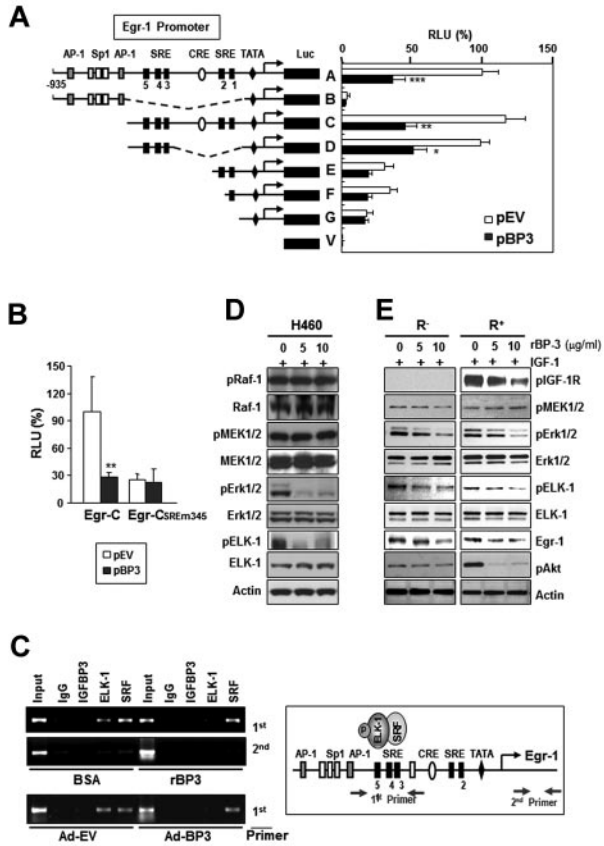

Figure 5. IGFBP-3 inhibits *Egr-1* transcription by inactivating Erk-Elk1 and Elk1 binding to SRE sites in the *Egr-1* promoter. (A-B) IGFBP-3's effects on *Egr-1* promoter activity. H460 cells were transiently cotransfected with Egr-1 Luc constructs (A) or an Egr-1 Luc construct carrying mutations in the 3 5′-SRE sites (SRE 3, 4, and 5; B), along with an empty vector (pEV) or pBP-3. The important genetic elements in the *Egr-1* regulatory region are shown, including the SRE sites, CRE sites, GC, and TATA boxes. The data are the mean ± SD from 3 independent experiments, with 4 replications per experiment. $^*P < .05$, $^{**}P < .01$, $^{***}P < .001$ compared with pEV-transfected cells. (C) IGFBP-3 reduces in vivo binding of Elk-1 to the *Egr-1* promoter. H460 cells, treated with rBP-3 or bovine serum albumin or infected with Ad-BP-3 or Ad-EV, cross-linked and immunoprecipitated with antibodies specific for IGFBP-3, Elk-1, SRF, or a normal serum control antibody (immunoglobulin). The second primer denotes PCR samples using a pair of negative control primers corresponding to the exon 1 sequence of the *Egr-1* gene. (D-E) Western blot analysis for the indicated proteins in H460 cells (D) and R^- and R^+ cells (E) treated with the indicated concentrations of rBP-3 for 2 days and stimulated with IGF-1 for 15 minutes.

contrast, removal of regions upstream of the SRE 1 or 2 sites (E and F constructs) led to a dramatic reduction in *Egr-1* promoter's activity and response to IGFBP-3 expression. Loss of all 5 SRE sites and 2 CRE sites (B construct) led to a total elimination of *Egr-1* promoter activity. In contrast, pBP-3 had no effect on the activity of the *Egr-1* promoter that carried mutations in the 3 5′-SRE sites (SRE 3, 4, and 5; *C*SREm345 construct; Figure 5B).

These findings suggest that the regions upstream of SRE 1 and 2, especially the 3 5′-SRE sites (SRE 3, 4, and 5), contain promoter elements that are regulated by IGFBP-3. The *Egr-1* promoter sequence that encompasses SRE sites 3-5 contains a cluster of Ets motifs (GGA sequence),[38] and these SRE sites and adjacent Ets motifs are continuously occupied by ternary complex factors transcription factors.[39-41] The authors of previous studies have shown that Elk-1, in combination with SRF, participates in the initiation of *Egr-1* transcription.[42] Hence, we hypothesized that IGFBP-3 treatment would inhibit the binding of Elk-1 or SRF to the *Egr-1* promoter, leading to reduced *Egr-1* transcription. We performed a ChIP assay by using 2 primer sets that encompassed the 5′-SRE sites or the first exon (as a negative control) and H460 cells treated with Ad-BP-3 or rBP-3. IGFBP-3 did not interact directly with the SRE sites and did not affect SRF's binding to these sites (Figure 5C). In contrast, IGFBP-3 markedly reduced Elk-1's binding to the 5′-SRE sites. The immunoprecipitates with preimmune serum (immunoglobulin) showed no significant binding to these sites. These results suggest that IGFBP-3 regulates *Egr-1* transcription by indirectly inhibiting Elk-1's binding to the 5′-SRE sites in the *Egr-1* promoter.

The authors of previous studies have indicated that transcriptional Egr-1 activation is regulated by Elk-1 phosphorylation through the MEK/Erk signaling cascade,[20] which is required to recruit SRF to the SREs in the *Egr-1* promoter.[43] Thus, we determined whether IGFBP-3 interfered with the Raf-MAPK-Elk phosphorylation cascade in H460 cells. A Western blot analysis revealed that phosphorylated Erk1/2 (pErk1/2) and phosphorylated Elk-1 (pElk-1) expression was dramatically reduced by IGFBP-3 treatment, whereas total and phosphorylated Raf and MEK1/2 levels were not affected (Figure 5D). Likewise, pBP-3 transfection led to reduced pErk1/2 expression, with no change in pMEK1/2 levels (supplemental Figure 3). An additional experiment using R^- and R^+ cells treated with rBP-3 and stimulated with IGF-1 resulted in reduced pErk1/2, pElk-1, and Egr-1 levels, with no change in pMEK1/2 levels in both cell lines (Figure 5E). In contrast, neither pIGF-1R nor pAkt levels were affected in rBP-3–treated R^- cells. Together, these findings suggest that IGFBP-3 inhibits Erk1/2 and Elk-1 activation through IGF-1–independent mechanisms, leading to reduced binding of Elk-1 to SREs in the *Egr-1* promoter and *Egr-1* transcription suppression.

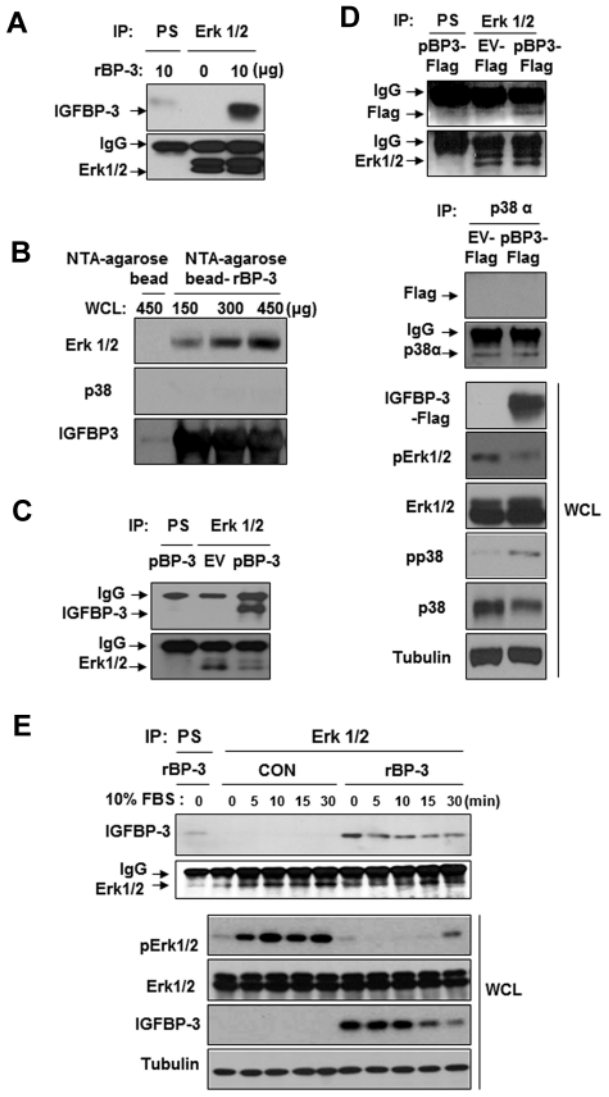

Figure 6. IGFBP-3 binds to and inactivates Erk. (A,C-D) H1299 cells were pretreated with rBP-3 for 3 hours (A) or transiently transfected with pEV or pBP-3 (C), or with pEV-Flag or pBP-3-Flag (D) for 2 days. Lysates from H1299 cells were used for immunoprecipitation with rabbit anti-Erk1/2 antibody. Erk1/2, Flag, IGFBP-3, and p38α were detected by Western blotting. Whole cell lysates (WCLs) were subjected to a Western blot assay for phospho-Erk and phospho-p38 to determine specific inhibition of Erk by IGFBP-3. EV: empty vector. pBP-3-Flag: pCMV6-IGFBP-3-Flag. (B) Ni-NTA bead-bound his-tagged rBP-3 was incubated with H1299 whole cell lysate (150, 300, or 450 μg) for 5 hours before being washed and subjected to Western blot analysis for Erk1/2, p38α, and IGFBP-3. (E) H1299 cells were incubated with rBP-3 for 3 hours and stimulated with 10% FBS; samples were removed at different time points, as shown. The cell lysates were used for immunoprecipitation with rabbit anti-Erk antibody. Western blotting was used to detect IGFBP-3 and Erk from immunoprecipitation or whole cell lysates.

IGFBP-3 binds to and inactivates Erk1/2

We determined the IGF-independent mechanisms by which IGFBP-3 may deregulate Erk1/2 activation. IGFBP-3 has been shown to act independently of the IGF system by binding to its own receptors or other cellular proteins, although the mechanism by which this occurs has not been clearly identified. Therefore, we determined whether IGFBP-3 interacted with Erk1/2 using H1299 cells that do not express IGFBP-3.[44] First, we performed coimmunoprecipitation assays by using H1299 cell lysates that had been pretreated with rBP-3. H1299 cell immunoprecipitation with the use of an anti-Erk1/2 antibody, followed by Western blotting for IGFBP-3, revealed an association between Erk1/2 and rBP-3 (Figure 6A). Second, we determined in vitro whether IGFBP-3 directly interacts with Erk1/2. rBP-3 protein conjugated to NTA-agarose beads was incubated with H1299 cell lysates, washed, electrophoresed, and immunoblotted for Erk1/2 and p38. We found an interaction between IGFBP-3 and Erk1/2 that increased with the amount of the cell lysate added (Figure 6B). However, we did not detect an interaction between p38α and IGFBP-3.

Because large amounts of recombinant protein may cause coimmunoprecipitation artifacts and binding of cellular extracts to IGFBP-3 conjugated to affinity beads may not establish that IGFBP-3 interacts with Erk1/2 in vivo, we performed coimmunoprecipitation assays by using H1299 cell lysates that had been transfected with expression vectors carrying IGFBP-3 (pBP-3; Figure 6C) or Flag-tagged

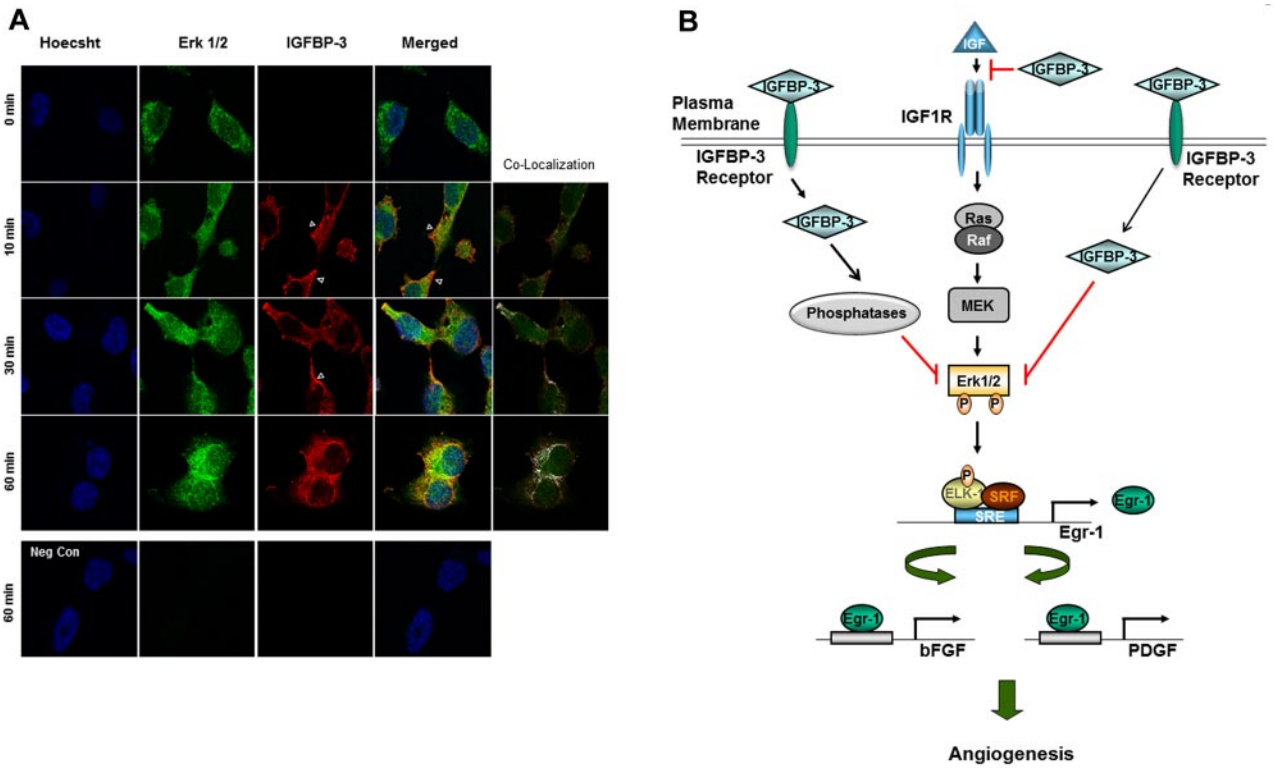

Figure 7. Translocalization and colocalization of rBP-3 with Erk in H1299 cells. (A) H1299 cells on cover slips were treated with rhIGFBP-3 (10 μg/mL) and fixed at 0, 10, 30, and 60 minutes after being washed 3 times in PBS. Nuclei (blue) were stained with Hoechst 33342 (1 μg/mL). Erk1/2 (green) was stained with mouse anti-Erk antibody and secondary antibodies conjugated with Alexa Fluor 488. IGFBP-3 (red) was stained with rabbit anti-IGFBP-3 antibody and secondary antibodies conjugated with Alexa Fluor 568. For the negative control, cells treated with rhIGFBP-3 for 60 minutes were stained with secondary but not primary antibodies. Neg Con: negative control. Colocalization map: schematic plot of colocalization; white dots represent the colocalization of Erk and IGFBP-3. The empty arrowhead indicates IGFBP-3 accumulation near the cell membrane. (B) Schematic model of IGFBP-3's angiogenesis inhibition. IGFBP-3 inhibits tumor angiogenesis by IGF-dependent and -independent mechanisms. In the IGF-independent mechanism, IGFBP-3 directly binds to and inactivates Erk1/2, prevents Elk-1 activation and binding between activated Elk-1 and *Egr-1* promoter, and inhibits expression of Egr-1 and its target genes, including bFGF and PDGF, resulting in suppression of angiogenesis and tumor growth.

IGFBP-3 (pBP-3-Flag; Figure 6D). We found an association between Erk1/2 and IGFBP-3 in these cells, further confirming an Erk1/2-IGFBP-3 interaction. In contrast, a control immunoprecipitation using an anti-p38α antibody revealed that p38α was not associated with IGFBP-3 (Figure 6D bottom). IGFBP-3-Flag expression induced a marked decrease in Erk phosphorylation, with a slight increase in p38α phosphorylation. These findings suggest a direct and specific interaction between Erk1/2 and IGFBP-3. Thus, the interaction between IGFBP-3 and Erk does not appear to be an artifact of the high IGFBP-3 concentration.

We then correlated Erk1/2 activation with the association between IGFBP-3 and Erk1/2 by incubating H1299 cells with rBP-3 in serum-free conditions and analyzing samples obtained at several time points up to 30 minutes after stimulation with 10% FBS. IGFBP-3 was strongly associated with Erk1/2 under the serum-starved condition (Figure 6E). We found that 10% FBS stimulated Erk1/2 activation in control cells; however, Erk1/2 remained inactive in rBP-3–treated cells in which IGFBP-3 associated with Erk1/2. IGFBP-3 levels in H1299 cells gradually decreased 15 minutes after FBS stimulation, and Erk1/2 was rephosphorylated. These findings suggest that IGFBP-3 binds to Erk1/2, obstructing its activation and downstream signaling cascades.

Transcolocalization of IGFBP-3 with Erk in H1299 cells

We performed confocal microscopy to determine whether exogenously supplied recombinant IGFBP-3 protein entered the cytosol and interacted with Erk. Serum-starved H1299 cells were treated with rBP-3 (10 μg/mL) for 1 hour; the cells were collected after 0, 10, 30, and 60 minutes and subjected to immunofluorescence staining with antibodies against IGFBP-3 or Erk1/2. As shown in Figure 7A, IGFBP-3 was localized near the membrane and in the cytosol 10 minutes after treatment and translocalized more to the cytosol by 60 minutes. Furthermore, IGFBP-3 and Erk1/2 colocalization at the cytoplasmic and perinuclear regions was markedly increased after 60 minutes. Interestingly, nuclear colocalization of IGFBP-3 and Erk1/2 was not detected, suggesting that IGFBP-3 binds and inactivates Erk1/2, resulting in suppression of Erk1/2 nuclear localization.

Discussion

IGFBP-3 is known to have IGF-independent antiangiogenic antitumor activities; however, mechanisms by which the IGF-independent activities of IGFBP-3 are mediated are not clearly understood. In this article, we have demonstrated a novel principal mechanism by which IGFBP-3 blocks tumor angiogenesis induced by NSCLC cells, including blocking the autocrine and paracrine loops of angiogenic factors by inhibiting the production of angiogenic factors such as bFGF and PDGF. IGFBP-3 appears to bind to and inactivate Erk1/2, which results in Elk-1 inactivation and Elk-1–SRE binding suppression in the *Egr-1* promoter. Ultimately, this inhibits the transcription of *Egr-1* and its target genes, including bFGF and PDGF.

Because IGFBP-3 has been shown to inhibit vascular endothelial cell survival[45,46] and induce tumor vasculature normalization,[47] it is believed to have antiangiogenic properties. In support of this notion, IGFBP-3–mediated antitumor activities have been found to involve angiogenesis suppression in various cancer types.[7,8,45] However, to date, the mechanisms by which IGFBP-3 regulates angiogenesis are not understood.

We investigated the mechanisms that mediate IGFBP-3's antiangiogenic activity and found that it regulates the expression of *bFGF* and *PDGF,* potent angiogenic factors, in NSCLC, HNSCC, and vascular endothelial cells. Because the Egr-1 transcription factor plays a role in regulating these angiogenic factors' expression by binding to the G/C-rich consensus element in their promoters, we determined effects of IGFBP-3 on Egr-1 expression. As expected, IGFBP-3 decreased *Egr-1* promoter activity and expression; it also led to reduced transcription of Egr-1 target genes, including *bFGF* and *PDGF*. Furthermore, Egr-1 overexpression restored the *bFGF* promoter and angiogenic activities that had been suppressed by IGFBP-3. Therefore, IGFBP-3 may regulate tumor angiogenesis through mechanisms that involve Egr-1, a transcription factor for bFGF and PDGF expression.

IGFBP-3 leads to decreased clusterin expression, which is induced by stress-induced Egr-1 transactivation through IGF-1R-Src-MEK-Erk signal transduction cascade activation.[48] Hence, the inhibitory effect of IGFBP-3 on Egr-1 expression and the resultant reduction in *bFGF* and *PDGF* transcription may have occurred through IGF-dependent mechanisms. However, Egr-1 regulation by IGFBP-3 appears to include novel IGF-independent mechanisms for the following reasons: (1) both wild-type IGFBP-3 and the non-IGF–binding IGFBP-3-ggg mutant suppressed the *Egr-1* promoter activity that had been stimulated by mitogenic and nonmitogenic stimuli in H1299, IGF-1R–null (R^-), and IGF-1R–positive (R^+) cells; and (2) Egr-1 overexpression abrogated the antiangiogenic activity of wild-type IGFBP-3 and the IGFBP-3-ggg mutant in NSCLC cells. Our gross promoter deletion and mutation analyses revealed that the SREs and their adjacent Ets sites are critical to the IGFBP-3–mediated reduction in *Egr-1* transcription. Importantly, our ChIP assay results showed that Elk-1's binding to SRE sites 3-5 was inhibited by IGFBP-3 treatment, whereas SRF binding was not affected. This pattern of constitutive binding by SRF without ternary complex formation is consistent with some[49,50] SRE-mediated transcription models. One possible mechanism of the IGFBP-3–mediated down-regulation of Elk-1 binding is inactivation of the Ras-Raf-MEK1/2-Erk1/2 signaling cascade, which phosphorylates and activates Elk-1 and regulates SRE-Ets–mediated *Egr-1* transcription.[49] The Ras-Raf-MEK1/2-Erk1/2 pathway regulates endothelial cell behavior during angiogenesis by stimulating cell proliferation, survival, migration, and invasion.[51,52] MEK1 knockout mice have defects in angiogenesis in the placenta, resulting in embryonic lethality.[53] Surprisingly, our biochemical analysis revealed that rBP-3 treatment resulted in Erk1/2 inactivation and suppression of Elk-1 and Egr-1 expression without concordant inactivation of MEK1/2 in NSCLC, R^+, and R^- cells. These findings demonstrate that IGFBP-3 can inactivate Erk/Elk-1 independent of MEK-1.

Scaffolding proteins, such as Ras kinase suppressor, MAPK organizer-1, and MEK partner-1, are known as regulators of the Ras-Raf-MEK signaling pathway.[54] This knowledge led us to begin investigating the potential involvement of these scaffolding proteins in IGFBP-3–mediated Erk1/2 inactivation. However, we detected no interactions among these scaffolding proteins and IGFBP-3 in H1299 or H460 cells that had been transfected with pBP-3 or infected with Ad-BP-3 (data not shown). Furthermore, interaction between these scaffolding proteins and signaling components of Ras-Raf-MEK-Erk signaling was not appreciably changed by the IGFBP-3 expression. These findings suggest that IGFBP-3 inactivates Erk1/2 through mechanisms that are independent of these scaffolding proteins. Surprisingly, our data clearly demonstrated that IGFBP-3 can directly interact with Erk1/2, leading to Erk1/2 activity suppression. This interaction appeared to be Erk1/2-specific because the high level of IGFBP-3 obtained after treatment with recombinant protein or transient transfection with mammalian expression vector did not induce p38 binding.

In summary, our data provide a model of an IGF-independent mechanism through which IGFBP-3 inhibits the Erk1/2-Elk-1 activation loop and thus reduces Egr-1 expression. The intracellular translocalization of IGFBP-3 may have been mediated by membrane receptors, as proposed in previous studies.[55-57] In this study, recombinant IGFBP-3 translocated through the membranes into the cytoplasm. Additional mechanisms underlying the IGFBP-3–mediated inactivation of Erk1/2 should be explored (such as whether IGFBP-3's binding to surface receptors triggers phosphatases to dephosphorylate Erk1/2), our current data provide a schematic model in which IGFBP-3 directly binds to Erk1/2 and inhibits its activation, thereby preventing Elk-1 phosphorylation. IGFBP-3's dissociation from Erk1/2 during mitogen stimulation allows Erk1/2 activation, leading to Elk-1–induced expression of *Egr-1*, a master transcription factor that regulates genes that are strongly implicated in tumor growth and angiogenesis. Ultimately, this activation stimulates the Egr-1–mediated transcriptional events observed in cancer cells (Figure 7B).

Antiangiogenic therapies currently in clinical trials induce acquired resistance in cells by causing them to shift to other growth factor-induced angiogenesis mechanisms. Therefore, IGFBP-3's ability to regulate multiple potent angiogenic factors makes it an attractive antiangiogenic, antineoplastic agent. However, because reduced tumor vascularization after antiangiogenic therapy could induce hypoxia and thus promote the spread of cancer cells toward a more oxygenated environment,[58] extensive studies are needed before clinical trials in which IGFBP-3 overexpression is induced are considered. In this work, we did not determine the exact mechanisms by which IGFBP-3 enters cells and by which serum stimulation induces IGFBP-3 dissociation from Erk1/2, although serum stimulation may activate proteases, including various MMPs, that cause IGFBP-3's degradation.[59-61] Further studies are warranted to understand the molecular mechanisms of IGFBP-3-Erk1/2 interaction.

Acknowledgments

The authors are grateful to Warren Davis (Medical University of South Carolina) and David M. Cohen (Oregon Health and Science University) for generously donating plasmids.

This work was supported by National Institutes of Health grants R01 CA100816 and R01 CA109520 (H.-Y.L.) and P50 CA907007 (S.M.L.). This research is supported in part by the National Institutes of Health through M. D. Anderson's Cancer Center Support Grant CA016672. Specifically, this study was performed by use of the microscopy equipment that is part of the Flow Cytometry and Cellular Imaging Core Facility at M. D. Anderson.

Authorship

Contribution: J.-H.K., D.S.C., O.-H.L., and S.-H.O. performed the in vitro experiments; S.-H.O. contributed to the animal experiments; S.M.L. provided clinical input and financial support; and J.-H.K. and H.-Y.L. designed the research and wrote the paper.

Conflict-of-interest disclosure: The authors declare no competing financial interests.

The current affiliation for O.-H.L. is the Severance Integrative Research Institute for Cerebral & Cardiovascular Diseases, Yonsei University Health System, Seoul, Republic of Korea. The current affiliation for S.-H.O is the Division of Cancer Biology, National Cancer Center, Goyang-si, Republic of Korea.

Correspondence: Ho-Young Lee, PhD, Research Institute of Pharmaceutical Sciences, College of Pharmacy, Seoul National University, 599 Gwanak-ro, Gwanak-gu, Seoul 151-742, Republic of Korea; e-mail: hylee135@snu.ac.kr.

References

1. van Moorselaar RJ, Voest EE. Angiogenesis in prostate cancer: its role in disease progression and possible therapeutic approaches. *Mol Cell Endocrinol.* 2002;197(1-2):239-250
2. Ferrara N. VEGF and the quest for tumour angiogenesis factors. *Nat Rev Cancer.* 2002;2(10):795-803.
3. Folkman J. Angiogenesis: an organizing principle for drug discovery? *Nat Rev Drug Discov.* 2007;6(4):273-286.
4. Firth SI, Kaufman PL, De Jean BJ, Byers JM, Marshak DW. Innervation of the uvea by galanin and somatostatin immunoreactive axons in macaques and baboons. *Exp Eye Res.* 2002;75(1):49-60.
5. Granata R, Trovato L, Garbarino G, et al. Dual effects of IGFBP-3 on endothelial cell apoptosis and survival: involvement of the sphingolipid signaling pathways. *FASEB J.* 2004;18(12):1456-1458.
6. Lee CY, Lee HP, Jeong JH, et al. Effects of restricted feeding, low-energy diet, and implantation of trenbolone acetate plus estradiol on growth, carcass traits, and circulating concentrations of insulin-like growth factor (IGF)-I and IGF-binding protein-3 in finishing barrows. *J Anim Sci.* 2002;80(1):84-93.
7. Liu B, Lee KW, Anzo M, et al. Insulin-like growth factor-binding protein-3 inhibition of prostate cancer growth involves suppression of angiogenesis. *Oncogene.* 2007;26(12):1811-1819.
8. Oh SH, Kim WY, Kim JH, et al. Identification of insulin-like growth factor binding protein-3 as a farnesyl transferase inhibitor SCH66336-induced negative regulator of angiogenesis in head and neck squamous cell carcinoma. *Clin Cancer Res.* 2006;12(2):653-661.
9. Bhattacharyya N, Pechhold K, Shahjee H, et al. Nonsecreted insulin-like growth factor binding protein-3 (IGFBP-3) can induce apoptosis in human prostate cancer cells by IGF-independent mechanisms without being concentrated in the nucleus. *J Biol Chem.* 2006;281(34):24588-24601.
10. Ikonen M, Liu B, Hashimoto Y, et al. Interaction between the Alzheimer's survival peptide humanin and insulin-like growth factor-binding protein 3 regulates cell survival and apoptosis. *Proc Natl Acad Sci U S A.* 2003;100(22):13042-13047.
11. Lee HY, Chun KH, Liu B, et al. Insulin-like growth factor binding protein-3 inhibits the growth of non-small cell lung cancer. *Cancer Res.* 2002;62(12):3530-3537.
12. Li H, Bubley GJ, Balk SP, et al. Hypoxia-inducible factor-1alpha (HIF-1alpha) gene polymorphisms, circulating insulin-like growth factor binding protein (IGFBP)-3 levels and prostate cancer. *Prostate.* 2007;67(12):1354-1361.
13. Cohen DM. Urea-inducible Egr-1 transcription in renal inner medullary collecting duct (mIMCD3) cells is mediated by extracellular signal-regulated kinase activation. *Proc Natl Acad Sci U S A.* 1996;93(20):11242-11247.
14. Chen GJ, Forough R. Fibroblast growth factors, fibroblast growth factor receptors, diseases, and drugs. *Recent Patents Cardiovasc Drug Discov.* 2006;1(2):211-224.
15. Worden B, Yang XP, Lee TL, et al. Hepatocyte growth factor/scatter factor differentially regulates expression of proangiogenic factors through Egr-1 in head and neck squamous cell carcinoma. *Cancer Res.* 2005;65(16):7071-7080.
16. Shimoyamada H, Yazawa T, Sato H, et al. Early growth response-1 induces and enhances vascular endothelial growth factor-a expression in lung cancer cells. *Am J Pathol.* 2010;177(1):70-83.
17. Khachigian LM. Early growth response-1: blocking angiogenesis by shooting the messenger. *Cell Cycle.* 2004;3(1):10-11.
18. Fahmy RG, Dass CR, Sun LQ, Chesterman CN, Khachigian LM. Transcription factor Egr-1 supports FGF-dependent angiogenesis during neovascularization and tumor growth. *Nat Med.* 2003;9(8):1026-1032.
19. Fahmy RG, Khachigian LM. Suppression of growth factor expression and human vascular smooth muscle cell growth by small interfering RNA targeting EGR-1. *J Cell Biochem.* 2007;100(6):1526-1535.
20. Guha M, O'Connell MA, Pawlinski R, et al. Lipopolysaccharide activation of the MEK-ERK1/2 pathway in human monocytic cells mediates tissue factor and tumor necrosis factor alpha expression by inducing Elk-1 phosphorylation and Egr-1 expression. *Blood.* 2001;98(5):1429-1439.
21. Lucerna M, Mechtcheriakova D, Kadl A, et al. NAB2, a corepressor of EGR-1, inhibits vascular endothelial growth factor-mediated gene induction and angiogenic responses of endothelial cells. *J Biol Chem.* 2003;278(13):11433-11440.
22. Lee CT, Park KH, Yanagisawa K, et al. Combination therapy with conditionally replicating adenovirus and replication defective adenovirus. *Cancer Res.* 2004;64(18):6660-6665.
23. Kim MS, Kwon HJ, Lee YM, et al. Histone deacetylases induce angiogenesis by negative regulation of tumor suppressor genes. *Nat Med.* 2001;7(4):437-443.
24. Oh SH, Woo JK, Jin Q, et al. Identification of novel antiangiogenic anticancer activities of deguelin targeting hypoxia-inducible factor-1 alpha. *Int J Cancer.* 2008;122(1):5-14.
25. Oh SH, Jin Q, Kim ES, Khuri FR, Lee HY. Insulin-like growth factor-I receptor signaling pathway induces resistance to the apoptotic activities of SCH66336 (lonafarnib) through Akt/mammalian target of rapamycin-mediated increases in survivin expression. *Clin Cancer Res.* 2008;14(5):1581-1589.
26. Kim WY, Oh SH, Woo JK, Hong WK, Lee HY. Targeting heat shock protein 90 overrides the resistance of lung cancer cells by blocking radiation-induced stabilization of hypoxia-inducible factor-1alpha. *Cancer Res.* 2009;69(4):1624-1632.
27. Kim JH, Tuziak T, Hu L, et al. Alterations in transcription clusters underlie development of bladder cancer along papillary and nonpapillary pathways. *Lab Invest.* 2005;85(4):532-549.
28. Lee HY, Moon H, Chun KH, et al. Effects of insulin-like growth factor binding protein-3 and farnesyltransferase inhibitor SCH66336 on Akt expression and apoptosis in non-small-cell lung cancer cells. *J Natl Cancer Inst.* 2004;96(20):1536-1548.
29. Goldhar AS, Vonderhaar BK, Trott JF, Hovey RC. Prolactin-induced expression of vascular endothelial growth factor via Egr-1. *Mol Cell Endocrinol.* 2005;232(1-2):9-19.
30. Han JY, Oh SH, Morgillo F, et al. Hypoxia-inducible factor 1alpha and antiangiogenic activity of farnesyltransferase inhibitor SCH66336 in human aerodigestive tract cancer. *J Natl Cancer Inst.* 2005;97(17):1272-1286.
31. Biesiada E, Razandi M, Levin ER. Egr-1 activates basic fibroblast growth factor transcription. Mechanistic implications for astrocyte proliferation. *J Biol Chem.* 1996;271(31):18576-18581.
32. Jimenez SK, Sheikh F, Jin Y, et al. Transcriptional regulation of FGF-2 gene expression in cardiac myocytes. *Cardiovasc Res.* 2004;62(3):548-557.
33. Silha JV, Gui Y, Mishra S, Leckstrom A, Cohen P, Murphy LJ. Overexpression of gly56/gly80/gly81-mutant insulin-like growth factor-binding protein-3 in transgenic mice. *Endocrinology.* 2005;146(3):1523-1531.
34. Datta R, Rubin E, Sukhatme V, et al. Ionizing radiation activates transcription of the EGR1 gene via CArG elements. *Proc Natl Acad Sci U S A.* 1992;89(21):10149-10153.
35. Lo LW, Cheng JJ, Chiu JJ, Wung BS, Liu YC, Wang DL. Endothelial exposure to hypoxia induces Egr-1 expression involving PKCalpha-mediated Ras/Raf-1/ERK1/2 pathway. *J Cell Physiol.* 2001;188(3):304-312.
36. Lange-Carter CA, Johnson GL. Ras-dependent growth factor regulation of MEK kinase in PC12 cells. *Science.* 1994;265(5177):1458-1461.
37. Sell C, Dumenil G, Deveaud C, et al. Effect of a null mutation of the insulin-like growth factor I receptor gene on growth and transformation of mouse embryo fibroblasts. *Mol Cell Biol.* 1994;14(6):3604-3612.
38. Bernal-Mizrachi E, Wen W, Srinivasan S, Klenk A, Cohen D, Permutt MA. Activation of Elk-1, an Ets transcription factor, by glucose and EGF treatment of insulinoma cells. *Am J Physiol Endocrinol Metab.* 2001;281(6):E1286-E1299.
39. Watson DK, McWilliams MJ, Lapis P, Lautenberger JA, Schweinfest CW, Papas TS. Mammalian ets-1 and ets-2 genes encode highly conserved proteins. *Proc Natl Acad Sci U S A.* 1988;85(21):7862-7866.
40. Watson DK, Robinson L, Hodge DR, Kola I, Papas TS, Seth A. FLI1 and EWS-FLI1 function as ternary complex factors and ELK1 and SAP1a function as ternary and quaternary complex factors on the Egr1 promoter serum response elements. *Oncogene.* 1997;14(2):213-221.
41. Whitmarsh AJ, Shore P, Sharrocks AD, Davis RJ. Integration of MAP kinase signal transduction pathways at the serum response element. *Science.* 1995;269(5222):403-407.
42. Treisman R. Ternary complex factors: growth factor regulated transcriptional activators. *Curr Opin Genet Dev.* 1994;4(1):96-101.
43. Gille H, Kortenjann M, Strahl T, Shaw PE. Phosphorylation-dependent formation of a quaternary

complex at the c-fos SRE. *Mol Cell Biol.* 1996; 16(3):1094-1102.

44. Chang YS, Wang L, Liu D, et al. Correlation between insulin-like growth factor-binding protein-3 promoter methylation and prognosis of patients with stage I non-small cell lung cancer. *Clin Cancer Res.* 2002;8(12):3669-3675.
45. Franklin SL, Ferry RJ Jr, Cohen P. Rapid insulin-like growth factor (IGF)-independent effects of IGF binding protein-3 on endothelial cell survival. *J Clin Endocrinol Metab.* 2003;88(2):900-907.
46. Yamada PM, Lee KW. Perspectives in mammalian IGFBP-3 biology: local vs. systemic action. *Am J Physiol Cell Physiol.* 2009;296(5):C954-C976.
47. Delafontaine P, Song YH, Li Y. Expression, regulation, and function of IGF-1, IGF-1R, and IGF-1 binding proteins in blood vessels. *Arterioscler Thromb Vasc Biol.* 2004;24(3):435-444.
48. Criswell T, Beman M, Araki S, et al. Delayed activation of insulin-like growth factor-1 receptor/Src/MAPK/Egr-1 signaling regulates clusterin expression, a pro-survival factor. *J Biol Chem.* 2005; 280(14):14212-14221.
49. Clarkson RW, Shang CA, Levitt LK, Howard T, Waters MJ. Ternary complex factors Elk-1 and Sap-1a mediate growth hormone-induced transcription of egr-1 (early growth response factor-1) in 3T3-F442A preadipocytes. *Mol Endocrinol.* 1999;13(4):619-631.
50. Drewett V, Molina H, Millar A, Muller S, von Hesler F, Shaw PE. DNA-bound transcription factor complexes analysed by mass-spectrometry: binding of novel proteins to the human c-fos SRE and related sequences. *Nucleic Acids Res.* 2001;29(2):479-487.
51. Berra E, Milanini J, Richard DE, et al. Signaling angiogenesis via p42/p44 MAP kinase and hypoxia. *Biochem Pharmacol.* 2000;60(8):1171-1178.
52. Liotta LA, Kohn EC. The microenvironment of the tumour-host interface. *Nature.* 2001;411(6835): 375-379.
53. Giroux S, Tremblay M, Bernard D, et al. Embryonic death of Mek1-deficient mice reveals a role for this kinase in angiogenesis in the labyrinthine region of the placenta. *Curr Biol.* 1999;9(7):369-372.
54. Kolch W. Coordinating ERK/MAPK signalling through scaffolds and inhibitors. *Nat Rev Mol Cell Biol.* 2005;6(11):827-837.
55. Oh Y, Muller HL, Lamson G, Rosenfeld RG. Insulin-like growth factor (IGF)-independent action of IGF-binding protein-3 in Hs578T human breast cancer cells. Cell surface binding and growth inhibition. *J Biol Chem.* 1993;268(20):14964-14971.
56. Yamanaka Y, Fowlkes JL, Wilson EM, Rosenfeld RG, Oh Y. Characterization of insulin-like growth factor binding protein-3 (IGFBP-3) binding to human breast cancer cells: kinetics of IGFBP-3 binding and identification of receptor binding domain on the IGFBP-3 molecule. *Endocrinology.* 1999;140(3):1319-1328.
57. Ingermann AR, Yang YF, Han J, et al. Identification of a novel cell death receptor mediating IGFBP-3-induced anti-tumor effects in breast and prostate cancer. *J Biol Chem.* 2010;285(39): 30233-30246.
58. Pennacchietti S, Michieli P, Galluzzo M, Mazzone M, Giordano S, Comoglio PM. Hypoxia promotes invasive growth by transcriptional activation of the met protooncogene. *Cancer Cell.* 2003;3(4):347-361.
59. Fowlkes JL, Serra DM, Bunn RC, Thrailkill KM, Enghild JJ, Nagase H. Regulation of insulin-like growth factor (IGF)-I action by matrix metalloproteinase-3 involves selective disruption of IGF-I/IGF-binding protein-3 complexes. *Endocrinology.* 2004;145(2):620-626.
60. Miyamoto S, Yano K, Sugimoto S, et al. Matrix metalloproteinase-7 facilitates insulin-like growth factor bioavailability through its proteinase activity on insulin-like growth factor binding protein 3. *Cancer Res.* 2004;64(2):665-671.
61. Sadowski T, Dietrich S, Koschinsky F, Sedlacek R. Matrix metalloproteinase 19 regulates insulin-like growth factor-mediated proliferation, migration, and adhesion in human keratinocytes through proteolysis of insulin-like growth factor binding protein-3. *Mol Biol Cell.* 2003; 14(11):4569-4580.

An Open-Label, Multicenter, Three-Stage, Phase II Study of S-1 in Combination with Cisplatin as First-Line Therapy for Patients with Advanced Non-small Cell Lung Cancer

Alan Sandler, MD, Charles Graham, MD,† Maria Baggstrom, MD,‡ Roy Herbst, MD, PhD,§ Christopher Zergebel, BS,‖ Kaku Saito, MS,‖ and Dennie Jones, MD¶*

Introduction: S-1 is a rationally designed oral agent that combines the 5-fluorouracil prodrug tegafur with gimeracil and oteracil, which inhibit 5-fluorouracil degradation by dihydropyrimidine dehydronase and phosphorylation within the gastrointestinal tract, respectively, to increase antineoplastic activity while reducing gastrointestinal toxicity. We investigated the activity and toxicity of S-1 in combination with cisplatin in patients with unresectable non-small cell lung cancer (NSCLC).

Methods: Cisplatin, 75 mg/m^2, was administered intravenously on day 1, with S-1, 25 mg/m^2 PO two times a day, days 1 to 14, every 21 days for a maximum of six cycles. Primary end point was overall response.

Results: A total of 58 patients received at least one cycle of protocol-specified therapy. The best overall response rate was 23.2% (95% confidence interval: 13.0–36.4), and the disease control rate was 67.9%. The median progression-free survival was 4.0 months (95% confidence interval: 3.3–5.5). There did not appear to be any relationship between response to therapy and tumor histology. The most frequently reported adverse events of G3 or more (≥10%) were neutropenia (28%), hyponatremia (19%), diarrhea (17%), hypokalemia (12%), fatigue (10%), dehydration (10%), and deep vein thrombosis (10%).

Conclusions: Although the S-1 + cisplatin regimen used in this study appeared to have a similar level of antitumor activity and toxicity to that of established cisplatin-based doublets in NSCLC, the protocol-specified criteria of sufficient efficacy to warrant further study with an objective response rate ≥30% was not achieved. Therefore, while S-1 appears to be a promising agent in NSCLC, further evaluation should be conducted to determine the optimal S-1-based regimen to take forward for additional study.

*Oregon Health and Science University, Portland, Oregon; †Charleston Cancer Center, Charleston, South Carolina; ‡Washington University School of Medicine, St. Louis, Missouri; §M. D. Anderson Cancer Center, Houston, Texas; ‖Taiho Pharma USA, Princeton, New Jersey; and ¶University of New Mexico, Albuquerque, New Mexico.

Disclosure: Kaku Saito and Christopher Zergebel are employees of Taiho Pharma, USA, Inc. All other authors report no involvements that might raise the question of bias.

Address for correspondence: Alan Sandler, MD, Oregon Health and Science University, 3181 SW Sam Jackson Park Road, MC: L586, Portland, OR 97239. E-mail: sandlera@ohsu.edu

ISSN: 1556-0864/11/0608-1400

Key Words: Lung cancer, Non-small cell, S-1, Cisplatin, Fluoropyrimidines, Clinical trial.

(*J Thorac Oncol.* 2011;6: 1400–1406)

Lung cancer is the second most common form of cancer and the leading cause of cancer death in both men and women in the United States. Data from the American Cancer Society projected more than 219,440 new cases of lung cancer in 2009.[1] Lung cancer is still a highly lethal malignancy in both genders, with a 5-year survival rate that is less than 15%.

Chemotherapy for stage IV non-small cell lung cancer (NSCLC) is still suboptimal, and for all intents and purposes, metastatic lung cancer remains incurable. The currently accepted frontline therapy for unresectable NSCLC is platinum-based doublet therapy with or without biological compounds.[2] The standard of care for most "fit" patients is a combination of cisplatin or carboplatin with a taxane (paclitaxel or docetaxel), vinorelbine, a topoisomerase inhibitor (irinotecan or topotecan), pemetrexed, or gemcitabine.[3] However, in multiple randomized multi-institutional trials, each of the doublets has a comparable response rate of approximately 20%, median progression-free survival (PFS) of 4 to 5 months, median overall survival of 8 to 10 months, and 1-year survival of 35 to 40%. Toxicities, although manageable, can be considerable, including myelosuppression and neutropenic fever, neuropathy, and gastrointestinal toxicities. Recently, with an appreciation of the influence of histology on response and survival associated with certain regimens, a modest improvement (median survival of 12 months) has been observed with the addition of the vascular endothelial growth factor inhibitor bevacizumab to platinum-based therapy in nonsquamous carcinomas, and the utilization of pemetrexed was limited to the same patient population.[4] While this modest progress is encouraging, it is clear that other agents and regimens must be evaluated.

5-Fluorouracil (5-FU), one of the most underutilized antineoplastic agents, has minimal activity against NSCLC, potentially due to an overexpression of dihydropyrimidine dehydronase (DPD).[5,6] The most recent studies have evaluated bolus infusions of 5-FU, usually in combination with other agents such as cisplatin and etoposide or a vinca

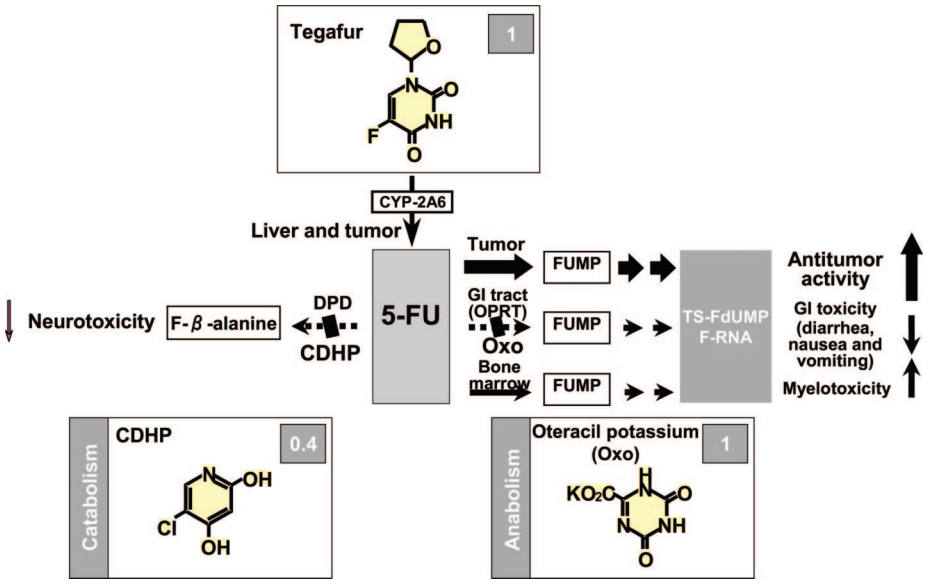

FIGURE 1. Components of S-1 and role in the metabolism of 5-fluorouracil.

alkaloid, or radiotherapy.[7–11] Single agent 5-FU is modestly active in combination with leucovorin, with a 16% objective response rate noted in one study.[9] Although 5-FU may be more active when administered continuously, prolonged infusion is cumbersome for most patients. To date, there have only been a few prior reports of the oral fluoropyrimidine, tegafur and uracil, and capecitabine administered to patients with NSCLC.[11–16]

S-1 is a novel oral fluoropyrimidine that combines tegafur (5-fluoro-1-[tetrahydro-2-furyl]uracil), a prodrug of 5-FU, with two modulators, gimeracil (5-chloro-2,4-dihydroxypyridine, CDHP), which inhibits 5-FU degradation by DPD inhibition, and oteracil potassium (monopotassium 1,2,3,4-tetrahydro-2,4-dioxo-1,3,5-triazine-6-carboxylate), which inhibits 5-FU phosphorylation in the digestive tract (Figure 1).[17] CDHP is about 180 times more potent than uracil in inhibiting DPD in both the tumor and the liver, thus allowing greater concentrations of 5-FU to go though the anabolic pathway than that of tegafur and uracil alone.[18] S-1 is rationally designed to achieve enhanced antitumor activity while decreasing gastrointestinal tract toxicity. S-1 is currently marketed in Japan, South Korea, China, and Singapore for the treatment of cancers of the stomach. In Japan, phase II trials of S-1 have shown promising efficacy (response rate: 33–47%, median survival time: 11–16 months) and tolerability as first-line chemotherapy for patients with advanced NSCLC.[19,20] Based on evidence of benefit in prior studies, and as the ultimate outcome of systemic therapy in NSCLC is still poor, we investigated a combination of S-1 with cisplatin in patients with advanced NSCLC.

MATERIALS AND METHODS

Study Design

This was an open-label, multicenter, single-arm, three-stage, phase II study evaluating the efficacy and safety of S-1 in combination with cisplatin in patients who have not received any prior therapy for advanced NSCLC. The three stages of this study corresponded to a run-in tolerability stage (stage 1), a futility stage (stage 2), and a decision stage (stage 3). The run-in tolerability stage was conducted at a limited number of sites to assess any additional toxicity associated with a more frequent schedule of administration of cisplatin (75 mg/m^2 every 3 weeks) versus the dosing regimen established in a prior phase I study in patients with advanced gastric cancer (75 mg/m^2 every 4 weeks).[21] Stage 2 was conducted to ensure that the treatment combination was sufficiently efficacious to expose a sufficient number of patients to be able to make a decision (stage 3) whether this combination treatment warranted further evaluation in future studies.

Eligibility

All patients were required to have a histologic or cytologic diagnosis of NSCLC that was either locally advanced but not amenable to treatment with radiotherapy or surgery or metastatic disease. Mixed small cell and non-small cell histologies were not allowed. Other eligibility criteria included an Eastern Cooperative Oncology Group (ECOG) performance status 0 to 1; age 18 years or older; using effective contraception; and have evidence of good end-organ function (absolute neutrophil count $>1500/\mu$l, platelet count $>100{,}000/\mu$l, calculated creatinine clearance ≥ 60 ml/min, and bilirubin $\leq 1.5 \times$ normal). Patients were excluded if they were either pregnant or lactating; had a myocardial infarction; had other active malignancy; had prior chemotherapy for metastatic disease (prior chemotherapy for adjuvant or neoadjuvant therapy was allowed provided it was completed at least 12 months earlier); had prior radiotherapy to an indicator lesion unless there was objective evidence of tumor growth in that lesion; had evidence of uncontrolled symptomatic metastatic disease of the central nervous system; had received either radiotherapy or surgery within 2 weeks; had any investigational agent, either currently or within the past

30 days; or had any comorbid condition that, in the view of the attending physician, might place the patient at an increased risk for treatment complications. All patients were required to provide signed informed consent.

Treatment Plan

Study Evaluations

Within 1 week of the initiation of therapy, all patients were required to undergo a baseline evaluation, including a medical history and physical examination, complete blood count with leukocyte differential, and serum chemistries. A computed tomography or magnetic resonance imaging scan for tumor measurement was to be obtained within 4 weeks of therapy. Blood counts were repeated weekly during each cycle, along with the serum chemistries, before each cycle. Repeat radiographic evaluation was performed before every other cycle until the observation of progressive disease (PD) to document tumor response.

Chemotherapy Guidelines

All patients received S-1, 25 mg/m^2, administered orally twice daily from days 1 through 14, and cisplatin, 75 mg/m^2, administered intravenously (IV) as a 1- to 3-hour infusion on day 1 of each cycle after the morning dose of S-1. A recovery period followed on days 15 through 21. This regimen was repeated every 3 weeks for a maximum of six cycles.

Determination of Toxicity and Response

All patients were eligible for evaluation of toxicity, even if they were unable to complete the first cycle. Patients were monitored for safety using adverse event (AE) information, physical examinations, the ECOG scale, vital signs, and laboratory evaluations. AEs were graded using National Cancer Institute (NCI) Common Toxicity Criteria version 3.0 (CTC v3.0).

On-site tumor assessments were performed by the investigator and local radiologist, and the results of those assessments were used to determine whether to continue or discontinue treatment. Tumor scans were collected and forwarded to the Core Imaging Laboratory (ICON Medical Imaging) for independent reader review. Scans/assessments were collected on an end of every even-cycle schedule; however, if a patient responded, response confirmation was to be obtained through tumor assessments/scans at least 4 weeks after the first documentation of response. Patients then returned to their original even-cycle schedule of assessments. The same schedule was followed for clinical assessments; however, if the patient developed PD during clinic visits, study treatment was discontinued. After discontinuation of study treatment for reasons other than withdrawal of consent or PD, patients were followed for tumor response every 6 weeks until disease progression or initiation of new anticancer therapy. Treatment decisions by the investigator were based on objective tumor assessments made according to the RECIST criteria of unidimensional evaluation. The determination of antitumor efficacy, as determined by an independent reader, was also based on those criteria.

Statistical Considerations

Study Design

This study was designed as an exploratory, proof of concept study in three stages to evaluate the tolerability and antitumor activity of S-1 in combination with cisplatin in patients with advanced NSCLC. The study design reflects the classical two-stage Simon design, with the exception that the first stage is divided into two parts: (a) the run-in tolerability stage and (b) the futility stage. The treatment regimen of S-1 25 mg/m^2 combined with cisplatin 75 mg/m^2 administered on a 21-day cycle as used in this study was similar to the maximum tolerated dose of S-1 25 mg/m^2 combined with cisplatin 75 mg/m^2 for 4 weeks, which was established in a phase I dose-escalation study in patients with advanced gastric cancer.[21] However, in this study, cisplatin was administered every 3 weeks to keep the cisplatin dose intensity in the 21 to 30 mg/m^2/wk range, rather than every 4 weeks, as in the previous study. The run-in tolerability stage assessed any additional toxicity associated with a more frequent schedule of administration of cisplatin.

In this study, a response rate of 35% or higher would be considered as a good indicator for further development, whereas a response rate of 20% or lower would be considered poor and not supportive of future development. Based on the exact binomial probability distribution approach published by Richard Simon,[22] the sample size would be 53 for a "Minimax Design" with P1 = 0.35, P0 = 0.20, with $\alpha = 0.05$ (one sided), $\beta = 0.2$. For the first and second stage combined, the sample size would be 31. The trial could go on to the third stage only if 7 of 31 (23%) or more patients had achieved a confirmed response (complete response [CR] or partial response [PR]) in the first two stages. To be considered sufficiently efficacious to warrant further study, the criteria to proceed to stage 3 needed to be met and, by the end of the trial, there needed to be 16 of 53 patients (30%) or more who had achieved a confirmed response. Simon's "Minimax Design" was chosen over his "Optimal Design," as it minimized the maximum sample size when the criteria for proceeding to the second stage were met, which was the expectation based on S-1 performance in studies previously conducted in United States and Japan. Assuming a 10% rate for loss to follow-up and/or nonevaluability for the response rate assessment, it was projected that a total of 60 patients would be enrolled in the study. The primary end point, overall response rate (ORR), was used as a screening end point in this exploratory, proof of concept study in patients with advanced NSCLC.

Efficacy. The primary efficacy population included all patients in the safety population who met the key eligibility criteria. All efficacy parameters were analyzed using data from this population, including the primary efficacy end point, ORR, based on the best overall response for each patient. For ORR, the determination of an efficacious result was based on the two-stage "Minimax" methodology described by Richard Simon (i.e., there must be 30% or more patients who achieved a confirmed response to be considered efficacious at the end of the study).

The time to the first CR or PR, the duration of the CR or PR, and PFS were estimated using Kaplan-Meier methodology.

Safety. Hematology were assessed weekly, and blood biochemistry, urinalysis, and physical findings/vital signs were assessed triweekly. Other safety data (vital signs, ECOG performance status, and clinical laboratory results) were summarized descriptively. Any AEs were evaluated for grading, duration, and S-1 causality according to the NCI-CTC v3.0.

RESULTS

Patient Demographics

A total of 60 patients were enrolled, of which 58 received the study drug. Two patient discontinued before treatment due to AE. The majority of the patients were white (46 of 58, 79%) (Table 1). More than half of the patients (34 of 58, 59%) had histologic/cytologic classification of adenocarcinoma. Fifty-two patients (90%) had stage IV NSCLC, and 6 (10%) had stage IIIB NSCLC. At study entry, approximately 60% of patients had an ECOG performance status of 1, while the remainder had ECOG scores of 0. Most patients (51 of 58, 88%) had not had prior resections. Seventeen of 58 (29%) patients had prior radiotherapy; none of the patients had received systemic anticancer therapy before study entry. Among the 58 treated patients, at baseline, 57 patients had measurable disease based on the investigator assessment. A majority of those patients (50 of 57, 88%) had two or more target lesions at the time of study entry.

TABLE 1. Patient Characteristics (n = 58)

	n	%
Age, years		
Median (range)	63.0	(40–84)
Gender, n (%)		
Male	37	64
Female	21	36
ECOG PS, n (%)		
0	23	40
1	35	60
Race		
White	46	79
African American	7	12
Asian	2	3
Other	3	5
BSA, m^2		
Median (range)	1.86	(1.33–2.30)
Histological classification		
Adenocarcinoma	34	59
Squamous cell	10	17
Large cell	3	5
Other	11	19
Stage, TNM classification		
Stage IIIB	6	10
Stage IV	52	90
Sites of metastatic disease at baseline		
Lymph nodes	42	72
Lung	30	52
Liver	14	24
Bone	21	36
CNS	3	5
Other	20	35
Number of target lesions		
1	7	12
2	16	28
3	12	21
>3	22	39
Prior surgery		
Not resected	51	88
Partially resected	1	2
Resected	6	10
Prior radiotherapy		
Yes	17	29
No	41	71

Responses to Therapy

The ORR for the first 31 patients (stages 1 and 2) was 36% (11 of 31) by the investigator assessment; therefore, the study proceeded to stage 3. Based on independent reader assessments, the best ORR was with 13 patients achieving a PR, 25 (45%) patients with stable disease, and 14 (25%) patients with PD, while 4 (7%) patients were not evaluable. The overall response was 23% (95% CI: 13.0–36.4), and the disease control rate was 68% (95% CI: 54.0–79.7) (Table 2). There was no evidence of any interaction of tumor histology with objective response to therapy, although the study was not powered to evaluate such potential interactions (Table 2). A total of 10 patients presented with squamous cell carcinoma; 2 (20%) experienced a PR on independent review, while the ORR was 24% (11 of 46) in patients with nonsquamous cell carcinoma. For those patients responding to treatment, the median duration of response was 4.2 months ($n = 13$) based on the independent review assessments. For all patients, the Kaplan-Meier estimate for median PFS was 4.0 months (95% CI: 3.3–5.5) based on independent review assessments (Figure 2).

Toxicity

No dose-limiting toxicities were observed for six patients at stage 1. Therefore, the study proceeded to stage 2. A total of 58 patients in all stages received at least one dose of S-1 and were included in the safety population. The median number of cycles of study treatment delivered was 4. More than 55% of patients initiated at least four cycles of treatment, and 36% had all six cycles initiated. Median relative dose intensity was 0.90 (SD, 0.17; range, 0.38–1.22) for S-1 and 0.94 for cisplatin (SD, 0.17; range, 0–1.03).

All 58 (100%) patients experienced at least one AE (Table 3). Twenty-four (41%) patients experienced grade 3 AEs and 16 (28%) experienced grade 4 AEs. The most frequently reported AEs of grade 3 or more (≥10%) were neutropenia (28%), hyponatremia (19%), diarrhea (17%), hypokalemia (12%), fatigue (10%), dehydration (10%), and deep vein thrombosis (10%). Only one patient (2%) experienced a treatment-related deep vein thrombosis. A total of

TABLE 2. Response Rate by Independent Assessment (n = 56)

	Total (n = 56)	Patients with Squamous cell carcinoma (n = 10)	Patients with Non-squamous cell carcinoma (n = 46)
Response, n (%)			
Complete response	0 (0)	0 (0)	0 (0)
Partial response	13 (23)	2 (20)	11 (24)
Stable disease	25 (45)	4 (40)	21 (46)
Progressive disease	14 (25)	3 (30)	11 (24)
Not evaluable*	4 (7)	1 (10)	3 (7)
Overall response rate, n (%)	13 (23)	2 (20)	11 (24)
95% CI	13.0–36.4	—	—
Disease control rate, n (%)	38 (67.9)	6 (60.0)	32 (69.6)
95% CI	54.0–79.7	—	—

*No post-baseline assessments.

TABLE 3. Hematological and Non-hematological Adverse Events

	Any		> = G3	
	n	%	n	%
Leukopenia	8	14	3	5
Neutropenia	22	38	16	28
Anemia	30	52	2	3
Thrombocytopenia	7	12	2	3
Anorexia	17	29	1	2
Nausea	42	72	5	9
Vomiting	28	48	4	7
Fatigue	34	59	6	10
Diarrhea	29	50	10	17
Dehydration	15	26	6	10
Stomatitis	6	10	0	0
Constipation	22	38	1	2
Abdominal pain	10	17	3	5
Weight decreased	13	22	2	3
Rash	6	10	0	0
Dizziness	15	26	1	2
Hyponatraemia	15	26	11	19
Hypokalaemia	12	21	7	12
Hypotension	13	22	3	5
Deep Vein Thrombosis	7	12	6	10

three patients died due to treatment-related AEs that occurred at any time during the study (including events with onset >30 days after the last dose of study drug): neutropenic sepsis and multiorgan failure (one patient), renal failure (one patient), and sepsis and multiorgan failure (one patient). Twenty-two of the 58 (38%) patients discontinued their study participation due to objective disease progression. Remaining patients discontinued the study due to completion of all six cycles of study-specified treatment (28%), AEs (14%), investigator judgment (9%), noncompliance (3%), death (3%), requiring more than 3 weeks to recover from a prior treatment cycle (2%), intercurrent illness (2%), or other reasons (2%).

DISCUSSION

Disseminated NSCLC remains a frustrating disease to treat, with poor responses to treatment in most of the patients. Although treatment with chemotherapy may offer some palliative benefit, the survival benefit of platinum-based chemotherapy, still considered the "gold standard," is modest and measured in weeks. We need to identify and evaluate new agents and combinations that may offer improvements in response rate and survival. Equally important is to identify regimens that may be equivalent in activity to the current standard regimens but with less toxicity.

Conventional 5-FU has not provided clinically relevant responses in most patients with NSCLC. An explanation of

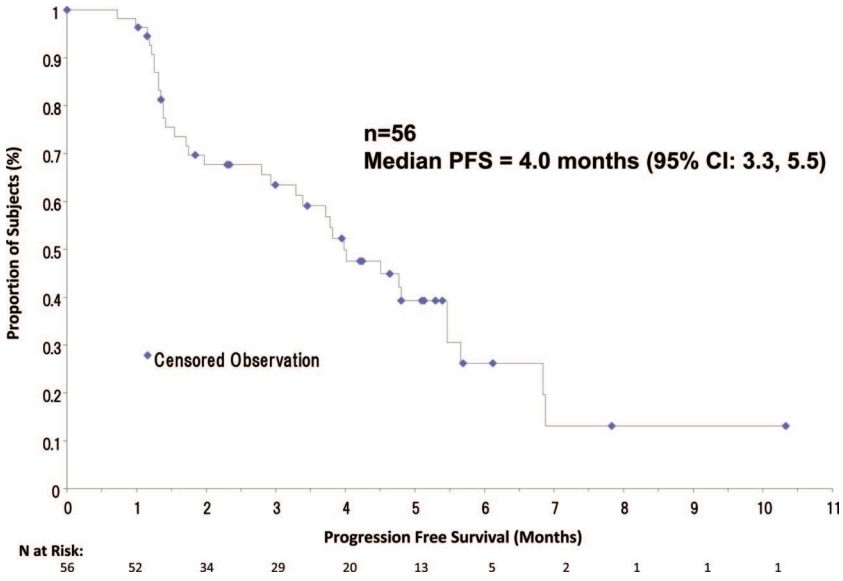

FIGURE 2. Progression-free survival by independent assessment ($n = 56$).

this failure may be that the majority of patients with NSCLC have been shown to have relatively high DPD activity.[5,6] When 5-FU is administered intravenously alone, 90% of the drug is rapidly catabolized in the liver by DPD and excreted in the urine as α-fluoro-β-alanine. S-1 is a new oral pyrimidine fluoride-derived anticancer agent in which tegafur is combined with two classes of modulators, gimeracil (CDHP) and oteracil potassium (Oxo). This combination drug is being developed to enhance the clinical advantage of an oral fluoropyrimidine and ameliorate the disadvantage of gastrointestinal toxicity. Within the patient population with high DPD activity, more than 60% have been shown to have low thymidylate synthase (TS) activity while 25% have high TS activity. Without inhibition of the high DPD activity, conventional 5-FU and 5-FU prodrugs are considered to be rapidly destroyed, significantly limiting the amount of 5-FU that is available for the anabolic pathway. Because S-1 contains CDHP, an inhibitor of DPD, catabolism is significantly slowed, allowing large amounts of 5-FU to be available for the anabolic pathway. In fact, two phase II studies with S-1 in patients with NSCLC conducted in Japan demonstrated promising efficacy with an acceptable safety profile.[19,20]

Cisplatin is the backbone of treatment regimens for patients with advanced NSCLC (stage IIIb/stage IV). Cisplatin as a single agent has limited antitumor activity. Sandler et al.[23] reported an ORR for cisplatin alone in NSCLC of 11.1% (CR: 0.4%, PR: 10.7%). The higher ORR observed with cisplatin + S-1 in this study (23%) underlines that S-1 has an antitumor effect in patients with advanced NSCLC.

This is one of the first studies in North America to demonstrate that a fluoropyrimidine has an antitumor effect in patients with NSCLC; this builds on Japanese experience with this agent when administered as a single agent or in combination with cisplatin or irinotecan.[24] The prior lack of efficacy with 5-FU could be explained by the high DPD activity in NSCLC, as a component of S-1 inhibits the DPD enzyme and could explain the activity of S-1 in this patient population. A separate pilot trial by Sagar et al.[16] also demonstrated some potential benefit to a combination of capecitabine and carboplatin but at dose levels that proved too toxic for further evaluation. The study results are comparable to results obtained using established cisplatin-based regimens for treatment of patients with advanced NSCLC (stage IIIb/stage IV). Schiller et al.[25] conducted a randomized trial to compare the efficacy of three commonly used regimens with that of a reference regimen of cisplatin/paclitaxel. The cisplatin dose in the cisplatin/paclitaxel regimen and the cisplatin/docetaxel regimen was 75 mg/m^2 every 3 weeks, the same as used in this study. The ORRs using cisplatin with paclitaxel and cisplatin with docetaxel were 21% and 17%, respectively. Median time to progression was 3.4 months (2.8–3.9 months) for cisplatin/paclitaxel and 3.7 months (2.9–4.2 months) for cisplatin/docetaxel. The primary objective of this study of an ORR of $\geq$30% could not be reached. One of the reasons for this might be the lower dosage of S-1 in the study compared with that in Japanese studies.[20,24,26,27] However, the higher dosage of S-1 (30 mg/m^2) was not safe when combined with cisplatin 75 mg/m^2 on day 1 in a phase I dose-escalation study in patients with advanced gastric cancer.[21] Therefore, we investigated the combination regimen of the established dosage of S-1 (25 mg/m^2) and the standard dosage of cisplatin (75 mg/m^2) in this study. In fact, the results indicate that the doublet cisplatin + S-1 may have antitumor activity comparable to that of established cisplatin-based doublets. Ichinose et al.[20] and Kubota et al.[26] investigated the regimen of S-1 in combination with cisplatin on day 8, which shows promising results. Therefore, it is necessary to find the best regimen of S-1 + cisplatin combination in a randomized study in the future.

As with all cisplatin-based regimens, the S-1 + cisplatin regimen used in this study was associated with significant toxicity.[25,28–32] More than 55% of patients initiated at least four cycles of treatment, and 36% had six cycles initiated. Across all cycles, 42% of patients experienced AEs with maximum grade 3 toxicity, and 28% of patients experienced AEs with maximum grade 4 toxicity. This overall toxicity is lower than that observed with the treatment regimens of cisplatin/paclitaxel or cisplatin/docetaxel, for which maximum grade 4 toxicity was observed in 68% and 61% of patients, respectively.[25] The most common toxic effect of platinum-based doublet therapy is bone marrow suppression, particularly neutropenia and its consequences. In this study of S-1 + cisplatin, the incidence of grade 3 or 4 neutropenia was 28%, lower than that observed with established therapy regimens of cisplatin/paclitaxel (75%) or cisplatin/docetaxel (69%).[25] The incidence of death due to toxicity (3 of 58, 5%) observed in this study is consistent with that observed with other established regimens in advanced NSCLC, including cisplatin + taxanes therapies.[22]

While the S-1 + cisplatin regimen is active, the initial impression from this multicenter phase II trial is that it is unlikely to be superior to currently approved platinum-doublet regimens, which are currently administered in North America. For this reason, the present regimen would not be taken forward into a phase III trial. However, there is evidence that S-1 may be synergistic with other agents as well: preclinical data indicates that the epidermal growth factor receptor tyrosine kinase inhibitor gefitinib may enhance S-1 activity via downregulation of TS activity.[33] In addition, the combination of S-1 and docetaxel exhibited downregulation of both DPD and TS and did so to a greater extent than the combination of docetaxel and 5-FU.[34] An additional report suggests that histone deacetylase inhibitors may at least partially reverse fluoropyrimidine resistance by downregulating TS expression, although it is unclear whether this will enhance S-1 activity specifically.[35]

In summary, S-1 alone, and in combination with cisplatin, appears to be active in NSCLC. This is similar to the findings of Japanese investigators. In Japan, a phase III trial is being conducted by comparing S-1 + cisplatin versus cisplatin + docetaxel as first-line therapy for the patients with advanced NSCLC.[36] It also appears that the S-1 contributes activity in this regimen, as the platinums that are currently available in North America (cisplatin and carboplatin) actually have very limited activity as single agents in this disease. While this combination appears to be a potential treatment

regimen for the population of patients with NSCLC, this doublet does not appear to be superior to other platinum-based doublet regimens. However, in light of a growing body of data of other agents, which are already used for the therapy for NSCLC and may be associated with true synergy, further in vitro and clinical evaluation of S-1 is warranted to determine the potential optimal treatment regimen in this spectrum of diseases.

ACKNOWLEDGMENTS

Supported by Taiho Pharma, USA, Inc.

REFERENCES

1. American Cancer Society. Cancer Facts & Figures 2009. Atlanta, GA: American Cancer Society; 2009. Available at: http://www.cancer.org/downloads/STT/500809web.pdf. Accessed October 17, 2009.
2. Sandler A, Gray R, Perry MC, et al. Paclitaxel-carboplatin alone or with bevacizumab for non-small-cell lung cancer. *N Engl J Med* 2006;355:2542–2550.
3. NCCN Clinical Practice Guidelines in Oncology: Non-small Cell Lung Cancer. National Comprehensive Cancer Network, V.2.2010. Available at: http://www.nccn.org/professionals/physician_gls/PDF/nscl.pdf. Accessed April 20, 2010.
4. Scagliotti GV, Parikh P, von Pawel J, et al. Phase III study comparing cisplatin plus gemcitabine with cisplatin plus pemetrexed in chemotherapy-naive patients with advanced-stage non-small-cell lung cancer. *J Clin Oncol* 2008;26:3543–3551.
5. Fukui Y, Oka T, Nagayama S, et al. Thymidylate synthase, dihydropyrimidine dehydrogenase, orotate phosphoribosyltransferase mRNA and protein expression levels in solid tumors in large scale population analysis. *Int J Mol Med* 2008;22:709–716.
6. Fukushima M, Morita M, Ikeda K, et al. Population study of expression of thymidylate synthase and dihydropyrimidine dehydrogenase in patients with solid tumors. *Int J Mol Med* 2003;12:839–844.
7. Yang CT, Chang WC, Chen LH, et al. Concurrent 5-fluorouracil, leucovorin, etoposide, cisplatin and radiotherapy for locally advanced non-small cell lung cancer. *Changgeng Yi Xue Za Zhi* 1997;20:187–194.
8. Ball D, Smith J, Bishop J, et al. A phase III study of radiotherapy with and without continuous-infusion fluorouracil as palliation for non-small-cell lung cancer. *Br J Cancer* 1997;75:690–697.
9. Crawford J, O'Rourke M, Schiller JH, et al. Randomized trial of vinorelbine compared with fluorouracil plus leucovorin in patients with stage IV non-small-cell lung cancer. *J Clin Oncol* 1996;14:2774–2784.
10. Nakano T, Ikegami H, Nakamura S, et al. A phase II study of cisplatin, vindesine and continuously infused 5-fluorouracil in the treatment of advanced non-small-cell lung cancer. Osaka Lung Cancer Chemotherapy Study Group. *Br J Cancer* 1996;73:1096–1100.
11. Tanaka F, Yanagihara K, Ohtake Y, et al. p53 status predicts the efficacy of postoperative oral administration of tegafur (FT) for completely resected non-small cell lung cancer (NSCLC) (Meeting abstract). Proceedings of the Annual Meeting of the American Society of Clinical Oncology 1997;16:A1746.
12. Xu G, Rong T, Lin P. Adjuvant chemotherapy following radical surgery for non-small-cell lung cancer: a randomized study on 70 patients. *Chin Med J (Engl)* 2000;113:617–620.
13. Tanaka F, Miyahara R, Ohtake Y, et al. Advantage of post-operative oral administration of UFT (tegafur and uracil) for completely resected p-stage I-IIIa non-small cell lung cancer (NSCLC). *Eur J Cardiothorac Surg* 1998;14:256–262.
14. Wada H, Hitomi S, Teramatsu T. Adjuvant chemotherapy after complete resection in non-small-cell lung cancer. West Japan Study Group for Lung Cancer Surgery. *J Clin Oncol* 1996;14:1048–1054.
15. Wada H, Miyahara R, Tanaka F, et al. Postoperative adjuvant chemotherapy with PVM (Cisplatin + Vindesine + Mitomycin C) and UFT (Uracil + Tegafur) in resected stage I-II NSCLC (non-small cell lung cancer): a randomized clinical trial. West Japan Study Group for lung cancer surgery (WJSG). *Eur J Cardiothorac Surg* 1999;15:438–443.
16. Sagar B, Estaphan F, Spell DW, et al. A pilot phase II study of capecitabine with carboplatin in patients with advanced nonsmall cell lung cancer. *Int J Oncol* 2009;6, No. 1.
17. Shirasaka T, Shimamoto Y, Ohshimo H, et al. Development of a novel form of an oral 5-fluorouracil derivative (S-1) directed to the potentiation of the tumor selective cytotoxicity of 5-fluorouracil by two biochemical modulators. *Anticancer Drugs* 1996;7:548–557.
18. Tatsumi K, Fukushima M, Shirasaka T, et al. Inhibitory effect of pyrimidine, barbituric acid and pyridine derivatives on 5-fluorouracil degradation in rat liver extracts. *Jpn J Cancer Res* 1987;78:748–755.
19. Kawahara M, Furuse K, Segawa Y, et al; S-1 Cooperative Study Group (Lung Cancer Working Group). Phase II study of S-1, a novel oral fluorouracil, in advanced non-small-cell lung cancer. *Br J Cancer* 2001;85:939–943.
20. Ichinose Y, Yoshimori K, Sakai H, et al. S-1 plus cisplatin combination chemotherapy in patients with advanced non-small cell lung cancer: a multi-institutional phase II trial. *Clin Cancer Res* 2004;10:7860–7864.
21. Ajani JA, Faust J, Ikeda K, et al. Phase I pharmacokinetic study of S-1 plus cisplatin in patients with advanced gastric carcinoma. *J Clin Oncol* 2005;23:6957–6965.
22. Simon R. Optimal two-stage designs for phase II clinical trials. *Control Clin Trials* 1989;10:1–10.
23. Sandler J, Nemunaitis J, Denham C, et al. Phase III study of cisplatin with or without gemcitabine in patients with advanced non-small cell lung cancer. *J Clin Oncol* 2000;18:122–130.
24. Okamoto I, Nishimura T, Miyazaki M, et al. Phase II study of combination therapy with S-1 and irinotecan for advanced non-small cell lung cancer: West Japan Thoracic Oncology Group 3505. *Clin Cancer Res* 2008;14:5250–5254.
25. Schiller JH, Harrington D, Belani CP, et al. Comparison of chemotherapy regimens for advanced non-small cell lung cancer. *N Engl J Med* 2002;346:92–98.
26. Kubota K, Sakai H, Yamamoto N, et al. A multi-institution phase I/II trial of triweekly regimen with S-1 plus cisplatin in patients with advanced non-small cell lung cancer. *J Thorac Oncol* 2010;5:702–706.
27. Satouchi M, Kotani Y, Katakami N, et al. Randomized phase II study of two different schedules of gemcitabine and oral S-1 in chemo-naïve patients with advanced non-small cell lung cancer. *J Thorac Oncol* 2010;5:696–701.
28. Thienelt CD, Bunn PA Jr, Hanna N, et al. Multicenter phase I/II study of cetuximab with paclitaxel and carboplatin in untreated patients with stage IV non-small-cell lung cancer. *J Clin Oncol* 2005;23:8786–8793.
29. Millward MJ, Bishop JF, Friedlander M, et al. Phase II trial of a 3-hour infusion of paclitaxel in previously untreated patients with advanced non-small-cell lung cancer. *J Clin Oncol* 1996;14:142–148.
30. Zalcberg J, Millward M, Bishop J, et al. Phase II study of docetaxel and cisplatin in advanced non-small-cell lung cancer. *J Clin Oncol* 1998;16:1948–1953.
31. Hanna N, Bunn PA Jr, Langer C, et al. Randomized phase III trial comparing irinotecan/cisplatin with etoposide/cisplatin in patients with previously untreated extensive-stage disease small-cell lung cancer. *J Clin Oncol* 2006;24:2038–2043.
32. Herbst RS, O'Neill VJ, Fehrenbacher L, et al. Phase II study of efficacy and safety of bevacizumab in combination with chemotherapy or erlotinib compared with chemotherapy alone for treatment of recurrent or refractory non small-cell lung cancer. *J Clin Oncol* 2007;25:4743–4750.
33. Okabe T, Okamoto I, Tsukioka S, et al. Synergistic antitumor effect of S-1 and the epidermal growth factor receptor inhibitor gefitinib in non-small cell lung cancer cell lines: role of gefitinib-induced down-regulation of thymidylate synthase. *Mol Cancer Ther* 2008;7:599–606.
34. Wada Y, Yoshida K, Suzuki T, et al. Synergistic effects of docetaxel and S-1 by modulating the expression of metabolic enzymes of 5-fluorouracil in human gastric cancer cell lines. *Int J Cancer* 2006;119:783–791.
35. Lee J-H, Park J-H, Jung Y, et al. Histone deacetylase inhibitor enhances 5-fluorouracil cytotoxicity by down-regulating thymidylate synthase in human cancer cells. *Mol Cancer Ther* 2006;5:3085–3095.
36. Okamoto I, Fukuoka M. S-1: a new oral fluoropyrimidine in the treatment of patients with advanced non-small-cell lung cancer. *Clin Lung Cancer* 2009;10:290–294.

Original Article

Early Findings on Toxicity of Proton Beam Therapy With Concurrent Chemotherapy for Nonsmall Cell Lung Cancer

Samir Sejpal, MD[1]; Ritsuko Komaki, MD[1]; Anne Tsao, MD[2]; Joe Y. Chang, MD, PhD[1]; Zhongxing Liao, MD[1]; Xiong Wei, MD[1]; Pamela K. Allen, PhD[1]; Charles Lu, MD[2]; Michael Gillin, PhD[3]; and James D Cox, MD[1]

BACKGROUND: Concurrent chemoradiation therapy, the standard of care for locally advanced nonsmall cell lung cancer (NSCLC), can cause life-threatening pneumonitis and esophagitis. X-ray (photon)-based radiation therapy (RT) often cannot be given at tumoricidal doses without toxicity to proximal normal tissues. We hypothesized that proton beam therapy for most patients with NSCLC could permit higher tumor doses with less normal-tissue toxicity than photon RT delivered as 3-dimensional conformal RT (3D-CRT) or intensity-modulated RT (IMRT). **METHODS:** We compared the toxicity of proton therapy+concurrent chemotherapy in 62 patients with NSCLC (treatment period 2006-2008) with toxicity for patients with similar disease given 3D-CRT+chemotherapy (n = 74; treatment period 2001-2003) or IMRT+chemotherapy (n = 66; treatment period 2003-2005). Proton therapy to the gross tumor volume was given with weekly intravenous paclitaxel (50 mg/m^2) and carboplatin (area under the curve 2 mg/mL/min). The primary endpoint was toxicity (Common Terminology Criteria for Adverse Events version 3.0). **RESULTS:** Median follow-up times were 15.2 months (proton), 17.9 months (3D-CRT), and 17.4 months (IMRT). Median total radiation dose was 74 Gy(RBE) for the proton group versus 63 Gy for the other groups. Rates of severe (grade $\geq$3) pneumonitis and esophagitis in the proton group (2% and 5%) were lower despite the higher radiation dose (3D-CRT, 30% and 18%; IMRT, 9% and 44%; $P<.001$ for all). **CONCLUSIONS:** We found that higher doses of proton radiation could be delivered to lung tumors with a lower risk of esophagitis and pneumonitis. A randomized comparison of IMRT versus proton therapy is underway. ***Cancer*** **2011;117:3004-13.** © *2011 American Cancer Society.*

KEYWORDS: lung cancer, toxicity, protein therapy, esophagitis, pneumonitis.

Lung cancer is the most common cause of death from cancer in the United States and in most urbanized countries. More than three-quarters of patients have the nonsmall cell lung cancer (NSCLC) histotype. Surgical resection is the preferred treatment for localized NSCLC, but more than one-third of patients present with locally advanced, unresectable tumors. Concurrent radiation therapy and chemotherapy is believed to offer these patients the highest potential for prolonged disease-free and overall survival.[1]

The main problems associated with concurrent chemoradiation therapy for lung cancer are acute and subacute toxicity, primarily esophageal reactions with odynophagia and treatment-related pneumonitis that can be life-threatening or lethal. These toxic effects adversely affect quality of life for the patients and limit the dose of radiation that can be administered. Advances in radiation techniques such as highly conformal intensity-modulated radiation therapy (IMRT) or proton therapy may reduce the risk of pneumonitis.[2]

Proton beam therapy differs from traditional x-ray (photon) therapy in that the maximum dose is concentrated in the tumor and the dose beyond the tumor is negligible. Treatment planning studies suggest that higher tumor doses can be achieved with proton therapy than with advanced x-ray techniques for locally advanced NSCLC, with a lower risk of common side effects.[3]

Corresponding author: James D Cox, MD, Department of Radiation Oncology, Unit 97, The University of Texas MD Anderson Cancer Center, 1515 Holcombe Boulevard, Houston, TX 77030; jcox@mdanderson.org

[1]Department of Radiation Oncology, The University of Texas MD Anderson Cancer Center, Houston, Texas; [2]Department of Thoracic/Head & Neck Medical Oncology, The University of Texas MD Anderson Cancer Center, Houston, Texas; [3]Department of Radiation Physics, The University of Texas MD Anderson Cancer Center, Houston, Texas

Portions of this study were presented at the Chicago Multidisciplinary Symposium in Thoracic Oncology, November 13-15, 2008, Chicago, Illinois, and the 47th International Conference of the Proton Therapy Co-Operative Group, May 19-24, 2008, Jacksonville, Florida.

DOI: 10.1002/cncr.25848, **Received:** August 19, 2010; **Revised:** October 7, 2010; **Accepted:** November 10, 2010, **Published online** January 24, 2011 in Wiley Online Library (wileyonlinelibrary.com)

Proton therapy was initiated at The University of Texas MD Anderson Cancer Center in May 2006 with a specific program in combined-modality treatment for NSCLC. We report here our early experience with acute and subacute toxicity from proton therapy and concurrent chemotherapy for locally advanced NSCLC.

MATERIALS AND METHODS

Patients

Between May 2006 and June 2008, 62 consecutive patients with locally advanced, unresectable NSCLC were enrolled in 1 of 2 phase 2 clinical trials that had been approved by the MD Anderson Cancer Center institutional review board. All participants provided written informed consent. The first protocol (NCT00495170) enrolled patients with previously untreated stage 3 NSCLC (according to the 2002 staging system of the American Joint Committee on Cancer[4]). The other protocol (NCT00991094) had more permissive inclusion criteria, allowing enrollment of patients with NSCLC at any stage, prior malignant tumors, and postoperative recurrences. Patients in the second protocol were typically selected for proton therapy because of comorbid conditions, especially limited pulmonary function. This early report of acute toxicity includes patients from both trials.

Pretreatment Evaluation and Exclusion Criteria

Findings from a complete history and physical examination, including performance status, weight loss, and concurrent nonmalignant disease, were recorded. Exclusion criteria were prior thoracic irradiation, malignant pleural effusion, Karnofsky performance status[5] score <60, and weight loss $>10\%$ during the 6 months before diagnosis. Laboratory studies included complete blood counts with differential and platelet count and measurement of serum creatinine, blood urea nitrogen, electrolytes, lactate dehydrogenase, aspartate aminotransferase, alanine aminotransferase, alkaline phosphatase, and total bilirubin levels. Plain chest films, computed tomography (CT) of the thorax and upper abdomen, and positron emission tomography (PET) were required. Mediastinal lymph nodes suspected of harboring disease but with negative PET findings were sampled via mediastinoscopy with biopsy or by bronchoscopy with endobronchial ultrasonography and fine needle aspiration. CT or magnetic resonance imaging scans of the brain were required before proton therapy; pulmonary function tests were recommended but not required. Disease was staged according to the 2002 criteria of the American Joint Committee on Cancer.[4]

Treatments

Radiation therapy

All patients in the proton group received concurrent proton therapy and chemotherapy; no patient in the proton group received x-ray (photon) irradiation as any component of treatment. Proton therapy was delivered using a variable energy synchrotron in doses expressed as Gy(RBE), where Gy is the absorbed dose and RBE (relative biological effectiveness) is the radiation weighting factor, which was 1.1. We used 3-dimensional (3D) conformal techniques to plan and deliver the proton therapy, with 2-4 fields used for each patient.[3] Treatment simulations took place while the patients lay supine, with arms extended over the head, in a custom-fitted vacuum cushion (Vac-Lok, CIVCO Medical Solutions, Kalona, Iowa) that also immobilized the lower extremities. Four-dimensional CT[6] was used to identify the path of the tumors throughout the respiratory cycle. Tumor delineation was aided by PET. Gross tumor volume (GTV) included all nodal disease documented via imaging (CT or PET) or tissue analysis (mediastinoscopy or bronchoscopy). Ipsilateral hilar lymph nodes were included in the GTV if mediastinal or subcarinal lymph nodes showed evidence of disease. Contralateral mediastinal, contralateral hilar, or supraclavicular lymph nodes were included in the GTV only when those nodes showed abnormalities on imaging or pathological analysis. For the 26 patients (42%) who received induction chemotherapy, the GTV consisted of gross disease measured after chemotherapy plus any lymph node stations considered abnormal before chemotherapy. An 8-mm margin was extended beyond the GTV for presumed microscopic tumor extension. Another 5-mm margin was added to account for range and set-up uncertainties.

Constraints on the radiation doses to specific organs were:

Spinal cord: 0% to receive $\geq$45 Gy(RBE);

Normal lung: $<35\%$ to receive 20 Gy(RBE); mean dose to entire lung: <20 Gy(RBE);

Heart: $<100\%$ to receive 40 Gy(RBE); $<50\%$ to receive 50 Gy(RBE);

Esophagus: $<50\%$ to receive 60 Gy(RBE).

Chemotherapy

All patients received concurrent carboplatin-and-paclitaxel chemotherapy as weekly intravenous infusions

during proton therapy. Paclitaxel was administered at 50 mg/m^2 of body surface area, and carboplatin was given at an area under the curve level of 2 mg/mL/min. Standard anti-emetics were allowed at the discretion of the medical oncologist. Concurrent chemotherapy could be withheld or the doses modified if toxicity was encountered as follows. If the absolute neutrophil count decreased to <1000/μL or the platelet count decreased to <75,000/μL, carboplatin and paclitaxel were withheld until the myelosuppression resolved. If grade 3 dysphagia appeared, weekly carboplatin and paclitaxel were withheld and then readministered at 50% of the original dose at the discretion of the medical oncologist.

Neoadjuvant and adjuvant chemotherapy at systemic doses were allowed in either trial. The choice of chemotherapy type, dosing, and timing was at the discretion of the treating physicians. Only the chemotherapy given concurrently with the proton therapy was standardized.

Treatment Evaluation

Patients were evaluated at least weekly during treatment, at 4-6 weeks after treatment, and then every 3 months for 2 years and every 6 months thereafter. Adverse events were scored using Common Terminology Criteria version 3.0. The first follow-up visit included an interval medical history and physical examination, hematological studies, chest x-ray, and CT examination. A follow-up PET examination was conducted during the first 3 to 4 months after treatment. Thereafter, chest x-ray plus CT examinations were alternated with PET examinations.

Data on survival, time to progression, and failure patterns are being collected in the ongoing phase 2 trials. Early information on survival is reported here for completeness.

Comparison Groups

This report focuses on early toxicity of proton beam therapy and concurrent chemotherapy. The results are compared with historical results from 2 previously approved retrospective chart reviews of toxicity after x-ray (photon) RT (either IMRT[2,7] or 3D conformal RT [3D-CRT][8]) with concurrent chemotherapy as definitive treatment for locally advanced, unresectable NSCLC. Concurrent chemoradiation therapy has been the standard of care at the MD Anderson Cancer Center since the 1990s, although radiation delivery techniques evolved from 2-dimensional CRT to 3D-CRT in the late 1990s and then to IMRT in the early 2000s. We chose 2 comparison groups because the National Comprehensive Cancer Network still considers 3D-CRT with concurrent chemotherapy the standard of care for NSCLC (http://www.nccn.org/professionals/physician_gls/PDF/nscl.pdf) and because our institutional experience suggests that IMRT is associated with less pulmonary toxicity than 3D-CRT.[7] The median radiation dose in both comparison groups was 63 Gy; the survey periods were 2001-2003 for 3D-CRT and 2003-2005 for IMRT.[2,7,8]

Statistical Analyses

Stata/SE 11.1 (Stata Corp LP, College Station, Texas) was used for data analyses. Pearson's chi-square test was used to assess measures of association in frequency tables. Survival was calculated using the Kaplan-Meier method. The equality of means for continuous variables was assessed using t tests. $P \leq .05$ was considered statistically significant. Statistical tests were based on a 2-sided significance level. Mantel-Haenszel estimates were used to assess specific interactions between disease stage and toxicity grade by treatment group.

RESULTS

Patient characteristics, treatment characteristics, and follow-up information for all 3 groups are shown in Table 1. Thirty-seven patients were enrolled in the prospective trial of proton beam therapy for previously untreated stage 3 NSCLC, and 25 patients were enrolled in the trial that allowed disease at other stages. The median total proton dose was 74 Gy(RBE). Details of concurrent chemotherapy are also shown in Table 1. The median number of concurrent weekly chemotherapy cycles was 6; 23% of patients experienced treatment delays, 13% required chemotherapy dose reductions, and 10% did not complete the full course of concurrent chemotherapy. Twenty-six patients received neoadjuvant chemotherapy (median 3 cycles of systemic dose chemotherapy). Eight patients were known to proceed to adjuvant chemotherapy after a median 2 cycles of concurrent treatment.

Toxicity for all 3 patient groups is shown in Table 2. No differences in hematological toxicity (anemia, thrombocytopenia, neutropenia, and leukopenia) were found between groups (data not shown). The most common toxicity of concurrent proton therapy and chemotherapy (experienced by 60 patients [97%]) was dermatitis; in most cases this was mild, with only 15 patients (24%) experiencing grade 3 reactions. Esophageal reactions, usually odynophagia, were observed in 49 (79%) patients; 27 (43%) patients experienced grade 2 or higher reactions

Table 1. Baseline and Treatment Characteristics of Patients Treated With Photons Versus Protons

Characteristic	3D Conformal Concurrent Chemoradiation (n=74)	IMRT Concurrent Chemoradiation (n=66)	Proton Beam Concurrent Chemoradiation (n=62)	*P*
Treatment period	2001-2003	2003-2005	2006-2008	
Age, y, median (range)	61 (38-81)	62 (38-82)	67 (38-81)	.04[a]
Sex				
Men	37 (50%)	40 (61%)	34 (55%)	.453[b]
Women	37 (50%)	26 (39%)	28 (45%)	
Karnofsky performance score				
100	0	2 (3%)	1 (2%)	.05[b]
90	22 (30%)	9 (13%)	22 (35%)	
80	44 (59%)	39 (59%)	29 (47%)	
70	4 (5%)	13 (20%)	7 (11%)	
60	4 (5%)	3 (5%)	3 (5%)	
Weight loss				
<5%	71 (96%)	58 (88%)	48 (77%)	.005[b]
≥5%	3 (4%)	8 (12%)	14 (23%)	
Tumor histology				
Squamous	27 (36%)	17 (26%)	25 (40%)	.19[b]
Nonsquamous	47 (64%)	49 (74%)	37 (60%)	
Ethnicity				
White	65 (88%)	46 (70%)	37 (60%)	.001[b]
Nonwhite	9 (12%)	20 (30%)	25 (40%)	
Prior malignancy				
Yes	10 (14%)	18 (27%)	17 (27%)	.13[b]
No	64 (86%)	48 (73%)	45 (73%)	
Clinical disease stage				
1B	0	0	2 (3%)	.002[b]
2A	2 (3%)	0	0	
2B	2 (3%)	3 (5%)	5 (8%)	
3A	30 (41%)	15 (23%)	25 (40%)	
3B	34 (46%)	38 (58%)	17 (27%)	
4	6 (8%)	7 (11%)	5 (8%)	
Recurrent	0	3 (4%)	8 (13%)	
Lymph node involvement				
Yes	59 (80%)	60 (91%)	50 (81%)	.151[b]
No	15 (20%)	6 (9%)	12 (19%)	
Tumor location				
Left lung	30 (41%)	22 (33%)	28 (45%)	.68[b]
Right lung	43 (58%)	42 (64%)	33 (53%)	
Mediastinum	1 (1%)	2 (3%)	1 (2%)	
Total radiation dose, median (range)	63 Gy (60-69.9)	63 Gy (60-76)	74 Gy(RBE) (63-80.95)	<.001[a]
Gross tumor volume, cm^3, median (range)	141.1 (6.2-1186.1)	203.1 (20.9-817.9)	67.45 (4.1-753.2)	.04[a]
Radiation therapy completed				
Yes	74	63	61	.151[b]
No	0	3	1	
Delay until completion of radiation, d				
≤5	4	22	6	.442[b]
>5	1	2	2	
Induction chemotherapy				
Yes	42 (57%)	22 (33%)	23 (37%)	.01[b]
No	32 (43%)	44 (67%)	39 (63%)	

(Continued)

Table 1. (Continued)

Characteristic	3D Conformal Concurrent Chemoradiation (n=74)	IMRT Concurrent Chemoradiation (n=66)	Proton Beam Concurrent Chemoradiation (n=62)	*P*
No. of induction chemotherapy cycles				
0	32	44	39	
1	1	5	1	
2	24	9	8	
3	12	5	4	
4+	3	0	6	
Unknown	2	3	4	
Concurrent chemotherapy				
Yes	74	66	62	
No	0	0	0	
No. of concurrent chemotherapy cycles				
1	1	0	0	
2	2	1	2	
3	1	6	2	
4	2	2	1	
5	0	5	1	
6	67	43	54	
7	0	0	2	
Unknown	1	9	0	
Adjuvant chemotherapy				
Yes	15 (20%)	32 (48%)	9 (14%)	<.001[b]
No	59 (80%)	34 (52%)	53 (86%)	
No. adjuvant chemotherapy cycles				
1	0	0	4	
2	4	11	2	
3	3	11	2	
4+	5	0	1	
Unknown	3	10	0	
Vital status at last follow-up				<.001[b]
Alive with disease	4	4	20	
Alive without disease	9	11	20	
Alive, disease status unknown	1	0	0	
Dead of disease	40	38	18	
Dead of intercurrent disease	0	5	1	
Dead of unknown causes	20	8	3	
Follow-up time, mo, median (range)				<.001[a]
All patients	17.9 (2.3-76.1)	17.4 (1.8-65.5)	15.2 (3.3-27.4)	
Patients alive at last follow-up	63.3 (24.0-79.1)	45.6 (1.8-65.5)	15.2 (5.2-27.4)	

3D indicates 3-dimensional; IMRT, intensity-modulated radiation therapy.
[a] Analysis of variance.
[b] Chi-square test.

(ie, symptomatic and affecting eating or swallowing, with intravenous fluids indicated for <24 hours), but only 3 (5%) patients experienced grade 3 reactions (ie, symptomatic and severely affecting eating/swallowing, with intravenous fluids, tube feedings, or total parenteral nutrition indicated for ≥24 hours). Treatment-related pneumonitis was noted in 49 patients (79%), but only 1 (2%) patient experienced pneumonitis of grade 3 or higher (ie, symptomatic [rather than only visible on radiography], interfering with activities of daily living, and requiring supplemental oxygen) (Table 2). Because differences in tumor volume (67 cm^3 for the proton group, 141 cm^3 for the 3D-CRT group, and 203 cm^3 for the IMRT group [Table 1]) could have influenced these results, we

Table 2. Acute Nonhematologic Toxicity After Photon Versus Proton Therapy for Nonsmall Cell Lung Cancer

Toxicity and Treatment	Grade 0	Grade 1	Grade 2	Grade 3	Grade 4	Grade 5	Unknown	*P*
Esophagitis								<.001
Chemotherapy+3D-CRT	3 (4)	25 (34)	33 (45)	13 (18)	0	0	0	
Chemotherapy+IMRT	4 (6)	9 (14)	24 (36)	26 (39)	3 (4.5)	0	0	
Chemotherapy+PBT	13 (21)	22 (35.5)	24 (39)	3 (5)	0	0	0	
Pneumonitis								<.001
Chemotherapy+3D-CRT	23 (31)	9 (12)	20 (27)	22 (30)	0	0	0	
Chemotherapy+IMRT	19 (29)	24 (36)	17 (26)	4 (6)	0	2 (3)	0	
Chemotherapy+PBT	13 (21)	30 (48)	18 (29)	1 (2)	0	0	0	
Dermatitis								<.001
Chemotherapy+3D-CRT	6 (8)	54 (73)	9 (12)	5 (7)	0	0	0	
Chemotherapy+IMRT	5 (8)	33 (50)	17 (26)	11 (17)	0	0	0	
Chemotherapy+PBT	2 (3)	22 (35.5)	23 (37)	15 (24)	0	0	0	
Fatigue								.002
Chemotherapy+3D-CRT	0	20 (24)	28 (34)	24 (29)	2 (2)	0	0	
Chemotherapy+IMRT	12 (18)	16 (24)	27 (41)	10 (15)	1 (1.5)	0	0	
Chemotherapy+PBT	3 (5)	12 (19)	32 (52)	12 (19)	3 (5)	0	0	

All data are expressed as No. of patients (%).
3D-CRT indicates 3-dimensional conformal radiation therapy; IMRT, intensity-modulated radiation therapy; PBT, proton beam therapy.

Table 3. Acute Grade ≥2 Nonhematologic Toxicity After Photon Versus Proton Therapy for Nonsmall Cell Lung Cancer According to Gross Tumor Volume

Toxicity and Treatment	Gross Tumor Volume											
	≤50 cm^3		≤100 cm^3		≤200 cm^3		≤300 cm^3		≤400 cm^3		≤500 cm^3	
	Events (%)	*P*	Events (%)	*P*	Events (%)	*P*	Events (%)	*P*	Events (%)	*P*	Events (%)	*P*
Esophagitis												
Chemotherapy+3D-CRT	6 (67)	.160	16 (62)	.013	27 (55)	<.001	32 (57)	<.001	38 (61)	<.001	41 (60)	<.001
Chemotherapy+IMRT	3 (100)		6 (75)		22 (79)		33 (80)		35 (80)		43 (83)	
Chemotherapy+PBT	11 (48)		19 (45)		24 (44)		25 (44)		25 (42)		26 (43)	
Pneumonitis												
Chemotherapy+3D-CRT	7 (78)	.017	17 (65)	<.001	31 (63)	<.001	36 (64)	<.001	37 (60)	<.001	38 (56)	<.001
Chemotherapy+IMRT	1 (33)		3 (38)		11 (39)		17 (41)		18 (41)		19 (37)	
Chemotherapy+PBT	4 (17)		10 (24)		17 (31)		17 (30)		18 (31)		18 (30)	
Dermatitis												
Chemotherapy+3D-CRT	0 (0)	.035	5 (19)	.03	8 (16)	.001	10 (18)	<.001	12 (19)	<.001	13 (19)	<.001
Chemotherapy+IMRT	1 (33)		3 (38)		10 (36)		16 (39)		17 (39)		21 (40)	
Chemotherapy+PBT	14 (61)		16 (38)		33 (60)		35 (61)		37 (63)		37 (62)	
Fatigue												
Chemotherapy+3D-CRT	5 (56)	.671	16 (62)	.227	33 (67)	.001	37 (66)	.001	43 (69)	<.001	49 (72)	.001
Chemotherapy+IMRT	2 (67)		6 (75)		16 (57)		23 (56)		24 (55)		29 (56)	
Chemotherapy+PBT	18 (78)		30 (71)		40 (73)		42 (74)		44 (75)		45 (75)	

3D-CRT indicates 3-dimensional conformal radiation therapy; IMRT, intensity-modulated radiation therapy; PBT, proton beam therapy.

compared toxicity according to tumor volume and found that rates of grade ≥2 pneumonitis were lower after proton therapy at every tumor volume (Table 3). We further found that disease stage was related to the severity of esophagitis in the 3D-CRT group, but not to the severity of pneumonitis, dermatitis, or fatigue in any treatment group (Table 4). Finally, we found that toxicity from concurrent proton therapy and chemotherapy was not affected by receipt of neoadjuvant therapy, with no differences observed in the incidence or severity of esophagitis, pneumonitis, fatigue, dermatitis, or hematological variables (data not shown).

Table 4. Disease Stage and Acute Toxicity After Photon Versus Proton Therapy for Nonsmall Cell Lung Cancer

Toxicity and Disease Stage	Treatment and Toxicity Grade																	
	3D-CRT						IMRT						PBT					
	0	1	2	3	4	5	0	1	2	3	4	5	0	1	2	3	4	5
Esophagitis[a]																		
1B	—	—	—	—	—	—	—	—	—	—	—	—	0	1	1	0	0	0
2A	0	0	2	0	0	0	—	—	—	—	—	—	—	—	—	—	—	—
2B	1	0	0	1	0	0	1	0	1	1	0	0	3	2	0	0	0	0
3A	0	14	13	3	0	0	1	5	5	4	0	0	4	11	10	0	0	0
3B	2	9	16	7	0	0	2	3	15	16	2	0	3	3	9	2	0	0
4	0	2	2	2	0	0	0	1	3	2	1	0	2	0	2	1	0	0
Recurrent	—	—	—	—	—	—	0	0	0	3	0	0	1	5	2	0	0	0
Pneumonitis[b]																		
1B	—	—	—	—	—	—	—	—	—	—	—	—	0	1	1	0	0	0
2A	0	0	1	1	0	0	—	—	—	—	—	—	—	—	—	—	—	—
2B	1	0	1	0	0	0	0	1	1	1	0	0	0	3	2	0	0	0
3A	8	5	9	8	0	0	6	2	6	1	0	0	2	15	7	1	0	0
3B	9	4	9	12	0	0	12	15	7	2	0	2	5	7	5	0	0	0
4	5	0	0	1	0	0	0	4	3	0	0	0	2	2	1	0	0	0
Recurrent	—	—	—	—	—	—	1	2	0	0	0	0	4	2	2	0	0	0
Dermatitis[c]																		
1B	—	—	—	—	—	—	—	—	—	—	—	—	0	2	0	0	0	0
2A	0	2	0	0	0	0	—	—	—	—	—	—	—	—	—	—	—	—
2B	0	2	0	0	0	0	1	1	1	0	0	0	0	2	1	2	0	0
3A	3	22	3	2	0	0	0	10	2	3	0	0	1	9	12	3	0	0
3B	3	24	4	3	0	0	3	16	12	7	0	0	1	4	7	5	0	0
4	0	4	2	0	0	0	1	3	2	1	0	0	0	0	3	2	0	0
Recurrent	—	—	—	—	—	—	0	3	0	0	0	0	0	5	0	3	0	0
Fatigue[d]																		
1B	—	—	—	—	—	—	—	—	—	—	—	—	0	0	1	0	1	0
2A	0	1	0	1	0	0	—	—	—	—	—	—	—	—	—	—	—	—
2B	0	0	0	2	0	0	2	1	0	0	0	0	0	1	3	1	0	0
3A	0	10	13	7	0	0	3	3	7	2	0	0	2	5	15	3	0	0
3B	0	8	12	13	1	0	6	10	15	6	1	0	0	3	9	4	1	0
4	0	1	3	1	1	0	1	1	4	1	0	0	0	0	2	3	0	0
Recurrent	—	—	—	—	—	—	0	1	1	1	0	0	1	3	2	1	1	0

3D-CRT indicates 3-dimensional conformal radiation therapy; IMRT, intensity-modulated radiation therapy; PBT, proton beam therapy.
[a] $P = .042$ for 3D-CRT, .333 for IMRT, and .155 for PBT (Mantel-Haenszel, not significant).
[b] $P = .412$ for 3D-CRT, .388 for IMRT, and .655 for PBT (Mantel-Haenszel, not significant).
[c] $P = .953$ for 3D-CRT, .537 for IMRT, and .315 for PBT.
[d] $P = .324$ for 3D-CRT, .911 for IMRT, and .237 for PBT.

Preliminary findings on survival are as follows. Median overall survival times were 17.7 months for the 3D-CRT group, 17.6 months for the IMRT group, and 24.4 months for the proton therapy group (log-rank $P = 0.1061$ [not significant]).

DISCUSSION

This is the first report of proton beam therapy with concurrent chemotherapy for NSCLC that permits evaluation of acute and subacute toxicity. We recognize that any comparison of treatment outcomes that involves 1 or more retrospective components will be associated with selection bias; nevertheless, we believe that historical comparisons such as the ones made here are important.

Unresectable NSCLC is far more common and lethal than the other diseases treated with proton therapy to date. Concurrent chemoradiation therapy has emerged as the treatment of choice for unresectable NSCLC, but the sensitivity of the normal lung limits the radiation doses that can be delivered. Local control rates at conventional radiation doses are poor, ranging from 20% to 50%, depending on the method of evaluation.[9] Findings from a phase 1/2 trial by the Radiation Therapy Oncology Group (RTOG),[10] a phase 1 trial by the North Central Cancer Treatment Group,[11] and a phase 2 trial by the

Table 5. Pneumonitis and Esophagitis in Other Trials of Chemoradiation Therapy for Locally Advanced Nonsmall Cell Lung Cancer

Study	No. of Patients	Esophagitis, %	Pneumonitis, %
Bradley et al[10]	53	40[a]	23
Socinski et al[12]	37	16	11
Antonadou et al[15]	73	84	56
Komaki et al[16]	62	35	16
Leong et al[17]	60	15	NR
Senzer[18]	100	21	NR
Movsas et al[19]	243	34	16.7
Wei et al[20]	215	20.5	NR
Current study	62	5	2

All toxicities are grade ≥3 unless noted otherwise.
NR indicates not reported.
[a] Grade ≥2 esophagitis; grade ≥3 esophagitis not reported.

Cancer and Leukemia Group B[12] confirm that the maximum tolerated dose of x-ray (photon) therapy, given as 3D-CRT with paclitaxel- and carboplatin-based chemotherapy, is 74 Gy. If the use of protons allowed the radiation dose to the tumor to be increased without increasing the toxicity of the concurrent treatment, this could be an important factor in improving outcome.

Concurrent chemoradiation therapy has been the standard of care for locally advanced NSCLC at the MD Anderson Cancer Center since the 1990s. The transition from 2D-RT to 3D-CRT took place in 1997.[13,14] The transition from 3D-CRT to IMRT occurred in 2004, and results comparing these 2 techniques have been reported elsewhere.[2,7] Studies of tumor motion and methods of managing it also took place during 2003-2005[6] and were used as the basis for addressing tumor motion with IMRT and with proton therapy. Nevertheless, when this report was written, IMRT was not considered standard throughout the United States, which led to our including a comparison group treated with 3D-CRT as well as another group treated with IMRT during the past decade.

This report focuses only on acute and subacute toxicity, because our follow-up time is too short to evaluate tumor control and survival. Findings from other trials of concurrent chemoradiation therapy for NSCLC are shown in Table 5.[10,12,15-20] Notably, our median total dose from proton therapy as reported here was 74 Gy(RBE), which is more than 15% higher than the standard 63-Gy dose used in most NSCLC trials such as RTOG 9410.[21] Both phase 2 trials that used 74 Gy (photons) with carboplatin and paclitaxel[10,12] have shown substantially higher rates of severe (grade ≥3) pneumonitis than the current experience (Table 5). Rates of severe esophagitis are more difficult to compare directly, because the RTOG report[10] included only grade ≥2 esophagitis. Nevertheless, the rate of grade ≥2 esophagitis in that study (40%) compared favorably with the rate in the current study (43%).

Treatment-related pneumonitis is the most serious adverse effect of radiation or chemoradiation in NSCLC. It occurs predominantly within 6 months of treatment[22] and can contribute to the death of patients. In the MD Anderson Cancer Center experience with 3D-CRT given at a median total dose of 63 Gy, 32% of patients had treatment-related pneumonitis of grade 3 or higher.[2] Pneumonitis is well known to be related to the volume of normal lung irradiated[22-25]; hence in cooperative group studies, a limit is placed on the volume of normal lung that can receive a total dose of 20 Gy or more. Findings from treatment planning studies[3] suggest that proton beam therapy could decrease the volume of normal lung irradiated compared with x-ray treatments (3D-CRT and IMRT) even while delivering higher total radiation doses to the tumor. Our experience to date supports this hypothesis.

Esophageal reactions are rarely life-threatening, but the odynophagia resulting from concurrent chemoradiation therapy can profoundly hinder quality of life during treatment and for weeks thereafter. Such reactions are relatively common (Tables 2, 4, 5); in an RTOG study of the cytoprotectant amifostine to reduce dysphagia and odynophagia from concurrent chemoradiation for NSCLC,[19] the rate of severe (≥grade 3) esophageal reactions was 34% in the control (no-amifostine) group (n = 122). In the present study, we found that proton beam therapy produced severe esophagitis in only 5% of patients.

The relatively high rate of dermatitis in the proton group probably reflects the higher surface dose of protons versus photons and the use of relatively few proton beams (2-4 per patient) to minimize the exposure of normal lung tissue. In any event, dermatitis associated with proton therapy was rarely severe (24% grade 3 and no grade 4-5 [Table 2]) and was effectively treated with supportive measures without the need to delay therapy.

Our study did have several shortcomings related to the use of retrospective data for comparison, including substantial differences in pretreatment assessments (especially imaging) and treatment-planning capabilities[7] over the periods of study and the heterogeneity of the patient populations. The difference in baseline GTV between the 3 groups in particular could be attributable to heterogeneity of disease stage, but also to the increasing use of more rigorous evaluations of nodal disease (eg, PET, endoscopic ultrasonography) and the development of highly

conformal planning and delivery techniques over the periods of study, both of which might be expected to lead to smaller GTVs. The proton therapy group was itself somewhat heterogeneous because of the inclusion of 25 patients with any stage (including recurrent) disease; however, a separate analysis of only those patients with previously untreated stage 3 disease showed similar rates of grade 3 toxicity (dermatitis 13.3%, esophagitis 6.7%, pneumonitis 3.3%) and no grade 4-5 toxicity.[26] Moreover, our analysis of toxicity according to GTV revealed that most toxicities were independent of tumor size within the groups and that the rate of pneumonitis was lower in the proton group regardless of tumor size (Table 3) and disease stage (Table 4). Despite these acknowledged shortcomings, it seemed important nevertheless to have clinical data on the potential toxicity of proton therapy before proceeding to a randomized trial, particularly one involving a higher total radiation dose. Some strengths that may warrant such comparisons include the consistency of normal-tissue dose constraints over the 3 treatment periods (2001-2003 for 3D-CRT, 2003-2005 for IMRT, and 2006-2008 for proton therapy). These dose constraints were derived from those used by the RTOG, of which MD Anderson Cancer Center has been a participating member for more than 2 decades. Moreover, tumor motion has been accounted for in the same way since 2004; specifically, 4-dimensional CT scanning is used during treatment simulation and planning to develop individualized GTVs and clinical target volumes.

This promising early experience with concurrent chemotherapy and proton therapy has led us to design a prospective randomized comparative trial of proton therapy versus IMRT, both with concurrent chemotherapy, for stage 2/3 NSCLC (ClinicalTrials.gov identifier NCT00495040). In that trial, patients are randomly assigned to receive IMRT+chemotherapy or proton beam therapy+chemotherapy. Both arms require that the GTV be treated to the same total dose [74 Gy of IMRT; 74 Gy(RBE) of proton therapy] in the same fractionation [2 Gy or 2 Gy(RBE) per fraction]. Primary endpoints are local tumor control and severe (≥grade 3) treatment-related pneumonitis. This trial, a joint effort between Massachusetts General Hospital and MD Anderson Cancer Center, is supported in part by a grant from the National Cancer Institute (P01CA021239).

CONFLICT OF INTEREST DISCLOSURES

Funding was provided by The University of Texas MD Anderson Cancer Center.

REFERENCES

1. Furuse K, Fukuoka M, Kawahara M, et al. Phase III study of concurrent versus sequential thoracic radiotherapy in combination with mitomycin, vindesine, and cisplatin in unresectable stage III non-small-cell lung cancer. *J Clin Oncol*. 1999;17:2692-2699.
2. Yom SS, Liao Z, Liu HH, et al. Initial evaluation of treatment related pneumonitis (TRP) in advanced-stage non-small-cell lung cancer patients treated with concurrent chemotherapy and intensity modulated radiotherapy. *Int J Radiat Oncol Biol Phys*. 2007;68:94-102.
3. Chang JY, Zhang X, Wang X, et al. Significant reduction of normal tissue dose by proton radiotherapy compared with three-dimensional conformal or intensity modulated radiation therapy in stage I or stage III non-small-cell lung cancer. *Int J Radiat Oncol Biol Phys*. 2006;65:1087-1096.
4. Greene FL, Page DL, Fleming ID, et al, eds. American Joint Committee on Cancer Staging Manual. 6th ed. New York, NY: Springer; 2002.
5. Karnofsky DA, Burchenal JH. The clinical evaluation of chemotherapeutic agents in cancer. In: Macleod CM, ed. Evaluation of Chemotherapeutic Agents. New York, NY: Columbia University Press; 1949:191-205.
6. Liu HH, Balter P, Tutt T, et al. Assessing respiration-induced tumor motion and internal target volume using 4-dimensional computed tomography for radiotherapy of lung cancer. *Int J Radiat Oncol Biol Phys*. 2007;68:531-540.
7. Liao ZX, Komaki R, Thames HD Jr, et al. Influence of technologic advances on outcomes in patients with unresectable, locally advanced non-small-cell lung cancer receiving concomitant chemoradiotherapy. *Int J Radiat Oncol Biol Phys*. 2010;76:775-781.
8. Wang S, Liao Z, Liu HH, et al. Initial evaluation of clinical and dosimetric parameters associated with treatment-related pneumonitis in patients with non-small-cell lung cancer treated with concurrent chemotherapy and three-dimensional conformal radiotherapy. *Int J Radiat Oncol Biol Phys*. 2006;66:1399-1407.
9. Arriagada R, Le Chevalier T, Quoix E, et al. ASTRO plenary: effect of chemotherapy on locally advanced non-small cell lung carcinoma: a randomized study of 353 patients. GETCB (Groupe d'Etude et Traitement des Cancers Bronchiques), FNCLCC (Federation Nationale des Centres de Lutte contre le Cancer) and the CEBI trialists. *Int J Radiat Oncol Biol Phys*. 1991;20:1183-1190.
10. Bradley JD, Bae K, Graham MV, et al. Primary analysis of the phase II component of a phase I/II dose intensification study using three-dimensional conformal radiation therapy and concurrent chemotherapy for patients with inoperable non-small-cell lung cancer: RTOG 0117. *J Clin Oncol*. 2010;28:2475-2480.
11. Schild SE, McGinnis WL, Graham D, et al. Results of a phase I trial of concurrent chemotherapy and escalating doses of radiation for unresectable non-small cell lung cancer. *Int J Radiat Oncol Biol Phys*. 2006;65:1106-1111.
12. Socinski MA, Blackstock AW, Bogart JA, et al. Randomized phase II trial of induction chemotherapy followed by concurrent chemotherapy and dose-escalated thoracic conformal radiotherapy (74 Gy) in stage III non-small-cell lung cancer: CALGB 30105. *J Clin Oncol*. 2008;26:2457-2463.
13. Fang LC, Komaki R, Allen PK, et al. Comparison of outcomes for patients with medically inoperable stage I non-small-cell cancer treated with two-dimensional vs. three-dimensional radiotherapy. *Int J Radiat Oncol Biol Phys*. 2006;66:108-116.

14. Zinner RG, Komaki R, Cox JD, et al. Dose escalation of gemcitabine is possible with concurrent chest three-dimensional rather than two-dimensional radiotherapy: a phase I trial in patients with stage III non-small-cell lung cancer. *Int J Radiat Oncol Biol Phys*. 2009;73:119-127.
15. Antonadou D, Throuvalas N, Petridis A, et al. Effect of amifostine on toxicities associated with radiochemotherapy in patients with locally advanced non-small-cell lung cancer. *Int J Radiat Oncol Biol Phys*. 2003;57:402-408.
16. Komaki R, Lee JS, Milas L, et al. Effects of amifostine on acute toxicity from concurrent chemotherapy and radiotherapy for inoperable non-small-cell lung cancer: report of a randomized comparative trial. *Int J Radiat Oncol Biol Phys*. 2004;58:1369-1377.
17. Leong SS, Tan EH, Fong KW, et al. Randomized double-blind trial of combined modality treatment with or without amifostine in unresectable stage III non-small-cell lung cancer. *J Clin Oncol*. 2003;21:1767-1774.
18. Senzer N. A phase III randomized evaluation of amifostine in stage IIIA/IIIB non-small cell lung cancer patients receiving concurrent carboplatin, paclitaxel, and radiation therapy followed by gemcitabine and cisplatin intensification. Preliminary findings. *Semin Oncol*. 2002;29:38-41.
19. Movsas B, Scott C, Langer C, et al. Randomized trial of amifostine in locally advanced non-small-cell lung cancer patients receiving chemotherapy and hyperfractionated radiation: Radiation Therapy Oncology Group trial 98-01. *J Clin Oncol*. 2005;23:2145-2154.
20. Wei X, Liu H, Tucker SL, et al. Risk factors for acute esophagitis in non-small cell lung cancer patients treated with concurrent chemotherapy and three-dimensional conformal radiotherapy. *Int J Radiat Oncol Biol Phys*. 2006;66:100-107.
21. Curran WJ Jr, Scott C, Langer C, et al. Long-term benefit is observed in a phase III comparison of sequential vs concurrent chemoradiation for patients with unresected stage III NSCLC. RTOG 9410 [abstract]. *Proc Am Soc Clin Oncol*. 2003;22:621.
22. Graham MV, Purdy JA, Emami B, et al. Clinical dose-volume analysis for pneumonitis after 3D treatment for non-small cell lung cancer. *Int J Radiat Oncol Biol Phys*. 1999;45:323-329.
23. Hernando ML, Marks LB, Bentel GC et al. Radiation-induced pulmonary toxicity: a dose-volume histogram analysis in 201 patients with lung cancer. *Int J Radiat Oncol Biol Phys*. 2001;51:650-659.
24. Willner J, Jost A, Baier K, et al. A little to a lot or a lot to a little? An analysis of pneumonitis risk from dose-volume parameters of the lung in patients with lung cancer treated with 3-D conformal radiotherapy. *Strahlenther Onkol*. 2003;179:548-556.
25. Tsujino K, Mirota S, Endo M, et al. Predictive value of dose-volume histogram parameters for predicting radiation pneumonitis after concurrent chemoradiation for lung cancer. *Int J Radiat Oncol Biol Phys*. 2003;55:110-115.
26. Chang JY, Komaki R, Bucci MK, et al. Failure pattern and toxicity of concurrent proton therapy and chemotherapy for stage III non-small cell lung cancer [abstract 2590]. *Int J Radiat Oncol Biol Phys*. 2009;75(3 suppl):S446.

Original Study

Long-Term Safety and Tolerability of Sorafenib in Patients with Advanced Non–Small-Cell Lung Cancer: A Case-Based Review

Alex A. Adjei,[1] George R. Blumenschein, Jr.,[2] Sumithra Mandrekar,[3] Shauna Hillman,[3] Ulrich Gatzemeier,[4] David Heigener[4]

Abstract

Background: Sorafenib, a small-molecule inhibitor of multiple kinases involved in tumor growth and progression, is approved for the treatment of advanced renal-cell carcinoma and advanced hepatocellular carcinoma. Encouraging activity and good tolerability of daily oral sorafenib, either as a single agent or in combination with gefitinib, have been demonstrated in phase I-II trials in patients with advanced non–small-cell lung cancer (NSCLC). Currently, minimal data are available describing the long-term safety and tolerability of sorafenib in patients with NSCLC. **Materials and Methods:** We describe a series of 12 patients with advanced NSCLC (derived from 1 phase I and 2 phase II trials) who achieved long-term (ie, > 12 months) disease control and continued to receive sorafenib alone or in combination with gefitinib beyond the end of the study in which they were enrolled. **Results:** The safety profile of sorafenib administered on a long-term basis did not differ significantly from that seen previously in the shorter term. The majority of adverse events (AEs) were Grade 1-2 in severity. Five of the 12 patients experienced no ≥ Grade 3 AEs. There was no evidence of increased frequency or severity of AEs over time, or of late AEs, and no patient in this series discontinued study treatment because of AEs. **Conclusion:** In patients with advanced NSCLC who achieve a prolonged response or stable disease with sorafenib given as a single agent or as part of a combination regimen, sorafenib treatment could be continued until disease progression without major long-term safety or tolerability problems.

Clinical Lung Cancer, Vol. 12, No. 4, 212-7 © 2011 Published by Elsevier Inc.
Keywords: Anti-angiognesis, Epidermal growth factor receptor, Gefitinib, Multikinase inhibitor, Toxicity, Tyrosine kinase

Introduction

Non–small-cell lung cancer (NSCLC) accounts for 85% of all lung cancer diagnoses.[1] Patients with NSCLC typically present late in the course of the disease. Despite the wide variety of agents used to treat NSCLC, prognosis remains poor. In general, 5-year survival rates for lung cancer do not exceed 15%,[2] and only 1% of patients with advanced, metastatic NSCLC at diagnosis live for 5 years.[3]

Chemotherapeutic options for patients with NSCLC include platinum-based doublet chemotherapy in the first-line setting, and docetaxel, pemetrexed, gemcitabine, and vinorelbine at first and/or subsequent relapses.[4,5] However, outcomes following cytotoxic chemotherapy remain unsatisfactory, and the side effects associated with these regimens can significantly impair quality of life. Moreover, elderly patients and/or those with poor performance status are often unsuitable for cytotoxic chemotherapy. Targeted therapies, many of which are cytostatic in nature, can result in disease stability and sometimes result in tumor response with an improved side effect profile compared with cytotoxic chemotherapy.[6-9] Targeted therapies may therefore offer the potential for long-term treatment, thereby facilitating effective disease control and the maintenance of functional status.

Several targeted therapies inhibit the activity of epidermal growth factor receptor (EGFR), an important regulator of proliferation in cancer cells. Two EGFR tyrosine kinase inhibitors (TKIs) are approved as second- or third-line therapy for NSCLC: erlotinib and gefitinib. In April 2010, erlotinib was also approved as maintenance treatment for patients with locally advanced or metastatic NSCLC. Both of these agents have demonstrated an acceptable tolerability profile, with diarrhea and rash being the most commonly reported

[1]Roswell Park Cancer Institute, Buffalo, NY
[2]University of Texas, MD Anderson Cancer Center, Houston, TX
[3]Mayo Clinic, Rochester, MN
[4]Hospital Grosshansdorf, Grosshansdorf, Germany

Submitted: Aug 11, 2010; Revised: Sep 27, 2010; Accepted: Oct 1, 2010

Address for correspondence: Alex A. Adjei, MD, PhD, Roswell Park Cancer Institute, Elm and Carlton Streets, Buffalo, NY 14263
Fax: 716-845-3423; e-mail contact: alex.adjei@roswellpark.org

1525-7304/$ - see frontmatter © 2011 Published by Elsevier Inc.
doi: 10.1016/j.cllc.2011.03.021

adverse events (AEs) in clinical trials.[7,9] Targeting a single signaling pathway, however, may not be sufficient to prevent the growth of many tumors, and the efficacy of EGFR TKIs in NSCLC appears to be closely related to the presence of EGFR mutations.[10-12] Another signaling pathway that has been targeted in NSCLC is that regulated by vascular endothelial growth factor (VEGF), a mediator of angiogenesis. The anti-VEGF monoclonal antibody bevacizumab, in combination with platinum-based doublets, is active in NSCLC,[13] and combinations of bevacizumab with erlotinib[14] or cisplatin/gemcitabine[15,16] have yielded particularly encouraging results.

Sorafenib is a small-molecule inhibitor of several protein kinases, including Raf serine/threonine kinases, the proangiogenic VEGF receptors (VEGFR)-1, VEGFR-2, VEGFR-3, and platelet-derived growth factor receptor (PDGFR)-β tyrosine kinases.[17] It therefore inhibits both tumor-cell proliferation and tumor angiogenesis. Sorafenib blocks proliferation of tumor cells by inhibiting the Raf/MEK/ERK pathway at the level of Raf kinase, as well as inhibiting angiogenesis by targeting VEGFR-2 and -3 and PDGFR. Sorafenib, administered at a dose of 400 mg twice a day (b.i.d.), is approved by the European Medicines Agency for the treatment of advanced renal cell carcinoma (RCC; patients who have failed or are unsuitable for cytokine therapy) and hepatocellular carcinoma (HCC),[18] and by the US Food and Drug Administration for the treatment of advanced RCC and unresectable HCC.[19] Sorafenib and has also shown antitumor activity in clinical trials in patients with other solid tumors.[6,20-24] Phase III studies in RCC and HCC established the safety profile of sorafenib, with the majority of AEs being mild-to-moderate in severity and manageable.[25-27] In these trials, the most common AEs in the sorafenib groups included diarrhea, fatigue, and skin problems such as rash and hand and foot skin reaction (HFSR).

Sorafenib is currently under investigation in NSCLC and a variety of other tumor types, including thyroid, breast, ovarian, and prostate cancers, gastrointestinal stromal tumor, malignant melanoma, acute myelogenous leukemia, and central nervous system tumors. Studies typically employ a dosing schedule of 400 mg b.i.d. given in repeated cycles of 28 days. Sorafenib, either alone or in combination with another agent, demonstrated activity in NSCLC in 3 phase I-II studies.[6,20,23] In a phase I study in 31 patients with refractory or recurrent NSCLC treated with sorafenib in combination with the EGFR TKI gefitinib,[6] 1 patient achieved a partial response (PR) and 20 achieved stable disease (SD) (13 patients maintained SD for $\geq$ 4 months). The majority of AEs were Grade 1-2, and the most frequent Grade 3-4 AEs were diarrhea and elevated alanine aminotransferase (ALT). In a single agent, phase II "window of opportunity" study of sorafenib in 25 patients with previously untreated stage IIIB-IV NSCLC,[20] 3 patients (12%) achieved a PR and 7 (28%) achieved SD. Fatigue, diarrhea, and dyspnea were the most common AEs. There was 1 Grade 4 pulmonary hemorrhage. In another phase II study,[23] sorafenib given as a single agent elicited SD in 30 (59%) out of 51 evaluable patients with advanced, recurrent NSCLC. Tumor shrinkage was observed in 15 (29%) evaluable patients. Again, sorafenib was generally well tolerated; the most frequent drug-related AEs were diarrhea, HFSR, fatigue, and nausea.

A phase III trial of sorafenib in combination with carboplatin and paclitaxel in patients with advanced NSCLC has been conducted. However, this study did not meet its primary endpoint of improved overall survival compared with carboplatin and paclitaxel plus placebo.[28] These findings suggest that the use of sorafenib in combination with chemotherapy as a first-line treatment for patients with NSCLC needs further consideration and evaluation. There may also be a role for sorafenib as a single agent in the treatment of NSCLC in the second- and third-line settings.

Promising preliminary results of a randomized discontinuation study of single-agent sorafenib versus placebo in patients with NSCLC who had progressed on chemotherapy (n = 342) suggest that sorafenib in the third-line setting may prolong progression-free survival in heavily pretreated patients with slowly growing disease.[29] Again, sorafenib was well tolerated, with fatigue (11.3%) and HFSR (9%) being the most frequently reported Grade 3-4 toxicities.

The dosing schedule for sorafenib involves continuous treatment until progression; hence, patients who benefit from sorafenib treatment are likely to continue to receive therapy over a long period. There are minimal data on the long-term safety and tolerability of sorafenib in NSCLC. We therefore retrospectively analyzed the case histories of 12 patients from 3 studies[6,20,23] who maintained a response of SD or better for longer than 12 months, and thus continued to receive sorafenib throughout this period.

Case Series

Data are reported for 12 patients who continued sorafenib therapy for a period of more than 1 year. Four cases of stage IIIB (with effusion)/IV NSCLC (previously untreated) were derived from a phase II trial of sorafenib alone,[20] 2 cases of relapsed or refractory stage IV NSCLC were derived from a phase II sorafenib alone trial,[23] and 6 cases of advanced, refractory or recurrent disease were derived from a phase I dose-escalation study of sorafenib in combination with gefitinib.[6] The studies were approved by the appropriate ethics committees and institutional review boards, and all patients provided informed consent. The number of patients in the original study samples and long-term sorafenib treatment subsets, as well the median duration of treatment in each of the long-term sorafenib treatment subsets, are summarized in Table 1.[6,20,23] The 12 patients included in the case series achieved clinical benefit from sorafenib treatment and tolerated sorafenib well; hence, at the discretion of the respective investigators, they continued to receive sorafenib treatment on a long-term basis. Four of the 12 patients had previously received chemotherapy for NSCLC; 3 of these had also undergone surgery, and 1 had undergone radiotherapy. Two patients had undergone surgery alone. One patient (sorafenib alone; previously untreated) was of Asian origin; the remainder were Caucasian. Baseline demographic and disease characteristics of the 12 patients included in this case series are shown in Table 2.

Sorafenib Treatment

Patients were scheduled to receive oral sorafenib (Bayer Pharmaceuticals Corporation) at the standard dose of 400 mg b.i.d., either alone or in combination with gefitinib (AstraZeneca) 250 mg once per day (q.d.). The 6 patients from the sorafenib alone trials received 16-37 cycles of sorafenib, and those in the combination trial received 18-31 cycles of sorafenib plus gefitinib (Table 3).

The dose of sorafenib could be reduced, or sorafenib treatment could be delayed or interrupted, for AEs at any time during treatment at the discretion of the investigator. In general, dose delay refers

Table 1 Studies From Which Cases Were Derived, Number of Cases Derived From Each Study, and Median Duration of Sorafenib Therapy in Long-Term Treatment Subsets

Study	Treatment Regimen	N[a]	n[b]	Median Duration of Sorafenib Therapy in Long-Term Treatment Subgroup, Days (Range)
Front-Line, Window-of-Opportunity, Phase II Sorafenib Alone Trial[20] **(Data not shown)**	**Sorafenib** 400 mg b.i.d. in previously untreated patients	25	4	587 (457-761)
Phase II, Uncontrolled Sorafenib Alone Trial[23]	**Sorafenib** 400 mg b.i.d. in patients with recurrent NSCLC	52	2	68 (1-344)
Phase I Trial of Sorafenib in Combination With Gefitinib[6]	**Sorafenib** 200 mg-400 mg b.i.d. plus **Gefitinib** 250 mg q.d.	32	6	104 (12-368)

Abbreviations: b.i.d. = twice per day; NSCLC = non–small-cell lung cancer; q.d. = once per day.
[a] Number of evaluable patients in original study sample.
[b] Number of patients who received long-term treatment with sorafenib and are included in case series.

Table 2 Baseline Demographic, Disease Characteristics, and Treatment History

Patient	Demographics			Disease Characteristics				Treatment History		
	Age (Years)	Sex	Ethnicity	ECOG PS	Date of Diagnosis	Stage at Study Entry	Histology	Previous Surgery	Previous Radiotherapy	Previous Chemotherapy
Sorafenib Alone (400 mg b.i.d.)										
I	38	F	Caucasian	0	Apr 26 2001	IV	AdenoCA	Yes	No	Cetuximab/vinorelbine/cisplatin
II	51	F	Caucasian	0	Jun 23 2003	IV	AdenoCA	No	Yes	Carboplatin/etoposide
III	60	F	Caucasian	0	Feb 24 2005	IV	NA	No	No	No
IV	61	M	Caucasian	0	Jun 19 1998	IV	NA	Yes	No	No
V	58	F	Asian	0	Mar 5 2005	IIIB (pleural effusion)	NA	No	No	No
VI	74	F	Caucasian	0	Apr 7 2005	IV	NA	No	No	No
Sorafenib 400 mg b.i.d. plus Gefitinib 250 mg q.d.										
VII	70	M	Caucasian	0	Jan 5 2004	IB	BAC	No	No	No
VIII	46	F	Caucasian	0	Feb 25 2002	IIIB	AdenoCA	Yes	No	Gemcitabine/pemetrexed
IX	67	F	Caucasian	0	Mar 2 2004	IV	BAC	No	No	No
X	74	M	Caucasian	0	Mar 15 2004	IV	AdenoCA	Yes	No	No
XI	69	F	Caucasian	1	Apr 19 2000	IB	BAC	Yes	No	Gemcitabine/pemetrexed
XII	73	F	Caucasian	1	1999	IIIB	AdenoCA	No	No	No

Abbreviations: AdenoCA = adenocarcinoma; BAC = bronchoalveolar carcinoma; b.i.d. = twice per day; ECOG PS = Eastern Cooperative Oncology Group performance status; F = female; M = male.

to a halt in dose because of unforeseen circumstances, whereas dose interruption refers to a planned pause in treatment; for example, to allow resolution of an AE. In 1 of the sorafenib alone trials,[20] 1 patient received only 200 mg b.i.d. for the first cycle because of an error, but did receive 400 mg in subsequent cycles; and 2 patients (patients IV and VI) had multiple dose modifications. In the combination therapy trial,[6] 3 patients (patients VIII, IX, and XI) had their sorafenib dose reduced from 400 to 200 mg b.i.d. because of AEs (after 1, 4, and 6 cycles of treatment, respectively), and they remained at this dose for all subsequent cycles. Another patient (patient XII) received 400 mg in the first cycle, 400 to 800 mg q.d. in cycles 2 and 3, and 200 mg q.d. from cycle 4. Dose interruptions and dose delays were relatively rare; however, more patients receiving combination therapy required dose delay (4 versus 2 patients) or dose interruption (5 versus 3 patients) compared with those treated with sorafenib alone. The most common reasons for sorafenib dose reduction, interruption, or delay were HFSR and fatigue.

Safety and Tolerability

In all patients studied here, sorafenib (either alone or in combination with gefitinib) was generally well tolerated over the long term. The majority of AEs were Grades 1-2, and 5 of the 12 patients had no AEs greater in severity than grade 2. A wider variety and number of Grade 1-2 AEs were reported in patients with previously untreated NSCLC who received sorafenib alone, than in patients with recurrent NSCLC although this may be a consequence of different reporting methods between studies. The majority of treatment-related AEs occurred over just a few cycles of treatment (between 1 and 7 cycles in duration). However, the following AEs were more persistent and continued through numerous cycles in some patients: diarrhea (be-

Table 3 Sorafenib Dosing and Dose Reductions, Interruptions, and Delays

Patient	Date of First Sorafenib Dose	First Sorafenib Dose (mg per day)	Subsequent Sorafenib Doses (mg per day)	Total Number of 28-day Cycles	Cycles with Sorafenib Dose Interruption	Cycles with Sorafenib Dose Delay
Sorafenib Alone (400 mg b.i.d.)						
I	May 04	400	800 c 2 onward	34	None	None
II	Sep 04	800	800 all cycles	37	None	None
III	Mar 05	800	800 all cycles	16	None	None
IV	Mar 05	800	400 c 10; 600 c 11-14; 400 c 15 onward	19	2, 9, 14, 18-19	None
V	June 05	800	800 all cycles	23	19-20	14, 20, 22
VI	Apr 05	800	400 c 2-5; 200 c 6 onward	26	1, 5, 26	2-3, 5-6, 8-9, 16-17, 22, 25
Sorafenib 400 mg b.i.d. plus Gefitinib 250 mg q.d.						
VII	May 04	800	800 all cycles	31	1, 24	None
VIII	May 04	800	400 c 2 onward	28	2, 8, 27-28	2, 10
IX	Jul 04	800	400 c 5 onward	26	1, 2, 4, 12, 18-30	1, 5, 10
X	Jun 04	800	800 all cycles	18	None	None
XI	Sep 04	800	400 c 7 onward	26	1, 7, 12, 26	1, 12
XII	Dec 04	400	800 in c 2; 400 c 3; 200 q.d., c 4 onward	19	1, 2, 4, 7, 18	4

Abbreviations: b.i.d. = twice per day; c = cycle; q.d. = once per day.

tween 0 and 26 cycles in total), fatigue (between 0 and 28 cycles), HFSR (between 0 and 5 cycles), alopecia (between 0 and 35 cycles), rash/itch (between 0 and 32 cycles), and anorexia (between 0 and 13 cycles). Aminotransferase elevations were reported in 8 patients; these elevations were of grade 1-2 in all but 2 patients (Grade 3 elevated ALT or aspartate aminotransferase [AST]), generally reported early in the treatment (between cycles 1 and 3), and lasted for 0 to 28 cycles, depending on the patient. Other Grade 1-2 AEs included skin rash, cramps, and mucositis, reported at varying stages of treatment. The only AEs reported later than cycle 18 that had not been seen earlier in at least 1 patient were paresthesia in the toes, bronchus hemorrhage, limb edema, dizziness, back pain, and skin pain, all of which were Grade 1-2 in severity. In general, the patterns of AEs associated with sorafenib alone and combination therapy were consistent.

The only Grade 3-4 AE associated with sorafenib alone was diarrhea (Table 4). Grade 3-4 AEs were more common in patients receiving combination therapy than in those receiving sorafenib alone (Figure 1[6,20,23]). Grade 3-4 AEs among patients receiving combination therapy included cough, elevated transaminases, and diarrhea. Grade 3-4 AEs deemed probably or possibly related to treatment were diarrhea, elevated transaminases, and cough. Grade 3-4 AEs deemed unrelated to study treatment were elevated lipase, elevated uric acid, coronary artery atherosclerosis, chest pressure, and viral gastroenteritis. There were no specific patient characteristics that appeared to suggest differences in the tolerability of long-term sorafenib, and the pattern and severity of AEs did not indicate any worsening of toxicity, or emergence of new toxicities, during long-term treatment with sorafenib.

Response To Therapy

Patients were selected for this analysis on the basis that they maintained SD or better for at least 13 cycles of treatment. All 6 patients who received sorafenib alone eventually had disease progression after 16-37 cycles of treatment. Similarly, all 6 patients who received sorafenib plus gefitinib experienced disease progression 18-31 cycles after the initiation of therapy (Table 5).

Discussion

Patients with advanced NSCLC currently have a very poor prognosis, with 2% to 10% of patients (stages III and IV) surviving 5 years after diagnosis.[3] Furthermore, for most patients, NSCLC presents a considerable burden of symptoms that can profoundly reduce quality of life.[30] Therapy for patients with advanced NSCLC must therefore offer sustained antitumor activity, control the disease and its symptoms, and have an acceptable safety/tolerability profile.

In this case series of 12 patients who experienced continuous benefit for more than 12 months during therapy with sorafenib alone or combination therapy with gefitinib, the safety and tolerability profile remained constant throughout prolonged therapy. Few treatment-related AEs were of Grade ≥ 3 in severity, and when these did occur they were generally of short duration, and resolution was achieved by reduction, interruption, or delay of sorafenib dosing. This observation is consistent with that of other investigators with experience treating patients for more than 6 months with sorafenib.[31]

Overall, long-term toxicities observed in this case series were consistent with those seen in other trials evaluating sorafenib in NSCLC. Common AEs included diarrhea, HFSR, rash, elevated ALT, and fatigue, which were also common toxicities in shorter-term studies of

Table 4 Treatment Cycles in Which Grade 3-4 AEs Were Reported

Patient	Grade 3-4 AEs Possibly/Probably Related to Study Treatment				Grade 3-4 AEs Not Related to Study Treatment				
	Cough	Elevated AST	Elevated ALT	Diarrhea	Elevate Lipase	Elevated Uric Acid	Coronary Artery Atherosclerosis	Chest Pressure	Viral Gastroenteritis
Sorafenib Alone									
IV	–	–	–	9	–	–	–	–	–
Sorafenib plus Gefitinib									
VII	–	–	–	–	–	–	24	23	–
VIII	28	–	1	–	–	1	–	–	–
IX	–	–	–	4	–	–	–	–	–
X	–	–	–	10	–	–	–	–	–
XI	–	–	–	–	1	–	–	–	11
XII	–	3	–	–	–	–	–	–	–

Abbreviations: AE = adverse event; ALT = alanine aminotransferase; AST = aspartate aminotransferase.

Figure 1 Number of Patients With Advanced NSCLC Treated With Sorafenib Alone (n = 6)[20,23] or a Combination of Sorafenib plus Gefitinib (n = 6)[6] Who Experienced ≥ 1 Grade 3-4 AE, ≥ 1 Sorafenib Dose Delay, or ≥ 1 Sorafenib Dose Interruption

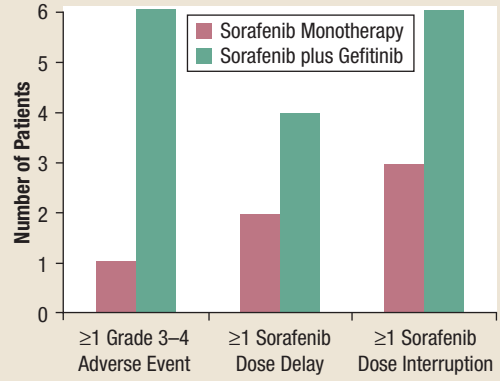

Abbreviations: AE = adverse event; NSCLC = non–small-cell lung cancer.

Table 5 Response to Treatment and Outcome

Patient	Total Cycles	Best Response	Current Status
Sorafenib Alone			
I	34	SD	PD[a]
II	37	SD	PD
III	16	SD	PD
IV	19	SD	PD
V	23	PR	PD
VI	26	SD	PD
Sorafenib plus Gefitinib			
VII	31	SD	PD
VIII	28	SD	PD
IX	26	SD	PD
X	18	SD	PD
XI	26	SD	PD
XII	19	SD	PD

Abbreviations: PD = progressive disease; PR = partial response; SD = stable disease.
[a] PD after 34 months; patient died 5 months later.

sorafenib.[20,25,28,29] In our case series and in these trials, sorafenib-related AEs were both predictable and manageable. The most frequent AE of any grade in this case series was diarrhea, a recognized side effect of both sorafenib[25-27] and gefitinib.[32] Diarrhea accounted for 3 of the 11 Grade ≥ 3 AEs and was the only Grade ≥ 3 AE to occur with sorafenib alone. Experience with sorafenib in patients with RCC has demonstrated that diarrhea is often easily manageable with dietary modification and standard antidiarrhea treatments.[33,34] Although dose interruption may be necessary in severe cases, diarrhea rarely necessitates discontinuation of sorafenib.

Cardiovascular AEs were relatively rare, and no bleeding events were reported. Three patients receiving therapy with sorafenib alone experienced hypertension; all cases were of Grade 1-2 in severity. Hypertension has previously been associated with sorafenib therapy in patients with RCC[25] 1 incidence of coronary artery atherosclerosis, although this was not deemed to be related to the study treatment.

In this case series, there was no evidence of an increasing need to modify dose frequency with prolonged sorafenib treatment. For all patients who had their dose reduced for toxicity, dose reduction usually occurred during the first few cycles of therapy, with no dose reduction needed after cycle 7 for 11 of the 12 patients, and none needed after cycle 14 for any of the patients. This suggests that, for any patient who may require dose reduction, the optimal tolerated dose of sorafenib may be established early in treatment. Dose interruptions and delays because of AEs occurred throughout treatment in some patients, but with no suggestion of increased AE incidence in

later cycles. All patients were able to maintain the dose of sorafenib established during the first year of treatment until progression, with no withdrawals for late toxicity.

There is currently an unmet need for effective and well tolerated second- and third-line therapeutic options for NSCLC. Presently, chemotherapy for NSCLC can prolong survival and maintain quality of life for patients with good performance status at baseline; however, the majority of patients with advanced-stage disease experience disease progression within 3 months of initiation of second-line therapy.[35] This retrospective case series suggests that sorafenib may be successfully administered for long periods of time without significant safety or tolerability issues.

Conclusion

In the 12 patients included in this retrospective case-based analysis, prolonged sorafenib therapy (> 1 year) was well tolerated, suggesting that patients with NSCLC can achieve long-lasting disease control with sorafenib without serious treatment-related sequelae. The clinical evaluation of sorafenib in patients with NSCLC should be continued.

Acknowledgement

Two of the 3 studies from which cases were derived (Adjei AA, Molina JR, Mandrekar SJ, et al. *Clin Cancer Res* 2007; 13:2684-91; Blumenschein GR Jr, Gatzemeier U, Fossella F, et al. *J Clin Oncol* 2009; 27:4274-80) were designed, sponsored, and administered by Bayer HealthCare Pharmaceuticals and Onyx Pharmaceuticals. Study sponsors were involved in the collection of data from only 1 of the 3 studies; this aside, data collection, analysis, and interpretation was carried out by the authors.

The authors thank John Bull, GeoMed, Macclesfield, UK (funded by Bayer HealthCare Pharmaceuticals) and John D. Zoidis, MD, Bayer HealthCare Pharmaceuticals, Montville, NJ for writing and editorial support.

Disclosure

Dr Gatzemeier has received honoraria from Roche, Bayer HealthCare, Onyx, AstraZeneca, Lilly, and Novartis, and has served on advisory boards for Bayer HealthCare, Mundipharma, Roche, Lilly, and AstraZeneca. Dr Heigener has received honoraria from AstraZeneca. Dr Blumenschein has received research funding from Bayer HealthCare. Drs Adjei, Mandrekar, and Hillman have no conflicts of interest to declare.

References

1. American Cancer Society. Cancer Facts & Figures 2009. Available at: http://www.cancer.org/downloads/STT/500809web.pdf. Accessed May 26, 2010.
2. Parkin DM, Bray F, Ferlay J, et al. Global cancer statistics, 2002. *CA Cancer J Clin* 2005; 55:74-108.
3. American Cancer Society. Detailed Guide: Lung Cancer–Non-Small Cell. How Is Non-Small Cell Lung Cancer Staged? Available at: http://www.cancer.org/docroot/CRI/content/CRI_2_4_3x_How_Is_Non-Small_Cell_Lung_Cancer_Staged.asp?rnav=cri. Accessed May 26, 2010.
4. National Comprehensive Cancer Network. NCCN Clinical Practice Guidelines in Oncology Non-Small Cell Lung Cancer V.2.2010. Available at: http://www.nccn.org/professionals/physician_gls/PDF/nscl.pdf. Accessed May 26, 2010.
5. Pfister DG, Johnson DH, Azzoli CG, et al. American Society of Clinical Oncology treatment of unresectable non-small cell lung cancer guideline: update 2003. *J Clin Oncol* 2004; 22:330-53.
6. Adjei AA, Molina JR, Mandrekar SJ, et al. Phase I trial of sorafenib in combination with gefitinib in patients with refractory or recurrent non-small cell lung cancer. *Clin Cancer Res* 2007; 13:2684-91.
7. Cho BC, Im K-C, Park M-S, et al. Phase II study of erlotinib in advanced non–small-cell lung cancer after failure of gefitinib. *J Clin Oncol* 2007; 25:2528-33.
8. Nakatomi K, Soda H, Kitazaki T, et al. Long-term survival in three patients with metastatic non-small cell lung cancer treated with gefitinib. *Lung Cancer* 2006; 52:253-5.
9. Reck M, Gatzemeier U. Benefit in lung function improvement and side-effect profile of long-term responders: an analysis of 14 NSCLC patients treated for at least 9 months with gefitinib. *Lung Cancer* 2005; 50:107-14.
10. Lynch TJ, Bell DW, Sordella R, et al. Activating mutations in the epidermal growth factor receptor underlying responsiveness of non-small-cell lung cancer to gefitinib. *N Engl J Med* 2004; 350:2129-39.
11. Paez JG, Janne PA, Lee JC, et al. EGFR mutations in lung cancer: correlation with clinical response to gefitinib therapy. *Science* 2004; 304:1497-500.
12. Pao W, Miller V, Zakowski M, et al. EGF receptor gene mutations are common in lung cancers from "never smokers" and are associated with sensitivity of tumors to gefitinib and erlotinib. *Proc Natl Acad Sci U S A* 2004; 101:13306-11.
13. Sandler A, Gray R, Perry MC, et al. Paclitaxel-carboplatin alone or with bevacizumab for non-small-cell lung cancer. *N Engl J Med* 2006; 355:2542-50.
14. Herbst RS, O'Neill VJ, Fehrenbacher L, et al. Phase II study of efficacy and safety of bevacizumab in combination with chemotherapy or erlotinib compared with chemotherapy alone for treatment of recurrent or refractory non small-cell lung cancer. *J Clin Oncol* 2007; 25:4743-50.
15. Reck M, von Pawel J, Zatloukal P, et al. Phase III trial of cisplatin plus gemcitabine with either placebo or bevacizumab as first-line therapy for nonsquamous non-small-cell lung cancer: AVAiL. *J Clin Oncol* 2009; 27:1227-34.
16. Reck M, von Pawel J, Zatloukal P, et al. Overall survival with cisplatin-gemcitabine and bevacizumab or placebo as first-line therapy for nonsquamous non-small-cell lung cancer: results from a randomised phase III trial (AVAiL). *Ann Oncol* 2010; 21:1804-9.
17. Wilhelm SM, Adnane L, Newell P, et al. Preclinical overview of sorafenib, a multikinase inhibitor that targets both Raf and VEGF and PDGF receptor signaling. *Mol Cancer Ther* 2008; 7:3129-40.
18. European Medicines Agency. Nexavar Summary of Product Characteristics. 2006. Available at: http://www.emea.europa.eu/humandocs/PDFs/EPAR/nexavar/emea-combined-h690en.pdf. Accessed May 26, 2010.
19. Nexavar (sorafenib) tablets [prescription information]: Wayne, NJ. Bayer HealthCare Pharmaceuticals; 2009. Available at: http://berlex.bayerhealthcare.com/html/products/pi/Nexavar_PI.pdf. Accessed May 26, 2010.
20. Dy GK, Hillman SL, Rowland KM Jr, et al. A front-line window of opportunity phase 2 study of sorafenib in patients with advanced nonsmall cell lung cancer. North Central Cancer Treatment Group Study N0326. *Cancer* 2010; 116:5686-93.
21. Duran I, Hotte SJ, Hirte H, et al. Phase I targeted combination trial of sorafenib and erlotinib in patients with advanced solid tumors. *Clin Cancer Res* 2007; 13:4849-57.
22. Escudier B, Lassau N, Angevin E, et al. Phase I trial of sorafenib in combination with IFN alpha-2a in patients with unresectable and/or metastatic renal cell carcinoma or malignant melanoma. *Clin Cancer Res* 2007; 13:1801-9.
23. Blumenschein GR Jr, Gatzemeier U, Fossella F, et al. Phase II, multicenter, uncontrolled trial of single-agent sorafenib in patients with relapsed or refractory, advanced non–small-cell lung cancer. *J Clin Oncol* 2009; 27:4274-80.
24. Liu B, Barrett T, Choyke P, et al. A Phase II study of BAY 43-9006 (Sorafenib) in patients with relapsed non-small cell lung cancer (NSCLC). *J Clin Oncol* 2006; 24(Suppl):676S Abstract 17119.
25. Escudier B, Eisen T, Stadler WM, et al. Sorafenib in advanced clear-cell renal-cell carcinoma. *N Engl J Med* 2007; 356:125-34.
26. Llovet JM, Ricci S, Mazzaferro V, et al. Sorafenib in advanced hepatocellular carcinoma. *N Engl J Med* 2008; 359:378-90.
27. Cheng A-L, Kang TK, Chen Z, et al. Efficacy and safety of sorafenib in patients in the Asia-Pacific region with advanced hepatocellular carcinoma: a phase III randomized, double-blind, placebo-controlled trial. *Lancet Oncol* 2009; 10:25-34.
28. Scagliotti G, Novello S, von Pawel J, et al. Phase III study of carboplatin and paclitaxel alone or with sorafenib in advanced non-small-cell lung cancer. *J Clin Oncol* 2010; 28:1835-42.
29. Schiller J, Lee J-W, Hanna NH, et al. A randomized discontinuation phase II study of sorafenib vs placebo in patients with non-small cell lung cancer (NSCLC) who failed at least two prior chemotherapy regimens: E2501. *International Association for the Study of Lung Cancer 13th World Conference on Lung Cancer. San Francisco, CA: July 31-August 4, 2009* Abstract C1.6.
30. Temel JS, Pirl WF, Lynch TJ. Comprehensive symptom management in patients with advanced-stage non-small-cell lung cancer. *Clin Lung Cancer* 2006; 7:241-9.
31. Flaherty KT, Brose MS. Sorafenib-related hand–foot skin reaction improves, not worsens, with continued treatment. *Clin Cancer Res* 2009; 15:7749.
32. Kim ES, Hirsh V, Mok T, et al. Gefitinib versus docetaxel in previously treated non-small-cell lung cancer (INTEREST): a randomized phase III trial. *Lancet* 2008; 372:1809-18.
33. Wood LS, Manchen B. Sorafenib: a promising new targeted therapy for renal cell carcinoma. *Clin J Oncol Nurs* 2007; 11:649-56.
34. Grünwald V, Heinzer H, Fiedler W. Managing side effects of angiogenesis inhibitors in renal cell carcinoma. *Onkologie* 2007; 30:519-24.
35. Bunn PA, Thatcher N. Systemic treatment for advanced (stage IIIb/IV) non-small cell lung cancer: more treatment options; more things to consider. Conclusion. *Oncologist* 2008; 13(Suppl 1):37-46.

Invest New Drugs (2011) 29:499–505
DOI 10.1007/s10637-009-9380-z

PHASE III STUDIES

Pharmacokinetic study of the phase III, randomized, double-blind, multicenter trial (TRIBUTE) of paclitaxel and carboplatin combined with erlotinib or placebo in patients with advanced Non-small Cell Lung Cancer (NSCLC)

Hai T. Tran · Ralph G. Zinner · George R. Blumenschein Jr. · Yun W. Oh · Vassiliki A. Papadimitrakopoulou · Edward S. Kim · Charles Lu · Mubashira Malik · Bert L. Lum · Roy S. Herbst

Received: 18 April 2007 / Accepted: 17 December 2009 / Published online: 22 January 2010

Summary *Purpose* To assess the pharmacokinetics and evaluate potential drug-drug interactions between erlotinib, paclitaxel and carboplatin. *Experimental Design* 1,079 previously untreated patients with advanced NSCLC were enrolled and randomized in a phase III trial (TRIBUTE) to receive either erlotinib or placebo in combination with paclitaxel 200 mg/m2 IV over 3 h and carboplatin at a calculated dose to achieve an AUC 6 mg·min/mL. To determine possible drug-drug interaction with this combination, a subset of 24 (12 erlotinib, 12 placebo) patients were enrolled onto an intensive pharmacokinetic (IPK) substudy group at a single site. All IPK patients received either erlotinib 150 mg/day or placebo-controlled tablets. Analyses were completed using validated analytical methodologies. Non-compartmental modeling was utilized to estimate PK parameters. *Results* Complete blood sampling for pharmacokinetic analysis was obtained in 21 of 24 patients. Mean $AUC_{0-\tau}$ for erlotinib and the OSI-420 metabolite were 29,997 ng·h/mL and 3,020 ng·h/mL, respectively. Mean (SD) paclitaxel clearances ($L/h/M^2$) were 11.7 (3.4) and 12.7 (6.7) in the placebo and erlotinib treatment groups, respectively. The resultant paclitaxel $AUC_{0-\infty}$ (ng·h/mL) was 18,400 (5,300) for the placebo group and 17,800 (5,500) for the erlotinib group. For carboplatin, the mean (SD) clearances (L/h) were 16.8 (3.9) and 16.1 (4.4) for the placebo and erlotinib groups, respectively. The resultant carboplatin $AUC_{0-\infty}$ (ng/mL·h) were 49,900 (9,700) for the placebo group and 48,400 (11,900) for the erlotinib group. No significant differences were observed in these paclitaxel or carboplatin pharmacokinetic group comparisons. *Conclusions* The addition of erlotinib to a standard chemotherapy regimen for NSCLC did not alter the systemic exposures ($AUC_{0-\infty}$) of paclitaxel ($p=0.80$) and carboplatin ($p=0.756$) when erlotinib-treated patients were compared to placebo-treated patients. The pharmacokinetics of erlotinib and its metabolite OSI-420 did not appear to be altered by the concomitant administration of paclitaxel and carboplatin.

Keywords Erlotinib · NSCLC · Lung cancer · EGFR inhibitor · Pharmacokinetics

This research was supported by a grant from Genentech, Inc., an ASCO Career Development Award, and an M. D. Anderson Cancer Center Physician Scientist Program Award to Dr. Roy S. Herbst.

H. T. Tran (✉) · R. G. Zinner · G. R. Blumenschein Jr. · V. A. Papadimitrakopoulou · E. S. Kim · C. Lu · R. S. Herbst
Department of Thoracic/Head and Neck Medical Oncology, The University of Texas M. D. Anderson Cancer Center, 1515 Holcombe Blvd, Box 432, Houston, TX 77030, USA
e-mail: htran@mdanderson.org

Y. W. Oh
School of Medicine, Georgetown University, Washington, DC, USA

M. Malik · B. L. Lum
Genentech, Inc., South San Francisco, CA, USA

Introduction

Erlotinib (OSI-774, Tarceva®, Genentech, Inc, South San Francisco, CA USA) is a novel, orally bioavailable

inhibitor of tyrosine kinase with potent and reversible binding to the epidermal growth factor receptor (HER1/EGFR) [1]. Preclinical studies have demonstrated an additive effect when erlotinib is combined with cytotoxic agents including paclitaxel and cisplatin [2, 3]. Erlotinib has demonstrated activity as a single agent in patients with advanced NSCLC [4, 5]. Recent clinical trials with the combination of erlotinib and various chemotherapeutic agents have shown promising effects [6, 7]. Specifically, results from a phase II trial studying the combination of erlotinib with one of the accepted standard chemotherapy doublets consisting of paclitaxel and a platinum agent showed durable objective responses [6]. With this as a base, a phase III randomized, placebo-controlled trial of paclitaxel and carboplatin with or without erlotinib in chemotherapy-naïve patients with advanced NSCLC (TRIBUTE) was conducted in several institutions. The clinical results of this study have been reported elsewhere [8].

Erlotinib's principal metabolic pathway is via CYP3A4 forming several metabolites including the equipotent active metabolite, OSI-420 [9]. Since both paclitaxel and erlotinib utilize CYP3A4 as a metabolic pathway [10, 11], a subset of patients was enrolled onto an intensive pharmacokinetic (IPK) substudy to determine the possible drug-drug interactions with this combination. All IPK patients received either erlotinib 150 mg/day or placebo-controlled tablets.

Patients and methods

Patient eligibility

Inclusion required histologically documented stage IIIB or stage IV NSCLC; age ≥18 years; and Eastern Cooperative Oncology Group (ECOG) performance status of 0 or 1. Exclusion criteria included prior systemic chemotherapy for NSCLC; symptomatic or untreated brain metastases, prior exposure to agents directed at the HER axis; unstable systemic disease that would potentially preclude chemotherapy treatment with or without erlotinib; inadequate hematologic (granulocytes ≤1.5/mL), renal (creatinine >1.5× upper limit of normal [ULN]), or hepatic function (liver function tests > 2.5×ULN). EGFR protein expression determination (by IHC methodology) was not an a priori condition for enrollment.

All patients provided informed consent which was approved from the ethics committee at each center. The study followed the Declaration of Helsinki and good clinical practice guidelines [12].

Treatment protocol and pharmacokinetic sampling strategy

In the TRIBUTE trial, 1079 previously untreated patients with advanced NSCLC were enrolled and randomized to receive either erlotinib or placebo in combination with paclitaxel 200 mg/M^2 administered intravenously over 3 h and carboplatin at a calculated dose to provide an AUC= 6 mg·min/mL administered intravenously over 1 h. To determine possible drug-drug interactions with this combination, a subset of 24 randomized patients were enrolled onto an IPK substudy at the University of Texas M.D. Anderson Cancer Center (12 erlotinib, 12 placebo). All IPK patients provided informed consent separately from the main clinical study to participate in this substudy and were randomized to receive either daily oral erlotinib (150 mg) or identical placebo tablets concurrently with chemotherapy. In the overall phase III study randomization was stratified by disease stage (IIIB; IV), weight loss during the previous 6 months (≤5%; >5%), tumor measurability (measurable; non-measurable), and treatment center. Patients received a maximum of six cycles of paclitaxel and carboplatin every 3 weeks in the absence of disease progression.

The pharmacokinetic sampling strategy was such that at cycle 1, erlotinib was not started until 2 days after administration of chemotherapy to allow for the assessment of paclitaxel and carboplatin pharmacokinetics in the absence of erlotinib. From day 2 onward, patients were administered erlotinib on a daily schedule so that at cycle 2 steady-state erlotinib concentrations would be achieved, based on previous half-life estimates [4]. In the IPK substudy concomitant use potent inhibitors or inducers of CYP4503A drug metabolism enzymes were not allowed.

Pharmacokinetic, bioanalytical, and statistical methods

Blood collection for the pharmacokinetic study of erlotinib, paclitaxel and carboplatin was completed with the schedule as listed on Table 1. For isolation of plasma, collected blood samples were centrifuged at 1500 RPM for 10 min at 5°C. For the analysis of carboplatin plasma-ultrafiltrate (free platinum), an additional step using Centrifree® micropartition device (Millipore, Massachusetts, USA) was used to obtain an ultrafiltrate of human plasma. All processed samples were transferred into appropriately labeled vials and stored frozen (−80°C) until analysis.

All drug analyses were completed by a contract service (MDS Pharma Services, St. Laurent, Quebec, Canada) utilizing appropriate and validated assays (on file at MDS Pharma Services, St. Laurent, Quebec, Canada). For erlotinib, sample preparation consisted of a liquid-liquid extraction method. The concentrations of erlotinib and OSI-420 in plasma were determined by a liquid chromatography tandem mass spectrometry (LC/MS/MS) method. The equally active demethylated metabolites, OSI-420 and OSI-413 were reported as one concentration value (OSI-420) since they exist as isomers and cannot be individually

Table 1 IPK blood collection schedule

Drug to be analyzed	Drug sampling cycle	Drug sampling time
Erlotinib, OSI-420	Cycle 1	Predose
	Cycle 2	Predose and 0.25, 0.5, 1, 2, 3, 4, 6, 8, and 12 h and 1, 2, and 7 days post first elotinib dose
Paclitaxel	Cycle 1, 2	Predose and 0[a], 0.25, 0.5, 0.75, 1, 2, 3, 5, 9, 21, and 45 h post end of paclitaxel infusion
Carboplatin	Cycle 1, 2	Predose and 0[a], 0.25, 0.5, 1.5, 2.5, 4.5, 8.5, and 20.5 h post end of carboplatin infusion

[a] Blood samples taken 5 min prior to end of infusion

distinguished using this analytical method. The limit of quantitation (LOQ) was set at the concentration of the lowest non-zero standard (1 ng/mL for erlotinib and 0.998 ng/mL for OSI-420).

A solid phase extraction method was utilized to isolate paclitaxel. The extracts were analyzed using a LC/MS/MS method with an assay range of 5.02–5022.86 ng/mL. The LOQ was set at the concentration of the lowest non-zero standard (5.02 ng/mL). Concentrations of carboplatin in plasma ultrafiltrates were analyzed for the presence of platinum using validated flameless atomic absorption spectroscopy (FAAS) utilizing a graphite furnace. This method detected elemental platinum only and not carboplatin. Thus, all of the values calculated from the calibration curve were converted to an equal molar amount of carboplatin. The assay range was 51.08–2247.32 ng/mL. The LOQ was set at the concentration of the lowest non-zero standard, 51.08 ng Pt/mL. Pharmacokinetic parameters for erlotinib, paclitaxel and carboplatin were estimated using standard non-compartmental methods (WinNonlin [version 3.1]; Pharsight Corporation, Mountain View, CA).

The IPK study was designed to allow comparison of PK parameters between patients receiving erlotinib or placebo in combination with paclitaxel and carboplatin. To assess if erlotinib had an effect on the pharmacokinetics of paclitaxel or carboplatin, the parameters between the two groups were compared using the two-sample rank sum nonparametric test with a priori level of significance of P=.05.

Results

Twenty-four patients (12 in each group, erlotinib and placebo) consented to the trial and participated in this IPK sub-study; the characteristics of these patients are listed in Table 2. Among the 12 patients in the erlotinib-treated group, blood samplings were adequate for pharmacokinetic analysis in nine patients. Two patients developed acute hypersensitivity reactions to paclitaxel and withdrew consent for further blood collection for pharmacokinetic analysis. One patient withdrew consent to have any blood collection done prior to start of therapy.

Paclitaxel blood sampling was adequate for pharmacokinetic analysis in 21 of 24 patients. Paclitaxel pharmacokinetic parameters in the two groups of patients, those treated with erlotinib or placebo, are summarized in Table 3. No differences in the pharmacokinetics of paclitaxel were observed between the two groups. The exposure ($AUC_{0-\infty}$ [ng·h/mL]) of paclitaxel was similar in the erlotinib and placebo-treated patients, with mean (SD) values of 18,400 (5,300) in the placebo-treated group and 17,800 (5,500) in the erlotinib-treated group (p=0.886). A concentration-time plot for mean (+/− SE) values at nominal times following the end of paclitaxel infusion for the two treatment groups is illustrated in Fig. 1. These results suggest erlotinib does not result in an alteration of paclitaxel pharmacokinetics.

Carboplatin blood sampling was adequate to allow for pharmacokinetic determinations in 21 of 24 patients enrolled in the substudy. The pharmacokinetic parameters of carboplatin in the two groups of patients, those treated with erlotinib or placebo are listed in Table 3. There were no differences between the two group's drug exposures. Overall, $AUC_{0-\infty}$ of carboplatin was similar between the erlotinib and placebo-treated patients, with mean (SD) $AUC_{0-\infty}$ (ng·h/mL) values of 49,900 (9,700) in placebo-treated patients and 48,400 (11,900) (ng·h/mL) in erlotinib-treated patients (p= 0.696). There was a trend for a shorter ultrafilterable carboplatin t½ in the erlotinib-treated patients. A concentration-time plot of mean (+/− SE) values at nominal times following the end of carboplatin infusion for the two treatment groups is illustrated in Fig. 2. These

Table 2 Patient characteristics

Characteristic	Group 1 (n=9) Erlotinib + Paclitaxel + Carboplatin	Group 2 (n=12) Placebo + Paclitaxel + Carboplatin
Age (years)		
Median (Range)	61 (38–69)	59.5 (36–73)
Gender (M/F)	9/1	8/4
PS (ECOG) 0/1	2/8	4/8

PS performance status, *ECOG* Eastern Cooperative Oncology Group

Table 3 Summary of the pharmacokinetic parameters of paclitaxel and carboplatin with either erlotinib or placebo

	Group 1 (n=9) Erlotinib + Paclitaxel + Carboplatin	Group 2 (n=12) Placebo + Paclitaxel + Carboplatin	p value
Paclitaxel			
CL (L/h/M^2)	12.7±6.7	11.7±3.4	0.696
$T_{1/2}$ (h)	9.7±5.5	12.3±1.7	0.166
Vd (L/M^2)	72.5±29.2	84.0±20.8	0.166
$AUC_{0-\infty}$ (ng·h/mL)	17,800±5,500	18,400±5,300	0.886
Carboplatin			
CL (L/h)	16.1±4.4	16.8±3.9	0.644
$T_{1/2}$ (h)	2.8±0.6	3.3±0.3	0.030
Vd (L)	46.9±16.3	53.3±14.5	0.303
$AUC_{0-\infty}$ (ng·h/mL)	48,400±11,900	49,900±9,700	0.696

Data are means ± SD

CL clearance, $T_{1/2}$ half-life, *Vd* volume of distribution, $AUC_{0-\infty}$ area under the concentration-time curve from time 0 to infinity

Carboplatin was measured as ultrafilterable platinum concentrations

results suggest erlotinib does not alter the pharmacokinetic behavior of carboplatin.

Erlotinib patients had received a minimum of 21 (range 21–22) single daily doses of erlotinib at the time of the pharmacokinetic analysis and were presumed to be at steady state based on previous reported terminal half-life estimates of approximately 18 h. The pharmacokinetic data for erlotinib and its metabolite, OSI-420, are summarized in Table 4. The mean (SD) C_{max} for erlotinib and OSI-420

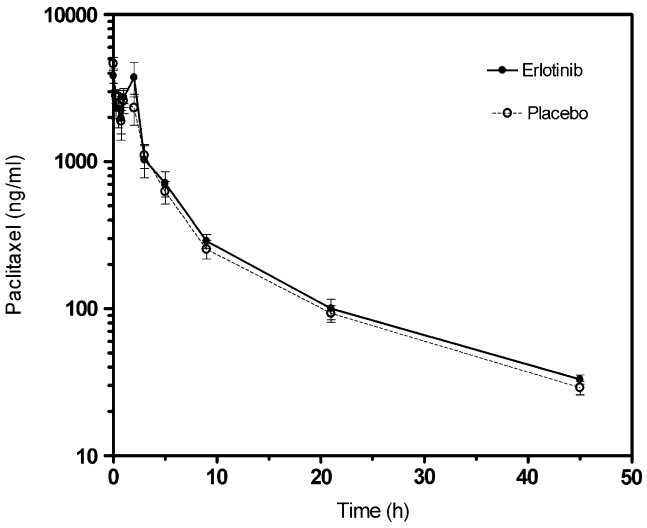

Fig. 1 Concentration-time plot for paclitaxel from patients in the erlotinib (*closed circle*)- and placebo (*open circle*)-treatment group (values are mean ± standard error of the mean)

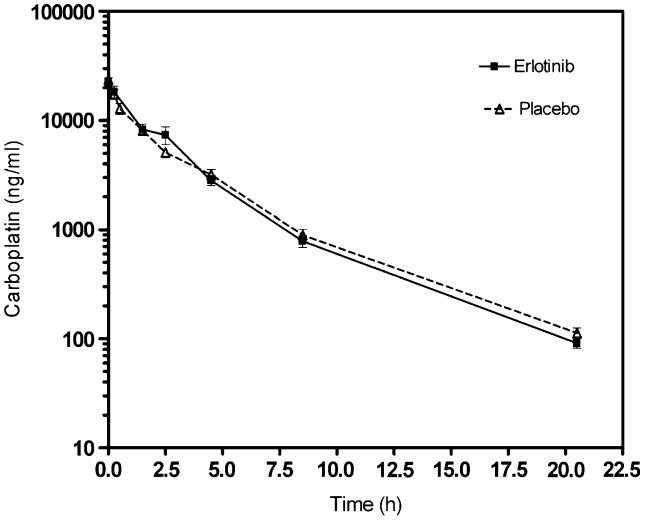

Fig. 2 Concentration-time plot for carboplatin from patients in the erlotinib- (*closed circle*) and placebo (*open circle*)-treatment group (values are mean ± standard error of the mean). Carboplatin was measured as ultrafilterable platinum concentrations

were 1,703.6 (519.3) ng/mL and 130.9 (49.4) ng/mL, respectively. The $AUC_{0-\tau}$ estimates were 29,997 (9,713) ng·h/mL for erlotinib and 3,020 (1,293) ng·h/mL for the metabolites. The mean (SD) $AUC_{0-\tau}$ ratio of metabolites (OSI-420) to parent was 0.10 (0.04) and the mean (SD) percentage of free (non-protein bound) erlotinib and metabolites were 4.1 (0.6) % and 6.2 (0.5) %, respectively. Figure 3 depicts the concentration-time profile of erlotinib and OSI-420 following oral administration during steady state.

The non-hematologic adverse events occurring in greater than 25% of patients in the overall phase III study are listed in Table 5. As expected, more erlotinib-associated adverse events including diarrhea and rashes were observed in the erlotinib-treated group versus the placebo-treated group. The incidence of anticipated low (grades 1, 2) or high grade (grades 3, 4) chemotherapy related toxicity, such as alopecia, vomiting, neutropenia, or peripheral neuropathy, did not appear to be exacerbated by erlotinib treatment (Table 5).

Table 4 Mean erlotinib and OSI-420 pharmacokinetic data when administered in combination with paclitaxel and carboplatin

No. patients = 9	C_{max} (ng/ml)	T_{max} (h)	$AUC_{0-\tau}$ (ng·h/mL)
Erlotinib	1,703.6 (519.3)	5.5 (3.8)	29,997 (9,713)
OSI-420	130.9 (49.4)	6.3 (3.8)	3,020 (1,293)

Data are means with SD in parentheses

C_{max} maximum observed concentration (ng/mL), T_{max} time to maximum observed concentration, $AUC_{0-\tau}$ area under the concentration-time curve from time 0 to Tau (dosing interval), *CL/Fss* apparent clearance at steady state

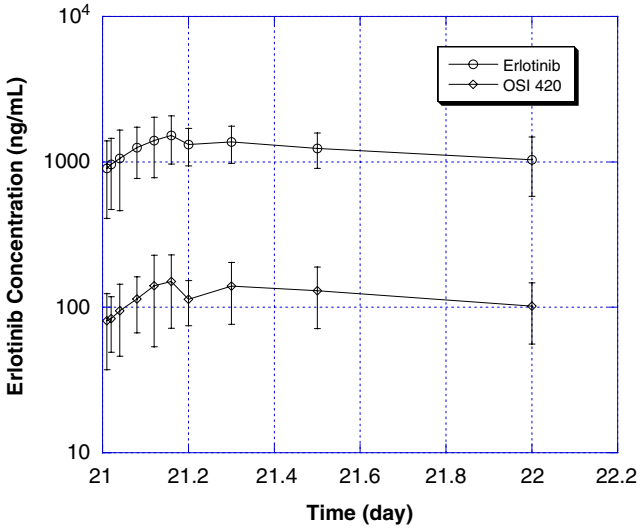

Fig. 3 Concentration-time plot for erlotinib following oral administration

Discussion

The pharmacokinetic data for erlotinib and its' major active metabolite, OSI-420 in this IPK sub-study are similar to those previously reported in a phase I single agent study [5]. The observed median (range) $AUC_{0-\tau}$ of 33,046 (13,069–42,401) ng·h/mL was similar to that reported previously (24,900 (8,660–67,000) ng·h/mL) in a Phase 1 study. These results suggest that the concomitant administration of carboplatin or paclitaxel did not markedly alter erlotinib pharmacokinetics. Additionally, the $AUC_{0-\tau}$ ratio of metabolite to erlotinib to the primary metabolite, OSI-420, observed in this study were also similar to that previously reported, suggesting that concomitant administration of erlotinib with chemotherapy did not markedly alter the metabolism of erlotinib.

Since paclitaxel and erlotinib share the same drug metabolism enzyme, CYP3A4, there is a theoretical potential for a drug-drug interaction. In this study, in cycle 1 patient did not receive erlotinib until two days following chemotherapy, followed by continuous daily dosing of erlotinib, which allowed reaching steady state concentrations by the time of cycle 2. This design allowed study of the effect of erlotinib on the pharmacokinetics of the chemotherapeutic agents. Concomitant administration of erlotinib did not alter the behavior of carboplatin and paclitaxel. Although we observed a trend for a decrease in the t½ of carboplatin in the erlotinib-treated group, the effect was slight and the AUC was not altered. The reasons or this is unknown but is possibly due to variability in the curvature between the alpha and beta phases of the concentration-time profile and the number of points describing the terminal elimination phase. Of note, paclitaxel principal metabolic fate is not CYP3A4 but via CYP2C8 to form the 6a-OH metabolite. So while there is a potential for a drug-drug interaction, the likelihood appears small and was not observed in this study. Similarly, other investigators have also reported that erlotinib did not alter the disposition of either paclitaxel or docetaxel in two previous phase Ib combination studies [13, 14]. In addition, our results are similar to those reported in a phase 1b study combining erlotinib with carboplatin and paclitaxel 6). In this previous study, there was no evidence of a pharmaco-

Table 5 Adverse events occurring in ≥25% of subjects receiving paclitaxel, carboplatin with erlotinib or placebo

Intensive Safety Population	Placebo (*N*=208)		Erlotinib (*N*=209)	
Adverse events*	Grade 1/2	Grade 3/4	Grade 1/2	Grade 3/4
Total	203 (97.6%)	157 (75.5%)	204 (97.4%)	164 (78.5%)
Nausea	111 (53.4%)	12 (5.8%)	120 (57.4%)	8 (3.8%)
Fatigue	104 (50.0%)	13 (6.3%)	100 (47.8%)	12 (5.7%)
Alopecia	118 (56.7%)	0 (0.0%)	103 (49.3%)	1 (0.5%)
Diarrhea NOS	70 (33.7%)	10 (4.8%)	116 (55.5%)	26 (12.4%)
Anemia NOS	74 (35.6%)	13 (6.3%)	92 (44.0%)	16 (7.7%)
Rash NOS	56 (26.9%)	2 (1.0%)	114 (54.5%)	15 (7.2%)
Constipation	93 (44.7%)	4 (1.9%)	68 (32.5%)	3 (1.4%)
Vomiting NOS	65 (31.3%)	10 (4.8%)	64 (30.6%)	10 (4.8%)
Arthralgia	64 (30.8%)	8 (3.8%)	66 (31.6%)	6 (2.9%)
Neutropenia	22 (10.6%)	47 (22.6%)	27 (12.9%)	46 (22.0%)
Anorexia	50 (24.0%)	2 (1.0%)	59 (28.2%)	4 (1.9%)
Dyspnea	41 (19.7%)	13 (6.3%)	37 (17.7%)	15 (7.2%)
Cough	46 (22.1%)	0 (0.0%)	54 (25.8%)	1 (0.5%)
Insomnia	43 (20.7%)	2 (1.0%)	51 (24.4%)	4 (1.9%)
Peripheral neuropathy NOS	51 (24.5%)	4 (1.9%)	34 (16.3%)	0 (0.0%)

NOS not otherwise specified, Intensive Safety Population: a subject who received at least one dose of study drug and who is in complete safety collection

kinetic interaction between paclitaxel and erlotinib, while a small (~11%) but statistically significant increase in AUC values of total platinum was observed during erlotinib treatment. These findings are unlikely to bear clinical relevance, since unbound carboplatin is the bioactive species [10].

The degree of erlotinib protein binding in this study was similar to that reported previously as a single agent [4] and suggests that the chemotherapeutic agents did not result in a plasma protein-binding displacement interaction. Such an interaction could predispose to an enhanced toxicity; however, this was not observed in this phase III trial. Table 5 lists the non-hematologic adverse events occurring in greater than 25% of patients in the overall phase III study and as anticipated, there are more presumed EGFR-associated adverse events including diarrhea and rashes observed in the erlotinib-treated group. However, theses frequencies are similar to those reported in the single agent trials [4, 14]. In addition, erlotinib when combined with paclitaxel and carboplatin does not result in an increased incidence in anticipated low (grades 1, 2) or high grade (grades 3, 4) chemotherapy related toxicity, such as alopecia, vomiting, neutropenia, or peripheral neuropathy.

Although this Phase III study did not allow the assessment of erlotinib PK in a controlled fashion as a single agent, exposure and free concentrations were similar to those observed of historical data. In addition to enhanced toxicity as a result of increased systemic exposure, toxicity could also result from an enhanced effect in the absence of increased exposure. However, this does not appear to be the case (Table 5).

Randomized controlled trials have demonstrated survival benefit in patients treated with single agent erlotinib in second or third line treatment NSCLC (BR.21 study) or in combination with gemcitabine as first line treatment of advanced pancreatic adenocarcinoma [14, 15]. Two large phase III trials (TRIBUTE, TALENT) of erlotinib in combination with platinum-based chemotherapy doublet showed no survival benefit [8, 16]. Our pharmacokinetic substudy suggests the lack of benefit in these two phase III trials are unlikely attributable to a drug interactions resulting in a lower systemic exposure to the chemotherapeutic agents.

References

1. Pollack VA, Savage DM, Baker DA, Tsaparikos KE, Sloan DE, Moyer JD, Barbacci EG, Pustilnik LR, Smolarek TA, Davis JA, Vaidya MP, Arnold LD, Doty JL, Iwata KK, Morin MJ (1999) Inhibition of epidermal growth factor receptor-associated tyrosine phosphorylation in human carcinomas with CP-358, 774: dynamics of receptor inhibition in situ and antitumor effects in athymic mice. J Pharmacol Exp Ther 291:739–748
2. Data on file with OSI Pharmaceuticals
3. Higgins B, Kolinsky K, Smith M, Beck G, Rashed M, Adames V, Linn M, Wheeldon E, Gand L, Birnboeck H, Hoffmann G (2004) Antitumor activity of erlotinib (OSI-774, Tarceva) alone or in combination in human non-small cell lung cancer tumor xenograft models. Anticancer Drugs 15:503–512
4. Hidalgo M, Siu LL, Nemunaitis J, Rizzo J, Hammond LA, Takimoto C, Eckhardt SG, Tolcher A, Britten CD, Denis L, Ferrante K, Von Hoff DD, Silberman S, Rowinsky EK (2001) Phase I and pharmacologic study of OSI-774, an epidermal growth factor receptor tyrosine kinase inhibitor, in patients with advanced solid malignancies. J Clin Oncol 19:3267–3279
5. Soulieres D, Senzer NN, Vokes EE, Hidalgo M, Agarwala SS, Siu LL (2004) Multicenter phase II study of erlotinib, an oral epidermal growth factor receptor tyrosine kinase inhibitor, in patients with recurrent or metastatic squamous cell cancer of the head and neck. J Clin Oncol 22:77–85
6. Patnaik A, Wood D, Tolcher AW, Hamilton M, Kreisberg JI, Hammond LA, Schwartz G, Beeram M, Hidalgo M, Mita MM, Wolf J, Nadler P, Rowinsky EK (2006) Phase I, pharmacokinetic, and biological study of erlotinib in combination with paclitaxel and carboplatin in patients with advanced solid tumors. Clin Cancer Res 12:7406–7413
7. Ratain MJ, George CM, Janisch L, Kindler HL, Ryan C, Wood DL, Nadler PI, Vokes EE (2002) Phase I trial of erlotinib (OSI-774) in combination with gemcitabine (G) and cisplatin (P) in patients with advanced solid tumors. Proc Am Soc Clin Oncol 21:76 (Abstract 2115)
8. Herbst RS, Prager D, Hermann R, Fehrenbacher L, Johnson BE, Sandler A, Kris MG, Tran HT, Klein P, Li X, Ramies D, Johnson DH (2005) TRIBUTE Investigator Group. TRIBUTE: a phase III trial of erlotinib hydrochloride (OSI-774) combined with carboplatin and paclitaxel chemotherapy in advanced non-small-cell lung cancer. J Clin Oncol 23:5892–5899
9. Ling J, Johnson K, Miao Z, Rakhit A, Pantze M, Hamilton M, Lum B, Prakash C (2006) Metabolism and excretion of erlotinib, a small molecule inhibitor of epidermal growth factor receptor tyrosine kinase, in healthy male volunteers. Drug Metab Dispos 34:420–426
10. Canal PR (1998) Cisplatin, carboplatin, and platinum analogs. In: Growchow LB, Ames MM (eds) A clinicians guide to chemotherapy pharmacokinetics and pharmacodynamics. Williams and Wilkins, Baltimore, pp 345–374
11. Relling M, Sonnichen D (1998) Paclitaxel and Docetaxel. In: Growchow LB, Ames MM (eds) A clinicians guide to chemotherapy pharmacokinetics and pharmacodynamics. Williams and Wilkins, Baltimore, pp 3375–3394
12. Declaration of Helsinki. Adopted by the 18th World Medical Assembly, Helsinki, Finland, June 1964, amended by the 29th World Medical Assembly, Tokyo, Japan, October 1975, and the 35th World Medical Assembly, Venice, Italy, October, 1983
13. Foursorouzesh B, Hidalgo M, Takimoto C, de Bono JS, Forero L, Muralidhar B, Malik S, Patnaik A, Rizzo J, Hammond LA, Schwartz G, Goetz A, Mays T, Kiene A, Norris J, Tolcher A, Rowinsky EK, Nadler P, Wood D, Zitelli A (2002) Phase I, pharmacokinetic (PK), and biological studies of the epidermal growth factor-tyrosine kinase (EGFR-TK) inhibitor OSI-774 in combination with docetaxel. Proc Am Soc Clin Oncol 21:21 (Abstract 81)
14. Shepherd FA, Pereira JR, Ciuleanu T, Tan EH, Hirsh V, Thongprasert S, Campos D, Maoleekoonpiroj S, Smylie M, Martins R, van Kooten M, Dediu M, Findlay B, Tu D, Johnston D, Bezjak A, Clark G, Santabárbara P, Seymour L (2005) National Cancer Institute of Canada Clinical Trials Group. Erlotinib in previously treated non-small-cell lung cancer. N Engl J Med 353:123–132

15. Moore MJ, Goldstein D, Hamm J, Figer A, Hecht JR, Gallinger S, Au HJ, Murawa P, Walde D, Wolff RA, Campos D, Lim R, Ding K, Clark G, Voskoglou-Nomikos T, Ptasynski M, Parulekar W (2007) National Cancer Institute of Canada Clinical Trials Group. Erlotinib plus gemcitabine compared with gemcitabine alone in patients with advanced pancreatic cancer: a phase III trial of the National Cancer Institute of Canada Clinical Trials Group. J Clin Oncol 25:1960–1966

16. Gatzemeier U, Pluzanska A, Szczesna A, Kaukel E, Roubec J, De Rosa F, Milanowski J, Karnicka-Mlodkowski H, Pesek M, Serwatowski P, Ramlau R, Janaskova T, Vansteenkiste J, Strausz J, Manikhas GM, Von Pawel J (2007) Phase III study of erlotinib in combination with cisplatin and gemcitabine in advanced non-small-cell lung cancer: the Tarceva Lung Cancer Investigation Trial. J Clin Oncol 25(12):1545–1552

Differential Impacts of Insulin-Like Growth Factor-Binding Protein-3 (IGFBP-3) in Epithelial IGF-Induced Lung Cancer Development

Woo-Young Kim, Mi-Jung Kim,* Hojin Moon,* Ping Yuan, Jin-Soo Kim, Jong-Kyu Woo, Guangcheng Zhang, Young-Ah Suh, Lei Feng, Carmen Behrens, Carolyn S. Van Pelt, Hyunseok Kang, J. Jack Lee, Waun-Ki Hong, Ignacio I. Wistuba, and Ho-Young Lee

Departments of Thoracic Head and Neck Medical Oncology (W.-Y.K., J.-S.K., J.-K. W., G.Z., C.B., W.-K.H., I.I.W., H.-Y.L.), Pathology (M.-J.K., P.Y., C.B., I.I.W.), Genetics (Y.-A.S.), Biostatistics (L.F., J.J.L.), and Veterinary Medicine and Surgery (C.S.V.P.), The University of Texas M.D. Anderson Cancer Center, and The University of Texas Graduate School of Biomedical Sciences (J.J.L., H.-Y.L.), Houston, Texas 77030; College of Pharmacy (H.-Y.L.), Seoul National University, Seoul 151-742, Korea; School of Pharmacy (W.Y.K.), Sookmyung Women's University, Seoul 140-742, Korea; Department of Mathematics and Statistics (H.M.), California State University, Long Beach, California 90840; and Columbia University College of Physicians and Surgeons (H.K.), New York, New York 10032

The IGF axis has been implicated in the risk of various cancers. We previously reported a potential role of tissue-derived IGF in lung tumor formation and progression. However, the role of IGF-binding protein (IGFBP)-3, a major IGFBP, on the activity of tissue-driven IGF in lung cancer development is largely unknown. Here, we show that IGF-I, but not IGF-II, protein levels in non-small-cell lung cancer (NSCLC) were significantly higher than those in normal and hyperplastic bronchial epithelium. We found that IGF-I and IGFBP-3 levels in NSCLC tissue specimens were significantly correlated with phosphorylated IGF-IR (pIGF-IR) expression. We investigated the impact of IGFBP-3 expression on the activity of tissue-driven IGF-I in lung cancer development using mice carrying lung-specific human *IGF-I* transgene (*Tg*), a germline-null mutation of *IGFBP-3*, or both. Compared with wild-type ($BP3^{+/+}$) mice, mice carrying heterozygous ($BP3^{+/-}$) or homozygous ($BP3^{-/-}$) deletion of *IGFBP-3* alleles exhibited decreases in circulating IGFBP-3 and IGF-I. Unexpectedly, IGF^{Tg} mice with 50% of physiological IGFBP-3 ($BP3^{+/-}$; IGF^{Tg}) showed higher levels of pIGF-IR/IR and a greater degree of spontaneous or tobacco carcinogen [4-(methylnitrosamino)-1-(3-pyridyl)-1-butanone]-induced lung tumor development and progression than did the IGF^{Tg} mice with normal ($BP3^{+/+}$; IGF^{Tg}) or homozygous deletion of *IGFBP-3* ($BP3^{-/-}$; IGF^{Tg}). These data show that IGF-I is overexpressed in NSCLC, leading to activation of IGF-IR, and that IGFBP-3, depending on its expression level, either inhibits or potentiates IGF-I actions in lung carcinogenesis. **(*Endocrinology* 152: 2164–2173, 2011)**

The IGF play a pivotal role in cell proliferation, survival, and metabolism, and their signaling is associated with cancer, because it is required for cell transformation. IGF-I is unique among cellular growth factors in being synthesized by the liver and peripheral tissues, thus being both a tissue growth factor and an endocrine hormone (1–3). The IGF-I receptor (IGF-IR) binds to both IGF-I and IGF-II, and activated IGF-IR transfers the activated signal, mainly through phosphatidylinositol 3-kinase/AKT and MAPK (2, 3). The IGF-II receptor binds to IGF-II but has no in-

ISSN Print 0013-7227 ISSN Online 1945-7170
Printed in U.S.A.

doi: 10.1210/en.2010-0693 Received June 23, 2010. Accepted March 8, 2011.
First Published Online March 29, 2011

* M.-J. K. and H.M. contributed equally to this research.

Abbreviations: hIGF-I, Human IGF-I; IGFBP, IGF-binding protein; IGF-IR, IGF-I receptor; IHC, immunohistochemical; mIGF, murine IGF; NNK, 4-(methylnitrosamino)-1-(3-pyridyl)-1-butanone; NSCLC, non-small-cell lung cancer; pIGF-IR, phosphorylated IGF-IR; TMA, tissue microarray.

trinsic tyrosine kinase activity. Thus, the effects of IGF are mediated mainly through the IGF-IR.

Epidemiological studies have found that a high serum level of IGF-I is a risk factor for several types of cancer, including lung (4), prostate (5), breast (premenopausal) (6), and colon cancers (7). However, following studies have shown inconsistent findings regarding the link between the serum levels of IGF-I and lung cancer risk (4, 8, 9). The impact of the serum level of IGF-I on the risk of developing lung cancer, therefore, remains ambiguous. We have recently demonstrated that airway lung epithelial cells produce IGF (IGF-I and -II) in an autocrine manner, leading to deregulation of IGF-IR activation (10). Additionally, we showed that lung-specific overexpression of IGF-I in mouse promotes lung tumor development and progression, which is accelerated by the tobacco carcinogens 4-(methylnitrosamino)-1-(3-pyridyl)-1-butanone (NNK) and benzo[*a*]pyrene. These findings indicate the importance of peripheral tissue-derived IGF-I in lung cancer development, providing an explanation for the apparent inconsistent findings (4, 8, 9) in which circulating IGF were mainly analyzed.

IGF bioavailability is regulated by a family of six IGF-binding proteins (IGFBP), of which IGFBP-3 is the major IGF carrier protein in the serum (11). Previous studies have demonstrated that the serum IGF-I level in mice is significantly reduced when IGFBP-3, IGFBP-4, and IGFBP-5 are lost (12), and reduced levels of circulating IGF-I delay the onset of mammary tumor formation and suppress growth and metastasis of colon cancer (13, 14). In another murine model, however, prostate tumor development was suppressed by increased levels of circulating IGFBP-3 (15). In addition to its modulatory effect on IGF action, IGFBP-3 has IGF-independent antiproliferative and proapoptotic effects (16). These findings have led investigators to question whether IGFBP-3 plays a positive or negative role in IGF-promoted tumor development.

The association between high plasma levels of IGFBP-3 and reduced lung cancer risk was reported years ago (17). Recent studies have also demonstrated that inverse correlation between circulating IGFBP-3 and lung cancer risk (8, 18). However, other studies showed positive correlation between IGFBP-3 level and lung cancer risk (19). Therefore, the association between circulating levels of IGFBP-3 and the risk of lung cancer is not conclusive yet.

In the current study, we determined 1) the expression of the IGF-I and IGF-II in human non-small-cell lung cancer (NSCLC) and adjacent normal tissues and correlated that expression with the activation of IGF-IR/IR, 2) the link between IGFBP-3 expression and IGF-IR/IR activation in the lungs, and 3) the impact of IGFBP-3 expression levels in IGF-I-mediated pathogenesis of spontaneous and NNK-initiated lung carcinogenesis by using tissue microarrays (TMA) of human NSCLC and a mouse model of lung carcinogenesis composed of a lung-specific human *IGF-I* transgene (IGF^{Tg}) with or without a germline-null mutation of IGFBP-3. The data described herein demonstrate the positive and negative impacts of IGFBP-3 on IGF-IR activation in tumor development and progression.

Materials and Methods

Case selection and TMA construction

Archived formalin-fixed, paraffin-embedded normal/preneoplastic tissue samples and tumor samples resected from patients with NSCLC were obtained from the previously described tissue bank at The University of Texas M.D. Anderson Cancer Center (10). Tissue specimens had been collected between 1997 and 2003 from 353 lung tumors (234 adenocarcinomas and 119 squamous cell carcinomas) and were classified according to the 2004 World Health Organization classification system (20).

To assess the immunohistochemical (IHC) expression of IGF-I, IGF-II, and phosphorylated IGF-IR (pIGF-IR)/IR in the early pathogenesis of NSCLC, we studied formalin-fixed, paraffin-embedded material placed in TMA from 52 normal bronchial epithelia, 61 bronchial hyperplasias, and 32 squamous dysplasia and carcinomas *in situ* as well as 52 normal alveoli, 37 atypical adenomatous hyperplasias, and four cases of alveolar bronchiolization. After histological examination, TMA were constructed from selected NSCLC specimens by obtaining three 1-mm-diameter cores from each tumor. The clinicopathological features of lung cancer cases studied are shown in Supplemental Table 1 (published on The Endocrine Society's Journals Online web site at http://endo.endojournals.org).

IHC staining and evaluation of TMA

IHC staining procedures were performed as described previously (10). Cytoplasmic expression was blindly analyzed and quantified by two independent pathologists (P.Y. and I.I.W.), who were also unaware of the patients' outcomes, using a four-value scale of staining intensity (0, 1+, 2+, and 3+) and a percentage (0–100%) for extent of reactivity. A final cytoplasmic expression score was obtained by multiplying the intensity and extent of reactivity values (range, 0–300). Nuclear expression was quantified on a range of 0–100, according to the percentage of positive nuclei among all tumor or epithelial cells present in the TMA core specimens. The antibodies used for the staining were the following: IGF-I (Santa Cruz Biotechnology, Santa Cruz, CA), IGF-II (Upstate/Millipore, Billerica, MA), IGFBP-3 (Diagnostic Systems Laboratories, Webster, TX), and pIGF-IR/IR (Invitrogen, Carlsbad, CA).

Mice

Mice carrying lung-specific human IGF^{Tg} in *FVB/NJ* background were described previously (10, 21). Briefly, IGF^{Tg} mice convey the DNA encoding 3.7 kb of human surfactant protein C gene promoter region followed by the cDNA of human *IGF-I* and express human IGF-I (hIGF-I) in alveolar type II cells of lung, not in the plasma. Germline mutant *IGFBP-3* mice (12) were a gift from Dr. John Pintar (Rutgers University, Piscataway, NJ).

The *IGFBP-3* null mutation was transferred to *FVB/NJ*-background mice via backcrossing six times. Male *IGFBP-3* heterozygous mutant *IGF* transgenic ($BP3^{+/-}$;IGF^{Tg}) mice were mated to female *IGFBP-3* heterozygous ($BP3^{+/-}$) mice to produce the following six genotypes: $BP3^{+/+}$, $BP3^{+/-}$, $BP3^{-/-}$, $BP3^{+/+}$;IGF^{Tg}, $BP3^{+/-}$;IGF^{Tg}, and $BP3^{-/-}$;IGF^{Tg}. *IGF* transgene genotyping was performed as previously described (10, 21). An *IGFBP-3* forward primer, an *IGFBP-3* reverse primer, and a *Neo* reverse primer (TGTCCTCACTCCTATCTGGGA, ACTCCAGGGACTCTGGTCTTC, and TCGGCAGGAGCAAGGTGAGAT, respectively) were used for *IGFBP-3* genotyping. All mouse maintenance and experiments were performed according to a protocol preapproved by M.D. Anderson's Institutional Animal Care and Use Committee.

Histology and IHC of mouse lung tissues

At age 14–15 months, mice were euthanized for pathological examination of their lungs. Lung tissue specimens were fixed in formalin, dehydrated, and processed for embedding in paraffin. Every 20th 5-μm section of the paraffin blocks (20 sections total per mouse) was evaluated after hematoxylin and eosin staining by two pathologists including one animal pathologist. Adenoma and adenocarcinoma were diagnosed according to histological criteria described previously (10).

Statistical analysis

Statistical analysis of IGF-I, IGF-II, IGFBP-3, and pIGF-IR/IR expression levels was performed according to patient baseline characteristics. The independent-samples *t* test or ANOVA test were used to compare these expressions in different subgroups defined by categorical variables. Pearson correlation coefficient was used to estimate the correlation between the IGF-I/II and pIGF-IR/IR expression scores. The Student's *t* test and Fisher exact test were performed to compare the lung tumor development in mice. All of the statistical tests performed were two sided, and *P* values ≤ 0.05 were considered statistically significant. If the *P* value was >0.05 but <0.10, we considered the difference to represent a trend in the data and noted this trend. All analyses were conducted using SAS (SAS Institute, Cary, NY) or SPSS (SPSS, Chicago, IL).

ELISA

Serum levels of murine IGF (mIGF) and IGFBP-3 (mIGFBP-3) were measured by using a sandwich method with the following antibodies: antimouse IGF-I, biotinylated antimouse IGF-I, antimouse IGFBP-3, and biotinylated antimouse IGFBP-3 (R&D Systems, Minneapolis, MN; FAF02, BAF791, MAB775, and BAF775, respectively). The ELISA plate and avidin/*para*-nitrophenylphosphate were obtained from Corning (Lowell, MA) and Invitrogen, respectively. The sensitivities of the ELISAs were 0.3 and 4 ng/ml for mIGF and mIGFBP-3, respectively. The serum IGF was extracted by using a standard acid-ethanol extraction method (22). No cross-reactivity between hIGF and mIGF was observed.

Results

IGF axis protein expression is associated with lung cancer

We have shown overexpression of IGF (IGF-I and -II) and pIGF-IR/IR in human preneoplastic bronchial epithelial lesions and in lung tumors formed in mice with lung-specific overexpression of IGF-I (10), suggesting that an increase in autocrine IGF level and subsequent activation of IGF-IR are common events in the early stages of lung cancer development. These findings led us to hypothesize that tissue-derived IGF could promote progression of lung cancer. To test the hypothesis, we performed IHC analysis to evaluate expression of IGF in TMA, which were composed of 353 biopsy specimens of lung adenocarcinoma (n = 234) and squamous cell carcinoma (n = 119) and the adjacent normal tissues. A summary of the clinicopathological features of this study with the staining is described in Supplemental Table 1. Consistent with previous findings (10), IGF-I and -II staining was primarily cytoplasmic (Fig. 1). Although IGF-I staining was not associated with age, sex, or race of the patients (Supplemental Table 2), IGF-II staining was associated with gender, with a higher level in male patients. Interestingly, the expression level of IGF-I was significantly higher in NSCLC tissues than in normal tissue specimens, whereas IGF-II staining did not show such difference (Fig. 2A).

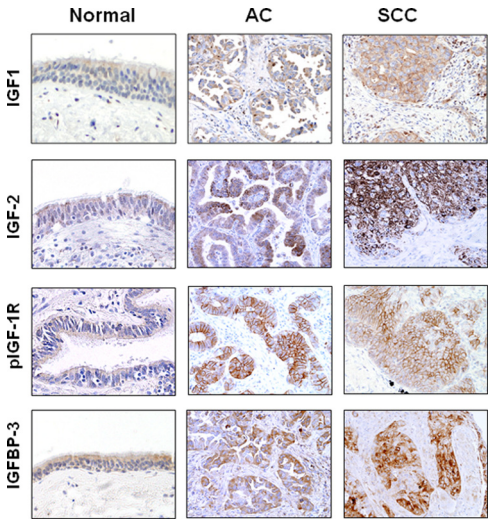

FIG. 1. Expression of IGF-I, IGF-II, pIGF-IR, and IGFBP-3 in specimens of human NSCLC. Adenocarcinomas (AC), squamous cell carcinomas (SCC), and adjacent normal tissues are shown after IHC staining.

To assess whether the increased levels of IGF were associated with activation of IGF-IR, we performed IHC analysis in the same cohort of NSCLC patients using an antibody against pIGF-IR/IR (Tyr^{1131}/Tyr^{1146}); staining appeared in the cell membrane and/or cytoplasm in 35.4% of the specimens (102 of 288 cases) (Fig. 1). Expressions of IGF-I, but not IGF-II, were significantly correlated with levels of pIGF-IR/IR staining in the membrane suggests that tissue-derived IGF-I could, in part, account for activation of IGF-IR/IR in NSCLC. However, the correlation was not robust (Fig. 2B), suggesting that other factors could have been involved in the regulation of IGF-IR/IR phosphorylation in NSCLC. In addition to the well-

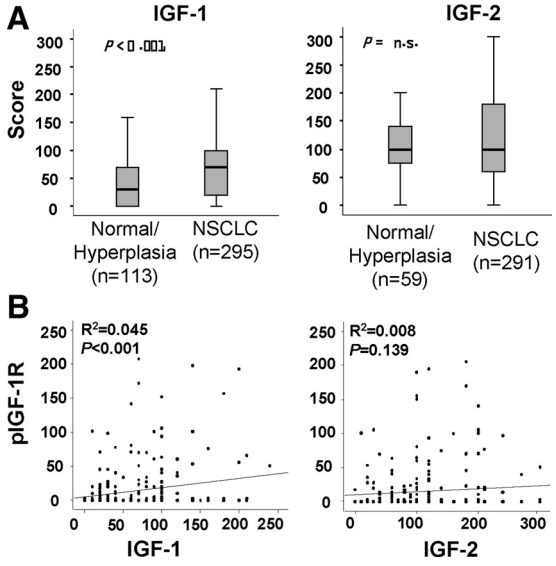

FIG. 2. IGF-I and IGF-II expression and IGF-IR activation in NSCLC. A, Expression of IGF-I and IGF-II in cancer specimens and normal/ hyperplastic lung tissues; B, correlation among IGF-I, IGF-II, and pIGF-IR/IR expression levels. Positive correlations were observed between IGF-I and pIGF-IR/IR but not between IGF-II and pIGF-IR/IR. n.s., Not significant; R^2, Pearson's coefficient.

known function in regulating bioavailability of IGF, IGFBP-3 is believed to potentiate IGF-I-induced signaling and proliferative activities depending on cellular context (23). However, the stimulatory effects of IGFBP-3 has remained elusive in NSCLC. Hence, we evaluated IGFBP-3 expression in the same specimens and assessed correlation between levels of staining for pIGF-IR/IR and IGFBP-3. We observed that the specimen that expresses IGFBP-3 at the highest quartile expresses greater pIGF-IR/IR than do the specimens at first or second to third quartile (Fig. 3). This result suggests a possibility that high expression of IGFBP-3 is associated functionally with activated IGF-IR/IR signaling in NSCLC.

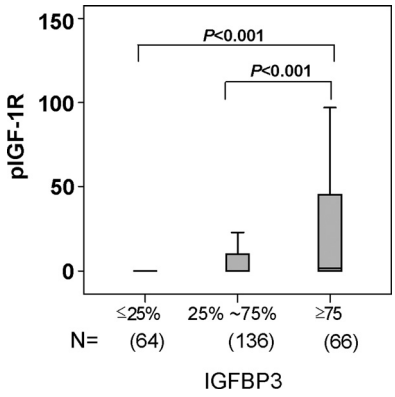

FIG. 3. Elevated pIGF-IR/IR expression in higher IGFBP-3-expressing NSCLC specimens. The box plot shows pIGF-IR/IR expression levels among 266 cases of NSCLC. The specimen with the highest quartile expression of IGFBP-3 (n = 66, ≥75%) showed significantly higher pIGF-IR/IR expression compared with the specimen with the lowest quartile expression of IGFBP-3 (n = 64, ≤25%) or medium expression of IGFBP-3 (n = 136, 25–75%). The *boxes* represent the central two quartiles (first and third quartiles), and the *bar within the box* represents the median value of pIGF-IR/IR staining.

Circulating IGF-I level is dependent on level of IGFBP-3 expression but does not determine level of IGF-IR activation in peripheral lung tissues

IGFBP-3 has been suggested to induce both inhibition and potentiation of IGF activity, whereas results from *in vivo* studies largely support the concept that IGFBP-3 enhances IGF activity by providing a stable serum reservoir of bioactive IGF-I (16, 24). Given the controversial findings on the impact of IGFBP-3 on IGF action in tumor development (13–15), we decided to investigate the role of IGFBP-3 in lung pathogenesis promoted by tissue-derived IGF in a more defined system using a transgenic mouse model. To this end, we generated mice with lung-specific IGF-I overexpression and variable levels of IGFBP-3 expression. The breeding scheme and nomenclature of the mice in this study are shown in Fig. 4A. Offspring genotypes occurred at expected Mendelian ratios; the offspring were fertile and had normal growth rates, suggesting that the genetic changes did not alter normal development. We first determined whether germline deletion of *IGFBP-3* resulted in changes in the levels of IGFBP-3 and IGF in circulation. A mouse IGFBP-3-specific ELISA showed no detectable levels of IGFBP-3 in the serum of $BP3^{-/-}$ and $BP3^{-/-}$;IGF^{Tg} mice (Fig. 4B) as expected. $BP3^{+/-}$ and $BP3^{+/-}$;IGF^{Tg} mice, which lost one allele of the *IGFBP-3* gene, had approximately 50% lower serum levels of IGFBP-3 than wild-type ($BP3^{+/+}$) mice. A mouse IGF-specific ELISA revealed that the serum levels of mIGF-I in $BP3^{+/-}$ and $BP3^{-/-}$ mice were about 80 and 45% of those in the $BP3^{+/+}$ mice, respectively, regardless of the lung-specific expression of the human *IGF-I* transgene (Fig. 3C). The serum levels of hIGF-I in the IGF^{Tg} mice were under the detection limit (6 ng/ml), indicating no significant hIGF-I secretion into circulation (data not shown). Thus, we had six cohorts with three expression levels of systemic IGF-I and IGFBP-3, with or without the lung-specific *IGF-I* transgene, as summarized in Supplemental Table 3. We examined the expression levels of pIGF-IR/IR in the lungs of these six mice groups. IHC staining analysis of pIGF-IR and IGF-IR on the lung tissues revealed that pIGF-IR staining levels normalized by that of total IGF-IR levels in the $BP3^{+/-}$;IGF^{Tg} mice group were greatest among all of the groups (Supplemental Fig. 1 and Fig. 4D), suggesting the partial loss of IGFBP-3 was more effective in activating IGF-IR than was the complete loss of IGFBP-3.

Impact of variable levels of IGFBP-3 on the effects of tissue-derived IGF-I in lung tumor development

We assessed whether changes in IGFBP-3 expression affect lung tumor development and progression in IGF^{Tg}

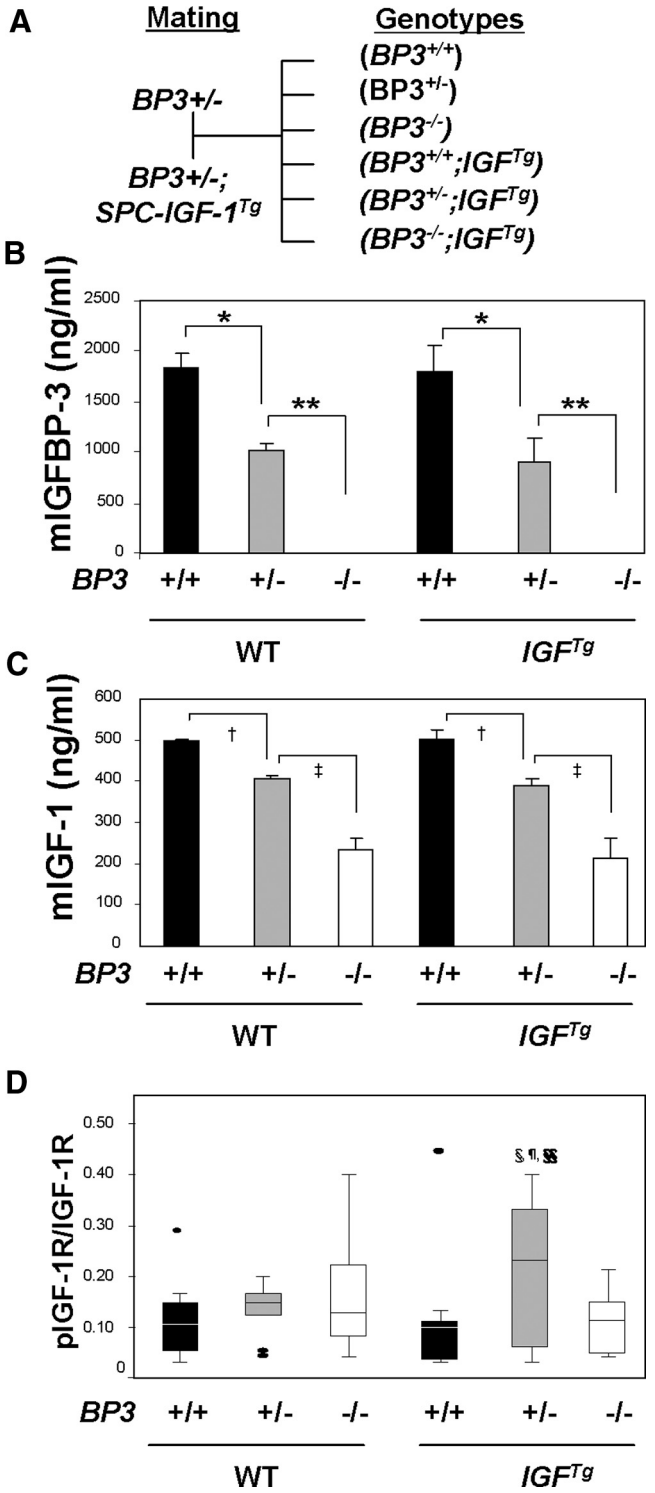

FIG. 4. The status of IGF and IGFBP-3 concentrations in serum and IGF-IR/IR activation in lungs of *IGF* transgenic and *IGFBP-3*-null mice. A, Schematic of mating strategy used to get mice with the six genotypes of *IGF* and *IGFBP-3*; n = 4 in each group, triplicate samples. B, Expression level of IGFBP-3 in serum. *, $P < 0.01$; **, $P < 0.001$. C, Circulating expression levels of mIGF. †, $P < 0.01$; ‡, $P < 0.001$; n = 4 in each group, triplicate samples. D, IHC analysis of total IGF-IR and pIGF-IR expression on bronchial epithelium. Blindly scored expression levels of pIGF-IR *vs.* IGF-IR are plotted for the mice genotypes. Each *bar* represents median, quartile, and range. Student's *t* test was used to obtain *P* values (§, ¶, §§, $P < 0.05$ compared with $BP3^{+/+}$, $BP3^{+/-}$;IGF^{Tg}, and $BP3^{-/-}$;IGF^{Tg}, respectively); n = 10 in each group. WT, Wild type.

mice. Because the tumor incidence in *FVB*-background mice increases with age (25), we ensured that the mice in each group were comparable in age at the time of analysis. Because a few IGF^{Tg} mice develop benign tumors (adenoma) at over 1 yr of age (10, 21), we evaluated 14- to 15-month-old mice. Gross appearance of representative dissected lungs is shown in the *left panels* of Fig. 5. We were able to find several small lung tumors across all genotypes, including control mice, consistent with previous findings in age-matched mice with *FVB* background (25). The tumors in the wild-type mice were small and all ad-

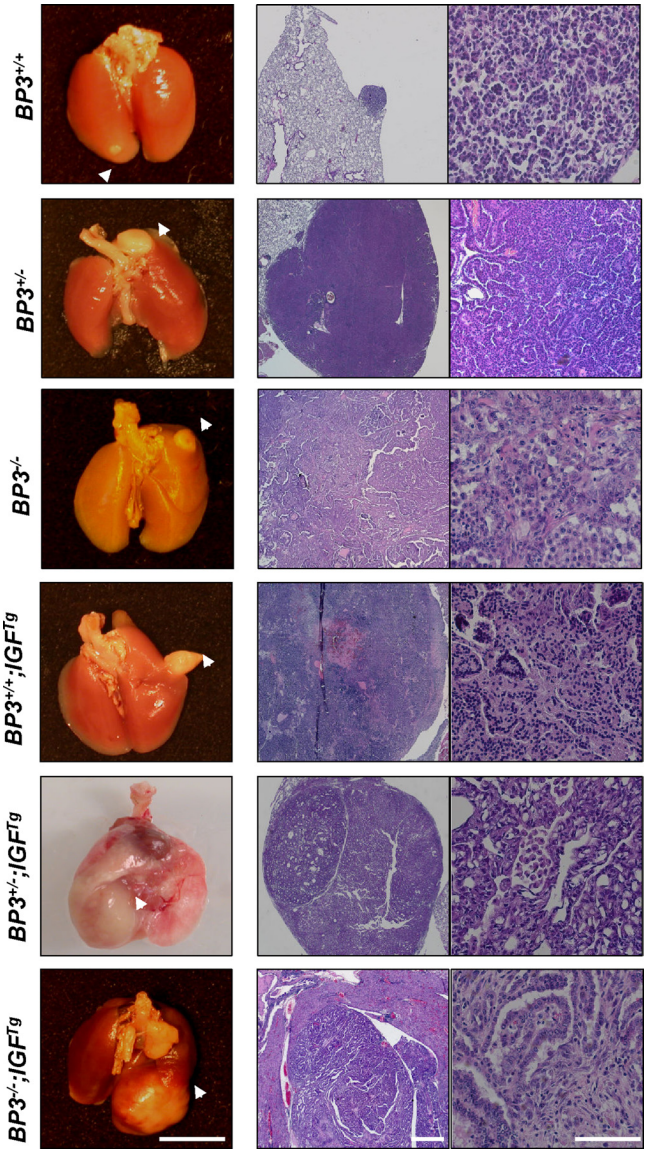

FIG. 5. Lung tumor development in *IGFBP-3* mutant and/or IGF^{Tg} mice. Profiles of spontaneous lung adenocarcinomas from 14- to 15-month-old *IGFBP-3* mutant and/or IGF^{Tg} mice. All tumors were histologically evaluated after sectioning and hematoxylin and eosin staining. *Top* ($BP3^{+/+}$), Papillary adenomas; all others, adenocarcinomas. Magnification, ×4 (*left panels*), ×25 (*middle panels*), and ×400 (*right panels*). Notable are the invasive cancer cells in $BP3^{+/-}$;IGF^{Tg} and $BP3^{-/-}$;IGF^{Tg} mice. *Scale bars*, 3 mm (*left panels*), 200 μm (*middle panels*), and 100 μm (*right panels*).

enomas (Fig. 5, *top*). Tumors larger than 3 mm in diameter and histological feature of adenocarcinoma were observed only in mice with the *IGF* transgene with and without the *IGFBP-3* deletion mutation (Fig. 5). Intensive quantitative and pathological microscopic analysis of the lungs of mice (n = 305) of all six genotypes ($BP3^{+/+}$, $BP3^{+/-}$, $BP3^{-/-}$, $BP3^{+/+}$;IGF^{Tg}, $BP3^{+/-}$;IGF^{Tg}, and $BP3^{-/-}$;IGF^{Tg}; n = 49, 53, 46, 82, 34, and 41, respectively) revealed that mice with $IGF\text{-}I^{Tg}$ and/or the *IGFBP-3* deletion mutation had a greater incidence of spontaneous lung tumors than $BP3^{+/+}$ mice (Fig. 6A). Furthermore, $BP3^{+/-}$;IGF^{Tg} mice showed the greatest tumor incidence and multiplicity (Fig. 6, A and B) than any of the other genotypes. Specifically, they showed a significantly greater mean tumor multiplicity than did $BP3^{+/+}$;IGF^{Tg} ($P < 0.05$) or $BP3^{-/-}$;IGF^{Tg} ($P < 0.01$) mice, suggesting that IGF-I-induced lung tumor formation is enhanced by reduction, but not complete loss, of IGFBP-3 expression. To assess the impact of IGFBP-3 levels on IGF-I-promoted lung tumor progression, we performed histopathological analysis of tumor tissues from mice in the six cohorts. No adenocarcinomas were observed in the $BP3^{+/+}$ mice, whereas mice from all other groups had developed adenocarcinomas and adenomas at the time of dissection. Consistent with their having the greatest tumor incidence and multiplicity, the $BP3^{+/-}$;IGF^{Tg} mice exhibited the most frequent incidence and multiplicity of adenocarcinomas (Fig. 5, C and D).

Impact of variable levels of IGFBP-3 on adenocarcinoma progression in mice with lung-specific IGF-I overexpression

Upon finding that pIGF-IR was activated by tissue IGF expression or loss of one *IGFBP-3* allele, we questioned whether the effect of IGF-IR signaling on lung cancer is at the initiation of lung carcinogenesis or at progression to lung cancer. To address this question, we explored the impact of changes in IGFBP-3 expression on lung cancer development initiated by the tobacco carcinogen NNK. Mice were treated with NNK (3 μmol, ip, once a week for 7 wk) from 8 months of age, and the resulting tumors were examined 6 months later (Fig. 6). The incidence of neoplastic lesions (hyperplasia, adenoma, and adenocarcinoma) reached 80–90% and did not differ significantly among the six genotypes (Fig. 7A). The NNK exposure enhanced lung cancer development in $BP3^{+/-}$, $BP3^{-/-}$, $BP3^{+/-}$;IGF^{Tg}, and $BP3^{-/-}$;IGF^{Tg} mice; NNK-treated mice showed about 2- to 3-fold increases in incidence and multiplicity of adenocarcinomas compared with untreated mice (compare Figs. 6 and 7). In contrast, NNK-exposed $BP3^{+/+}$ and $BP3^{+/+}$;IGF^{Tg} mice showed no detectable difference in tumor progression compared with the unexposed mice. Consistent with their having the greatest spontaneous tumor incidence and multiplicity (Fig. 6), $BP3^{+/-}$;IGF^{Tg} mice revealed the greatest malignant tumor (adenocarcinoma) development than did any other genotype. However, the difference from the $BP3^{-/-}$;IGF^{Tg} mice did not reach statistical significance. It is possible that the advantage in tumor development in the $BP3^{+/-}$;IGF^{Tg} mice over the $BP3^{-/-}$;IGF^{Tg} mice was lost in the NNK-induced cancer formation, or the difference was simply because the size of the experimental group was not big enough to reveal the difference (total 88 in the NNK-

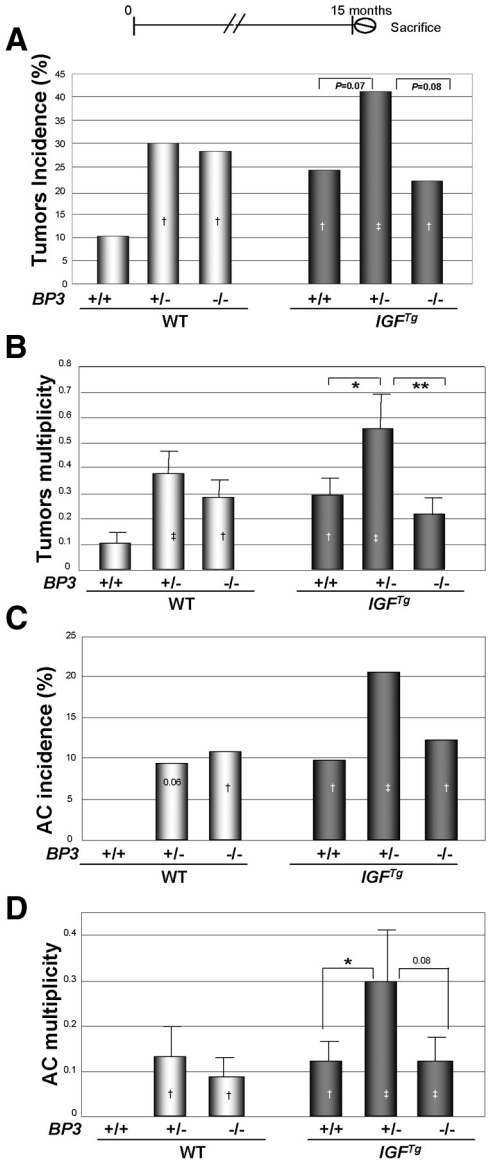

FIG. 6. Expression of *IGF* and *IGFBP-3* and lung tumor development. A, Incidence (percentage) of tumor [adenoma plus adenocarcinoma (AC)] formation per mouse; B, multiplicity of tumors per mouse; C, incidence (percentage) of AC formation per mouse; D, multiplicity of AC per mouse. The Fisher exact test (incidence) and Student's *t* test (multiplicity) were used to obtain *P* values. †, $P < 0.05$; ‡, $P < 0.01$ compared with $BP3^{+/+}$; *, $P < 0.05$; **, $P < 0.01$ compared with $BP3^{+/+}$;IGF^{Tg} or $BP3^{-/-}$;IGF^{Tg}, respectively. *P* values >0.05 but <0.1 are noted. WT, Wild type.

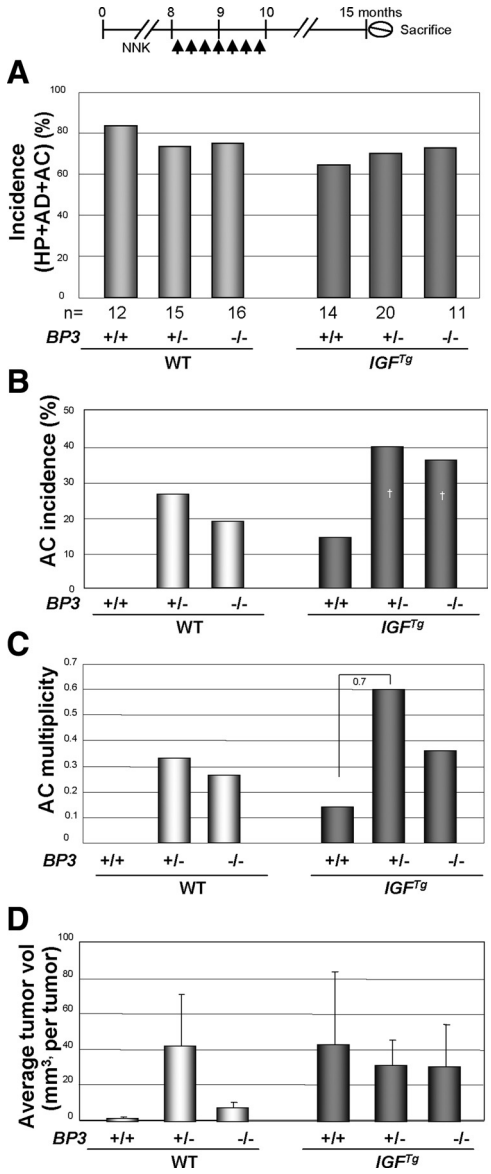

FIG. 7. Expression of IGF and IGFBP-3 and lung tumor promotion. A, The incidence of pathological lesions including hyperplasia (HP), adenomas (AD), and adenocarcinomas (AC) in mice treated with NNK are combined and shown by genotype; B and C, incidence (percentage) (B) and multiplicity (C) of AC formation per mouse (*, $P <$ 0.05; *P* values >0.05 but <0.1 are noted); D, the average volume of the tumors. The Fisher exact test (incidence) and Student's *t* test (multiplicity and average tumor volume) were used to obtain *P* values. (†, $P < 0.05$; ‡, $P < 0.01$ compared with $BP3^{+/+}$; *, $P < 0.05$, compared with $BP3^{+/+}$;IGF^{Tg}; *P* values >0.05 but <0.1 are noted). WT, Wild type.

treated group in Fig. 7, and a total of 305 were used in the spontaneous tumor group in Fig. 6).

The facts that IGF-IR activation was strongest and the lung tumor development and progression are greatest in the $BP3^{+/-}$;IGF^{Tg} mice (Figs. 4D, 6A, and 7B) clearly indicate that neither high level of expression nor complete depletion of IGFBP-3 promotes activation of IGF-IR and development of lung cancer. Notably, average tumor volume did not show a significant difference among the IGF^{Tg}, $BP3^{+/-}$;IGF^{Tg}, and $BP3^{-/-}$;IGF^{Tg} mice (Fig. 7D), suggesting that reduced levels of IGFBP-3 expression are implicated in the progression but not the growth of lung tumors.

Discussion

IGFBP-3 has been associated with both inhibitory and stimulating activity of proliferation and apoptosis in a variety of human cancer cells (26–32). Several *in vitro* studies have noted switches of IGFBP-3 bioactivity from antiproliferative to proliferative (33, 34) or from proapoptotic to antiapoptotic (35, 36). Hence, characterization of IGFBP-3's impact on cell proliferation and apoptosis is an area of active research. This study shows *in vivo* evidence that IGFBP-3 can have stimulatory or inhibitory effects on IGF bioactivity and tumor formation and progression in the lung depending on its expression level. Through the use of tumor samples from patients with NSCLC, we found that 1) the levels of tissue-derived IGF-I significantly correlated with pIGF-IR/IR in tumor samples from patients with NSCLC, although the correlation was not robust, and 2) IGFBP-3 expression levels positively correlated with pIGF-IR/IR expression. Through the use of lung-specific *IGF-I* transgenic mice (21) in which expression of IGFBP-3 was suppressed by knocking out the *IGFBP-3* genes, we further demonstrated that IGFBP-3 has a positive and a negative role in IGF-I actions and lung carcinogenesis depending on its expression level. It is likely that, if expressed at physiological levels, IGFBP-3 binds to IGF, leading to suppression of IGF actions on cell proliferation. When expressed at the decreased levels, IGF should be rapidly released from IGFBP-3, resulting in activation of the IGF-IR pathway. When IGFBP-3 is completely lost, however, IGF-I, which requires IGFBP-3 for stability, is degraded quickly, leading to IGF-IR inactivation.

Several investigations have shown the importance of IGF-IR signaling in the development of human cancers. A case-control study using samples from lung cancer patients and control subjects showed that high plasma levels of IGF-I were associated with an increased risk of lung cancer (4). A prospective cohort study, however, did not support the importance of circulating IGF-I and IGFBP-3 in lung cancer risk (8, 9). The inconsistency of these findings could be due to the fact that local production of IGF was not considered in those analyses. Our previous and current findings show that 1) expression of IGF and an associated activation of IGF-IR/IR were significantly increased in human bronchial preneoplastic (10) and NSCLC specimens compared with normal bronchial tis-

sue samples, and 2) lung tumor formation and progression is increased in mice with lung-specific IGF^{Tg}, especially when exposed to tobacco carcinogens (10).

Because tissue IGF bioactivity is regulated in large part by IGFBP-3, IGFBP-3 has been expected to be a major determinant of IGF action. Indeed, the case-control retrospective and prospective studies have found inverse correlations between circulating levels of IGFBP-3 and the risk of developing lung cancer (4, 8). IGFBP-3 has also been shown to suppress the activity of IGF-I at the tissue level *in vitro* and *in vivo* (37). We have demonstrated that overexpression of IGFBP-3 introduced by an adenoviral vector suppresses IGF-IR activation and induces apoptosis in NSCLC cells *in vitro* and *in vivo* (26). These findings indicate the inhibitory effects of IGFBP-3 on the action of IGF-I in cancer. However, occasional positive correlation between circulating IGFBP-3 and premenopausal breast cancer has been reported (38, 39). Furthermore, there is ample evidence for high expression of IGFBP-3 in a variety of cancer types, including breast, prostate, and renal cancers (40–43). Moreover, tumor size or a malignant phenotype correlate with IGFBP-3 expression levels in a number of cancers (36, 40, 42, 44, 45). These controversial findings could have been due to the complex role of IGFBP-3 in IGF-I action (46, 47) and IGF-independent suppressive effects on cell growth (48) as well as its procancerous activity regardless of its role in regulating bioavailability of IGF (23, 49).

In the present study, we show high tissue expression of IGFBP-3 in a positive correlation with pIGF-IR level in NSCLC, suggesting that increased levels of IGFBP-3 could be implicated in the activation of IGF-IR. Because the antibody we used for the human TMA for pIGF-IR detection recognizes the activated form of both IGF-IR and IR, it is possible that the signaling we observed includes the activated form of IR. IGF-IR and IR, which form heterodimers and can be activated by IGF, are closely related in structure (50) and function (51–53). Hence, the positive correlation between expression levels of IGFBP-3 and pIGF-IR/IR in NSCLC shown in the current study suggests that increased levels of IGFBP-3 could have played a positive role in activation of the IGF signaling pathway.

To determine the actual impact of IGFBP-3 expression on the bioactivity of IGF-I and lung tumorigenesis, we established a mouse model with various levels of IGFBP-3 expression (normal, reduced, and absent) by mating IGF^{Tg} mice (21) with *IGFBP-3* knockout mice. We observed that 50% ($BP3^{+/-}$) or complete loss ($BP3^{-/-}$) of IGFBP-3 expression led to reduction in serum level of IGF-I by about 19–23 or 54–58%, respectively. Given that 80% of circulating IGF bind to IGFBP-3 (16), decreases of less than 60% in the level of circulating IGF-I in the $BP3^{-/-}$ mice indicated possible compensation by other IGFBP family members. However, we were not able to detect any compensatory increase of IGFBP, including IGFBP-2 and -4, in $BP3^{+/-}$ and $BP3^{-/-}$ mice (data not shown). Nevertheless, given a previous finding of significantly delayed carcinogenesis/cancer cell growth in liver-specific IGF-null mice (13), which had only 10–25% of the normal serum IGF level, we expected that the 19–58% reduction in the level of circulating IGF-I would suppress lung cancer development. However, the mice with reduced or loss of IGFBP-3 expression ($BP3^{+/-}$, $BP3^{-/-}$) had obviously greater overall tumor incidence and multiplicity than in the wild-type mice ($BP3^{+/+}$) mice. These results, which contradict previous reports showing a positive correlation between circulating IGF-I and cancer development (54), indicate the importance of tissue-derived (rather than serum) IGF-I in its bioavailability in lung epithelial cells during the process of lung tumor formation. The increased tumor incidence in $BP3^{+/-}$ and $BP3^{-/-}$ mice compared with that in $BP3^{+/+}$ mice could have resulted from the decrease or loss of IGFBP-3's IGF-I-independent antiproliferative activity, but the greater tumor development and progression in $BP3^{+/-}$ mice than in $BP3^{-/-}$ mice does not support that notion. Our observations, including 1) the increased tumor incidence and multiplicity in $BP3^{+/-}$ mice, especially when IGF-I was overexpressed in the lung, and 2) the accelerated tumor progression in $BP3^{+/-}$;IGF^{Tg} mice compared with $BP3^{+/+}$;IGF^{Tg} mice or $BP3^{-/-}$;IGF^{Tg} mice provide novel *in vivo* evidence that support a significant role for IGFBP-3 in potentiating IGF action.

The accelerated tumor progression in $BP3^{+/-}$;IGF^{Tg} mice could have resulted simply from accelerated transformation of lung epithelial cells and/or enhanced initiation and promotion of lung tumors owing to activation of IGF-IR. However, $BP3^{+/-}$;IGF^{Tg} mice had the greater multiplicity of adenocarcinomas with local invasion than did $BP3^{+/+}$;IGF^{Tg} mice or $BP3^{-/-}$;IGF^{Tg} mice after lung tumor initiation was synchronized by NNK injection. These findings strongly imply a role of IGFBP-3 in both lung tumor formation and progression. The advanced pathogenesis in $BP3^{+/-}$;IGF^{Tg} mice can be explained by increased net tissue bioavailability of IGF-I regardless of the loss of circulating IGF-I as a benefit from partial depletion of tissue levels of IGFBP-3. Supporting this hypothesis is our finding that $BP3^{+/-}$;IGF^{Tg} mice had greater IGF-IR activation than did $BP3^{+/+}$;IGF^{Tg} mice. However, the more severe phenotype and the greater IGF-IR activation in $BP3^{+/-}$;IGF^{Tg} mice than in $BP3^{-/-}$;IGF^{Tg} mice supports the protective role of IGFBP-3 in IGF action; *e.g.* the complete loss of IGFBP-3 could have resulted in the suppression of IGF signaling. These results

emphasize the critical function of IGFBP-3 as a reservoir for IGF bioactivity as suggested by the previous reports in certain contexts (16, 24). Another possible explanation is that IGFBP-3 mediates procancer activity through unknown novel mechanisms independent of its modulation of IGF signaling. Indeed, IGFBP-3 directly interacts with the integrin or caveolin and propagates the mitotic signal downstream (49). Nevertheless, these findings suggest that IGFBP-3 can either suppress or enhance lung tumor formation and progression depending on the level of expression.

In summary, our findings using human patient tumor specimens and an *in vivo* mouse system demonstrate that 1) expression of IGF-I is higher in NSCLC than in normal tissue, 2) lung tumor development and progression are mainly regulated by levels of tissue-derived IGF-I but not circulating IGF-I, 3) decreased but not completely absent expression of IGFBP-3 elevates local availability of IGF-I in lung tissue and increases the risk of lung cancer, and 4) IGFBP-3 may not only suppress but also enhance IGF-I actions on and risk of developing lung cancer. In light of these issues, further studies with liver- and lung-specific IGFBP-3-null mice are warranted to confirm the role of IGFBP-3 in lung cancer development. Our findings also indicate that attempts to modulate serum or tissue levels of IGFBP-3 in cancer therapy must be approached with caution.

Acknowledgments

Address all correspondence and requests for reprints to: Ho-Young Lee, Ph.D., College of Pharmacy, Seoul National University, Sillim 9 Dong, 599 Kwanakro, Kwanak-Gu, Seoul 151-742, Korea. E-mail: hylee135@snu.ac.kr.

This work was supported by National Institutes of Health Grants R01 CA109520 and CA100816-01A1 (to H.-Y. L.) and in part by grants from the National Foundation for Cancer Research, the Department of Defense, the VITAL program (W81XWH-04-1-0142), and the BATTLE program (W81XWH-06-1-0303) (to W.-K.H.).

Current address for M.-J.K.: Department of Pathology, University of Ulsan College of Medicine, Asan Medical Center, Seoul 138-736, Korea.

Disclosure Summary: The authors do not have any conflicts of interest to disclose.

References

1. **Yakar S, Liu JL, Stannard B, Butler A, Accili D, Sauer B, LeRoith D** 1999 Normal growth and development in the absence of hepatic insulin-like growth factor I. Proc Natl Acad Sci USA 96:7324–7329
2. **Pollak MN** 2004 Insulin-like growth factors and neoplasia. Novartis Found Symp 262:84–98; discussion 98–107, 265–108
3. **Pollak M** 2008 Insulin and insulin-like growth factor signalling in neoplasia. Nat Rev Cancer 8:915–928
4. **Yu H, Spitz MR, Mistry J, Gu J, Hong WK, Wu X** 1999 Plasma levels of insulin-like growth factor-I and lung cancer risk: a case-control analysis. J Natl Cancer Inst 91:151–156
5. **Chan JM, Stampfer MJ, Giovannucci E, Gann PH, Ma J, Wilkinson P, Hennekens CH, Pollak M** 1998 Plasma insulin-like growth factor-I and prostate cancer risk: a prospective study. Science 279:563–566
6. **Hankinson SE, Willett WC, Colditz GA, Hunter DJ, Michaud DS, Deroo B, Rosner B, Speizer FE, Pollak M** 1998 Circulating concentrations of insulin-like growth factor-I and risk of breast cancer. Lancet 351:1393–1396
7. **Ma J, Pollak M, Giovannucci E, Chan JM, Tao Y, Hennekens C, Stampfer MJ** 2000 A prospective study of plasma levels of insulin-like growth factor I (IGF-I) and IGF-binding protein-3, and colorectal cancer risk among men. Growth Horm IGF Res 10(Suppl A):S28–S29
8. **London SJ, Yuan JM, Travlos GS, Gao YT, Wilson RE, Ross RK, Yu MC** 2002 Insulin-like growth factor I, IGF-binding protein 3, and lung cancer risk in a prospective study of men in China. J Natl Cancer Inst 94:749–754
9. **Lukanova A, Toniolo P, Akhmedkhanov A, Biessy C, Haley NJ, Shore RE, Riboli E, Rinaldi S, Kaaks R** 2001 A prospective study of insulin-like growth factor-I, IGF-binding proteins-1, -2 and -3 and lung cancer risk in women. Int J Cancer 92:888–892
10. **Kim WY, Jin Q, Oh SH, Kim ES, Yang YJ, Lee DH, Feng L, Behrens C, Prudkin L, Miller YE, Lee JJ, Lippman SM, Hong WK, Wistuba II, Lee HY** 2009 Elevated epithelial insulin-like growth factor expression is a risk factor for lung cancer development. Cancer Res 69:7439–7448
11. **Firth SI, Kaufman PL, De Jean BJ, Byers JM, Marshak DW** 2002 Innervation of the uvea by galanin and somatostatin immunoreactive axons in macaques and baboons. Exp Eye Res 75:49–60
12. **Ning Y, Schuller AG, Bradshaw S, Rotwein P, Ludwig T, Frystyk J, Pintar JE** 2006 Diminished growth and enhanced glucose metabolism in triple knockout mice containing mutations of insulin-like growth factor binding protein-3, -4, and -5. Mol Endocrinol 20:2173–2186
13. **Wu Y, Yakar S, Zhao L, Hennighausen L, LeRoith D** 2002 Circulating insulin-like growth factor-I levels regulate colon cancer growth and metastasis. Cancer Res 62:1030–1035
14. **Wu X, Tortolero-Luna G, Zhao H, Phatak D, Spitz MR, Follen M** 2003 Serum levels of insulin-like growth factor I and risk of squamous intraepithelial lesions of the cervix. Clin Cancer Res 9:3356–3361
15. **Silha JV, Sheppard PC, Mishra S, Gui Y, Schwartz J, Dodd JG, Murphy LJ** 2006 Insulin-like growth factor (IGF) binding protein-3 attenuates prostate tumor growth by IGF-dependent and IGF-independent mechanisms. Endocrinology 147:2112–2121
16. **Baxter RC** 1994 Insulin-like growth factor binding proteins in the human circulation: a review. Horm Res 42:140–144
17. **Yu H, Rohan T** 2000 Role of the insulin-like growth factor family in cancer development and progression. J Natl Cancer Inst 92:1472–1489
18. **Wakai K, Ito Y, Suzuki K, Tamakoshi A, Seki N, Ando M, Ozasa K, Watanabe Y, Kondo T, Nishino Y, Ohno Y** 2002 Serum insulin-like growth factors, insulin-like growth factor-binding protein-3, and risk of lung cancer death: a case-control study nested in the Japan Collaborative Cohort (JACC) Study. Jpn J Cancer Res 93:1279–1286
19. **Spitz MR, Barnett MJ, Goodman GE, Thornquist MD, Wu X, Pollak M** 2002 Serum insulin-like growth factor (IGF) and IGF-binding protein levels and risk of lung cancer: a case-control study nested in the beta-Carotene and Retinol Efficacy Trial Cohort. Cancer Epidemiol Biomarkers Prev 11:1413–1418
20. **Beasley MB, Brambilla E, Travis WD** 2005 The 2004 World Health

Organization classification of lung tumors. Semin Roentgenol 40: 90–97
21. **Frankel SK, Moats-Staats BM, Cool CD, Wynes MW, Stiles AD, Riches DW** 2005 Human insulin-like growth factor-IA expression in transgenic mice promotes adenomatous hyperplasia but not pulmonary fibrosis. Am J Physiol Lung Cell Mol Physiol 288:L805–L812
22. **Chestnut RE, Quarmby V** 2002 Evaluation of total IGF-I assay methods using samples from type I and type II diabetic patients. J Immunol Methods 259:11–24
23. **Martin JL, Lin MZ, McGowan EM, Baxter RC** 2009 Potentiation of growth factor signaling by insulin-like growth factor-binding protein-3 in breast epithelial cells requires sphingosine kinase activity. J Biol Chem 284:25542–25552
24. **Clemmons DR** 1997 Insulin-like growth factor binding proteins and their role in controlling IGF actions. Cytokine Growth Factor Rev 8:45–62
25. **Huang P, Duda DG, Jain RK, Fukumura D** 2008 Histopathologic findings and establishment of novel tumor lines from spontaneous tumors in FVB/N mice. Comp Med 58:253–263
26. **Lee HY, Chun KH, Liu B, Wiehle SA, Cristiano RJ, Hong WK, Cohen P, Kurie JM** 2002 Insulin-like growth factor binding protein-3 inhibits the growth of non-small cell lung cancer. Cancer Res 62:3530–3537
27. **Baxter RC** 2001 Signalling pathways involved in antiproliferative effects of IGFBP-3: a review. Mol Pathol 54:145–148
28. **Oh Y, Müller HL, Lamson G, Rosenfeld RG** 1993 Insulin-like growth factor (IGF)-independent action of IGF-binding protein-3 in Hs578T human breast cancer cells. Cell surface binding and growth inhibition. J Biol Chem 268:14964–14971
29. **Rajah R, Valentinis B, Cohen P** 1997 Insulin-like growth factor (IGF)-binding protein-3 induces apoptosis and mediates the effects of transforming growth factor-beta1 on programmed cell death through a p53- and IGF-independent mechanism. J Biol Chem 272: 12181–12188
30. **Bhattacharyya N, Pechhold K, Shahjee H, Zappala G, Elbi C, Raaka B, Wiench M, Hong J, Rechler MM** 2006 Nonsecreted insulin-like growth factor binding protein-3 (IGFBP-3) can induce apoptosis in human prostate cancer cells by IGF-independent mechanisms without being concentrated in the nucleus. J Biol Chem 281:24588–24601
31. **Butt AJ, Fraley KA, Firth SM, Baxter RC** 2002 IGF-binding protein-3-induced growth inhibition and apoptosis do not require cell surface binding and nuclear translocation in human breast cancer cells. Endocrinology 143:2693–2699
32. **Liu B, Lee HY, Weinzimer SA, Powell DR, Clifford JL, Kurie JM, Cohen P** 2000 Direct functional interactions between insulin-like growth factor-binding protein-3 and retinoid X receptor-α regulate transcriptional signaling and apoptosis. J Biol Chem 275:33607–33613
33. **Butt AJ, Martin JL, Dickson KA, McDougall F, Firth SM, Baxter RC** 2004 Insulin-like growth factor binding protein-3 expression is associated with growth stimulation of T47D human breast cancer cells: the role of altered epidermal growth factor signaling. J Clin Endocrinol Metab 89:1950–1956
34. **Firth SM, Fanayan S, Benn D, Baxter RC** 1998 Development of resistance to insulin-like growth factor binding protein-3 in transfected T47D breast cancer cells. Biochem Biophys Res Commun 246:325–329
35. **McCaig C, Perks CM, Holly JM** 2002 Intrinsic actions of IGFBP-3 and IGFBP-5 on Hs578T breast cancer epithelial cells: inhibition or accentuation of attachment and survival is dependent upon the presence of fibronectin. J Cell Sci 115:4293–4303
36. **Granata R, Trovato L, Garbarino G, Taliano M, Ponti R, Sala G, Ghidoni R, Ghigo E** 2004 Dual effects of IGFBP-3 on endothelial cell apoptosis and survival: involvement of the sphingolipid signaling pathways. FASEB J 18:1456–1458
37. **Ali O, Cohen P, Lee KW** 2003 Epidemiology and biology of insulin-like growth factor binding protein-3 (IGFBP-3) as an anti-cancer molecule. Horm Metab Res 35:726–733
38. **Krajcik RA, Borofsky ND, Massardo S, Orentreich N** 2002 Insulin-like growth factor I (IGF-I), IGF-binding proteins, and breast cancer. Cancer Epidemiol Biomarkers Prev 11:1566–1573
39. **Yu H, Jin F, Shu XO, Li BD, Dai Q, Cheng JR, Berkel HJ, Zheng W** 2002 Insulin-like growth factors and breast cancer risk in Chinese women. Cancer Epidemiol Biomarkers Prev 11:705–712
40. **Rocha RL, Hilsenbeck SG, Jackson JG, Lee AV, Figueroa JA, Yee D** 1996 Correlation of insulin-like growth factor-binding protein-3 messenger RNA with protein expression in primary breast cancer tissues: detection of higher levels in tumors with poor prognostic features. J Natl Cancer Inst 88:601–606
41. **Singh D, Febbo PG, Ross K, Jackson DG, Manola J, Ladd C, Tamayo P, Renshaw AA, D'Amico AV, Richie JP, Lander ES, Loda M, Kantoff PW, Golub TR, Sellers WR** 2002 Gene expression correlates of clinical prostate cancer behavior. Cancer Cell 1:203–209
42. **Yu H, Levesque MA, Khosravi MJ, Papanastasiou-Diamandi A, Clark GM, Diamandis EP** 1996 Associations between insulin-like growth factors and their binding proteins and other prognostic indicators in breast cancer. Br J Cancer 74:1242–1247
43. **Chuang ST, Patton KT, Schafernak KT, Papavero V, Lin F, Baxter RC, Teh BT, Yang XJ** 2008 Over expression of insulin-like growth factor binding protein 3 in clear cell renal cell carcinoma. J Urol 179:445–449
44. **Granata R, Trovato L, Lupia E, Sala G, Settanni F, Camussi G, Ghidoni R, Ghigo E** 2007 Insulin-like growth factor binding protein-3 induces angiogenesis through IGF-I- and SphK1-dependent mechanisms. J Thromb Haemost 5:835–845
45. **Hansel DE, Rahman A, House M, Ashfaq R, Berg K, Yeo CJ, Maitra A** 2004 Met proto-oncogene and insulin-like growth factor binding protein 3 overexpression correlates with metastatic ability in well-differentiated pancreatic endocrine neoplasms. Clin Cancer Res 10: 6152–6158
46. **De Mellow JS, Baxter RC** 1988 Growth hormone-dependent insulin-like growth factor (IGF) binding protein both inhibits and potentiates IGF-I-stimulated DNA synthesis in human skin fibroblasts. Biochem Biophys Res Commun 156:199–204
47. **Conover CA** 1992 Potentiation of insulin-like growth factor (IGF) action by IGF-binding protein-3: studies of underlying mechanism. Endocrinology 130:3191–3199
48. **Gill ZP, Perks CM, Newcomb PV, Holly JM** 1997 Insulin-like growth factor-binding protein (IGFBP-3) predisposes breast cancer cells to programmed cell death in a non-IGF-dependent manner. J Biol Chem 272:25602–25607
49. **Burrows C, Holly JM, Laurence NJ, Vernon EG, Carter JV, Clark MA, McIntosh J, McCaig C, Winters ZE, Perks CM** 2006 Insulin-like growth factor binding protein 3 has opposing actions on malignant and nonmalignant breast epithelial cells that are each reversible and dependent upon cholesterol-stabilized integrin receptor complexes. Endocrinology 147:3484–3500
50. **Lawrence MC, McKern NM, Ward CW** 2007 Insulin receptor structure and its implications for the IGF-1 receptor. Curr Opin Struct Biol 17:699–705
51. **Belfiore A** 2007 The role of insulin receptor isoforms and hybrid insulin/IGF-I receptors in human cancer. Curr Pharm Des 13:671–686
52. **Belfiore A, Frasca F, Pandini G, Sciacca L, Vigneri R** 2009 Insulin receptor isoforms and insulin receptor/insulin-like growth factor receptor hybrids in physiology and disease. Endocr Rev 30:586–623
53. **Heuson JC, Legros N** 1972 Influence of insulin deprivation on growth of the 7,12-dimethylbenz (a) anthracene-induced mammary carcinoma in rats subjected to alloxan diabetes and food restriction. Cancer Res 32:226–232
54. **Wu X, Yu H, Amos CI, Hong WK, Spitz MR** 2000 Joint effect of insulin-like growth factors and mutagen sensitivity in lung cancer risk. J Natl Cancer Inst 92:737–743

Efficacy of bevacizumab plus erlotinib versus erlotinib alone in advanced non-small-cell lung cancer after failure of standard first-line chemotherapy (BeTa): a double-blind, placebo-controlled, phase 3 trial

Roy S Herbst, Rafat Ansari, Frederique Bustin, Patrick Flynn, Lowell Hart, Gregory A Otterson, Gordana Vlahovic, Chang-Heok Soh, Paula O'Connor, John Hainsworth

Lancet 2011; 377: 1846–54

See Comment page 1810

Department of Thoracic/Head and Neck Medical Oncology, The University of Texas, MD Anderson Cancer Center, Houston, TX, USA (R S Herbst MD); **Michiana Hematology/Oncology, South Bend, IN, USA** (R Ansari MD); **Centre Hospitalier Regional de la Citadelle, Liege, Belgium** (F Bustin MD); **Minnesota Oncology Hematology PA, Maplewood, MN, USA** (P Flynn MD); **Florida Cancer Specialists, Fort Myers, FL, USA** (L Hart MD); **Ohio State University Medical Center, Columbus, OH, USA** (G A Otterson MD); **Duke University Medical Center, Durham, NC, USA** (G Vlahovic MD); **Genentech, South San Francisco, CA, USA** (C-H Soh PhD, P O'Connor MD); **and Sarah Cannon Research Institute, Nashville, TN, USA** (J Hainsworth MD)

Correspondence to:
Dr Roy S Herbst, Yale Cancer Center, 333 Cedar Street, PO Box 208028, New Haven, CT 06520–8028, USA
roy.herbst@yale.edu

Summary

Background Bevacizumab and erlotinib target different tumour growth pathways with little overlap in their toxic-effect profiles. On the basis of promising results from a phase 1/2 trial assessing safety and activity of erlotinib plus bevacizumab for recurrent or refractory non-small-cell lung cancer (NSCLC), we aimed to assess efficacy and safety of this combination in a phase 3 trial.

Methods In our double-blind, placebo-controlled, randomised phase 3 trial (BeTa), we enrolled patients with recurrent or refractory NSCLC who presented to 177 study sites in 12 countries after failure of first-line treatment. Patients were randomly allocated in a one-to-one ratio to receive erlotinib plus bevacizumab (bevacizumab group) or erlotinib plus placebo (control group) according to a computer-generated randomisation sequence by use of an interactive voice response system. The primary endpoint was overall survival in all enrolled patients. Patients, study staff, and investigators were masked to treatment assignment. We assessed safety by calculation of incidence of adverse events and tissue was collected for biomarker analyses. This trial is registered with ClinicalTrials.gov, number NCT00130728.

Findings Overall survival did not differ between 317 controls and 319 patients in the bevacizumab group (hazard ratio [HR] 0·97, 95% CI 0·80–1·18, p=0·7583). Median overall survival was 9·3 months (IQR 4·1–21·6) for patients in the bevacizumab group compared with 9·2 months (3·8–20·2) for controls. Progression-free survival seemed to be longer in the bevacizumab group (3·4 months [1·4–8·4]) than in the control group (1·7 months [1·3–4·1]; HR 0·62, 95% CI 0·52–0·75) and objective response rate suggested some clinical activity of bevacizumab and erlotinib. However, these secondary endpoint differences could not be defined as significant because the study prespecified that the primary endpoint had to be significant before testing of secondary endpoints could be done, to control type I error rate. In the bevacizumab group, 130 (42%) of 313 patients with safety data had a serious adverse event, compared with 114 (36%) controls. There were 20 (6%) grade 5 adverse events, including two arterial thromboembolic events, in the bevacizumab group, and 14 (4%) in the control group.

Interpretation Addition of bevacizumab to erlotinib does not improve survival in patients with recurrent or refractory NSCLC.

Funding Genentech.

Introduction

Lung cancer is the leading cause of cancer-related deaths worldwide.[1–3] 1·5 million people were diagnosed with the disease in 2008 and more than 1·3 million died.[1] Non-small-cell lung cancers (NSCLCs) account for more than 85% of all lung cancers;[1] about 75% of patients with NSCLC present with advanced-stage (unresectable or metastatic) disease.

Erlotinib is a small-molecule inhibitor of the epidermal growth factor receptor (EGFR), a tyrosine kinase receptor,[4,5] which is approved by the US Food and Drug Administration for treatment of patients with locally advanced or metastatic NSCLC whose disease has not responded to more than one previous chemotherapy regimen.[4,5] A phase 3 study[5] showed that second-line or third-line monotherapy with erlotinib improved overall survival in patients with NSCLC.

The recombinant, anti-vascular endothelial growth factor (anti-VEGF) monoclonal antibody bevacizumab, combined with paclitaxel and carboplatin, was approved by the US Food and Drug Administration for first-line treatment of patients with unresectable, locally advanced, recurrent, or metastatic non-squamous NSCLC.[6] A phase 3 study showed this combination significantly improved overall survival and progression-free survival in patients with NSCLC compared with carboplatin and paclitaxel alone.[7,8] Another phase 3 trial[9] showed that the addition of bevacizumab to cisplatin and gemcitabine improved progression-free survival and objective responses rates for first-line treatment of non-squamous NSCLC; however, overall survival was not improved.

Bevacizumab and erlotinib target different tumour growth pathways (angiogenesis and EGFR activity,

respectively) with little overlap in their toxic-effect profiles. These two drugs have potentially complementary mechanisms to control tumour growth.[10–14]

The safety and activity of combination erlotinib-bevacizumab were assessed in a phase 1/2 trial[15] for patients with relapsed and refractory non-squamous NSCLC. The combination dose was established at 15 mg/kg bevacizumab once every 3 weeks and 150 mg erlotinib once per day. The objective response rate in 34 patients in phase 2 was 20%, disease-control rate was 85%, and median overall survival was 12·6 months.[15]

In a multicentre phase 2 trial[16] of patients with relapsed and refractory non-squamous NSCLC who were randomly allocated to receive erlotinib plus bevacizumab, bevacizumab and chemotherapy, or chemotherapy alone, median overall survival was better in the groups that received bevacizumab (13·7 months for erlotinib plus bevacizumab and 12·6 months for bevacizumab and chemotherapy) than it was with chemotherapy alone (8·6 months); safety data favoured the erlotinib plus bevacizumab group.

In this phase 3 trial, we aimed to further assess the efficacy of bevacizumab in combination with erlotinib compared with erlotinib and placebo in patients with recurrent or refractory advanced-stage NSCLC who had disease progression during or after first-line therapy.

Methods

Study design and participants

In our international, double-blind, placebo-controlled phase 3 trial (BeTa), we enrolled patients who presented to 177 study sites in 12 countries with cytologically or histologically confirmed advanced-stage NSCLC that was recurrent or refractory after standard first-line chemotherapy or chemoradiotherapy. Patients were eligible if they were aged 18 years or older and had Eastern Cooperative Oncology Group performance status scores of 2 or lower. Patients with squamous cell carcinoma were eligible if their disease was extrathoracic or if intrathoracic lesions were peripheral. Patients with a history of brain metastases who were treated with a minimum of whole-brain radiotherapy and with no ongoing dexamethasone requirement, patients requiring anticoagulation (low-molecular-weight heparins only), and patients who had received neoadjuvant and adjuvant therapy for stage I–IIIa disease were also eligible.

Patients were ineligible for inclusion if they had had a myocardial infarction within the previous 6 months, unstable angina, congestive heart failure, symptomatic arrhythmia, substantial peripheral vascular disease, uncontrolled hypertension, history of gross haemoptysis, presence of a cavitary lesion or tumour invading or abutting major blood vessels, bleeding diathesis or coagulopathy, abnormal haematological values, abnormal liver function tests, used warfarin or equivalents, used aspirin or non-steroidal anti-inflammatory drugs, a surgical procedure on-study or within 28 days before randomisation, previous treatment with anti-EGFR or anti-angiogenesis agents, another invasive cancer within 5 years before randomisation, neurosurgery for brain metastases within 6 months of day 0, and brain biopsy within 3 months of day 0.

All enrolled patients provided signed informed consent and consented to analysis of archival diagnostic tissue if available. Institutional review board approval was obtained at every study site.

Randomisation and masking

Patients were randomly allocated in a one-to-one ratio to receive erlotinib plus bevacizumab (bevacizumab group) or erlotinib plus placebo (control group) by use of an interactive voice-response system with a computer-generated allocation sequence. Staff at Genentech (South San Fransisco, CA, USA), investigators, and patients were masked to treatment assignment. Patients were stratified by sex, baseline Eastern Cooperative Oncology Group performance status score (0 or 1 *vs* 2), smoking history (never *vs* current or previous), and study site. Unmasked adverse events data were provided every month to an independent data and safety monitoring board.

Procedures

Patients received placebo or bevacizumab administered at 15 mg/kg by intravenous infusion on the first day of 3-week cycles (±4 days). Erlotinib was taken orally at 150 mg per day, beginning on the first day of the first cycle. Patients remained on treatment until there was documented evidence of radiographic or clinical disease

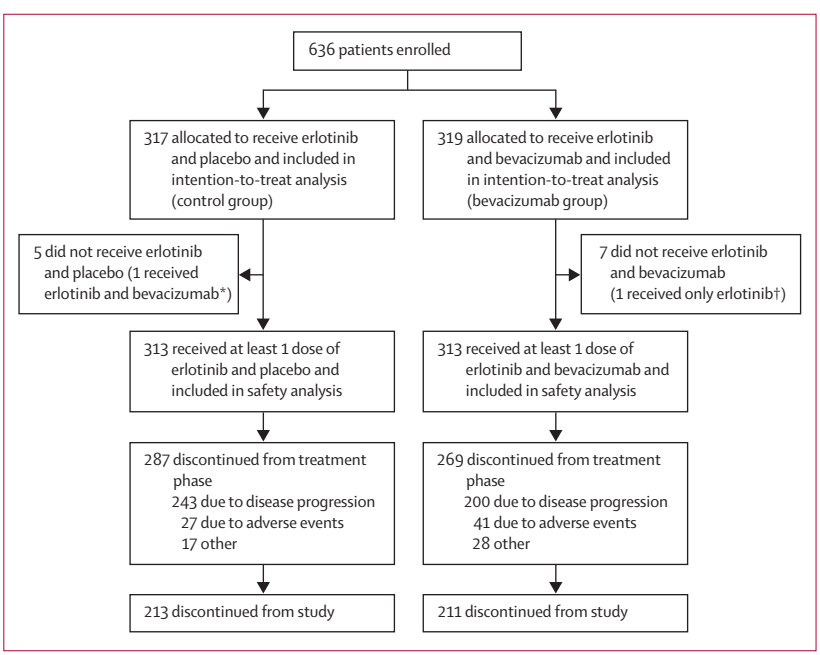

Figure 1: **Trial profile**

*This patient was analysed as part of the bevacizumab group for safety analyses. †This patient was analysed as part of the control group for safety analyses.

progression or unmanageable toxic effects. If toxic effects were caused by bevacizumab, patients could continue on erlotinib until disease progression or unmanageable toxic effects. Patients who discontinued erlotinib received no further study treatment. Subsequent therapy was provided at the treating doctor's discretion. All patients were followed-up for survival until death, loss to follow-up, or study termination by the sponsor, whichever occurred first.

	Control group (n=317)	Bevacizumab group (n=319)
Sex		
Men	170 (54%)	171 (54%)
Women	147 (46%)	148 (46%)
Age, years	65·0 (10·3)	64·8 (10·4)
Race		
White	257 (81%)	264 (83%)
Black	33 (10%)	21 (7%)
Asian/Pacific islander	18 (6%)	23 (7%)
Hispanic	8 (3%)	10 (3%)
American Indian/Alaskan native	1 (<1%)	0
Other	0	1 (<1%)
Smoking history		
Never	33 (10%)	34 (11%)
Previous	212 (67%)	237 (74%)
Current	72 (23%)	48 (15%)
ECOG performance status score		
0	121/317 (38%)	129/318 (41%)
1	176/317 (56%)	166/318 (52%)
2	20/317 (6%)	23/318 (7%)
Time since initial diagnosis		
<6 months	78/312 (25%)	77/313 (25%)
6–12 months	122/312 (39%)	120/313 (38%)
>12 months	112/312 (36%)	116/313 (37%)
Histology		
Large-cell carcinoma	25 (8%)	23 (7%)
Adenocarcinoma	235 (74%)	242 (76%)
Squamous	17 (5%)	11 (3%)
Other*	40 (13%)	43 (13%)
Patients with treated brain metastases	30 (9%)	38 (12%)
EGFR status		
FISH positive	43/102 (42%)	33/102 (32%)
FISH negative	59/102 (58%)	69/102 (68%)
IHC positive	119/161 (74%)	135/184 (73%)
IHC negative	42/161 (26%)	49/184 (27%)
EGFR mutant	18/170 (11%)	12/185 (6%)
EGFR wild-type	152/170 (89%)	173/185 (94%)
Kras mutation status		
Mutant	38/178 (21%)	48/190 (25%)
Wild-type	140/178 (79%)	142/190 (75%)

Data are n (%), mean (SD), or n/n with assessable tissue and test results (%). ECOG=Eastern Cooperative Oncology Group. EGFR=epidermal growth factor receptor. FISH=fluorescence in-situ hybridisation. IHC=immunohistochemistry. *Includes bronchoalveolar carcinoma and tumours defined as not otherwise specified or other.

Table 1: **Demographics and baseline characteristics, including biomarkers**

We undertook clinical and laboratory assessments at baseline and every 6 weeks to week 24, and every 12 weeks thereafter. Tumour responses were investigator-assessed according to Response Evaluation Criteria in Solid Tumours (RECIST) 1.0.[17]

Adverse events were graded according to US National Cancer Institute Common Toxicity Criteria for Adverse Events version 3.0. Patients were assessed for all grades of adverse events, serious adverse events (including grade ≥3 pulmonary haemorrhage or grade ≥2 symptomatic central nervous system haemorrhage), and adverse events requiring study-drug interruption or discontinuation.

At study entry, tumour biopsy material was requested from patients to assess EGFR and *Kras* expression. Archival tumour tissue samples were collected with accompanying pathology reports. For those patients with data for biomarker expression, we did EGFR fluorescence in-situ hybridisation (FISH) analyses with a PathVysion kit (Abbott Molecular, Des Plaines, IL, USA). High EGFR copy number was defined as high polysomy (≥4 gene copies in ≥40% of cells) or amplification (≥2 genes or chromosomes or ≥15 gene copies in ≥10% of cells). Immunohistochemical analysis of EGFR was done with PharmDx kits (DAKO, Glostrup, Denmark); positive EGFR expression was defined as EGFR staining of more than 10% of tumour cells. Highly sensitive analyses of *EGFR* somatic gene mutations in exons 18–21 and *Kras* mutations in exons 2 and 3 were done by use of denaturing HPLC (Transgenomics, Omaha, NE, USA).

The primary efficacy endpoint was overall survival. Secondary endpoints included progression-free survival, objective response rate, duration of objective response, safety, and assessment of associations between efficacy endpoints and expression of EGFR and *Kras* biomarkers. Overall survival was defined as time from randomisation to death from any cause. Progression-free survival was defined as time from randomisation to documented disease progression, as determined by investigator with use of RECIST, or death on study treatment (from any cause within 30 days of last dose), whichever occurred first.

Statistical analyses

We designed the study to detect 33% improvement in median survival, which required 417 deaths to provide 83% power for final analysis of overall survival. We planned an interim efficacy analysis after 280 deaths had occurred (~67% of required deaths for final analysis); the significance level for comparisons of overall survival was established from the Lan-DeMets α spending function with an O'Brien-Fleming boundary of 0·0124 at 67% event time and 0·0462 at final analysis.

At the interim and final efficacy analyses, all patients randomly allocated to treatment groups were included in survival analyses (intention-to-treat analysis). Only patients with measurable disease at baseline were

included in the analysis of objective response and the exploratory analysis of disease control.

We used stratified Cox proportional hazard models to estimate hazard ratios (HRs) and 95% CIs for overall survival and progression-free survival in the intention-to-treat population. We used a two-sided log-rank test, stratified by randomisation stratification factors apart from study site to compare overall survival and progression-free survival between trial groups. To control the overall type I error rate at the 5% level for efficacy endpoints, we used fixed-sequence testing, requiring that the primary endpoint be significant before statistical testing of key secondary endpoints.[18,19] We estimated median and IQRs for overall survival and progression-free survival with Kaplan-Meier methods. IQRs are shown throughout the manuscript in parentheses after medians. 95% CIs for median time-to-events were calculated by the Brookmeyer and Crowley method[20] where indicated.

We assessed overall and progression-free survival in subpopulations of patients (eg, biomarker-defined subgroups) with an unstratified Cox proportional hazards model and Kaplan-Meier method. Differences in treatment effects between subgroups were assessed by testing the interaction effect between treatment groups and characteristics of patients. Statistical analyses were done with SAS versions 9.1 and 9.2.

This trial is registered with ClinicalTrials.gov, number NCT00130728.

Role of the funding source

The study sponsor (Genentech) was involved in study design, data collection, data analysis, and interpretation of results, working closely with the investigators. All authors had full access to all the data in the study and had final responsibility for the decision to submit for publication.

Results

Between June 8, 2005, and April 16, 2008, we enrolled 636 patients at 177 study sites in 12 countries and randomly allocated 319 patients to the bevacizumab group and 317 to the control group (figure 1, table 1). 200 (63%) patients in the bevacizumab group discontinued treatment because of disease progression, compared with 243 (77%) in the control group.

Baseline characteristics were much the same between treatment groups (table 1). 448 (70%) of 636 patients had previously received carboplatin as first-line therapy and 113 (18%) had received cisplatin; other frequently used drugs included taxanes (294 [46%] patients received paclitaxel and 132 [21%] received docetaxel) and gemcitabine (148 [23%]). Rates of response to previous first-line treatment were balanced between groups. 68 (11%) of 636 patients entered the study with treated brain metastases. 613 (98%) of 626 treated patients used concomitant medications during treatment, including steroids, anti-emetics, analgesics, or other drugs.

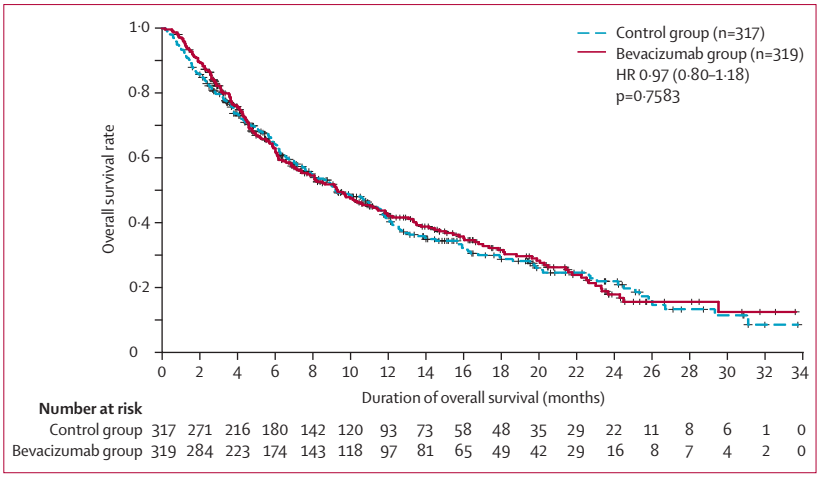

Figure 2: **Kaplan-Meier curves for overall survival**
Overall survival is shown for assessable patients randomly allocated to erlotinib plus bevacizumab (bevacizumab group) or erlotinib plus placebo (control group). The p value for overall survival is based on a stratified log-rank test; stratification factors were Eastern Cooperative Oncology Group performance status, smoking history, and sex.

We did the interim efficacy analysis on Feb 7, 2008, after 284 deaths (68% of 417 deaths required for final analysis), at which point the data monitoring committee recommended that the study continue. Median follow-up time for patients who were randomly allocated to treatment groups was 19 months (IQR 11–25 months; range 0·2–34 months).

Overall survival did not differ between the patients in the bevacizumab group and controls (figure 2 and figure 3). Median overall survival was about 9·2–9·3 months in both groups (figure 3). In the Kaplan-Meier analysis, 1-year survival was 42·1% in the bevacizumab group and 40·7% in the control group.

Figure 4 shows progression-free survival and table 2 shows an analysis of objective response rate. Median progression-free survival was 3·4 months (IQR 1·4–8·4) in the bevacizumab group compared with 1·7 months (1·3–4·1) in the control group (figure 4). The objective response rate in the bevacizumab group was much higher than it was in the control group (table 2). Three patients had a complete response after treatment with bevacizumab compared with one patient in the control group (table 2). Median duration of overall response seemed to be longer in the bevacizumab group than in the control group (table 2). The disease control rate was 45% (136 patients) in the bevacizumab group and 34% (104 patients) in the control group. Because of the prespecified use of fixed-sequence testing to control the overall type I error rate, we did not compare secondary efficacy results statistically.

A subgroup analyses of 67 patients who never smoked suggested a possible improvement in overall survival in the bevacizumab group compared with the control group (HR 0·44, 95% CI 0·21–0·94; figure 3).

477 (75%) of 636 enrolled patients had tumour tissue available for biomarker analyses. 390 patients (202 in

	All patients	Control group		Bevacizumab group		Hazard ratio (95% CI)	p value for interaction
		Patients	Median overall survival, months (IQR)	Patients	Median overall survival, months (IQR)		
Overall	636	317	9·2 (3·8–20·2)	319	9·3 (4·1–21·6)	0·97 (0·80–1·18)	NA
Age							0·8143
<65 years	309	156	9·2 (4·2–23·1)	153	9·7 (4·2–24·3)	0·94 (0·71–1·25)	
≥65 years	327	161	9·1 (3·7–16·8)	166	8·6 (4·1–18·2)	0·98 (0·76–1·28)	
Sex							0·7108
Men	341	170	7·9 (3·7–16·1)	171	8·1 (4·2–17·8)	0·94 (0·73–1·22)	
Women	295	147	11·5 (4·1–24·5)	148	10·2 (4·1–23·3)	1·01 (0·76–1·35)	
Race							0·0974
White	521	257	9·1 (3·8–19·5)	264	8·2 (3·8–19·9)	1·02 (0·83–1·26)	
Black	54	33	7·9 (3·4–20·2)	21	15·4 (7·4–20·5)	0·72 (0·36–1·43)	
Asian or Pacific islander	41	18	9·9 (3·2–NR)	23	NR (22·6–NR)	0·33 (0·09–1·22)	
Hispanic	18	8	NR (5·8–NR)	10	6·5 (4·3–21·7)	3·55 (0·77–16·49)	
Baseline ECOG score							0·8642
0	250	121	13·9 (7·6–25·1)	129	14·7 (5·8–24·3)	1·04 (0·74–1·46)	
1	342	176	6·7 (2·9–16·1)	166	7·4 (3·6–17·3)	0·93 (0·73–1·20)	
2	43	20	2·4 (1·0–11·0)	23	5·9 (2·3–11·2)	0·92 (0·45–1·85)	
Smoking history							0·0295
Never	67	33	9·2 (4·5–29·3)	34	NR (9·3–NR)	0·44 (0·21–0·94)	
Current or previous	569	284	9·1 (3·7–19·8)	285	8·1 (3·7–19·9)	1·06 (0·87–1·29)	
Histology							0·5349
Other	83	40	11·0 (2·6–17·9)	43	11·8 (4·5–29·5)	0·78 (0·46–1·35)	
Large-cell carcinoma	48	25	6·8 (4·2–20·2)	23	13·3 (5·8–22·5)	0·69 (0·34–1·41)	
Adenocarcinoma	477	235	9·3 (4·0–22·7)	242	9·1 (3·7–20·5)	1·07 (0·85–1·33)	
Squamous-cell carcinoma	28	17	5·1 (3·6–11·8)	11	5·0 (3·8–10·2)	0·91 (0·36–2·33)	
Time since initial diagnosis of NSCLC							0·1838
<6 months	155	78	5·7 (2·1–13·9)	77	4·4 (2·6–9·1)	1·31 (0·91–1·87)	
6–12 months	242	122	9·2 (3·7–19·8)	120	9·2 (4·4–22·2)	0·92 (0·67–1·26)	
>12 months	228	112	11·3 (5·8–23·1)	116	16·0 (6·2–23·7)	0·84 (0·60–1·18)	
Biomarker-defined subgroups of patients							
EGFR mutation status							0·1826
Mutant	30	18	20·2 (16·4–31·1)	12	NR (22·6–NR)	0·44 (0·11–1·67)	
Wild-type	325	152	9·1 (3·8–18·6)	173	8·1 (3·8–17·3)	1·11 (0·86–1·44)	
EGFR FISH status							0·5113
Positive	76	43	11·6 (5·1–20·2)	33	6·2 (2·6–15·0)	1·43 (0·83–2·47)	
Negative	128	59	8·9 (3·4–18·6)	69	6·2 (3·8–17·3)	1·14 (0·76–1·70)	
EGFR immunohistochemistry status							0·6124
Positive	254	119	11·0 (3·8–22·7)	135	8·5 (4·2–21·4)	1·07 (0·79–1·45)	
Negative	91	42	7·0 (3·2–12·6)	49	9·2 (3·6–12·2)	0·92 (0·57–1·50)	
Kras mutation status							0·6699
Mutant	86	38	12·6 (6·3–22·7)	48	10·3 (4·8–21·4)	1·23 (0·72–2·08)	
Wild-type	282	140	9·7 (4·0–19·8)	142	8·2 (3·8–19·6)	1·08 (0·81–1·43)	

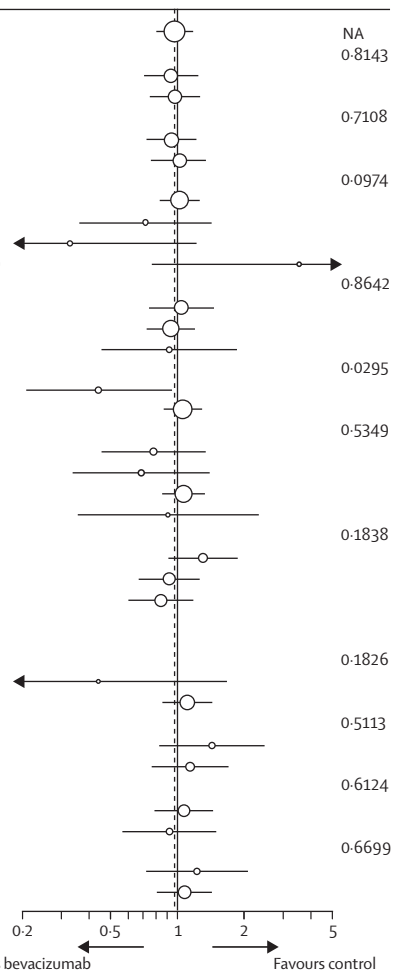

Figure 3: **Forest plot for subpopulations of patients defined by demographics and baseline characteristics, including biomarker expression**
Dashed line shows hazard ratio for the overall population. Overall survival hazard ratios were estimated by use of an unstratified Cox model. FISH=fluorescence in-situ hybridisation. NA=not assessable. NR=not reached. ECOG=Eastern Cooperative Oncology Group. NSCLC=non-small-cell lung cancer. EGFR=epidermal growth factor receptor.

the bevacizumab group and 188 in the control group) had results for at least one of the following tests: EGFR immunohistochemistry, EGFR FISH, *EGFR* mutation status, and *Kras* mutation status. 355 (56%) patients had assessable tests for *EGFR* mutations and 368 (58%) had assessable tests for *Kras* mutations. Figure 3 shows overall survival for patients with available tissue and assessable results. Although subgroup analysis of suggested overall survival seemed to favour bevacizumab in patients with *EGFR*-mutated tumours compared with those with *EGFR*-wild-type tumours, the difference did not achieve significance (p=0·1826). Survival outcomes were similar between patients with tumours with *Kras* mutations and those that were *Kras* wild-type. Progression-free survival outcomes were much the same in patients with tumours with *EGFR* mutations and those that were *EGFR* wild-type (data not shown).

188 (60%) of 313 patients in the bevacizumab group had grade 3 or 4 adverse events, compared with 151 (48%) of 313 controls (table 3). Incidence of grade 3 arterial thromboembolic events was higher in the bevacizumab group than it was in the control group, but was much the same as previously reported rates in patients with advanced NSCLC who were treated with bevacizumab.[6,7] 15 patients (5%) in the bevacizumab group and four (1%) in the control group had grade 3 or 4 hypertension, and no patients had grade 5 hypertension (table 3).

There were 20 (6%) grade 5 adverse events in the bevacizumab group, compared with 14 (4%) in the control group, most commonly dyspnoea (three events *vs* two events), pneumonia (two *vs* four events), and pulmonary embolism (one event in each group). Two deaths due to bleeding (pulmonary haemorrhage and gastrointestinal haemorrhage) occurred in the bevacizumab group, compared with none in the control group. No bleeding events of grade 3 or higher (including central nervous system haemorrhage) were reported in 68 patients entering the study with treated brain metastases.

41 patients (13%) in the bevacizumab group discontinued treatment because of adverse events, compared with 27 (9%) in the control group (figure 1).

Patients in the bevacizumab group received a mean dose of 132·2 mg (SD 25·8) erlotinib per day for a duration of 152·2 days (173·4); controls received a mean dose of 139·3 mg (20·8) erlotinib every day for a duration of 101·5 days (119·0). Patients in the bevacizumab group received a median of 4 (IQR 2–9; range 1–47) doses of bevacizumab, compared with a median of 2 (IQR 2–6; range 0–37) doses of placebo in the control group.

In the bevacizumab group, 24 (8%) of 319 patients received bevacizumab in subsequent lines of therapy, compared with 38 (12%) of 317 patients in the control group. In the bevacizumab group, 164 (51%) of 319 patients received one or more subsequent therapies (most commonly pemetrexed or gemcitabine) after discontinuation of study treatment, compared with 193 (61%) of 317 in the control group.

Discussion

We assessed the efficacy of addition of bevacizumab to erlotinib in patients with recurrent, advanced, or metastatic NSCLC after failure of standard first-line chemotherapy, and showed that addition of bevacizumab to erlotinib did not improve overall survival (figure 2). Bevacizumab added to erlotinib seemed to prolong progression-free survival, objective response rate, and duration of response compared with erlotinib alone; median progression-free survival and objective response rates were about double those in the control group. However, because of our prespecified use of fixed-sequence testing, the secondary endpoints were not compared statistically.

Results from our subset analyses for survival were generally consistent with overall trial results. Most subpopulations of patients derived a benefit to progression-free survival but not overall survival from the addition of bevacizumab. Although a few subsets of patients in the bevacizumab group showed longer survival than did those in the control group, the sample sizes were small and CIs were wide; hence, these subgroup results should be interpreted with caution.

This trial had limitations, including the absence of accounting for crossover effects of a potentially active therapy (eg, bevacizumab) on overall survival. More

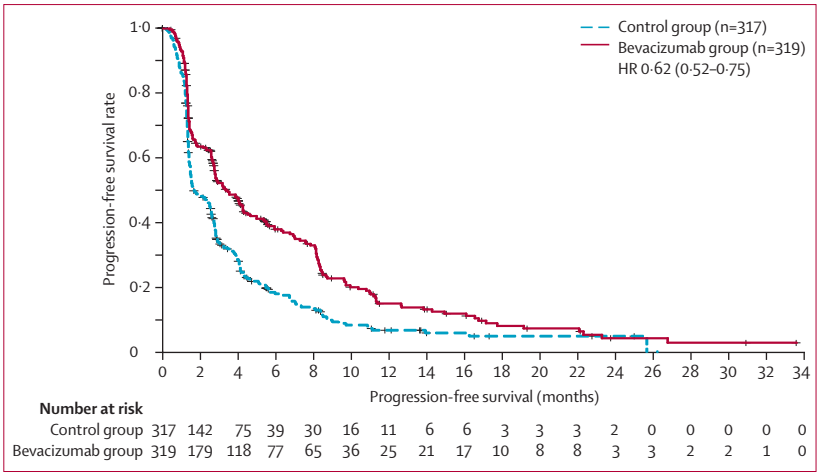

Figure 4: **Kaplan-Meier curves for progression-free survival**
Progression-free survival is shown for assessable patients in the bevacizumab group (randomly allocated to erlotinib plus bevacizumab) and control group (randomly allocated to erlotinib plus placebo). Because of the prespecified use of fixed sequence testing to control the overall type I error rate, which required that the primary endpoint (overall survival) be significant before statistical testing of key secondary endpoints, progression-free survival results could not be defined as significant.

	Control group (n=306)	Bevacizumab group (n=301)
Objective response	19 (6%)	38 (13%)
Complete response	1 (<1%)	3 (1%)
Partial response	18 (6%)	35 (12%)
Stable disease	85 (28%)	98 (33%)
Progressive disease	154 (50%)	112 (37%)
Disease control rate		
Complete response, partial response, or stable disease	104 (34%)	136 (45%)
Median duration of objective response, months	8·4 (3·5–14·9, 3·4–14·9)	9·7 (6·9–19·5, 5·7–19·5)

Data are n (%) or median (95% CI, IQR).

Table 2: **Response rates, disease control rates, and duration of objective response in patients with measurable disease at baseline**

	Control group (n=313)	Bevacizumab group (n=313)
Any adverse event	309 (99%)	312 (>99%)
Any serious adverse event	114 (36%)	130 (42%)
Any grade ≥3 adverse event	Grade 3/4: 151 (48%); grade 5: 14 (4%)	Grade 3/4: 188 (60%); grade 5: 20 (6%)
Haemorrhage	Grade 3/4: 7 (2%)	Grade 3/4: 8 (3%); grade 5: 2 (1%)
Pulmonary haemorrhage	Grade 3/4: 1 (<1%)	Grade 3/4: 2 (1%); grade 5: 1 (<1%)
CNS haemorrhage	0	Grade 3/4: 1 (<1%)
Arterial thromboembolic event	Grade 3/4: 1 (<1%)	Grade 3/4: 10 (3%); grade 5: 2 (1%)
Hypertension	Grade 3/4: 4 (1%)	Grade 3/4: 15 (5%)
Interstitial lung disease-like events	Grade 3/4: 1 (<1%); grade 5: 1 (<1%)	Grade 3/4: 1 (<1%); grade 5: 1 (<1%)
Rash	Grade 3/4: 19 (6%)	Grade 3/4: 49 (16%)

Data are for the safety-assessable patient population. CNS=central nervous system.

Table 3: **Adverse events**

Panel: Research in context

Systemic review

We searched the PubMed database for articles published in English between Jan 15, 2001 and Jan 15, 2011 with the search terms "lung cancer", "angiogenesis", and "epidermal growth factor" to identify preclinical data and clinical trials in lung cancer that assessed epidermal growth factor receptor (EGFR) and angiogenesis inhibitors. We identified 240 reports, including 12 reports of clinical trials targeting EGFR and angiogenesis pathways in combination in lung cancer.

Interpretation

Preclinical data suggest an enhanced benefit of dual inhibition of the EGFR and angiogenesis pathways in lung cancer. These findings, together with our experience in phase 1 and phase 2 trials of erlotinib and bevacizumab, support this combination therapy in non-small-cell lung cancer.[15,16] Indeed, clinical trials of inhibitors targeting EGFR and angiogenesis showed an increase in progression-free survival in several studies, underlining a probable advantage of targeting both pathways concurrently. However, the combination therapies described in our and most of the other studies failed to enhance overall survival in patients with advanced disease. These results emphasise the challenge overall survival provides as a primary endpoint in a population of patients with refractory non-small-cell lung cancer and the need for predictive biomarkers to select patients who will most probably benefit from concurrent inhibition of the EGFR and angiogenesis pathways.

patients in the control group than in the bevacizumab group received subsequent lines of therapy during follow-up, including subsequent treatment with bevacizumab, which could have confounded the comparison of overall survival between the two cohorts. Reports of an overall survival benefit in the setting of refractory NSCLC have become more difficult in recent years, because of the increased number of moderately active agents available for subsequent treatment. A predictive tissue marker was not identified in this study, although our biomarker analysis was done with samples obtained by surgery or for diagnostic intent (rather than new biopsies), potentially restricting the value of this biomarker analysis.

Several preclinical studies[10–13] showed an enhanced benefit from combination EGFR and angiogenesis inhibitors (panel). A preclinical study[14] in an orthotopic lung cancer model showed that inhibition of EGFR and VEGFR signalling led to profound antiangiogenic, antivascular, and antitumour effects.[14] The hypothesis was therefore made that combination of erlotinib and bevacizumab would be more clinically effective than would erlotinib monotherapy, while maintaining acceptable toxic effects. Furthermore, studies[21,22] have suggested that blocking of VEGFR and EGFR signalling could overcome primary or acquired resistance to EGFR inhibitors in xenograft models. Second-line NSCLC treatment with vandetanib, a drug targeting both angiogenesis and EGFR activity, has led to prolonged progression-free survival in two clinical trials,[23,24] although overall survival was not improved.

EGFR expression, overexpression, and mutation have been implicated in the pathogenesis of NSCLC,[25–30] suggesting that patients who are EGFR positive (by immunohistochemistry or FISH analyses) or who have *EGFR* mutations might derive increased benefit from EGFR-targeted therapies. In a subgroup analysis of EGFR mutation status, the HR for overall survival was apparently lower in patients with *EGFR*-mutant tumours than in patients with wild-type tumours. However, this result should be interpreted with caution because only 30 patients in the study had *EGFR*-mutated tumours and the 95% CIs for the HRs were wide (upper limits >1·0) and overlapping.

Predictive markers show responses to treatment, whereas prognostic markers show the natural history of disease. Predictive conclusions about the role of biomarkers in erlotinib treatment cannot be made because both treatment groups contained erlotinib. However, the *EGFR* mutation data do support *EGFR* mutation as a prognostic marker for NSCLC. Activation of mutations in *Kras* occur in 30% of NSCLCs and might indicate poor prognosis or mediate resistance to EGFR inhibitors.[31,32] By contrast with previous reports, the *Kras* data in our study do not support *Kras* mutation status as an independent marker of poor prognosis for NSCLC.

Both regimens were well tolerated, although patients given bevacizumab had slightly more toxic effects than did controls, with an increased proportion of grade 5 events. The toxic effects of erlotinib and bevacizumab that we noted were consistent with the known individual drug toxic-effect profiles; no new safety signals were reported. The incidence of events related to bevacizumab, including arterial thromboembolic events, venous thromboses, and haemorrhages, was consistent with previously reported data for bevacizumab.[6] Events typically associated with erlotinib, such as diarrhoea, nausea, and vomiting, were reported at much the same rates in both groups. The incidence of rash associated with erlotinib was higher in the bevacizumab group, although in most cases rash was manageable and did not lead to substantial treatment discontinuation. The increased overall incidence of adverse events in the bevacizumab group probably reflects some additive effects of the drug combination, and the greater median length of time on-study for patients receiving erlotinib and bevacizumab.

In summary, erlotinib and bevacizumab given to patients with advanced-stage NSCLC after failure of standard first-line chemotherapy did not result in improved overall survival compared with erlotinib and placebo. Although we could not assess significance,

potential clinical activity of the combination is suggested by possible improvements in progression-free survival and objective response rates and the tolerable safety profile, which supports the hypothesis that the combination could be useful in treatment of NSCLC. However, the absolute improvement in median progression-free survival (6 weeks; figure 4) by this combination will need to be balanced against the slightly increased rate of toxic effects and cost, perhaps requiring more detailed analysis of patient-derived outcomes.

A trial[33] testing the addition of erlotinib to bevacizumab maintenance in patients without progressive disease after four cycles of chemotherapy and bevacizumab showed improved progression free survival but not overall survival compared to bevacizumab alone. Our trial did not test a maintenance concept but instead was designed to detect a survival improvement for the combination of bevacizumab and erlotinib in a more advanced population of patients that had progressed after front-line treatment. Both studies suggest that despite improvements in several efficacy endpoints, improving survival remains a challenge in the treatment of NSCLC. Therefore, optimisation of outcomes from a combination of bevacizumab and erlotinib will probably require new techniques to prospectively identify subsets of patients who are most likely to benefit from this treatment.

Contributors

RSH, RA, FB, PF, LH, GAO, GV, PO'C, and JH contributed to study design, data collection, analysis, and interpretation, and writing of the manuscript. C-HS contributed to data analysis and interpretation and writing of the manuscript.

Conflicts of interest

Genentech funded this clinical trial. RSH, LH, PF, and GAO have received funding from Genentech. RSH has consulted for Genentech, OSI, and Roche. GAO has consulted for Genentech and Abraxis. PF has consulted for Genentech, participated in speakers' bureaux for Genentech and OSI Pharmaceuticals, and grant funding from the Metro Minnesota Community Clinical Oncology Program, a non-profit research program sponsored by NCI. GV has consulted for Genentech and participated in speakers' bureaux for Genentech and Sanofi-Aventis. C-HS and PO'C have been employed by Genentech and were stockholders with Roche.

Acknowledgments

We thank the patients and study investigators who participated in this study, Christopher Bowden (Genentech, South San Franscisco, CA, USA) for critical review and input, and Abie Craiu (Genentech), Bich Tran (MD Anderson Cancer Center, Houston, TX, USA), and Joerg Jacoby (MD Anderson Cancer Center) for assistance with preparation of the manuscript. RSH was supported in part by the US National Institutes of Health through the MD Anderson's Cancer Center Support Grant CA016672.

References

1 Jemal A, Bray F, Center MM, Ferlay J, Ward E, Forman D. Global cancer statistics. *CA Cancer J Clin* 2011; **61:** 69–90.

2 Jemal A, Siegel R, Xu J, Ward E. Cancer statistics, 2010. *CA Cancer J Clin* 2010; **60:** 277–300.

3 Pazdur R, Coia LR, Hoskins WJ, Wagman LD. Cancer management: a multidisciplinary approach, 8th edn. Manhasset, NY, USA: CMP Healthcare Media, 2004.

4 Erlotinib (Tarceva) [package insert]. South San Francisco, CA, USA: Genentech, 2007.

5 Shepherd FA, Rodrigues Pereira J, Ciuleanu, et al. Erlotinib in previously treated non-small-cell lung cancer. *N Engl J Med* 2005; **353:** 123–32.

6 Bevacizumab (Avastin) [package insert]. South San Francisco, CA, USA: Genentech, 2007.

7 Sandler A, Gray R, Perry MC, et al. Paclitaxel–carboplatin alone or with bevacizumab for non-small-cell lung cancer. *N Engl J Med* 2006; **355:** 2542–50.

8 Johnson DH, Fehrenbacher L, Novotny WF, et al. Randomized phase II trial comparing bevacizumab plus carboplatin and paclitaxel with carboplatin and paclitaxel alone in previously untreated locally advanced or metastatic non-small-cell lung cancer. *J Clin Oncol* 2004; **22:** 2184–91.

9 Reck M, von Pawel J, Zatloukal P, et al. Phase III trial of cisplatin plus gemcitabine with either placebo or bevacizumab as first-line therapy for nonsquamous non-small-cell lung cancer: AVAiL. *J Clin Oncol* 2010; **27:** 2415–22.

10 Ciardiello F, Bianco R, Damiano V, et al. Antiangiogenic and antitumor activity of anti-epidermal growth factor receptor C225 monoclonal antibody in combination with vascular endothelial growth factor antisense oligonucleotide in human GEO colon cancer cells. *Clin Cancer Res* 2000; **6:** 3739–47.

11 Shaheen RM, Ahmad SA, Liu W, et al. Inhibited growth of colon cancer carcinomatosis by antibodies to vascular endothelial and epidermal growth factor receptors. *Br J Cancer* 2001; **85:** 584–89.

12 Bozec A, Sudaka A, Fischel JL, et al. Combined effects of bevacizumab with erlotinib and irradiation: a preclinical study on a head and neck cancer orthotopic model. *Br J Cancer* 2008; **99:** 93–99.

13 Schicher N, Paulitschke V, Swoboda A, et al. Erlotinib and bevacizumab have synergistic activity against melanoma. *Clin Cancer Res* 2009; **15:** 3495–502.

14 Wu W, Onn A, Isobe T, et al. Targeted therapy of orthotopic human lung cancer by combined vascular endothelial growth factor and epidermal growth factor receptor signaling blockade. *Mol Cancer Ther* 2007; **6:** 471–83.

15 Herbst RS, Johnson DH, Mininberg E, et al. Phase I/II trial evaluating the anti-vascular endothelial growth factor monoclonal antibody bevacizumab in combination with the HER-1/epidermal growth factor receptor tyrosine kinase inhibitor erlotinib for patients with recurrent non-small-cell lung cancer. *J Clin Oncol* 2005; **23:** 2544–55.

16 Herbst RS, O'Neill VJ, Fehrenbacher L, et al. Phase II study of efficacy and safety of bevacizumab in combination with chemotherapy or erlotinib compared with chemotherapy alone for treatment of recurrent or refractory non small-cell lung cancer. *J Clin Oncol* 2007; **25:** 4743–50.

17 Eisenhauer EA, Therasse P, Bogaerts J, et al. New response evaluation criteria in solid tumours: revised RECIST guideline (version 1.1). *Eur J Cancer* 2009; **45:** 228–47.

18 Dmitrienko A, Molenberghs G, Chuang-Stein C, Offen W. Analysis of clinical trials using SAS. Cary, NC, USA: SAS Institute, 2005.

19 Westfall PH, Krishen A. Optimally weighted, fixed sequence and gatekeeper multiple testing procedures. *J Stat Planning Inference* 2001; **99:** 25–40.

20 Brookmeyer R, Crowley J. A confidence interval for median survival time. *Biometrics* 1982; **38:** 29–41.

21 Ciardiello F, Bianco R, Caputo R, et al. Antitumor activity of ZD6474, a vascular endothelial growth factor receptor tyrosine kinase inhibitor, in human cancer cells with acquired resistance to antiepidermal growth factor receptor therapy. *Clin Cancer Res* 2004; **10:** 784–93.

22 Naumov GN, Nilsson MB, Cascone T, et al. Combined vascular endothelial growth factor receptor and epidermal growth factor receptor (EGFR) blockade inhibits tumor growth in xenograft models of EGFR inhibitor resistance. *Clin Cancer Res* 2009; **15:** 3484–94.

23 Herbst RS, Sun Y, Eberhardt WEE, et al. Vandetanib plus docetaxel versus docetaxel as second-line treatment for patients with advanced non-small-cell lung cancer (ZODIAC): a double-blind, randomised, phase 3 trial. *Lancet Oncol* 2010; **11:** 619–26.

24 Natale RB, Bodkin D, Govindan R, et al. Vandetanib versus gefitinib in patients with advanced non-small-cell lung cancer: results from a two-part, double-blind, randomized phase II study. *J Clin Oncol* 2009; **27:** 2523–29.

25 Hirsch FR, Varella-Garcia M, Dziadziuszko R, et al. Fluorescence in situ hybridization subgroup analysis of TRIBUTE, a phase III trial of erlotinib plus carboplatin and paclitaxel in non-small cell lung cancer. *Clin Cancer Res* 2008; **14:** 6317–23.

26 Andratschke NH, Dittmann KH, Mason KA, et al. Epidermal growth factor receptor as a target to improve treatment of lung cancer. *Clin Lung Cancer* 2004; **5:** 340–52.

27 Roskoski R Jr. The ErbB/HER receptor protein-tyrosine kinases and cancer. *Biochem Biophys Res Commun* 2004; **319:** 1–11.

28 Lynch TJ, Bell DW, Sordella R, et al. Activating mutations in the epidermal growth factor receptor underlying responsiveness of non-small-cell lung cancer to gefitinib. *N Engl J Med* 2004; **350:** 2129–39.

29 Paez JG, Jänne PA, Lee JC. EGFR mutations in lung cancer: correlation with clinical response to gefitinib therapy. *Science* 2004; **304:** 1497–500.

30 Pao W, Miller V, Zakowski M, et al. EGF receptor gene mutations are common in lung cancers from "never smokers" and are associated with sensitivity of tumors to gefitinib and erlotinib. *Proc Natl Acad Sci USA* 2004; **101:** 13306–11.

31 Eberhard DA, Johnson BE, Amler LC, et al. Mutations in the epidermal growth factor receptor and in KRAS are predictive and prognostic indicators in patients with non-small-cell lung cancer treated with chemotherapy alone and in combination with erlotinib. *J Clin Oncol* 2005; **23:** 5900–09.

32 Miller VA, Riely GJ, Zakowski MF, et al. Molecular characteristics of bronchioloalveolar carcinoma and adenocarcinoma, bronchioloalveolar carcinoma subtype, predict response to erlotinib. *J Clin Oncol* 2008; **26:** 1472–78.

33 Miller VA, O'Connor P, Soh C, Kabbinavar F, for the ATLAS Investigators. A randomized, double-blind, placebo-controlled, phase IIIb trial (ATLAS) comparing bevacizumab (B) therapy with or without erlotinib (E) after completion of chemotherapy with B for first-line treatment of locally advanced, recurrent, or metastatic non-small cell lung cancer (NSCLC). *Proc Am Soc Clin Oncol* 2009; **27:** LBA8002 (abstr).

DOI: 10.1093/jnci/djr075
Advance Access publication on April 11, 2011.

ARTICLE

Genome-Wide Association Study of Survival in Non–Small Cell Lung Cancer Patients Receiving Platinum-Based Chemotherapy

Xifeng Wu, Yuanqing Ye, Rafael Rosell, Christopher I. Amos, David J. Stewart, Michelle A.T. Hildebrandt, Jack A. Roth, John D. Minna, Jian Gu, Jie Lin, Shama C. Buch, Tomoko Nukui, Jose Luis Ramirez Serrano, Miquel Taron, Adrian Cassidy, Charles Lu, Joe Y. Chang, Scott M. Lippman, Waun Ki Hong, Margaret R. Spitz, Marjorie Romkes, Ping Yang

Manuscript received July 15, 2010; revised February 2, 2011; accepted February 15, 2011.

Correspondence to: Xifeng Wu, MD, PhD, Department of Epidemiology, The University of Texas MD Anderson Cancer Center, 1515 Holcombe Blvd, Unit 1340, Houston, TX 77030 (e-mail: xwu@mdanderson.org).

Background Interindividual variation in genetic background may influence the response to chemotherapy and overall survival for patients with advanced-stage non–small cell lung cancer (NSCLC).

Methods To identify genetic variants associated with poor overall survival in these patients, we conducted a genome-wide scan of 307 260 single-nucleotide polymorphisms (SNPs) in 327 advanced-stage NSCLC patients who received platinum-based chemotherapy with or without radiation at the University of Texas MD Anderson Cancer Center (the discovery population). A fast-track replication was performed for 315 patients from the Mayo Clinic followed by a second validation at the University of Pittsburgh in 420 patients enrolled in the Spanish Lung Cancer Group PLATAX clinical trial. A pooled analysis combining the Mayo Clinic and PLATAX populations or all three populations was also used to validate the results. We assessed the association of each SNP with overall survival by multivariable Cox proportional hazard regression analysis. All statistical tests were two-sided.

Results SNP rs1878022 in the chemokine-like receptor 1 (*CMKLR1*) was statistically significantly associated with poor overall survival in the MD Anderson discovery population (hazard ratio [HR] of death = 1.59, 95% confidence interval [CI] = 1.32 to 1.92, $P = 1.42 \times 10^{-6}$), in the PLATAX clinical trial (HR of death = 1.23, 95% CI = 1.00 to 1.51, $P = .05$), in the pooled Mayo Clinic and PLATAX validation (HR of death = 1.22, 95% CI = 1.06 to 1.40, $P = .005$), and in pooled analysis of all three populations (HR of death = 1.33, 95% CI = 1.19 to 1.48, $P = 5.13 \times 10^{-7}$). Carrying a variant genotype of rs10937823 was associated with decreased overall survival (HR of death = 1.82, 95% CI = 1.42 to 2.33, $P = 1.73 \times 10^{-6}$) in the pooled MD Anderson and Mayo Clinic populations but not in the PLATAX trial patient population (HR of death = 0.96, 95% CI = 0.69 to 1.35).

Conclusion These results have the potential to contribute to the future development of personalized chemotherapy treatments for individual NSCLC patients.

J Natl Cancer Inst 2011;103:817–825

Lung cancer causes approximately 28% of cancer-related deaths per year in the United States and has remained the leading cause of all cancer deaths for the past decade with a 5-year survival rate of 15% (1). Non–small cell lung cancer (NSCLC) accounts for more than 80% of all lung cancers and is often diagnosed at an advanced stage. Disease stage and performance status are two of the most important clinical factors used to determine prognosis and guide treatment options for NSCLC patients. Platinum-based chemotherapy is the main treatment option for advanced-stage NSCLC patients and has demonstrated improved overall survival (2,3). Unfortunately, response to platinum-based chemotherapy varies among patients with similar clinical characteristics (4). Therefore, identification of biomarkers that can better predict a patient's clinical outcome might prove helpful in guiding the physician in the selection of an optimal treatment regimen.

Germline genetic variations, such as single-nucleotide polymorphisms (SNPs), have attracted much attention as potential predictors of overall survival for NSCLC patients treated with platinum-based chemotherapy (2,5–8). A majority of these studies have applied a candidate gene approach requiring a priori knowledge of SNPs and gene function. For example, studies focused on the association between genetic variants in DNA repair pathway genes and clinical outcome have assumed that suboptimal DNA repair capacity influences individual responses to chemotherapy and overall survival. However, the results have often been conflicting and difficult to replicate (8).

Recently, several genome-wide association studies have been completed with the aim of identifying genetic variants influencing the risk of lung cancer (9–13). The availability of the data from the patient population of our previous genome-wide association studies

CONTEXT AND CAVEATS

Prior knowledge

Although platinum-based chemotherapy is the main treatment for non–small cell lung cancer (NSCLC), most patients either do not respond to the therapy or develop resistance. Variation among patients might account for at least some of the variability in response and response duration.

Study design

A genome-wide scan for genetic variants associated with decreased overall survival was performed in a population of NSCLC patients who received platinum-based chemotherapy with or without radiation. Variants highly statistically significantly associated with decreased overall survival in the initial discovery population were validated in two independent patient populations as well as in pooled analyses.

Contribution

A genetic variation in the chemokine-like receptor 1 (*CMKLR1*) gene was statistically significantly associated with decreased overall survival in the three individual populations as well as in pooled analyses.

Implications

NSCLC patients carrying a genetic variation in *CMKLR1* may not respond to platinum-based chemotherapy. This study demonstrates an analytical approach to identify genetic factors associated with clinical outcomes that could be used to develop refined treatment strategies for these patients.

Limitations

There are no previous reports of *CMKLR1* or its protein being associated with lung cancer. Further studies are necessary to confirm a role and elucidate a mechanism for this G-protein-coupled receptor in NSCLC and resistance to platinum-based chemotherapeutic agents.

From the Editors

for lung cancer risk together with data from additional patients selected from our ongoing epidemiological lung cancer study at MD Anderson Cancer Center provided us with the opportunity to comprehensively examine genome-wide genetic data to identify common genetic variants associated with overall survival for NSCLC. To construct a relatively homogeneous treatment regimen, this study was restricted to patients who did not receive surgery and were treated with platinum-based chemotherapy with or without radiation. We implemented a three-stage study design with a fast-track replication for 60 selected SNPs in an independent NSCLC patient cohort at Mayo Clinic followed by further validation for seven SNPs in NSCLC patients who received cisplatin and docetaxel as part of the PLATAX clinical trial.

Methods

MD Anderson Discovery Population

All participants were selected from 1235 newly diagnosed histologically confirmed lung cancer patients. Of these 1235 patients, 1154 patients from our recent genome-wide association studies of lung cancer risk (9) and an additional 81 lung cancer patients from an ongoing epidemiological lung cancer study at the University of Texas MD Anderson Cancer Center were included in the analysis. All patients were recruited from January 1, 1995, to December 30, 2007, and had a median lag time of 34 days between the date of initial diagnosis and the start of chemotherapy. To be eligible for this study, patients had to be white ever-smokers with stage III or IV NSCLC without surgery or other prior therapy and treated at MD Anderson Cancer Center with first-line platinum-based chemotherapy with or without radiotherapy. In total, 327 NSCLC patients were selected for inclusion in the discovery phase. We also performed a separate analysis on 213 NSCLC patients with incurable stage IIIB (wet) and IV disease. All study participants gave written informed consent, and the study was approved by the Institutional Review Board of the University of Texas MD Anderson Cancer Center.

Mayo Clinic Validation Population

Of the 945 lung cancer patients who received platinum-based chemotherapy recruited from the Mayo Clinic (14), we applied the same eligibility criteria as was used in the discovery step and identified 315 NSCLC patients who met the criteria outlined above. Patients were recruited from January 1, 1997, to December 30, 2008, and had a median lag time of 25 days between the date of initial diagnosis and the start of chemotherapy. All study participants gave written informed consent, and the study was approved by the Institutional Review Board of the Mayo Foundation.

PLATAX Validation Population

Specimens from 420 NSCLC stage III and IV patients who received chemotherapy (cisplatin and docetaxel) within the pharmacogenomic, open-label, single-arm multicenter PLATAX trial were included in the validation analysis. Lag time for each patient was less than 1 month. Specimen collection was performed as part of a collaborative study under a Grupo Espanol de Cancer de Pulmon (Spanish Lung Cancer Group) Clinical Research Ethics Committee–approved protocol involving multiple institutions in Spain (a complete list of participating Spanish hospitals is found in the Notes). All patients provided written informed consent and de-identified specimens, and patient data were sent to the University of Pittsburgh (Pittsburgh, PA) for genotyping analyses under a separately approved Institutional Review Board protocol.

Genotyping

Genotypes were generated using Illumina's HumanHap300 BeadChip (San Diego, CA) for the 1154 patients included in our previous genome-wide association studies of lung cancer risk (9). We carried out genotyping for an additional 81 patients from MD Anderson Cancer Center using Illumina's HumanHap317 BeadChip. The analysis focused on 307 260 SNPs that were included in both chips and passed quality control filters including call rate of at least 95% and minor allele frequencies of at least 0.01. All 1235 specimens had call rates greater than 95%, reported gender consistent with X chromosome heterozygosity, and passed additional quality control tests for duplicate sample detection and outlier sample detection implemented in the software package PLINK (version 1.03, http://pngu.mgh.harvard.edu/~purcell/plink/) (15). Genotyping for the Mayo Clinic validation population was

performed in the Mayo Clinic Genomic Shared Resources facilities using the SNPstream genotyping platform (Beckman Coulter, Fullerton, CA) and TaqMan assays (Applied Biosystems, Foster City, CA) according to the manufacturer's instructions. Genotyping was performed at the University of Pittsburgh using a custom Illumina GoldenGate panel (Illumina) and TaqMan assays following standard protocols.

Statistical Analysis

We assessed three genetic models of inheritance (dominant, recessive, and additive) using the discovery dataset for each SNP by multivariable Cox proportional hazard regression analysis. Adjustments for age (continuous), sex (male or female), pack-years (continuous), clinical stage (IIIA, IIIB [dry], IIIB [wet], or IV), and pretreatment performance status (0, 1, or 2–4) were made with the use of STATA software (version 10; STATA Corporation, College Station, TX). The model with the smallest *P* value was used to measure the statistical significance of the association between each SNP and overall survival for the genome-wide SNP data. Only the dominant model was considered when the rare homozygous genotype was less than 5% in both living and deceased patients. Overall survival time was defined as the time from the date of chemotherapy start to the date of death or the date of last follow-up, whichever came first. Kaplan–Meier curves and log-rank tests were used to calculate the survival difference associated with individual genotypes. All statistical tests were two-sided.

All patients from the discovery population were used to determine population substructure using the software packages PLINK and EIGENSTRAT (version 3.0, http://genepath.med.harvard.edu/~reich/Software.htm) (16). The 1235 patients were classified into 27 strata on the basis of genetic similarity using PLINK clustering analysis. When restricted to the 327 patients analyzed in the discovery phase, 22 strata were identified. Analysis using EIGENSTRAT software and principle component analysis identified the five top eigenvalues from the 1235 available eigenvalues. Multivariable Cox regression analyses were used to allow for potential population substructure by two separate analyses (one with the PLINK identified strata and the other with the five eigenvectors from EIGENSTRAT).

We divided the data equally using two approaches—by randomly splitting the data into training and test sets and by assigning alternating samples into training and test sets according to the date of sample collection. For SNPs showing statistically significant differences in patients with stage III and IV disease, a SNP was selected for validation in the Mayo Clinic validation population if it was statistically significantly associated with overall survival in the training and testing sets generated by both approaches or if it was among the top 20 statistically significant SNPs identified in the training and testing sets generated by either approach. For SNPs statistically significantly associated with overall survival by analysis of the subgroup of specimens from patients with stage IIIB (wet) and IV disease, a SNP was selected for validation if it was one of the top 20 SNPs with a statistically significant association with overall survival in both the training and testing sets, generated by either approach (Supplementary Table 1, available online).

The analysis of specimens from the Mayo Clinic validation studies was performed using multivariable Cox regression analysis with adjustment variables identical to those of the initial scan. Seven SNPs showing consistent association with overall survival, resulting in the corresponding hazard ratios in the MD Anderson and Mayo Clinic studies, were selected for further replication in the PLATAX clinical trial samples (Supplementary Table 1, available online). Multivariable Cox regression analysis with adjustments for age, sex, clinical stage, and pretreatment performance status (same as above definitions) was used to investigate an association between a SNP and overall survival. Smoking history was not available for these patients, so the data were not adjusted for this variable. To summarize results for the discovery set and the two validation studies, we performed pooled analysis to obtain the summary hazard ratio and 95% confidence interval (CI). We tested the proportional-hazards assumption on the basis of Schoenfeld residuals. Data from MD Anderson, Mayo Clinic, and the PLATAX clinical trial satisfied the proportionality assumption with $P = .21$, $P = .48$, and $P = .15$, respectively, when rs1878022 and all covariates were included in the analysis.

Haploview software (version 4.1, http://www.broad.mit.edu/mpg/haploview/) was used to determine pair-wise linkage disequilibrium structure across the genomic region under study (17). To impute SNPs in the region containing susceptibility loci, we used MACH software (http://www.sph.umich.edu/csg/abecasis/MaCH) and haplotype information for the multimarker tags from the International HapMap Project release 22, human genome build 36 (www.hapmap.org).

We constructed receiver operating characteristic curves and calculated the area under the curve (AUC) to evaluate the specificity and sensitivity of predicting 1-year survival for the pooled dataset by clinical and epidemiological variables and by the combination of clinical, epidemiological, and genetic variables. We used 1000 bootstrapping samples to compute a 95% bias-corrected confidence interval for the difference of the AUCs between the two models to determine the statistical significance of adding genetic markers to the model.

Results

The initial genome-wide scan was performed for 307 260 SNPs that passed strict quality control measures. In the discovery phase, we observed 31 751 SNPs that met our selection criteria ($P < .05$; among them, 20 with $P < 10^{-5}$ and one with $P < 10^{-6}$) for the analysis focused on stage III and IV NSCLC patients (Figure 1, A). When the analysis was restricted to only stage IIIB (wet) and IV patients, 30 258 SNPs ($P < .05$; among them, 15 with $P < 10^{-5}$ and three with $P < 10^{-6}$) were identified (Figure 1, B). In a sensitivity analysis, we performed two separate analyses (one with clusters from PLINK and the other with eigenvectors from EIGENSTRAT) to assess the potential effect of population substructure using multivariable Cox regression analysis. The data indicated that the patient population is relatively ethnically homogeneous and the observed associations were not driven by potential population substructure (Supplementary Table 2, available online).

To determine which associations identified in the discovery phase were robust, we identified 60 SNPs (Supplementary Table 1, available online) to perform a fast-track validation study using an independent NSCLC patient cohort from the Mayo Clinic

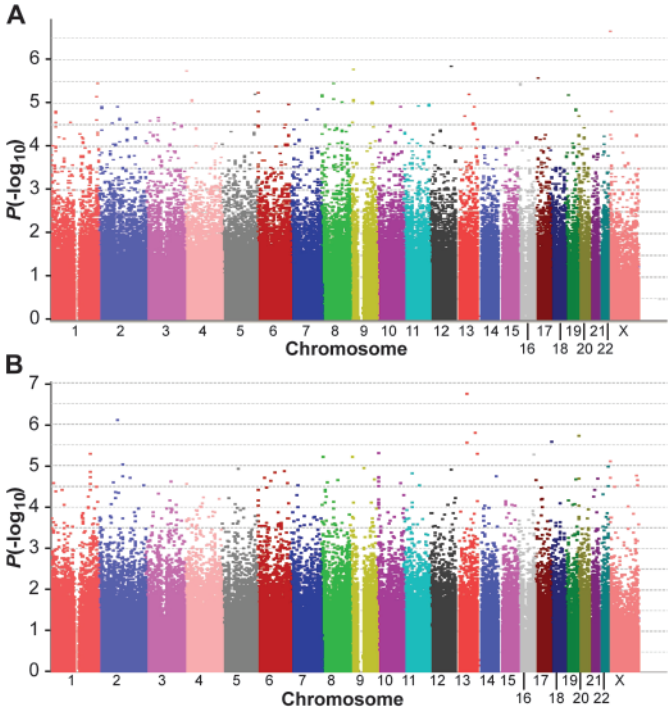

Figure 1. Genome-wide association study results for overall survival by chromosome in the MD Anderson discovery population. Associations are expressed as $-\log_{10}(P)$. *P* values were from multivariable Cox proportional hazards models and were two-sided. **A**) Association analysis of overall survival in 327 non–small cell lung cancer (NSCLC) patients who were in stage III and IV and had received first-line platinum-based chemotherapy with or without radiation plotted by individual chromosomes for the whole genome. **B**) Association analysis of overall survival in 213 NSCLC patients who were in stage IIIB (wet) and IV and had received first-line platinum-based chemotherapy with or without radiation plotted by individual chromosomes for the whole genome.

following the same eligibility criteria as the discovery population (Table 1). As summarized in Table 2, under the additive model, rs1878022 was statistically significantly associated with poor overall survival in the MD Anderson discovery population (hazard ratio [HR] of death = 1.59, 95% CI = 1.32 to 1.92, $P = 1.42 \times 10^{-6}$), and the difference in survival time was dependent on the number of variant alleles carried by the patient ($P = 0.001$) (Figure 2). This association reached borderline statistical significance in the Mayo Clinic validation population (HR of death = 1.16, 95% CI = 0.95 to 1.41, $P = .15$) but was associated with survival time differences in patients with different genotypes (homozygous common genotype [TT] vs heterozygous genotype [TC] vs homozygous variant genotype [CC], $P = .04$) (Figure 2).

Another candidate SNP, rs10937823, was associated with statistically significantly poorer survival in the MD Anderson discovery dataset (HR of death = 2.40, 95% CI = 1.67 to 3.43, $P = 1.80 \times 10^{-6}$), the Mayo Clinic validation dataset (HR of death = 1.45, 95% CI = 1.02 to 2.08, $P = .04$), and the combined MD Anderson and Mayo Clinic dataset (HR of death = 1.82, 95% CI = 1.42 to 2.33, $P = 1.73 \times 10^{-6}$). In the combined dataset, the median survival time for individuals with the common homozygous genotype (16.05 months) was statistically significantly longer than the mean survival time for those carrying the variant-containing genotypes (10.72 months, $P = 6.76 \times 10^{-5}$).

In a sensitivity analysis, we repeated the analysis for rs1878022 by restricting to all patients who had chemotherapy treatment before 2004, 2005, and 2006 (ie, those patients who had at least 5, 4, and 3 years of follow-up). The associations between overall survival and rs1878022 were very similar to the overall analysis, and for the Mayo study, we observed stronger association with poor overall survival when the follow-up was longer. We also assessed the effect on overall survival of rs1878022 in patients who received radiotherapy as part of their treatment regimen. In both the MD Anderson and Mayo Clinic populations, the results were similar between the two treatment groups (MD Anderson: chemotherapy and radiotherapy, HR of death = 1.50, 95% CI = 1.16 to 1.94, vs chemotherapy only, HR of death = 1.64, 95% CI = 1.22 to 2.20; Mayo Clinic: chemotherapy and radiotherapy, HR of death = 1.17, 95% CI = 0.90 to 1.52, vs chemotherapy only, HR

Table 1. Characteristics of study populations

Study population characteristics	MD Anderson discovery	Mayo Clinic validation	PLATAX validation for rs10937823	PLATAX validation for rs1878022
Total No. of patients	327	315	420	277
Median survival time, mo	12.83	16.28	8.88	8.88
Age, median (range), y	61 (31–81)	65 (34–88)	59 (31–80)	59 (31–80)
Sex, No. (%)				
Male	195 (60)	200 (63)	350 (83)	232 (84)
Female	132 (40)	115 (37)	70 (17)	45 (16)
Clinical stage, No. (%)				
Stage IIIA	45 (14)	59 (19)		
Stage IIIB	90 (27)	81 (26)	66 (16)	44 (16)
Stage IV	192 (59)	175 (56)	354 (84)	233 (84)
Performance status*, No. (%)				
0	76 (26)	98 (32)	114 (27)	80 (29)
1	186 (63)	151 (50)	296 (71)	191 (69)
2–4	34 (11)	53 (18)	8 (2)	5 (2)
Smoking status, No. (%)				
Former	165 (50)	198 (63)	Unknown	Unknown
Current and recent quitter	162 (50)	117 (37)	Unknown	Unknown
Pack-years, median (range)	40 (0.1–153)	44 (0.5–182)	Unknown	Unknown

* Among patients with performance status information available.

Table 2. Summary results for rs1878022 analysis*

Study populations	Dead, No. (%)	Alive, No. (%)	HR (95% CI)	*P*†
MD Anderson for discovery analysis				
TT	106 (40.0)	39 (62.9)	1 (referent)	—
TC	121 (45.7)	21 (33.9)	1.72 (1.29 to 2.30)	2.07×10^{-4}
CC	38 (14.3)	2 (3.2)	2.42 (1.62 to 3.62)	1.65×10^{-5}
P_{trend}	NA	NA	1.59 (1.32 to 1.92)‡	1.42×10^{-6}
Mayo Clinic for validation analysis				
TT	115 (42.3)	20 (50.0)	1 (referent)	—
TC	127 (46.7)	16 (40.0)	1.07 (0.83 to 1.39)	.59
CC	30 (11.0)	4 (10.0)	1.49 (0.95 to 2.33)	.08
P_{trend}	NA	NA	1.16 (0.95 to 1.41)‡	.15
PLATAX for validation analysis				
TT	86 (39.6)	32 (55.2)	1 (referent)	—
TC	104 (47.9)	24 (41.4)	1.39 (1.03 to 1.86)	.03
CC	27 (12.4)	2 (3.5)	1.37 (0.86 to 2.16)	.18
P_{trend}	NA	NA	1.23 (1.00 to 1.51)§	.05
Mayo Clinic and PLATAX for pooled validation analysis	489	98	1.22 (1.06 to 1.40)||	.005
Overall pooled population	754	160	1.33 (1.19 to 1.48)||	5.13×10^{-7}

* CC = homozygous variant genotype, CI = confidence interval, HR = hazard ratio, NA = not applicable, TC = heterozygous genotype, TT = homozygous common genotype.

† *P* values were calculated by multivariable Cox proportional hazards models and statistical tests were two-sided.

‡ Hazard ratio under the additive model adjusted for age (continuous), sex (male or female), pack-years (continuous), clinical stage (IIIA, IIIB [dry], IIIB [wet] or IV), and pretreatment performance status (0, 1, or 2–4).

§ Hazard ratio under the additive model adjusted age (continuous), sex (male or female), clinical stage (IIIB [wet] or IV), and pretreatment performance status (0, 1, or 2–4).

|| Hazard ratio under the additive model adjusted for age (continuous), sex (male or female), clinical stage (IIIA, IIIB [dry], IIIB [wet] or IV), pretreatment performance status (0, 1, or 2–4), and study site (MD Anderson, Mayo Clinic, or PLATAX).

of death = 1.23, 95% CI = 0.89 to1.69) with overlapping 95% confidence intervals.

To further provide evidence that these genetic loci are associated with poor overall survival in patients receiving platinum-based chemotherapy, we analyzed rs1878022 and rs10937823 in patients enrolled in the PLATAX clinical trial. Under the dominant model, rs10937823 was non-statistically significantly associated with poor overall survival in the PLATAX validation population (HR of

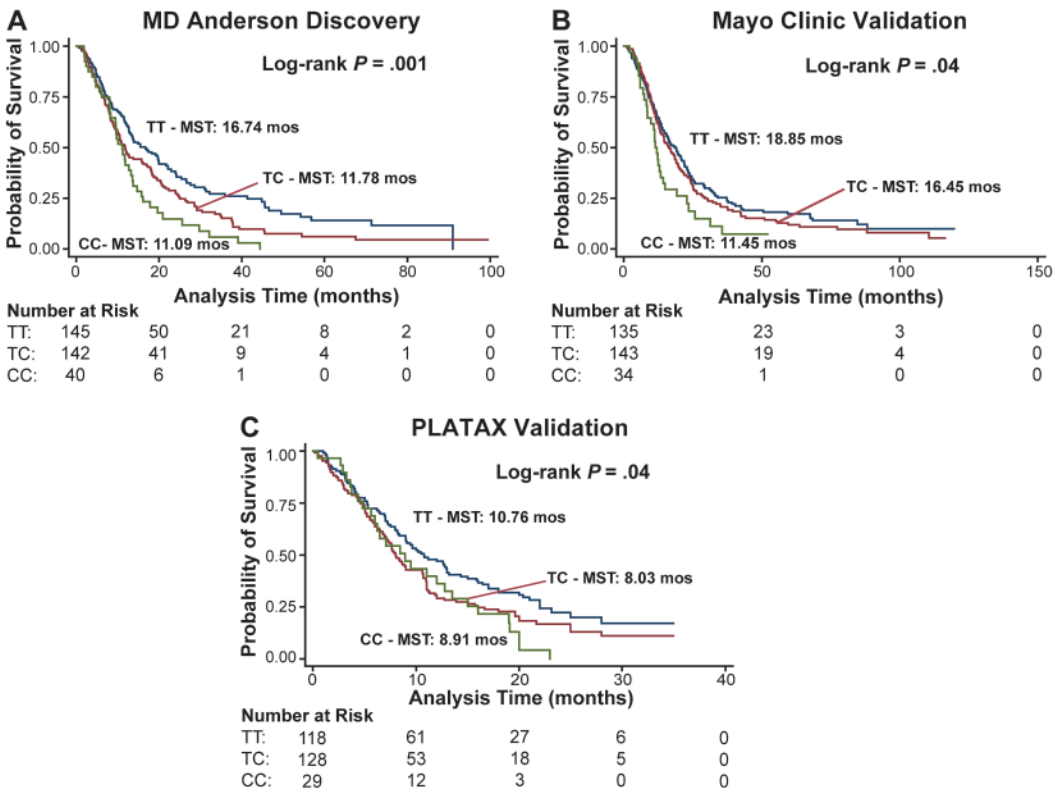

Figure 2. Kaplan–Meier curves of overall survival in non–small cell lung cancer patients who received platinum-based chemotherapy by rs1878022 genotype. Overall survival is shown for **A**) the MD Anderson discovery set, **B**) the Mayo Clinic validation set, and **C**)the PLATAX validation set. The absolute numbers of patients at risk are listed below each Kaplan–Meier curve. CC = homozygous variant genotype, MST = median survival, TC = heterozygous genotype, TT = homozygous common genotype. Log-rank *P* values were calculated by the two-sided log-rank test.

death = 0.96, 95% CI = 0.69 to 1.35, $P = .84$). Also, rs1878022 was validated in the PLATAX population (HR of death = 1.23, 95% CI = 1.00 to 1.51, $P = .05$) (Table 2). However, a statistically significant difference in median survival times (log-rank $P = .04$) was evident based on the number of variant alleles. Patients with the common genotype had a mean survival time of 10.76 months compared with 8.03 and 8.91 months for patients carrying the heterozygous genotype and the variant genotype, respectively (Figure 2). This association was stronger in a pooled analysis of the two validation datasets (HR of death = 1.22, 95% CI = 1.06 to 1.40, $P = .005$) and was highly statistically significant overall using data from all three studies (HR of death = 1.33, 95% CI = 1.19 to 1.48, $P = 5.13 \times 10^{-7}$).

SNP rs1878022 is located on chromosome 12q23.3 within the intron of the chemokine-like receptor 1 gene (*CMKLR1*). Haplotype analysis of the genomic region surrounding rs1878022 indicated rs1878022 was not in high linkage disequilibrium with any neighboring SNPs, thus rs1878022 is not located in any major haplotype blocks within this region of the chromosome (Figure 3). Imputation of HapMap SNPs within this genomic region confirmed

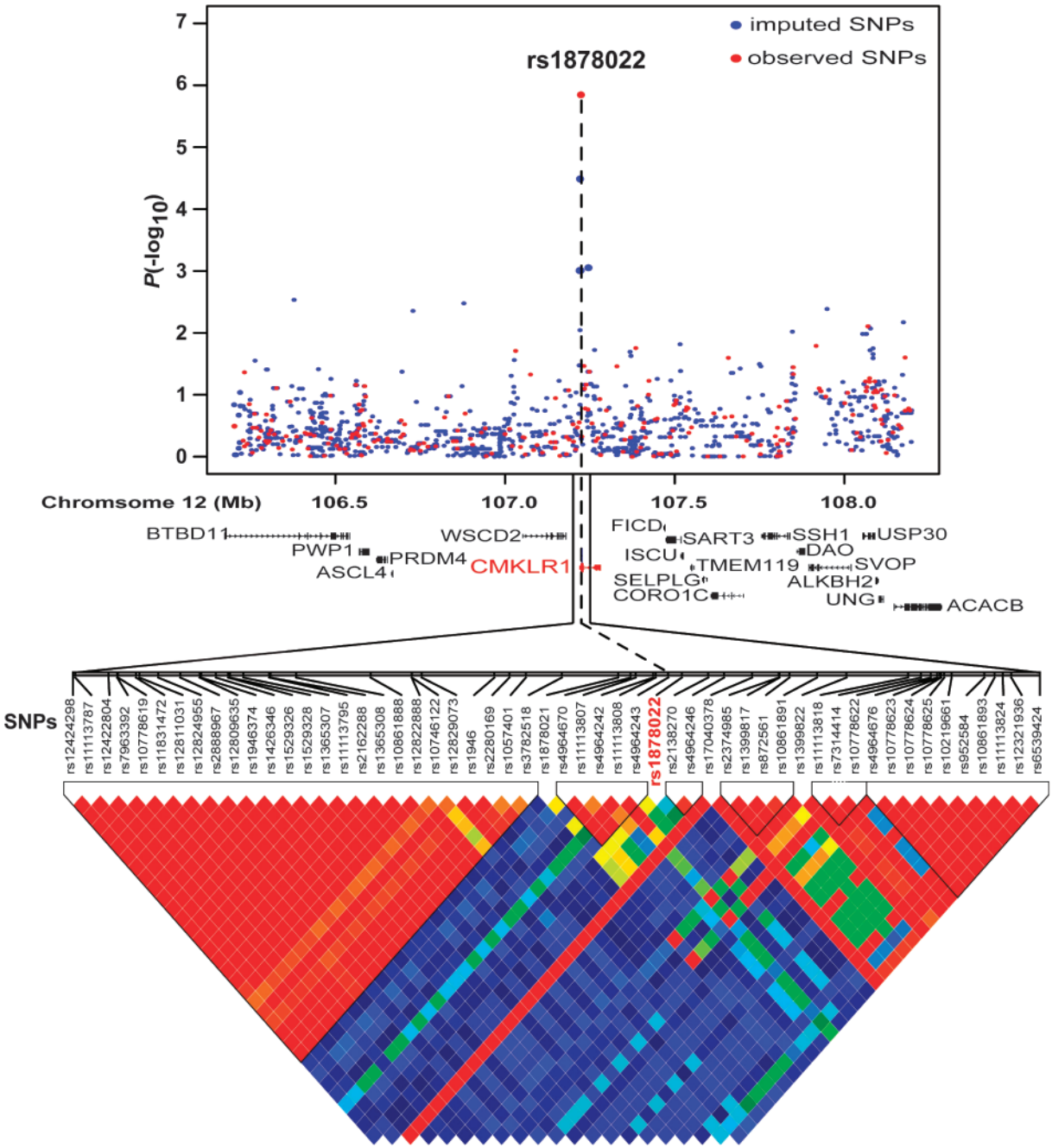

Figure 3. Linkage disequilibrium structure and association of observed and imputed single-nucleotide polymorphisms (SNPs) surrounding rs1878022 on chromosome 12. The linkage disequilibrium structure was created with the GOLD heat map Haploview 4.0 color scheme using the standardized disequilibrium coefficient, D′, with associations expressed as $-\log_{10}(P)$ and calculated by the multivariable Cox proportional hazard model.

these findings, and no other SNPs demonstrated a statistically significant association with poor overall survival in NSCLC patients as calculated using this method.

We created two prediction models based on 1-year survival for the pooled dataset to investigate the clinical relevance of rs1878022. The AUC based on the clinical and epidemiological variables (age, sex, clinical stage, and pretreatment performance status) was 69.1%, demonstrating reasonable predictive power. The addition of the single SNP to the model increased the AUC to 70.5%. Results based on 1000 bootstrapping samples showed that the distribution of the difference of the AUCs has a 95% bias-corrected confidence interval of 0.4% to 3.4%, indicating a statistically significant improvement in prediction of decreased overall survival in NSCLC patients after adding rs1878022 to the model.

Discussion

To better understand the genetic factors modulating response to platinum-based therapy in stage III and IV patients, we used a three-stage analytical approach that took advantage of two of the largest lung NSCLC patient cohorts in the United States and patients from a large multicenter clinical trial. Our data identified a common genetic polymorphism in *CMKLR1* that is statistically significantly associated with decreased overall survival. An additional candidate SNP was also identified that was non-statistically significantly associated with an increased risk of poor outcome in our study populations but may reach statistical significance after further analyses in a larger patient population. This is the first genome-wide study, to our knowledge, taking an unbiased non candidate gene–driven approach to investigate the genetic factors influencing overall survival for advanced-stage NSCLC patients receiving platinum-based chemotherapy.

Previous candidate gene studies have indicated that genetic variation in genes within the platinum drug action pathway may be associated with response to chemotherapy (18). However, the observed effect of each individual SNP is modest with a stronger association in combined analyses of multiple risk alleles (8). Linkage studies using lymphoblastoid cell lines from pedigrees of Caucasian individuals have indicated that approximately 47% of the variation in susceptibility to cisplatin-induced cytotoxicity is because of heritable factors (19). These results indicate that there are unidentified genetic factors playing a major role in determining patient responses to platinum-based chemotherapeutics. Genome-wide association studies of cisplatin cytotoxicity in lymphoblastoid cell lines have also been performed and identified several novel associations between genetic variation and cytotoxicity (20,21). Similar to the findings of our study, the variants identified in these previous reports were located within genes not previously considered as candidates for chemotherapy response.

The validated SNP rs1878022 is an intronic variant located within *CMKLR1* on human chromosome 12. This gene encodes for a seven transmembrane G-protein coupled receptor (also known as the ChemR23 protein) that is involved in several cellular pathways, including inflammation, adipogenesis, and osteoblastogenesis (22–25). Although primarily expressed on dendritic cells and macrophages, high CMKLR1 protein expression has been previously reported in lung tissue (25). Binding to this receptor by its ligands chemerin and resolvin E1 has been shown to activate multiple downstream signaling pathways including phosphoinositide-3 kinase/AKT, mitogen-activated protein kinase (MAPK), and extracellular signal-related kinase 1 and 2 (ERK1/2) (24–27), and more recently, endothelial cell expression and angiogenesis (27). Expression of *CMKLR1* was found to be higher in normal mucosa of patients with esophageal squamous dysplasia patients whose disease had progressed (28). However, to date, no studies have been published reporting an association between either *CMKLR1* or its protein and lung cancer. Further studies are needed to elucidate the function of *CMKLR1* and its protein specifically within the context of lung cancer and to determine how genetic variation within this gene modulates these functions resulting in differences in advanced-stage NSCLC patients' responses to platinum-based chemotherapeutics.

The SNP rs10937823 was statistically associated with decreased overall survival in the MD Anderson and Mayo Clinic patient populations, but not associated with decreased overall survival in patients enrolled in the PLATAX clinical trial. This genetic variant is located within an intron, a gene encoding for the poorly characterized SORCS2 protein. SORCS2 contains a VPS10 domain that is known to have a role in intracellular trafficking and lysosomal processing (29). Other members of this gene family with VPS10 domains, such as sortilin (*SORT1*), are known to be responsible for both trafficking and regulation of neurotrophin signaling (30). However, SORCS2 is mainly located on the cell surface and is not believed to have a major role in cellular trafficking (31), in part because its VPS10 domain differs from that of other members of the family (32). SORCS2 is highly expressed in the brain and central nervous system during development (33,34), and protein expression has been detected in the developing and adult lung (32,34). Although the exact function of this receptor is unclear, several gene expression studies have hypothesized a role for *SORCS2* in breast cancer clinical outcome (35) and lymphatic metastasis after treatment for oral carcinoma (36). Also, SORCS2 gene expression was strongly related to sensitivity to chemotherapeutics in human gastric cancer cell lines in vitro (37). Our data indicate that rs10937823 may be associated with overall survival in NSCLC patients. Additional studies are necessary to determine the function of SORCS2 in NSCLC and further establish rs10937823 as a candidate SNP for poor overall survival in this patient population.

Somatic alterations in tumor tissues are immensely useful in characterizing the molecular changes that occur during cancer development and may aid in selecting the appropriate targeted therapy for those patients with specific mutations (38). However, platinum-based chemotherapy is often used to treat patients for whom surgery is not an option because of disease severity or other preexisting conditions, making it difficult to screen for somatic alterations if tumor specimens are limited. Because of these characteristics, it may be difficult to screen for somatic alterations due to lack of tumor availability and underscores the need to identify germline genetic variations that can be used as prognostic and predictive markers. Furthermore, platinum-based chemotherapy is also used in the adjuvant setting before surgery. Germline SNPs are stable markers that do not vary with disease severity and can be screened for using DNA isolated from a blood sample before

treatment. Identification of these common genetic polymorphisms that can reliably predict response to chemotherapy has the potential to guide personalized therapeutic prediction.

Our study has two limitations that are major concerns inherent of any genome-wide approach—multiple comparisons and the presence of false-positive findings. To address these issues, we used a three-stage study design in multiple independent populations using a progressively smaller panel of candidate SNPs. The study design allows for validation of any findings from the large discovery population that is more prone to false-positive findings, SNPs that remain statistically significantly associated with decreased overall survival across all study populations have a high likelihood of being true-positive findings, thus reducing the need for strict multiple comparison correction. Future studies to replicate our data in other patient populations with similar treatment regimens are necessary to confirm the conclusions of our study.

Because of the widespread use of platinum-based chemotherapy to treat advanced-staged NSCLC, it is difficult to establish SNPs as pharmacogenetic markers specific for response to treatment or more general prognostic markers. This distinction would only be possible with a parallel analysis in a platinum-based chemotherapy-naive patient population. Nevertheless, by focusing on a select homogenous population of NSCLC patients, we are able to determine that a statistically significant increase in risk of death is present in patients with specific genetic variants when treated with platinum-based chemotherapy. There was only a moderate statistically significant increase in risk of death associated with either of the two candidate SNPs. However, the combinatorial effect of multiple SNPs and potential unidentified gene–gene interactions may result in a stronger association between genetic variants and risk of death in NSCLC. This has been previously demonstrated for risk models developed for prostate and breast cancers (39,40). Together with epidemiology, demographic, clinical, and other genetic risk factors, our findings have the potential to influence personalized treatment by identifying patients who would respond best to a specific treatment regimen.

Advanced-stage NSCLC patients are commonly treated with platinum-based chemotherapy. Although this course of treatment has been shown to increase overall survival, many patients develop resistance or dose-limiting side effects to these agents and even with therapy, the 1-year survival rate is 29% (41). To the best of our knowledge, this is the first genome-wide study to assess the genetic factors influencing overall survival for advanced-stage NSCLC patients receiving platinum-based chemotherapy. This study provides additional biomarkers that can be integrated with known epidemiological, clinical, and genetic risk factors to potentially identify patients who are more likely to respond to chemotherapy, thereby helping the physician develop individualized treatment regimens.

References

1. American Cancer Society. *Cancer Facts and Figures 2008.* Atlanta, GA: American Cancer Society; 2008.
2. Gurubhagavatula S, Liu G, Park S, et al. XPD and XRCC1 genetic polymorphisms are prognostic factors in advanced non-small-cell lung cancer patients treated with platinum chemotherapy. *J Clin Oncol.* 2004;22(13):2594–2601.
3. Tibaldi C, Giovannetti E, Vasile E, et al. Correlation of CDA, ERCC1, and XPD polymorphisms with response and survival in gemcitabine/cisplatin-treated advanced non-small cell lung cancer patients. *Clin Cancer Res.* 2008;14(6):1797–1803.
4. Schiller JH, Harrington D, Belani CP, et al. Comparison of four chemotherapy regimens for advanced non-small-cell lung cancer. *N Engl J Med.* 2002;346(2):92–98.
5. Booton R, Ward T, Heighway J, et al. Xeroderma pigmentosum group D haplotype predicts for response, survival, and toxicity after platinum-based chemotherapy in advanced nonsmall cell lung cancer. *Cancer.* 2006;106(11):2421–2427.
6. Kim SH, Juhnn YS, Song YS. Akt involvement in paclitaxel chemoresistance of human ovarian cancer cells. *Ann N Y Acad Sci.* 2007;1095(1):82–89.
7. Matakidou A, el Galta R, Webb EL, et al. Genetic variation in the DNA repair genes is predictive of outcome in lung cancer. *Hum Mol Genet.* 2007;16(19):2333–2340.
8. Wu X, Lu C, Ye Y, et al. Germline genetic variations in drug action pathways predict clinical outcomes in advanced lung cancer treated with platinum-based chemotherapy. *Pharmacogenet Genomics.* 2008;18(11):955–965.
9. Amos CI, Wu X, Broderick P, et al. Genome-wide association scan of tag SNPs identifies a susceptibility locus for lung cancer at 15q25.1. *Nat Genet.* 2008;40(5):616–622.
10. Hung RJ, McKay JD, Gaborieau V, et al. A susceptibility locus for lung cancer maps to nicotinic acetylcholine receptor subunit genes on 15q25. *Nature.* 2008;452(7187):633–637.
11. McKay JD, Hung RJ, Gaborieau V, et al. Lung cancer susceptibility locus at 5p15.33. *Nat Genet.* 2008;40(12):1404–1406.
12. Thorgeirsson TE, Geller F, Sulem P, et al. A variant associated with nicotine dependence, lung cancer and peripheral arterial disease. *Nature.* 2008;452(7187):638–642.
13. Wang Y, Broderick P, Webb E, et al. Common 5p15.33 and 6p21.33 variants influence lung cancer risk. *Nat Genet.* 2008;40(12):1407–1409.
14. Yang P, Allen MS, Aubry MC, et al. Clinical features of 5,628 primary lung cancer patients: experience at Mayo Clinic from 1997 to 2003. *Chest.* 2005;128(1):452–462.
15. Purcell S, Neale B, Todd-Brown K, et al. PLINK: a tool set for whole-genome association and population-based linkage analyses. *Am J Hum Genet.* 2007;81(3):559–575.
16. Price AL, Patterson NJ, Plenge RM, Weinblatt ME, Shadick NA, Reich D. Principal components analysis corrects for stratification in genome-wide association studies. *Nat Genet.* 2006;38(8):904–909.
17. Barrett JC, Fry B, Maller J, Daly MJ. Haploview: analysis and visualization of LD and haplotype maps. *Bioinformatics.* 2005;21(2):263–265.
18. Hildebrandt MA, Gu J, Wu X. Pharmacogenomics of platinum-based chemotherapy in NSCLC. *Expert Opin Drug Metab Toxicol.* 2009;5(7):745–755.
19. Dolan ME, Newbold KG, Nagasubramanian R, et al. Heritability and linkage analysis of sensitivity to cisplatin-induced cytotoxicity. *Cancer Res.* 2004;64(12):4353–4356.
20. Huang RS, Duan S, Shukla SJ, et al. Identification of genetic variants contributing to cisplatin-induced cytotoxicity by use of a genomewide approach. *Am J Hum Genet.* 2007;81(3):427–437.
21. Shukla SJ, Duan S, Badner JA, Wu X, Dolan ME. Susceptibility loci involved in cisplatin-induced cytotoxicity and apoptosis. *Pharmacogenet Genomics.* 2008;18(3):253–262.
22. Muruganandan S, Roman AA, Sinal CJ. Role of chemerin/CMKLR1 signaling in adipogenesis and osteoblastogenesis of bone marrow stem cells. *J Bone Miner Res.* 2010;25(2):222–234.
23. Bozaoglu K, Bolton K, McMillan J, et al. Chemerin is a novel adipokine associated with obesity and metabolic syndrome. *Endocrinology.* 2007;148(10):4687–4694.
24. Roh SG, Song SH, Choi KC, et al. Chemerin—a new adipokine that modulates adipogenesis via its own receptor. *Biochem Biophys Res Commun.* 2007;362(4):1013–1018.
25. Wittamer V, Franssen JD, Vulcano M, et al. Specific recruitment of antigen-presenting cells by chemerin, a novel processed ligand from human inflammatory fluids. *J Exp Med.* 2003;198(7):977–985.

26. Ohira T, Arita M, Omori K, Recchiuti A, Van Dyke TE, Serhan CN. Resolvin E1 receptor activation signals phosphorylation and phagocytosis. *J Biol Chem.* 2010;285(5):3451–3461.
27. Kaur J, Adya R, Tan BK, Chen J, Randeva HS. Identification of chemerin receptor (ChemR23) in human endothelial cells: chemerin-induced endothelial angiogenesis. *Biochem Biophys Res Commun.* 2010;391(4): 1762–1768.
28. Joshi N, Johnson LL, Wei WQ, et al. Gene expression differences in normal esophageal mucosa associated with regression and progression of mild and moderate squamous dysplasia in a high-risk Chinese population. *Cancer Res.* 2006;66(13):6851–6860.
29. Westergaard UB, Sorensen ES, Hermey G, et al. Functional organization of the sortilin Vps10p domain. *J Biol Chem.* 2004;279(48):50221–50229.
30. Willnow TE, Petersen CM, Nykjaer A. VPS10P-domain receptors—regulators of neuronal viability and function. *Nat Rev Neurosci.* 2008;9(12): 899–909.
31. Hermey G, Sjogaard SS, Petersen CM, Nykjaer A, Gliemann J. Tumour necrosis factor alpha-converting enzyme mediates ectodomain shedding of Vps10p-domain receptor family members. *Biochem J.* 2006;395(2):\285–293.
32. Hampe W, Rezgaoui M, Hermans-Borgmeyer I, Schaller HC. The genes for the human VPS10 domain-containing receptors are large and contain many small exons. *Hum Genet.* 2001;108(6):529–536.
33. Hermey G, Plath N, Hubner CA, Kuhl D, Schaller HC, Hermans-Borgmeyer I. The three sorCS genes are differentially expressed and regulated by synaptic activity. *J Neurochem.* 2004;88(6):1470–1476.
34. Rezgaoui M, Hermey G, Riedel IB, Hampe W, Schaller HC, Hermans-Borgmeyer I. Identification of SorCS2, a novel member of the VPS10 domain containing receptor family, prominently expressed in the developing mouse brain. *Mech Dev.* 2001;100(2):335–338.
35. Finak G, Bertos N, Pepin F, et al. Stromal gene expression predicts clinical outcome in breast cancer. *Nat Med.* 2008;14(5):518–527.
36. Watanabe H, Mogushi K, Miura M, et al. Prediction of lymphatic metastasis based on gene expression profile analysis after brachytherapy for early-stage oral tongue carcinoma. *Radiother Oncol.* 2008;87(2):237–242.
37. Jung JJ, Jeung HC, Chung HC, et al. In vitro pharmacogenomic database and chemosensitivity predictive genes in gastric cancer. *Genomics.* 2009; 93(1):52–61.
38. Ding L, Getz G, Wheeler DA, et al. Somatic mutations affect key pathways in lung adenocarcinoma. *Nature.* 2008;455(7216):1069–1075.
39. Zheng SL, Sun J, Wiklund F, et al. Cumulative association of five genetic variants with prostate cancer. *N Engl J Med.* 2008;358(9):910–919.
40. Mealiffe ME, Stokowski RP, Rhees BK, Prentice RL, Pettinger M, Hinds DA. Assessment of clinical validity of a breast cancer risk model combining genetic and clinical information. *J Natl Cancer Inst.* 2010;102(21):1618–1627.
41. Burdett S, Stephens R, Stewart L, et al. Chemotherapy in addition to supportive care improves survival in advanced non-small-cell lung cancer: a systematic review and meta-analysis of individual patient data from 16 randomized controlled trials. *J Clin Oncol.* 2008;26(28):4617–4625.

Funding

The study was supported in part by National Institutes of Health (R01CA111646 and P50CA070907 to X.W., R01CA55769 to M.R.S., R01CA121197 to C.I.A., R01CA084354 and R01CA115857 to P.Y., P50CA090440 and 5U01CA114771 to M.R.).

Notes

M. Romkes and P. Yang contributed equally to this work.

The participating institutions from Spain include Hospital Doce de Octubre, Madrid; Xeral Cies de Vigo, Vigo; Catalan Institute of Oncology, Badalona; Clinica Sagrado Corazon, Sevilla; Hospital General Yague, Burgos; Hospital La Princesa, Madrid; Catalan Institute of Oncology, Girona; Hospital de Leon, Leon; Hospital General de Valencia, Valencia; Hospital Arnau de Vilanova, Valencia; Catalan Insitute of Oncology, Bellvitge; Hospital Clinico San Carlos, Madrid; Hospital General de Asturias, Oviedo; Hospital Alcoy, Alicante; Autonomous University of Madrid, Madrid.

The sponsors had no role in the design or conduct of the study; collection, management, analysis, or interpretation of the data; and preparation, review, or approval of the article.

Affiliations of authors: Department of Epidemiology (XW, YY, CIA, MATH, JG, JL, AC, MRS), Department of Thoracic Head and Neck Medical Oncology (DJS, CL, SML, WKH), Department of Thoracic Cardiovascular Surgery (JAR), and Department of Radiation Oncology (JYC), The University of Texas MD Anderson Cancer Center, Houston, TX; Medical Oncology Service, Department of Medicine, Catalan Institute of Oncology, Hospital Germans Trias i Pujol and Autonomous University of Barcelona, Badalona, Spain (RR, JLRS, MT); Department of Internal Medicine and Pharmacology, Hamon Center for Therapeutic Oncology Research, The University of Texas Southwestern Medical Center, Dallas, TX (JDM); Department of Medicine, University of Pittsburgh and University of Pittsburgh Cancer Institute, Pittsburgh, PA (SCB, TN, MR); Department of Health Sciences Research, Mayo Clinic College of Medicine, Rochester, MN (PY).

Published OnlineFirst January 21, 2011; DOI:10.1158/1078-0432.CCR-10-1412

Clinical Cancer Research

Imaging, Diagnosis, Prognosis

Abnormalities of the *TITF-1* Lineage-Specific Oncogene in NSCLC: Implications in Lung Cancer Pathogenesis and Prognosis

Ximing Tang[1], Humam Kadara[1], Carmen Behrens[1], Diane D. Liu[3], Yun Xiao[7], David Rice[4], Adi F. Gazdar[5,6], Junya Fujimoto[1], Cesar Moran[2], Marileila Varella-Garcia[7], J. Jack Lee[3], Waun Ki Hong[1], and Ignacio I. Wistuba[1,2]

Abstract

Purpose: Emerging evidence suggests that aberrant expression of oncogenes contributes to development of lung malignancy. The thyroid transcription factor 1 (*TITF-1*) gene functions as a lineage survival gene abnormally expressed in a significant fraction of non–small cell lung cancers (NSCLC), in particular lung adenocarcinomas.

Experimental Design: To better characterize *TITF-1* abnormality patterns in NSCLC, we studied *TITF-1*'s gene copy number using FISH and quantitative PCR, as well as its protein expression by immunohistochemistry analysis in a tissue microarray comprising surgically resected NSCLC ($N = 321$) including 204 adenocarcinomas and 117 squamous cell carcinomas (SCC). *TITF-1* copy number and protein expression were correlated with patients' clinicopathologic characteristics, and in a subset of adenocarcinomas with *EGFR* and *KRAS* mutation status.

Results: We found that increased TITF-1 protein expression was prevalent in lung adenocarcinomas only and was significantly associated with female gender ($P < 0.001$), never-smokers ($P = 0.004$), presence of *EGFR* mutations ($P = 0.05$), and better overall survival (all stages, $P = 0.0478$; stages I and II, $P = 0.002$). *TITF-1* copy number gain(CNG) was detected by FISH analysis in both adenocarcinomas (18.9%; high CNG, 8.3%) and SCCs (20.1%; high CNG, 3.0%), and correlated significantly with the protein product ($P = 0.004$) and presence of *KRAS* mutations ($P = 0.008$) in lung adenocarcinomas. Moreover, multivariate analysis revealed that *TITF-1* copy number gain was an independent predictor of poor survival of NSCLC ($P = 0.039$).

Conclusions: Our integrative study demonstrates that the protein versus genomic patterns of *TITF-1* have opposing roles in lung cancer prognosis and may occur preferentially in different subsets of NSCLC patients with distinct oncogene mutations. *Clin Cancer Res; 17(8); 2434–43. ©2011 AACR.*

Introduction

It is estimated that lung cancer is the leading cause of cancer-related deaths in the United States (1). The majority of diagnosed lung cancers are non–small cell lung cancers (NSCLC) which include 2 major histological subtypes; lung adenocarcinomas and squamous cell carcinomas (SCC; ref 2). Lung adenocarcinomas and SCCs appear to develop progressively by different pathogenic phases; SCCs typically develop near the central airways, whereas lung adenocarcinomas occur predominantly in the lung periphery (3). Therefore, it is plausible to assume that characterization of molecular and biological markers for better understanding the similarities and differences in the development of the different subtypes of NSCLC will favorably impact the clinical management of this deadly disease (4).

It has been suggested that lineage-specific genes, that play important roles in normal developmental processes such as organogenesis or tissue homeostasis and remain to be expressed or become amplified during an acquired pathological condition, are crucial for maintenance of the disease state (5, 6). Moreover, lineage-oncogenes have been shown to be important for mediating the prosurvival properties of cancer cells of different histopathological characteristics; for example, adenocarcinomas versus SCCs (5). In addition, tumor cells are addicted to aberrant and growth-promoting cell signaling mediated by lineage-specific oncogenes (7), for example, the presence of the BCR–ABL fusion oncoprotein in chronic myelogenous leukemia (CML; ref 8), mutations in the *KIT* oncogene in gastrointestinal stromal tumors (GISTs; ref 9) and mutations in

Authors' Affiliations: Departments of [1]Thoracic/Head and Neck Medical Oncology, [2]Pathology, [3]Biostatistics, and [4]Thoracic and Cardiovascular Surgery, The University of Texas MD Anderson Cancer Center, Houston, Texas; [5]The Hamon Center for Therapeutic Oncology Research and [6]Department of Pathology, The University of Texas Southwestern Medical Center, Dallas, Texas; and [7]Department of Medicine/Medical Oncology and Pathology, The University of Colorado Cancer Center, Aurora, Colorado

Note: Supplementary data for this article are available at Clinical Cancer Research Online (http://clincancerres.aacrjournals.org/).

Corresponding Author: Ignacio I. Wistuba, Departments of Pathology and Thoracic/Head and Neck Medical Oncology, University of Texas MD Anderson Cancer Center, Houston, TX. Phone: 713-563-9184; Fax: 713-563-1848; E-mail: iiwistuba@mdanderson.org

doi: 10.1158/1078-0432.CCR-10-1412

Published OnlineFirst January 21, 2011; DOI:10.1158/1078-0432.CCR-10-1412

Translational Relevance

Thyroid transcription factor 1 (TITF-1) is a transactivating factor with important functions in the normal peripheral lung and that exhibits dysregulated expression in non–small cell lung cancers (NSCLC) and amplification in a significant fraction of lung tumors typical of a lineage-specific oncogene. We tested the hypothesis that the abnormal expression of TITF-1 at the protein and DNA levels may occur in different subsets of patients with distinct clinicopathological and unique molecular features. We demonstrated significant association of TITF-1 protein expression and copy number gain with favorable and poor prognosis, respectively, in NSCLC patients. Importantly, we unraveled distinct correlations between TITF-1 protein expression and copy number gain of the gene with mutations in the *EGFR* and *KRAS* oncogenes, respectively, in lung adenocarcinoma. Our findings, suggest that lung adenocarcinomas exhibiting elevated protein or copy gain of TITF-1 may be of different cell lineage populations with distinct oncogene mutation patterns, and therefore subject to dissimilar anticancer therapies.

the epidermal growth factor receptor (*EGFR*) in lung adenocarcinomas (10–12).

NK2 homeobox 1 (NKX2.1) otherwise known as thyroid transcription factor 1 (TITF-1) is a homeodomain-containing transactivating factor predominantly expressed in the terminal lung bronchioles and lung periphery in the developing and adult mouse (13–15). In addition, TITF-1 is crucial for branching morphogenesis during normal lung development (14–17) and transactivates the expression of the surfactant proteins (SP) such as SPs-A, -B, and -C which are in turn typically expressed in the Clara cells and are important for the differentiation of alveolar type II pneumocyte cells in the peripheral lung (18–20). More recently, TITF-1 expression and function have been shown to be important in the etiology of congenital pulmonary disease (21) and NSCLC (22–24). *TITF-1* is part of the 14q13.3 cytoband locus which is amplified in a significant fraction of lung tumors (22, 24). In addition, knockdown of TITF-1 expression by RNA interference results in lung adenocarcinoma cell growth inhibition and apoptosis demonstrating a lineage-specific dependency of lung adenocarcinomas on TITF-1 (22–24). In contrast to the expected prosurvival properties of a cell lineage oncogene, TITF-1 protein expression by immunohistochemistry is a marker of favorable prognosis in NSCLC patients (25–28) and is associated with good prognosis in early-stage (stage-I) lung adenocarcinoma patients (29). More recently, amplification of the *TITF-1* gene has been identified in lung SCCs (28) despite lack of protein expression; however, the relevance of this copy number gain to the clinical outcome of NSCLC patients is still unclear, although Weir and colleagues reported no significant difference in patient survival between adenocarcinoma tumors with or without amplification of *TITF-1* (24).

In this study, we sought to investigate protein and copy number levels of the *TITF-1* gene in NSCLC patients and correlate, in parallel, both levels of analyses with the clinicopathological and molecular features of the patients. We demonstrate the significant and close association of TITF-1 protein with the protein expression of all 3 SPs tested. In addition, we find a significant association of TITF-1 protein expression and copy gain with favorable and poor prognosis, respectively, in lung adenocarcinoma patients, despite a significant positive correlation between the gene's copy number and protein expression. Lastly, we unravel distinct significant correlations between TITF-1 protein expression and DNA copy gain with mutations in the lung adenocarcinoma-prevalent *EGFR* and *KRAS* oncogenes.

Methods

Human lung tissues and tissue microarray

All human tissues were obtained from the Lung Cancer Specialized Program of Research Excellence (SPORE) Tissue Bank at the MD Anderson Cancer Center. For each tissue sample, the percentage of malignant tissue was calculated and the cellular composition of specimens was determined by histological examination (I.I.W.) following Hematoxylin-Eosin (H&E) staining.

Specimens resected from NSCLC patients with stages I to IV disease according to the revised International System for Staging Lung Cancer (30) who had no prior chemotherapy or radiotherapy were used for tissue microarray (TMA) analysis by immunohistochemistry. Clinicopathological characteristics of the patients are summarized in Supplementary Table S1. Patients who had smoked at least 100 cigarettes in their lifetime were defined as smokers. Samples were fixed in formalin, embedded in paraffin, stained with H&E, and reviewed by an experienced pathologist (I.I.W.). The 321 tissue specimens collected from 321 patients included 117 SCCs and 204 adenocarcinomas. All tumors and lesions were classified according to the World Health Organization (WHO) 2004 criteria as previously described (31). The TMAs were prepared with a manual tissue arrayer (Advanced Tissue Arrayer ATA100, Chemicon International) using 1-mm-diameter cores in triplicate for tumors. Sections were then determined if they were suitable for analysis of TITF-1 protein expression by immunohistochemistry and *TITF-1* amplification by FISH analysis. Of the entire TMA set, 179 and 170 adenocarcinomas were used for immunohistochemistry and FISH analyses, respectively. In addition, 117 and 99 lung SCC sections were used for immunohistochemistry and FISH analyses, respectively. Moreover, 151 lung adenocarcinomas were subsequently analyzed for correlation of TITF-1 expression by immunohistochemistry and FISH analyses. Furthermore, data on *EGFR* and *KRAS* mutational status were available and conducted on 178 and 120 lung adenocarcinoma sections, respectively.

Published OnlineFirst January 21, 2011; DOI:10.1158/1078-0432.CCR-10-1412

Immunohistochemistry analysis

Tissue section slides were baked at 56°C overnight, then deparaffinized in xylene and rehydrated through a graded series of ethanol concentrations. Antigen retrieval was carried out using a decloaker for analysis of SP-B expression and a steamer (PH = 9, 20 minutes) for assessment of TITF-1 protein expression. Intrinsic peroxidase activity was blocked by 3% hydrogen peroxide in H_2O_2 for 15 minutes and 5% goat serum (Sigma) solution was used for blocking nonspecific antibody binding by incubating at room temperature for 60 minutes. Slides were then incubated at room temperature for 1 hour with primary antibodies raised against TITF-1 (dilution 1:100, clone 8G7G3/1, Cell Marque), SP-A (dilution 1:150, clone PE10, Thermo Scientific), SP-B (dilution 1:150, clone SPB02, Thermo Scientific), and SP-C (dilution 1:300, Chemicon). After 3 washes in Tris-buffered saline with Tween-20 (TBST) for 5 minutes each, the slides were incubated with Dako Envision + Dual Link for 30 minutes at room temperature. Following 3 additional washes in TBST, the slides were incubated with Dako chromogen substrate for 5 minutes and were counterstained with hemotoxylin for 5 minutes. The slides were read under microscope. Two pathologists (X.T. and I.W.) examined both the intensity and extent of immunostaining by light microscopy using a ×20 magnification objective. Cytoplasmic and nuclear expression were quantified using a 4-value intensity score (0, none; 1+, weak; 2+, moderate; and 3+, strong) and the percentage (0–100%) of the extent of reactivity. A final expression score was obtained by multiplying the intensity and reactivity extension values (range, 0–300).

FISH analysis

TITF-1 DNA was originally provided by Dr. Wam Lam (British Columbia Cancer Research Center, Vancouver, British Columbia, Canada). The DNA was labeled with Spectrum Red conjugated dUTP (Abbott Laboratories) using the Vysis Nick translation kit, according to the manufacturer's instructions. A chr14 control probe (14q11) was prepared using the BAC clone RP11–324B11 and labeled with Spectrum Green-conjugated dUTP using the same procedure as described above for the *TITF-1* probe. The FISH assay was conducted on the TMAs using a standard protocol (32). Briefly, slides were incubated for 4 hours at 56°C, deparaffinized in Citri-Solv (Thermo Fisher Scientific), and were hydrated. The slides were then incubated in 2× saline–sodium citrate (SSC) buffer at 75°C for 10 to 13 minutes, digested in 0.25 mg/mL proteinase K/2× SSC at 45°C for 10 to 13 minutes, washed in 2× SSC for 5 minutes, and dehydrated. Following application of the probe mixtures, samples were denaturated for 15 minutes at 80°C and incubated at 37°C for 48 hours, after which post-hybridization washes were carried out with 2× SSC/0.3% NP40 (pH 7.0–7.5) at 72°C for 2 minutes. Slides were then washed in 2× SSC for 2 min, dehydrated and chromatin was counterstained with 4′,6-diamidino-2-phenylindole (DAPI; 0.3 μg/mL in Vectashield mounting medium, Vector Laboratories). Analysis was carried out in epifluorescence microscope using single interference filters sets for green (fluorescein isothiocyanate, FITC), red (Texas Red), and blue (DAPI) as well as dual (red/green) band pass filters. Monochromatic images were captured and merged using the CytoVision workstation (Genetix). The quality of the preparation and the intensity of the fluorescence signal were variable per slide and per tissue core. The assay was repeated once for each array to obtain results in higher number of cores. Specimens displaying a gene signal number per cell of 4 or greater were considered to exhibit copy number gain (4–10 signals, low copy gain; greater than 10 signals, high level of copy number gain). The maximum value among the 3 cores was considered to represent each case.

DNA extraction and quantitative PCR

NSCLC tissues (n = 82, 53 adenocarcinomas and 29 SCCs) were dissected from formalin-fixed paraffin-embedded (FFPE) Hematoxylin-stained tissue sections using manual microdissection under stereomicroscope to ensure that tumor cell proportions are greater than 70% for subsequent DNA extraction. Tumor DNA was extracted using the PicoPure DNA extraction Kit (Arcturus) according to the manufacturer's instructions. Two μL of DNA was added to a 20 μL of final volume reaction mixture consisting of 10 μL of Power SYBR Green PCR Master Mix (Applied Biosystems) and 0.5 μmol/L of each of forward and reverse primers spanning the *TITF-1* gene (forward, 5′-gctgtgcgtttgtcgcttac-3′; reverse, 5′-ccatgccgctcatgttca-3′). *β-actin* gene was used as an endogenous reference gene. TaqMan Control Human Genomic DNA (Applied Biosystems) was amplified as a standard control for calibration. All samples and standard DNA reactions were carried out in triplicates. Quantitative PCR (qPCR) was carried out using an ABI 7300 Real-Time PCR System Sequence (Applied Biosystems) at 50°C for 2 minutes, 95°C for 10 minutes, followed by 40 cycles at 95°C for 15 seconds and 60°C for 1 minutes. The quantity of the target genes were normalized using the level of the *β-actin* gene, and expressed as relative quantities (RQ) compared with the value of the Human Genomic DNA. RQ equal or larger than 2 was considered as gene copy gain.

EGFR and *KRAS* mutational status

Exons 18 and 21 of *EGFR* and exons 1 and 2 of *KRAS* were PCR-amplified using DNA extracted from microdissected tumor cells, as previously described (33). Each PCR was carried out using HotStarTaq Master Mix (Qiagen) for 40 cycles at 94°C for 30 seconds, at annealing temperature for 30 seconds, and 72°C for 30 seconds, followed by a 7-minute extension at 72°C. All primer sequence and annealing temperatures are list in Supplementary Table S2. PCR products were directly sequenced using the Applied Biosystems PRISM dye terminator cycle sequencing method (Perkin-Elmer Corp.). Sequence variants were confirmed by independent PCR amplifications from at least 2 independent microdissections and in both directions.

Published OnlineFirst January 21, 2011; DOI:10.1158/1078-0432.CCR-10-1412

Statistical analyses

Data were summarized using descriptive statistics and frequency tabulation. Associations between categorical variables were assessed via cross-tabulation, chi-squared tests, and Fisher's exact tests. Differences in continuous markers between groups were tested using the rank-based nonparametric Wilcoxon-rank sum test or Kruskal–Wallis tests. Survival rates were calculated using the Kaplan–Meier method for estimation of survival probability. Univariate and multicovariate Cox proportional hazard models were applied to assess the effects of covariates on overall and recurrence-free survival. All computations were done in Statistical analysis Software (SAS; Cary) and S-plus 7.0 (TIBCO software Inc.).

Results

Immunohistochemical expression of TITF-1, SP-A, SP-B, and SP-C proteins in NSCLC

We assessed the protein expression of TITF-1 and the SPs, SP-A, SP-B, and SP-C which are typically transactivated by TITF-1 (18–20), in a series of lung adenocarcinomas ($n = 179$) and SCCs ($n = 117$) by immunohistochemistry. TITF-1 protein expression was mainly nuclear (Fig. 1A), prevalent in lung adenocarcinomas (68.7% with TITF-1 protein greater than 0) and absent in SCCs (all zero TITF-1 protein; $P < 0.0001$; Supplementary Table S3). Similarly, the immunohistochemical protein expression (greater than a score of zero) of SP-A and SP-B was mainly cytoplasmic (Fig. 1A) and only evident in lung adenocarcinomas (19.8% and 16.4%, respectively) and was absent in SCC ($P < 0.0001$; Supplementary Table S3). In contrast, SP-C protein was expressed in both NSCLC subtypes as 84.5% of lung adenocarcinomas and 93.6% of SCCs exhibited an SP-C expression score of greater than zero (Supplementary Table S3). A significant positive correlation was found between the expression of any of the 3 SPs analyzed and TITF-1 expression when lung adenocarcinoma patients were stratified by the absence or presence of TITF-1 immunoreactivity (Table 1).

We then correlated TITF-1 protein expression with other clinicopathological features besides histology (Table 2). TITF-1 protein expression was significantly associated with female gender ($P = 0.0001$), never- compared with ever-smokers ($P < 0.001$), and never- compared with former- or current-smokers ($P = 0.0004$; Table 2).

We next asked whether TITF-1 protein expression exhibits prognostic properties in lung adenocarcinomas, the NSCLC subtype where it is predominantly expressed. Lung adenocarcinoma patients with higher than the median expression of TITF-1 protein ($\geq$125) exhibited favorable survival compared with patients with lower expression (less than total score of 125; $P = 0.0478$ of the log-rank test) with a HR of 0.639 (Fig. 1B). Similar results were obtained when stages I and II lung adenocarcinoma patients ($n = 140$) were analyzed alone using the same cut-off for TITF-1 protein expression ($P = 0.01$ of the log-rank test, HR = 0.485; Fig. 1C). In contrast to those findings, no significant association was found between TITF-1 protein expression and recurrence-free survival in lung adenocarcinoma patients (data not shown). In addition, multivariate Cox proportional hazard regression analysis revealed that TITF-1 protein expression was not an independent predictor of overall or recurrence-free survival in lung adenocarcinoma (data not shown).

TITF-1 gene amplification in NSCLC and association with clinicopathological features

We next assessed the gene dosage levels of the *TITF-1* gene in NSCLC patients by 2 different methodologies, copy

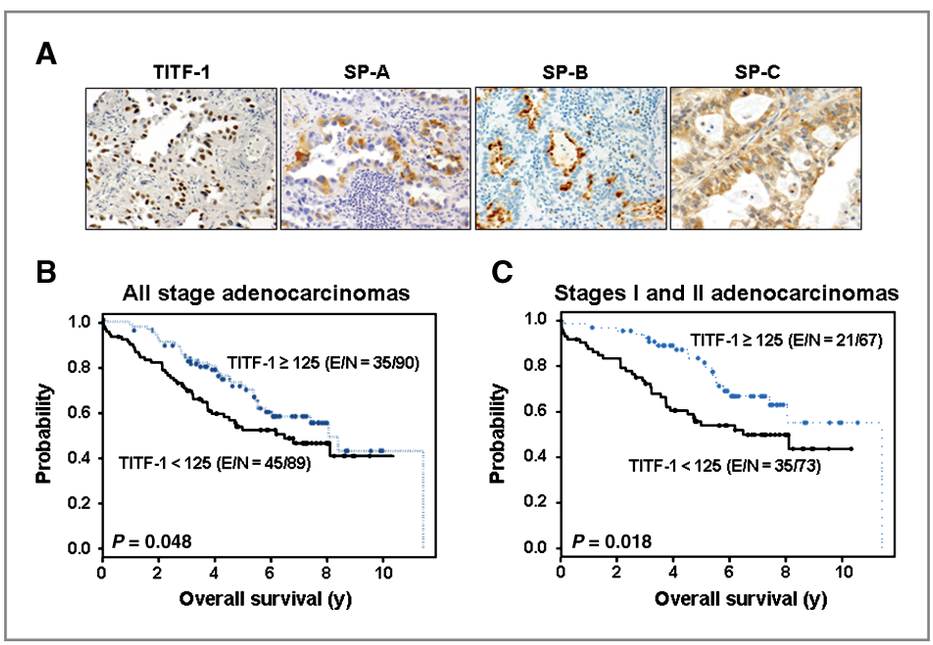

Figure 1. TITF-1 immunohistochemical expression in NSCLC. A, representative photomicrographs of the immunohistochemical expression of TITF-1, SP-A, SP-B, and SP-C. Kaplan–Meier survival probability plots of all stages (B) and stages I and II only (C) lung adenocarcinoma patients stratified by TITF-1 protein expression. *P* values were obtained by the log-rank test. E/N, censored events/total number of cases.

Published OnlineFirst January 21, 2011; DOI:10.1158/1078-0432.CCR-10-1412

Table 1. Correlation of the immunohistochemical protein expression of TITF-1 and the SP-A, SP-B, and SP-C SPs in lung adenocarcinomas

Covariate (*n*)	Covariate expression (*n*)	TITF-1 negative, *n* (%)	TITF-1 positive, *n* (%)	*P*
SP-A (171)	Negative (135)	49 (36)	86 (64)	0.004
	Positive (36)	4 (11)	32 (89)	
SP-B (168)	Negative (137)	47 (34)	90 (66)	0.002
	Positive (31)	2 (7)	29 (94)	
SP-C (171)	Negative (23)	14 (61)	9 (39)	0.0005
	Positive (148)	37 (25)	111 (75)	

NOTE: *P* values were obtained by the Fisher's exact test. TITF-1 immunoreactivity greater than zero was considered positive.

number gain and amplification by FISH (170 lung adenocarcinomas and 99 SCCs) and copy gain by qPCR in 46 lung adenocarcinomas and 36 SCCs. *TITF-1* copy number gain by FISH was found in 18.9% of lung adenocarcinomas and in 20.2% of lung SCCs (Fig. 2A and Supplementary Table S4). A high level of *TITF-1* copy number gain (>10 copies) was found in 8.3% and 3.0% of lung adenocarcinomas and SCCs, respectively (Supplementary Table S4). Two lung adenocarcinoma cases and 1 case of lung SCC were found to have greater than 20 signals per cell; the high level of *TITF-1* copy gain by FISH detected in the SCC case is depicted in Supplementary Figure 1. We then determined to correlate TITF-1 protein with its DNA copy gain in lung adenocarcinomas as both variables were assessed and found in these set of patients. A significant positive correlation was found between the TITF-1 protein expression (as a continuous score variable) with the presence of *TITF-1* copy gain assessed by FISH ($P = 0.004$; Fig. 2B) in lung adenocarcinomas. The mean and median of the TITF-1 protein score, assessed by immunohistochemical analysis, were 200.69 ± 115.73 and 240 (min, 0; max, 300), respectively, in *TITF-1* FISH-positive lung adenocarcinoma patients ($n = 29$) and 127.1 ± 122.61 and 93 (min, 0; max, 300), respectively, in *TITF-1* FISH-negative adenocarcinoma specimens ($n = 122$).

We also assessed *TITF-1* copy number gain by qPCR in a subset of patients that we had analyzed by FISH ($n = 82$, 46 lung adenocarcinomas and 36 SCCs). A similar percentage of lung adenocarcinomas (18.4%) and SCCs (18.2%) exhibited greater than 3 copies of *TITF-1* analyzed by qPCR (Supplementary Table S5). Similar to the FISH analysis, a slightly higher percentage of lung adenocarcinomas (10.2%) displayed a higher ratio (≥ 5) of *TITF-1* copy gain than that of SCCs (4.6%, Supplementary Table S5). Moreover, we found a significant correlation between levels of *TITF-1* copy gain by FISH and qPCR analyses in both lung adenocarcinomas ($P = 0.0037$) and lung SCCs ($P = 0.048$). The mean and median levels of relative *TITF-1* RQ by qPCR in *TITF-1* FISH-positive lung adenocarcinomas ($n = 11$) were 5.12 ± 5.55 and 3.41 (min, 0.53; max, 21), compared with 2.49 ± 4.31 and 1.41 (min, 0.48; max, 24.22) in FISH-negative adenocarcinomas ($n = 35$). In addition, the mean and median levels of *TITF-1* RQ assessed by qPCR in *TITF-1* FISH-positive SCCs ($n = 9$) were 13.61 ± 24.16 and 2.23 (min, 0.82; max, 74.93), compared with 1.64 ± 1.18 and 1.28 (min, 0.56; max, 4.8) in *TITF-1* FISH-negative SCCs.

We next investigated the role of *TITF-1* copy number gain by FISH in prognosis of both lung adenocarcinoma and SCC patients because we detected *TITF-1* gain in both

Table 2. Association of TITF-1 protein expression with NSCLC histology, gender, tobacco history, and smoking habits

Covariate	Covariate type (*n*)	TITF-1 negative, *n* (%)	TITF-1 positive, *n* (%)	*P*
Gender	Female (148)	65 (43.9)	83 (56.1)	<0.0001
	Male (135)	95 (70.4)	40 (29.6)	
Tobacco history	Never (53)	17 (32.1)	36 (67.9)	0.0001
	Ever (229)	142 (62)	87 (38)	
Smoking habit	Never (53)	17 (32.1)	36 (67.9)	0.0004
	Former (140)	86 (61.4)	54 (38.6)	
	Current (89)	56 (62.9)	33 (37.1)	
Histology	Adenocarcinoma (179)	56 (31.3)	123 (68.7)	<0.0001
	SCC (104)	104 (100)	0 (0)	

P values were obtained by the Fisher's exact test.

Published OnlineFirst January 21, 2011; DOI:10.1158/1078-0432.CCR-10-1412

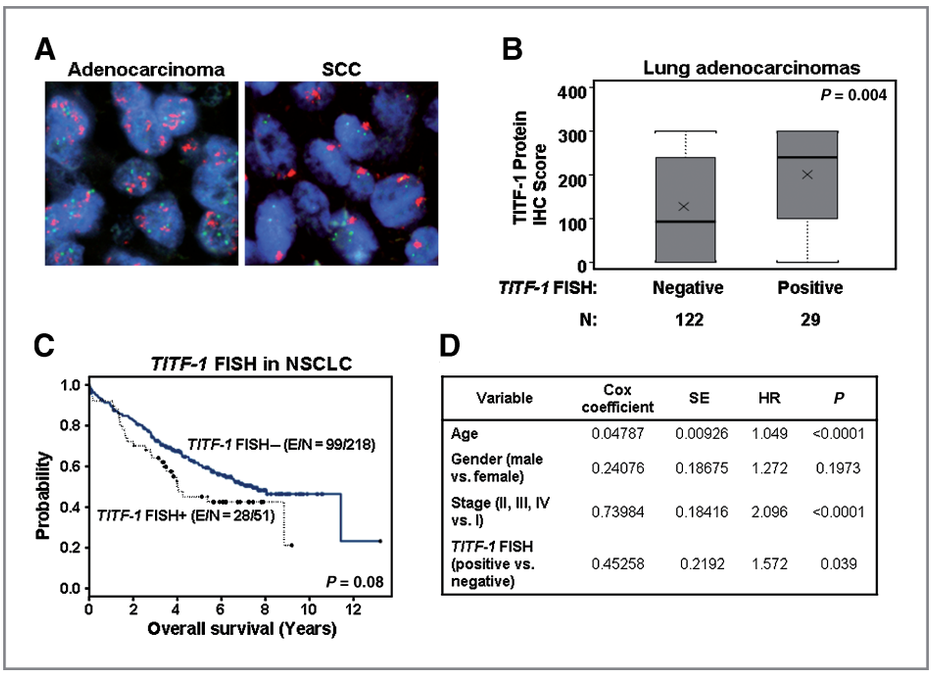

Figure 2. *TITF-1* copy number gain in NSCLC. A, representative photomicrographs (magnification ×1000) of lung adenocarcinoma (left) and SCC (right) cells with copy number gain of *TITF-1*. B, statistically significant differences in TITF-1 protein score between lung adenocarcinomas with and without *TITF-1* copy gain by FISH. *P* value was determined by the nonparametric Wilcoxon-rank sum test. C, Kaplan–Meier curves of the overall survival of NSCLC patients ($n = 269$) based on the presence or absence of *TITF-1* copy number gain by FISH. D, Cox proportional multivariate hazard model of overall survival of NSCLC patients.

subtypes of NSCLC. NSCLC patients with *TITF-1* copy number gain (low and high) by FISH ($n = 51$, 33 adenocarcinomas and 18 SCCs) displayed a trend for poorer survival ($P = 0.08$) compared with NSCLC patients lacking *TITF-1* copy number gain ($n = 218$, 137 adenocarcinomas and 81 SCCs). However, multivariate Cox proportional hazard regression analysis revealed that copy number gain of the *TITF-1* gene by FISH was an independent predictor of poor survival in NSCLC alone with age ($P < 0.0001$), and stage-I disease ($P < 0.0001$; Fig. 2D). Similar results were obtained when NSCLC patients were dichotomized on the basis of the presence or absence of high level of *TITF-1* copy gain (>10 signals; data not shown).

Association of TITF-1 protein and copy number gain with *EGFR* and *KRAS* mutations in lung adenocarcinoma

Molecular abnormalities in the expression or function of *KRAS* and *EGFR* contribute to tumor development and progression and therefore serve as crucial targets for molecularly driven target-specific therapies (2, 34). We had previously investigated the prevalence of *EGFR* and *KRAS* mutations in our clinical sample sets and correlated the extent of the mutations of those 2 oncogenes with patients' clinicopathological features (33, 35). However, the relationship of TITF-1 abnormalities with the mutational pattern of oncogenes prevalent in lung adenocarcinoma, for example, *EGFR* and *KRAS*, is not well understood. Therefore, we sought to correlate the presence of mutations in the *KRAS* and *EGFR* oncogenes with DNA copy gain and protein levels of the *TITF-1* gene. Interestingly, the protein levels and gene dosage extent of *TITF-1* exhibited different correlation patterns. TITF-1 protein expression as a continuous variable displayed border-line significant positive correlation with the presence of *EGFR* mutations ($P = 0.05$; Supplementary Fig. 2). The mean and median levels of TITF-1 immunohistochemical protein in *EGFR* mutant lung adenocarcinomas ($n = 22$) were 183.94 ± 124.58 and 225 (min, 0; max, 300), compared with 124.62 ± 121.06 and 100 (min, 0; max, 300) in *EGFR* wild-type adenocarcinomas ($n = 137$). No significant differences were found in TITF-1 protein expression between *KRAS* mutant ($n = 10$; mean, 126.67 ± 127.57; median, 75) and wild type ($n = 94$; mean, 112.78 ± 117.68; median, 66.67) lung adenocarcinomas. On the other hand, *TITF-1* copy gain by FISH displayed a significant positive correlation with the presence of *KRAS* mutations as 55% or 6 of 11 *KRAS* mutant patients exhibited *TITF-1* copy number gain compared with 15.9% of patients with wild-type *KRAS* (14 of 88 patients; $P = 0.008$ of the Fisher's exact test; Table 3). Moreover and in accordance with the analysis of TITF-1 protein expression as a continuous variable, 64% of lung adenocarcinoma patients with mutant *EGFR* exhibited a TITF-1 protein score greater than or equal to 200 compared with 33% of patients with wild-type *EGFR* ($P = 0.006$; Table 3). These new findings further demonstrate the dissimilarities between the extent of protein and DNA of *TITF-1* in lung adenocarcinomas with *EGFR* versus *KRAS* mutations.

Discussion

In this study, we investigated the protein and DNA copy number gain of the *TITF-1* cell lineage gene in a TMA comprised mainly of lung adenocarcinomas and SCCs and in correlation with molecular and

Published OnlineFirst January 21, 2011; DOI:10.1158/1078-0432.CCR-10-1412

Table 3. Significant positive associations of *TITF-1* copy number and TITF-1 protein expression with mutations in *KRAS* and *EGFR*, respectively

		***TITF-1* FISH**		**TITF-1 IHC $\geq$ 200[a]**	
Covariate	**Covariate type**	***n* Positive/total (%)**	***P***	***n* Positive/total (%)**	***P***
EGFR	Mutant	5/16 (31)	0.338	14/22 (64)	0.006
	wild type	27/133 (20)	45/137 (33)		
KRAS	Mutant	6/11 (55)	0.008	3/10 (30)	0.933
	wild type	14/88 (16)	27/94 (29)		

P values were obtained by the Fisher's exact test.
[a]TITF-1 immunoreactivity greater than or equal to 200 was considered positive.

clinicopathological features. We found that immunohistochemical protein expression of TITF-1 is prevalent in lung adenocarcinomas and absent in SCCs, correlates positively and significantly with the protein expression of the SP-A, SP-B, and SP-C SPs and with female gender and never smoking status. Moreover, copy gain of *TITF-1* DNA, assessed by FISH, was observed in both adenocarcinomas and SCCs and correlated positively and significantly with TITF-1 protein in lung adenocarcinomas as well as copy gain in NSCLC assessed by qPCR. Interestingly, while higher expression of TITF-1 protein was predictive of favorable prognosis in lung adenocarcinomas, *TITF-1* copy number gain was an indicator of poor survival in NSCLC. Lastly, TITF-1 protein and DNA copy gain exhibited distinct correlations with oncogene mutation status in lung adenocarcinomas as the former correlated significantly with *EGFR* mutations, whereas the latter was associated with mutations in *KRAS*. The opposing prognostic, clinicopathological and molecular characteristics of TITF-1 protein expression and copy number gain suggest that different subsets of NSCLC patients may express TITF-1 through different cellular mechanisms.

Our findings on the association of higher levels of TITF-1 protein expression with favorable prognosis and overall survival are in accordance with previous findings by independent groups (25–29). In this study, we further investigated TITF-1 protein expression in clinical samples of NSCLC by correlating its expression with that of 3 SPs, SP-A, SP-B, and SP-C. We unraveled significant associations of TITF-1 protein expression with that of the 3 SPs. It is noteworthy that staining patterns of TITF-1 in the developing and adult lung are very similar to those observed for the 3 SPs (18–20, 36). Moreover, TITF-1 is known to facilitate the differentiation of alveolar type II cells, in part, by transactivating the expression of the 3 surfactant genes following direct binding on their promoter regions (18–20, 36). It is worthy to mention that the combined use of Napsin A, an aspartic proteinase involved in the maturation of SP-B, and TITF-1 results in improved sensitivity and specificity for identifying pulmonary adenocarcinoma in primary lung tumors and in metastatic settings (37). Here, we provide new evidence of positive association of TITF-1 protein and that of the 3 major SPs in clinical specimens of human lung adenocarcinoma. These findings raise the possibility of the combined use of TITF-1 and SP expression in the diagnosis of pulmonary adenocarcinomas as the usage of TITF-1 with any of the SPs may increase the number of adenocarcinoma cases with positive expression of either marker.

We tested the association of TITF-1 protein expression with prognosis in lung adenocarcinomas because we only noted the protein in this subtype of NSCLC. In contrast, we analyzed the prognostic capacity of *TITF-1* copy number gain in lung adenocarcinomas and SCCs as we detected increased *TITF-1* gene dosage in both subtypes of NSCLC. It is worthwhile to note, that Kwei and colleagues previously demonstrated amplification of *TITF-1* assessed by comparative genomic hybridization (CGH) in both lung adenocarcinomas and SCCs, albeit at a lower frequency (11% and 3%, respectively; ref 22). In the present study, we detected *TITF-1* both low and high copy number gain in 20.1% of lung SCCs assessed. Specifically, 17.2% of lung SCCs exhibited low level of amplification (4–10 copies, data not shown) and 3% (3 cases) displayed high level of *TITF-1* copy number gain (>10 copies, Supplementary Table S4), which is similar to the rate of amplification found in lung SCC in the previously reported CGH study by Kwei and colleagues (22). Interestingly, we also found that 1 case of lung SCC harbored greater than 20 copies of *TITF-1* (Supplementary Fig. 1). It is worthwhile to note that a recent study by Bass and colleagues using single nucleotide polymorphism (SNP) arrays showed the absence of *TITF-1* amplification in a set of lung SCCs ($n = 47$; ref 5). In our study and as mentioned before, only 3 of 99 lung SCCs were found to display more than greater than 10 signals of *TITF-1* per cell that we considered to harbor high copy gain of the gene rather than amplification. Due to the lack normalization to DNA content, a shortcoming in our FISH analysis, it is not clear whether specimens displaying high level of *TITF-1* copy number gain actually harbor amplified *TITF-1*.

We found a significant positive correlation between TITF-1 protein expression and DNA copy number levels assessed by FISH analysis in lung adenocarcinomas. Previously, Perner and colleagues demonstrated a similar positive

Published OnlineFirst January 21, 2011; DOI:10.1158/1078-0432.CCR-10-1412

correlation between the protein products and the DNA copy gain levels of the *TITF-1* gene (28). Moreover, we further demonstrated that, unlike the association of TITF-1 protein with overall survival of lung adenocarcinoma patients, *TITF-1* copy gain by FISH analysis appears to be a marker of poor prognosis in NSCLC. We also attempted to investigate the survival of lung adenocarcinoma patients alone with *TITF-1* copy number gain stratified by the presence or absence of TITF-1 protein expression. Lung adenocarcinoma patients with copy number gain of *TITF-1* displayed worse survival than adenocarcinoma patients with both copy gain and protein expression (data not shown), demonstrating the association of *TITF-1* copy number gain and TITF-1 protein expression with poor and good prognosis, respectively, in the lung adenocarcinoma population alone. The better survival correlations with TITF-1 protein and worse outcomes associated with *TITF-1* copy gain are in close agreement with those reported earlier by Barletta and colleagues (38). It is uncertain why protein levels and DNA copy gain of *TITF-1* have opposing associations with prognosis of NSCLC patients including lung adenocarcinomas alone. However, it is worthwhile to mention that oncogene copy number gain is a feature of cell lineage genes that elicit prosurvival functions important for the population of cells expressing the oncogene or for the pathological condition, that is, cancer, whose cells are driven by amplification of the oncogene (5, 6). In this context, it is not surprising that NSCLC patients exhibiting copy number gain of the *TITF-1* gene display poor survival and these findings no longer become counterintuitive. Moreover, it is plausible to suggest that *TITF-1* copy number gain may be more reliable than protein expression for studying cell lineage patterns of expression in NSCLC. It is noteworthy that TITF-1 protein was found to be elevated in primary lung adenocarcinoma compared with matched metastatic lesions in the brain (39). This is in accordance with our findings and the results of previous reports by other groups (25–29) on the utility of TITF-1 protein expression as a marker of favorable prognosis in lung cancer. Interestingly, Tanaka and colleagues reported that *TITF-1* gene dosage, which we demonstrated in this study to be a marker of dismal prognosis in NSCLC, was higher in metastatic sites compared with primary lung tumors (23). Therefore, our current findings and previous reports by others suggest that lung adenocarcinoma cells with either elevated TITF-1 protein expression or copy gain of the *TITF-1* gene may originate from different cell populations with dissimilar biological properties and effects on patient clinical outcome. Congruent with this probable thought, is our novel finding that TITF-1 protein expression and *TITF-1* gene copy number were associated with mutations in different oncogenes in lung adenocarcinomas. Our current study shed light on positive associations between *TITF-1* gene dosage and protein expression level with mutations in the *KRAS* and *EGFR* oncogenes, respectively. It is noteworthy, that overexpression of *HRAS* inhibits the mRNA and protein levels of TITF-1 as well as its transcriptional factor function (40). Thus, it is plausible to suggest that *TITF-1* copy number gain is favored in lung adenocarcinomas with mutant *KRAS*. Since, mutations in *EGFR* and *KRAS* occur almost mutually exclusively in lung adenocarcinomas (2), our results suggest that elevated expression of TITF-1 may be variably controlled (copy gain versus transcription) in distinct subsets of lung adenocarcinoma patients. Moreover, the association of TITF-1 protein, but not copy gain, with *EGFR* mutations is in accordance with our finding on the increased levels of TITF-1 protein in never-smoker compared with ever-smoker lung cancer patients.

It has been suggested that other genes within the *TITF-1* amplicon (14q13.3) may facilitate, cooperate with, or even enhance the prosurvival biological properties of *TITF-1* (22, 24, 41, 42). Kwei and colleagues and Weir and colleagues reported the location of several genes within the *TITF-1* amplicon including the paired box transcriptional factor family member *PAX9* and *NKX2.8* (22, 24). It is worthy to note that Kendal and colleagues demonstrated that coamplified *TITF-1*, *PAX9*, and *NKX2.8* exhibit oncogenic cooperation and cell prosurvival and proliferative properties (42). Overexpression of both TITF-1 and NKX2.8 simultaneously in BEAS-2B immortalized human bronchial epithelial cells elicited the highest increase in cell colony growth compared with single-gene transfected cells (42). Moreover, pathway genes signatures that overlap downstream of both *TITF-1* and *NKX2.8* defined lung adenocarcinoma patients with most dismal prognosis compared with signatures downstream of either transcriptional factor alone (41). It is therefore tempting to speculate that co-amplification or copy gain of *NKX2.8* and/or *PAX9* together with *TITF-1* may contribute to the observed poor survival patterns observed in NSCLC patients exhibiting copy gain of the *TITF-1* gene compared with patients with exhibiting only elevated expression of the protein product of this cell lineage gene. It is also plausible that *TITF-1* copy gain and its correlation with important biological outcomes in NSCLC may only be a surrogate marker, for example, in SCCs, of another molecular defect in a gene nearby or within the 14q13.3 amplicon, for example *NKX2.8* or *PAX9*. It is worthwhile to mention that *NKX2.8* displays dissimilar patterns of expression relative to those of TITF-1 in the developing and adult mouse lung (43). Therefore, it is possible that expression of the NKX2.8 protein or its copy number gain may subdivide patients exhibiting positive expression of TITF-1 protein into subsets with different clinical outcomes. Moreover, lung SCC patients with copy number gain of the *TITF-1* gene, as shown in this study and previously (28, 38), may display positive expression of the NKX2.8 protein and that transactivation of *TITF-1* may be inhibited in lung SCCs and not in adenocarcinomas by yet unknown mechanisms.

In summary and herein, we further highlight the cell lineage pattern of *TITF-1* in human NSCLC and its correlation at the protein level with that of SPs in clinical specimens of lung adenocarcinoma. Moreover, we demonstrate that TITF-1 protein and gene dosage are associated with discordant clinical outcomes. We also noted in lung SCCs

Published OnlineFirst January 21, 2011; DOI:10.1158/1078-0432.CCR-10-1412

TITF-1 copy number gain in the absence of protein expression which warrants future studies. Furthermore, we highlight previously unknown associations of *TITF-1* gene dosage and protein expression with differing oncogene mutation patterns suggesting that lung adenocarcinomas exhibiting elevated protein or amplification of the gene may be further divided into different cell lineage subsets that can be subject to distinct treatment strategies.

Disclosure of Potential Conflicts of Interest

No potential conflicts of interest were disclosed.

Grant Support

This study was supported in part by grants from the Department of Defense (W81XWH-04-1-0142 to W.K. Hong and I.I. Wistuba) and by the Specialized Program of Research Excellence in Lung Cancer Grants P50CA70907 (A.F. Gazdar and I.I. Wistuba) and P50CA58187 (M.V. Garcia) as well as Cancer Center Support Grant CA-16672 from the National Cancer Institute.

The costs of publication of this article were defrayed in part by the payment of page charges. This article must therefore be hereby marked *advertisement* in accordance with 18 U.S.C. Section 1734 solely to indicate this fact.

Received May 25, 2010; revised December 7, 2010; accepted January 7, 2011; published OnlineFirst January 21, 2011.

References

1. Jemal A, Siegel R, Xu J, Ward E. Cancer Statistics, 2010. CA Cancer J Clin 2010;60:277–300.
2. Herbst RS, Heymach JV, Lippman SM. Lung cancer. N Engl J Med 2008;359:1367–80.
3. Wistuba II, Gazdar AF. Lung cancer preneoplasia. Annu Rev Pathol 2006;1:331–48.
4. Wistuba II. Genetics of preneoplasia: lessons from lung cancer. Curr Mol Med 2007;7:3–14.
5. Bass AJ, Watanabe H, Mermel CH, Yu S, Perner S, Verhaak RG, et al. SOX2 is an amplified lineage-survival oncogene in lung and esophageal squamous cell carcinomas. Nat Genet 2009;41:1238–42.
6. Garraway LA, Sellers WR. Lineage dependency and lineage-survival oncogenes in human cancer. Nat Rev Cancer 2006;6:593–602.
7. Weinstein IB. Cancer. Addiction to oncogenes—the Achilles heal of cancer. Science 2002;297:63–4.
8. Kantarjian H, Sawyers C, Hochhaus A, Guilhot F, Schiffer C, Gambacorti-Passerini C, et al. Hematologic and cytogenetic responses to imatinib mesylate in chronic myelogenous leukemia. N Engl J Med 2002;346:645–52.
9. Demetri GD, von Mehren M, Blanke CD, Van den Abbeele AD, Eisenberg B, Roberts PJ, et al. Efficacy and safety of imatinib mesylate in advanced gastrointestinal stromal tumors. N Engl J Med 2002;347:472–80.
10. Lynch TJ, Bell DW, Sordella R, Gurubhagavatula S, Okimoto RA, Brannigan BW, et al. Activating mutations in the epidermal growth factor receptor underlying responsiveness of non-small-cell lung cancer to gefitinib. N Engl J Med 2004;350:2129–39.
11. Paez JG, Jänne PA, Lee JC, Tracy S, Greulich H, Gabriel S, et al. EGFR mutations in lung cancer: correlation with clinical response to gefitinib therapy. Science 2004;304:1497–500.
12. Pao W, Miller V, Zakowski M, Doherty J, Politi K, Sarkaria I, et al. EGF receptor gene mutations are common in lung cancers from "never smokers" and are associated with sensitivity of tumors to gefitinib and erlotinib. Proc Natl Acad Sci U S A 2004;101:13306–11.
13. Gontan C, de Munck A, Vermeij M, Grosveld F, Tibboel D, Rottier R. Sox2 is important for two crucial processes in lung development: branching morphogenesis and epithelial cell differentiation. Dev Biol 2008;317:296–309.
14. Minoo P, Su G, Drum H, Bringas P, Kimura S. Defects in tracheoesophageal and lung morphogenesis in Nkx2.1(−/−) mouse embryos. Dev Biol 1999;209:60–71.
15. Yuan B, Li C, Kimura S, Engelhardt RT, Smith BR, Minoo P. Inhibition of distal lung morphogenesis in Nkx2.1(−/−) embryos. Dev Dyn 2000;217:180–90.
16. Bingle CD. Thyroid transcription factor-1. Int J Biochem Cell Biol 1997;29:1471–3.
17. Kimura S, Hara Y, Pineau T, Fernandez-Salguero P, Fox CH, Ward JM, et al. The T/ebp null mouse: thyroid-specific enhancer-binding protein is essential for the organogenesis of the thyroid, lung, ventral forebrain, and pituitary. Genes Dev 1996;10:60–9.
18. Bohinski RJ, Di Lauro R, Whitsett JA. The lung-specific surfactant protein B gene promoter is a target for thyroid transcription factor 1 and hepatocyte nuclear factor 3, indicating common factors for organ-specific gene expression along the foregut axis. Mol Cell Biol 1994;14:5671–81.
19. Ikeda K, Clark JC, Shaw-White JR, Stahlman MT, Boutell CJ, Whitsett JA. Gene structure and expression of human thyroid transcription factor-1 in respiratory epithelial cells. J Biol Chem 1995;270:8108–14.
20. Minoo P, Hu L, Xing Y, Zhu NL, Chen H, Li M, et al. Physical and functional interactions between homeodomain NKX2.1 and winged helix/forkhead FOXA1 in lung epithelial cells. Mol Cell Biol 2007;27:2155–65.
21. Krude H, Schütz B, Biebermann H, von Moers A, Schnabel D, Neitzel H, et al. Choreoathetosis, hypothyroidism, and pulmonary alterations due to human NKX2-1 haploinsufficiency. J Clin Invest 2002;109:475–80.
22. Kwei KA, Kim YH, Girard L, Kao J, Pacyna-Gengelbach M, Salari K, et al. Genomic profiling identifies TITF1 as a lineage-specific oncogene amplified in lung cancer. Oncogene 2008;27:3635–40.
23. Tanaka H, Yanagisawa K, Shinjo K, Taguchi A, Maeno K, Tomida S, et al. Lineage-specific dependency of lung adenocarcinomas on the lung development regulator TTF-1. Cancer Res 2007;67:6007–11.
24. Weir BA, Woo MS, Getz G, Perner S, Ding L, Beroukhim R, et al. Characterizing the cancer genome in lung adenocarcinoma. Nature 2007;450:893–8.
25. Barlési F, Pinot D, Legoffic A, Doddoli C, Chetaille B, Torre JP, et al. Positive thyroid transcription factor 1 staining strongly correlates with survival of patients with adenocarcinoma of the lung. Br J Cancer 2005;93:450–2.
26. Berghmans T, Mascaux C, Martin B, Ninane V, Sculier JP. Prognostic role of thyroid transcription factor-1 in stage III non-small cell lung cancer. Lung Cancer 2006;52:219–24.
27. Berghmans T, Paesmans M, Mascaux C, Martin B, Meert AP, Haller A, et al. Thyroid transcription factor 1–a new prognostic factor in lung cancer: a meta-analysis. Ann Oncol 2006;17:1673–6.
28. Perner S, Wagner PL, Soltermann A, LaFargue C, Tischler V, Weir BA, et al. TTF1 expression in non-small cell lung carcinoma: association with TTF1 gene amplification and improved survival. J Pathol 2009;217:65–72.
29. Anagnostou VK, Syrigos KN, Bepler G, Homer RJ, Rimm DL. Thyroid transcription factor 1 is an independent prognostic factor for patients with stage I lung adenocarcinoma. J Clin Oncol 2009;27:271–8.
30. Mountain CF. Revisions in the International System for Staging Lung Cancer. Chest 1997;111:1710–7.
31. Behrens C, Feng L, Kadara H, Kim HJ, Lee JJ, Mehran R, et al. Expression of interleukin-1 receptor-associated kinase-1 in non-small cell lung carcinoma and preneoplastic lesions. Clin Cancer Res; 16:34–44.
32. Cappuzzo F, Marchetti A, Skokan M, Rossi E, Gajapathy S, Felicioni L, et al. Increased MET gene copy number negatively affects survival of surgically resected non-small-cell lung cancer patients. J Clin Oncol 2009;27:1667–74.
33. Tang X, Varella-Garcia M, Xavier AC, Massarelli E, Ozburn N, Moran C, et al. Epidermal growth factor receptor abnormalities in the pathogen-

Published OnlineFirst January 21, 2011; DOI:10.1158/1078-0432.CCR-10-1412

esis and progression of lung adenocarcinomas. Cancer Prev Res (Phila Pa) 2008;1:192–200.
34. Sun S, Schiller JH, Spinola M, Minna JD. New molecularly targeted therapies for lung cancer. J Clin Invest 2007;117:2740–50.
35. Massarelli E, Varella-Garcia M, Tang X, Xavier AC, Ozburn NC, Liu DD, et al. KRAS mutation is an important predictor of resistance to therapy with epidermal growth factor receptor tyrosine kinase inhibitors in non-small-cell lung cancer. Clin Cancer Res 2007;13:2890–6.
36. Maeda Y, Dave V, Whitsett JA. Transcriptional control of lung morphogenesis. Physiol Rev 2007;87:219–44.
37. Bishop JA, Sharma R, Illei PB. Napsin A and thyroid transcription factor-1 expression in carcinomas of the lung, breast, pancreas, colon, kidney, thyroid, and malignant mesothelioma. Hum Pathol; 41:20–5.
38. Barletta JA, Perner S, Iafrate AJ, Yeap BY, Weir BA, Johnson LA, et al. Clinical significance of TTF-1 protein expression and TTF-1 gene amplification in lung adenocarcinoma. J Cell Mol Med 2009;13: 1977–86.
39. McDonald JM, Pelloski CE, Ledoux A, Sun M, Raso G, Komaki R, et al. Elevated phospho-S6 expression is associated with metastasis in adenocarcinoma of the lung. Clin Cancer Res 2008;14: 7832–7.
40. De Vita G, Bauer L, da Costa VM, De Felice M, Baratta MG, De Menna M, et al. Dose-dependent inhibition of thyroid differentiation by RAS oncogenes. Mol Endocrinol 2005;19:76–89.
41. Hsu DS, Acharya CR, Balakumaran BS, Riedel RF, Kim MK, Stevenson M, et al. Characterizing the developmental pathways TTF-1, NKX2-8, and PAX9 in lung cancer. Proc Natl Acad Sci U S A 2009; 106:5312–7.
42. Kendall J, Liu Q, Bakleh A, Krasnitz A, Nguyen KC, Lakshmi B, et al. Oncogenic cooperation and coamplification of developmental transcription factor genes in lung cancer. Proc Natl Acad Sci U S A 2007;104:16663–8.
43. Tian J, Mahmood R, Hnasko R, Locker J. Loss of Nkx2.8 deregulates progenitor cells in the large airways and leads to dysplasia. Cancer Res 2006;66:10399–407.

DOI: 10.1093/jnci/djr523
Advance Access publication on January 13, 2012.

ARTICLE

Effect of *KRAS* Oncogene Substitutions on Protein Behavior: Implications for Signaling and Clinical Outcome

Nathan T. Ihle, Lauren A. Byers, Edward S. Kim, Pierre Saintigny, J. Jack Lee, George R. Blumenschein, Anne Tsao, Suyu Liu, Jill E. Larsen, Jing Wang, Lixia Diao, Kevin R. Coombes, Lu Chen, Shuxing Zhang, Mena F. Abdelmelek, Ximing Tang, Vassiliki Papadimitrakopoulou, John D. Minna, Scott M. Lippman, Waun K. Hong, Roy S. Herbst, Ignacio I. Wistuba, John V. Heymach, Garth Powis

Manuscript received March 29, 2011; revised October 28, 2011; accepted November 22, 2011.

Correspondence to: Garth Powis, DPhil, Department of Experimental Therapeutics, MD Anderson Cancer Center, 1400 Holcombe Blvd, FC6.3044, Unit 422, Houston, TX 77030 (e-mail: gpowis@mdanderson.org).

Background Mutations in the v-Ki-ras2 Kirsten rat sarcoma viral oncogene homolog (*KRAS*) play a critical role in cancer cell growth and resistance to therapy. Most mutations occur at codons 12 and 13. In colorectal cancer, the presence of any mutant KRas amino acid substitution is a negative predictor of patient response to targeted therapy. However, in non–small cell lung cancer (NSCLC), the evidence that *KRAS* mutation is a predictive factor is conflicting.

Methods We used data from a molecularly targeted clinical trial for 215 patients with tissues available out of 268 evaluable patients with refractory NSCLC to examine associations between specific mutant KRas proteins and progression-free survival and tumor gene expression. Transcriptome microarray studies of patient tumor samples and reverse-phase protein array studies of a panel of 67 NSCLC cell lines with known substitutions in KRas and in immortalized human bronchial epithelial cells stably expressing different mutant KRas proteins were used to investigate signaling pathway activation. Molecular modeling was used to study the conformations of wild-type and mutant KRas proteins. Kaplan–Meier curves and Cox regression were used to analyze survival data. All statistical tests were two-sided.

Results Patients whose tumors had either mutant KRas-Gly12Cys or mutant KRas-Gly12Val had worse progression-free survival compared with patients whose tumors had other mutant KRas proteins or wild-type KRas ($P = .046$, median survival = 1.84 months) compared with all other mutant KRas (median survival = 3.35 months) or wild-type KRas (median survival = 1.95 months). NSCLC cell lines with mutant KRas-Gly12Asp had activated phosphatidylinositol 3-kinase (PI-3-K) and mitogen-activated protein/extracellular signal-regulated kinase kinase (MEK) signaling, whereas those with mutant KRas-Gly12Cys or mutant KRas-Gly12Val had activated Ral signaling and decreased growth factor–dependent Akt activation. Molecular modeling studies showed that different conformations imposed by mutant KRas may lead to altered association with downstream signaling transducers.

Conclusions Not all mutant KRas proteins affect patient survival or downstream signaling in a similar way. The heterogeneous behavior of mutant KRas proteins implies that therapeutic interventions may need to take into account the specific mutant KRas expressed by the tumor.

J Natl Cancer Inst 2012;104:228–239

Approximately 30% of all human cancers have a mutation in the v-Ki-ras2 Kirsten rat sarcoma viral oncogene homolog (*KRAS*), which encodes a GTPase that is essential for normal signaling; mutant *KRAS* plays a critical role in cancer cell growth and resistance to therapy (1). In colorectal cancer, the presence of a *KRAS* mutation predicts resistance to therapies that target the epidermal growth factor receptor (EGFR) and is predictive of poor prognosis (2). Less clear is the role of *KRAS* mutations as a predictive factor in non–small cell lung cancer (NSCLC): Some studies have shown a weak association with resistance to treatment and other studies have shown no association (3).

KRAS mutations in patient tumors are limited to a few sites; most mutations occur in codon 12, whereas codons 13, 10, and 61 are much less frequently mutated (1). Codon 12 or 13 *KRAS* mutations result in base changes that lead to amino acid substitutions that lock the KRas protein in an active state (4). The frequency and spectrum of *KRAS* mutations in codons 12 and 13 differs among cancer types. For example, the most common *KRAS*

mutation in colorectal tumors, as in most solid tumors including NSCLCs in nonsmoking patients, is a G to A transition (92% of mutations); a G to A transition at codon 12 and/or codon 13 results in KRas proteins in which the wild-type glycine (Gly) residue is replaced by an aspartate (Asp; approximately 50% of tumors), a valine (Val; 28% of tumors), or a cysteine (Cys; 9% of tumors) (1,5,6). In NSCLC in patients who smoke, the most common *KRAS* mutation is a G to T transversion (84% of mutations), and the most common amino acid replacements at codon 12 and/or codon 13 are Cys (47% of tumors), Val (24%), Asp (15%), and alanine (7%) (1,6–8).

KRas has the ability to activate multiple downstream signaling pathways that have been implicated as independent drivers of tumorigenesis, including those involving phosphatidylinositol 3-kinase (PI-3-K), mitogen-activated protein/extracellular signal-regulated kinase kinase (MEK), v-ral simian leukemia viral oncogene homolog ras related (Ral), mammalian target of rapamycin (mTOR), and p70 S6 kinase (9). In this study, we used data from a recently completed biopsy-required, biomarker-driven, molecularly targeted multi-arm trial in patients with refractory NSCLC to examine the associations between mutant KRas proteins bearing different amino acid substitutions and patient response to molecularly targeted therapy. We analyzed tumor transcriptome microarray data for expression of cell cycle genes. We used a panel of NSCLC cell lines with known amino acid substitutions in KRas to identify pathways activated by the different mutant KRas proteins. Finally, we used molecular modeling to examine interactions between wild-type and mutant KRas proteins and downstream signaling transducers.

CONTEXT AND CAVEATS

Prior knowledge

KRas protein is a GTPase involved in signal transduction, and mutant KRas plays a critical role in cancer cell growth and resistance to therapy. Mutant KRas proteins with any amino acid substitution are a negative predictor of patient response to targeted therapy in colorectal cancer. However, there is inconsistent evidence that mutant *KRAS* is a predictive factor in non–small cell lung cancer (NSCLC).

Study design

Data from a clinical trial of patients with refractory NSCLC were used to examine associations between specific mutant KRas proteins and patient response to molecularly targeted therapy and tumor gene expression. Microarray analysis was used to identify signaling pathways activated in 67 NSCLC lines that expressed different mutant KRas proteins.

Contribution

Mutant KRas-Gly12Cys and mutant KRas-Gly12Val were associated with decreased progression-free survival compared with other mutant KRas or wild-type KRas. NSCLC cell lines with mutant KRas-Gly12Asp had activated phosphatidylinositol 3-kinase and mitogen-activated protein/extracellular signal-regulated kinase kinase signaling, whereas those with mutant KRas-Gly12Cys or mutant KRas-Gly12Val had activated Ral signaling and decreased growth factor–dependent Akt activation.

Implication

Therapeutic interventions may need to take into account the specific mutant KRas protein expressed by the tumor.

Limitations

Only the major forms of mutant KRas in NSCLC and three downstream signaling pathways were considered. The patient response results may only be applicable to the types of molecularly targeted agents used in the clinical trial.

From the Editors

Methods

BATTLE Clinical Trial

To analyze associations between specific mutant KRas amino acid substitutions and patient survival, we used data from the prospective phase II Biomarker-integrated Approaches of Targeted Therapy for Lung Cancer Elimination (BATTLE) trial in patients with refractory NSCLC who had agreed to a baseline tumor biopsy (10). The BATTLE trial used an adaptive method to randomly assign patients with refractory NSCLC who agreed to a have a baseline biopsy of their tumor to one of four trial arms testing treatments with erlotinib, vandetanib, bexarotene and erlotinib, or sorafenib. The primary endpoint of the trial was disease control rate at 8 weeks. Radiographic imaging of tumors was reviewed to determine suitability of patients for biopsy. Patients who were 18 years of age or older and had an adequate performance status (Eastern Cooperative Oncology Group grade 0–2) were eligible for the trial. Although previous treatment with erlotinib was allowed, patients who had received erlotinib were excluded from the erlotinib-containing study arms. Patients with stable (for at least 4 weeks) or treated brain metastases were included in the trial. All participants provided written informed consent. The BATTLE trial enrolled 341 patients, and, among them, 255 were randomly assigned. Of the 341 patients enrolled, 268 had tumor tissue available for *KRAS* mutation analysis, and of these, 48 had a mutant *KRAS* in their tumor. Of the 255 patients who were randomly assigned, 215 had tumor tissue available for *KRAS* mutation analysis and were also evaluable for the progression-free survival.

Microarray Analysis of Patient Tumor Gene Expression Profiles

We conducted microarray analysis of mRNA expression on frozen tumor core biopsy samples from 101 patients who had been randomly assigned to a BATTLE treatment arm (27 to erlotinib, eight to erlotinib and bexarotene, 47 to sorafenib, and 19 to vandetanib) and were evaluable for 8-week disease control. Core tumor biopsy samples were taken from each patient before treatment at either the primary lung tumor or a metastatic site. Approximately one-third of the core from each sample was used for total RNA extraction and global gene expression analysis. RNA was extracted from tissue embedded in Tissue-Tek OCT compound (Ted-Pella Inc, Reding, CA) using the RNeasy Mini Kit (Qiagen, Valencia, CA) including on-column DNase (Qiagen, Valencia, CA) digestion as described by the manufacturer's protocol. Hematoxylin- and eosin-stained sections of all of the samples were available to check for the presence of cancer cells. RNA

quantification was done using a Nanodrop Technologies ND-1000 spectrophotometer (Thermo Scientific, Wilmington, DE). All RNA samples were serially diluted in RNAse-free water to obtain a 250-pg/μL stock solution. RNA quality was ensured by analyzing a separation trace of RNA using the RNA6000 PicoAssay for the Bioanalyzer 2100 (Agilent Technologies, Palo Alto, CA). Aliquots of RNA were prepared and stored at −80°C. Each aliquot was used once. The decision to submit the RNA sample for amplification was based on its purity (ie, ratio of the absorbance at 260 nm to that at 280 nm [260/280 ratio] ≥2.0), and an RNA integrity number (RIN) greater than 7 or when the RIN number was low or not available, the presence of an electrophoretic trace on a case-by-case basis. We used 0.5–50 ng of RNA for amplification, which was performed using a WT-Amplification Pico kit (NuGEN, San Carlos, CA). The amplification products were labeled using an FL-Ovation cDNA Biotin Module V2 (NuGEN) according to the manufacturers' protocols. The quantity and quality of the amplified cRNA was reassessed with the use of an ND 1000 spectrophotometer and Agilent Bioanalyzer (Agilent Technologies). When the RIN was lower than 7, amplification and labeling were repeated. Hybridization mixtures were prepared according to Affymetrix procedures (Affymetrix, Santa Clara, CA) to accommodate 5 μg of cDNA targets from NuGEN amplification with an RNA integrity number greater than 7. Hybridization was performed with the use of a Human Gene 1.ST platform (Affymetrix) according to the manufacturer's protocols. All steps from hybridization to the generation of raw microarray data were carried out at the University of Texas MD Anderson Cancer Center Microarray and Affymetrix Facility. Gene chips were scanned using an Affymetrix 7G scanner (Affymetrix), and images (DAT files) were converted to CEL files using GCOS software (Affymetrix).

Cells and Culture Conditions

A panel of 67 NSCLC cell lines (11,12) were provided by Dr J. D. Minna and grown in RPMI-1640 medium (Hyclone, Logan, UT) with 10% fetal bovine serum (FBS; Aleken Biologicals, Nash, TX) as previously described. Immortalized human bronchial epithelial cells with specific short hairpin RNA (shRNA) knockdown of p53 mRNA (HBECsiP53) (13,14) were maintained in K-SFM medium containing 50 μg/mL of bovine pituitary extract (BPE) and 5 ng/mL of epidermal growth factor (EGF) (all from Life Technologies, Carlsbad, CA). All cell lines were tested to confirm the absence of mycoplasma using an e-Myco PCR detection kit (Boca Scientific, Boca Raton, FL). The identities of the NSCLC cell lines were confirmed through DNA fingerprinting by the University of Texas MD Anderson Cancer Center Characterized Cell Line Core Service at the time of total protein lysate preparation. Mutant *KRAS*-transfected HBECsiP53 were sequenced to confirm the specific *KRAS* mutation (Supplementary Figure 1, available online).

Preparation of Protein Lysates and Reverse-Phase Protein Array (RPPA)

For each cell line including HBECsiP53, we prepared a protein lysate from cells harvested from subconfluent cultures that were incubated for 24 hours in medium containing no or 10% FBS. For total protein lysate preparation, the medium was removed, and the cells were washed twice with ice-cold phosphate-buffered saline (PBS)–containing Complete protease inhibitor cocktail tablets and PhosSTOP Phosphatase inhibitor cocktail tablets (two tablets each per 500 mL PBS; Roche Applied Science, Mannheim, Germany) and 1 mM Na_3VO_4. Lysis buffer (1% Triton X-100, 50 mM HEPES [pH 7.4], 150 mM NaCl, 1.5 mM $MgCl_2$, 1 mM EGTA, 100 mM NaF, 10 mM $Na_4P_2O_7$, 10% glycerol, 1 mM phenylmethylsulfonyl fluoride, 1 mM Na_3VO_4, and 10 μg/mL aprotinin) was added to the cells, and samples were vortexed frequently on ice for 20 minutes, followed by microcentrifugation at 18 000*g* for 10 minutes. Cleared supernatants were collected, and protein was measured using a BCA protein assay kit (Pierce Biotechnology Inc, Rockford, IL). Specific signaling proteins and phosphoproteins were then quantified by RPPA, using mouse monoclonal antibodies specifically validated for RPPA use (listed in Supplementary Table 1, available online) at optimized concentrations as previously described (12). Lysate was applied to slides for RPPA analysis. For each cell line, a serial dilution of five concentrations of the lysate was deposited on slides using a pin-based Aushon's 2470 microarrayer (Aushon Biosystems, Billerica, MA), with 10% of the samples replicated for quality control. Immunostaining was performed with the use of an automated autostainer (BioGenex, San Ramon, CA). Each array was incubated with primary antibody, and signal was detected using a catalyzed signal amplification system (Dako Cytomation California Inc, Carpinteria, CA). After quantification, the data were logarithmically transformed (base 2) for further processing and analysis.

Immunoblotting and Immunoprecipitation

Cells were washed twice with ice-cold PBS and then once with a lysis buffer containing 50 mmol/L HEPES (pH 7.5), 50 mmol/L NaCl, 0.2 mmol/L NaF, 0.2 mmol/L Na_3VO_4, 1 mmol/L phenylmethylsulfonyl fluoride, 20 μg/mL aprotinin, 20 μg/mL leupeptin, 1% Nonidet P-40, and 0.25% sodium deoxycholate. The protein concentration of each cell lysate was determined by the BCA protein assay (Pierce Biotechnology), and 50 μg of each lysate was boiled for 5 minutes in a denaturing buffer containing 0.25 mol/L Tris–HCl (pH 6.8), 35% glycerol, 8% sodium dodecyl sulfate, and 10% 2-mercaptoethanol, loaded on a 10% acrylamide–bisacrylamide gel, and resolved by electrophoresis at 150 V for 40 minutes. Proteins were electrophoretically transferred to a nitrocellulose membrane. The membrane was preincubated for 30 minutes in a blocking buffer (137 mmol/L NaCl, 2.7 mmol/L KCl, 897 mmol/L $CaCl_2$, 491 mmol/L $MgCl_2$, 3.4 mmol/L Na_2HPO_4, 593 mmol/L KH_2PO_4, and 5% bovine serum albumin) and then incubated overnight with rabbit monoclonal anti-phospho-Akt (Thr308), phospho-Akt (Ser473), anti-phospho-p70 S6 kinase (Thr389), or anti-Akt antibodies or rabbit polyclonal anti-phospho-Mapk (Thr202/Tyr204) antibodies (1:1000 dilution; Cell Signaling Technology, Danvers, MA). A goat polyclonal anti-lamin A/C antibody and a mouse monoclonal anti–β-actin antibody (Santa Cruz Biotechnology, Santa Cruz, CA) were used at 1:2000 dilution. Horseradish peroxidase–coupled donkey anti-rabbit immunoglobulin G secondary antibody (1:2000 dilution; GE Healthcare, Piscataway, NJ) was used for primary antibody detection, and a Western Lightening chemiluminescence kit (Perkin Elmer, Waltham, MA) was used to detect antibody

binding to the membrane. For measurement of active RalA and RalB, we used RalA and RalB activation kits (Millipore, Billerica, MA). Briefly, to measure active (ie, GTP-bound) RalA or RalB, HBECsiP53 cells were incubated for 1 hour at 4°C with Ral binding protein conjugated to beads. The beads were isolated by centrifugation at 18 000*g*, washed with PBS, denatured, and subjected to electrophoresis on polyacrylamide gels. RalA and RalB were detected by immunoblotting using a Renaissance chemiluminescence system (NEN, Boston, MA) on Kodak X-Omat Blue ML film (Eastman Kodak, Rochester, NY)

Lentiviral Vector Construction

Lentiviral vectors expressing wild-type *KRAS*, mutant *KRAS*-Gly12Cys, or mutant *KRAS*-Gly12Asp were constructed from a previously described vector, pLenti6-*KRAS*-V12 (14), using a site-directed mutagenesis kit (Stratagene, La Jolla, CA) according to the manufacturer's instructions. Correct sequences were confirmed by sequencing for all vectors. Viral transduction was performed as described previously (13) by transiently transfection of each viral vector into 293FT packaging cells with Viral Power Packaging Mix (Invitrogen, Carlsbad, CA) according to the manufacturer's instructions. Virus-containing medium was harvested 48–96 hours later and filtered through a 0.45-μm filter. HEBECsiP53 cells were stably infected with virus-containing media and 4 μg/mL polybrene (Sigma, St Loius, MO) for 16 hours followed by selection for 5 days in 2 μg/mL blasticidin (Invitrogen). All variants of *KRAS* were confirmed by DNA sequencing (Supplementary Figure 1, available online). RNA was extracted from the transformed cells and reverse transcribed to cDNA using an iScript cDNA Synthesis kit (Bio-Rad, Hercules, CA). cDNA was amplified using primers that bind either side of the codon 12 mutation (Forward primer: 5′-GACTGAATATAAACTTGTG GTAGTTGGACCT-3′; Reverse primer: 5′-TCCTCTTGACC TGCTGTGTCG-3′) and HotStar Taq polymerase (Qiagen, Germantown, MD), and the amplified products were purified with the use of a QiaQuick CleanUp kit (Qiagen, Germantown, MD). Products were sequenced using the forward primer and Big Dye Terminator v3.1 chemistry (Applied Biosystems, Foster City, CA) on an Applied Biosystems 3730xl instrument and purified with the use of Sephadex G-50 in Millipore Multiscreen plates (Millipore).

HBECsiP53 Plastic and Soft Agar Growth Assays

For cell growth assays on plastic, 2000 HBECsiP53 *KRAS*-transfected or wild-type cells were plated per well in 96-well plates (Griener, Monroe, SC) and allowed to attach for 16 hours. At various times up to 100 hours of growth, cell number was measured using phenazine methosulfate (Sigma-Aldrich, St Louis, MO) activation of methylthiazol tetrazolium (Promega, Madison, WI) and colorimetric measurement at 490 nm using a FLUOstar Omega Spectrometer (BMG Labtech, Cary, NC). Readings for eight wells were averaged per time point. Each plate contained four wells with no cells as a control background reading, which was subtracted from the samples from that plate. The experiment was performed in triplicate three times. Soft agar growth assays were performed as previously described (13). Briefly, HBECsiP53 cells were seeded at 1000 cells per well in 12-well plates in triplicate in K-SFM medium supplemented with 20% FBS, 50 μg/mL BPE, and 5 ng/mL EGF and incubated for 4 weeks. The cells were stained with 0.005% crystal violet and colonies (defined as >50 cells) were counted at ×4 magnification. Results are the average of three experiments.

Molecular Modeling

We retrieved the structures of Harvey rat sarcoma viral oncogene homolog (HRas) proteins in the PI-3-K/HRas complex (Protein Data Bank entry code: 1HE8) (15) and ral guanine nucleotide dissociation stimulator (RaLGDS)/HRas heterotetramer complex (Protein Data Bank entry code: 1LFD) (16) from the Protein Data Bank and used them as templates to build molecular models of wild-type KRas, mutant KRas-Gly12Cys, and mutant KRas-Gly12Asp. The homology models were energetically minimized using the NAMD software (17), and the resulting KRas homology models were superimposed to the HRas protein in 1HE8 and 1LFD, thus generating three PI-3-K/KRas complexes and three RaLGDS/KRas complexes. Molecular dynamics simulations of various forms of KRas in complex with PI-3-K or RaLGDS were carried out as previously described (14). The topology and parameter for GTP were generated as the chimeric analog of ATP and guanine using the CHARMM27 force field (18). Each protein complex was solvated in a water box in which every protein atom was at least 8 Å away from the boundary of the box. Sodium chloride at 100 mM was added to the water box to neutralize the system charges. Following equilibration of the system for 400 picoseconds, we then conducted 8-nanosecond molecular dynamics simulations while recording the trajectory (snapshot structures of the simulated system) every 200 femtoseconds. Trajectories of the last 6 nanoseconds for the six protein complexes were superimposed using the WORDOM software (19). The average structure for each protein complex was calculated with WORDOM and then optimized with the carbon-tethered energy minimization method of the Molecular Operating Environment software package (Chemical Computing Group, Montreal, Canada) to reduce structural defects. The snapshot structures of each protein complex were taken every 100 picoseconds, and we used the ZRANK program (20) to calculate the ZRANK score, an estimate of the relative binding affinities of different forms of KRas to PI-3-K or RaLGDS in which a lower score indicates tighter binding.

Statistical Analysis

Descriptive statistics were used to summarize all data. Dot plots, bar charts, and box plots were used where appropriate to provide a graphic assessment of the distributions of the data. Colony numbers for the soft agar growth assay for different cell line groups were compared using one-way analysis of variance. The Kaplan–Meier method was used to estimate the survival function for progression-free survival, and multivariable Cox regression analysis was applied to the patient survival data. The effects of multiple treatments, subtypes of KRas mutation, and their interactions were controlled for by Cox regression. Unsupervised cluster analysis was used for the microarray and RRPA data using the Pearson correlation distance between proteins, Euclidean distance between cell lines, and Ward linkage rule. The statistical analyses of microarray data were performed using R Development

Core Team (version 2.7.0, 2010; R Foundation for Statistical Computing, Vienna, Austria. ISBN 3-900051-07-0; URL http://www.R-project.org). RRPA data were logarithmically transformed (base 2) for processing and analysis. We chose a somewhat arbitrary false discovery rate of 0.3 because it struck a good balance between the number of statistically significant markers and a reasonable *P* value threshold for statistical significance. As a result, we selected 66 statistically significant markers, with a corresponding *P* value of .015, for the cluster analysis. All statistical tests were performed with a two-sided 5% type I error rate.

Results

Association Between KRas Proteins and NSCLC Patient Survival

The recently completed BATTLE trial for patients with refractory NSCLC who received either erlotinib, vandetanib, bexarotene and erlotinib, or sorafenib reported that grouping all *KRAS* mutations together was not associated with either overall survival or progression-free survival (*P* = .086) (10). We examined whether specific *KRAS* mutations were associated with survival. Of the 341 patients enrolled in the BATTLE trial, 268 had tumor *KRAS* mutation analysis performed. Of those patients, 48 had a *KRAS* mutation: one patient (2%) had a mutation at codon 10, 42 (88%) had a mutation at codon 12, two (4%) had a mutation at codon 13, and three (6%) had a mutation at codon 61 (Table 1). We also analyzed the BATTLE data for the association between different amino acid substitutions in mutant KRas and progression-free survival. Among the 255 patients who were randomly assigned to a treatment group, 215 had tissues available for the *KRAS* mutation analysis and were evaluable for the progression-free survival. We found that 43 patients had mutant KRas: 24 patients had Cys or Val substitution at codon 12 and 19 patients had other amino acids substitutions at codon 12 (Figure 1, A). Mutant KRas-Gly12Cys and KRas-Gly12Val was associated with a statistically significantly decreased progression-free survival (*P* = .046, median survival = 1.84 months) compared with all other mutant KRas (median survival = 3.35 months) or wild-type KRas (median survival = 1.95 months) (Figure 1, A). The negative association between a Cys or Val substitution at codon 12 and progression-free survival was most pronounced for patients in the sorafenib treatment arm (*P* = .026) (Figure 1, B). Although only three patients in the vandetanib arm had either mutant KRas-Gly12Cys or mutant KRas-Gly12Val, we observed a statistically significant association between these mutations and with decreased progression-free survival (*P* = .001). There was no association between tumors that expressed mutant KRas-Gly12Cys or mutant KRas-Gly12Val and progression-free survival in either erlotinib treatment arm; we suspect this is because of the high incidence of multiple EGFR mutations that was seen in the NSCLC patients in the BATTLE trial (10).

Table 1. KRas mutation status of all BATTLE* trial patients with available tumor tissue (n = 268)

Amino acid substitution or mutated codon	Patient population distribution		
	Cys or Val (n = 26)	Other amino acid (n = 22)	Wild type (n = 220)
Amino acid at codon of interest			
Gly	0	0	220
Ala	0	5	0
Asp	0	11	0
Cys	17	0	0
Val	8	0	0
Cys and Val	1	0	0
Other	0	6	0
Mutated codon			
None	0	0	220
10	0	1	0
12	26	16	0
13	0	2	0
61	0	3	0

* BATTLE stands for Biomarker-based Approaches of Targeted Therapy for Lung Cancer Elimination. This is a biomarker-based adaptive random trial in stage IV recurrent non–small cell lung cancer patients to evaluate the 8-week disease control rate of four regiments of targeted agents.

Tumor Microarray Transcriptome Analysis

We next performed a supervised cluster analysis of microarray transcriptome data from tumors from the BATTLE trial to identify genes whose expression differed statistically significantly between tumors that expressed either mutant KRas-Gly12Cys or mutant KRas-Gly12Val and those that expressed other mutant forms of KRas. We identified genes that most accurately defined the differences between these two mutant KRas groups, thereby allowing clustering of the patients into two groups (Figure 1, C; Supplementary Data, available online). Genes that defined the two groups included the cell cycle regulators *PLK1* (polo-like kinase 1), *CCNB1* (cyclin B), and *CCNE1* (cyclin E), whose expression was lower in tumors expressing either mutant KRas-Gly12Cys or mutant KRas-Gly12Val and higher in the remaining mutant KRas tumors, compared with tumors expressing wild-type KRas.

Effect of Mutant Forms of KRas on Downstream Signaling in NSCLC Cell Lines

To examine the effect of mutant forms of KRas on protein signal transduction, we conducted a comprehensive RRPA analysis across a panel of 67 genetically characterized NSCLC cell lines comparing specific signaling protein expression in lines that expressed either mutant KRas-Gly12 or 13 Cys or mutant KRas-Gly12Val (n = 13 cell lines), with cell lines that expressed any other mutant KRas (n = 9 cell lines) and wild-type KRas (n = 45 cell lines). Neither phosphorylated Mek nor phosphorylated p38 showed statistically significant differences in expression levels between cell lines that had either mutant KRas-Gly12Cys or mutant KRas-Gly12Val, and those that had other mutant forms of KRas or wild-type KRas (Figure 2, A and B). However, phosphorylated Akt levels were decreased in cell lines that expressed either mutant KRas-Gly12Cys or mutant KRas-Gly12Val compared with cells lines that expressed other mutant KRas (*P* = .009) or wild-type KRas (*P* = .020) (Figure 2, C). These findings were confirmed by immunoblot analysis of whole-cell lysates for a set of seven NSCLC cell lines with KRas codon 12 mutations (Figure 2, D).

To study the signaling and growth effects of different KRas mutations in a uniform cell background, we stably expressed the

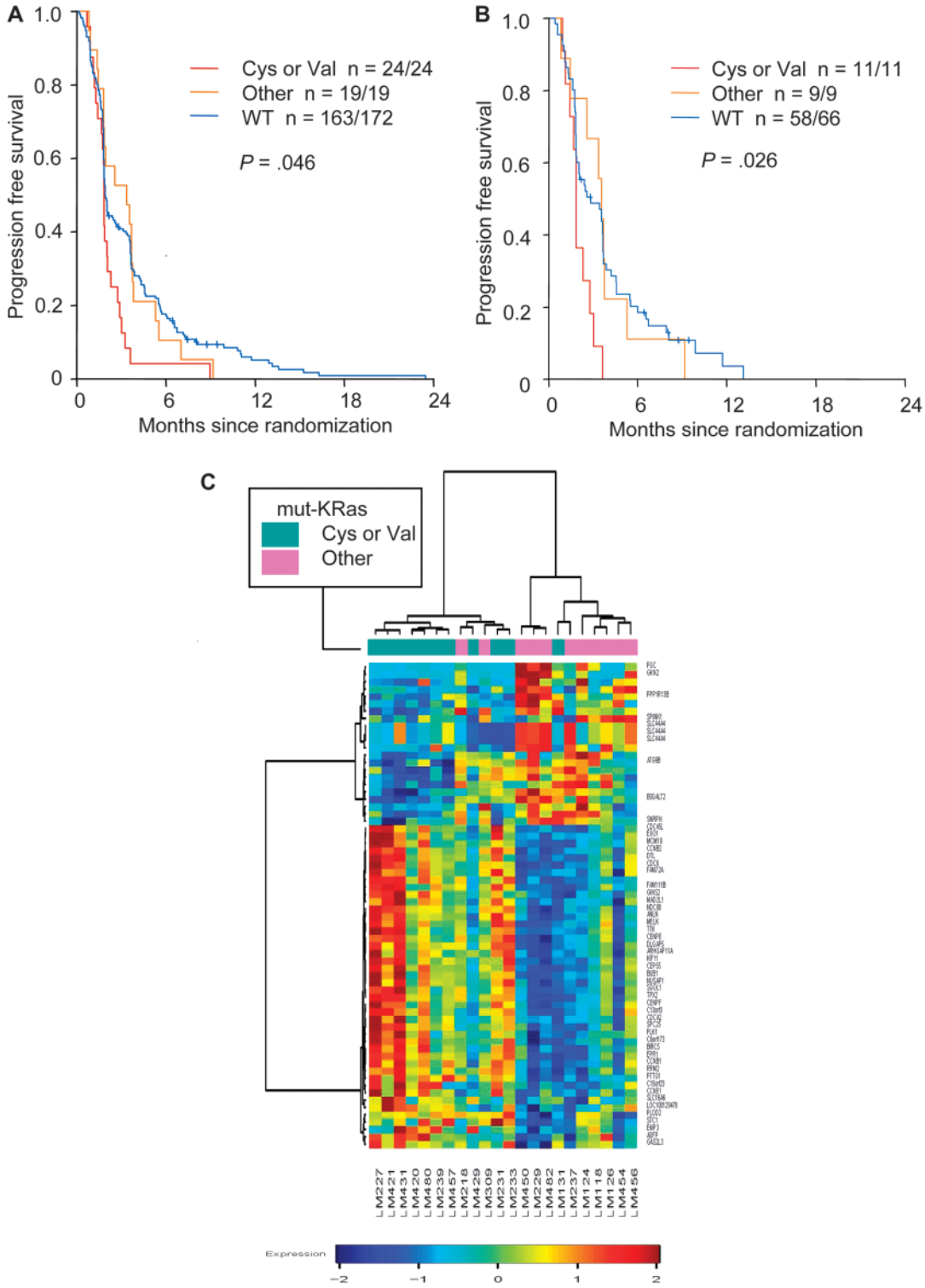

Figure 1. Mutant KRas-Gly12Cys and mutant KRas-Gly12Val and response in refractory non–small cell lung cancer (NSCLC). Kaplan–Meier plots of progression-free survival (PFS) for NSCLC patients in the BATTLE trial by tumor KRas mutation for (**A**) all treatments and (**B**) for sorafenib-treated patients. n = *a*/*b* indicates "*a*" total number of events in "*b*" patients in each category. Data were analyzed by the log-rank test. *P* values are two-sided. **C**) Cluster analysis of microarray data from patients treated in BATTLE trial of genes that most accurately define the differences between mutant KRas-Gly12Cys or mutant KRas-Gly12Val, and other mutant KRas tumors. The false discovery rate was chosen as 0.3. **Red dots** indicate genes known to be involved in cell cycle regulation. Panel A: The numbers at risk at 3, 6, and 12 months were 4, 1, 0 for Cys/Val; 10, 2, 0 for other; and 67, 29, 6 for wild-type KRas groups, respectively. The corresponding PFS (95% confidence intervals [CIs]) were 0.17 (95% CI = 0.07 to 0.41), 0.04 (95% CI = 0.01 to 0.28), and NA (not applicable) for the Cys/Val group; 0.53 (95% CI = 0.34 to 0.81), 0.11 (95% CI = 0.03 to 0.39), and NA for the other group; and 0.41 (95% CI = 0.34 to 0.49), 0.18 (95% CI = 0.13 to 0.25), and 0.05 (95% CI = 0.02 to 0.11) for the wild-type KRas group. Panel B: The numbers at risk at 3, 6, and 12 months were 2, 0, 0 for Cys/Val; 6, 1, 0, for other; and 29, 12, 1, for wild-type KRas groups, respectively. The corresponding PFS (95% CIs) were 0.18 (95% CI = 0.05 to 0.64), NA (NA) for the Cys/Val group; 0.67 (95% CI = 0.42 to 1.00), 0.11 (95% CI = 0.02 to 0.71), and NA for the other group; and 0.49 (95% CI = 0.38 to 0.63), 0.20 (95% CI = 0.12 to 0.33), and 0.04 (95% CI = 0.01 to 0.21) for the wild-type KRas group.

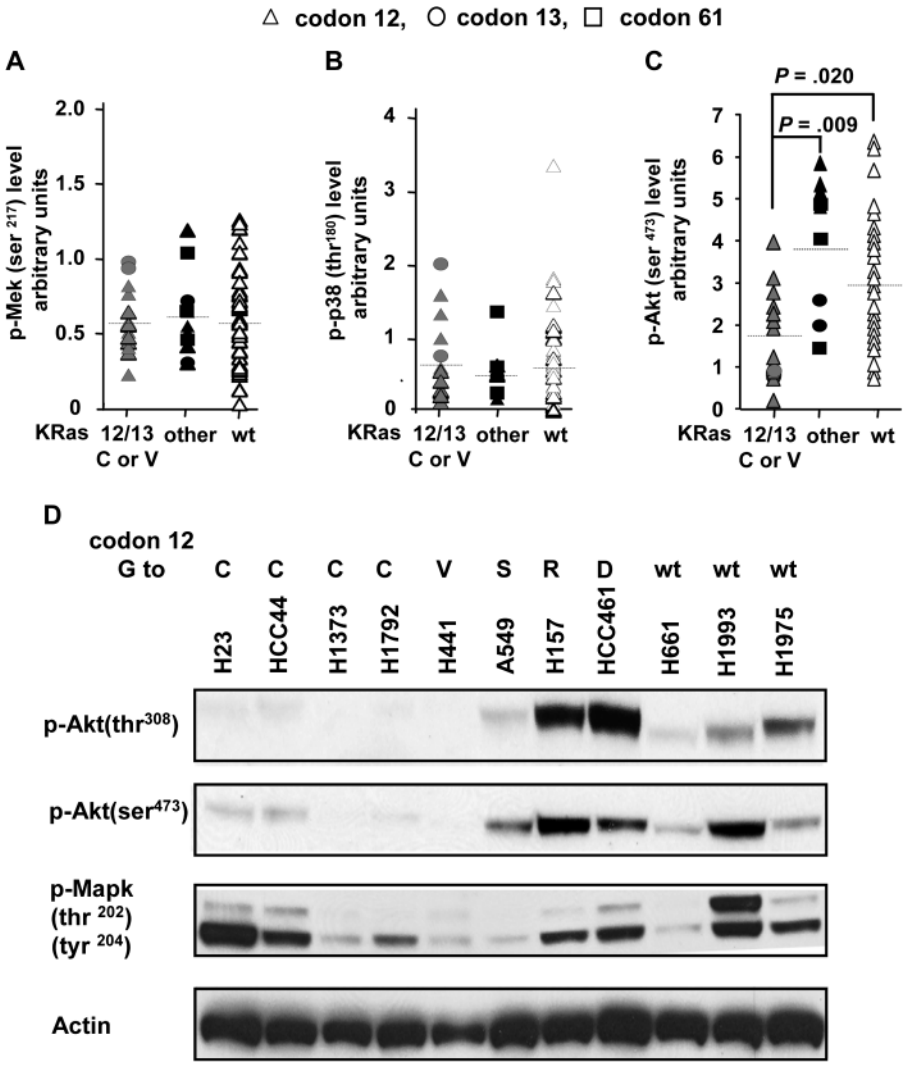

Figure 2. Mek and Akt signaling in non–small cell lung cancer (NSCLC) cell lines expressing mutant or wild-type KRas. Reverse-phase protein array levels of (**A**) phospho-Mek (ser[217]), (**B**) phospho-p38 (thr[180]), and (**C**) phospho-Akt (ser[473]) for a panel of 67 NSCLC cell lines expressing mutant or wild-type KRas. KRas 12/13 C or V = cell lines with mutant KRas-Gly12Cys or mutant KRas-Gly13Cys (n = 13) or mutant KRas-Gly12Val (n = 1); other = cell lines with other mutant KRas (n = 9), wt = cell lines with wild-type KRas (n = 45). **Horizontal bars** indicate the mean value for the group. *P* values are two-sided (Wilcoxon rank test). **D**) Immunoblot analysis of a smaller panel of 11 NSCLC cell lines expressing mutant KRas with different codon 12 amino acid substitutions or wild-type KRas with Gly (G) at codon 12. C = Cys; D = Asp; R = Arg; S = Ser; V = Val.

most common mutant KRas in colon cancer (KRas-Gly12Asp), the most common mutant KRas in NSCLC (KRas-Gly12Cys), and wild-type KRas in previously characterized immortalized human bronchial epithelial cells (13) with shRNA knockdown of p53 to repress the toxicity of KRas in transformed cells (HBECsiP53). The DNA from the expression plasmids was sequenced for all the cell lines to ensure that the plasmids were expressed and that mutant KRas was present (Supplementary Figure 1, available online). HBECsiP53 cells that expressed wild-type KRas or either mutant KRas grew at similar rates in two-dimensional culture on plastic surfaces, and all three grew faster than cells transfected with empty vector (Figure 3, A). However, HBECsiP53 cells expressing mutant KRas-Gly12Cys showed statistically significantly increased anchorage-independent growth measured by colony formation in soft agarose compared with HBECsiP53 cells expressing mutant KRas-Gly12Asp ($P = .008$) or cells expressing wild-type KRas ($P < .001$) (Figure 3, B). Immunoblot analysis revealed that HBECsiP53 cells expressing mutant KRas-Gly12Asp had elevated levels of phosphorylated Akt compared with cells expressing wild-type KRas or empty vector, whereas cells that expressed wild-type KRas or mutant KRas-Gly12Cys had decreased levels of phosphorylated Akt compared with mutant KRas-Gly12Asp cells (Figure 4, C). The KRas downstream effectors RalA and RalB were both found to be activated in HBECsiP53 cells that expressed mutant KRas-Gly12Cys or wild type KRas, but not in cells that expressed mutant KRas-Gly12Asp (Figure 3, D). The results suggest that different amino acid substitutions in mutant KRas may activate different downstream signaling pathways compared with wild-type KRas (ie, mutant KRas-Gly12Asp through phospho-Akt signaling and mutant KRas-Gly12Cys through Ral signaling).

mTOR and Akt Signaling in NSCLC Cell Lines Expressing Mutant KRas Proteins

Mutant KRas and growth factors both lead to Akt phosphorylation, which results in mTOR activation and increased protein translation and tumorigenesis (21). mTOR activation also leads to feedback repression of growth factor–mediated Akt signaling through its effector p70 S6 kinase. Because Gly12Cys is the predominant KRas mutation in lung cancer (5,7,8), we were intrigued by the lack of Akt phosphorylation in HBECsiP53 cells expressing mutant KRas-Gly12Cys, even though these cells were grown in the presence of FBS. We therefore examined growth factor

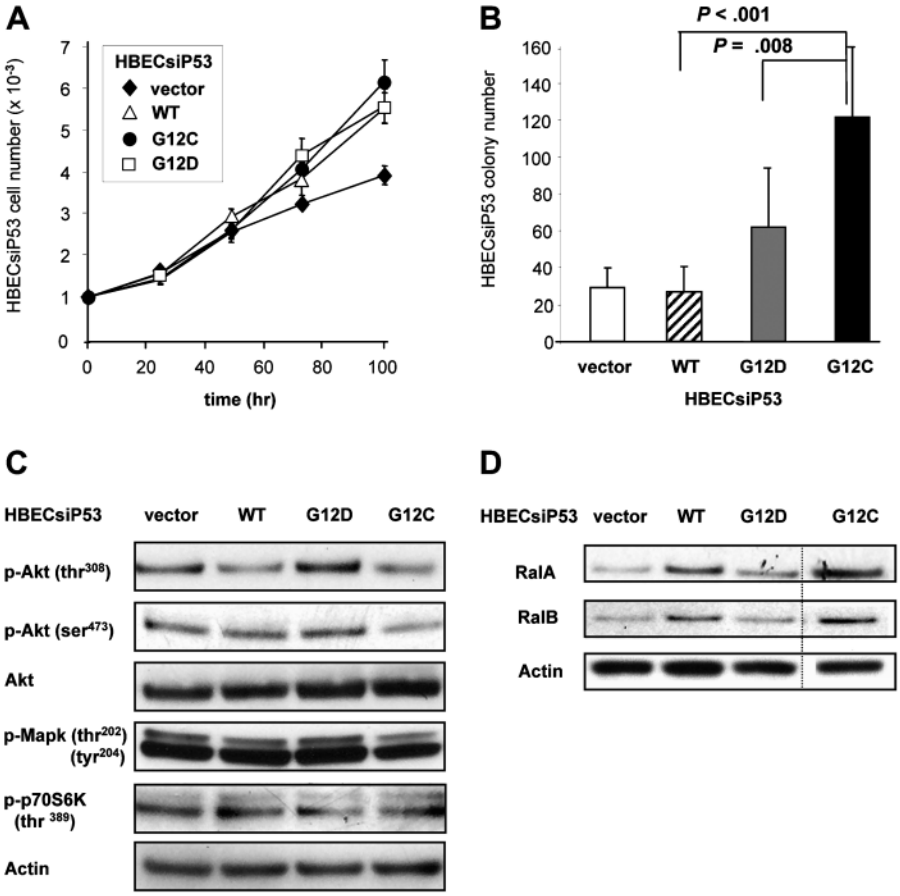

Figure 3. Signaling pathway activation in immortalized human bronchial epithelial cells with short hairpin RNA knockdown of p53 (HBECsiP53) stably transfected with *KRAS* expression plasmids. HBECsiP53 cells stably transfected with empty vector (vector), or vector coding for wild-type KRas (WT), mutant KRas-Gly12Cys (G12C), or mutant KRas-Gly12Asp (G12D) were grown on a plastic surface for 100 hrs (**A**) or in soft agarose for 4 weeks to assess anchorage-independent growth (**B**). Values are the mean of three experiments; **error bars** represent 95% confidence intervals. *P* values are two-sided (analysis of variance). **C**) Immunoblot analysis of Akt and Mapk pathway activation in the transfected HBECsiP53 cell lines. **D**) Pull-down assay for active RalA and RalB in the transfected HBECsiP53 cell lines. The experiments were repeated at least three times with similar results.

(ie, FBS)–mediated activation (ie, phosphorylation) of Akt as well as levels of phosphorylated p70 S6 kinase, which represses Akt activation by growth factors, in HBECsiP53 cells that expressed different mutant KRas proteins.

Despite the lower levels of phosphorylated Akt seen in NSCLC or HBEcsiP53 cells expressing either mutant KRas-Gly12Cys or mutant KRas-Gly12Val (Figures 1, C and 3, C), the levels of the mTOR effectors phospho-p70S6K and 4EBP were not statistically significantly changed compared with other mutant KRas or wild-type KRas cells (Figure 4, A and B). To examine the relationship between activation of the Akt pathway and mTOR activation, we subjected a panel of mutant KRas NSCLC cell lines to hierarchical clustering based on activation of downstream targets of Akt and mTOR signaling (Figure 4, B). We observed that NSCLC cells expressing mutant KRas-G12 or G13Cys or mutant KRas-G12Val had low levels of phospho-Akt (Figure 2, C) and no activation of phospho-Mek or phospho-p38, without or with serum (Supplementary Figure 2, available online). However, in the presence of serum, cell lines with mutant KRas-Gly12Cys or KRas-Gly12Val exhibited robust activation of the mTOR effector protein p70 S6 kinase compared with cell lines that expressed other mutant KRas proteins ($P = .02$) or wild-type KRas ($P = .01$). To determine if this p70 S6 kinase activation with KRas-Gly12Cys or KRas-Gly12Val contributed to our observation that mutant KRas-Gly12Cys or G12Val resulted in lower Akt activation, we treated KRas-transfected HBECsiP53 cell lines with the mTOR inhibitor rapamycin and examined its effects on signaling (Figure 4, C). Rapamycin inhibited activation of p70 S6 kinase in all of the transfected HBECsiP53 cell lines but induced activation of Akt in HBECsiP53 cells expressing wild-type KRas or mutant KRas-Gly12Cys. However, in HBECsiP53 cells expressing mutant KRas-Gly12Asp, Akt was constitutively activated, and rapamycin did not further increased the level of phosphorylated Akt, indicating that in these cells there was constitutive growth factor–independent activation of the signaling. Rapamycin had comparable effects on Akt activation in NSCLC cell lines expressing wild-type KRas, mutant KRas-Gly12Cys, and mutant KRas-Gly12Asp (Figure 4, D). Thus, these results suggest that Akt is constitutively activated by mutant KRas-Gly12Asp and is not inhibited by mTOR, whereas in cells that express wild-type KRas or mutant KRas-Gly12Cys, Akt activation is weak, inhibited by mTOR, and is presumably a consequence of stimulation by growth factors but not KRas.

Molecular Modeling Studies of KRas Proteins

Finally, we performed molecular modeling studies of the KRas proteins by using the available crystal structures of HRas (which has approximately 95% sequence identity to KRas) to create homology models of mutant KRas-Gly12Cys and mutant KRas-Gly12Asp, followed by molecular dynamics simulations for structural refinement. KRas interacts with its different downstream effectors by undergoing large conformational changes in the switch I and switch II regions of the protein that surround the amino acids corresponding to codons 12 and 13 (15,16). When

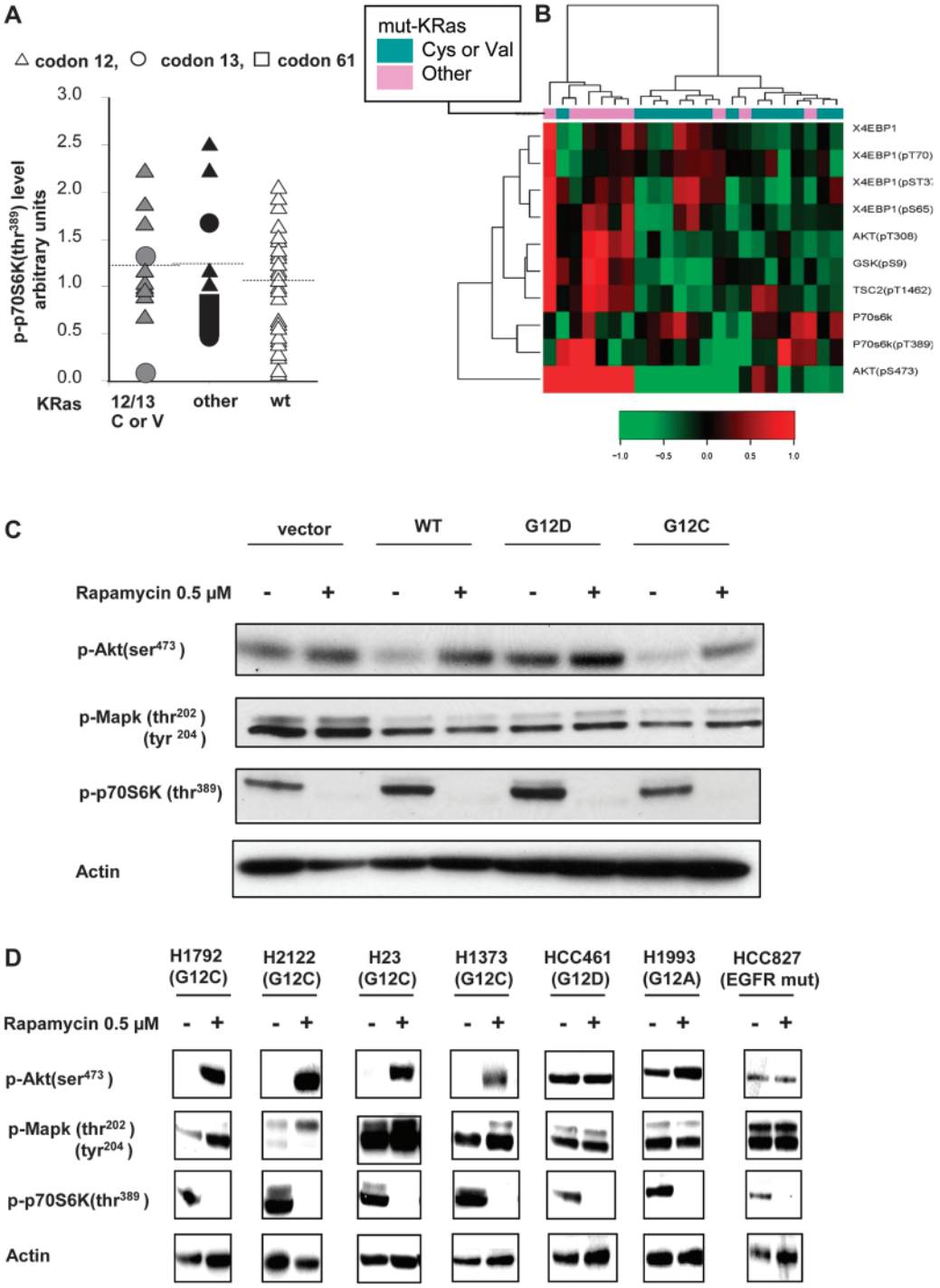

Figure 4. Signaling pathway activation in NSCLC cell lines expressing mutant or wild-type KRas. A) Phospho-p70 S6K (thr^{389}) levels measured by reverse-phase protein array in the panel of 67 NSCLC cell lines grown in medium containing 10% serum. KRas 12/13 C or V = cell lines with mutant KRas-Gly12Cys or mutant KRas-Gly13Cys (n = 13) or mutant KRas-Gly12Val (n = 1); other = cell lines with other mutant KRas (n = 9), wt = cell lines with wild type KRas (n = 45). **Horizontal dotted lines** indicate the mean value for the group. **B**) Two-way hierarchical clustering of NSCLC cell lines based on their expression of phosphorylated Akt and phosphorylated signaling proteins in related signaling pathways. Mutation type is indicated by the **color bar** above the heatmap: 14 cell lines with mutant KRas-Gly12Cys, mutant KRas-Gly13Cys, or mutant KRas-Gly12Val **(green–blue)** and 14 cell lines with other mutant KRas proteins (**pink**). **C**) Immunoblot analysis of Mapk, Akt, and p70 S6 kinase activation in transfected HBECsiP53 cells treated with the mTOR inhibitor rapamycin (0.5 μM) for 16 hours HBECsiP53 cells stably transfected with empty vector (vector), or vector coding for wild-type KRas (WT), mutant KRas-Gly12Cys (G12C), or mutant KRas-Gly12Asp (G12D). **D**) Immunoblot analysis of rapamycin-treated NSCLC cell lines expressing mutant KRas or mutant epidermal growth factor receptor (EGFR). The type of mutation is shown in parentheses.

KRas is bound to PI-3-K, the switch II regions of mutant KRas-Gly12Cys and wild-type KRas exist in a similar conformation that exposes the bound GTP to hydrolysis, thus inhibiting KRas activity. By contrast, a bulky side chain in mutant KRas-Gly12Asp results in electrostatic repulsion on Gly60 in switch II, which allows a hydrogen bond to form between the γ-phosphate of GTP

and Gly61, which protects the nucleotide from hydrolysis, thus stabilizing mutant KRas-Gly12Asp in its active form and activating its bound effector PI-3-K (Figure 5, A). Although PI-3-K and RaLGDS compete for activation by KRas (9), KRas activates these two proteins in very different ways: by direct binding of one KRas molecule to PI-3-K, whereas two KRas molecules form a homodimer to facilitate RaLGDS binding. In the latter case, the interaction of Tyr32 in one KRas molecule with GTP in the other KRas molecule is critical for RaLGDS binding and RalA and RalB activation (16). Our modeling suggests that in mutant KRas-Gly12Asp, the bulky Asp side chain causes steric interference of Tyr32 in switch I, which prevents homodimer formation and RaLGDS binding (Figure 5, B). By contrast, the smaller Cys residue of mutant KRas-Gly12Cys allows homodimer formation and Ral activation. Molecular dynamic and protein–protein docking data (Figure 5, C and D) show the results of these changes, with mutant KRas-Gly12Cys having a higher affinity for binding to RaLGDS and mutant KRas-Gly12Asp a higher affinity for PI-3-K than for RaLGDS.

Discussion

The recently completed BATTLE trial for patients with refractory NSCLC receiving either erlotinib, vandetanib, bexarotene and erlotinib, or sorafenib found that mutant *KRAS* was not associated with overall survival in any of the treatment groups (10). We reanalyzed the BATTLE data to examine associations between mutant KRas with specific amino acid substitutions and patient survival and found that either mutant KRas-Gly12Cys or mutant KRas-Gly12Val was associated with decreased progression-free survival compared with other mutant KRas or wild-type KRas. This is the first study to our knowledge to show an association between mutant KRas amino acid substitutions and response to molecularly targeted therapy in NSCLC.

There is already evidence that mutant KRas amino acid substitution could determine patient response. A study in colon cancer patients receiving EGFR inhibitors revealed that tumors with mutant KRas-Gly12Cys or KRas-Gly12Val are associated with rapid tumor progression and decreased patient survival compared with tumors with other mutant KRas proteins (mostly Gly12Asp) or wild-type KRas (6). A recent study has confirmed that different amino acid–substituted mutant KRas may also affect drug sensitivity of NSCLC patients (22).

Dysregulation of the cell cycle is a well-characterized feature of KRas-mediated tumorigenesis (23,24). Our analysis of tumor transcriptome microarray data from patients in the BATTLE trial provides the first indication to our knowledge that cell cycle signaling differs between the different forms of mutant KRas.

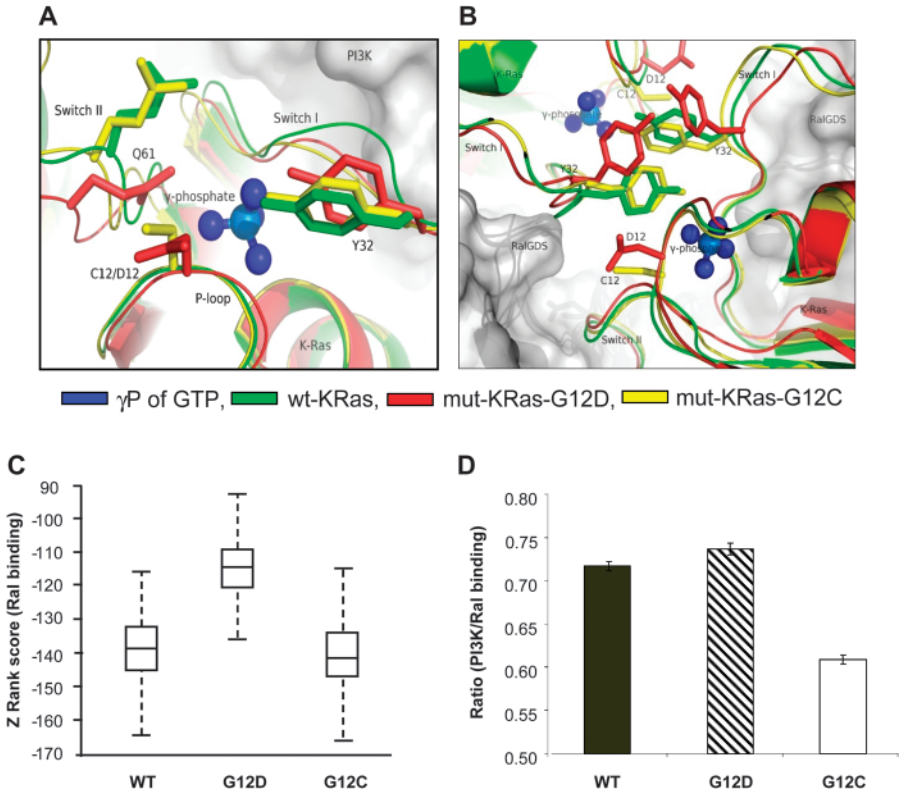

Figure 5. Molecular modeling of the KRas proteins. **A**) KRas with critical amino acid residues (depicted in **stick representations**) in association with phosphatidylinositol 3-kinase (PI-3-K) (depicted as a **gray surface**). In mutant KRas-Gly12Asp (**red**), the Switch II loop is pushed away from GTP (**blue**) by the large side chain of the Asp residue, thereby preventing GTP hydrolysis. Wild-type KRas (**green**) and mutant KRas-Gly12Cys (**yellow**) have similar conformations of Gln61 (Q61) that are open to GTP hydrolysis. Thus, in the presence of PI-3-K, mutant KRas-Gly12Asp is more firmly locked in the GTP-bound state compared with either wild-type or mutant KRas-Gly12Cys and thus constitutively active. **B**) KRas in association with RaLGDS (depicted as **gray surfaces**), the activator of RalA and RalB proteins. KRas exists as a homodimer, with Tyr32 (Y32) of one KRas molecule interacting with the γ-phosphate (**blue**) of another KRas molecule. The bulky side chain Asp residue in mutant KRas-Gly12Asp results in steric clashes with Y32, which impairs dimerization and, thus, binding and activation of RaLGDS. **C**) **Box plots** of predicted binding of wild-type KRas (WT), mutant KRas-Gly12Asp (G12D), and mutant KRas-Gly12Cys (G12C) to RaLGDS. The binding scores were calculated using the ZRANK program for 60 snapshot structures from the molecular dynamics simulations. The ZRANK score estimates the relative binding energy of protein–protein interactions, with a lower score indicating tighter binding. For each box, the **bottom and top lines** represent the 25th and 75th percentiles, respectively, and the **horizontal line** represents the median (50th percentile) of the ZRANK scores. The **error bars** represent the range from the minimum to the maximum of all ZRANK scores collected based on the 60 snapshot structures from the molecular dynamics simulations. **D**) Comparison of predicted binding of the various forms of KRas to RaLGDS with predicted binding of KRas to PI-3-K. The height (*y*-axis) of each panel represents the ratio of averaged binding of KRas to PI-3-K over binding to RaLGDS in terms of ZRANK scores. **Error bars** represent the standard error of the ratios (the corresponding 95% confidence intervals are 0.706 to 0.728 for the WT prediction, 0.723 to 0.751 for the G12D prediction, and 0.599 to 0.619 for the G12C prediction).

Specifically, we found that expression of the cell cycle regulators PLK1, cyclin B, and cyclin E was decreased in tumors with mutant KRas-Gly12Cys or KRas-Gly12Val compared with tumors with other mutant KRas proteins. Our RRPA analysis of a panel of genetically characterized NSCLC cell lines revealed that compared with cell lines expressing wild-type KRas, those with mutant KRas-Gly12Cys or Gly12Val had decreased levels of phosphorylated Akt, whereas those with other mutant KRas proteins had elevated levels of phosphorylated Akt. Transfection of immortalized, p53-deficient human bronchial epithelial HBECsiP53 cells with different mutant KRas expression plasmids also showed that overexpression of mutant KRas-Gly12Cys decreased phospho-Akt levels and increased Ral activation, whereas overexpression of mutant KRas-Gly12Asp increased phospho-Akt levels and decreased Ral activation compared with cells overexpressing wild-type KRas. Moreover, we found that HBECsiP53 cells overexpressing mutant KRas-Gly12Cys had lower Akt signaling, elevated Ral signaling, and increased anchorage-independent growth compared with HBECsiP53 cells overexpressing wild-type KRas. These findings are in agreement with a previous study (25) showing that Ral activation preferentially induces anchorage-independent growth in human cells, whereas Akt or Mek activation has only modest effects. These findings are also consistent with previous observations that when mutant KRas proteins were expressed in the lungs of mice, mutant KRas-Gly12Asp induced Raf and Akt activation (26), whereas mutant KRas-Gly12Cys resulted in Raf and Ral activation but minimal Akt activation regardless of the expression level of the mutant KRas protein (27,28).

Our data showed that mTOR may mediate some of the effects of different amino acid–substituted mutant KRas. We found that many NSCLC cell lines that had minimal Akt activation showed robust activation of the mTOR effector proteins p70 S6 kinase and 4E-BP. We found that inhibition of mTOR with rapamycin in NSCLC cells with mutant KRas-Gly12Cys resulted in decreased expression of p70 S6 kinase and an increase in phospho-Akt levels. The translational regulator mTOR is activated by Akt signaling, in addition to being activated by the Mapk and Ral signaling pathways (21). In addition, p70 S6 kinase downstream of mTOR has been shown to exert a regulatory feedback response that restricts growth factor signaling to the Akt pathway (29). Our results suggest that PI-3-K/Akt signaling is constitutively activated by mutant KRas-Gly12Asp and not subject to mTOR inhibition, whereas in cells expressing wild-type KRas or mutant KRas-GlyG12Cys, Akt activation is growth factor dependent and inhibited by mTOR.

KRas is known to interact with different downstream effectors by undergoing large conformational changes in the switch I and switch II regions of the protein surrounding codon 12 and 13 amino acids (15,16). Our molecular modeling studies showed that mutant KRas-Gly12Cys likely weakens the interaction with PI-3-K, whereas the bulky Asp of mutant KRas-Gly12Asp causes steric interference of KRas homodimer formation and RaLGDS binding, which is not seen with mutant KRas-Gly12Cys. These modeling results are in agreement with the results of our cellular studies showing that mutant KRas-Gly12Asp activated PI-3-K and Mek signaling, but not Ral, whereas mutant KRas-Gl12Cys fails to activate PI-3-K signaling.

The findings of this study showing different mechanisms for signaling through wild-type KRas, mutant KRas-Gly12Asp, and mutant KRas-Gly12Cys are summarized in Figure 6. Wild-type KRas activation results in signaling through Mek. Wild-type KRas has also been shown to activate Akt and RalA/B, although the conditions that dictate which pathway will be activated remain uncertain at this time. The Akt, Mek, and RalA/B pathways have all been shown capable of activating mTOR and its effector p70 S6 kinase, which serves as a negative regulator of growth factor receptor–regulated signaling to Akt. Other KRas effectors are likely also capable of regulating p70 S6 kinase. The KRas-Gly12Asp mutation preferably activates Akt signaling, making growth factor receptor Akt activation unnecessary and p70 S6 kinase inhibition irrelevant. In contrast, the KRas-Gly12Cys mutation preferentially activates RalA/B signaling over Akt and is able to suppress Akt activation through an Akt-independent activation of p70 S6 kinase. Other KRas effectors may also play a role in the signaling, but we have not considered them here.

Our observation that the substitution of different amino acids induces heterogeneous behavior in the KRas protein resulting in different signaling outputs has profound implications for identifying and treating KRAS-driven tumors. For example, it may be necessary to use different combinations of downstream signaling inhibitors when treating tumors with different mutant KRas amino acid substitutions.

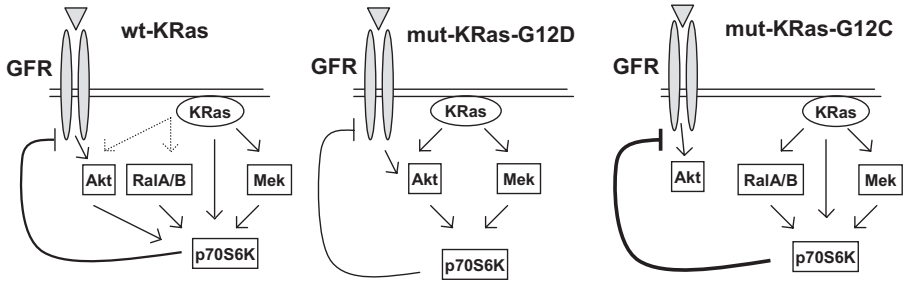

Figure 6. Proposed pathways of signaling by wild-type KRas, mutant KRas-Gly12Asp, and mutant KRas-Gly12Cys showing membrane growth factor receptor (GFR) or wild-type KRas (wt-KRas), mutant KRas-Gly12Asp (mut-KRas-G12D), and mutant KRas-Gly12Cys (mut-KRas-G12C) activation of Akt signaling (acting through PI-3-K), RalA and RalB signaling (acting through RaLGDS), and Mek signaling (acting through c-Raf). Forward transmission of signals is represented by **arrows**. **Solid lines** show established pathways, and **dashed lines** represent possible pathways. P70 S6 kinase (p70S6K) is activated and exerts feedback inhibition on GFR activation of Akt. The thickness of the lines indicates the strength of the feedback inhibition: weak inhibition by mutant KRas-Gly12Asp, moderate inhibition by wild-type KRas, and strong inhibition by mutant KRas-Gly12Cys.

This study focused on the major forms of mutant KRas in NSCLC, namely Gly12Cys (and Gly12Val) and Gly12Asp, and on the downstream signaling pathways involving PI-3-K/Akt, Mek, and Ral. We do not know how other forms of mutant KRas activate the pathways nor do we know how other known KRas downstream pathways [eg, Tiam1/Rac, PLCε/PKC, and Rassf1 (9)] may be affected by mutant KRas. Consequently, our findings that mutant KRas-Gly12Cys and mutant KRas-Gly12Val are associated with overall decreased patient progression-free survival compared with other forms of mutant KRas or wild-type KRas may only be applicable to the types of molecularly targeted agents used in the BATTLE study, which focused broadly on EGFR, VEGF, PI-3-K, and Mek signaling. Future studies will need to explore the role of mutant KRas and signaling pathways in the context of other agents in individual clinical trials.

References

1. Kranenburg O. The KRas oncogene: past, present and future. *Biochim Biophys Acta.* 2005;1756(2):81–82.
2. Raponi M, Winkler H, Dracopoli N. KRAS mutations predict response to EGFR inhibitors. *Curr Opin Pharmacol.* 2008;8(4):413–418.
3. Loriot Y, Mordant P, Deutsch E, Olaussen KA, Soria JC. Are RAS mutations predictive markers of resistance to standard chemotherapy? *Nat Rev Clin Oncol.* 2009;6(9):528–534.
4. Capella G, Cronauer-Mitra S, Peinado MA, Perucho M. Frequency and spectrum of mutations at codons 12 and 13 of the C-K-ras gene in human tumors. *Environ Health Perspect.* 1991;93:125–131.
5. Poorta M, Crous-Bou M, Wark PA, et al. Cigarette smoking and K-ras mutations in pancreas, lung and colorectal adenocarcinomas: etiopathogenic similarities, differences and paradoxes. *Mutat Res.* 2009;682(2–3):83–93.
6. Andreyev HJ, Norman AR, Cunningham D, et al. Kirsten ras mutations in patients with colorectal cancer: a multicenter "RASCAL" study. *J Nat Cancer Inst.* 1998;90(9):675–684.
7. Siegfried JM, Gillespie AT, Mera R, Casey TJ, Keohavong P, Testa JR. Prognostic value of specific KRAS mutations in lung adenocarcinoma. *Cancer Epidemiol Biomarkers Prev.* 1997;6(10):841–847.
8. Hunt JD, Strimas A, Martin JE, et al. Differences in KRAS mutation spectrum in lung cancer cases between African Americans and Caucasians after occupational or environmental exposure to known carcinogens. *Cancer Epidemiol Biomarkers Prev.* 2002;11(11):1405–1412.
9. Cully M, Downward J. SnapShot: Ras signaling. *Cell.* 2008;133(7):1292–1292.e1.
10. Kim ES, Herbst RS, Wistuba II, et al. The BATTLE trial: personalizing therapy for lung cancer. *Cancer Discov.* 2011;1(1):44–53.
11. Shames DS, Girard L, Gao B, et al. A genome-wide screen for promoter methylation in lung cancer identifies novel methylation markers for multiple malignancies. *PLoS Med.* 2006;3(12):e486.
12. Sullivan JP, Spinola M, Dodge M, et al. Aldehyde dehydrogenase activity selects for lung adenocarcinoma stem cells dependent on notch signaling. *Cancer Res.* 2010;70(23):9937–9948.
13. Sato M, Vaughan MB, Girard L, et al. Multiple oncogenic changes (K-RAS[V12], p53 knockdown, mutant EGFRs, p16 bypass, telomerase) are not sufficient to confer a full malignant phenotype on human bronchial epithelial cells. *Cancer Res.* 2006;66(4):2116–2128.
14. Vikis H, Sato M, James M, et al. EGFR-T790M is a rare lung cancer susceptibility allele with enhanced kinase activity. *Cancer Res.* 2007;67(10):4665–4670.
15. Pacold ME, Suire S, Perisic O, et al. Crystal structure and functional analysis of Ras binding to its effector phosphoinositide 3-kinase gamma. *Cell.* 2000;103(6):931–943.
16. Huang L, Hofer F, Martin GS, Kim SH. Structural basis for the interaction of Ras with RalGDS. *Nat Struct Biol.* 1998;5(6):422–426.
17. Phillips JC, Braun R, Wang W, et al. Scalable molecular dynamics with NAMD. *J Comput Chem.* 2005;26(16):1781–1802.
18. Gorfe AA, Grant BJ, McCammon JA. Mapping the nucleotide and isoform-dependent structural and dynamical features of Ras proteins. *Structure.* 2008;16(6):885–896.
19. Seeber M, Cecchini M, Rao F, Settanni G, Caflisch A, Wordom A. A program for efficient analysis of molecular dynamics simulations. *Bioinformatics.* 2007;23(19):2625–2627.
20. Pierce B, Weng ZP. ZRANK: reranking protein docking predictions with an optimized energy function. *Proteins.* 2007;67(4):1078–1086.
21. Dunlop EA, Tee AR. Mammalian target of rapamycin 1: signaling inputs, substrates and feedback mechanisms. *Cell Signal.* 2009;21(6):827–835.
22. Garassino MC, Marabese M, Rusconi P, et al. Different types of K-Ras mutations could affect drug sensitivity and tumour behaviour in non-small-cell lung cancer. *Ann Oncol.* 2011;22(1):235–237.
23. Fan J, Bertino J. KRas modulates the cell cycle via both positive and negative regulatory pathways. *Oncogene.* 1997;14(21):2595–2607.
24. Drosten M, Dhawahir A, Sum E, et al. Genetic analysis of Ras signaling pathways in cell proliferation, migration, and survival. *EMBO J.* 2010;29(6):1091–1104.
25. Hamad NM, Elconin JH, Kamoub AE, et al. Distinct requirements for Ras oncogenesis in human versus mouse cells. *Genes Dev.* 2002;16(16):2045–2057.
26. Tuveson DA, Shaw AT, Willis NA, et al. Endogenous oncogenic KRas (G12D) stimulates proliferation and widespread neoplastic and developmental defects. *Cancer Cell.* 2004;5(4):375–387.
27. Floyd HS, Farnsworth CL, Kock ND, et al. Conditional expression of the mutant Ki-Ras G12C allele results in formation of benign lung adenomas: development of a novel mouse lung tumor model. *Carcinogenesis.* 2005;26(12):2196–2206.
28. Dance-Barnes ST, Kock ND, Floyd HS, et al. Effects of mutant human Ki-Ras (G12C) gene dosage on murine lung tumorgenesis and signaling to downstream effectors. *Toxicol Appl Pharmacol.* 2008;231(12):77–84.
29. O'Reilly KE, Rojo F, She QB, et al. mTOR inhibition induces upstream receptor tyrosine kinase signaling and activates Akt. *Cancer Res.* 2006;66(3):1500–1508.

Funding

National Institutes of Health Grants (CA155196 to R.H., CA160398 to G.P.); DOD grant (W81XWH-6-1-0303 to W.K.H.); MD Anderson's Cancer Center Support Grant (P30 CA016672); and gift from the Perot Foundation (G.P.).

Notes

The study sponsors had no role in the design of the study; the collection, analysis, or interpretation of the data; the writing of the article; or the decision to submit the article for publication.

Affiliations of authors: Department of Experimental Therapeutics (NTI, LC, SZ, MFA, GP), Department of Thoracic Head and Neck Medical Oncology (LAB, ESK, PS, GRB, AT, XT, VP, SML, WKH, RSH, IIW, JVH), Department of Biostatistics (JJL, SL, JW, LD, KRC), and Department of Pathology (IIW); The Hamon Center for Therapeutic Oncology Research and Simmons Cancer Center, University of Texas Southwestern Medical Center, Dallas, TX (JEL, JDM).

OPEN ACCESS Freely available online

PLoS one

The Combination of RAD001 and NVP-BEZ235 Exerts Synergistic Anticancer Activity against Non-Small Cell Lung Cancer *In Vitro* and *In Vivo*

Cheng-Xiong Xu, Yikun Li, Ping Yue, Taofeek K. Owonikoko, Suresh S. Ramalingam, Fadlo R. Khuri, Shi-Yong Sun*

Department of Hematology and Medical Oncology, Emory University School of Medicine and Winship Cancer Institute, Atlanta, Georgia, United States of America

Abstract

The phosphoinositide 3-kinase (PI3K)-mammalian target of rapamycin (mTOR) signaling axis has emerged as a novel target for cancer therapy. Agents that inhibit PI3K, mTOR or both are currently under development. The mTOR allosteric inhibitor, RAD001, and the PI3K/mTOR dual kinase inhibitor, BEZ235, are examples of these agents. We were interested in developing strategies to enhance mTOR-targeted caner therapy. In this study, we found that BEZ235 alone effectively inhibited the growth of rapamycin-resistant cancer cells. Interestingly, the combination of sub-optimal concentrations of RAD001 and BEZ235 exerted synergistic inhibition of the growth of human lung cancer cells along with induction of apoptosis and G1 arrest. Furthermore, the combination was also more effective than either agent alone in inhibiting the growth of lung cancer xenografts in mice. The combination showed enhanced effects on inhibiting mTOR signaling and reducing the expression of c-Myc and cyclin D1. Taken together, our results suggest that the combination of RAD001 and BEZ235 is a novel strategy for cancer therapy.

Citation: Xu C-X, Li Y, Yue P, Owonikoko TK, Ramalingam SS, et al. (2011) The Combination of RAD001 and NVP-BEZ235 Exerts Synergistic Anticancer Activity against Non-Small Cell Lung Cancer *In Vitro* and *In Vivo*. PLoS ONE 6(6): e20899. doi:10.1371/journal.pone.0020899

Editor: Gen Sheng Wu, Wayne State University, United States of America

Received March 31, 2011; **Accepted** May 12, 2011; **Published** June 14, 2011

Funding: This study was supported by the Georgia Cancer Coalition Distinguished Cancer Scholar award, NIH R01 CA118450 and P01 CA116676 (Project 1), Department of Defense IMPACT (Imaging and Molecular Markers for Patients with Lung Cancer: Approaches with Molecular Targets, Complementary/Innovative Treatments, and Therapeutic Modalities) award W81XWH-05-0027 (Project 5), BATTLE (Biomarker-based Approaches of Targeted Therapy for Lung Cancer Elimination) award W81XWH-06-1-0303 (Project 4) and BESCT (Biology, Education, Screening, Chemoprevention and Therapy) award DAMD17-01-1-0689 (Project 2). The funders had no role in study design, data collection and analysis, decision to publish, or preparation of the manuscript.

Competing Interests: The authors have declared that no competing interests exist.

* E-mail: ssun@emory.edu

Introduction

K-Ras, LKB1 and epidermal growth factor receptor (EGFR) are frequently mutated in non-small cell lung cancer (NSCLC). These mutations result in aberrant activation of the phosphoinositide 3-kinase (PI3K)/Akt/mammalian target of rapamycin (mTOR) signaling pathway [1,2,3]. Therefore, the PI3K/Akt/mTOR signaling pathway has emerged as a promising therapeutic target for NSCLC.

RAD001 (Everolimus) is a derivative of rapamycin and is functionally similar to rapamycin as an allosteric inhibitor of mTOR. In patients with advanced renal cell cancer previously treated with VEGF targeted agents, RAD001 improves progression-free survival and has therefore been approved by the US Food and Drug Administration for this indication [4]. It has also been found to improve progression-free survival in patients with neuroendcorine cancers of the pancreas. In many other solid organ malignancies, RAD001 and other rapamycin analogues (rapalogs) the rapalogs exert modest anti-cancer effects, that though promising, are not sufficient to warrant monotherapy with these agents [5].

Recent efforts to improve the efficacy of the rapalogs have focused on developing novel combination strategies. NVP-BEZ235 (BEZ235) is a novel and orally administered dual PI3K and mTOR kinase inhibitor. This compound is a potent, reversible inhibitor of both class I PI3K and mTOR kinase catalytic activity by competing at their ATP-binding site [6]. BEZ235 is currently under evaluation in phase I/II clinical trials. In preclinical studies, BEZ235 induces striking anti-proliferative effects both in transgenic mice with oncogenic K-Ras-induced NSCLC and in NSCLC cell lines expressing oncogenic K-Ras. Moreover, it effectively sensitizes NSCLC cell lines expressing oncogenic K-Ras to the pro-apoptotic effects of ionizing radiation both *in vitro* and *in vivo* [7]. When BEZ235 was combined with a MEK inhibitor, marked synergy was achieved in shrinking K-Ras mutant murine lung cancers [8].

Like rapamycin, RAD001 causes Akt activation in human cancer cells including NSCLC cells while inhibiting the mTOR signaling [9]. We recently reported on the enhanced efficacy of the combination of RAD001 with a PI3K inhibitor on the growth of NSCLC cells both *in vitro* and *in vivo* [9]. Interestingly, BEZ235 could overcome rapamycin resistance as it effectively inhibited the growth of rapamycin- or RAD001-resistant NSCLC cells. Therefore we evaluated the effects of the combination of RAD001 and BEZ235 on the growth of NSCLC cells and found that the combination was more effective than either agent alone in inhibiting the growth of NSCLC cells both *in vitro* and *in vivo*. This report will primarily document our research findings in this regard.

Materials and Methods

Reagent

RAD001 and BEZ235 were supplied by Novartis Pharmaceuticals Corporation (East Hanover, NJ), dissolved in DMSO and stored at −80°C. Rabbit polyclonal anti-actin antibody was purchased from Sigma Chemical Co. (St. Louis, MO). Antibodies against Akt, p-Akt (S473), p-S6 (S235/S236), S6, p-4EBP1 (S65) p-4EBP1 (Thr37/46), 4EBP1, eIF4G, eIF4E, and poly(ADP-ribose)polymerase (PARP), respectively, were purchased from Cell Signaling Technology, Inc. (Beverly, MA). Goat polyclonal mTOR (FRAP; N-19) and mouse monoclonal c-Myc (9E10) antibodies were purchased from Santa Cruz Biotechnology, Inc. (Santa Cruz, CA), respectively. Rabbit polyclonal Rictor (BL2178) antibody was purchased from Bethyl Laboratories, Inc. (Montgomery, TX). Mouse monoclonal cyclin D1 antibody was purchased from Dako (Carpinteria, CA).

Cell Lines and Cell Culture

The human NSCLC cell lines A549, H460 and H157 were described previously [10]. HCC827 was purchased from the American Type Culture Collection ATCC (Manassas, VA). Rapamycin-resistant A549 cell line (A549-RR) was established previously [9]. These cell lines were grown in monolayer culture in RPMI 1640 medium supplemented with 5% fetal bovine serum (FBS) at 37°C in a humidified atmosphere consisting of 5% CO_2 and 95% air.

Growth Inhibition Assay

Cells were cultured in 96-well cell culture plates and treated the next day with the agents indicated. Viable cell number was estimated using the sulforhodamine B (SRB) assay, as previously described [10]. Combination index (CI) for drug interaction (e.g., synergy) was calculated using the CompuSyn software (ComboSyn, Inc.; Paramus, NJ).

Colony Formation Assay

The effects of the given drugs on colony formation on plates were measured as previously described [11].

Detection of Apoptosis

Apoptosis was evaluated by Annexin V staining using Annexin V-PE apoptosis detection kit purchased from BD Biosciences (San Jose, CA) according to the manufacturer's instructions.

Western Blot Analysis

Preparation of whole cell protein lysates and Western blot analysis were described previously [12,13].

m^7GTP Pull-down for Analysis of eIF4F Complex Formation

eIF4F complex in cell extracts was detected using affinity chromatography m^7GTP-Sepharose as described previously [14].

Detection of mTOR complexes (mTORCs)

mTORCs including mTORC1 and mTORC2 were immunoprecipitated with goat polyclonal mTOR (FRAP; N-19) antibody and followed with Western blotting to detect mTOR, raptor and rictor, respectively, as described previously [9].

Lung Cancer Xenografts and Treatments

Animal experiments were approved by the Institutional Animal Care and Use Committee (IACUC) of Emory University. The protocol number is 222-2008. Five- to 6-week old female athymic (nu/nu) mice were ordered from Taconic (Hudson, NY) and housed under pathogen-free conditions in microisolator cages with laboratory chow and water *ad libitum*. A549 cells at 5×10^6 in serum-free medium were injected s.c. into the flank region of nude mice. When tumors reached a size of approximately 100 mm^3, the mice were randomized into four groups (n = 6/group) according to tumor volumes and body weights for the following treatments: vehicle control, BEZ235 (20 mg/kg/day, og), RAD001 (3 mg/kg/day; og), and their combination. Tumor volumes were measured using caliper measurements once every two days and calculated with the formula $V = \pi(\text{length}\times\text{width}^2)/6$.

Statistic Analysis

The statistical significance of differences between two groups or among multiple groups was analyzed with two-sided unpaired Student's *t* tests (for equal variances) or with Welch's corrected *t* test (unequal variances) or one-way analysis of variance (ANOVA) by use of Graphpad InStat 3 software. Results were considered to be statistically significant at $P<0.05$.

Results

BEZ235 Effectively Inhibits the Growth of Rapamycin-resistant NSCLC Cells

In a prior study, we established a rapamycin-resistant cell line (i.e., A549-RR). This cell line is also resistant to RAD001 [9]. We anticipated that this cell line would be, at least in part, resistant to BEZ235 since it is a PI3K and mTOR dual inhibitor. Unexpectedly, BEZ235 demonstrated potent inhibition of the growth of A549-RR cells (Fig. 1A). Moreover, BEZ235 also induced apoptosis in A549-RR cells (Fig. 1B). In fact, the induction of apoptosis and growth inhibition with BEZ235 was slightly more effective in A549-RR cell than in the parent A549 cells (Fig. 1). Thus, rapamycin-resistant cells do not show cross-resistance to BEZ235.

The Combination of RAD001 and BEZ235 Synergistically Inhibits the Growth of NSCLC Cells along with Induction of Apoptosis and G1 arrest

We previously demonstrated that the combination of rapamycin or RAD001 with the PI3K inhibitor LY294002 resulted in enhanced growth-inhibitory effects against NSCLC cells both *in vitro* and *in vivo* [9,15]. We have now studied whether the combination of BEZ235 and RAD001 exerts augmented anti-cancer activity in NSCLC cells. Unexpectedly, we found that the combination of low concentrations of BEZ235 and RAD001 was much more potent than each single agent in inhibiting the growth of several NSCLC cell lines (e.g., A549, H460, H157 and HCC827). The CIs for most combinations were <1 (Fig. 2A, right panels), indicating synergistic effects on inhibiting the growth of NSCLC cells. In agreement, the combination of BEZ235 and RAD001 was significantly more potent than each single agent in inducing apoptosis (Fig. 2B) and G1 arrest (Fig. 2C) ($P<0.001$). Thus, enhanced induction of both apoptosis and cell cycle arrest contributes to augmented growth-inhibitory effects induced by the combination.

The Combination of RAD001 and BEZ235 Effectively Inhibits the Formation and Growth of NSCLC Cell Colonies

We further determined the long-term effects of the combination of RAD001 and BEZ235 on the growth of NSCLC cells in a colony formation assay. This assay allows us to repeat the treatments for a long time (e.g., 12 days). RAD001 at a dose of 1 nM and BEZ235 at 5 nM alone had minimal effect on suppression of colony formation

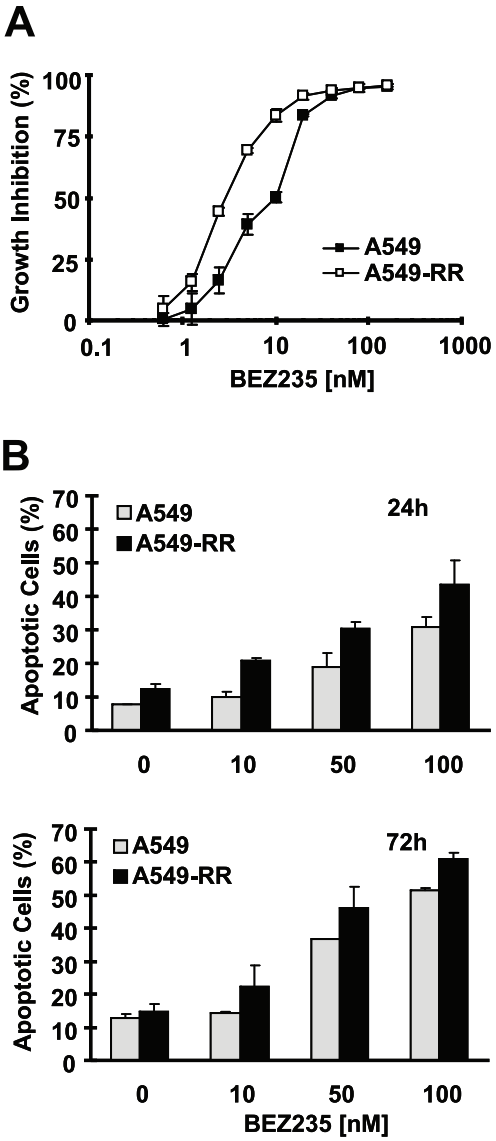

Figure 1. BEZ235 is effective in inhibiting the growth (*A*) and inducing apoptosis (*B*) of rapamycin-resistant cells. *A*, The indicated cell lines were seeded in 96-well plates and then treated with different concentrations of BEZ235 as indicated on the second day. After 3 days, the cell numbers were estimated using SRB assay. Points, means of four replicate determinations; bars, ± SD. *B*, The indicated cell lines were plated in 6-well plates and then treated next day with different concentrations of BEZ235 as indicated. After 24 and 72 h, the cells were harvested and subjected to detection of apoptosis using Annexin V staining. Columns, means of duplicate determinations; bars, ± SD.

doi:10.1371/journal.pone.0020899.g001

of the NSCLC cells; however the combination either eliminated the colony formation (e.g., A549) or drastically reduced the colony numbers (e.g., H460 and H157) (Fig. 3). Thus, it is clear that the combination is much more effective than either single agent in inhibiting the colony formation and growth of NSCLC cells ($P<0.001$). We also compared the effect of sequence of administration of the two agents on colony formation of NSCLC cells. Under the same experimental conditions described above, sequential treatments with RAD001 first followed by BEZ235 treatment (RAD001→BEZ235) or BEZ235 first followed by RAD001 treatment (BEZ235→RAD001) showed effects comparable to each alone with minimal suppression of the growth of NSCLC cell colonies. The concurrent combination of RAD001 and BEZ235 was much more potent than either sequential treatment in inhibiting the formation and growth of NSCLC colonies ($P<0.001$) (Fig. 2). Therefore, concurrent administration of RAD001 and BEZ235 is clearly superior to sequential treatments in inhibiting the growth of NSCLC cell colonies.

We further compared the effects of the combination of RAD001 and LY294002 with sequential treatments on colony formation of NSCLC cells. Consistently, the concurrent combination treatment, but not the sequential treatment either with RAD001 first followed by LY294002 or with LY294002 followed by RAD001, generated augmented effects on inhibiting the colony formation of NSCLC cells (Fig. S1).

The Combination of RAD001 and BEZ235 Exerts Augmented Activity against the Growth of NSCLC Xenografts in Nude Mice

Because of the promising growth-inhibitory effects of the RAD001 and BEZ235 combination in NSCLC cells *in vitro*, we then validated the efficacy of the combination against the growth of NSCLC tumors in mice. Both RAD001 and BEZ235 partially, but significantly, inhibited the growth of A549 xenografts ($P<0.01$); however the combination of RAD001 and BEZ235 was significantly more potent than each single agent in inhibiting the growth of the xenografts as measured by both tumor sizes and weights ($P<0.01$) (Figs. 4A and 4B). These *in vivo* data further demonstrate that the combination of RAD001 and BEZ235 displays augmented anticancer activity. We observed a higher degree of weight loss in mice treated with the combination (up to 19% of control mice) especially during the early treatment period. The weight difference at the end of the experiment improved to only 13% of control (Fig. 4C), suggesting possible adaptation and better tolerance of the combination treatment,

The Combination of RAD001 and BEZ235 Exerts Enhanced Effects on Suppression of the mTOR signaling and Downregulation of c-Myc and Cyclin D1

To gain insight into the mechanisms by which the combination of RAD001 and BEZ235 exert enhanced anticancer activity, we analyzed the effects of the combination on mTOR signaling and on the expression of its regulated proteins in comparison with either agent alone. At the tested doses, BEZ235 had a minimal effect on reduced p-S6 levels, but no effect on the levels of p-4EBP1 (both S65 and T37/46), c-Myc and cyclin D1. In fact, we observed increased levels of 4EBP1 (T37/46) (in both A549 and H157) and c-Myc (e.g., in H157). RAD001 at 2 nM strongly inhibited S6 and 4EBP1 (S65) phosphorylation, but did not reduce the levels of p-4EBP1 (T37/46), c-Myc and Cyclin D1. Similar to BEZ235, RAD001 also increased the levels of p-4EBP1 (T37/46) and c-Myc in both A549 and H157 cells. However the combination of RAD001 and BEZ235 either abrogated the increase in p-4EBP1 (T37/46) (e.g., in A549 cells) induced by the single agent or exerted enhanced effect on reducing p-4EBP1 (T37/46) levels (e.g., in H157 cells). Importantly, the combination of RAD001 and BEZ235 had augmented effects on decreasing the levels of c-Myc and cyclin D1 in both A549 and H157 cells in comparison with each single agent alone (Fig. 5).

RAD001 increased Akt phosphorylation in both A549 and H157 cell lines as we previously reported [9]. Interestingly, at low doses, BEZ235 also increased p-Akt levels. The presence of BEZ235 at the tested dose ranges either weakly reduced the levels of p-Akt induced by RAD001 (e.g., in A549 cells) or did not affect

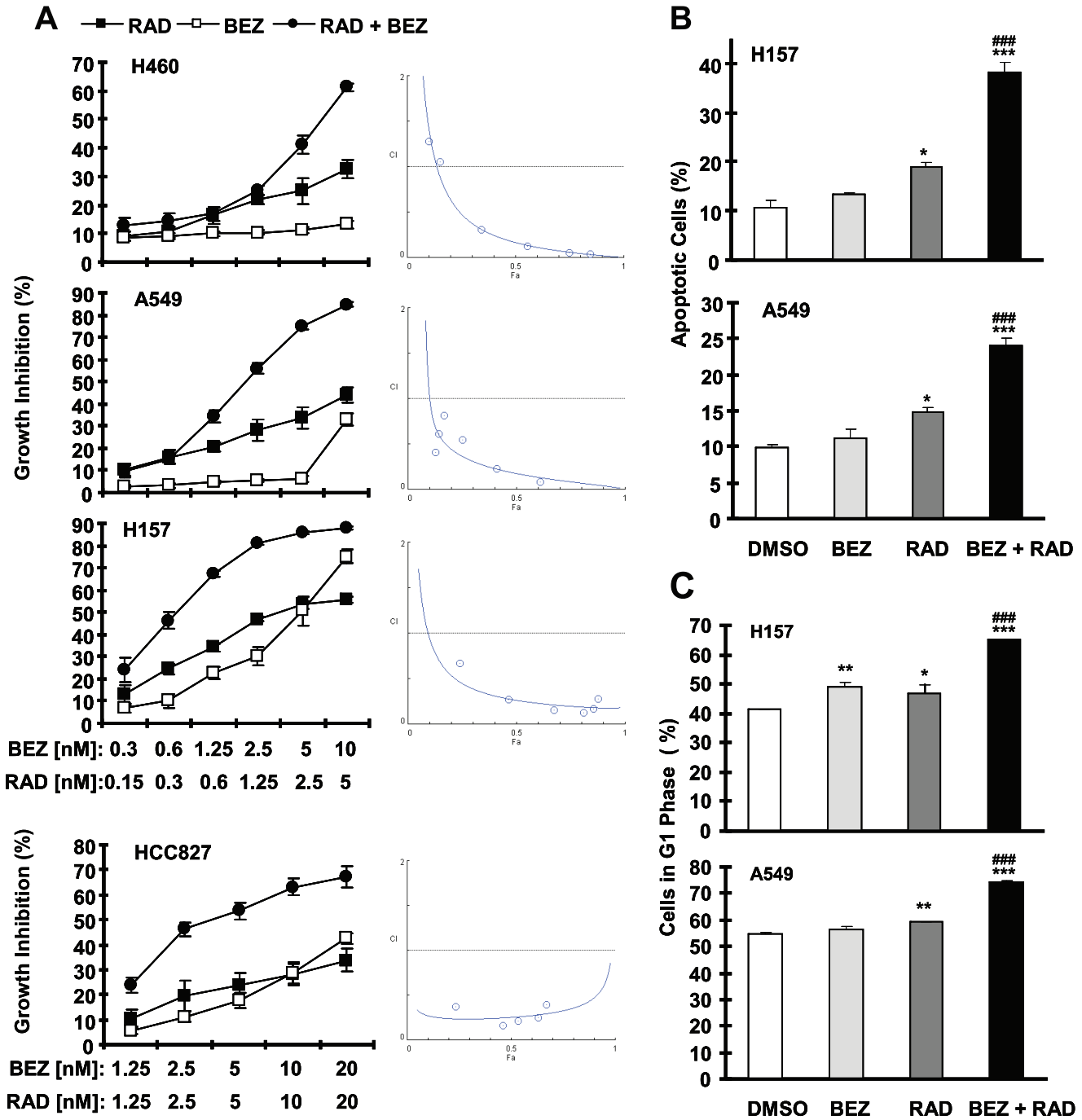

Figure 2. The combination of BEZ235 and RAD001 synergistically inhibits cell growth (*A*) and induces apoptosis (*B*) and cell cycle arrest (*C*) in NSCLC cells. *A*, the indicated cell lines were seeded in 96-well plates and then treated next day with different concentrations of BEZ235 (BEZ), RAD001 (RAD) and their respective combinations as indicated. After 3 days, the cell numbers were estimated using the SRB assay and CIs were calculated with CompuSyn software (right panels). Points, means of four replicate determinations; bars, ± SD. *B* and *C*, The indicated cell lines were seeded in 6-well plates and then treated with 10 nM BEZ235 alone, 2 nM RAD001 alone, and their combination. After 48 h, the cells were harvested for detection of apoptosis using Annexin V staining (*A*) and for cell cycle analysis with a flow cytometry (*C*). Columns, means of duplicate determinations; Bars, ± SD. *, $P<0.05$, ** $P<0.01$, and ***, $P<0.001$ compared with DMSO control; ###, $P<0.001$ compared with RAD001 or BEZ235 alone.

doi:10.1371/journal.pone.0020899.g002

RAD001-induced increase in p-Akt (e.g., in H157 cells) (Fig. 5). Thus, it seems that the RAD001 and BEZ235 combination can display enhanced effects on suppressing the mTOR signaling and the expression of its regulated proteins with limited or no inhibitory effects on Akt phophorylation.

The Combination of RAD001 and BEZ235 Exerts Enhanced Effects on Suppressing eIF4F Assembly

Since mTOR signaling is known to positively regulate cap-dependent translation initiation, we further analyzed the effects of

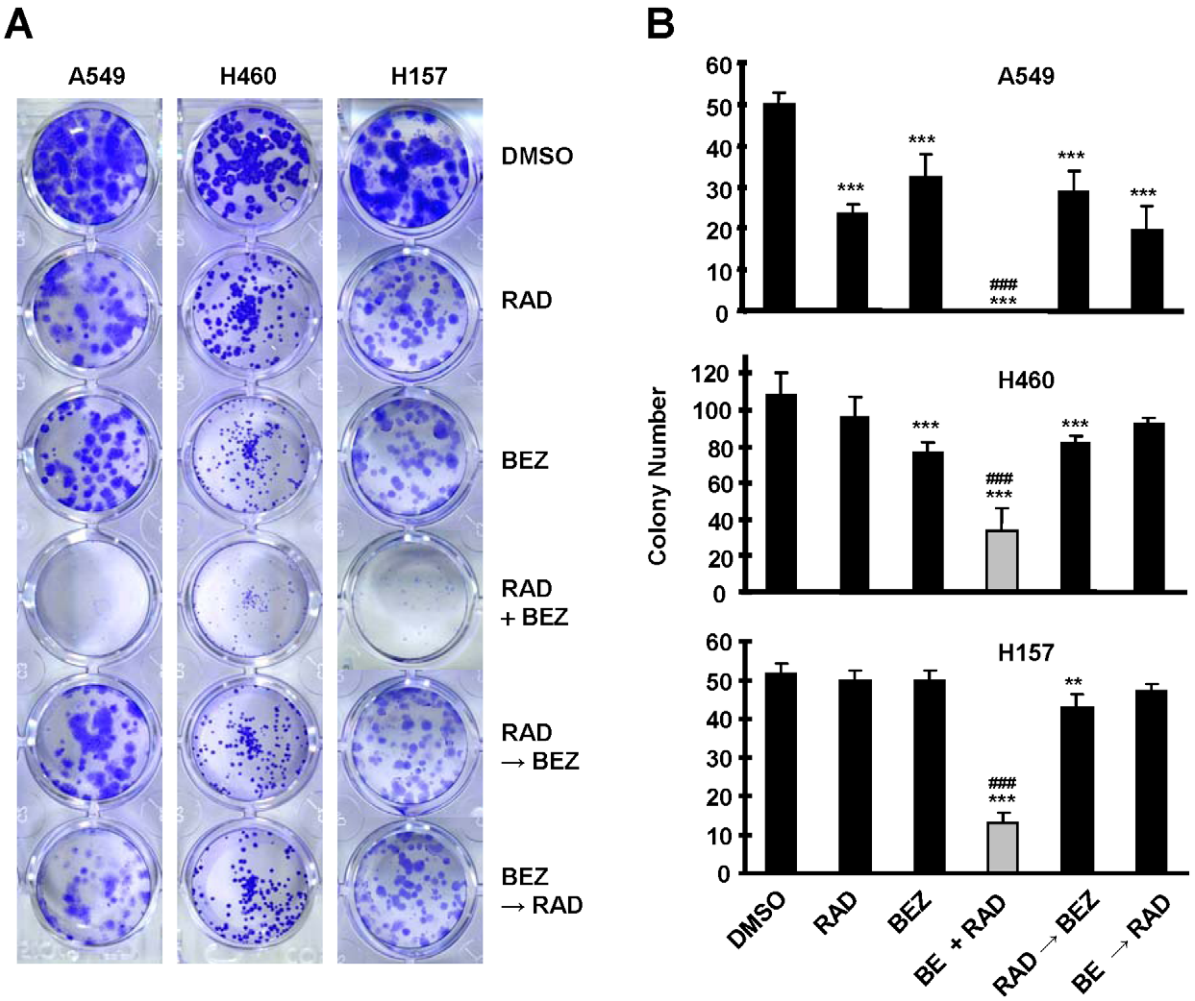

Figure 3. The concurrent combination of BEZ235 and RAD001 effectively inhibits colony formation ands growth of NSCLC cell. The indicated cell lines at a density of approximately 200 cells/well were seeded in 24-well plates. On the second day, the cells were treated with 1 nM RAD001 (RAD), 5 nM BEZ235 (BEZ) or their concurrent combinations (RAD+BEZ). The cells were also treated with 1 nM RAD001 for 6 days followed with 5 nM BEZ235 for another 6 days (RAD→BEZ) or with 5 nM BEZ for 6 days followed with 1 nM RAD001 for another 6 days (BEZ→RAD). After 12 days, the plates were stained for the formation of cell colonies with crystal violet dye. The picture of the colonies was then taken using a digital camera (*A*) and the colony numbers were counted (*B*). ***, $P<0.001$ compared with DMSO control; ###, $P<0.001$ compared with all other treatments.
doi:10.1371/journal.pone.0020899.g003

RAD001 and BEZ235 combination on the cap binding of eIF4E and eIF4G (e.g., eIF4F assembly) with the m^7GTP-Sepharose pull down assay. As presented in Fig. 5B, RAD0001 and BEZ235 alone reduced the amounts of eIF4G that interacted with eIF4E. However, the combination of RAD001 and BEZ235 was much more effective that either agent alone in decreasing the amounts of eIF4G binding to eIF4E. Theses results clearly indicate that the combination of RAD001 and BEZ235 exerts enhanced effects on suppressing the cap binding of eIF4E and eIF4G or eIF4F assembly.

The Combination of RAD001 and BEZ235 Does not Exhibit Enhanced Effects on Inhibiting the Assembly of mTORCs

It is known that the assembly or association of the mTOR with its partners (e.g., raptor and rictor) is essential for distinct enzyme activities and biological functions. RAD001, like rapamycin, suppresses mTOR signaling by inhibiting the assembly of the mTORCs [16]. Thus, we further determined whether the combination of RAD001 and BEZ235 exerted enhanced inhibitory effects on the assembly of the mTORCs including mTORC1 (mTOR/raptor) and mTORC2 (mTOR/rictor). To this end, we did immunoprecipitation (IP) with anti-mTOR antibody to pull down both mTORC1 and mTORC2 and then followed with Western blotting to detect raptor and rictor in the immunoprecipitates. As presented in Fig. 6, BEZ235 had minimal effects on reducing the levels of raptor and rictor in the immunoprecipitates, whereas RAD001 substantially reduced the levels of both raptor and rictor pulled down by mTOR antibody. The combination of RAD001 and BEZ235 had similar potency to RAD001 alone in reduction of the levels of raptor and rictor in the immunoprecipitates, indicating that the combination does not exhibit enhanced effects on inhibiting the assembly of mTORC1 and mTORC2.

Discussion

Development of rapamycin resistance is a critical issue in the treatment of cancer with rapamycin and its analogues [17].

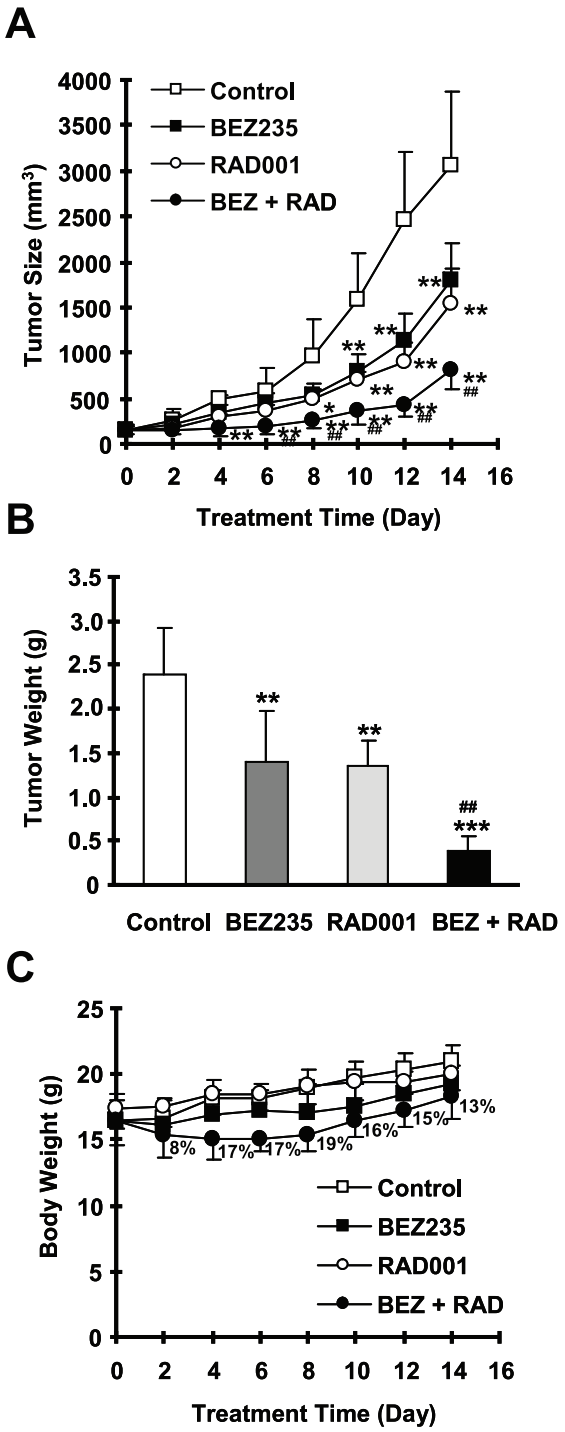

Figure 4. The combination of BEZ235 and RAD001 is significantly more effective than each single agent in suppressing the growth of NSCLC xenografts. A549 xenografts were treated (once a day) with vehicle control, RAD001 (3 mg/kg, og), BEZ235 (20 mg/kg, og) and their combination (BEZ+RAD) starting on the same day after grouping. Tumor sizes (*A*) and body weight (*C*) were measured once every two days. After 14 days, the mice were sacrificed and the tumors were removed and weighed (*B*). Each measurement is a mean ± SD (n = 6). The numbers in *C* represent body weight loss in the combination group compared with control group. * $P<0.05$ compared with vehicle control; ** $P<0.01$ compared with vehicle control; *** $P<0.001$ compared with vehicle control; ## $P<0.01$ compared with RAD001 or with BEZ235.
doi:10.1371/journal.pone.0020899.g004

BEZ235 is a PI3K and mTOR dual kinase inhibitor [6]. Our study demonstrated that BEZ235 inhibited the growth of rapamycin-resistant cells and induced apoptosis as effectively as it did in the matched parent cells. In fact, rapamycin-resistant cells were slightly more sensitive than their parental cells to BEZ235 (Fig. 1). These data suggest that rapamycin-resistant cells are not cross-resistant to BEZ235. Since this cell line had been shown to be fully resistant to RAD001, our findings suggest that BEZ235 inhibits the growth of cancer cells through different mechanisms from those that mediate the actions of rapalogs. It will be interesting to know if BEZ235 possess additional mechanism beyond dual inhibition of PI3K and BEZ235. Beside, our data also imply that BEZ235 can be used to overcome rapamycin resistance.

Although BEZ235 inhibits both PI3K and mTOR, in combination with RAD001, it exerts synergistic effects in inhibiting the growth of a panel of NSCLC cells as demonstrated in a 3-day monolayer culture (with the SRB assay) and in a long-term 12 days colony formation assay (Figs. 2 and 3). This synergy is likely due to enhanced effects on induction of cell cycle G1 arrest and apoptosis (Fig. 2). In agreement, the combination of RAD001 and BEZ235 was significantly more effective than either agent in inhibiting the growth of NSCLC xenografts in nude mice (Fig. 4). In the animal study, we noted that the combination initially caused significant loss of body weight (up to 19% of control); however, at the end of the experiment, mice receiving the combination treatment seemed to recover some of the weight loss (13% of control). This suggests that the mice can adapt and eventually tolerate the treatment with the combination of RAD001 and BEZ235. Nonetheless, we should aware potential enhanced adverse effects caused by the combination while the combination shows promising synergistic anticancer activity.

Treatment schedules may impact the final outcome of the given combinational therapy. In this study, we found that the sequential treatments with RAD001 followed by BEZ235 or with BEZ235 followed by RAD001 minimally inhibited the growth of NSCLC colonies; in contrast, the concurrent treatment of RAD001 and BEZ235 substantially inhibited growth of NSCLC colonies or eliminated the colony formation (Fig. 3). This is also true for the combination of rapamycin and LY294002 (Fig. S1). Our data suggests that the concurrent combination of RAD001 and BEZ235 may be optimal for further development of this combination.

The IC_{50}s (concentrations of inhibiting 50% cell growth) of BEZ235 in human NSCLC cells range from 10 nM to 100 nM (our unpublished data). In our combination experiments, we typically used low dose ranges of BEZ235 (e.g., 1–10 nM). At these doses, BEZ235 had a weak inhibitory effect on p-S6 phosphorylation but did not modulate p-4EBP1 phosphorylation or the levels of c-Myc and cyclin D1. At a dose of 2 nM, RAD001 effectively inhibited the phosphorylation of S6 and 4EBP1 (S65), but did not suppress 4EBP1 phosphorylation (T37/46) and c-Myc and cyclin D1 expression. However, the combination of RAD001 and BEZ235 effectively inhibited p-4EBP1 phosphorylation (at T37/46) and reduced the levels of c-Myc and cyclin D1 (Fig. 5A). Moreover, we showed that the combination of RAD001 and BEZ235 was much more potent than either single agent in inhibiting the cap binding of eIF4E and eIF4E or eIF4F assembly (Fig. 5B), implying that the combination exerts enhanced inhibitory effect on cap-dependent initiation. Since c-Myc and cyclin D1 are known to be regulated by the mTOR signaling through cap-dependent protein translation [18], our data indicate that the combination of RAD001 and BEZ235 exerts enhanced effect on inhibiting the mTOR signaling and the expression of its regulated oncogenic proteins (e.g., c-Myc and cyclin D1). This

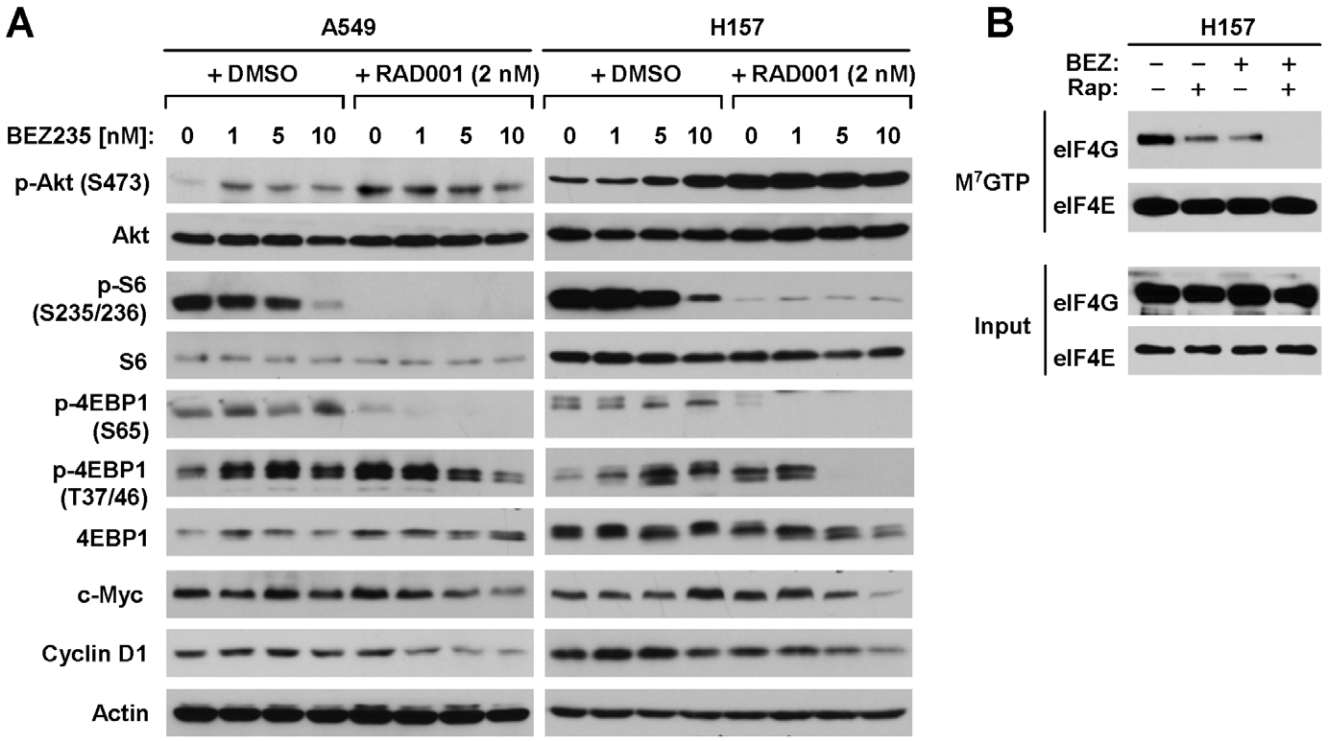

Figure 5. Effects of BEZ235 and RAD001 combination on the mTOR signaling (A), on the expression of mTOR-regulated proteins (A) and on the assembly of eIF4F complex (B). *A*, The indicated cell lines were plated in 10 cm-diameter cell culture dishes and treated next day with the given concentrations of BEZ-235 in the absence and presence of RAD001 for 24 h. The cells were then harvested for preparation of whole-cell protein lysates and subsequent Western blot analysis to detect the indicated proteins. *B*, The indicated cell lines were treated with 2 nM RAD001, 10 nM BEZ235 or their combination. After 24 h, the cells were harvested for preparation of whole-cell protein lysates and subsequent m^7GTP pull-down assay followed with Western blot analysis to detect the given proteins.
doi:10.1371/journal.pone.0020899.g005

effect may contribute to the synergistic activity against the growth of NSCLC cells *in vitro* and *in vivo* by the combination of RAD001 and BEZ235.

In this study, RAD001 increased Akt phosphorylation in both in A549 and H157 cells; this is in agreement with our previous reports [9]. At the concentrations tested (e.g., 1–10 nM), BEZ235 increased p-Akt levels as well. This observation is consistent with a previous report, in which BEZ235 was shown to increase Akt phosphorylation at low doses (e.g., 10 nM) [19]. It had been previously shown that higher concentrations of BEZ235 are needed (e.g., >100 nM) to inhibit Akt compared with that (e.g., >10 nM) required for inhibiting S6 phosphorylation [19]. Thus, it appears that BEZ235 primarily possesses mTOR-inhibitory activity at the low concentrations ranges. Accordingly, it is understandable that BEZ235 at low concentration ranges increases Akt phosphorylation as would be expected of a rapalog [9,15]. Interestingly, the combination of RAD001 and BEZ235 did not reduce p-Akt levels, which were as high as those in cells treated with RAD001 or BEZ235 alone (Fig. 5). Given that the combination of RAD001 and BEZ235 effectively inhibits the growth of NSCLC cells as discussed above, it appears that the combination of RAD001 and BEZ235 can exert enhanced anticancer activity with elevated levels of p-Akt.

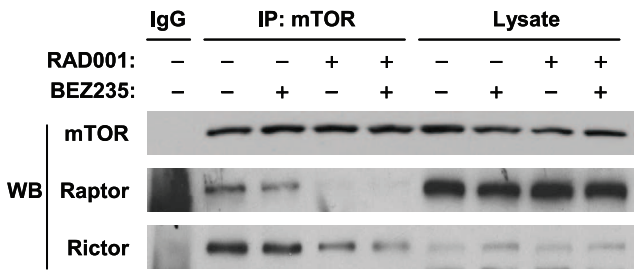

Figure 6. The combination of RAD001 and BEZ235 does not enhance disruption of mTORC assembly. A549 cells were treated with 2 nM RAD001, 10 nM BEZ235 or their combination. After 24 h, the cells were harvested for preparation of whole-cell protein lysates and subsequent IP-Western blotting.
doi:10.1371/journal.pone.0020899.g006

mTOR exerts its critical roles in promoting cell cycle progression and cell proliferation primarily through interactions with other proteins such as raptor (forming mTORC1) and rictor (forming mTORC2) [18,20]. mTORC2 is generally thought to be insensitive to rapalogs [18]. However, prolonged treatment with these mTOR inhibitors disrupts the assembly of the mTORC2 as demonstrated by us [9] and others [21]. In this study, after a 24 h treatment, RAD001, but not BEZ235, effectively inhibit the assembly or activity of both mTORC1 and mTORC2. The combination of RAD001 and BEZ235 did not further reduce the levels of raptor and rictor in the immunoprecipitates (Fig. 6), demonstrating that the combination does not display enhanced effects on inhibiting the assembly of mTORCs. Based on these observations, we speculate that the enhanced effects on suppression of the mTOR signaling by the combination is likely due to their distinctive effects on inhibiting the mTORC assembly and mTOR kinase activity. It is generally believe that a synergy is achieved through a corporation of two drugs functioning via

distinct mechanisms. Since BEZ235 effectively inhibits the growth of the rapamycin-resistant cells, it is also possible that the synergy between RAD001 and BEZ235 against the growth of lung cancer cells occurs through an unknown mechanism of BEZ235, which needs further investigation.

In summary, the current study has demonstrated that the combination of RAD001 and the PI3K/mTOR inhibitor BEZ235 exhibits synergistic inhibition on the growth of NSCLC cells *in vitro* and *in vivo* and thus represents a novel strategy to enhance the efficacy of mTOR-targeted cancer therapy. Our findings provide the rationale to evaluate this combination in clinical trials for patients with rapalog-sensitive and refractory malignancies.

Supporting Information

Figure S1 Concurrent combination of rapamycin and LY294002 is more effective than sequential treatments in inhibiting the formation and growth of NSCLC colonies. The indicated cell lines at a density of approximately 200 cells/well were seeded in 24-well plates. On the second day, cells were treated with 1 nM rapamycin (Rap) alone, 5 nM LY294002 (LY) alone, concurrent combination of rapamycin and LY294002 (Rap+LY), rapamycin for 3 days and then switched to LY294002 treatment (Rap→LY), LY294002 for 3 days and then switched to rapamycin treatment (LY→Rap). The same cycles of the treatments were repeated every 3 days. After 12 days, the plates were stained for the formation of cell colonies with crystal violet dye. The picture of the colonies was then taken using a digital camera (A) and the colonies were counted (*B*).
(PDF)

Acknowledgments

T.K.O., S.S.R., F.R.K. and S-Y.S. are Georgia Cancer Coalition Distinguished Cancer Scholars.

Author Contributions

Conceived and designed the experiments: C-XX S-YS. Performed the experiments: C-XX YL PY. Analyzed the data: C-XX S-YS. Contributed reagents/materials/analysis tools: TKO SSR FRK. Wrote the paper: TKO SSR FRK S-YS.

References

1. Shaw RJ, Bardeesy N, Manning BD, Lopez L, Kosmatka M, et al. (2004) The LKB1 tumorsuppressor negatively regulates mTOR signaling. Cancer Cell 6: 91–99.
2. Makowski L, Hayes DN (2008) Role of LKB1 in lung cancer development. Br J Cancer 99: 683–688.
3. Ding L, Getz G, Wheeler DA, Mardis ER, McLellan MD, et al. (2008) Somatic mutations affect key pathways in lung adenocarcinoma. Nature 455: 1069–1075.
4. Motzer RJ, Escudier B, Oudard S, Hutson TE, Porta C, et al. (2008) Efficacy of everolimus in advanced renal cell carcinoma: a double-blind, randomised, placebo-controlled phase III trial. Lancet 372: 449–456.
5. Abraham RT, Gibbons JJ (2007) The mammalian target of rapamycin signaling pathway: twists and turns in the road to cancer therapy. Clin Cancer Res 13: 3109–3114.
6. Maira SM, Stauffer F, Brueggen J, Furet P, Schnell C, et al. (2008) Identification and characterization of NVP-BEZ235, a new orally available dual phosphatidylinositol 3-kinase/mammalian target of rapamycin inhibitor with potent in vivo antitumor activity. Mol Cancer Ther 7: 1851–1863.
7. Konstantinidou G, Bey EA, Rabellino A, Schuster K, Maira MS, et al. (2009) Dual phosphoinositide 3-kinase/mammalian target of rapamycin blockade is an effective radiosensitizing strategy for the treatment of non-small cell lung cancer harboring K-RAS mutations. Cancer Res 69: 7644–7652.
8. Engelman JA, Chen L, Tan X, Crosby K, Guimaraes AR, et al. (2008) Effective use of PI3K and MEK inhibitors to treat mutant Kras G12D and PIK3CA H1047R murine lung cancers. Nat Med 14: 1351–1356.
9. Wang X, Yue P, Kim YA, Fu H, Khuri FR, et al. (2008) Enhancing mammalian target of rapamycin (mTOR)-targeted cancer therapy by preventing mTOR/raptor inhibition-initiated, mTOR/rictor-independent Akt activation. Cancer Res 68: 7409–7418.
10. Sun SY, Yue P, Dawson MI, Shroot B, Michel S, et al. (1997) Differential effects of synthetic nuclear retinoid receptor-selective retinoids on the growth of human non-small cell lung carcinoma cells. Cancer Res 57: 4931–4939.
11. Wang X, Hawk N, Yue P, Kauh J, Ramalingam SS, et al. (2008) Overcoming mTOR inhibition-induced paradoxical activation of survival signaling pathways enhances mTOR inhibitors' anticancer efficacy. Cancer Biol Ther 7: 1952–1958.
12. Liu X, Yue P, Zhou Z, Khuri FR, Sun SY (2004) Death receptor regulation and celecoxib-induced apoptosis in human lung cancer cells. J Natl Cancer Inst 96: 1769–1780.
13. Sun SY, Yue P, Wu GS, El-Deiry WS, Shroot B, et al. (1999) Mechanisms of apoptosis induced by the synthetic retinoid CD437 in human non-small cell lung carcinoma cells. Oncogene 18: 2357–2365.
14. Li Y, Yue P, Deng X, Ueda T, Fukunaga R, et al. (2010) Protein phosphatase 2A negatively regulates eukaryotic initiation factor 4E phosphorylation and eIF4F assembly through direct dephosphorylation of Mnk and eIF4E. Neoplasia 12: 848–855.
15. Sun SY, Rosenberg LM, Wang X, Zhou Z, Yue P, et al. (2005) Activation of Akt and eIF4E Survival Pathways by Rapamycin-Mediated Mammalian Target of Rapamycin Inhibition. Cancer Res 65: 7052–7058.
16. Guertin DA, Sabatini DM (2009) The pharmacology of mTOR inhibition. Sci Signal 2: pe24.
17. Huang S, Bjornsti MA, Houghton PJ (2003) Rapamycins: mechanism of action and cellular resistance. Cancer Biol Ther 2: 222–232.
18. Guertin DA, Sabatini DM (2007) Defining the role of mTOR in cancer. Cancer Cell 12: 9–22.
19. Serra V, Markman B, Scaltriti M, Eichhorn PJ, Valero V, et al. (2008) NVP-BEZ235, a dual PI3K/mTOR inhibitor, prevents PI3K signaling and inhibits the growth of cancer cells with activating PI3K mutations. Cancer Res 68: 8022–8030.
20. Wang X, Sun SY (2009) Enhancing mTOR-targeted cancer therapy. Expert Opin Ther Targets 13: 1193–1203.
21. Sarbassov dos D, Ali SM, Sengupta S, Sheen JH, Hsu PP, et al. (2006) Prolonged rapamycin treatment inhibits mTORC2 assembly and Akt/PKB. Mol Cell 22: 159–168.

RESEARCH PAPER

Cancer Biology & Therapy 12:6, 549-555; September 15, 2011; © 2011 Landes Bioscience

Augmentation of NVP-BEZ235's anticancer activity against human lung cancer cells by blockage of autophagy

Cheng-Xiong Xu, Liqun Zhao, Ping Yue, Guofu Fang, Hui Tao, Taofeek K. Owonikoko, Suresh S. Ramalingam, Fadlo R. Khuri and Shi-Yong Sun*

Department of Hematology and Medical Oncology; Emory University School of Medicine and Winship Cancer Institute; Atlanta, GA USA

Key words: BEZ235, PI3K, mTOR, autophagy, apoptosis, lung cancer

Autophagy is a cellular lysosomal degradation pathway essential for regulation of cell survival and death to maintain homeostasis. This process is negatively regulated by mammalian target of rapamycin (mTOR) signaling and often counteracts efficacy of certain cancer therapeutic agents. NVP-BEZ235 (BEZ235) is a novel, orally bioavailable dual PI3K/mTOR inhibitor that has exhibited promising activity against non-small cell lung cancer (NSCLC) in preclinical models. The current study focuses on evaluating the role of BEZ235 in regulating autophagy. BEZ235 was effective in inhibiting the growth of NSCLC cells including induction of apoptosis. It also potently induced the expression of type-II LC3, indicating induction of autophagy. When BEZ235 was used in combination with the lysosomal or autophagic inhibitor chloroquine (CQ), enhanced inhibitory effects on monolayer growth and colony formation of NSCLC cells was observed. In addition, enhanced induction of apoptosis was also detected in cells exposed to the combination of BEZ235 and CQ. Moreover, the combination of BEZ235 and CQ was more effective than each single agent alone in inhibiting the growth of NSCLC xenografts in nude mice. Thus, induction of autophagy by BEZ235 appears to be a survival mechanism that may counteract its anticancer effects. Based on these, we suggest a strategy to enhance BEZ235's anticancer efficacy by blockade of autophagy.

Introduction

Non-small cell lung cancer (NSCLC) has remained the leading cause of cancer-related deaths and has a poor 5-y survival rate (<16%) despite improvements in therapeutic options.[1] Thus novel agents or efficacious therapeutic regimens are urgently needed.

It is known that phosphoinositide-3-kinase (PI3K)/Akt signaling and its regulated mTOR axis promotes cancer cell proliferation and survival and is often activated in human cancers. Moreover, activation of this signaling pathway is associated with resistance to cytotoxic chemotherapy.[2,3] Therefore, targeting the PI3K/Akt/mTOR signaling pathway has become an attractive therapeutic strategy.[4,5] In NSCLC, the PI3K/Akt/mTOR signaling pathway is aberrantly activated, largely due to frequent mutations of its upstream regulators including K-Ras, LKB1 and epidermal growth factor receptor (EGFR).[6-8] Thus, the PI3K/Akt/mTOR signaling pathway is also a promising therapeutic target for NSCLC.

Consequently, small molecule drugs that target this signaling pathway have been actively developed and tested preclinically and clinically.[5,9,10] One such compound is NVP-BEZ235 (BEZ235), a novel and orally available dual PI3K and mTOR inhibitor. This compound potently and reversibly inhibits both class I PI3K and mTOR kinase catalytic activity by competing at their ATP-binding site.[11] BEZ235 is currently being studied in phase I/II clinical trials. A preclinical study has shown that BEZ235 causes marked tumor regression in mouse lung adenocracinomas initiated by expression of p110-α H1047R, but is ineffective in mutant K-Ras-initiated models unless combined with a MEK inhibitor.[12] In contrast, another recent study has demonstrated that BEZ235 effectively induces a striking growth-inhibitory effect against both oncogeneic K-Ras-induced lung adenocarcinomas in transgenic mice and human NSCLC xenografts harboring K-Ras mutation in nude mice.[13] In certain types of NSCLC (e.g., with EGFR mutation), BEZ235 alone does not induce apoptosis but does so when combined with a MEK inhibitor,[14] suggesting a necessity to combine with other agents to improve its anticancer efficacy.

Autophagy is a cellular lysosomal degradation pathway that is essential for regulation of cells survival and death to maintain cellular homeostasis.[15,16] One of the key regulators of autophagy is mTOR, which is the major inhibitory signal that shuts off autophagy in the presence of growth factors and abundant nutrients.[16] Accordingly, inhibition of mTOR signaling (e.g., by the mTOR inhibitor rapamycin) induces autophagy.[17] Autophagy can be either a pro-survival or death mechanism depending on

*Correspondence to: Shi-Yong Sun; Email: ssun@emory.edu
Submitted: 04/29/11; Revised: 05/23/11; Accepted: 06/08/11
DOI: 10.4161/cbt.12.6.16397

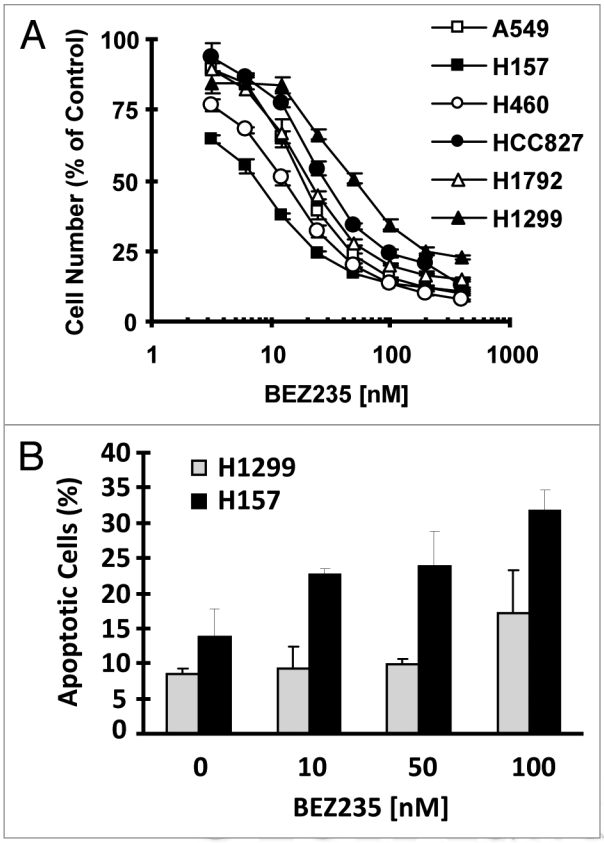

Figure 1. BEZ-235 inhibits cell growth (A) and induces apoptosis (B) in human lung cancer cells. (A) The indicated lung cancer cell lines were seeded in 96-well plates and then treated with different concentrations of BEZ235 as indicated on the second day. After 3 d, the cell numbers were estimated using the SRB assay. Points, means of four replicate determinations; bars, ± SD. (B) The indicated cell lines were plated in 6-well plates and then treated next day with different concentrations of BEZ235 as indicated. After 3 d, the cells were subjected to measurement of apoptosis using Annexin V staining. Columns, means of duplicate measurements; bars ± SD.

the circumstances,[15,16] thus generating variable impact on the outcome of cancer therapy.

In this study, we focused on addressing the role of BEZ235 on the induction of autophagy in human NSCLC cells and determining the impact of autophagy induction on its anticancer activity against NSCLC. We found that BEZ235 induced autophagy while inhibiting the growth of NSCLC cells. When combined with a lysosomal or authophagic inhibitor, the effects of BEZ235 on induction of apoptosis, inhibition of colony formation and suppression of xenografts in nude mice were substantially enhanced.

Results

BEZ235 inhibits cell growth and induces apoptosis in human NSCLC cells. To determine the effects of BEZ235 on the growth of human NSCLC cells, we treated a panel of NSCLC cell lines with various concentrations of BEZ235 (0.5–200 nM) for 3 d and then estimated cell numbers with the SRB assay. All six tested cell lines responded well to BEZ235 treatment. The IC_{50}s of BEZ235 for these cell lines were within the range of 10–50 nM (**Fig. 1A**). Moreover, we determined whether BEZ235 induces apoptosis in NSCLC cells. As presented in **Figure 1B**, BEZ235 induced apoptosis in both H157 and H1299 cells. However, H1299 cells were less sensitive than H157 cell to BEZ235-induced apoptosis. Nearly 10-fold higher concentrations of BEZ235 were required to induce apoptosis in H1299 cells compared with H157 (100 vs. 10 nM). Thus, it appears that NSCLC cell lines have variable sensitivities to undergo BEZ235-induced apoptosis.

BEZ235 inhibits Akt and mTOR signaling in human NSCLC cells. We next determined whether BEZ235 inhibits PI3K/Akt/mTOR signaling pathway in human NSCLC cells. We treated three NSCLC cell lines, H157, H1299 and A549, with increasing concentrations of BEZ235 for 12 h and then harvested the cells for detection of phosphorylation of certain key proteins in the signaling pathway by protein gel blot analysis. As shown in **Figure 2**, BEZ235 reduced the levels of p-Akt, p-4EBP1 and p-S6 in a concentration-dependent manner, indicating that BEZ235 inhibits the PI3K/Akt/mTOR signaling pathway in human NSCLC cells. Interestingly, we noted that BEZ235 at 10 nM increased p-Akt levels in H1299 cells although it inhibited Akt phosphorylation at high concentrations (e.g., 50–100 nM).

BEZ235 induces autophagy in human NSCLC cells. Given the critical role of mTOR in negatively regulating autophagy,[16,17] we then studied whether BEZ235 induces authophagy in human NSCLC cells. By protein gel blotting, we detected increased levels of type II LC3 (LC3-II) expression, a lysosome-bound form of LC3, in cells exposed to BEZ235 (**Fig. 3A**). Moreover, we detected punctate staining of YFP-LC3 in cells infected with lentiviral YFP-LC3 when exposed to BEZ235 ranging from 10–100 nM (**Fig. 3B**), indicating the formation of autophagosomes. Collectively, these data demonstrate that BEZ235 induces autophagy in human NSCLC cells.

Inhibition of autophagy enhances the effects of BEZ235 on suppressing cell growth and induction of apoptosis. Autophagy can be a cell survival or death mechanism.[18] To determine whether induction of autophagy by BEZ235 is a survival or death mechanism, we analyzed the effects of BEZ235 on cell growth and apoptosis in the presence of the lysosomal protease inhibitor chloroquine (CQ) in several human NSCLC cells. As shown in **Figure 4A**, the combination of BEZ235 and CQ was more potent than either agent alone in inhibiting the growth of the NSCLC cells lines ($p < 0.01$ or 0.001). Furthermore, we examined apoptosis in cells exposed to BEZ235 alone, CQ alone and their combination. As presented in **Figure 4B**, both BEZ235 and CQ had a weak effect on the induction of apoptosis in both A549 and H1299 cell lines; however, the combination of BEZ235 and CQ was much more potent than either agent alone in inducing apoptosis. The highest levels of cleaved PARP was observed in cells exposed to the combination than in cells exposed to either agent alone (**Fig. 4C**). Thus, it is clear that inhibition of autophagy enhances the ability of BEZ235 to induce apoptosis.

To further demonstrate the impact of autophagy blockade on BEZ235's effect on inhibition of NSCLC cell growth, we conducted a colony formation assay which allows for long-term

repeating treatments. As shown in **Figure 5**, BEZ235 alone at the tested conditions partially inhibited the growth of colony formation of NSCLC cells. In the presence of CQ, this effect was substantially enhanced in both A549 ($p < 0.001$) and H1299 ($p < 0.05$ or 0.001). In A549 cells, the combination of BEZ235 and CQ eliminated cell colonies in comparison with either agent alone that only partially inhibited the formation and growth of colonies. These results further support the notion that inhibition of autophagy enhances the effects of BEZ235 on inhibiting cell growth and inducing apoptosis.

BEZ235 combined with autophagy blockade exhibits enhanced antitumor activity against NSCLC xenografts in nude mice. We further tested whether inhibition of autophagy enhances the anticancer activity of BEZ235 in vivo. In A549 xenograft model, treatment with the BEZ235 alone or CQ alone did not significantly inhibit the growth of xenograft tumors; however the combination of BEZ235 and CQ significantly ($p < 0.001$) suppressed tumor growth compared with vehicle control treatment (**Fig. 6A**). The combination did not significantly reduce mouse body weight (**Fig. 6B**), indicating the lack of significant toxicity. These data provide in vivo evidence for enhancement of efficacy of BEZ235 by preventing autophagy.

Discussion

In the current study, we examined the effects of BEZ235 on the growth of a panel of NSCLC cell lines and found that BEZ235 effectively inhibited the growth of these cell lines with IC_{50}s of lower than 100 nM. Moreover, BEZ235 induced apoptosis in NSCLC cells as demonstrated in other types of cancer cells.[19,20] Thus, it is clear that BEZ235 is effective in inhibiting the growth of NSCLC cells. It was previously reported that BEZ235 treatment is ineffective in mutant K-Ras-initiated mouse lung adenocarcinoma model although generating marked tumor regression in mouse lung adenocracinomas initiated by mutant p110α.[12] In contrast to this study, another recent study has demonstrated that BEZ235 effectively induces a striking growth-inhibitory effect against both oncogeneic K-Ras-induced lung adenocarcinimas in transgenic mice and human NSCLC xenografts harboring K-Ras mutation in nude mice.[13] In our study, most of the tested cell lines (i.e., A549, H522, H460, H1792 and H157) have mutated K-Ras[21] and are equally sensitive as other cell lines without K-Ras mutation (e.g., HCC827) to BEZ235. Thus our findings support the efficacy of BEZ235 in NSCLC cells with K-Ras mutation.

The novel finding in this study is that BEZ235 potently induces autopagy in NSCLC cells while

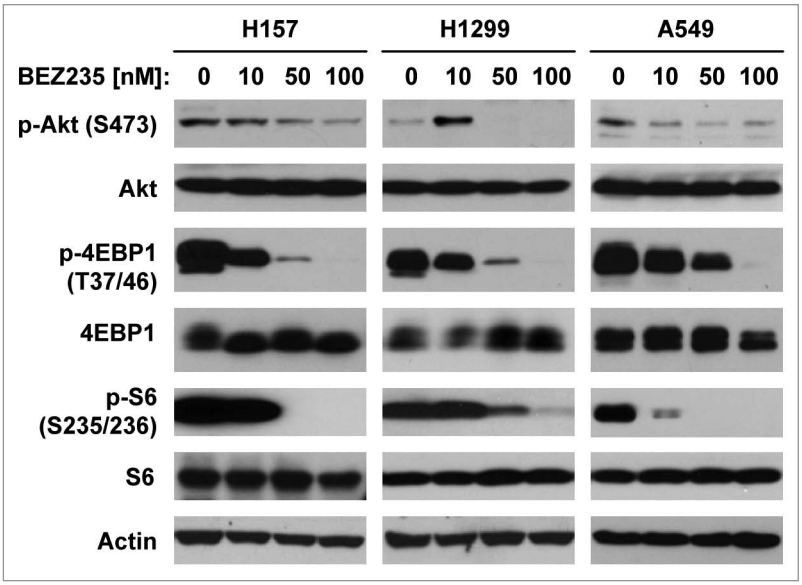

Figure 2. BEZ-235 inhibits Akt and mTOR signaling in human lung cancer cells. The indicated cell lines were plated in 10 cm-diameter cell culture dishes and treated next day with the given concentrations of BEZ-235 for 12 h. The cells were then harvested for preparation of whole-cell protein lysates and subsequent protein gel blot analysis.

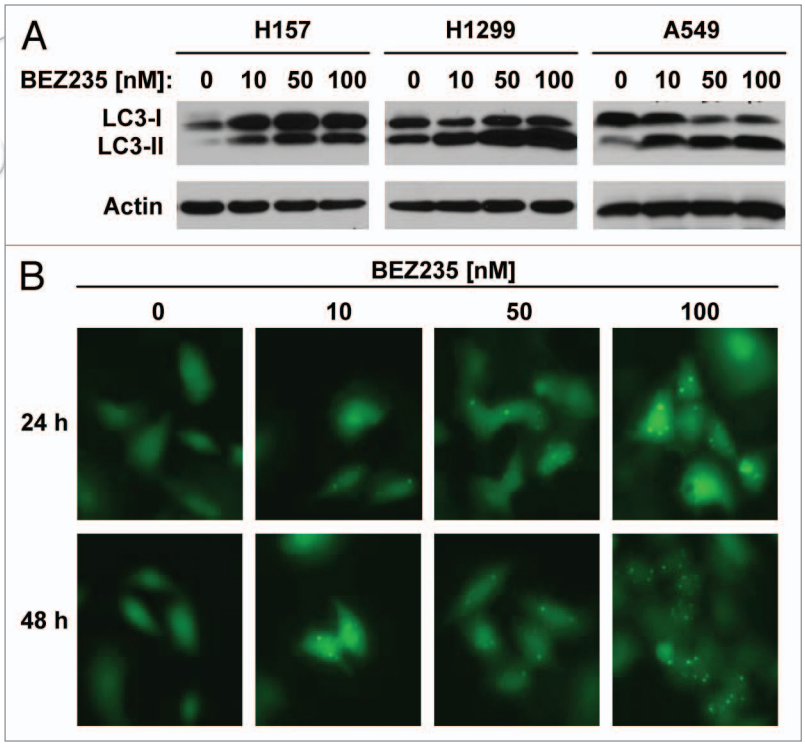

Figure 3. BEZ-235 induces type II LC3 expression. (A) The same whole-cell protein lysates as described in **Figure 2** were used for detection of LC3 with protein gel blot analysis. (B) A549/LC3-YFP cells were plated in 6-well plates and then treated with indicated concentrations of BEZ-235. After 24 and 48 h, fluorescence images recorded taken with a fluorescence microscopy.

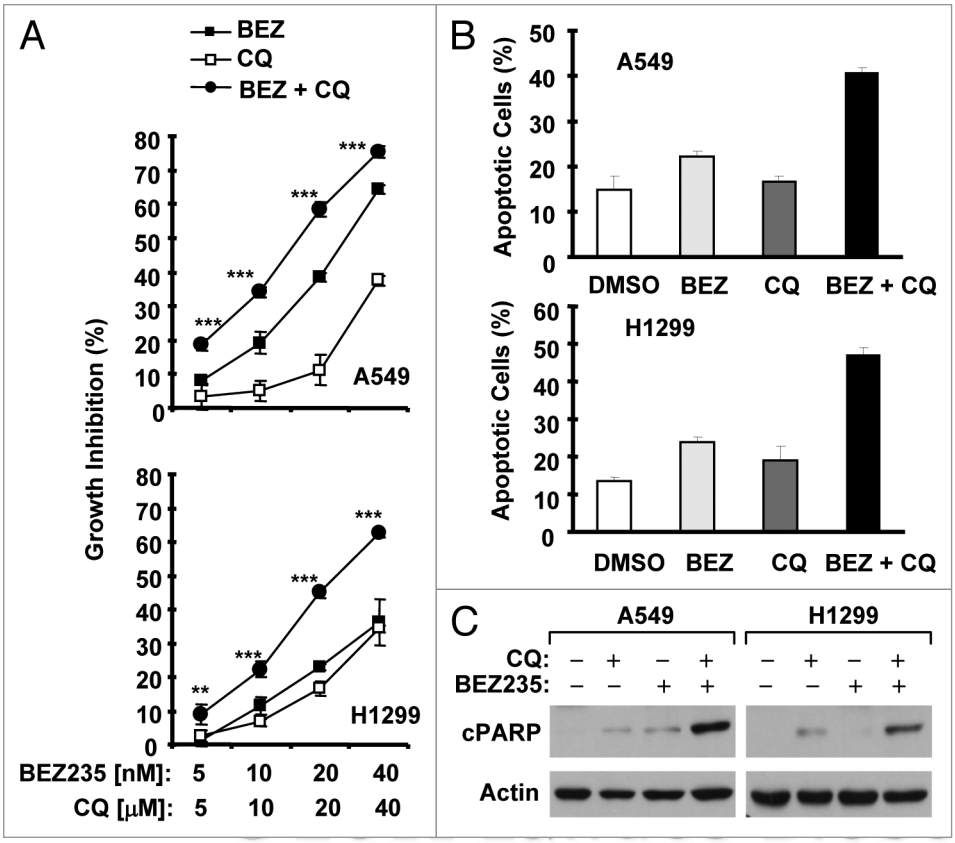

Figure 4. BEZ235 in combination with CQ exerts enhanced effects on inhibiting the growth (A) and on inducing apoptosis (B and C) of human lung cancer cells. (A) Given cell lines were seeded in 96-well plates and then treated next day with BEZ235, CQ and their combination as indicated for 3 d. The cell numbers were then estimated using the SRB assay. Points, mean of four replicate determinations; bars ± SD **p < 0.01 and ***p < 0.001 compared with BEZ235 alone or CQ alone. (B and C) The indicated cell lines were seeded in 6-well plates and then treated on the second day with 25 nM BEZ-235, 20 μM CQ and their combination. After 48 h, the cells were harvested for measurement of apoptosis using Annexin V staining (B) and for detection of PARP cleavage with protein gel blot analysis (C). Columns, means of duplicate measurements; bars ± SD.

inhibiting cell growth and initiates apoptosis, evidenced by detection of increased levels of LC3-II and punctate staining of YFP-LC3 bound in autophagosome. Considering the important role of mTOR in negatively regulating autophagy, it is not surprising to detect autophagy in cells exposed to BEZ235, a dual PI3K/mTOR inhibitor. Since autophagy can be either a pro-survival or death mechanism depending on the circumstances,[15,16] we were particularly interested in the impact of autopahgy induction on the anticancer effects of BEZ235. It was reported that dual inhibition of PI3K and mTOR with the combination of rapamycin and LY294002 in glioma cells exhibits enhanced antitumor effect by synergistic induction of autophagy.[22] In our study, induction of autophagy by BEZ235 is clearly a survival mechanism that counteracts its antitumor efficacy based on the following findings: (1) the combination of BEZ235 with the lysosomal inhibitor CQ exerts enhanced effects on inhibiting the growth of human NSCLC cells in a monolayer culture assay (**Fig. 4A**); (2) the combination exhibits enhanced effect on inhibiting the formation and growth of NSCLC cell colonies in a long-term colony formation assay (**Fig. 5A and B**); (3) the presence of CQ substantially augments BEZ235-induced apoptosis (**Fig. 4B and C**); and (4) BEZ235 and CQ combination is more effective than BEZ235 or CQ alone in inhibiting the growth of NSCLC xenografts in nude mice (**Fig. 6A**). Our findings are in agreement with a recent report that the combination of BEZ235 and CQ exerts enhanced effects on induction of apoptosis and on inhibition of xenograft growth in glioma cells.[23]

We noted that the combination of BEZ235 and CQ exhibited much more impressive suppression on colony formation in A549 than in H1299 cells (**Fig. 5**), suggesting that different NSCLC cell lines have varied sensitivities to the combination treatment. We noted that BEZ235 at 10 nM, a concentration used in the colony formation assay, actually increased p-Akt levels in H1299 cells. Under the same condition, BEZ235 reduced p-Akt levels in A549 cells (**Fig. 2**). This observation is consistent with a previous report, in which BEZ235 increased Akt phosphorylation in some cancer cell lines at low doses (e.g., 10 nM).[20] Whether Akt activation induced by the low dose of BEZ235 attenuates the efficacy of the combination of BEZ235 and CQ on the growth of some NSCLC cells needs further investigation.

In our study, BEZ235 at 10 nM, a concentration within the IC_{50} ranges in NSCLC cells (**Fig. 1A**), induced clear increase in LC3-II expression (**Fig. 3**), indicating that induction of autophagy in cells exposed to BEZ235 is a therapeutically relevant phenomenon. Thus, our finding on enhancement of efficacy of BEZ235 by blockade of autophagy may suggest a potential strategy to enhance therapeutic efficacy of dual targeting PI3K and mTOR signaling.

Materials and Methods

Reagent. BEZ235 was supplied by Novartis Pharmaceuticals Corporation (East Hanover, NJ), dissolved in DMSO and stored at -80°C. CQ and rabbit polyclonal anti-actin antibody were purchased from Sigma Chemical Co. (St. Louis, MO). Rabbit polyclonal antibodies against Akt, p-Akt (S473), p-p70S6K (T389), p70S6K, p-4EBP1 (Thr37/46), 4EBP1 and poly(ADP-ribose)polymerase (PARP), respectively, were purchased from Cell Signaling Technology, Inc. (Beverly, MA). Rabbit polyclonal microtubule-associated protein light chain 3 (LC3) antibody (NB100-2220) was purchased from Novus Biologicals, Inc. (Littleton, CO).

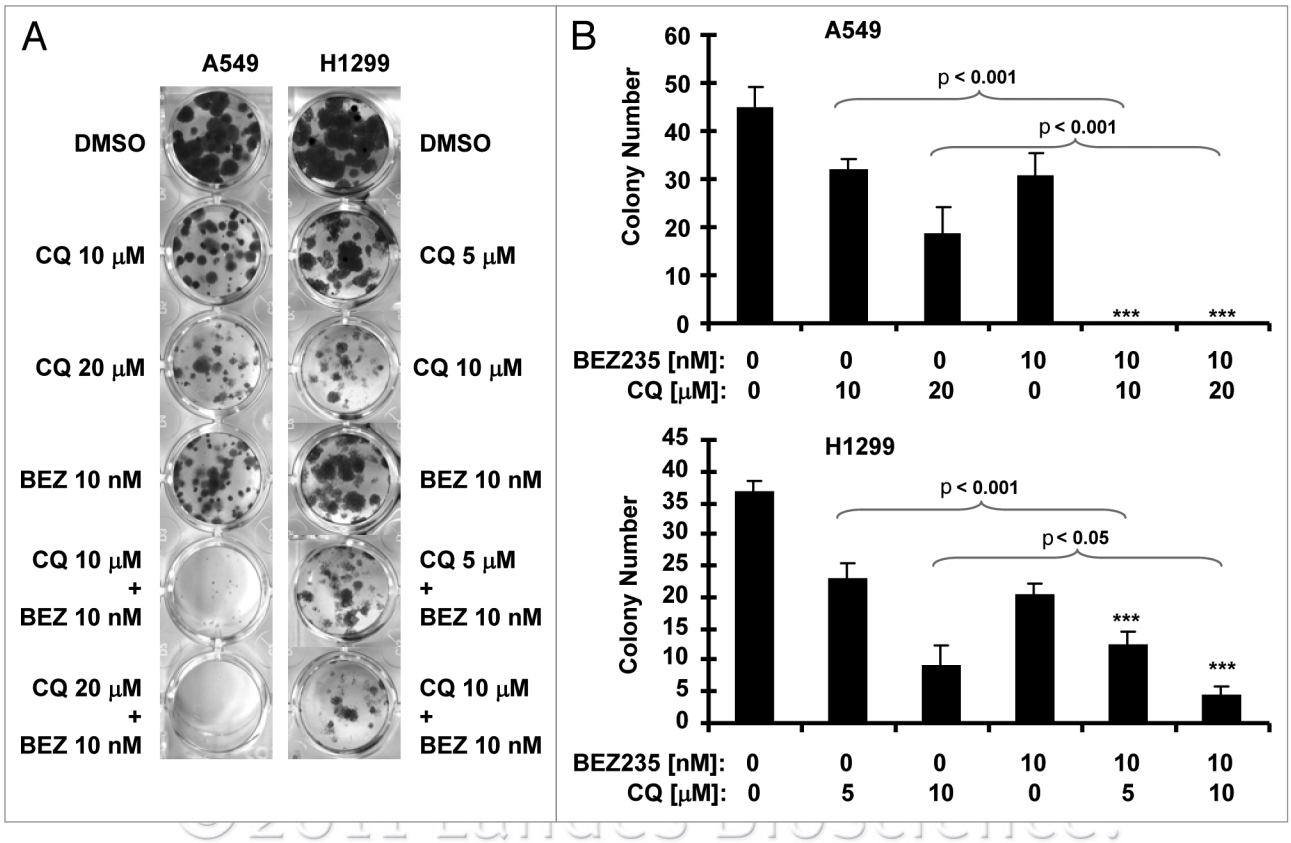

Figure 5. BEZ235 and CQ combination results in enhanced inhibitory effects on colony formation of lung cancer cells. The indicated cell lines at a density of approximately 200 cells/well were seeded in 24-well cell culture plates. On the second day, cells were treated with CQ, BEZ235 (BEZ), and their combinations as indicated. The same treatments were repeated every 3 d. After 12 d, the plates were stained for the formation of cell colonies with crystal violet dye. The representative pictures of the colonies were taken using a digital camera (A) and colonies were counted manually (B). Columns, means of four replicate measurements; bars ± SD ***p < 0.001 compared with BEZ235 (10 nM) alone.

Cell lines and cell culture. The human lung cancer cell lines used in this study were described previously in reference 24. A549/YFP-LC3 stable line was established by infecting A549 cells with lentiviruses carrying lentiviral YFP-LC3 expression construct as generated below. These cell lines were grown in monolayer culture in RPMI 1640 medium supplemented with 5% fetal bovine serum (FBS) at 37°C in a humidified atmosphere consisting of 5% CO_2 and 95% air.

Generation of lentiviral YFP-LC3 expression construct. LC3 cDNA, which was amplified with RT-PCR from total cellular RNA extracted from H157 cells with the following primers: LC3 BglII, 5'-ATA TAT AGA TCT CCG TCG GAG AAG ACC TTC-3', and LC3 EcoRI, 5'-GCG CGC GAA TTC TTA CAC TGA CAA TTT CAT-3', was cloned into pEYFP-C1 vector in the same reading frame with N-terminal YFP. The BamHI-YFP/LC3-EcoRI fragment was then obtained with PCR using the following primers and inserted into FUGW lentiviral vector[25] with BamHI and EcoRI link: BamHI YFP, 5'-ATA TAT GGA TCC ACC ATG GTG AGC AAG GGC-3' and LC3 EcoRI (same as above). The LC3 sequence was confirmed by sequencing.

Cell survival assay. Cells were cultured in 96-well cell culture plates and treated the next day with the agents indicated. Viable cell number was estimated using the sulforhodamine B (SRB) assay, as previously described in reference 24.

Colony formation assay. The effects of the given drugs on colony formation on plates were measured as previously described in reference 26.

Detection of apoptosis. Apoptosis was evaluated by Annexin V staining using Annexin V-PE apoptosis detection kit purchased from BD Biosciences (San Jose, CA) following the manufacturer's instructions. PARP cleavage was also detected by protein gel blotting as an additional indicator of apoptosis.

Protein gel blot analysis. Preparation of whole cell protein lysates and protein gel blot analysis were described previously in reference 27 and 28.

Lung cancer xenografts and treatments. Animal experiments were approved by the Institutional Animal Care and Use Committee (IACUC) of Emory University. Five- to six-week old female athymic (nu/nu) mice were ordered from Taconic (Hudson, NY) and housed under pathogen-free conditions in microisolator cages with laboratory chow and water ad libitum. A549 cells at 5 x 10^6 in serum-free medium were injected s.c. into the flank region of nude mice. When tumors reached certain size ranges (~100 mm^3), the mice were randomized into four groups (n = 6/group) according to tumor volumes and body weights for the following treatments: vehicle control, BEZ235 (30 mg/kg/day, og), CQ (50 mg/kg/day; ip), and their combination. Tumor

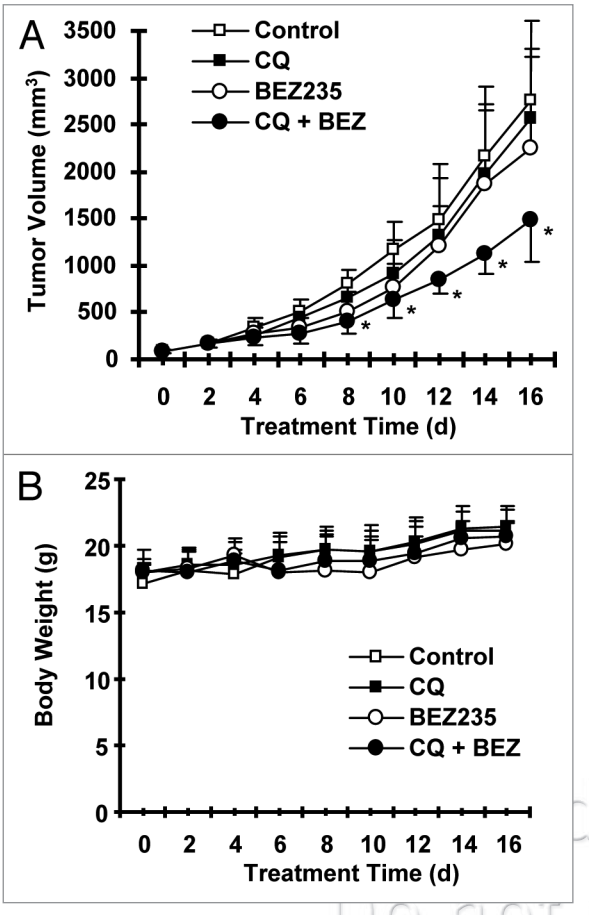

Figure 6. BEZ235 and CQ combination results in enhanced inhibitory effects on the growth of lung cancer xenograpts in mice. Mice with A549 xenograpts were treated with vehicle control, CQ (50 mg/kg) alone, BEZ-235 (30 mg/kg) alone and BEZ-235 plus CQ on the same day after grouping. After 16-d consecutive treatment (once daily), the mice were sacrificed. Tumor sizes (A) and body weight (B) were measured once every 2 d. Each measurement is a mean ± SD (n = 6). *p <0.001 compared with the vehicle control.

volumes were measured using caliper measurements once every 2 d and calculated with the formula V = π(length x width^2)/6.

Statistical analysis. The statistical significances among treatment groups in cell cultures were analyzed with one-way analysis of variance (ANOVA). The statistical significance of differences in tumor sizes between two groups was analyzed with two-sided unpaired Student's t-tests when the variances were equal or with Welch's corrected t-test when the variances were not equal. All of these analysese were done by use of Graphpad InStat 3 software (GraphPad Software; La Jolla, CA). Results were considered to be statistically significant at $p < 0.05$.

Disclosure of Potential Conflicts of Interest

No potential conflicts of interest were disclosed.

Acknowledgments

This study is supported by Georgia Cancer Coalition Distinguished Cancer Scholar award (to S.Y.S., T.K.O., S.S.R. and F.R.K.), NIH R01 CA118450 (S.Y.S.) and P01 CA116676 (Project 1 to F.R.K. and S.Y.S.), DOD IMPACT award W81XWH-05-0027 (Project 5 to F.R.K. and S.Y.S.), BATTLE award W81XWH-06-1-0303 (Project 4 to F.R.K. and S.Y.S.) and BESCT award DAMD17-01-1-0689 (Project 2 to F.R.K.). T.K.O., S.S.R., F.R.K. and S.Y.S. are Georgia Cancer Coalition Distinguished Cancer Scholars.

References

1. Jemal A, Siegel R, Xu J, Ward E. Cancer statistics. CA Cancer J Clin 2010; 60:277-300; PMID: 20610543; DOI: 10.3322/caac.20073.
2. West KA, Castillo SS, Dennis PA. Activation of the PI3K/Akt pathway and chemotherapeutic resistance. Drug Resist Updat 2002; 5:234-48; PMID: 12531180; DOI: 10.1016/S1368-7646(02)00120-6.
3. LoPiccolo J, Blumenthal GM, Bernstein WB, Dennis PA. Targeting the PI3K/Akt/mTOR pathway: effective combinations and clinical considerations. Drug Resist Updat 2008; 11:32-50; PMID: 18166498; DOI: 10.1016/j.drup.2007.11.003.
4. Shaw RJ, Cantley LC. Ras, PI(3)K and mTOR signalling controls tumour cell growth. Nature 2006; 441:424-30; PMID: 16724053; DOI: 10.1038/nature04869.
5. Hennessy BT, Smith DL, Ram PT, Lu Y, Mills GB. Exploiting the PI3K/AKT pathway for cancer drug discovery. Nat Rev Drug Discov 2005; 4:988-1004; PMID: 16341064; DOI: 10.1038/nrd1902.
6. Shaw RJ, Bardeesy N, Manning BD, Lopez L, Kosmatka M, DePinho RA, et al. The LKB1 tumor suppressor negatively regulates mTOR signaling. Cancer Cell 2004; 6:91-9; PMID: 15261145; DOI: 10.1016/j.ccr.2004.06.007.
7. Makowski L, Hayes DN. Role of LKB1 in lung cancer development. Br J Cancer 2008; 99:683-8; PMID: 18728656; DOI: 10.1038/sj.bjc.6604515.
8. Ding L, Getz G, Wheeler DA, Mardis ER, McLellan MD, Cibulskis K, et al. Somatic mutations affect key pathways in lung adenocarcinoma. Nature 2008; 455:1069-75; PMID: 18948947; DOI: 10.1038/nature07423.
9. Chen YL, Law PY, Loh HH. Inhibition of PI3K/Akt signaling: an emerging paradigm for targeted cancer therapy. Curr Med Chem Anticancer Agents 2005; 5:575-89; PMID: 16305480; DOI: 10.2174/156801105774574649.
10. Sawyers CL. Will mTOR inhibitors make it as cancer drugs? Cancer Cell 2003; 4:343-8; PMID: 14667501; DOI: 10.1016/S1535-6108(03)00275-7.
11. Maira SM, Stauffer F, Brueggen J, Furet P, Schnell C, Fritsch C, et al. Identification and characterization of NVP-BEZ235, a new orally available dual phosphatidylinositol-3-kinase/mammalian target of rapamycin inhibitor with potent in vivo antitumor activity. Mol Cancer Ther 2008; 7:1851-63; PMID: 18606717; DOI: 10.1158/1535-7163.MCT-08-0017.
12. Engelman JA, Chen L, Tan X, Crosby K, Guimaraes AR, Upadhyay R, et al. Effective use of PI3K and MEK inhibitors to treat mutant Kras G12D and PIK3CA H1047R murine lung cancers. Nat Med 2008; 14:1351-6; PMID: 19029981; DOI: 10.1038/nm.1890.
13. Konstantinidou G, Bey EA, Rabellino A, Schuster K, Maira MS, Gazdar AF, et al. Dual phosphoinositide-3-kinase/mammalian target of rapamycin blockade is an effective radiosensitizing strategy for the treatment of non-small cell lung cancer harboring K-RAS mutations. Cancer Res 2009; 69:7644-52; PMID: 19789349; DOI: 10.1158/0008-5472.CAN-09-0823.
14. Faber AC, Li D, Song Y, Liang MC, Yeap BY, Bronson RT, et al. Differential induction of apoptosis in HER2 and EGFR addicted cancers following PI3K inhibition. Proc Natl Acad Sci USA 2009; 106:19503-8; PMID: 19850869; DOI: 10.1073/pnas.0905056106.
15. Mizushima N, Levine B, Cuervo AM, Klionsky DJ. Autophagy fights disease through cellular self-digestion. Nature 2008; 451:1069-75; PMID: 18305538; DOI: 10.1038/nature06639.
16. Levine B, Kroemer G. Autophagy in the pathogenesis of disease. Cell 2008; 132:27-42; PMID: 18191218; DOI: 10.1016/j.cell.2007.12.018.
17. Rubinsztein DC, Gestwicki JE, Murphy LO, Klionsky DJ. Potential therapeutic applications of autophagy. Nat Rev Drug Discov 2007; 6:304-12; PMID: 17396135; DOI: 10.1038/nrd2272.
18. Levine B, Yuan J. Autophagy in cell death: an innocent convict? J Clin Invest 2005; 115:2679-88; PMID: 16200202; DOI: 10.1172/JCI26390.

19. Brachmann SM, Hofmann I, Schnell C, Fritsch C, Wee S, Lane H, et al. Specific apoptosis induction by the dual PI3K/mTor inhibitor NVP-BEZ235 in HER2 amplified and PIK3CA mutant breast cancer cells. Proc Natl Acad Sci USA 2009; 106:22299-304; PMID: 20007781; DOI: 10.1073/pnas.0905152106.
20. Serra V, Markman B, Scaltriti M, Eichhorn PJ, Valero V, Guzman M, et al. NVP-BEZ235, a dual PI3K/mTOR inhibitor, prevents PI3K signaling and inhibits the growth of cancer cells with activating PI3K mutations. Cancer Res 2008; 68:8022-30; PMID: 18829560; DOI: 10.1158/0008-5472.CAN-08-1385.
21. Mitsudomi T, Steinberg SM, Nau MM, Carbone D, D'Amico D, Bodner S, et al. p53 gene mutations in non-small-cell lung cancer cell lines and their correlation with the presence of ras mutations and clinical features. Oncogene 1992; 7:171-80; PMID: 1311061.
22. Takeuchi H, Kondo Y, Fujiwara K, Kanzawa T, Aoki H, Mills GB, et al. Synergistic augmentation of rapamycin-induced autophagy in malignant glioma cells by phosphatidylinositol-3-kinase/protein kinase B inhibitors. Cancer Res 2005; 65:3336-46; PMID: 15833867.
23. Fan QW, Cheng C, Hackett C, Feldman M, Houseman BT, Nicolaides T, et al. Akt and autophagy cooperate to promote survival of drug-resistant glioma. Sci Signal 2010; 3:81; PMID: 21062993; DOI: 10.1126/scisignal.2001017.
24. Sun SY, Yue P, Dawson MI, Shroot B, Michel S, Lamph WW, et al. Differential effects of synthetic nuclear retinoid receptor-selective retinoids on the growth of human non-small cell lung carcinoma cells. Cancer Res 1997; 57:4931-9; PMID: 9354460.
25. Lois C, Hong EJ, Pease S, Brown EJ, Baltimore D. Germline transmission and tissue-specific expression of transgenes delivered by lentiviral vectors. Science 2002; 295:868-72; PMID: 11786607; DOI: 10.1126/science.1067081.
26. Wang X, Hawk N, Yue P, Kauh J, Ramalingam SS, Fu H, et al. Overcoming mTOR inhibition-induced paradoxical activation of survival signaling pathways enhances mTOR inhibitors' anticancer efficacy. Cancer Biol Ther 2008; 7:1952-8; PMID: 18981735; DOI: 10.4161/cbt.7.12.6944.
27. Liu X, Yue P, Zhou Z, Khuri FR, Sun SY. Death receptor regulation and celecoxib-induced apoptosis in human lung cancer cells. J Natl Cancer Inst 2004; 96:1769-80; PMID: 15572759; DOI: 10.1093/jnci/djh322.
28. Sun SY, Yue P, Wu GS, El-Deiry WS, Shroot B, Hong WK, et al. Mechanisms of apoptosis induced by the synthetic retinoid CD437 in human non-small cell lung carcinoma cells. Oncogene 1999; 18:2357-65; PMID: 10327056; DOI: 10.1038/sj.onc.1202543.

Cancer Biology & Therapy 13:5, 272-280; March 2012; © 2012 Landes Bioscience

Elevated expression of eukaryotic translation initiation factor 4E is associated with proliferation, invasion and acquired resistance to erlotinib in lung cancer

Yikun Li,[1] Songqing Fan,[1,2] Junghui Koo,[1] Ping Yue,[1] Zhuo (Georgia) Chen,[1] Taofeek K. Owonikoko,[1] Suresh S. Ramalingam,[1] Fadlo R. Khuri[1] and Shi-Yong Sun[1,*]

[1]Department of Hematology and Medical Oncology; Emory University School of Medicine and Winship Cancer Institute; Atlanta, GA USA; [2]Department of Pathology; The Second Xiang-Ya Hospital; Central South University; Changsha; Hunan, China

Keywords: eIF4E, proliferation, invasion, erlotinib, resistance, lung cancer

Eukaryotic translation initiation factor 4E (eIF4E) is the rate-limiting factor for cap-dependent translation initiation, which is known to regulate oncogenesis. Elevated eIF4E and its negative impact on prognosis in human non-small cell lung cancer (NSCLC) have been reported previously. However, its potential as a therapeutic target and role in regulation of sensitivity to EGFR inhibitors is an area of ongoing investigations. In this study, we detected increased levels of eIF4E in 16 human NSCLC cell lines compared with their normal bronchial epithelial cells. Consistently, human tissue array analysis showed that eIF4E expression was significantly higher in human NSCLC tissues than normal tissues. Inhibition of eIF4E using eIF4E siRNA inhibited the growth and invasion of NSCLC cells. These data suggest that eIF4E overexpression plays a crucial role in positive regulation of the growth and invasion of NSCLC cells. By proteomics, we found that eIF4E levels were elevated in erlotinib-resistant cell lines compared with the sensitive parental cell line. In agreement, assembly of the eIF4F cap complex and several oncogenic proteins regulated by the cap-dependent translation mechanism, were also increased in erlotinib-resistant cells. Thus, erlotinib-resistant cells exhibit elevated eIF4E expression and cap-dependent translation. Inhibition of eIF4F with different means (e.g., gene knockdown) downregulated c-Met expression and partially restored cell sensitivity to erlotinib, suggesting that elevated eIF4E contributes to development of erlotinib resistance, likely through positive regulation of c-Met expression. Taken together, we suggest that elevated eIF4E in NSCLC cells is associated with proliferation, invasion and acquired erlotinib resistance.

Introduction

The long-established role of eukaryotic translation initiation factor 4E (eIF4E) in the cytoplasm is in the initiation of cap-dependent translation of cellular mRNAs. eIF4E is a cap-binding protein component of the eIF4F complex, which includes the RNA helicase eIF4A and the scaffolding protein eIF4G. Binding of eIF4E to the cap structure on the 5' end of cellular mRNAs recruits the eIF4F complex to the mRNA. As a result, the eIF4F complex can scan from the 5' cap through the untranslated region (5'-UTR), unwinding secondary structure to reveal the translation initiation codon, enable ribosome loading and facilitate final protein translation.[1,2] Thus, recruitment of mRNA to the ribosomal apparatus constitutes a key event in the initiation of translation of mRNAs that are otherwise translationally repressed due to their long 5'-UTRs.

Because eIF4E is the least abundant among these initiation factors and is considered to be the rate-limiting factor for cap-dependent translation initiation, changes in the levels of eIF4E profoundly affect translation rates. While increasing global protein synthesis rates, higher levels of eIF4E preferentially enhance the synthesis of potent growth promoting proteins and oncogenic proteins (e.g., c-Myc, cyclin D1, HIF-1 and Mcl-1), which usually have lengthy, G/C-rich and highly structured 5'-UTRs in the mRNAs and, under normal cellular conditions, are translationally repressed. By this mechanism, cancer-related events such as transformation, tumorigenesis, angiogenesis, invasion and metastasis could be facilitated.[1,3,4] It has been well documented that eIF4E expression is frequently elevated in many types of cancers and is associated with malignant progression. Inhibition of eIF4E effectively suppresses cellular transformation and tumor growth, invasiveness and metastasis.[3,5,6]

In human non-small cell lung cancer (NSCLC), elevated eIF4E expression has been documented in several previous studies in reference 7–10. Moreover, elevated eIF4E expression is associated with short survival of patients with NSCLC.[10-12] These

*Correspondence to: Shi-Yong Sun; Email: ssun@emory.edu
Submitted: 10/10/11; Revised: 12/01/11; Accepted: 12/02/11
http://dx.doi.org/10.4161/cbt.13.5.18923

results suggest that eIF4E may play an important role in positive regulation of the growth and other oncogenic phenotypes of NSCLC cells. However, whether eIF4E can serve as a good therapeutic target in NSCLC has not been demonstrated.

The epidermal growth factor receptor (EGFR) tyrosine kinase inhibitors (TKIs), erlotinib and gefitinib, are effective therapies for NSCLC patients with somatic mutations in EGFR. However, all patients eventually develop resistance (i.e., acquired resistance) to these agents.[13] Thus, there is an urgent need to understand the mechanism(s) of acquired resistance to develop effective strategies to overcome the resistance. Until now, two different EGFR-TKI resistance mechanisms have been described: i.e., a secondary EGFR mutation-790M and amplification of the c-Met oncogene.[13]

eIF4E has been suggested to be involved in resistance to chemotherapy and androgen ablation (in prostate cancer cells).[14,15] However, no study has linked eIF4E to EGFR-TKI resistance. Proteomics studies in comparing erlotinib-sensitive and resistant NSCLC cell lines uncovered an increase of eIF4E in erlotinib-resistant cells. Therefore, our present study analyzed eIF4E expression in human NSCLC cells and tissues, demonstrated its potential as a therapeutic target against NSCLC and elucidated its involvement in acquired EGFR-TKI resistance.

Results

Human NSCLC cells and tissues exhibit elevated eIF4E expression. We first examined eIF4E expression with western blotting in a panel of 16 NSCLC cell lines in comparison with two immortalized normal human bronchial epithelial (NHBE) cell lines (i.e., BEAS-2B and HBEC3KT). As presented in **Figure 1A**, all 16 NSCLC cell lines possessed much higher levels of eIF4E than both BEAS-2B and HBEC3KT cells, indicating that NSCLC cells exhibit elevated eIF4E expression. Moreover, we detected eIF4E expression with immunohistochemistry (IHC) in a tissue microarray (TMA) consisting of 40 cases of stage I–III lung cancer tissues (two cases of small cell lung cancer), 10 cases of metastatic cancer tissues from the primary lung cancer, and 9 cases of adjacent normal human lung tissues. In agreement with cell line data, we detected positive eIF4E staining in 71.1% (27/38) of NSCLC tissues, but only in 11.1% (1/9) of adjacent normal tissues (**Fig. 1B and C**). The eIF4E expression was significantly higher in NSCLC tissues than in adjacent normal tissues ($p = 0.0016$). Among these NSCLC tissues, we detected eIF4E expression in 92.3% (12/13) of squamous cell carcinoma, in 55.6% (10/18) of adenocarcinoma, and in 71.4% (5/7) of other NSCLC sub-types. Collectively, it is clear that eIF4E expression is elevated in human NSCLCs.

siRNA-mediated knockdown of eIF4E inhibits the growth of NSCLC cells. If elevated eIF4E is critical for the growth of NSCLC, we hypothesized that downregulation of eIF4E would result in inhibition of the growth of NSCLC cells. To verify this, we used eIF4E siRNA to downregulate eIF4E expression and then determined its impact on the growth of NSCLC cells. As shown in **Figures 2A, D and E**, transfection of eIF4E siRNA into four NSCLC cell lines (i.e., H157, A549, 801C and 801D) substantially reduced the levels of eIF4E in comparison with control siRNA, indicating successful knockdown of eIF4E. Consequently, we found that all eIF4E siRNA-transfected cell lines grew much slower than cell lines transfected with the control siRNA (**Fig. 2B**), indicating that silencing of eIF4E inhibits the growth of NSCLC cells. Moreover, we tested the effects of eIF4E siRNA transfection on the growth of NSCLC colonies on soft agar. Again, we detected much less colonies in cells transfected with eIF4E siRNA than in control siRNA-transfected cells (**Fig. 2C**), further indicating that inhibition of eIF4E expression suppresses the growth of NSCLC cells. Using cleaved PARP as a readout of apoptosis, we further determined whether knockdown of eIF4E induces apoptosis in the tested cell lines. As presented in **Figure 2D**, we detected cleaved form of PARP in eIF4E siRNA-transfected 801D cells, but not in eIF4E siRNA-transfected H157 cells. As a positive control, tumor necrosis factor-related apoptosis-inducing ligand induced strong cleavage of PARP in the both cell lines. Thus, knockdown of eIF4E induces a cell line-dependent apoptosis.

We also determined whether knockdown of eIF4E expression affected cap-dependent protein translation by detecting several proteins regulated by cap-dependent translation in eIF4E siRNA-transfected cells. As presented in **Figure 2E**, we detected reduced levels of c-Myc, cyclin D1, survivin and Mcl-1 in eIF4E siRNA-transfected H157 and 801D cells in comparison with control siRNA-transfected cells, suggesting that silencing of eIF4E expression in the tested cell systems inhibits cap-dependent translation.

Elevated eIF4E expression is associated with cell invasion. We detected that eIF4E levels were higher in 801D cells (a highly metastatic cell line) than in 801C cells (a low metastatic cell line) (**Fig. 3A**). Moreover, we noted that metastatic NSCLC tissues tended to have increased eIF4E staining rate than their matched primary tumor tissues (100 vs. 60%) (**Fig. 3B**). These data suggest that eIF4E may be involved in regulation of cancer metastasis. Therefore, we next determined whether inhibition of eIF4E expression impacted invasion of NSCLC cells. The matrigel chamber invasion assay showed that 801D cells had higher invasive capacity than 801C cells. Regardless, knockdown of eIF4E expression significantly reduced the number of invasive cells in both cell lines compared with control siRNA-transfected cells (**Fig. 3C and D**). Thus, inhibition of eIF4E expression suppresses the invasion of NSCLC cells, suggesting that elevated eIF4E expression is associated with positive regulation of cell invasion.

EGFR-TKI-resistant NSCLC cells possess elevated eIF4E expression and cap-dependent translation. In an effort to understand the biology of acquired EGFR-TKI resistance, we conducted proteomics by comparing HCC827/ER (derived from HCC827 with acquired resistance to erlotinib) with HCC827 cells using SILAC (stable isotope labeling with amino acids in cell culture) technique. Interestingly, eIF4E was among the proteins that were increased in HCC827/ER cells. By western blot analysis, we further confirmed increased eIF4E expression in HCC827/ER cells. In agreement, PC-9/GR cell also showed increased levels of eIF4E compared with PC-9 cells (**Fig. 4A**). Erlotinib treatment did not alter the expression of eIF4E both

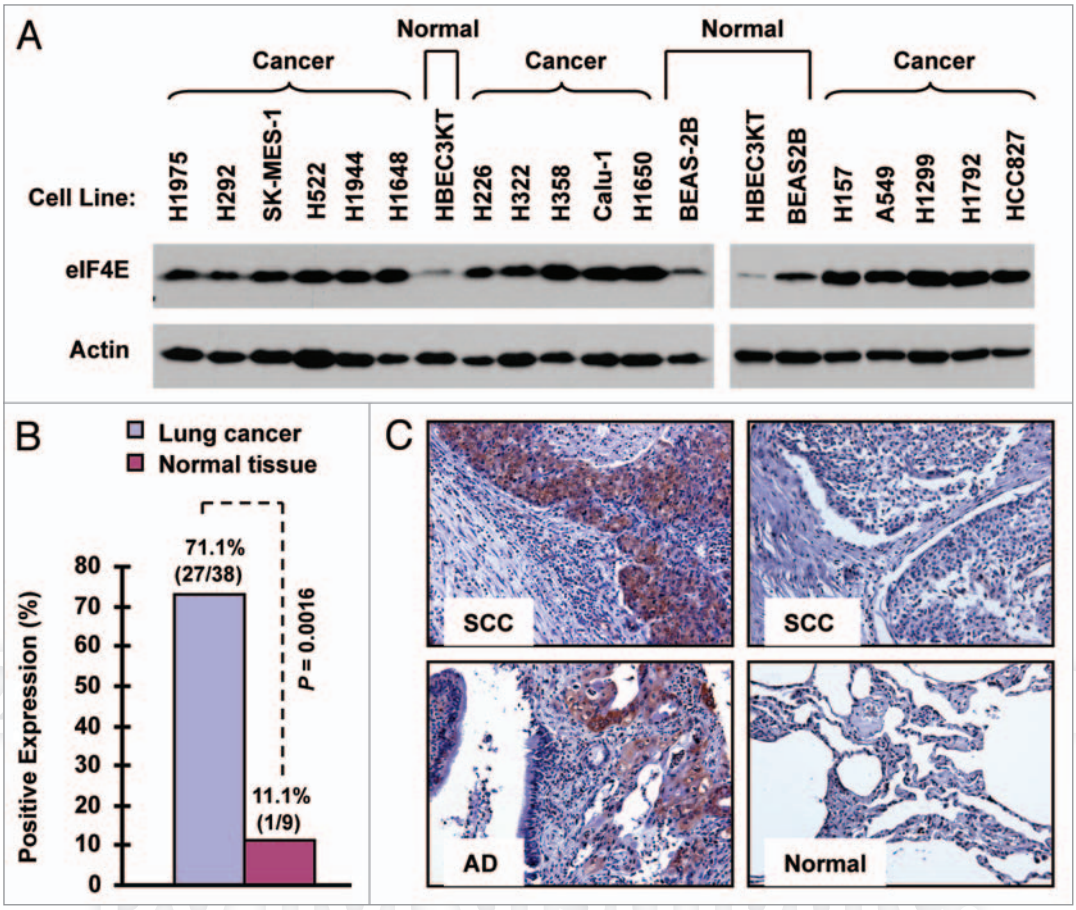

Figure 1. eIF4E expression is elevated in human NSCLC cell lines (A) and tissues (B and C). (A) Whole-cell protein lysates were extracted from the indicated normal and NSCLC cell lines and used for detection of eIF4E expression with western blotting. (B and C) eIF4E expression in human NSCLC tissues was detected with IHC and scored as positive or negative expression (B). The representative images were also presented (C). SCC, squamous cell carcinoma; AD, adenocarcinoma; Normal, adjacent normal lung tissue.

in HCC827 and HCC827/ER cells (**Fig. 4B**). By RT-PCR, we detected increased levels of eIF4E mRNA in HCC827/ER cells (**Fig. 4C**). Transfection of eIF4E promoter reporter plasmid (i.e., pGL3-eIF4E-luc) resulted in much higher luciferase activity in HCC827/ER cell than in HCC827 cells (**Fig. 4D**), indicating that HCC827/ER cells possess increased transcriptional activity of eIF4E. Thus, it appears that increased eIF4E in HCC827/ER cells occurs at the transcriptional level. Collectively, these data clearly demonstrate that eIF4E expression is upregulated in EGFR-TKI-resistant NSCLC cells.

Moreover, we analyzed whether EGFR-TKI resistant cells exhibit elevated cap-dependent translation by examining the formation of eIF4F complex and expression of proteins regulated by cap-dependent translation. Interestingly we found that both PC-9/GR and HCC827/ER cells expressed higher levels of eIF4G in addition to eIF4E than their corresponding counterparts. Accordingly, we detected more eIF4G bound to m^7GTP in both PC-9/GR and particularly HCC827/ER cells than their respective parent cells in our m^7GTP-pull down assay (**Fig. 5A**). This result indicates that EGFR-TKI-resistant NSCLC cells possess elevated eIF4F assembly. Furthermore, we detected higher levels of HIF1α, c-Myc and Mcl-1, which are typical proteins subject to regulation by the cap-dependent translation, in HCC827/ER cells than in HCC827 cells (**Fig. 5B**). Taken together we suggest that EGFR-TKI-resistant cells possess elevated cap-dependent translation.

Inhibition of eIF4E partially restores sensitivity of EGFR-TKI-resistant cells to erlotinib. If elevated eIF4E is involved in development of acquired resistance to EGFR-TKIs, we speculated that inhibition of eIF4E would overcome EGFR-TKI-resistance and restore the sensitivity of to EGFR-TKIs. To test this hypothesis, we used eIF4E siRNA to knock down eIF4E expression in HCC827/ER cells and then examined its impact on cell response to erlotinib. As presented in **Figure 6A**, erlotinib at 2 μM inhibited the growth of control siRNA-transfected HCC827/ER cells only by < 15%; however, it suppressed the growth of eIF4E siRNA-transfected HCC827/ER cells by > 55%, which was also greater than that cause by knockdown of eIF4E alone (< 35% growth inhibition). Thus, it is clear that silencing of eIF4E enhances the growth-inhibitory effect of erlotinib in HCC827/ER cells.

4EGI-1 is a small molecule that inhibits eIF4E and eIF4G interaction and cap-dependent translation.[16] Thus, we further determined whether addition of 4EGI-1 would enhance the

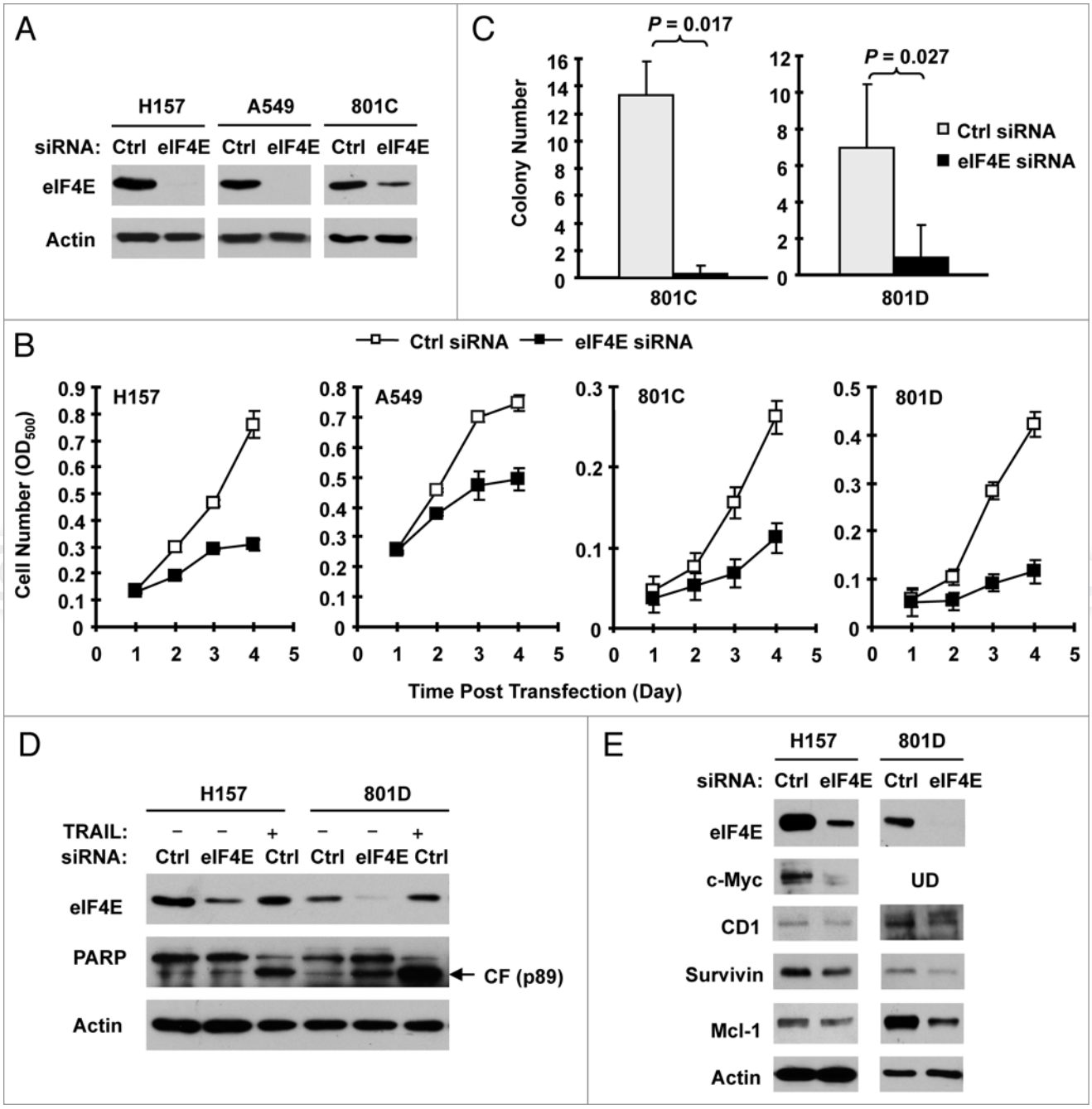

Figure 2. Knockdown of eIF4E (A, D and E) inhibits the growth of NSCLC cells (B and C) and induces apoptosis (D) with suppression of cap-dependent translation (E). (A and B) The indicated NSCLC cell lines were transfected with control (Ctrl) or eIF4E siRNA (20 nM) for 48 h and then subjected to western blot analysis for detection of eIF4E (A). The cells were also re-plated in 96-well plates. Cell numbers were estimated every 24 h with the SRB assay (B). The data are means ± SDs of four replicates. (C) 801-C and 801-D cells were transfected with control or eIF4E siRNA for overnight and equal numbers of cells were then used for soft agar in 35 mm diameter Petri dishes. After 14 d, colony numbers were counted and averaged from five random microscopic field or view. The final data are means ± SDs of triplicate independent determinations. The Student t-test was used to compare growth-inhibitory effects between two groups. (D and E) The indicated cell lines were transfected with control or eIF4E siRNA for 72 h (D) or 48 h (E). The cells were then harvested for preparation of whole-cell protein lysates and subsequent western blotting for detection of the given proteins. In (D) the control siRNA-transfected cells were exposed to 50 ng/ml tumor necrosis factor-related apoptosis-inducing ligand (TRAIL) for 20 h before harvesting the cells. UD, undetected.

growth inhibitory effects of erlotinib on HCC827/ER cells. In a 3 d assay, the combination of erlotinib and 4EGI-1 was more potent than either agent alone in inhibiting the growth of HCC827/ER cells. The combination indexes were < 1 for all combination treatments (**Fig. 6B**), indicating synergy between erlotinib and 4EGI-1 in inhibiting the growth of HCC827/ER cells. In agreement, the long-term colony formation assay generated similar results as presented in **Figure S1**. The presence of

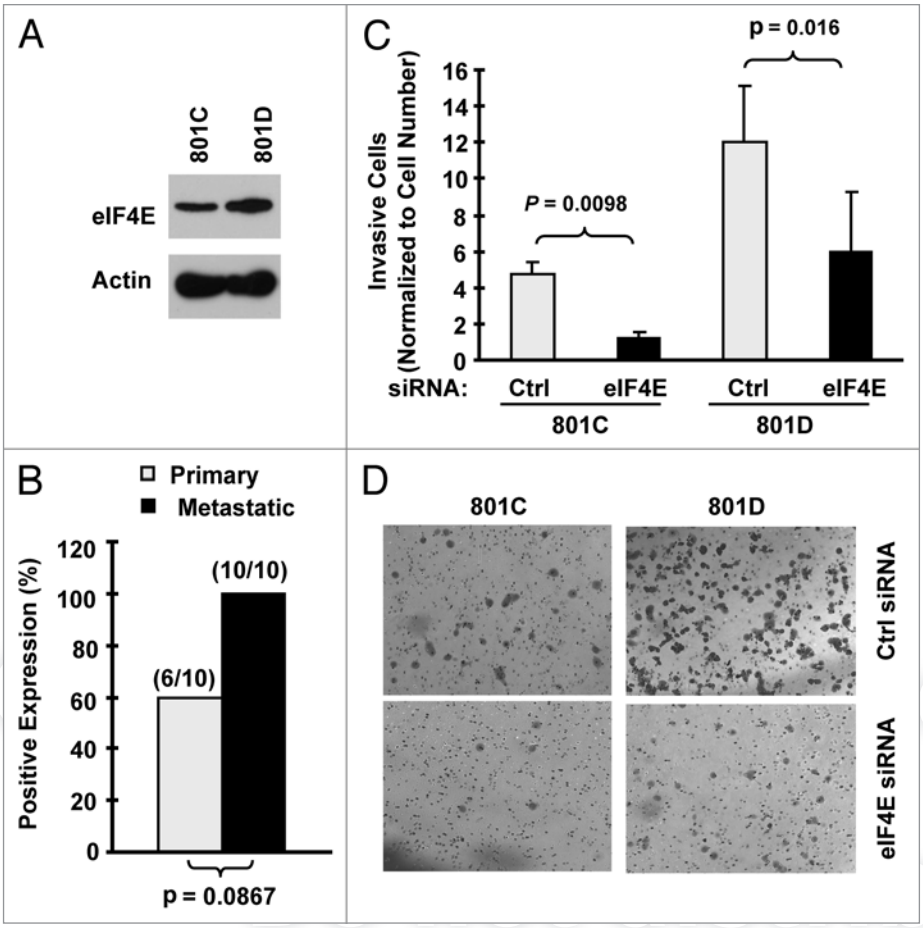

Figure 3. eIF4E expression is increased in metastatic NSCLC cells (A) and tissues (B) and is associated with cell invasion (C and D). (A) eIF4E expression in 801C and 801D cells was detected with western blot analysis. (B) eIF4E expression in primary and matched metastatic NSCLC tissues was detected with IHC. (C and D) Both 801C and 801D cells were transfected with control (Ctrl) or eIF4E siRNA for 48 h and then subjected to matrigel chamber invasion assay. After 36 h, the non-invaded cells and collagen matrix on top of the membranes were removed. Invasive cells on the bottoms of the membranes were counted and normalized by the live cells cultured under the same conditions (C). Representative images of invasive cells on the membranes were also shown (D). The data are means ± SDs of triplicate determinations. The Student t-test was used to compare inhibitory effects on invasion between two groups.

4EGI-1 enhanced the ability of erlotinib to inhibit the formation and growth of the colonies of HCC827/ER cells. Taken together, these results indicate that the combination of erlotinib and 4EGI-1 synergistically inhibits the growth of HCC827/ER cells.

eIF4G is also the major component in the eIF4F complex. Thus, we further knocked down eIF4G in HCC827/ER cells and analyzed its impact on cell sensitivity to erlotinib. As presented in **Figure 6C**, erlotinib at up 2 μM inhibited the growth of control siRNA-transfected HCC827/ER cells by approximately 25%, but the growth of eIF4G-transfected HCC827/ER cells by about 70%. Thus, the knockdown of eIF4G greatly sensitizes HCC827/ER cells to erlotinib, furthering the notion that inhibition of eIF4F cap complex restores TKI-resistant cells to TKIs.

Elevated eIF4E is associated with increased Met expression in TKI-resistant cells. c-Met amplification represents one of the major mechanisms accounting for EGFR TKI-resistance.[13] In HCC827/ER cells, c-Met expression is elevated compared with their parent HCC827 cells (**Fig. S2**). Since eIF4E is primarily involved in regulation of cap-dependent protein translation, we then asked whether elevated eIF4E enhances c-Met translation. To this end, we knocked down eIF4E and eIF4G, respectively, and then examined their impact on c-Met expression. Indeed, knockdown of either eIF4E or eIF4G reduced the levels of c-Met protein (**Fig. 7A and B**). Similarly, treatment of HCC827/ER cells with 4EGI-1 also reduced c-Met levels (**Fig. 7C**). These data collectively indicate that inhibition of eIF4F cap complex inhibits c-Met expression.

Discussion

In this study, we have shown that human NSCLC cell lines and tissues possess significantly elevated expression of eIF4E in comparison with their normal counterparts (**Fig. 1**). These findings are in agreement with previous observations.[7-10] In variance with a report that eIF4E is rarely increased in squamous cell carcinoma of lung,[7] we detected eIF4E expression in 92% (12/13) of squamous cell carcinoma. Nonetheless, our current and previous studies together clearly indicate that NSCLCs exhibit elevated eIF4E expression.

Given that elevated eIF4E expression is significantly associated with short survival of NSCLC patients,[10-12] it is plausible to speculate a role of eIF4E in positive regulation of the growth of NSCLC cells. Indeed, knockdown of eIF4E expression by siRNA in our study substantially inhibited the growth of NSCLC cells (**Fig. 2**), suggesting that eIF4E plays a critical role in mediating the growth of NSCLC cells. In this study, we found that knockdown of eIF4E induced apoptosis in 801D cells, but not in H157 cells although it effectively inhibited the growth of both cell lines, suggesting that inhibition of eIF4E inhibit the growth of cancer cells through growth arrest or both growth arrest and apoptosis. It has been recently shown that eIF4E-specific antisense oligonucleotides effectively inhibit the growth of cancer xenografts in mice with minimal toxicity,[17] hence providing robust validation for eIF4E-targeted cancer therapy. Our results also support eIF4E as a promising target for therapy of NSCLCs.

We noted that eIF4E knockdown potently reduced the levels of Mcl-1 in 801D cells, but only minimally in H157 cells even though it effectively decreased survivin levels in the both cell

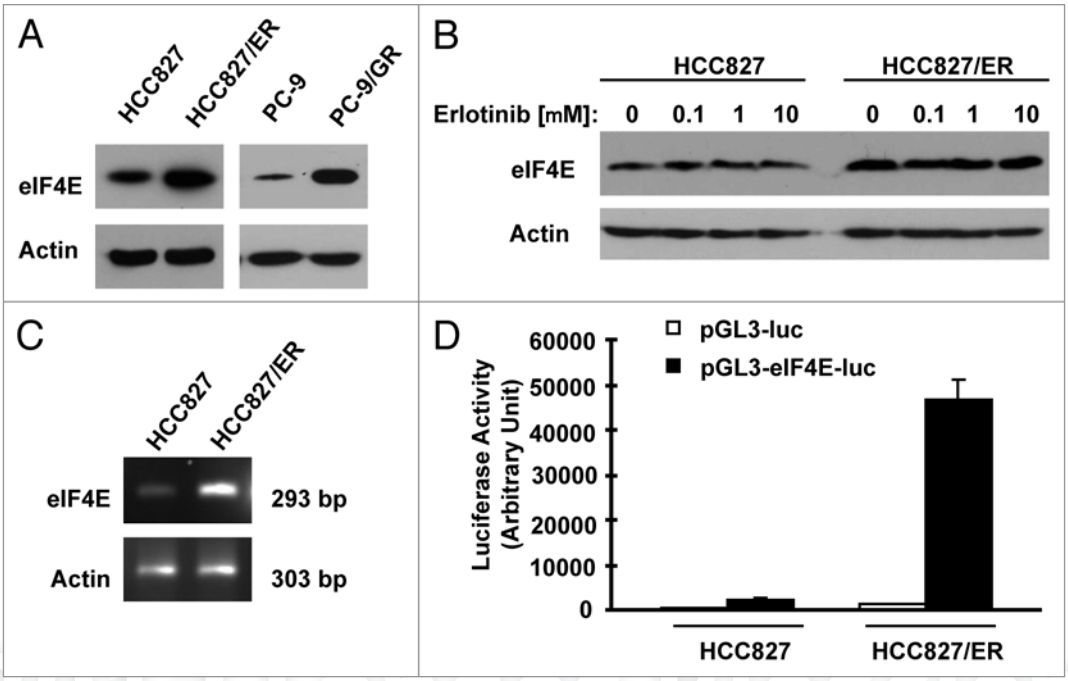

Figure 4. Erlotinib-resistant NSCLC cells possess elevated levels of eIF4E protein (A and B) and mRNA (C and D). (A and B) Whole-cell protein lysates were prepared from the indicated cell lines (A) or cell lines exposed to different concentrations of erlotinib for 6 h (B) and then used for western blot analysis to detect the given proteins as indicated. (C) Total cellular RNA was isolated from both parental and HCC827/ER cells for detection of eIF4E mRNA by RT-PCR. (D) eIF4E promoter activities in the given cell lines were performed with transfection of the given reporter constructs into HCC827 or HCC827/ER cells followed with a luciferase activity assay after 48 h. Each column represents the mean ± SD of triplicate determinations.

lines (**Fig. 2E**). Coincidentally, knockdown of eIF4E induced apoptosis in 801D cells, but not in H157 cells (**Fig. 2D**). Whether this suggests that Mcl-1 downregulation plays a critical role in mediating eIF4E inhibition-induced apoptosis needs further investigation.

The early work with antisense of eIF4E in Ras-transformed rat embryo fibroblasts showed that cells with reduced levels of eIF4E had delayed and reduced invasiveness and decreased experimental metastasis,[18] suggesting that eIF4E plays a role in regulation of invasion and metastasis.[1] In our study, we detected elevated eIF4E expression in metastatic NSCLC cells and tissues. Moreover, knockdown of eIF4E significantly inhibited invasion of NSCLC cells (**Fig. 3**), suggesting that elevated eIF4E expression is associated with positive regulation of invasion of NSCLC cells. Thus, our findings support the notion that eIF4E is involved in regulation of cancer invasion and metastasis.

Acquired resistance to EGFR-TKIs is a major obstacle and challenge in the treatment of NSCLCs with EGFR-TKIs.[13] Our exciting finding in this study that eIF4E expression is elevated in NSCLC cells with acquired resistance to EGFR-TKIs (e.g., HCC827/ER and PC-9/GR) is significant for future efforts to overcome EGFR-TKI resistance. Moreover we have shown that these EGFR-TKI-resistant NSCLC cells possess increased capacity of eIF4F assembly and elevated expression of oncogenic proteins known to be regulated by the cap-dependent translation mechanism (e.g., HIF1α, c-Myc and Mcl-1) (**Figs. 4 and**

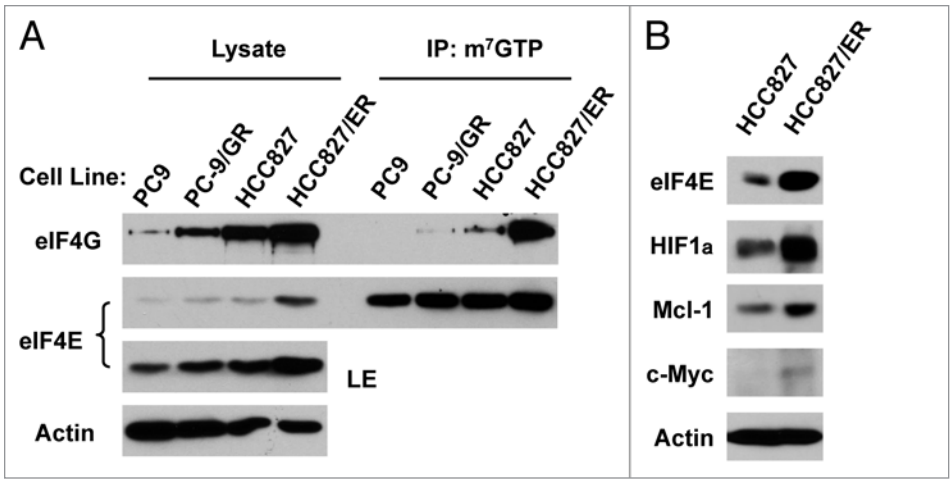

Figure 5. Erlotinib-resistance cells exhibit elevated eIF4F assembly (A) and expression of oncogenic proteins regulated by the cap-dependent translation (B). (A) Whole-cell protein lysates prepared from the given cell lines were used for m^{7}GTP pull-down assay followed with western blot analysis to detect the indicated proteins. LE, long exposure. (B) Whole-cell protein lysates were prepared from the indicated cell lines and then used for western blot analysis to detect the given proteins as indicated.

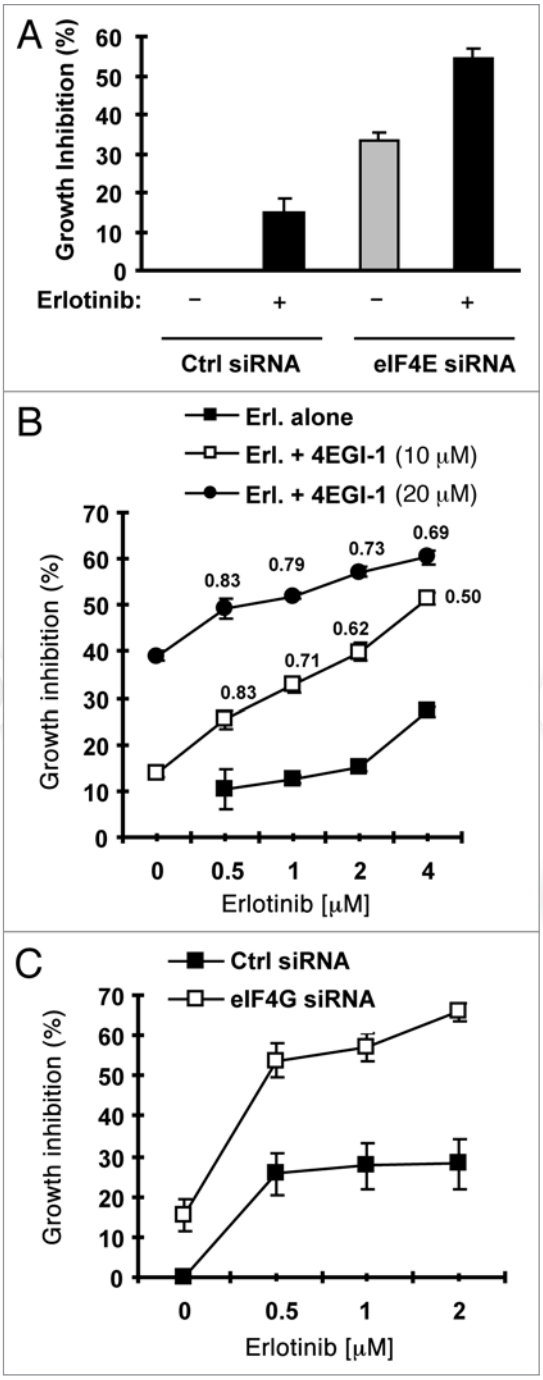

Figure 6. Inhibition of eIF4F formation by knocking down eIF4E (A) or eIF4G (C) or by inhibiting eIF4E and eIF4G interaction with 4EGI-1 (B) sensitizes erlotinib-resistant cells to erlotinib. (A) HCC828/ER cells were transfected with control (Ctrl) or eIF4E siRNA for overnight and then exposed to 2 μM erlotinib for 3 d. (B) HCC828/ER cells were treated with indicated concentrations of erlotinib in the absence and presence of 4EGI-1 for 3 d. (C) HCC828/ER cells were transfected with control (Ctrl) or eIF4G siRNA for overnight and then exposed to the indicated concentrations of erlotinib for 3 d. After the aforementioned treatments, the cell numbers were estimated by the SRB assay. The data are means ± SDs of four replicate determinations. The numbers by the lines in (B) are combination indexes for the combinations of erlotinib and 4EGI-1.

5). These results together indicate that eIF4E expression and cap-dependent translation are elevated in EGFR-TKI-resistant NSCLC cells. To the best of our knowledge, this is the first study that links eIF4E and cap-dependent translation to the acquired EGFR-TKI resistance of NSCLCs.

In our study, inhibition of eIF4F assembly by knocking down of eIF4E or eIF4G with eIF4E or eIF4G siRNA enhanced the effect of erlotinib against the growth of HCC827/ER cells. Moreover, the combination of erlotinib and 4EGI-1, an inhibitor of eIF4E and eIF4G interaction, synergistically inhibited the growth of HCC827/ER cells (**Figs. 6 and S2**). These data collectively suggest that elevated eIF4E expression is involved in development of acquired EGFR-TKI resistance. However, we noted that inhibition of eIF4F with the aforementioned approaches did not fully restore the sensitivity of HCC827/ER cell to erlotinib. Thus, we suggest that elevated eIF4E alone may not be sufficient to confer cell full resistance to EGFR-TKIs although it does contribute to development of acquired EGFR-TKI resistance.

One of the known mechanisms underlying acquired EGFR-TKI resistance is c-Met amplification.[13] Here, we showed that HCC827/ER cells possessed elevated expression of c-Met (**Fig. S2**). Importantly, we found that inhibition of eIF4F cap complex with either eIF4E or eIF4G siRNA or the small molecule 4EGI-1 reduced c-Met protein levels (**Fig. 7**), indicating that elevated eIF4E and cap-dependent cap initiation regulates c-Met expression. Thus, it is likely that elevated eIF4E contributes to development of acquired EGFR-TKI resistance through facilitating c-Met expression in addition to gene amplification. Our findings warrant further investigation in this direction.

Since we detected increased levels of eIF4E mRNA and transcriptional activity in HCC827/ER cells (**Fig. 4**), it appears that elevated eIF4E expression in EGFR-TKI-resistant cells occurs at the transcriptional level. Thus, our current findings warrant further study to fully elucidate the mechanisms by which eIF4E expression is upregulated in EGFR-TKI-resistant cells.

In summary, the current study has demonstrated that eIF4E expression is elevated in human NSCLCs. The elevated eIF4e expression is associated with positive regulation of cell proliferation and invasion of NSCLC cells and contributes to development of acquired resistance to EGFR-TKIs.

Materials and Methods

Reagents. Erlotinib and gefitinib were purchased from LC Laboratories. 4EGI-1 was purchased from EMD Chemicals, Inc. or Calbiochem. They were dissolved in DMSO at the concentration of 20 or 100 mM, and aliquots were stored at -80°C. Stock solutions were diluted to the appropriate concentrations with growth medium immediately before use. eIF4E, eIF4G, Mcl-1, survivin, PARP, p-EGFR (Tyr1068), EGFR, p-Erb3 (Tyr1289), p-Met (Tyr1234/1235), Met and Akt antibodies were purchased from Cell Signaling Technology, Inc. Rabbit anti-HIF-1α and p-Akt (S473) were purchased from Epitomics. Mouse monoclonal anti-c-Myc and rabbit anti-Erb3 antibodies were purchased from Santa Cruz Biotechnology, Inc. Mouse monoclonal cyclin D1 antibody (clone DCS-6) was purchased from Dako. Mouse

monoclonal anti-actin and anti-tubulin antibodies were purchased from Sigma Chemical Co., 7-methyl GTP (m^7GTP)-sepharose 4B was purchased from GE Healthcare Biosciences.

Cell lines and cell culture. H1975, HCC827 and H1650 were purchased from the American Type Culture Collection. The SV40-immortalized normal human bronchial epithelial (NHBE) cell line, BEAS-2B,[19] and other NSCLC cell lines were generously provided by Dr. R. Lotan (MD Anderson Cancer Center). The Cdk4/hTERT-immortalized NHBE cell line, HBEC3KT,[20] was obtained from Dr. J. Minna (University of Texas Southwestern Medical Center). PLA-801C and PLA-801D cell lines[21] were obtained from Dr. Y.L. Lu (Institute of Basic Medical Science, Academy of Military Medical Sciences). PC-9 and gefitinib-resistant PC-9 (PC-9/GR) cell lines were provided by Dr. P.A. Jänne (Dana Farber Cancer Institute). All NSCLC cell lines were cultured with RPMI 1640 containing 5% fetal bovine serum and HBEC3KT and BEAS-2B cells were cultured with K-SFM medium containing 50 μg/mL bovine pituitary extract and 5 ng/mL EGF (Life Technologies) at 37°C in a humidified atmosphere of 5% CO_2 and 95% air.

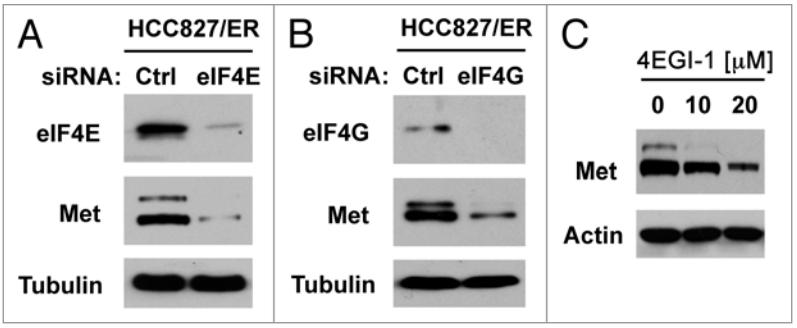

Figure 7. Inhibition of eIF4F formation by knocking down eIF4E (A) or eIF4G (B) or by inhibiting eIF4E and eIF4G interaction with 4EGI-1 (C) reduces c-Met protein levels. (A and B) HCC828/ER cells were transfected with control (Ctrl), eIF4E or eIF4G siRNA for 48 h. (C) HCC828/ER cells were treated with the indicated concentrations of 4EGI-1 for 24 h. After the aforementioned treatments, the cells were harvested for preparation of whole-cell protein lysates and subsequent western blotting.

Establishment of an erlotinib-resistant NSCLC cell line. The erlotinib-resistant HCC827 cell line (HCC827/ER) was established by exposing HCC827 cells to 3.5 μM erlotinib for 2 mo followed with one more month of exposure to 7.5 μM with 5 d drug on and 5 d drug off cycle. The resistant cell population was then routinely cultured with medium containing 1 μM erlotinib. HCC827/ER cell is also cross-resistant to gefitinib (**Fig. S2A**). Compared with HCC827 cells, HCC827/ER cells have down-regulated EGFR/p-EGFR and elevated levels of Met/p-Met, Akt/p-Akt and ERKs/p-ERKs, which are resistant to modulation by erlotinib (**Fig. S2B**). The resistance remains unchanged after withdrawal of erlotinib from culture medium for 6 mo, suggesting an irreversible phenotype (**Fig. S2C**).

Growth inhibition assay. Cell number in monolayer culture in 96-well plates was estimated by the sulforhodamine B (SRB) assay and the growth inhibition was calculated as previously described in reference 22. Combination index (CI) for drug interaction (e.g., synergy) was calculated using the CompuSyn software (ComboSyn, Inc.).

Colony formation assays. Colony formation assay on plastic surface was conducted in 6-well plate (approximately 600/well) as described previously in reference 23. To perform colony formation assay on soft agar, 0.5% bottom agar and 0.35% top agar were prepared and used for each 35 mm Petri dish. The top agar contained 5,000 cells. The dishes were cultured for 14 d and then stained with 0.005% crystal violet for 30 min. The colonies were then counted under a microscope.

Cell invasion assay. Cell invasion assay were performed using BD BioCoat™ Matrigel™ Invasion (BD Biosciences) coated with BD Matrigel Basement Membrane Matrix in a working concentration of 350 μg/ml. For each coated chamber, 25,000 cells in 500 μl of serum-free medium were seeded in the cell insert and pre-cultured for 8 h. After that, 750 μl complete medium supplemented with 10% fetal bovine serum was added to each lower chamber and culture for another 36 h. The invasive cells on the bottoms of the membranes were then counted after staining with Fisher Hema 3 Manual Staining System (Fisher Scientific) and normalized by live cells (determined by trypan blue) cultured at the same condition.

Western blot analysis. The procedures for preparation of whole-cell protein lysates and for western blotting were the same as described previously in reference 24.

IHC. Human lung cancer TMA was purchased from Imgenex (IMH-358). The TMA was stained with IHC using the EnVision + Dual Link System-HRP Kit (Dako) following the protocol. The rabbit polyclonal antibody against eIF4E (9742) was purchased from Cell signaling and used at 1:100 dilutions. eIF4E staining was scored as negative (<10% staining) and positive staining (≥ 10% staining), respectively.

m^7GTP pull-down for analysis of eIF4F complex. eIF4F complex in cell extracts was detected using affinity chromatography m^7GTP-sepharose as described previously in reference 25.

Small interfering RNA (siRNA)-mediated eIF4E and eIF4G knockdown. The siRNA duplexes for non-silencing control and eIF4E and their transfections were described previously in reference 25. eIF4G siRNA (sc-35286) was purchased from Santa Cruz Biotechnology.

Detection of eIF4E mRNA. The forward primer 5'-GGT TGC TAA CCC AGA ACA C-3' and reverse primer 5'-CAC TTC GTC TCT GCT GTT TG-3' were used for the RT-PCR to detect the eIF4E mRNA level. Forward primer 5'-GAA ACT ACC TTC AAC TCC ATC-3' and reverse primer 5'-CTA GAA GCA TTT GCG GTG GAC GAT GGA GGG GCC-5' were used to detect actin mRNA level as an internal control.

Construction of eIF4E reporter plasmid and luciferase activity assay. To make an eIF4E reporter construct, RT-PCR was used to amplify eIF4E promoter region (-1,507 to +72) from genomic DNA extracted from H157 cells using the following primers: forward 5'-GCG GGT ACC GCA CAG GCA GCC TGC ATA CA-3' and reverse 5'-CCC AAG CTT TCT CCT CTT CTG TAG TCG GGG G-3'. The final PCR product was

then cloned into pGL3-basic luciferase reporter vector (Promega Inc.) through KpnI and Hind III cloning sites to generate pGL3-eIF4E-luc construct. The transient transfection and subsequent luciferase assay have been described previously in reference 26.

Statistical analyses. The statistical significance between two groups was analyzed with two-sided unpaired Students t-tests or with Fishers exact test. All of these analyses were done by use of Graphpad InStat 3 software (GraphPad Software). Results were considered to be statistically significant at $p < 0.05$.

Disclosure of Potential Conflicts of Interest

No potential conflicts of interest were disclosed.

Acknowledgments

This study was supported by the Georgia Cancer Coalition Distinguished Cancer Scholar award (to S.Y.S.), NIH R01 CA118450 (S.Y.S.) and P01 CA116676 (Project 1 to F.R.K. and S.Y.S.), DOD BATTLE award W81XWH-06-1-0303 (Project 4 to F.R.K. and S.Y.S.) and Emory Winship Cancer Institute Cancer Cell Biology seed grant. S.S.R., T.K.O., F.R.K. and S.Y.S. are Georgia Cancer Coalition Distinguished Cancer Scholars.

Supplementary Material

Supplemental material can be found at:
www.landesbioscience.com/journals/cbt/article/18923/

References

1. De Benedetti A, Graff JR. eIF-4E expression and its role in malignancies and metastases. Oncogene 2004; 23:3189-99; PMID:15094768; http://dx.doi.org/10.1038/sj.onc.1207545.
2. Goodfellow IG, Roberts LO. Eukaryotic initiation factor 4E. Int J Biochem Cell Biol 2008; 40:2675-80; PMID:18069043; http://dx.doi.org/10.1016/j.biocel.2007.10.023.
3. Thumma SC, Kratzke RA. Translational control: a target for cancer therapy. Cancer Lett 2007; 258:1-8; PMID:17923280; http://dx.doi.org/10.1016/j.canlet.2007.08.022.
4. Graff JR, Zimmer SG. Translational control and metastatic progression: enhanced activity of the mRNA cap-binding protein eIF-4E selectively enhances translation of metastasis-related mRNAs. Clin Exp Metastasis 2003; 20:265-73; PMID:12741684; http://dx.doi.org/10.1023/A:1022943419011.
5. Graff JR, Konicek BW, Carter JH, Marcusson EG. Targeting the eukaryotic translation initiation factor 4E for cancer therapy. Cancer Res 2008; 68:631-4; PMID:18245460; http://dx.doi.org/10.1158/0008-5472.CAN-07-5635.
6. Clemens MJ. Targets and mechanisms for the regulation of translation in malignant transformation. Oncogene 2004; 23:3180-8; PMID:15094767; http://dx.doi.org/10.1038/sj.onc.1207544.
7. Rosenwald IB, Hutzler MJ, Wang S, Savas L, Fraire AE. Expression of eukaryotic translation initiation factors 4E and 2alpha is increased frequently in bronchioloalveolar but not in squamous cell carcinomas of the lung. Cancer 2001; 92:2164-71; PMID:11596034; http://dx.doi.org/10.1002/1097-0142(20011015)92:8<2164::AID-CNCR1559>3.0.CO;2-A.
8. Seki N, Takasu T, Mandai K, Nakata M, Saeki H, Heike Y, et al. Expression of eukaryotic initiation factor 4E in atypical adenomatous hyperplasia and adenocarcinoma of the human peripheral lung. Clin Cancer Res 2002; 8:3046-53; PMID:12374671.
9. Yang SX, Hewitt SM, Steinberg SM, Liewehr DJ, Swain SM. Expression levels of eIF4E, VEGF and cyclin D1, and correlation of eIF4E with VEGF and cyclin D1 in multi-tumor tissue microarray. Oncol Rep 2007; 17:281-7; PMID:17203162.
10. Wang R, Geng J, Wang JH, Chu XY, Geng HC, Chen LB. Overexpression of eukaryotic initiation factor 4E (eIF4E) and its clinical significance in lung adenocarcinoma. Lung Cancer 2009; 66:237-44; PMID:19261348; http://dx.doi.org/10.1016/j.lungcan.2009.02.001.
11. Seki N, Takasu T, Sawada S, Nakata M, Nishimura R, Segawa Y, et al. Prognostic significance of expression of eukaryotic initiation factor 4E and 4E binding protein 1 in patients with pathological stage I invasive lung adenocarcinoma. Lung Cancer 2010; 70:329-34; PMID:20621385; http://dx.doi.org/10.1016/j.lungcan.2010.03.006.
12. Khoury T, Alrawi S, Ramnath N, Li Q, Grimm M, Black J, et al. Eukaryotic initiation factor-4E and cyclin D1 expression associated with patient survival in lung cancer. Clin Lung Cancer 2009; 10:58-66; PMID:19289374; http://dx.doi.org/10.3816/CLC.2009.n.009.
13. Engelman JA, Janne PA. Mechanisms of acquired resistance to epidermal growth factor receptor tyrosine kinase inhibitors in non-small cell lung cancer. Clin Cancer Res 2008; 14:2895-9; PMID:18483355; http://dx.doi.org/10.1158/1078-0432.CCR-07-2248.
14. Wendel HG, De Stanchina E, Fridman JS, Malina A, Ray S, Kogan S, et al. Survival signalling by Akt and eIF4E in oncogenesis and cancer therapy. Nature 2004; 428:332-7; PMID:15029198; http://dx.doi.org/10.1038/nature02369.
15. Andrieu C, Taieb D, Baylot V, Ettinger S, Soubeyran P, De-Thonel A, et al. Heat shock protein 27 confers resistance to androgen ablation and chemotherapy in prostate cancer cells through eIF4E. Oncogene 2010; 29:1883-96; PMID:20101233; http://dx.doi.org/10.1038/onc.2009.479.
16. Moerke NJ, Aktas H, Chen H, Cantel S, Reibarkh MY, Fahmy A, et al. Small-molecule inhibition of the interaction between the translation initiation factors eIF4E and eIF4G. Cell 2007; 128:257-67; PMID:17254965; http://dx.doi.org/10.1016/j.cell.2006.11.046.
17. Graff JR, Konicek BW, Vincent TM, Lynch RL, Monteith D, Weir SN, et al. Therapeutic suppression of translation initiation factor eIF4E expression reduces tumor growth without toxicity. J Clin Invest 2007; 117:2638-48; PMID:17786246; http://dx.doi.org/10.1172/JCI32044.
18. Graff JR, Boghaert ER, De Benedetti A, Tudor DL, Zimmer CC, Chan SK, et al. Reduction of translation initiation factor 4E decreases the malignancy of ras-transformed cloned rat embryo fibroblasts. Int J Cancer 1995; 60:255-63; PMID:7829225; http://dx.doi.org/10.1002/ijc.2910600221.
19. Sun SY, Kurie JM, Yue P, Dawson MI, Shroot B, Chandraratna RA, et al. Differential responses of normal, premalignant and malignant human bronchial epithelial cells to receptor-selective retinoids. Clin Cancer Res 1999; 5:431-7; PMID:10037194.
20. Ramirez RD, Sheridan S, Girard L, Sato M, Kim Y, Pollack J, et al. Immortalization of human bronchial epithelial cells in the absence of viral oncoproteins. Cancer Res 2004; 64:9027-34; PMID:15604268; http://dx.doi.org/10.1158/0008-5472.CAN-04-3703.
21. Zhang JQ, Wang Y, Wang T, Du ZY, Xu YJ, Lu YL. Differentially expressed genes in human giant-cell lung cancer lines with different metastatic potentials. Zhonghua Zhong Liu Za Zhi 2004; 26:590-3; PMID:15634517.
22. Sun SY, Yue P, Dawson MI, Shroot B, Michel S, Lamph WW, et al. Differential effects of synthetic nuclear retinoid receptor-selective retinoids on the growth of human non-small cell lung carcinoma cells. Cancer Res 1997; 57:4931-9; PMID:9354460.
23. Wang X, Hawk N, Yue P, Kauh J, Ramalingam SS, Fu H, et al. Overcoming mTOR inhibition-induced paradoxical activation of survival signaling pathways enhances mTOR inhibitors' anticancer efficacy. Cancer Biol Ther 2008; 7:1952-8; PMID:18981735; http://dx.doi.org/10.4161/cbt.7.12.6944.
24. Sun SY, Rosenberg LM, Wang X, Zhou Z, Yue P, Fu H, et al. Activation of Akt and eIF4E Survival Pathways by Rapamycin-Mediated Mammalian Target of Rapamycin Inhibition. Cancer Res 2005; 65:7052-8; PMID:16103051; http://dx.doi.org/10.1158/0008-5472.CAN-05-0917.
25. Fan S, Li Y, Yue P, Khuri FR, Sun SY. The eIF4E/eIF4G interaction inhibitor 4EGI-1 augments TRAIL-mediated apoptosis through c-FLIP Downregulation and DR5 induction independent of inhibition of cap-dependent protein translation. Neoplasia 2010; 12:346-56; PMID:20360945.
26. Sun SY, Liu X, Zou W, Yue P, Marcus AI, Khuri FR. The Farnesyltransferase Inhibitor Lonafarnib Induces CCAAT/Enhancer-binding Protein Homologous Protein-dependent Expression of Death Receptor 5, Leading to Induction of Apoptosis in Human Cancer Cells. J Biol Chem 2007; 282:18800-9; PMID:17493934; http://dx.doi.org/10.1074/jbc.M611438200.

Print this Page

AACR ANNUAL MEETING
March 31- April 4, 2012 • Chicago, IL

Presentation Abstract

Abstract Number:	4819
Presentation Title:	Gene-expression profiles predict sorafenib efficacy in wild-type EGFR non-small cell lung cancer (NSCLC)
Presentation Time:	Tuesday, Apr 03, 2012, 3:20 PM - 3:35 PM
Location:	McCormick Place West (Level 1), Room W192
Author Block:	Pierre Saintigny[1], George R. Blumenschein, Jr.[1], Lixia Diao[1], Jing Wang[1], Kevin Coombes[1], Suyu Liu[1], Edward Kim[1], Anne Tsao[1], Roy Herbst[2], Christine Alden[1], Jack J. Lee[1], Ximing Tang[1], David Stewart[3], Merrill Kies[1], Frank Fossella[1], Hai Tran[1], Li Mao[4], Marshall Hicks[1], Jeremy Erasmus[1], Sanjay Gupta[1], Luc Girard[5], Michael Peyton[5], Suzanne Davis[1], Scott Lippman[1], Waun Ki Hong[1], John Minna[5], Ignacio Wistuba[1], John Heymach[1]. [1]UT MD Anderson Cancer Ctr., Houston, TX; [2]Yale Cancer Center, New Haven, CT; [3]University of Ottawa Faculty of Medicine, Canada, ON, Canada; [4]University of Maryland, Baltimore, MD; [5]UT Southwestern Medical Ctr., Dallas, TX
Abstract Body:	Background: Results from our Biomarkers-Integrated Approaches of Targeted Therapy for Lung Cancer Elimination (BATTLE) program suggest that patients with chemorefractory wild-type (wt) EGFR NSCLC including those with mutant KRAS may benefit from sorafenib. Using 3 different approaches, we tested the hypothesis that gene expression profiles from wild-type (wt) EGFR tumors may predict sorafenib efficacy by capturing effects on multiple targets. Material and Methods: Baseline tumor biopsies from 37 BATTLE patients (pts) with EGFR wt tumors and treated with sorafenib were profiled (Affymetrix Human Gene 1.ST), as well as 68 EGFR wt NSCLC cell lines with available IC50 to sorafenib (Illumina HumanWG-6 v3.0 expression beadchip). (i) We first developed an In vitro Sorafenib Signature (ISS). Correlation of IC50 with each individual probe expression level was computed. Most significant probes were summarized by the first principal component (PC), and correlated with IC50 of sorafenib. To validate the signature, the first PC was computed in BATTLE samples, and progression-free survival (PFS) of pts with high- vs. low-sensitivity signature was compared based on the median of the first PC. (ii) Alternatively, we developed a Clinical Sorafenib Signature (CSS) using BATTLE samples. We compared 23 (62%) pts who achieved 8-week disease control with 14 (38%) who did not (t-test). Most significant probesets were summarized by the first PC and PFS of pts with a high- vs. low-sensitivity signature were compared. To validate the signature, the first PC was computed in cell lines and correlated with IC50 of sorafenib. (iii) Finally, we tested a previously reported KRAS mutation gene expression signature derived by comparing genes differentially expressed in mutant vs. wt KRAS early stage resected lung adenocarcinomas, in 124 BATTLE samples including 24 mutant KRAS. Results: (i) The ISS included 50 probes. The first PC was correlated with the IC50 of sorafenib (rho = -0.71, $P < 0.0001$). The ISS was then tested in BATTLE and PFS was significantly different in pts with the high- (median PFS 3.61 months) vs. the low-sensitivity signature (median PFS 1.84 months, log-rank $P = 0.0263$). (ii) The CSS developed in BATTLE included 80 probesets summarized using the first PC. PFS was significantly different in pts with the high- vs. the low-sensitivity signature (log-rank $P < 0.0001$). The CSS was then tested in cell lines and the first PC was signicantly correlated with IC50 of sorafenib (rho = 0.24, $P = 0.0483$). (iii) Finally, the KRAS signature was significantly associated with KRAS mutation, but no association was observed with outcome in pts treated with sorafenib in BATTLE. Conclusion: We report 2 gene expression signatures, ISS and CSS, that predicted benefit from sorafenib in patients with chemorefractory NSCLC and in vitro sensitivity to sorafenib respectively. Further validation is planned in our ongoing BATTLE-2 program.

American Association for Cancer Research
615 Chestnut St. 17th Floor
Philadelphia, PA 19106